UNIVERSITY OF NOTTINGHAM

DEPARTMENT OF CIVIL ENGINEERING

Stress-Strain Relationships for Granular Materials under Repeated Loading

by

Philip Shaw, B.Sc.

November 1980

APPENDIX 6D

SIMPLE SHEAR TEST RESULTS - 1.5 mm MATERIAL

TEST	σ_v (kPa)	Final N cycles	$R_c(10)$
1B	284	5000	0.48
1BC	282	5000	0.47
2B	190	5000	0.48
2BC	190	5000	0.47
3B	97	5000	0.39
3BC	97	5000	0.45
1A	285	5000	0.46
1AC	283	5000	0.48
2A	190	5000	0.48
2AC	190	5000	0.50
3A	97	5000	0.62
3AC	97	5000	0.46

GENERAL TEST DATA - 1.5 mm MATERIAL

TEST RESULTS - 1.5 mm MATERIAL

TEST	τ (kPa)	LATERAL STRESS L (kPa) cycle 1		10		10^2		10^3		$5x10^3$	
		L1	L2	L1	L2	L1	L2	L1	L2	L1	L2
1B	+137	60.7	74.2	65.5	80.9	62.3	75.9	57.3	62.8	59.9	59.1
	-137	60.7	74.2	65.5	80.9	62.3	75.9	57.3	62.8	59.9	59.1
2B	+ 94	34.2	53.7	40.4	58.0	40.7	50.3	35.5	45.2	35.2	38.8
	- 94	34.2	53.7	40.4	58.0	40.7	50.3	35.5	45.2	35.2	38.8
3B	+ 37	19.6	38.9	19.7	37.1	19.8	37.2	19.9	31.4	19.9	29.5
	- 37	19.6	38.9	19.7	37.1	19.8	37.2	19.9	31.4	19.9	29.5
1BC	+134	70.4	93.5	60.9	90.5	57.8	81.5	52.9	62.5	55.3	58.6
	-134	70.4	93.5	60.9	90.5	57.8	81.5	52.9	62.5	55.3	58.6
	$\tau\&\sigma_v=0$	29.9	57.3	34.3	63.9	35.1	66.9	36.2	56.0	36.5	48.1
2BC	+ 92	50.2	59.7	50.6	62.1	48.8	66.5	41.5	57.2	41.9	51.5
	- 92	50.2	59.7	50.6	62.1	48.8	66.5	41.5	57.2	41.9	51.5
	$\tau\&\sigma_v=0$	20.1	19.9	20.2	27.9	20.3	30.2	18.9	26.8	19.4	23.0
3BC	+ 43	29.9	29.6	26.0	29.7	25.2	22.9	18.7	18.5	15.4	15.1
	- 43	29.9	29.6	26.0	29.7	25.2	22.9	18.7	18.5	15.4	15.1
	$\tau\&\sigma_v=0$	9.9	9.9	14.0	13.9	11.1	13.0	4.6	6.5	5.3	3.1

TEST RESULTS - 1.5 mm MATERIAL

TEST	τ (kPa)	LATERAL STRESS L (kPa) cycle 1		10		10^2		10^3		$5x10^3$	
		L1	L2	L1	L2	L1	L2	L1	L2	L1	L2
1A	132	49.9	69.2	52.2	59.6	58.4	53.8	59.1	49.6	37.6	38.9
	0	49.9	69.2	52.2	59.6	58.4	53.8	59.1	49.6	37.6	38.9
2A	101	45.7	49.2	39.9	39.5	39.9	37.6	34.8	28.5	30.2	17.7
	0	45.7	49.2	39.9	39.5	39.9	37.6	34.8	28.5	30.2	17.7
3A	60	29.9	39.5	23.9	33.6	22.2	27.9	17.6	19.4	4.0	17.6
	0	29.9	39.5	23.9	33.6	22.2	27.9	17.6	19.4	4.0	17.6
1AC	135	57.8	90.8	42.1	69.4	39.4	62.9	35.3	54.9	37.6	51.1
	$\tau\&\sigma_v=0$	17.8	21.6	19.9	29.6	19.2	34.8	16.9	32.6	21.1	30.7
2AC	105	58.9	54.5	45.4	39.1	34.5	28.3	36.0	28.7	36.7	22.1
	$\tau\&\sigma_v=0$	29.4	13.6	27.6	17.5	16.6	12.5	18.0	9.9	18.5	6.3
3AC	45	21.6	38.9	17.8	25.4	14.9	24.6	12.7	26.3	8.5	27.8
	$\tau\&\sigma_v=0$	3.9	9.7	3.9	9.7	3.1	10.9	2.7	10.5	2.4	7.9

TEST RESULTS - 1.5 mm MATERIAL

TEST	τ (kPa)	END STRESS E (kPa)									
		cycle 1		10		10^2		10^3		5×10^3	
		E1	E2	E1	E2	E1	E2	E1	E2	E1	E2
1B	+137	17.4	29.7	24.4	28.2	25.6	27.5	23.7	23.9	20.8	19.4
	-137	27.1	23.4	26.4	23.7	26.5	23.8	23.7	19.3	21.8	17.5
2B	+94	9.6	16.1	13.5	17.9	15.5	18.9	15.6	19.1	14.6	19.1
	-94	14.4	13.4	14.5	14.4	15.5	16.3	15.6	17.3	14.6	17.3
3B	+37	10.3	8.7	11.3	9.6	12.3	9.7	13.3	9.7	13.3	10.6
	-37	13.1	6.9	12.2	7.9	13.2	7.9	12.3	8.8	12.3	7.9
1BC	+134	16.3	21.5	17.5	20.8	17.6	20.9	16.7	21.9	16.7	20.0
	-134	21.1	18.8	20.3	27.1	20.5	19.1	18.7	20.2	16.7	20.2
	$\tau\&\sigma_V=0$	13.3	8.9	13.5	12.6	15.6	15.4	13.7	15.5	12.7	15.5
2BC	+92	9.6	14.3	13.5	13.5	15.6	14.5	15.6	14.6	13.7	13.7
	-92	12.5	10.7	12.6	10.8	13.6	11.8	13.7	11.8	12.7	11.8
	$\tau\&\sigma_V=0$	8.6	4.5	9.6	7.2	11.6	9.0	11.7	9.9	9.8	9.1
3BC	+43	4.7	7.1	6.7	8.0	6.7	8.0	5.8	9.9	4.8	8.9
	-43	7.6	7.1	7.6	6.2	6.7	7.1	5.8	8.0	4.8	8.1
	$\tau\&\sigma_V=0$	4.7	2.7	4.7	3.6	4.8	5.4	3.8	5.4	2.9	5.4

TEST RESULTS - 1.5 mm MATERIAL

TEST	τ (kPa)	END STRESS E (kPa)									
		cycle 1		10		10^2		10^3		5×10^3	
		E1	E2	E1	E2	E1	E2	E1	E2	E1	E2
1A	132	25.8	21.3	26.8	22.3	27.9	24.2	27.9	25.2	28.0	25.2
	0	23.8	24.0	24.9	24.1	25.9	25.9	26.0	26.9	25.1	27.0
2A	101	12.3	9.7	12.4	9.7	13.3	10.7	14.3	11.6	12.4	12.5
	0	11.4	10.6	11.4	10.6	12.4	11.6	13.4	13.4	11.5	13.4
3A	60	8.6	6.2	7.6	6.2	7.6	7.1	8.6	8.0	8.6	3.6
	0	7.6	7.1	7.6	7.1	7.6	7.1	8.6	8.0	9.6	1.8
1AC	135	23.8	17.7	22.0	11.6	20.2	8.1	18.4	7.2	16.5	5.4
	$\tau\&\sigma_v=0$	12.3	7.1	13.3	5.3	12.5	4.5	10.6	3.6	9.7	2.7
2AC	105	8.5	11.4	5.7	7.9	2.8	5.3	0.9	3.5	0.9	3.6
	$\tau\&\sigma_v=0$	1.9	4.4	1.9	4.4	0.9	2.6	0.0	1.8	0.0	1.8
3AC	45	14.1	6.1	12.3	4.4	12.3	3.5	9.5	2.7	5.7	0.9
	$\tau\&\sigma_v=0$	8.4	1.7	9.4	1.8	9.4	0.9	6.6	0.9	3.8	0.9

TEST	PERMANENT SHEAR STRAIN %				
	cycle 1	10	10^2	10^3	$5x10^3$
1A	1.70	2.04	2.53	2.97	3.21
1AC	1.30	1.81	2.45	3.04	3.24
2A	1.19	1.45	1.74	2.05	2.13
2AC	1.59	2.01	2.33	2.68	2.84
3A	0.79	0.94	1.15	1.31	1.37
3AC	1.19	1.65	2.19	2.69	3.01

TEST RESULTS - 1.5 mm MATERIAL

TEST	RESILIENT SHEAR STRAIN %				
	cycle 1	10	10^2	10^3	$5x10^3$
1B	4.24	2.12	1.78	1.67	1.65
1BC	3.49	2.11	1.75	1.62	1.61
2B	2.85	1.72	1.48	1.34	1.36
2BC	2.54	1.65	1.41	1.24	1.27
3B	1.75	1.01	0.89	0.81	0.79
3BC	1.52	1.00	0.83	0.79	0.75
1A	0.95	0.78	0.71	0.69	0.70
1AC	1.35	1.13	1.01	0.96	0.98
2A	0.76	0.60	0.57	0.52	0.55
2AC	1.02	0.77	0.68	0.64	0.57
3A	0.50	0.43	0.39	0.41	0.43
3AC	0.75	0.72	0.63	0.64	0.53

TEST	PERMANENT VOLUMETRIC STRAIN %				
	cycle 1	10	10^2	10^3	5×10^3
1B	2.63	3.61	4.23	4.76	4.99
2B	1.57	2.18	2.68	3.11	3.28
3B	0.95	1.31	1.66	2.02	2.22
1A	1.68	2.14	2.40	2.70	2.88
2A	0.84	1.11	1.31	1.53	1.59
3A	0.42	0.58	0.68	0.76	0.84

TEST RESULTS - 1.5 mm MATERIAL

TEST	σ_v	PERMANENT VOLUMETRIC STRAIN %				
		cycle 1	10	10^2	10^3	5×10^3
1BC	on	2.57	3.65	4.37	4.91	5.12
	off	1.91	2.93	3.80	4.43	4.67
2BC	on	1.21	1.94	2.46	2.95	3.09
	off	1.09	1.69	2.29	2.80	2.97
3BC	on	0.48	0.85	1.19	1.58	1.69
	off	0.42	0.81	1.15	1.56	1.66
1AC	on	2.11	2.52	3.13	3.82	3.99
	off	1.49	2.00	2.73	3.28	3.46
2AC	on	1.71	2.09	2.50	2.97	3.15
	off	1.33	1.74	2.19	2.67	2.86
3AC	on	1.03	1.40	1.76	2.22	2.41
	off	0.93	1.19	1.54	1.91	2.10

APPENDIX 6E

COMPARISON OF 3 mm AND 1.5 mm MATERIALS

BIDIRECTIONAL TESTS

3mm MATERIAL (ANSELL)

TEST	σ_v (kPa)	$R_c(10)$	Permanent Volumetric Strain % cycle 1	10	10^2	10^3	10^4
B11	285	0.53	0.49	1.77	2.97	4.05	4.77
BO7	190	0.51	0.18	0.86	1.58	2.24	2.72
BO1	95	0.32	0.06	0.12	0.26	0.47	0.66
			Resilient Shear Strain %				
B11	285	0.53	4.01	2.50	1.90	1.64	1.54
BO7	190	0.51	2.67	1.75	1.39	1.21	1.16
BO1	95	0.32	0.73	0.58	0.58	0.55	0.55

1.5mm MATERIAL

TEST	σ_v (kPa)	$R_c(10)$	Permanent Volumetric Strain % cycle 1	10	10^2	10^3	5×10^3
1B	285	0.48	2.63	3.61	4.23	4.76	4.99
2B	195	0.48	1.57	2.18	2.68	3.12	3.28
3B	97	0.39	0.95	1.31	1.66	2.02	2.22
			Resilient Shear Strain %				
1B	285	0.48	4.24	2.12	1.78	1.67	1.65
2B	195	0.48	2.85	1.71	1.48	1.34	1.36
3B	97	0.39	1.75	1.00	0.89	0.80	0.79

UNIDIRECTIONAL TESTS

3mm MATERIAL (ANSELL)

TEST	σ_v (kPa)	$R_c(10)$	cycle 1	10	10^2	10^3	$5x10^3$
			Permanent Shear Strain %				
A13	285	0.26	1.62	2.28	2.97	3.79	3.89
A06	190	0.21	0.98	2.27	1.66	2.11	2.44
A01	95	0.29	1.27	1.85	2.42	3.05	3.55
			Permanent Volumetric Strain %				
A13	285	0.26	0.39	0.64	1.00	1.45	1.51
A06	190	0.21	0.28	0.44	0.69	0.97	1.24
A01	95	0.29	0.14	0.27	0.47	0.71	0.96
			Resilient Shear Strain %				
A13	285	0.26	1.09	0.94	0.86	0.78	0.78
A06	190	0.21	0.73	0.59	0.55	0.50	0.50
A01	95	0.29	0.64	0.55	0.50	0.43	0.43

1.5mm MATERIAL

TEST	σ_v (kPa)	$R_c(10)$	cycle 1	10	10^2	10^3	$5x10^3$
			Permanent Shear Strain %				
1A	285	0.23	1.70	2.04	2.53	2.98	3.21
2A	197	0.25	1.19	1.45	1.74	2.05	2.13
3A	97	0.31	0.79	0.94	1.15	1.31	1.37
			Permanent Volumetric Strain %				
1A	285	0.23	1.68	2.14	2.40	2.70	2.88
2A	197	0.25	0.84	1.11	1.31	1.53	1.59
3A	97	0.31	0.42	0.58	0.68	0.76	0.84
			Resilient Shear Strain %				
1A	285	0.23	0.95	0.78	0.71	0.69	0.70
2A	197	0.25	0.76	0.60	0.57	0.52	0.55
3A	97	0.31	0.50	0.43	0.39	0.41	0.43

APPENDIX 7A

RESULTS FROM RAIL TRACK MODEL

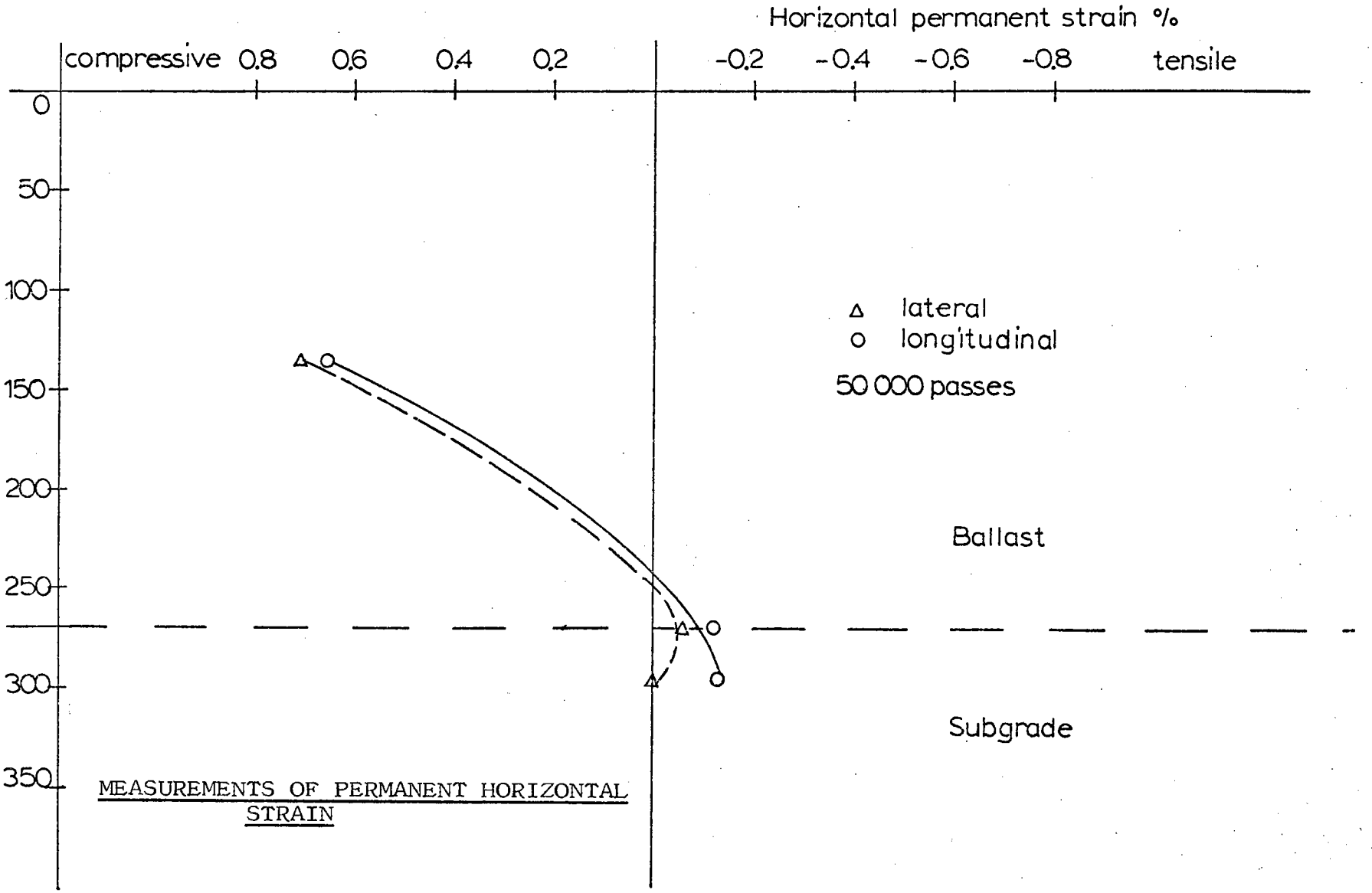

MEASUREMENTS OF PERMANENT HORIZONTAL STRAIN

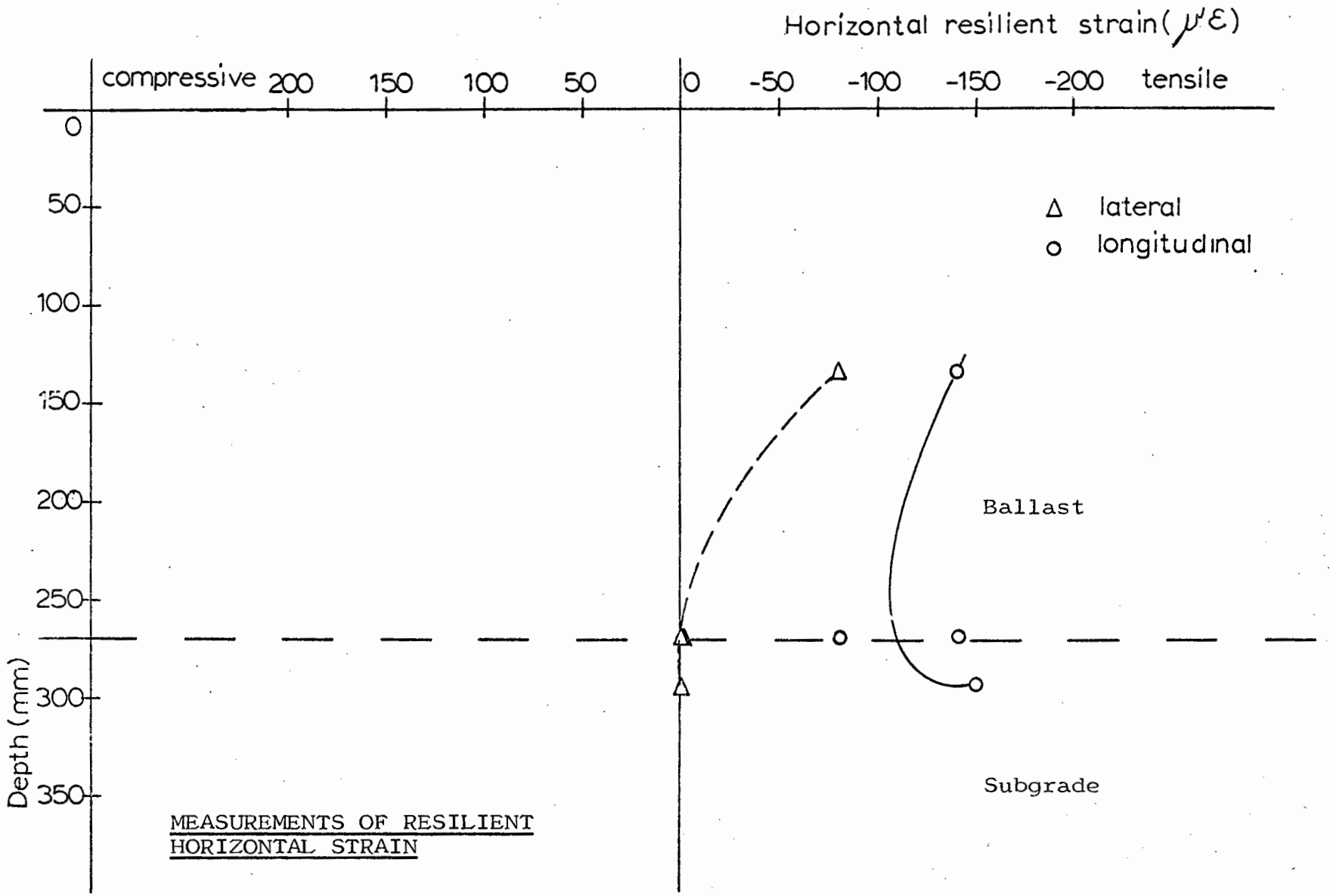

MEASUREMENTS OF RESILIENT HORIZONTAL STRAIN

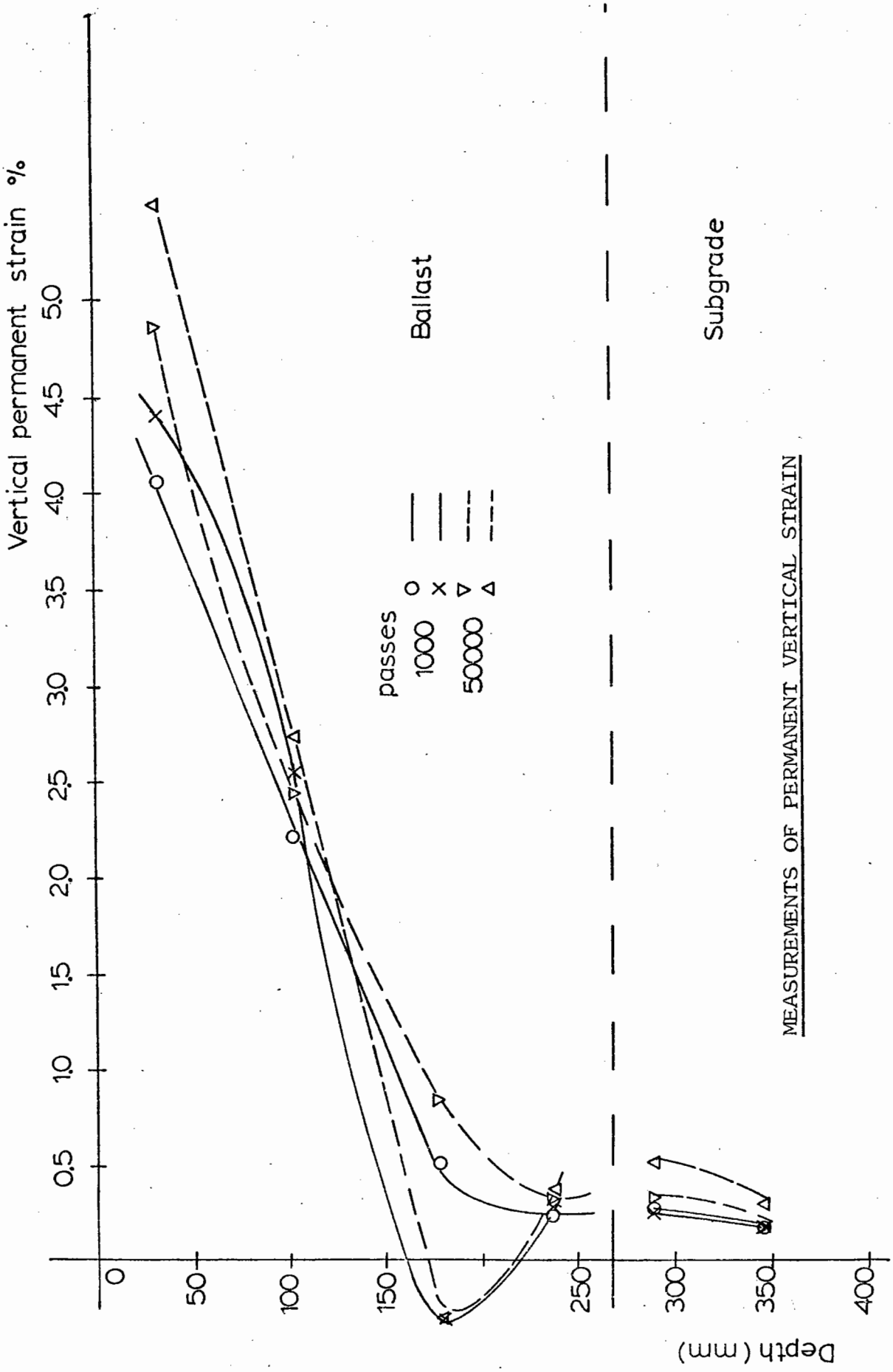

MEASUREMENTS OF PERMANENT VERTICAL STRAIN

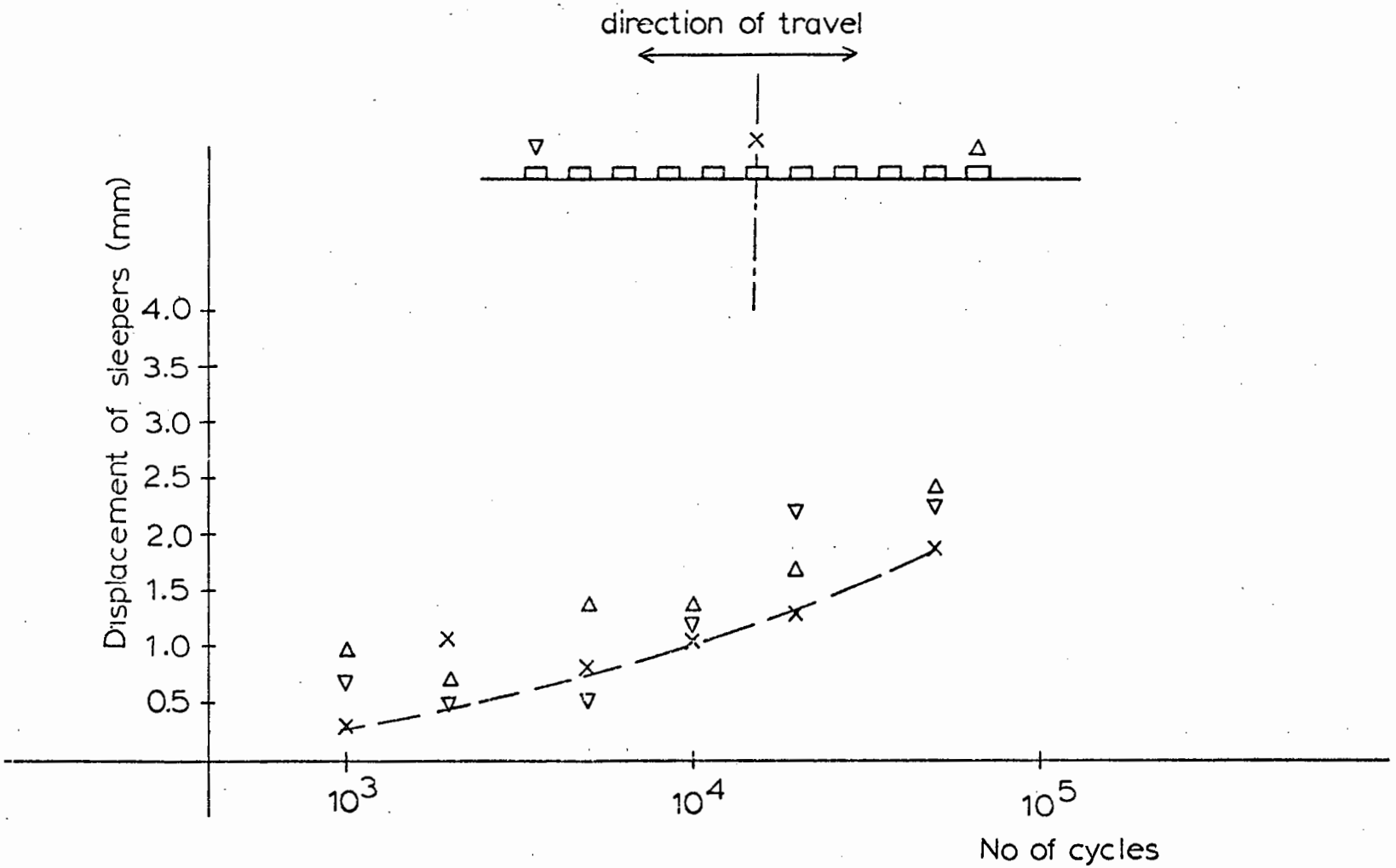

RELATIONSHIP OF PERMANENT DISPLACEMENT OF SLEEPERS WITH NUMBER OF CYCLES

UNIVERSITY OF NOTTINGHAM

DEPARTMENT OF CIVIL ENGINEERING

Stress-Strain Relationships for Granular Materials under Repeated Loading

by

Philip Shaw, BSc

Thesis submitted to the University of Nottingham
for the degree of Doctor of Philosophy

November 1980

ABSTRACT

The aim of the research was to characterise the behaviour of a granular material by means of laboratory testing. Servo-hydraulic triaxial equipment, a biaxial shear box and a simple shear apparatus were available and repeated load tests were conducted on a 3 mm single size crushed limestone material. The behaviour models developed were suitable for use in pavement analysis.

The resilient strain behaviour of the material was determined from repeated load triaxial testing and contours of resilient strain were drawn in the triaxial compression region. The contours were extended to triaxial extension and triaxial compression-extension stress states using a correction based on the ratio of the major to minor principal stresses. Results from repeated load biaxial tests showed that the resilient strain models could also be applied to $\sigma_1 \neq \sigma_2 \neq \sigma_3$ plane strain conditions. The resilient strain response of several other materials was investigated and similar models developed. Results were compared with those from a simple model relating resilient modulus to the sum of the principal stresses.

Test programmes to investigate permanent strain behaviour were conducted using the triaxial and biaxial equipment and models relating permanent shear strain rate to the distance of the stress path from the failure envelope were developed. Comparisons were made between the response of the single size material and that of a well graded material.

Modifications to the simple shear apparatus enabled normal stress on the sides and ends of the specimen to be measured. Tests with vertical load constant and cycled were conducted on the 3 mm crushed limestone material and results compared with those from previous research. Some problems were encountered in measuring lateral and end stresses and

a smaller material was selected for further testing. An attempt was made to correlate results from all three pieces of equipment.

The behaviour models were incorporated in a non-linear finite element program and used to analyse a number of road pavements. Predictions of stress and strain were compared with those obtained using the simple model relating resilient modulus and the stress state.

ACKNOWLEDGEMENTS

The author wishes to thank all those who have given help and advice in this research project, and in the preparation of the thesis. In particular:

Professor R.C. Coates, B.Sc.(Eng.), Ph.D., C.Eng., F.I.C.E., F.I.Struct.E., for providing all the facilities in the Department;

Dr S.F. Brown, B.Sc., Ph.D., C.Eng., M.I.C.E., F.I.H.E. and Professor R.W. Sparrow, B.A., B.A.I., Ph.D., C.Eng., M.I.C.E., for their helpful supervision of the work;

Mr D. Lockyer and Mr J. Moody for construction and maintenance of the apparatus;

Dr J.W. Pappin, B.E.(Hons.), M.E., Ph.D., C.Eng., M.I.C.E., for reading the draft of the thesis;

Miss J.L. Clerbaut for typing the thesis;

Sharon for preparation of diagrams and tables;

and all other members of staff in the Department and in the Faculty Workshops.

A research studentship provided by the Department of Education of Northern Ireland and the financial support of British Rail and the Transport and Road Research Laboratory are gratefully acknowledged.

CONTENTS

LIST OF SYMBOLS

E	Young's Modulus		
G	shear modulus		
K	bulk modulus		
M_R	resilient modulus of elasticity		
N	number of load cycles		
e	void ratio		
fnN	permanent shear strain shape function		
ℓ	stress path length in (p,q) stress space		
n	porosity		
$\sigma_1, \sigma_2, \sigma_3$	principal stresses		
$\sigma_x, \sigma_y, \sigma_z$	cartesian stresses		
σ_a	axisymmetric axial stress-triaxial axial stress		
σ_r	axisymmetric radial stress-triaxial radial stress		
σ_θ	axisymmetric tangential stress		
$\tau_{xy}, \tau_{xz}, \tau_{yz}$	shear stress		
ε_{ax}	axisymmetric axial strain-triaxial axial strain		
ε_{rad}	axisymmetric radial strain-triaxial radial strain		
$\varepsilon_x, \varepsilon_y, \varepsilon_z$	principal strains		
$\gamma_{xy}, \gamma_{xz}, \gamma_{yz}$	shear strains		
θ	sum of principal stresses		
ν	Poisson's Ratio		
p	normal stress	triaxial stresses $\frac{\sigma_a + 2\sigma_r}{3}$	three-dimensional stresses $\frac{\sigma_1 + \sigma_2 + \sigma_3}{3}$
q	deviator stress	$\sigma_a - \sigma_r$	$\frac{1}{\sqrt{2}}\left[(\sigma_1-\sigma_2)^2+(\sigma_2-\sigma_3)^2+(\sigma_3-\sigma_1)^2\right]^{\frac{1}{2}}$

v	volumetric strain	$\varepsilon_{ax} + 2\varepsilon_{rad}$	$\varepsilon_1 + \varepsilon_2 + \varepsilon_3$
ε	shear strain	$\frac{2}{3}(\varepsilon_{ax}-\varepsilon_{rad})$	$\frac{\sqrt{2}}{3}\left[(\varepsilon_1-\varepsilon_2)^2+(\varepsilon_2-\varepsilon_3)^2+(\varepsilon_3-\varepsilon_1)^2\right]^{\frac{1}{2}}$

Suffices

c	contour
m	mean
r	repeated (stress) or resilient (strain)
1	beginning of stress path
2	end of stress path

Compressive stresses and strains are taken as positive. Other symbols are defined and used in restricted conditions as required.

LIST OF FIGURES

CHAPTER ONE

INTRODUCTION

The construction or improvement of the transportation network is regarded as one of the most effective ways of promoting economic development of a country. This is evident from the considerable road and rail construction taking place in newly developing countries. Design involves the selection of materials and the determination of the thickness necessary to ensure that the resulting structure will carry traffic safely and at minimum cost.

In recent years, increased traffic loading has resulted in a rapid deterioration of the existing network in many countries generating considerable expenditure on maintenance. There is obviously a close relationship between construction and maintenance. A road which is generously designed will probably show a saving on maintenance but the initial investment will be too high. A lower design standard will reduce initial outlay but the cost of maintenance will soon become prohibitive.

Current design practice is still largely empirical, based on the findings of rather limited full scale test sections. Reliance on past experience can often be misleading, since experience gained at a particular site or in a particular country is dependent on a large number of changeable factors. At present road pavements in the UK tend to be predominantly of bituminous materials; however, with increasing oil prices and an expanding overseas work load, attention is being directed towards more efficient use of the properties of unbound materials. Traditional design methods cannot cope with changes in loading, construction materials or new construction techniques and this has led to the development of a

"structural" design method. The road pavement is treated as a structure and traffic loads are so distributed that the stresses and strains developed at all levels in the pavement are within the capabilities of the materials at those levels. The method therefore requires an understanding of the loading conditions and some fundamental knowledge of the stress-strain characteristics of the materials being used. The structural approach enables new loadings and materials to be handled as well as giving more attention to the important mechanical properties of the materials and is of more value than traditional methods.

The simplest type of analytical system is to consider the pavement as a structure of three or four layers, each layer being treated as linear elastic. This approach has been used extensively for resilient analysis (e.g. Peutz et al, 1968). Previous research (Hicks 1970, Allen and Thompson 1974, Brown 1974) has shown that the resilient behaviour of crushed rock or granular materials is very stress dependent and cannot be described using linear elastic theory alone. However, the method assumes that stress is proportional to strain and a constant Young's Modulus (E) and Poisson's ratio (ν) are specified for each material. The resilient modulus of a granular layer depends, among other things, on that of the material below and has an upper limit determined by the modulus of the underlying material. Generally, the modulus of the granular layer is not higher than $1\frac{1}{2}$ to $2\frac{1}{2}$ times that of the underlying soil (Heukelom and Klomp 1962). Experience has shown that in analysis a value for this modular ratio of about 2 is adequate for the design of pavements with asphalt bases. For situations in which the granular layer is not of major structural importance, this approximation is unlikely to lead to major errors. However, if the main structural layer of the pavement is composed of granular materials, then account has to be taken of their non-linear properties.

Single size granular materials are extensively used to provide a support system for railway tracks. The function of the granular layer is to spread the traffic loading in a manner which will not overload the supporting ground. Design philosophy for flexible road pavements is directed towards limiting permanent deformations to reasonable levels and preventing cracking of the bituminous bound layers. Structural maintenance of the pavement, if properly designed, should therefore be a rare event. However, in the railway track situation, where the only external constraint applied to the track to hold the geometry is the ballast, much higher levels of permanent deformation are experienced. Track maintenance, in the form of recompaction of the ballast to restore alignment and vertical profile of the track is therefore a regular feature of conventional rail track systems. Effective track maintenance procedures can only be developed if information is available on the ballast itself and how it behaves under the loading regime it experiences.

This dissertation is therefore devoted to investigating the stress-strain relationships of unbound granular materials by means of laboratory testing.

Material specimens may be subjected to either monotonic or repeated load tests. Material behaviour is completely different for the two loading conditions. In order to properly simulate field behaviour, it is necessary to subject the specimens to loads that will produce the same stress state as the passage of a wheel. The stresses acting in a pavement consist of repeated vertical and horizontal stresses and repeated reversing shear stresses (Fig. 1.1a). This is equivalent to variations in the magnitude of the principal stresses, σ_1, σ_2 and σ_3, accompanied by principal axes rotation (Fig. 1.1b). A repeated load triaxial apparatus, a repeated load biaxial shear box and a simple shear apparatus were available and an attempt has been made to investigate the response of unbound granular materials to these stress regimes.

FIG. 1.1 (a)

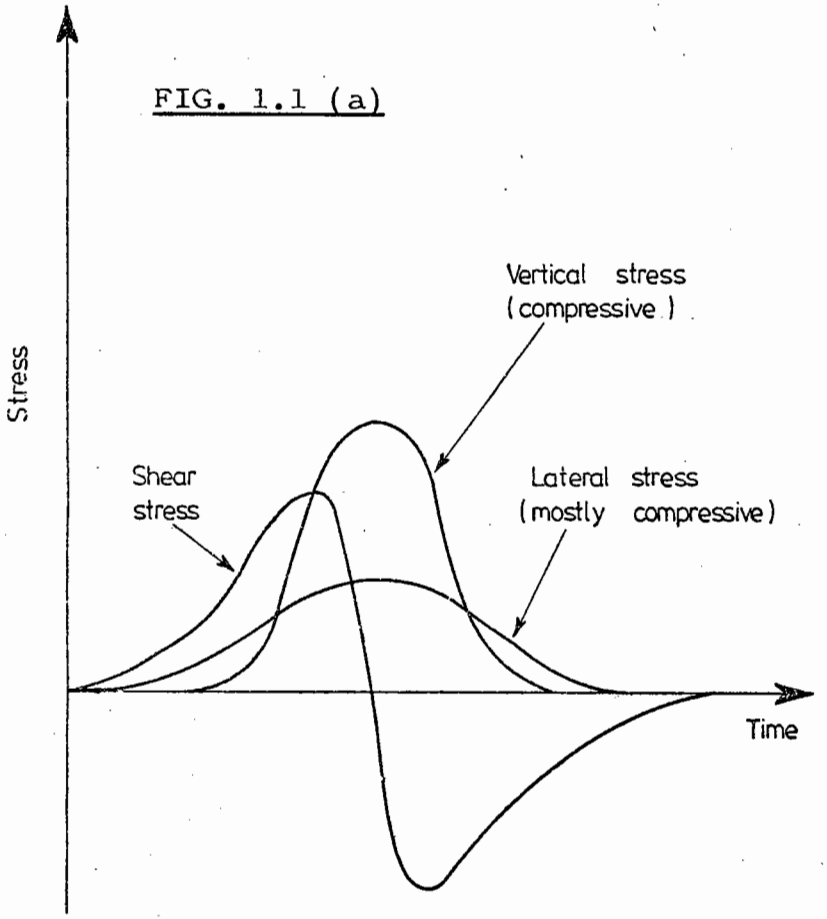

FIG. 1.1 (b)

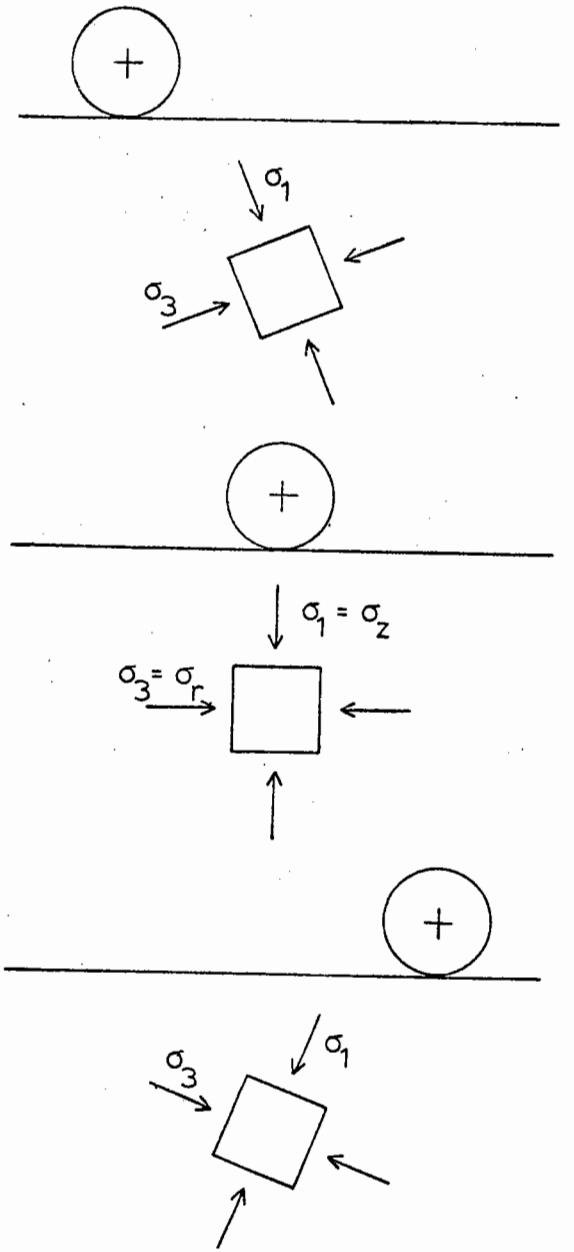

STRESSES BENEATH A ROLLING WHEEL LOAD

The material exhibits two distinct types of behaviour (Fig. 1.2). The first of these is the resilient (recoverable) response which is the rebound or "elastic" behaviour of the material under one application of load. The second is the permanent strain effect, which is the build up of irrecoverable strain after a number of load applications. Both properties are of importance to the pavement situation. The resilient characteristics are required to analyse the transient response of the structure to a single pass of a wheel load, and the irrecoverable properties are necessary to analyse the development of permanent strain.

A servo-hydraulic repeated load triaxial apparatus has been developed at the University of Nottingham (Boyce 1976, Pappin 1979). The apparatus was capable of cycling both cell pressure and axial load and was chosen because stress conditions are well defined and similar to those experienced by elements of material directly under a wheel load. Boyce and Pappin performed extensive repeated load tests on a well graded crushed limestone in an attempt to determine the resilient properties of the material. Models were developed relating the resilient strains to the applied stresses. The triaxial test is limited in that only principal stresses can be directly applied to a test specimen and because of the axisymmetric arrangement, two of these must necessarily be equal. During the passage of a wheel load, the principal stresses within elements gradually rotate (Fig. 1.1b) and this cannot be simulated by the triaxial apparatus. However, the apparatus was used as described in the following chapters in order that a comparison could be made between the behaviour of a single size crushed limestone material and that tested by Boyce and Pappin. A comparison was also made for results obtained using the three pieces of equipment available.

The biaxial shear box was designed by British Rail at the Technical

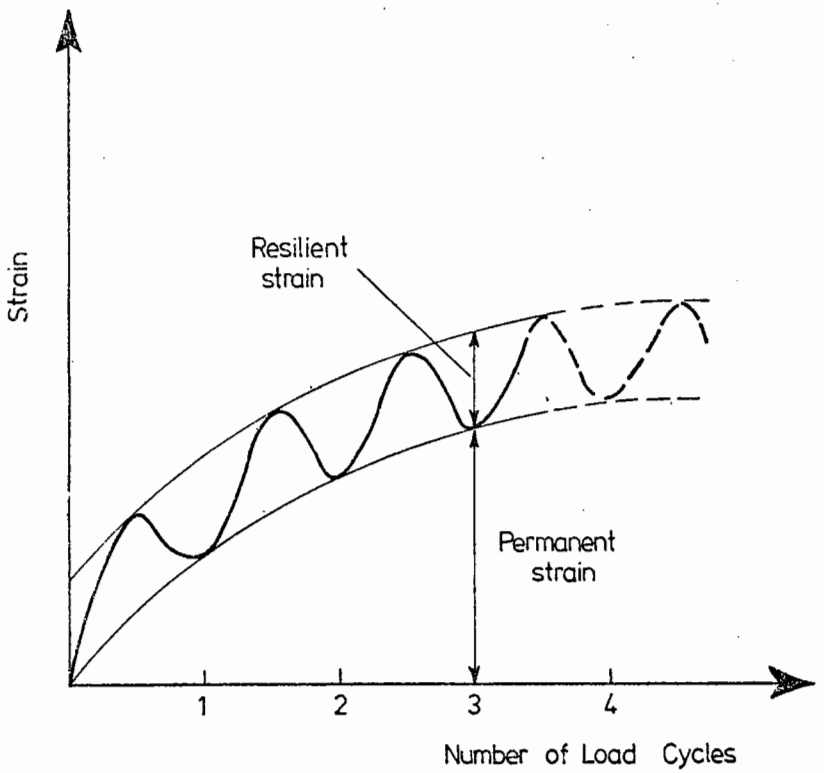

FIG. 1.2 COMPONENTS OF STRAIN IN THE REPEATED LOAD TRIAXIAL TEST

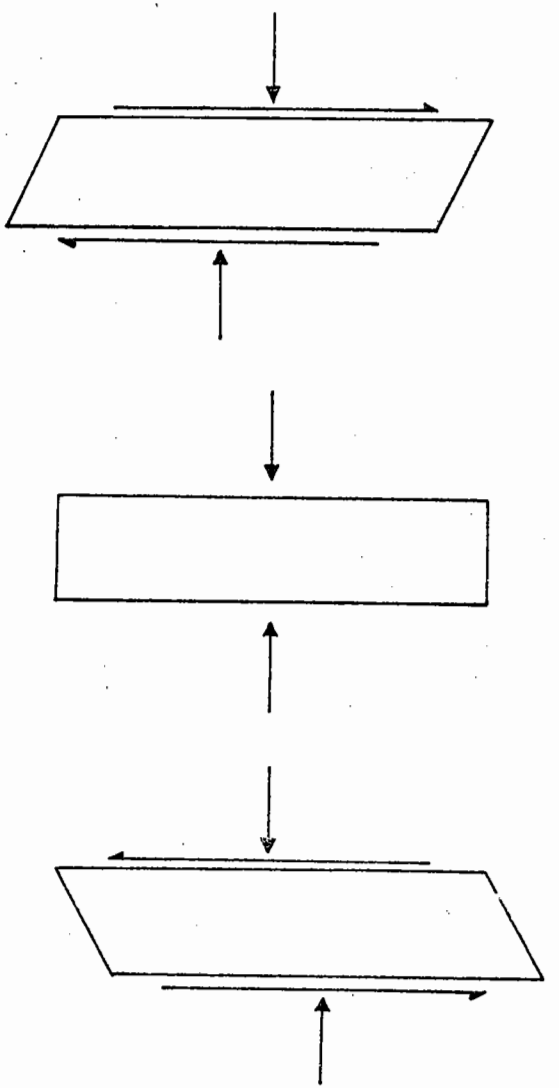

FIG. 1.3 SAMPLE DEFORMATION MODE IN THE SIMPLE SHEAR APPARATUS

Centre, Derby and was developed in connection with their track bed research programme. The apparatus could subject specimens to three independent principal stresses and repeated loads were applied using pneumatic rams operated by compressed air. The apparatus was used to investigate the effectiveness of tamping as a track bed maintenance procedure. Permanent deformation of the specimen due to repeated loading in the in situ vertical direction was firstly monitored and then observations made on the subsequent behaviour of the material after tamping by temporarily changing the direction of the principal stresses.

A rectangular simple shear apparatus capable of applying reversed shear stresses to specimens under plane strain conditions has been developed at Cambridge (Roscoe 1953). Financial restrictions ruled out any possibility of purchasing a Cambridge Simple Shear Apparatus (CSSA). However, a simpler model was developed at the University of Nottingham (Ansell 1977). The shear reversal is achieved by applying normal and shear loads to the top and bottom faces of the specimen as shown in Fig. 1.3. Ansell performed unidirectional and bidirectional tests on a single size crushed limestone material and subsequent chapters describe the continuation of this work.

To adequately examine the response of a material to different stress regimes, it is necessary to have some means of correlating results. This is best done by making a comparison of the stresses to which the specimens are subjected. The applied stresses in the triaxial and biaxial equipment are, by definition, principal stresses. However, the simple shear apparatus, as originally designed, only provided measurements of the vertical normal stress and horizontal shear stress on the top and bottom faces of the specimen respectively. This is not sufficient to determine the total stress state in the specimen. Considerable work has been conducted at Cambridge to design load cells to measure stresses

on the sides and ends of the CSSA (Bransby 1973). The original design of the Nottingham apparatus and the lack of funds encouraged the development of load cells at the University of Nottingham. Principal stresses could, therefore, be calculated to provide a means of correlating results from the three pieces of equipment. The repeated load triaxial apparatus is the most commonly used for pavement material characterisation. Comparisons of test results with those from other stress regimes provided some indication of the adequacy of the axisymmetric triaxial arrangement in modelling in situ stresses.

The major aim of the project was to establish stress-strain relationships for granular materials and these have subsequently been incorporated in non-linear finite element analysis of several road pavements.

CHAPTER TWO

REVIEW OF PREVIOUS WORK

2.1 INTRODUCTION

Effective, accurate methods of design for any structure require adequate knowledge of the properties of the materials which constitute the structure. Considerable work has been conducted to establish constitutive models for various materials used in pavement design. This chapter contains a review of some of the literature for both static and repeated load testing of granular materials for use in both pavement and permanent way. A short summary of the use of non-linear models in pavement analysis is also included.

The project is a continuation of the work by Ansell (1977) and Pappin (1979) who both conducted literature surveys. It is not the intention of the author to reproduce their reviews but rather to highlight some additional and some more recent developments in granular materials research.

2.2 EFFECTS OF TEST CONFIGURATION

It is essential that test conditions used to investigate the properties of materials simulate the in situ conditions as closely as possible. The stress regime in a road pavement and also in the rail track bed situation is such that the material is subjected to vertical and radial stress pulses, along with a shear stress reversal. Chapter 1 described this as being equivalent to variations in the magnitude of the principal stresses, σ_1, σ_2 and σ_3, accompanied by principal axes rotation.

The variation of stress with time for the road pavement situation is shown in Fig. 1.1. This is the stress regime which must be reproduced

as closely as possible in laboratory testing if results are to be used with some confidence in pavement design. Chapter 1 gives an introduction to the apparatus available at the University of Nottingham along with some details of their limitations.

The servo hydraulic triaxial equipment is capable of applying sinusoidal wave-shaped repeated confining and deviator stresses to a specimen 150 mm diameter by 300 mm long. The major limitations of the triaxial test are that only principal stresses may be applied, two of which must be equal because of the axial symmetry of the arrangement. The major principal stress can only act in either the vertical or horizontal direction limiting the rotation of the principal axes to a full right angle.

The biaxial shear box subjects 100 mm cubical specimens to $\sigma_1 \neq \sigma_2 \neq \sigma_3$ conditions. The apparatus involves plane strain and is limited to applying principal stresses only. The stress in the plane strain direction is measured using a load cell and the stresses in the remaining two directions are applied via air rams.

The simple shear apparatus is rectangular and applies shear reversal to specimens 140 mm x 210 mm x 30 mm deep under plane strain conditions. It is therefore possible to subject specimens to rotation of principal axes other than through a full right angle. The apparatus applies a vertical and shearing load as described in Chapter 1 and measurements of normal and shearing stresses enable principal stresses to be calculated.

For any project in which test results from several pieces of equipment are to be correlated, it is necessary to know the effects of test configuration on the measured soil properties.

Cornforth (1964) compared strengths of Brasted Sand in plane strain compression tests with those measured in triaxial tests at the

same placement density. During testing in the plane strain apparatus the relationship between the intermediate stress and the sum of the other two stresses was almost constant. It was found that strengths of the plane strain specimens were generally greater than the strengths of the corresponding triaxial specimens at the same placement density. However, the average ultimate strengths obtained in plane strain and triaxial compression testing were sufficiently close to be the same and independent of the intermediate principal stress.

Sutherland and Mesdary (1969) investigated the influence of the intermediate principal stress on the strength of sand. They tested a cuboidal specimen enclosed in a watertight membrane. The influence of σ_2' on ϕ' was observed over the range of σ_2' from σ_3' to σ_1'. Generally, the value of ϕ' was higher in the case of $\sigma_1' \neq \sigma_2' \neq \sigma_3'$. Results from cubical triaxial compression tests with $\sigma_2 = \sigma_3$, were compared with results from conventional cylindrical triaxial specimens and practically identical strengths were obtained.

Green and Reades (1975) investigated the effects of sample shape on the stress-strain characteristics of a sand. They used an independent stress control cell in which the three principal stresses or strains acting on a cuboidal sample could be independently controlled. The results from tests on a rectangular specimen were compared with those from a cylindrical specimen. Triaxial compression tests on specimens of differing densities revealed similar strengths for rectangular and circular specimens. The rectangular specimens, however, tended to show greater dilation and marginally lower axial strain at failure. A number of plane strain tests were also conducted. Green points out that plane strain testing generally results in greater experimental scatter, but failure tests under plane strain conditions tend to yield higher ϕ' values.

Comparisons of triaxial compression tests and plane strain tests by Lee (1970) also confirmed that plane strain tests produced greater ϕ' values for sand.

However, the major contribution of the work described in subsequent chapters is for repeated load testing. Little information was available, but Pyke (1978) reports on the effects of test configuration on measured soil properties under cyclic loading. Results of tests conducted on a dry, clean sand are presented for both triaxial and simple shear equipment. The simple shear apparatus was of the Norwegian Geotechnical Institute type (Section 2.5). By assuming K_o values for the simple shear apparatus and correcting triaxial data for anisotropy, it was possible to obtain similar values of shear modulus.

2.3 TESTING OF SINGLE SIZE MATERIAL

Raymond and Davies (1979) described monotonic tests on a dolomite railroad ballast. Triaxial compression and extension tests were performed at constant strain rate on saturated, drained specimens. It was found that the material had a higher friction angle in compression than in extension and strength envelopes based on Coulomb's failure criterion were found not to pass through the origin. The intercept was quite high in comparison with tests on sands and rounded gravel. It was suspected that this phenomenon was due to the angularity of the ballast particles and the fact that the ballast had 100% crushed faces.

Shenton (1974) conducted repeated load triaxial tests on a limestone ballast (Ballidon quarry) and found that settlement was proportional to the logarithm of the number of cycles of stress. Resilient response of the ballast was found to be virtually unaffected by frequency of loading and tended to stabilise after a relatively small number of cycles. A model relating permanent axial strain and number

of load cycles was developed as:

$$e_N = e_1(1 + 0.2 \log_{10} N) \qquad (2.1)$$

where e_1 and e_N are the permanent deformations at first and N^{th} load cycle respectively.

Raymond and Williams (1978) conducted repeated load triaxial tests on dolomite ballast. The test programme contained stress paths in both triaxial compression and extension. They found that under repeated load triaxial compression conditions, the ballast tended to become stiffer and then oscillate about a constant value after 10 000 cycles. Large amounts of permanent axial strain occurred during the first cycle and the amount of strain per cycle decreased with increasing number of cycles. Axial strain was observed to change approximately linearly with the logarithm of the number of cycles up to 100 000 cycles.

Sparrow (1976) described the initial design of a biaxial shear box built at the British Rail Technical Centre, Derby. The apparatus was suitably modified for use in this project (Chapter 4). The apparatus had the ability to test dry, granular materials under $\sigma_1 \neq \sigma_2 \neq \sigma_3$ conditions. Phillips (1975) presented results of tests carried out on a railway ballast which confirmed the strain relationship presented by Equation 2.1.

2.4 TESTING OF GRADED MATERIAL

A simple non-linear model relating resilient modulus and stress level is:

$$M_R = K_1 \theta^{K_2} \qquad (2.2)$$

The model is generally obtained from triaxial testing as described by Hicks and Monismith (1971). M_R is the resilient modulus, θ is the sum

of the principal stresses and K_1 and K_2 are material constants. Chapter 5 contains details on the development of the model and compares it with a more complex model, for both graded and single size materials.

Boyce (1976) and Pappin (1979), performed repeated load triaxial tests on graded specimens of a crushed limestone. Boyce conducted tests on dry specimens and Pappin continued research on the same material testing dry, saturated and partially saturated specimens. The work described in subsequent chapters is a continuation of that by Pappin, so his work is described in some detail.

Triaxial specimens were subjected to repeated load tests with confining stress both constant and cycled. The axial and radial deformations were monitored for each test.

The applied stresses were expressed in terms of:

$$\text{normal stress } p = \frac{1}{3}(\sigma_x + \sigma_y + \sigma_z) \tag{2.3}$$

$$\text{deviator stress } q = \frac{1}{\sqrt{2}}\{(\sigma_x-\sigma_y)^2 + (\sigma_y-\sigma_z)^2 + (\sigma_z-\sigma_x)^2 + 6\tau_{xy}^2 + 6\tau_{xz}^2 + 6\tau_{yz}^2\}^{\frac{1}{2}} \tag{2.4}$$

The resulting strains were expressed in terms of:

$$\text{volumetric strain } v = \varepsilon_x + \varepsilon_y + \varepsilon_z \tag{2.5}$$

and

$$\text{octahedral shear strain } \varepsilon = \frac{\sqrt{2}}{3}\{(\varepsilon_x-\varepsilon_y)^2 + (\varepsilon_y-\varepsilon_z)^2 + (\varepsilon_z-\varepsilon_x)^2 + \frac{3}{2}\gamma_{xy}^2 + \frac{3}{2}\gamma_{yz}^2 + \frac{3}{2}\gamma_{xz}^2\}^{\frac{1}{2}} \tag{2.6}$$

For the axisymmetric triaxial situation these reduce to:

$$p = (\sigma_a + 2\sigma_r)/3 \quad (2.7)$$

$$q = \sigma_a - \sigma_r \quad (2.8)$$

$$v = \varepsilon_{ax} + 2\varepsilon_{rad} \quad (2.9)$$

$$\varepsilon = \frac{2}{3}(\varepsilon_{ax} - \varepsilon_{rad}) \quad (2.10)$$

where σ_a and ε_{ax} are the axial stress and strain, σ_r is the confining stress and ε_{rad} is the radial strain.

The stress paths applied to the specimens by Boyce are shown in Fig. 2.1. Following these tests, which investigated resilient strain behaviour, Boyce developed a stress-strain relationship for the material. Pappin, however, found that the resilient strains could be expressed as a series of contours in (p,q) stress space as shown in Figs 2.2 and 2.3. Chapter 3 contains further details of the method by which the contours were developed and their interpretation. Assuming that the ratio of major to minor principal stress was constant, a correction was obtained which enabled stress paths in the triaxial extension region to be converted to equivalent triaxial compression stresses. The contour models developed for the compressive region of (p,q) stress space could therefore be applied to triaxial extension.

A model relating permanent shear strain to the maximum stress ratio (q/p) and the stress path length was also developed and is described in Chapter 3.

2.5 SIMPLE SHEAR TESTING AND STRESS ROTATION

The inability of the triaxial apparatus to produce gradual shear stress reversal has led to the development of several pieces of equipment capable of applying rotation of principal axes.

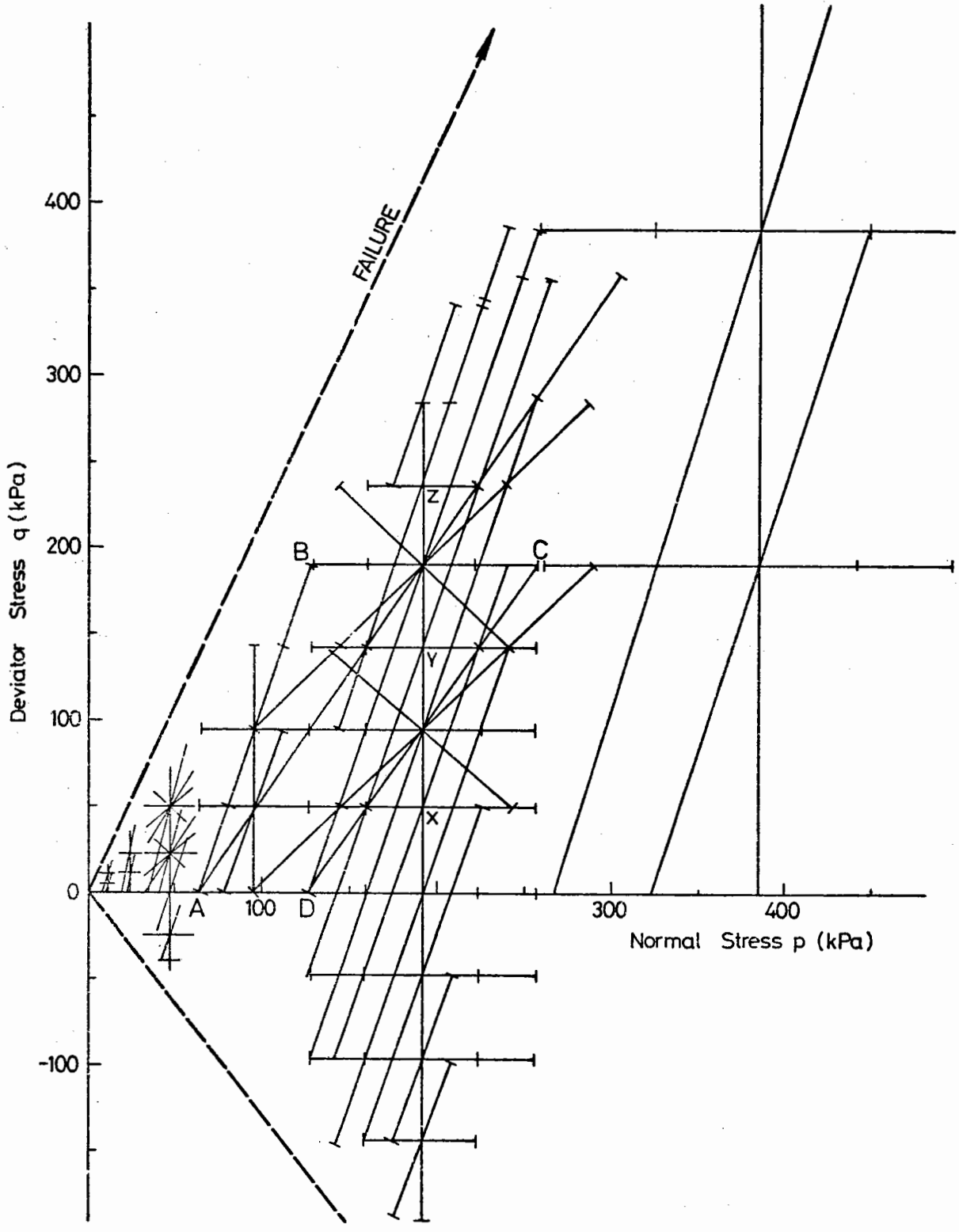

FIG. 2.1 STRESS PATHS TO INVESTIGATE RESILIENT STRAIN BEHAVIOUR (BOYCE 1976)

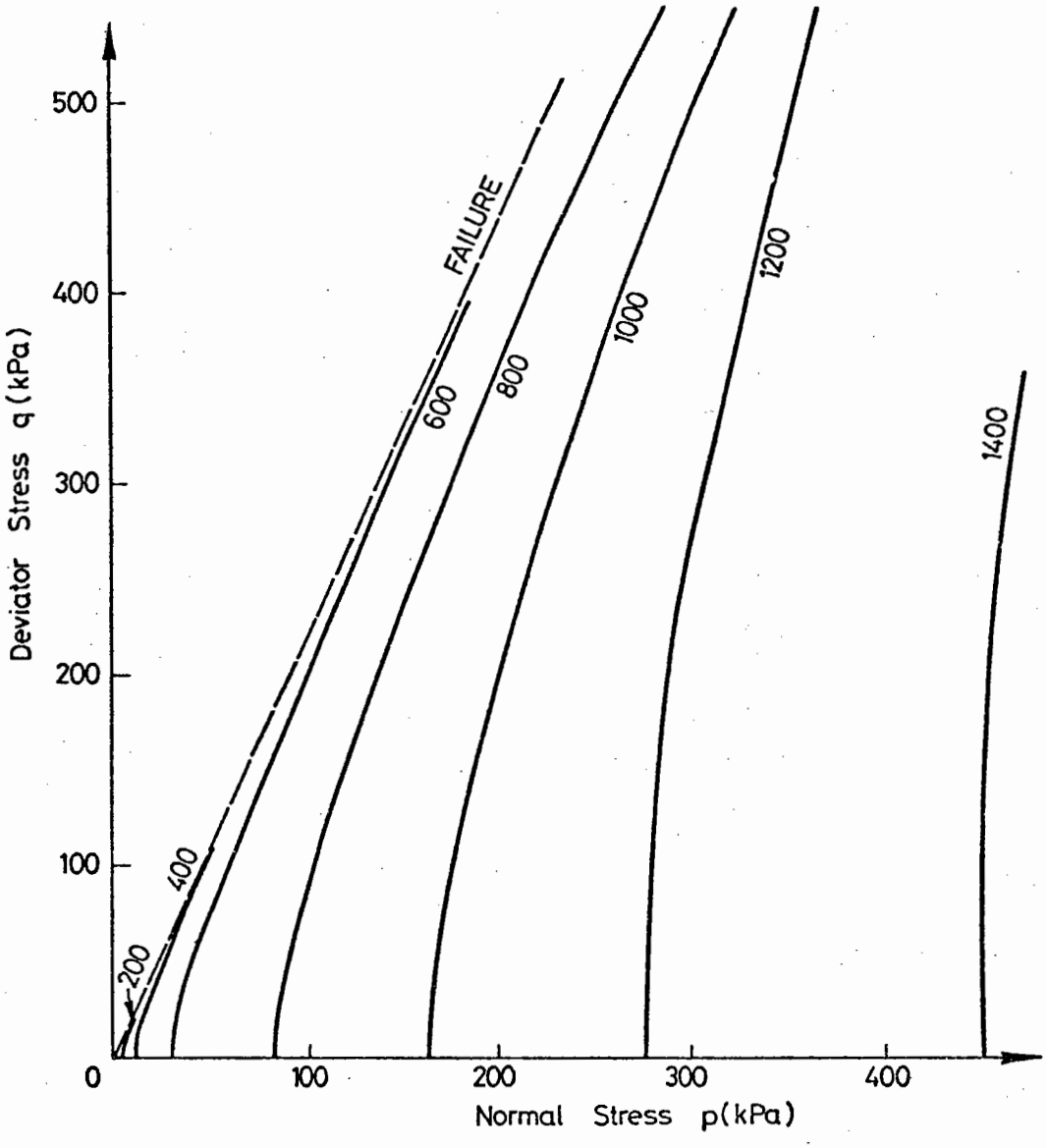

FIG. 2.2 CONTOURS OF VOLUMETRIC STRAIN IN (p,q) STRESS SPACE (PAPPIN 1979) (με)

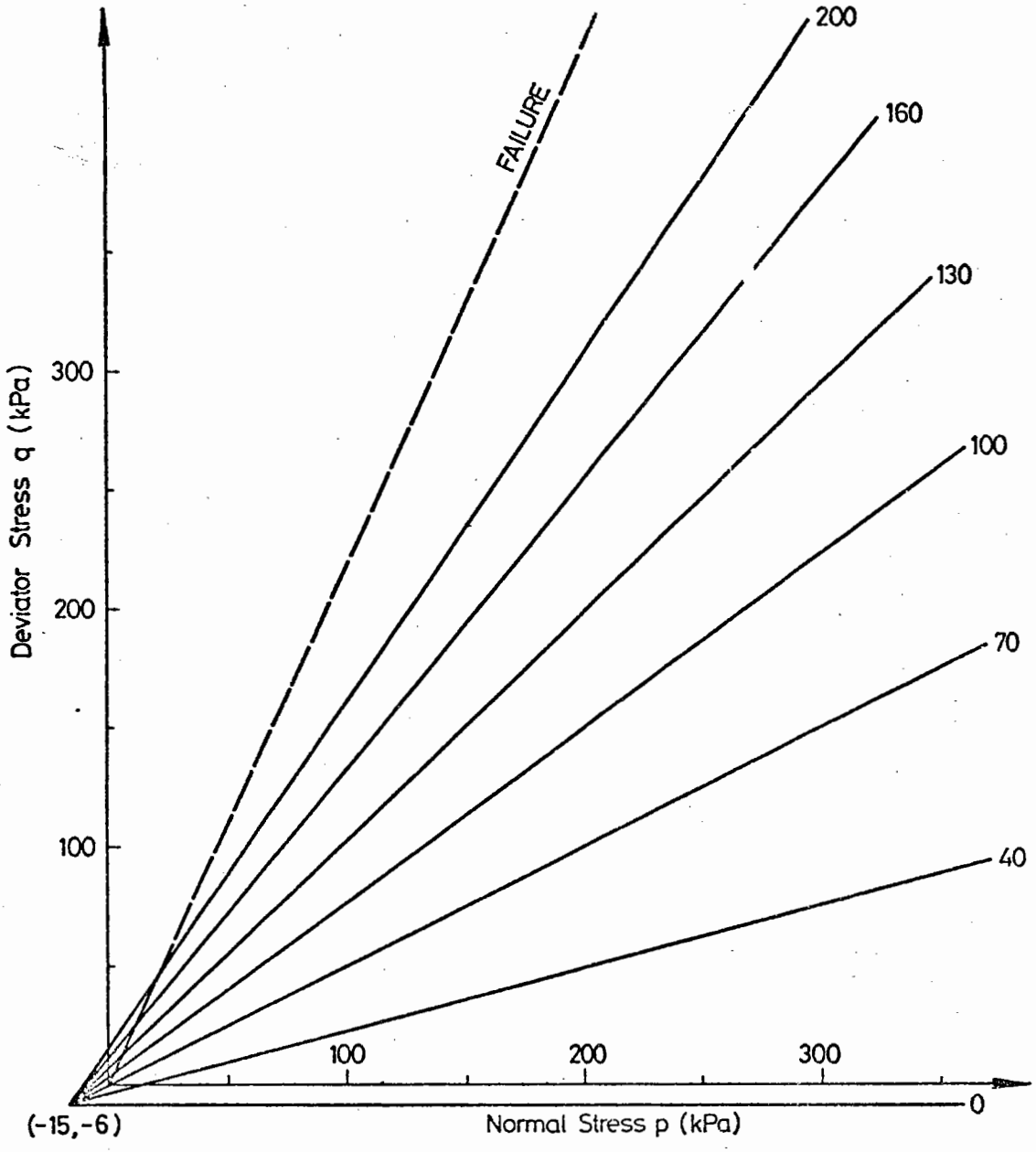

FIG. 2.3 CONTOURS OF NORMALISED SHEAR STRAIN IN (p,q) STRESS SPACE (PAPPIN 1979) (με)

Roscoe (1953) describes the original Cambridge Simple Shear Apparatus which could apply simple shear strain to a specimen 60 mm square by approximately 20 mm deep. This was an improvement on the standard direct shear box which constrained specimens to shear along a narrow plane at approximately mid-specimen depth. This tended to produce severe strain non-uniformities and by testing striped plasticene specimens in both pieces of equipment, Roscoe demonstrated the comparatively uniform strains produced in the new apparatus. The apparatus has subsequently been developed to an advanced stage where it is possible to obtain accurate measurements of stresses and strains in the specimen.

A different type of simple shear apparatus was developed at the Norwegian Geotechnical Institute (NGI) and is described by Bjerrum and Landva (1966). The specimen was an 80 mm diameter cylinder and approximately 10 mm deep surrounded by a confining rubber membrane reinforced by spiral binding wire.

More recently Arthur et al (1977) describes a new flexible boundary apparatus (Direct Shear Cell) having the ability to apply controlled rotation of principal stress axes. The specimen is enclosed in a thin unreinforced membrane and is subjected to plane strain. Both shear and normal stresses are applied to the specimen faces. The shear stress is applied via an inextensible reinforced rubber "pulling sheet" attached to each face by rubber strips glued at 5 mm intervals. Normal stresses are applied to the faces using reinforced rubber pressure bags, the stress being transmitted through the intervening rubber strips and sheets. A diagram of the apparatus is shown in Fig. 2.4. Careful manipulation of stress ratios enabled principal stress rotation to be achieved at any stage of testing.

Wood and Budhu (1980) discuss some of the inadequacies of the

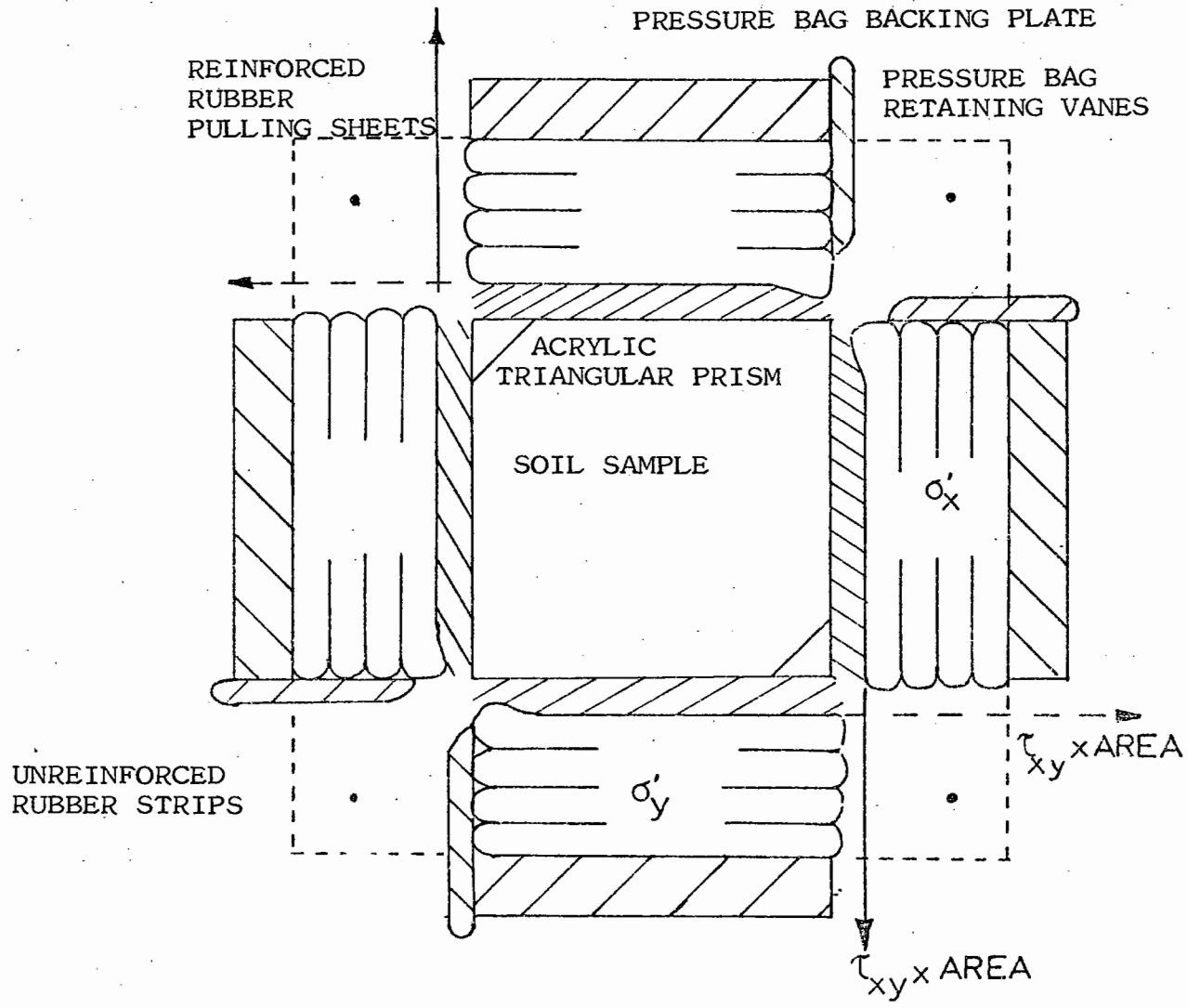

FIG. 2.4 FLEXIBLE BOUNDARY APPARATUS
(ARTHUR et al 1977)

Cambridge Simple Shear Apparatus. The main criticism is the lack of complementary shear stress on the specimen ends resulting in non-uniform shear stress distributions on the top and bottom boundaries of the specimen. These non-uniformities have led to the policy of surrounding the specimen with contact stress transducers. A circular simple shear apparatus similar to the NGI apparatus is also described in which only the average stresses applied to the horizontal boundaries of the specimen are measured. No measurement is made of the lateral stresses and the deformation is assumed uniform. Some comparisons of stress ratios obtained from central contact stress transducer readings in the square apparatus and those obtained by observing the average stresses recorded by the circular apparatus are presented. Generally, average stress ratios measured in monotonic and cyclic loading were lower than central stress ratios. The rectangular apparatus is principally a steel box but the circular apparatus is basically a specimen contained between horizontal boundaries and within a rubber membrane. A series of repeated load tests on Leighton Buzzard sand conducted in the rectangular shear box confirmed Youd's (1972) and Ansell's (1977) findings that two-way cyclic simple shear straining produced lower void ratios than can be produced by other simple means. Brown and Ansell (1980) suggest that if horizontal rather than vertical vibration were applied by rollers in the field, more efficient compaction may be achieved.

Arthur, Chua and Dunstan (1979) report the results of a number of cyclic load tests using the Direct Shear Cell. Tests on Leighton Buzzard sand were conducted in which the rotation of the major and minor principal stresses was entirely continuous. It was found that cyclic continuous rotation of the major principal stress direction resulted in large reductions of strength.

Youd (1975) presented data for lateral stresses in sands during cyclic loading. The tests were conducted in a Norwegian Geotechnical Institute type of simple shear apparatus. The horizontal stresses acting on the specimen were monitored with the aid of membranes in which strain gauge wire was used for reinforcement. Average horizontal normal stresses acting on the cylindrical specimen were calculated for changes in the electrical resistance of the reinforcing wire. The tests were performed on a dry sand of 0.36 mm mean particle size. They involved incrementally increasing and decreasing the vertical stress. The second phase of the experiment applied cyclic shear loading for a constant vertical stress and finally vertical stress was cycled in the absence of any shear load. Youd found that the value of K_o increased with increasing initial void ratio and appeared to be approximately consistent with Bishop's (1958) empirical relationship $K_o = 1 - \sin \phi'$. During repeated shear straining the coefficient of lateral stress increased with shear strain amplitude and cyclic number.

The increase in K_o appeared to be negligible for strain amplitudes less than 0.01% but was considerably higher at strain amplitudes near 1%. The amount of increase in the coefficient was greatest during the first cycle and diminished with cycle number thereafter. Prevost and Hoeg (1976) in a mathematical analysis of the simple shear apparatus evaluated the changes in lateral total stress and produced an expression for the induced change in octahedral normal total stress during a simple shear state of strain.

Roscoe, Bassett and Cole (1967) used the Cambridge Mk VI Simple Shear Apparatus to investigate the directions of the principal axes of stress and strain for Leighton Buzzard sand. Hill (1950) postulates that the principal axes of the plastic strain increment coincides with the principal axes of stress for a material which is exhibiting plastic

behaviour. For elastic conditions, it is the principal axes of strain increment and stress increment which coincide. Monotonic tests conducted on the sand revealed that the specimens tended to compact initially, but as peak shear stress ratios were approached, showed considerable expansion. It was found that the axes of strain increment and stress showed excellent agreement especially between minimum voids ratio and peak shear stress ratio conditions. The principal axes of strain increment and stress increment only appeared to coincide at very small strains. This indicated that the material could only be considered as elastic for a very limited range of strains and for the major part should be considered as a plastic media.

Wood, Drescher and Budhu (1979) make reference to the work of Roscoe and assuming that the principal axes of strain increment and stress coincide, have developed a technique for determining the stress state around a simple shear specimen. The method required only the applied vertical load and shear stress to be measured on the top and bottom boundaries of the specimen. The procedure is discussed in more detail in Chapter 6 where predictions are made of the stresses around the specimen in a simple shear apparatus at the University of Nottingham.

Ansell (1977) describes the development of the simple shear apparatus at the University of Nottingham. Repeated load bidirectional and unidirectional tests were conducted on a 3 mm single size crushed limestone. The simple shear behaviour of the material was characterised by a relatively large initial strain after which the rate of accumulation of permanent strain tended to decrease with number of cycles. Various empirical models for the response of the material were developed and presented in both graphical and mathematical form. A more detailed description of the apparatus as developed by Ansell and subsequent modifications are presented in Chapter 6.

2.6 APPLICATION OF CONSTITUTIVE MODELS TO PAVEMENT AND RAILWAY TRACK ANALYSIS

Although the majority of problems associated with maintenance of road and railway track structures are the result of permanent straining, it is of major importance that the resilient behaviour of the materials is fully understood. A knowledge of the transient properties enables the stress distribution to be accurately determined after which the permanent strain response of the structure can be investigated.

Granular materials exhibit non-linear resilient characteristics. However, many pavement structures are still analysed using layered elastic theory (e.g. Peutz, Van Kempen and Jones 1968). This necessitates the use of a constant Young's Modulus and Poisson's ratio for each material throughout the pavement structure. However, it is possible to model granular material response without linear elastic assumptions.

The relationship of Equation 2.2 has been used extensively in the United States for pavement analysis. Raad and Figueroa (1980) report the use of the model in finite element analysis. Prediction of stresses in the granular layer, however, tended to be high and a method was employed which modified the principal stresses so that they did not exceed the strength of the material as defined by the Mohr Coulomb failure envelope. Turcke and Raymond (1979) in a three-dimensional finite element analysis of a rail track structure, report the development of tensile stresses in the ballast. They used a technique where fictitious restraining forces were introduced to counteract the tensile principal stresses. Adegoke et al (1979) also report the use of Equation 2.2 to model the non-linear response of railway ballast.

Pappin (1979) describes the development of a non-linear finite element program which incorporates the resilient contour models described previously to model the granular layer. The program was used to predict

the response of test pavements to moving wheel loads. Brown et al (1980) describe the comparison between predicted and measured stresses and strains indicating that the program predicted resilient strains more accurately than transient stresses. However, the contour models did not predict tensile stresses in the granular layer.

CHAPTER THREE

THE REPEATED LOAD TRIAXIAL TEST

3.1 INTRODUCTION

A servo hydraulic repeated load triaxial apparatus has been developed at Nottingham over a number of years (Boyce 1976, Pappin 1979). This chapter gives a brief description of the equipment along with results from monotonic failure tests on a single size crushed limestone material.

Contour models of shear and volumetric strain produced from an extensive test programme are presented and compared with results obtained using a K-theta model. A test programme to investigate permanent strain behaviour is described and a model to predict permanent shear strain developed. The effects of permanent straining on resilient behaviour and static strength are also discussed. Tests conducted on several other materials are described and comments made on the suitability of contours for general use in modelling granular materials.

3.2 EQUIPMENT DESCRIPTION

3.2.1 Loading Equipment

The principal components of the servo-hydraulic equipment are shown in Fig. 3.1. The axial load and confining stresses were applied to specimens in a triaxial cell by hydraulic actuators. The axial load was continuously monitored by a load cell which formed an integral part of the load ram. The load cell output was compared with a load command signal by the electronic control system. An error signal was then applied to the servo-valve on the actuator so as to correct the load applied to that required. The confining stress was similarly controlled by the output of a pressure transducer in the cell fluid. The pressure

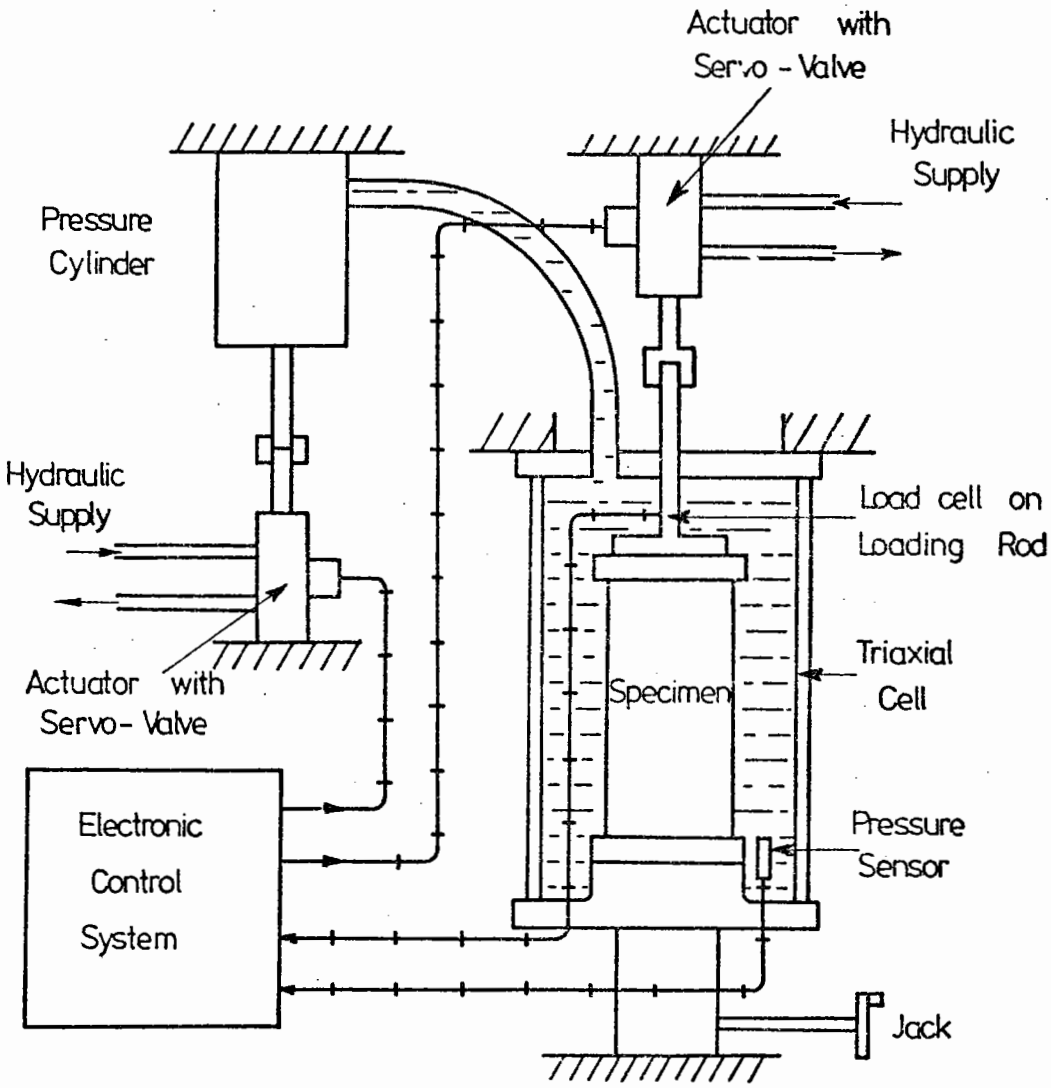

FIG 3.1 DIAGRAM OF LOADING EQUIPMENT

transducer consisted of a strain gauged diaphragm which directly measured the pressure difference across it. At cell pressures approaching zero, the servo-hydraulic system tended to respond sluggishly to command signals. To increase efficiency in this range it was possible to apply a back pressure to the specimen and, by increasing the cell pressure to a more acceptable value, retain the same effective cell pressure.

A back pressure equal to that on the specimen was applied to the pressure transducer so that direct readings of the effective cell pressure could be obtained. The two command signals were derived from the same waveform generator (Prosser type A100) which had the facilities for producing many different waveforms and had two sinusoidal outputs with variable phase difference. There were additional controls enabling the command signal to be taken from a ramp generator and the feedback to be taken from axial strain measurements, so that single load tests could be performed at a constant rate of strain.

3.2.2 Material

The material selected for testing was as used by Ansell (1977) in the simple shear apparatus. The size fraction passing 3/16 in. BS sieve and retained on No. 7 BS sieve was taken from a wet-mix base material as supplied by Amalgamated Roadstone Corporation, Chipping Sodbury. Full details of the physical properties of the material are given in Table 3.1.

3.2.3 Specimen Preparation

Each specimen was enclosed in two latex membranes. The inner one (0.3 mm thick) was held against the porous inner surface of a four piece former by an applied vacuum during specimen preparation. The outer one (0.5 mm thick) was added afterwards to cover any inner membrane punctures produced during compaction.

Table 3.1 Aggregate Properties

Property	Value	Size fraction
Specific gravity	2.71	All size fractions
Aggregate crushing value	19	
Aggregate abrasion value	7.4	
Angularity	10.1	1/2" - 3/8" sieves
Elongation	26%	
Flakiness	21%	

The technique used to measure strain required location studs to be attached to the inner membrane before it was placed inside the specimen former. These are discussed in the following section.

To reduce end platen restraint "free ends" were provided. This involved making a "sandwich" of high vacuum silicone grease and latex membrane on the top and bottom platens. The high vacuum silicone grease did not harden with time. Prior to specimen preparation, the bottom platen was placed on a vibrating table. The former with the inner membrane held inside, was then placed on top of the platen and clamped to the table (see Fig. 3.2). After each batch of material was placed in the former, it was tamped by hand and then vibrated for 30 seconds with a nominal surcharge placed on top to keep the surface level. Six consecutive periods of vibration were used of 5 seconds each, starting with the largest amplitude and decreasing to the smallest. The material was placed in four batches.

The top platen was then placed in position and the voids of the specimen were evacuated so that the former could be removed. The second membrane was placed over the specimen and both membranes were sealed by stretching 'O' rings over the platens. The density of each

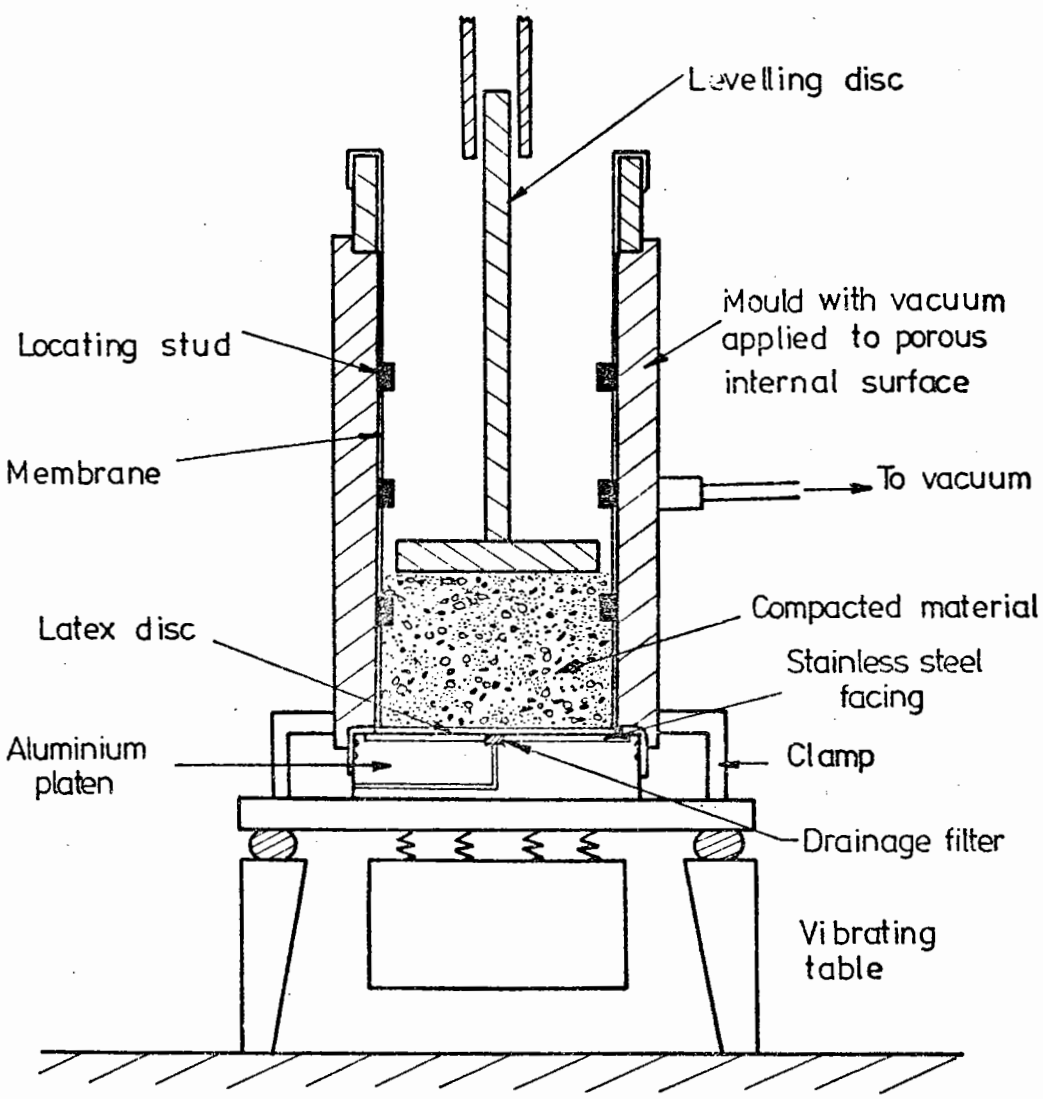

FIG. 3.2 SPECIMEN PREPARATION

specimen was estimated from the weight of material used and the external dimensions. This method of compaction produced an average density of 1.62 Mg/m^3.

3.2.4 Deformation Measurement

Strain measurements were taken from points on the specimen by means of location studs (Fig. 3.3). These have the advantage that using a vibrating table for compaction enabled the material to be compacted around the studs (Fig. 3.2). Each stud can be considered as an aggregate particle with an extension protruding through the membrane. Fig. 3.3 shows how the location studs were attached to the inner membtane and the procedure for sealing the outer membrane around the 6 BA rod protruding from each stud. The studs were attached to the inner membrane before it was placed inside the specimen former and the 6 BA rods were inserted after the outer membrane had been added. There were six studs on each sample 75 mm apart as shown in Fig. 3.4.

Axial strain was measured by four small LVDTs attached to the 6 BA rods and operating over separate gauge lengths as shown in Fig. 3.4. The LVDTs had a range of ±5 mm and a weight of about 10 g. Normally, measurements were taken with all four LVDTs, the outputs averaged electrically and the reading plotted on one channel of an ultra violet (U.V.) recorder.

Radial strain was measured by three strain rings (Fig. 3.5). These were made from araldite and weighed 27 g each. The rings were made narrower at the strain gauges to give increased sensitivity. Wiring with 600 Ω foil strain gauges produced sensitivities of about 0.9 mV/mm. The outputs were averaged electrically and the resulting value plotted on one channel of a U.V. recorder.

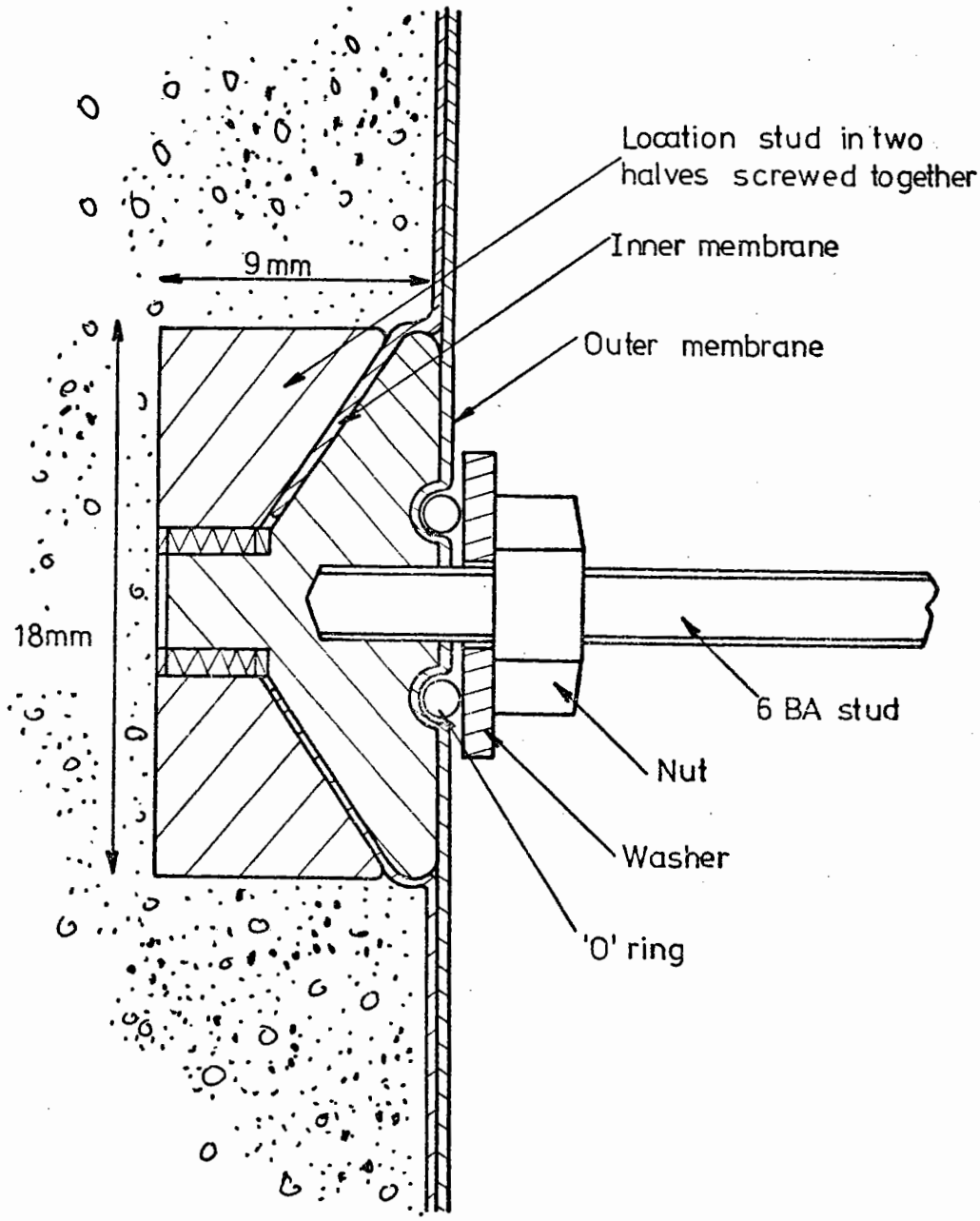

Scale : 5 times full size
Material : Brass

FIG. 3.3 LOCATION STUD FOR STRAIN TRANSDUCERS

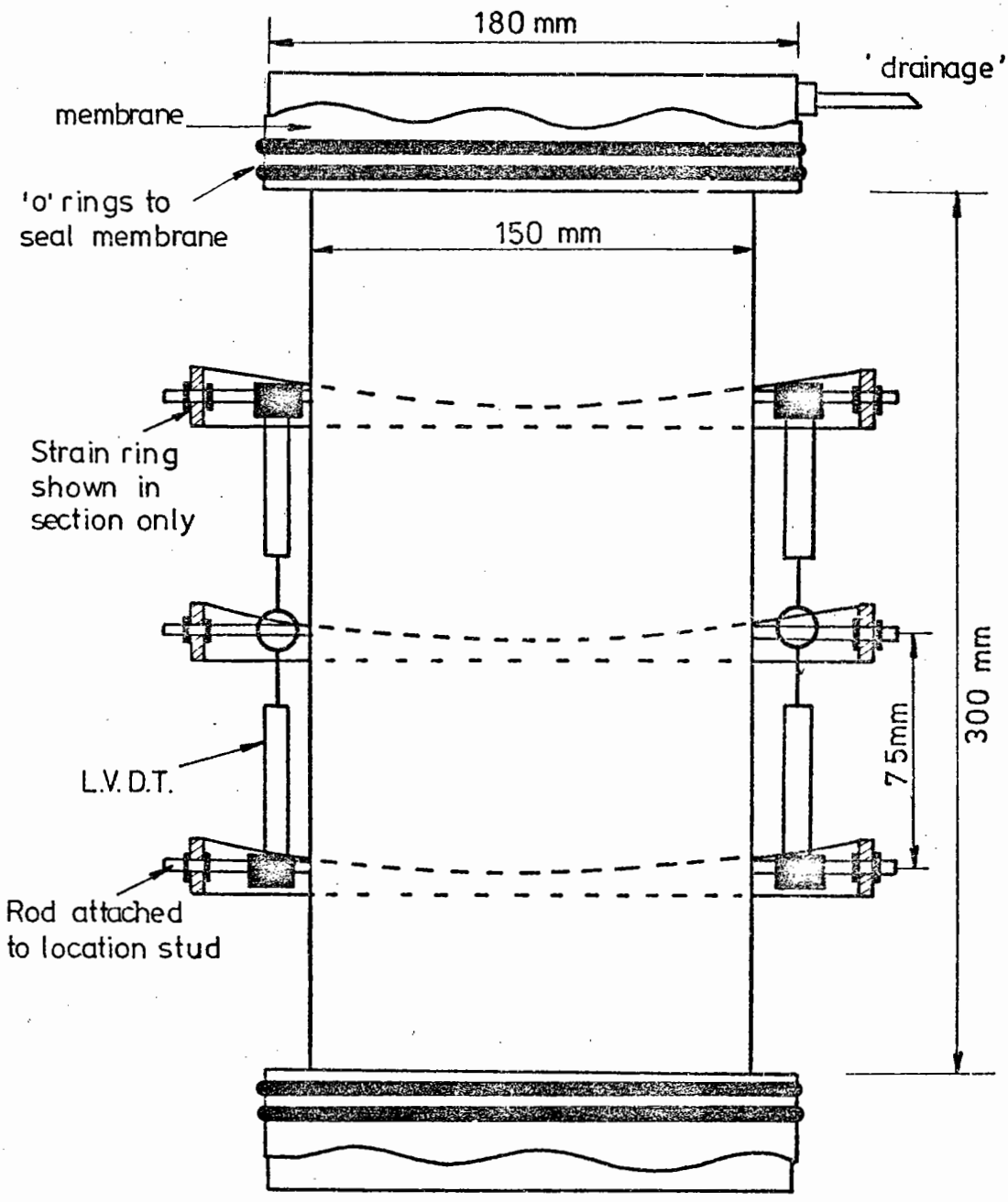

FIG. 3.4 POSITION OF STRAIN TRANSDUCERS

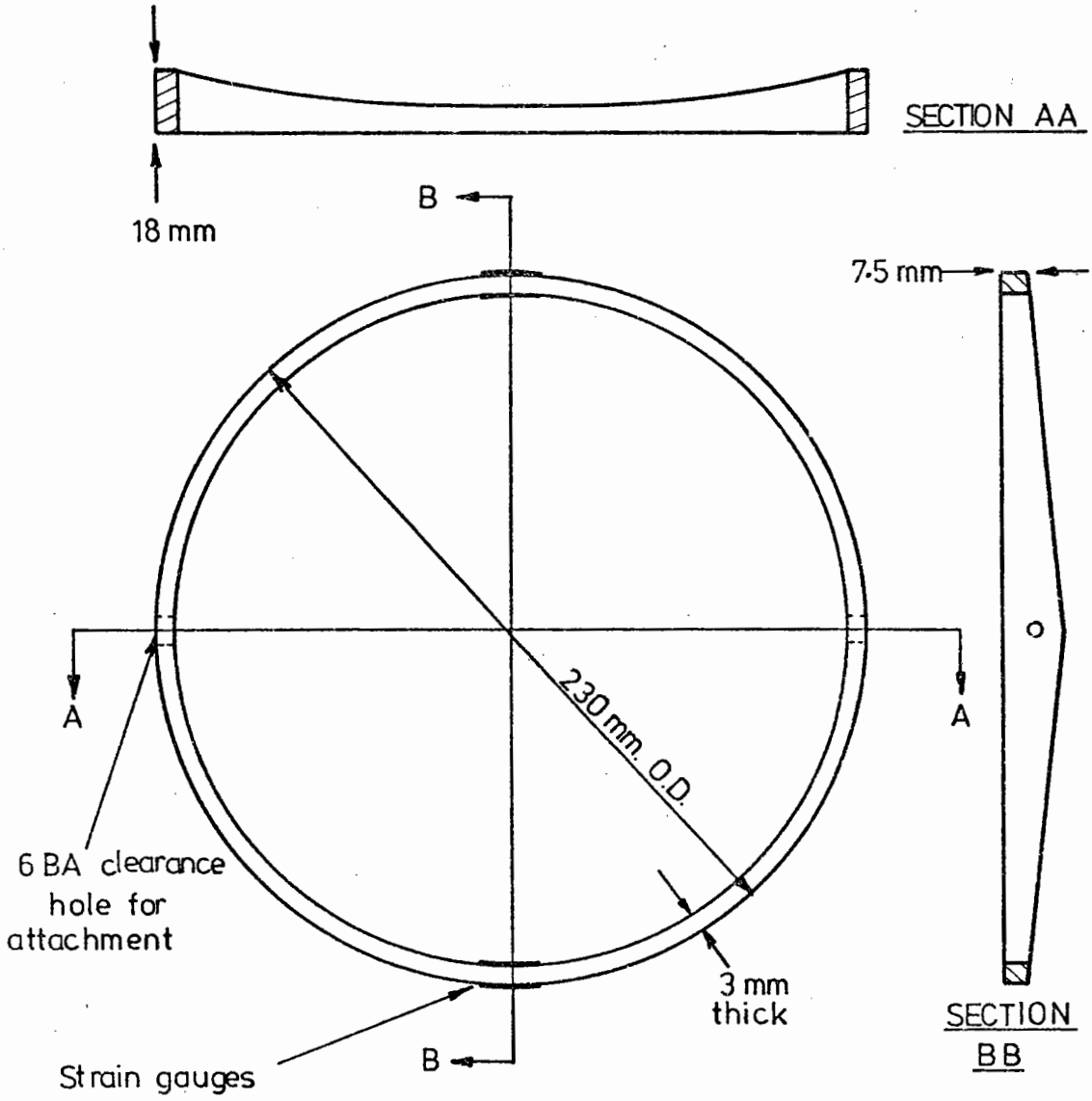

FIG. 3.5 ARALDITE STRAIN RING

3.2.5 Data Monitoring

An ultra violet chart recorder was used for recording all measurements of stress and strain. Six channels were normally used for the following parameters:

(1) Deviator stress

(2) Cell pressure

(3) Total axial strain

(4) Total radial strain

(5) Resilient axial strain

(6) Resilient radial strain

For the resilient strain readings, the strain signals were passed through a d.c. offset generator and then amplified (usually by a factor of 20 times). The offset generator ensured that the amplified strain signal remained on scale as permanent strain developed. Using this technique, resilient strains of 5 $\mu\varepsilon$ could be resolved even when superimposed on a large permanent strain.

3.2.6 Testing of Wet Materials

Although this project involved the testing of dry materials only, facilities were available for dealing with wet specimens. A full description of the facilities is presented by Pappin (1979) who conducted dry, saturated and partially saturated tests on a graded crushed limestone.

3.2.7 Stress Paths in the Triaxial Apparatus

The range of stresses which can be applied to unbound granular material in the triaxial test are shown in Fig. 3.6. Both triaxial compression and triaxial extension tests may be performed. The equipment was capable of applying a maximum confining stress of 400 kN/m^2 and a

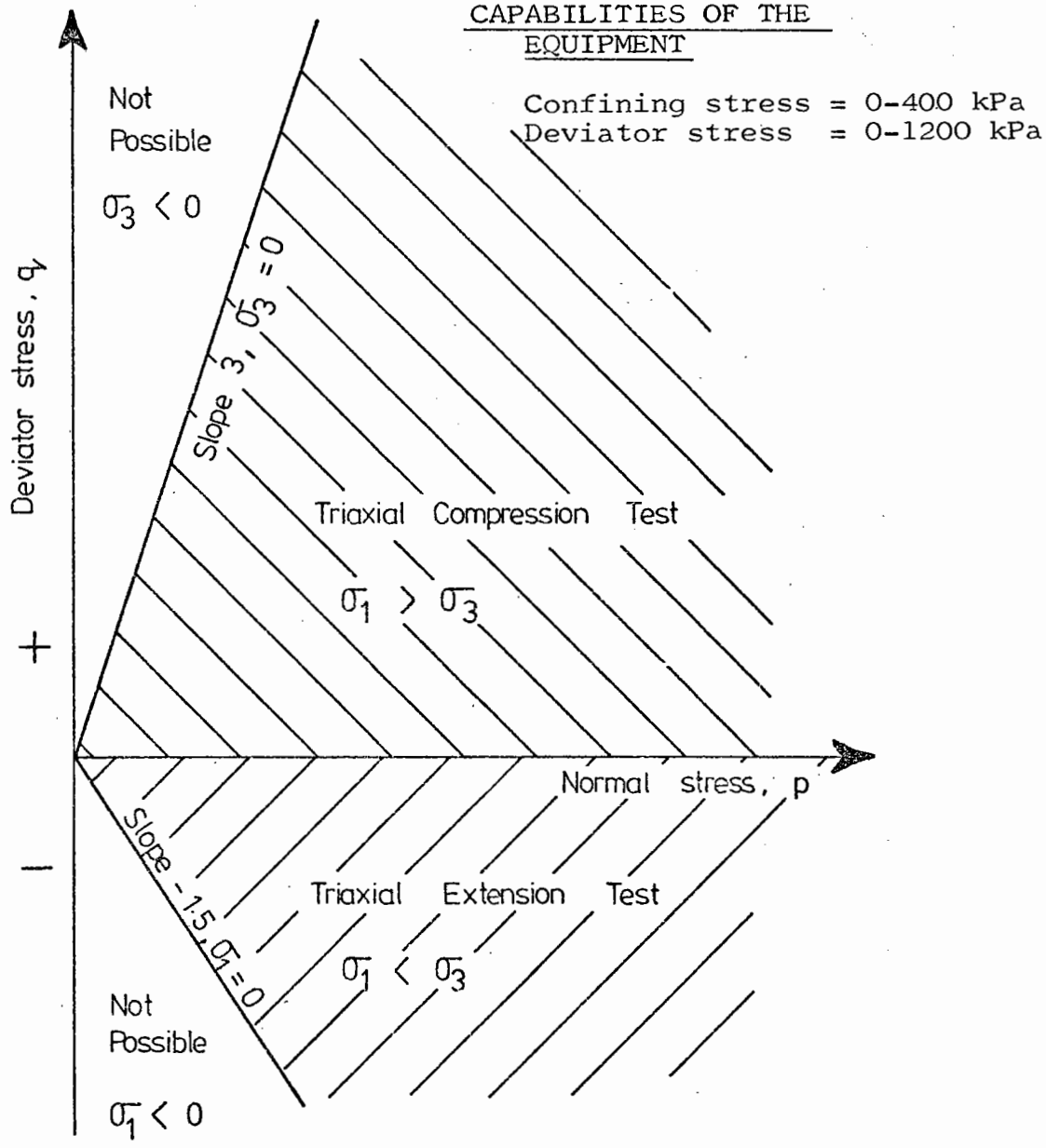

FIG. 3.6 RANGE OF STRESSES WHICH CAN BE APPLIED TO UNBOUND MATERIAL IN THE TRIAXIAL TEST

maximum deviator stress of 1200 kN/m^2.

It should be noted that in the triaxial test the major principal stress can only act in either the vertical or a horizontal direction. This means it is not possible to have rotation of the principal axes other than through a full right angle.

3.3 MONOTONIC FAILURE TESTING

Several compression and extension failure tests were carried out as presented in Figs 3.7 and 3.8. Due to the excessive strains produced in the single size material, it was not feasible to use the LVDTs and strain rings which normally monitor deformations. Axial strains were measured externally using a dial gauge attached to the loading ram. An area correction estimated from the total radial strain measured at the end of the test was applied in calculating the stress. The tests gave an average triaxial compression failure condition $q/p = 2.1$ ($\phi' = 51.3^o$) and average triaxial extension failure at $q/p = -1.47$. An extension failure of $q/p = -1.03$ was predicted using the Mohr Coulomb failure criterion based on a compression failure ratio of $q/p = 2.1$. Compared with the well graded material used by Pappin (1979), the uniformly graded material appears to have similar strength in compression but to be stronger in extension. Triaxial compression failure for the graded material was at $q/p = 2.2$ and triaxial extension failure at $q/p = -1.37$.

3.4 RESILIENT STRAIN BEHAVIOUR

3.4.1 Preliminary Repeated Load Tests

A preliminary test was conducted in which a limited number of stress paths were applied to one specimen, so that the influences of permanent strain and frequency could be assessed. The specimen was

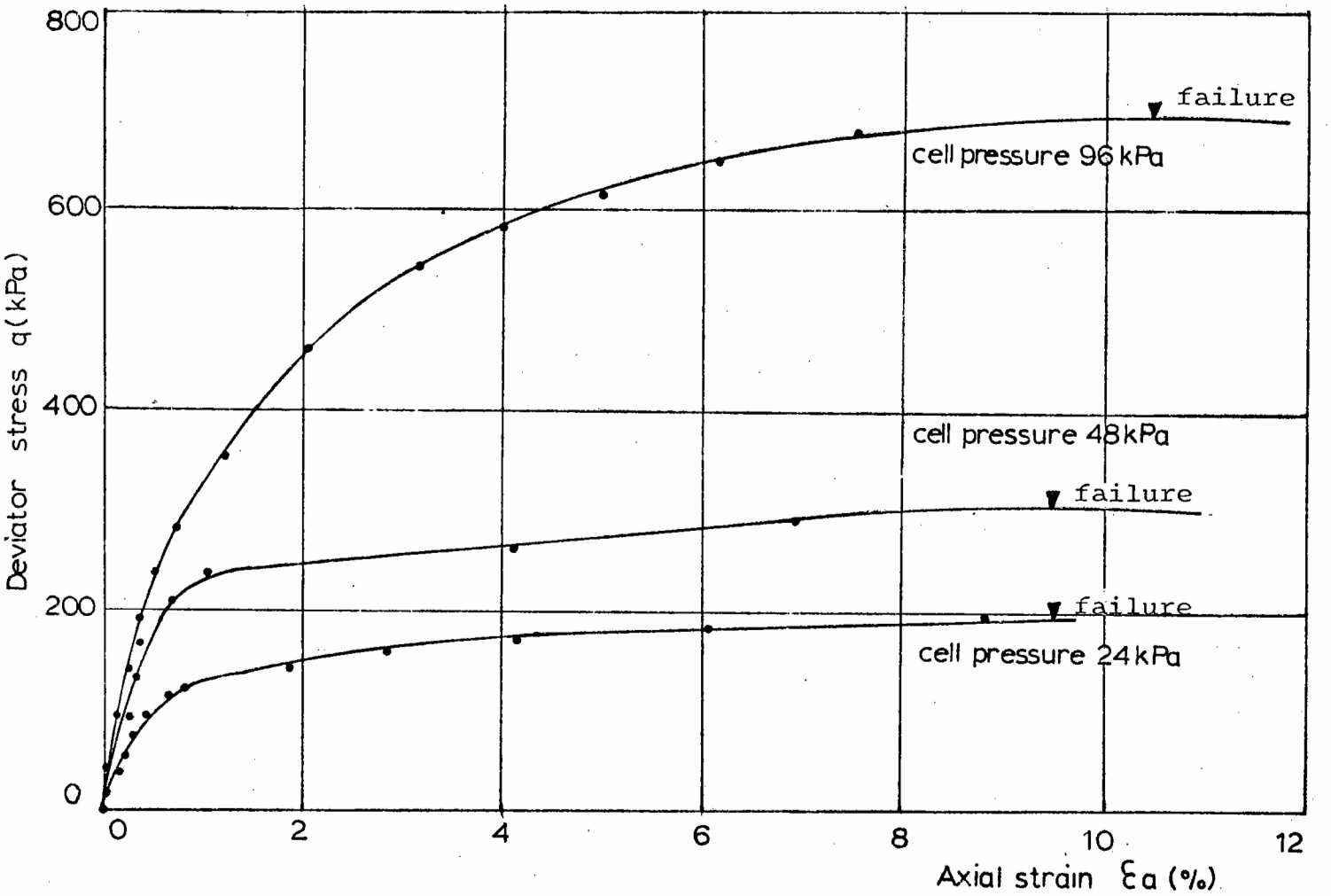

FIG. 3.7 MONOTONIC FAILURE TESTS - TRIAXIAL COMPRESSION

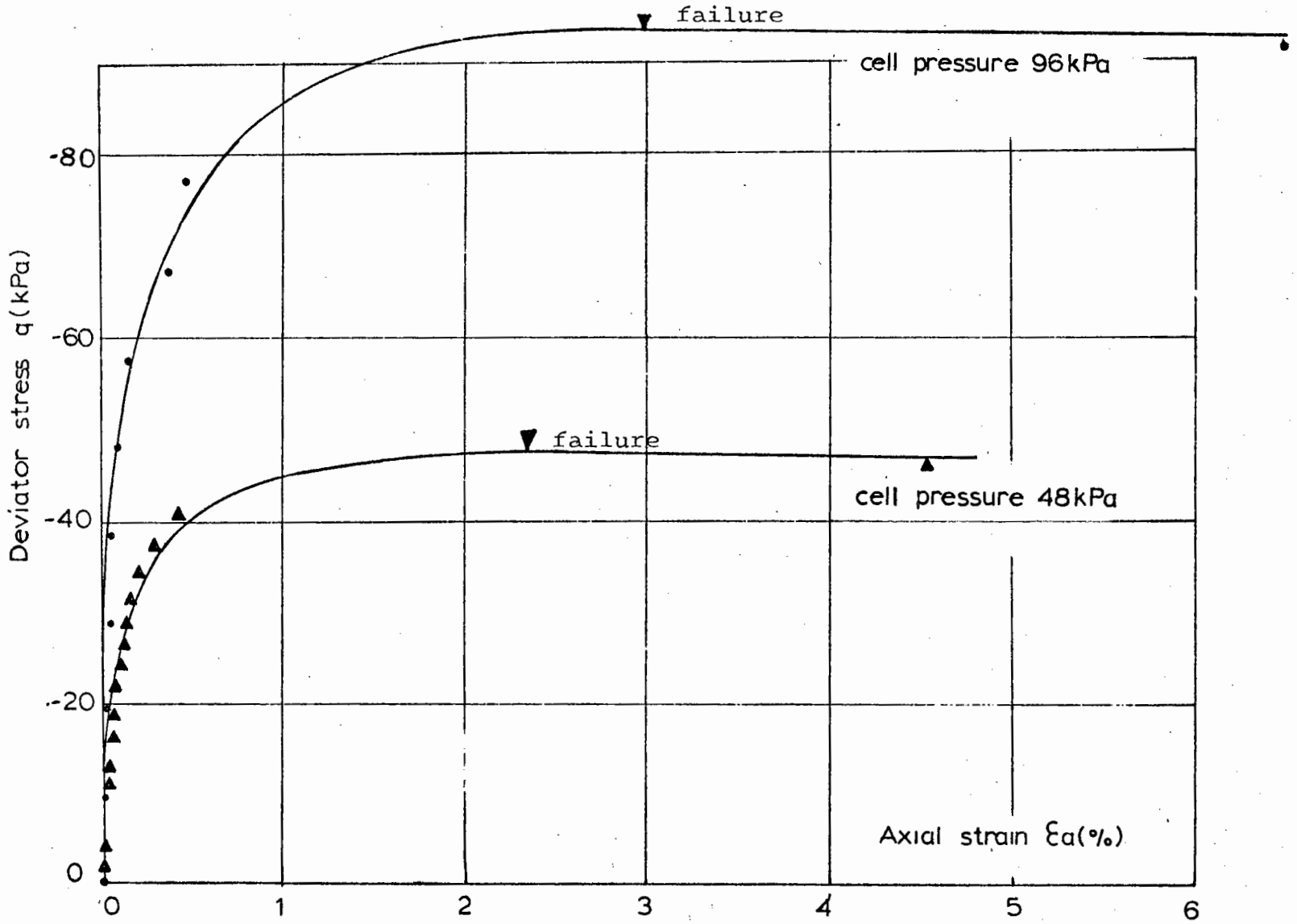

FIG. 3.8 MONOTONIC FAILURE TESTS - TRIAXIAL EXTENSION

prepared as detailed in Section 3.2.3 and subjected to a short test programme selected from the stress paths shown in Fig. 3.9.

The effect of frequency of load application on the resilient response of the material was also investigated for two of these paths at 0.1, 0.2, 0.5, 1 and 2 Hz.

Several thousand cycles of one stress path were then applied until some permanent strains developed when the test programme and frequency tests were repeated.

The resilient behaviour of the material was found to be similar for all frequencies and for differing magnitudes of permanent strain. It was decided that in line with the procedure adopted by Pappin (1979), the specimen should be subjected to several hundred cycles of load application before embarking on the complete testing programme. Section 3.8 indicates that for the single size material, resilient strains reached a steady value after about 200 cycles. The resilient behaviour for each stress path was observed over about ten cycles.

3.4.2 Full Test Programme

The repeated stress paths illustrated in Fig. 3.9 were applied to the specimens at various values of mean normal stress p_m.

The stress paths were defined by using the stress invariants:

$$p = (\sigma_1 + \sigma_2 + \sigma_3)/3 \tag{3.1}$$

$$q = \frac{1}{\sqrt{2}} \left[(\sigma_1-\sigma_2)^2 + (\sigma_2-\sigma_3)^2 + (\sigma_3-\sigma_1)^2\right]^{\frac{1}{2}} \tag{3.2}$$

For triaxial test conditions these reduce to:

$$p = \frac{\sigma_a + 2\sigma_r}{3} \tag{3.3}$$

$$q = \sigma_a - \sigma_r \tag{3.4}$$

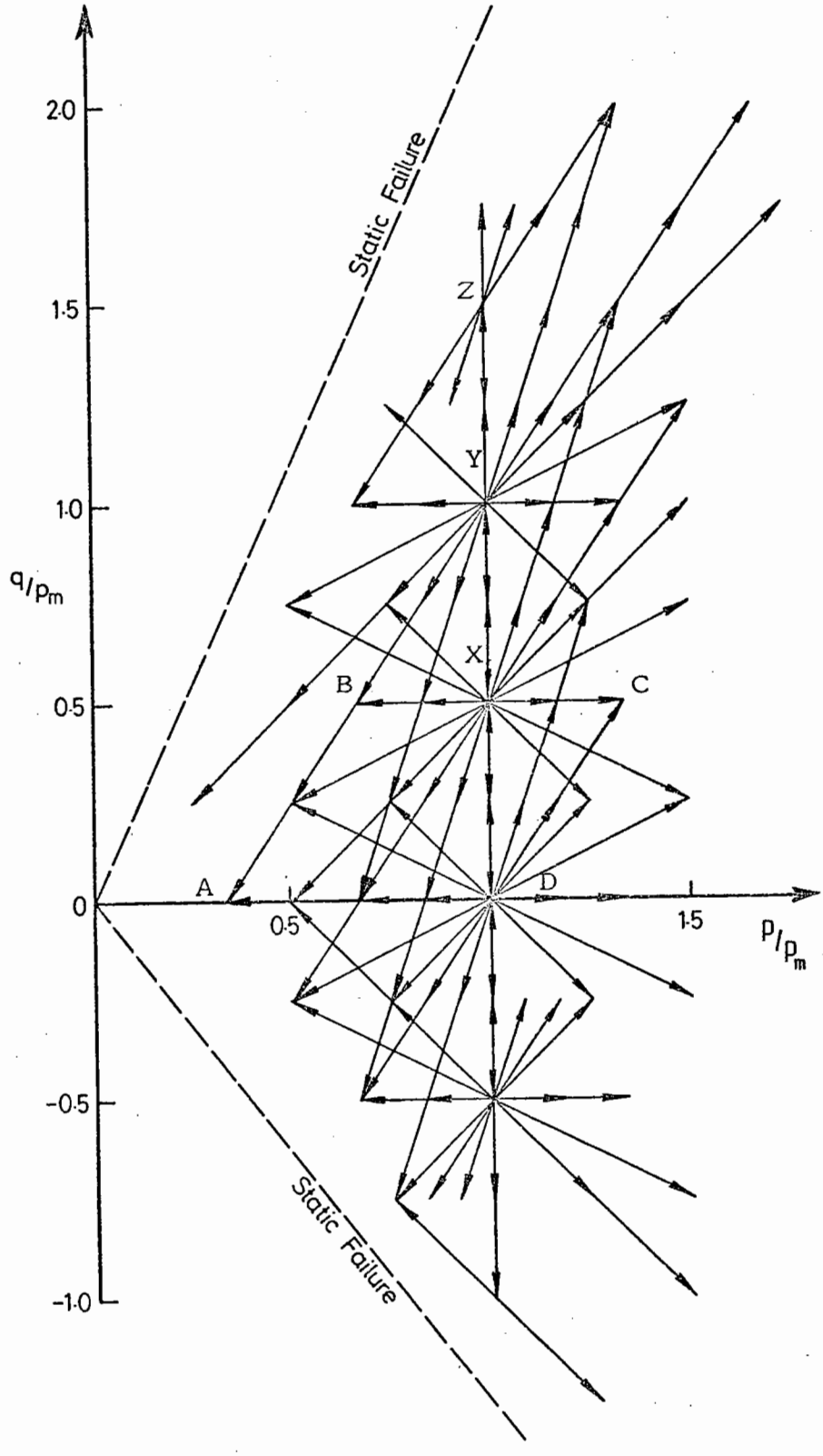

FIG. 3.9 COMPLETE SERIES OF STRESS PATHS APPLIED TO SPECIMEN AT ONE VALUE OF p_m

where σ_a and σ_r are the axial and radial stress. Each stress path could be totally defined using mean and repeated normal stress (p_m and p_r) and mean and repeated deviator stress (q_m and q_r) as shown in Fig. 3.10.

The complete series of stress paths (Fig. 3.9) was applied to three specimens at p_m values of 48, 96 and 192 kPa. Limitations on the magnitude of cell pressure enabled only a limited number of compression stress paths to be applied at a p_m of 384 kPa. The results for all three tests were averaged and are given in Appendix 3A.

The test programme included paths in the triaxial compression and extension regions as well as some in both. The specimens were therefore subjected to a comprehensive range of stress paths enabling the material response to be investigated for a wide range of loading conditions.

3.4.3 Triaxial Compression

In order that direct comparisons could be made between the behaviour of the single size material and the graded material tested by Pappin (1979), similar procedures were adopted for the analysis of the resilient strains.

Volumetric strain: The volumetric strains resulting from the stress paths shown in Fig. 3.9 were found to be commutable in stress space. That is, considering stress paths AB, BC, CD and DA and assuming zero volume change at point A, the sum of the strain from paths AB, BC, CD and DA resulted in zero. This may be expressed mathematically as:

$$v_{r(x-y)} + v_{r(y-z)} = v_{r(x-z)} \qquad (3.5)$$

for the points x, y and z in stress space, where v_r = resilient volumetric strain.

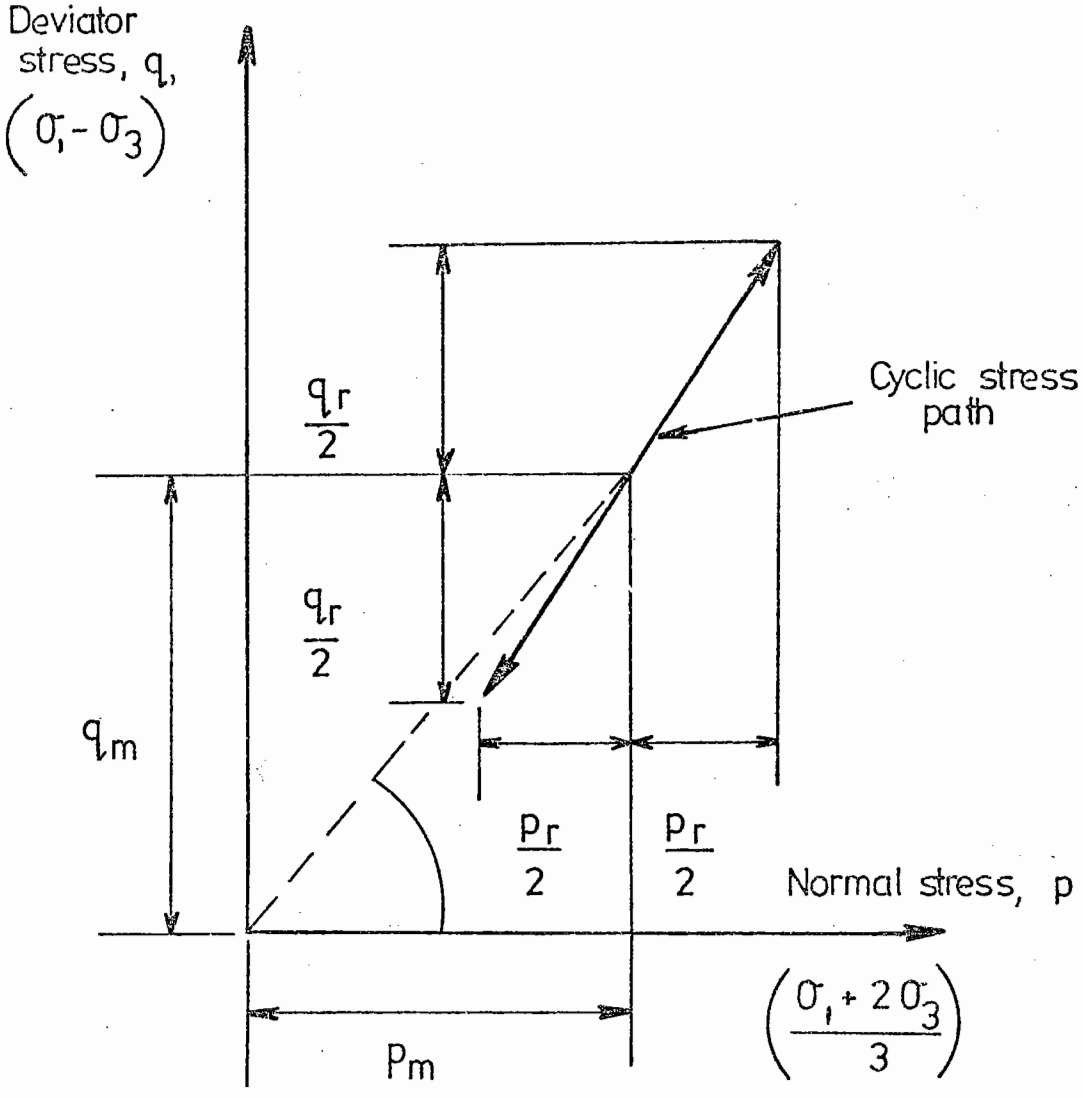

FIG. 3.10 COMPONENTS OF STRESS IN THE REPEATED LOAD TRIAXIAL TEST

Assuming that zero volumetric strain occurred at zero stress, a plot of resilient volumetric strain contours was drawn as shown in Fig. 3.11. The explanation of these contours is that if, for example, a stress path moves from a point on the 800 με contour to a point on the 1000 με contour, then a net compressive resilient volumetric strain of 200 με strain will have occurred. If a stress path begins and ends on the same contour, no net volume change will result.

These contours were then expressed mathematically in stress space. The relationship between p and volumetric strain when q = 0, was established by considering the intercept of the contours with the p axis (Fig. 3.12a). A multiplication factor dependent on the stress ratio, q/p, was then superimposed (Fig. 3.12b) to give:

$$v_c = \left(\frac{p}{A}\right)^{0.5}\left[1 - B(q/p)^C\right] \qquad (3.6)$$

where v_c is the contour value of resilient volumetric strain and A, B and C are constants, $A = 1.23 \times 10^{+8}$ kPa, B = 0.033, C = 3.5.

Assuming a stress path moved from stress (p_1, q_1) to (p_2, q_2), the resilient volumetric strain was calculated as:

$$v_r = A^{-0.5}\left[p_2{}^{0.5}\left[1 - B(q_2/p_2)^C\right] - p_1{}^{0.5}\left[1 - B(q_1/p_1)^C\right]\right] \qquad (3.7)$$

Figs 3.13 to 3.16 show comparisons of predicted and experimental resilient volumetric strains. The model is shown to perform satisfactorily at all stress levels.

Shear strain: On considering shear strain, it was found that, unlike volumetric strains, the results were not commutable. The sum of the resilient shear strains resulting from stress paths x to y and y to z did not equal that of path x to z (Fig. 3.9). This was in agreement with the finding of Pappin (1979) for the well graded material. This

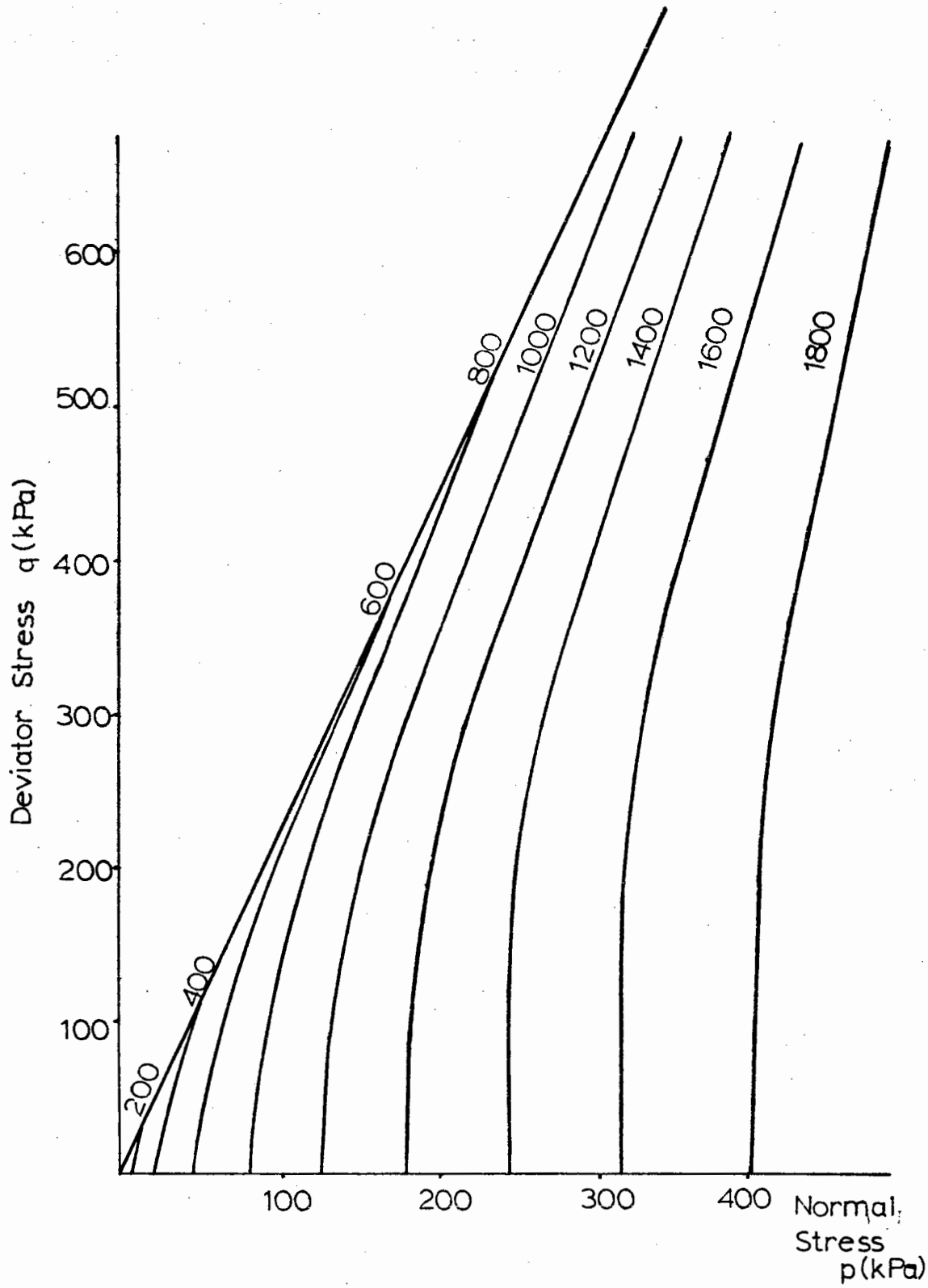

FIG. 3.11 CONTOURS OF VOLUMETRIC STRAIN IN (p,q) STRESS SPACE ($\mu\varepsilon$)

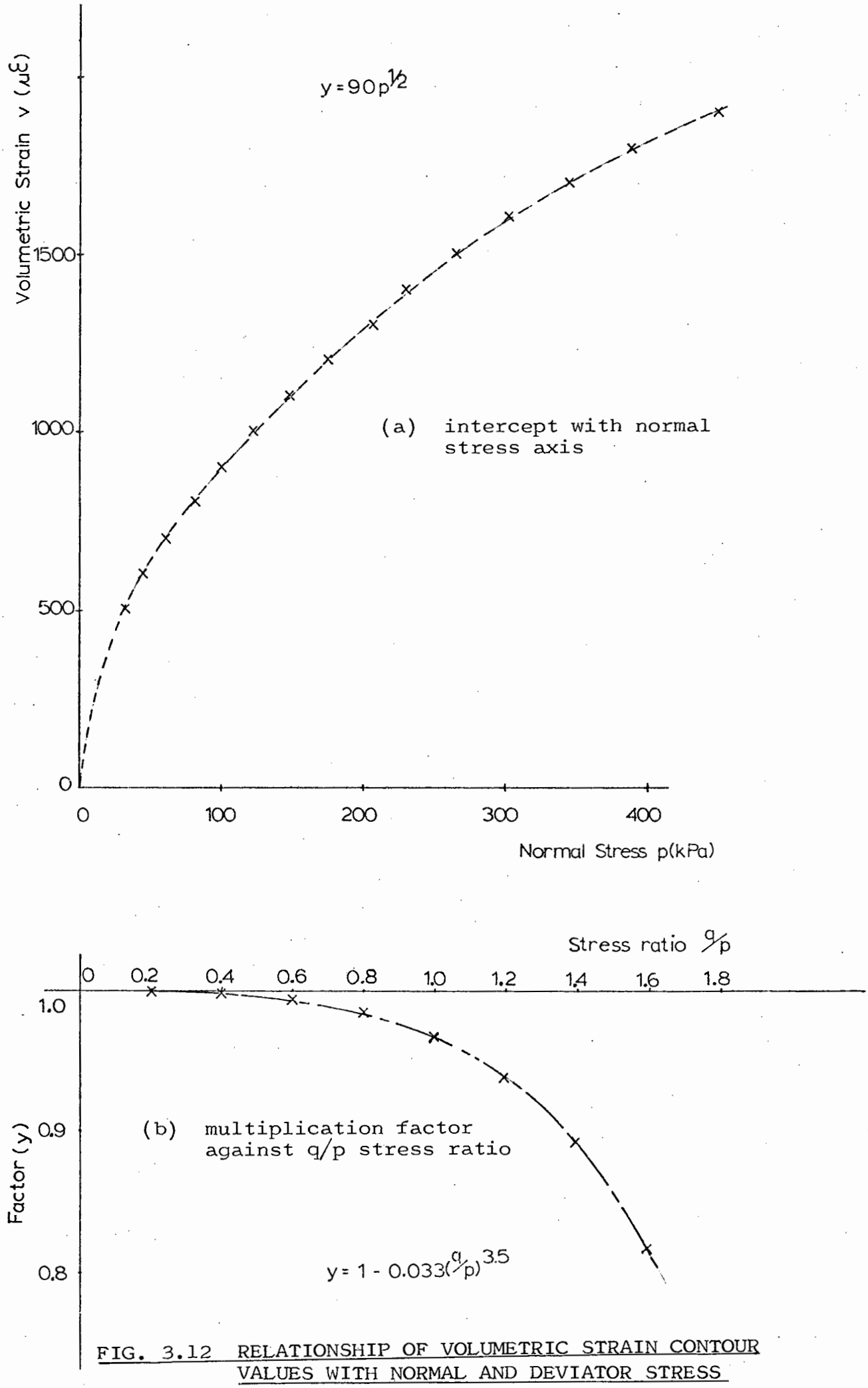

FIG. 3.12 RELATIONSHIP OF VOLUMETRIC STRAIN CONTOUR VALUES WITH NORMAL AND DEVIATOR STRESS

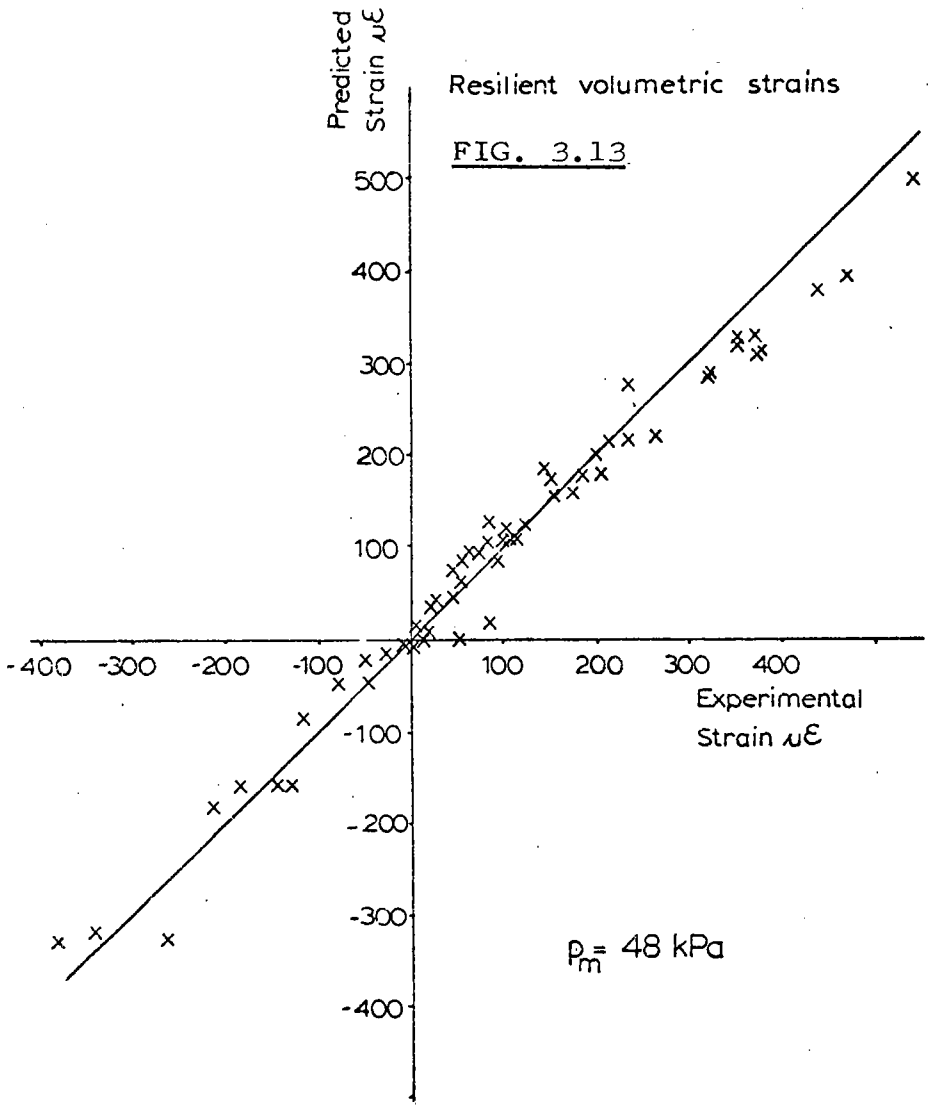

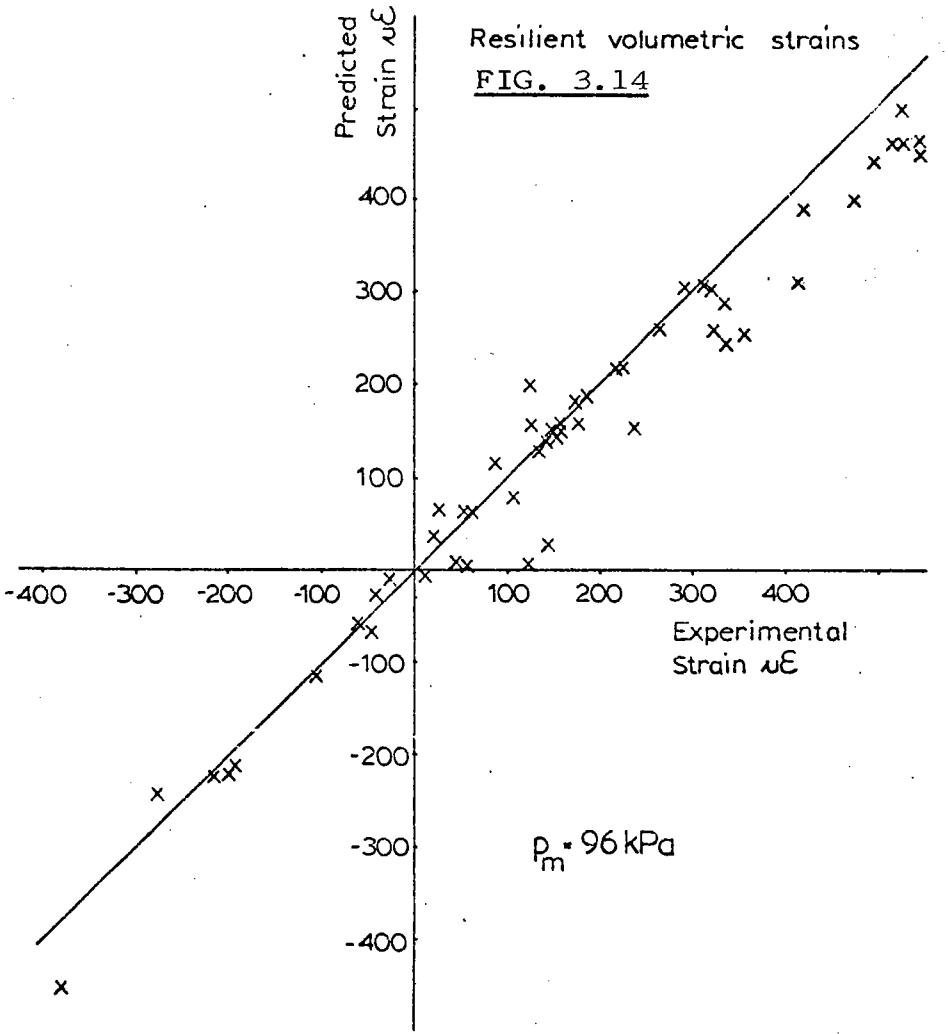

COMPARISON OF PREDICTED AND EXPERIMENTAL RESILIENT VOLUMETRIC STRAINS

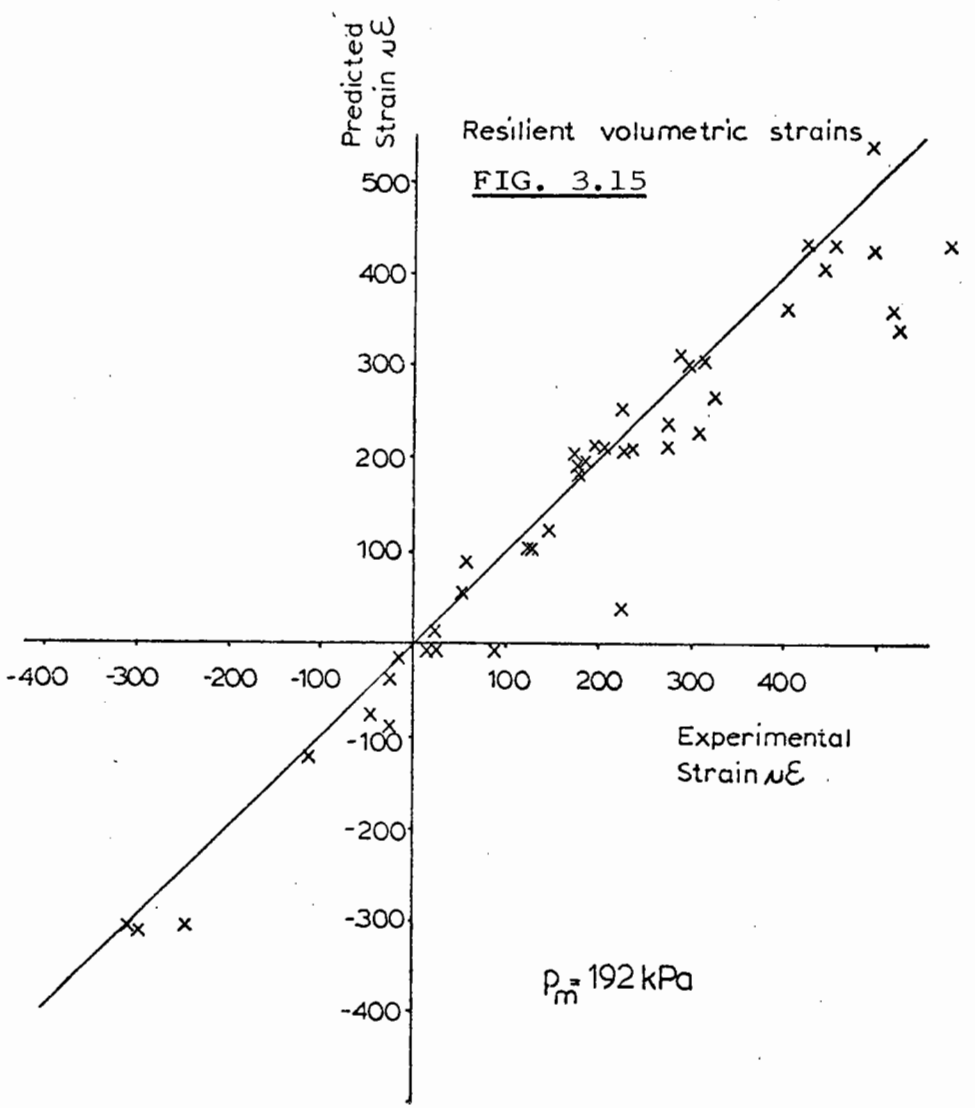

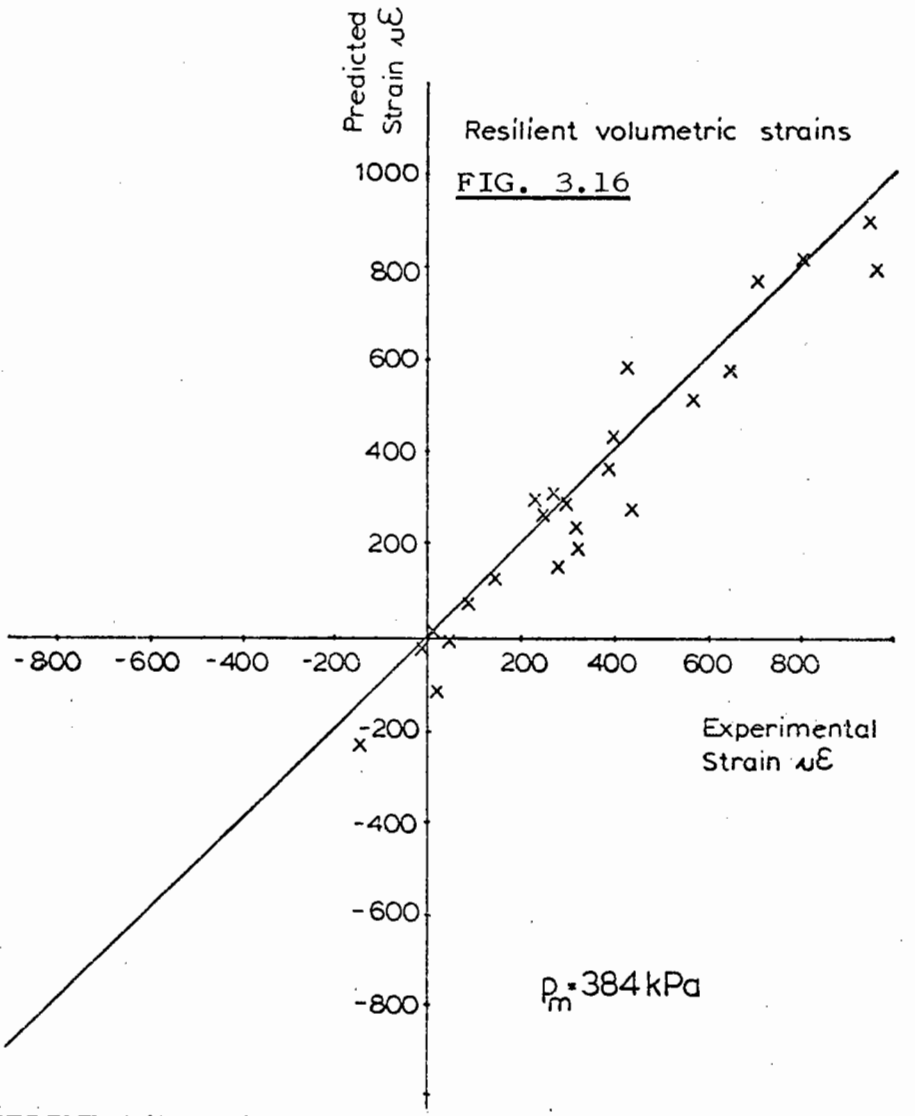

COMPARISON OF PREDICTED AND EXPERIMENTAL RESILIENT VOLUMETRIC STRAINS

indicated that shear strain is stress path dependent and implied that both the beginning and end point of a stress path due to additions of load must be included in any analysis predicting the shear strain occurring at the end point of that stress path.

At any constant mean stress (q_m and p_m) and constant q_r/p_r, the shear strain increased with stress path length:

$$\ell_r = (p_r^2 + q_r^2)^{\frac{1}{2}} \tag{3.8}$$

in the manner shown in Fig. 3.17. This behaviour was similar for all tested directions of q_r/p_r and can be described mathematically as:

$$\varepsilon_r = \varepsilon_o \times \left[\frac{\ell_r}{\ell_o}\right]^{1.45} \tag{3.9}$$

where ε_o = shear strain produced by stress path length ℓ_o

ε_r = " " " " " " " ℓ_r

The shear strains were then normalised such that for path xyz in Fig. 3.9, normalised shear strain xy plus normalised shear strain yz equalled the normalised shear strain produced by path xz. Hence:

$$\varepsilon_n = \varepsilon_o \times \frac{\ell_r}{\ell_o} = \varepsilon_r \times \frac{\ell_r}{\ell_o}\left[\frac{\ell_o}{\ell_r}\right]^{1.45} = \varepsilon_r \times \left[\frac{\ell_o}{\ell_r}\right]^{0.45} \tag{3.10}$$

A plot of normalised resilient shear strains in the compression region of (p,q) stress space was then drawn on a similar basis to that of the volumetric strain. It was found that ℓ_o in Equations 3.9 and 3.10 could be replaced by p_m. This agreed with the findings of Pappin (1979) and was found to be satisfactory.

The normalised resilient shear strain contours are shown in Fig. 3.18. The resulting contours are a series of straight lines radiating from the stress point p = -130 kPa, q = 0 kPa and having a value determined by the equation:

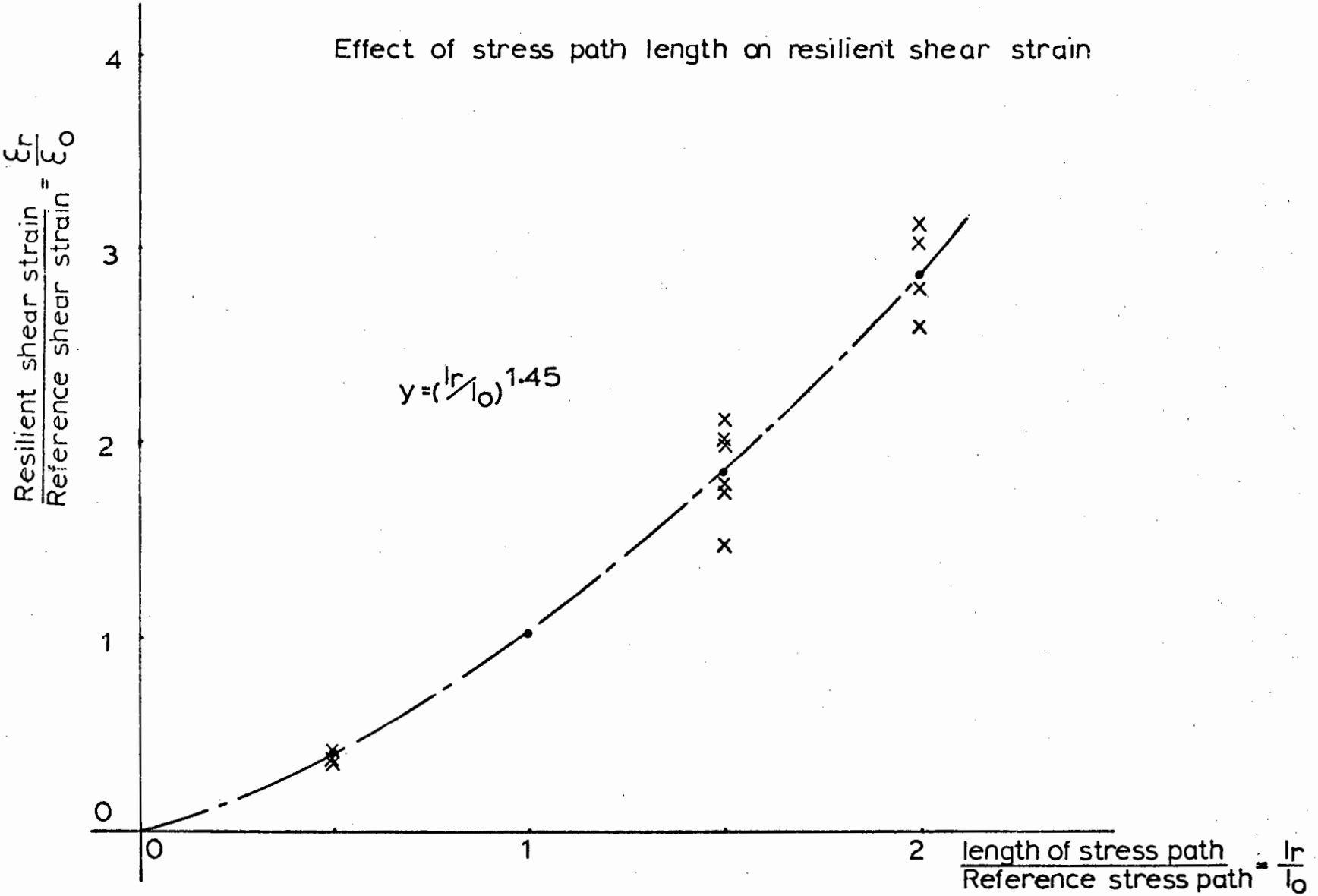

FIG. 3.17 EFFECT OF STRESS PATH LENGTH ON RESILIENT SHEAR STRAIN

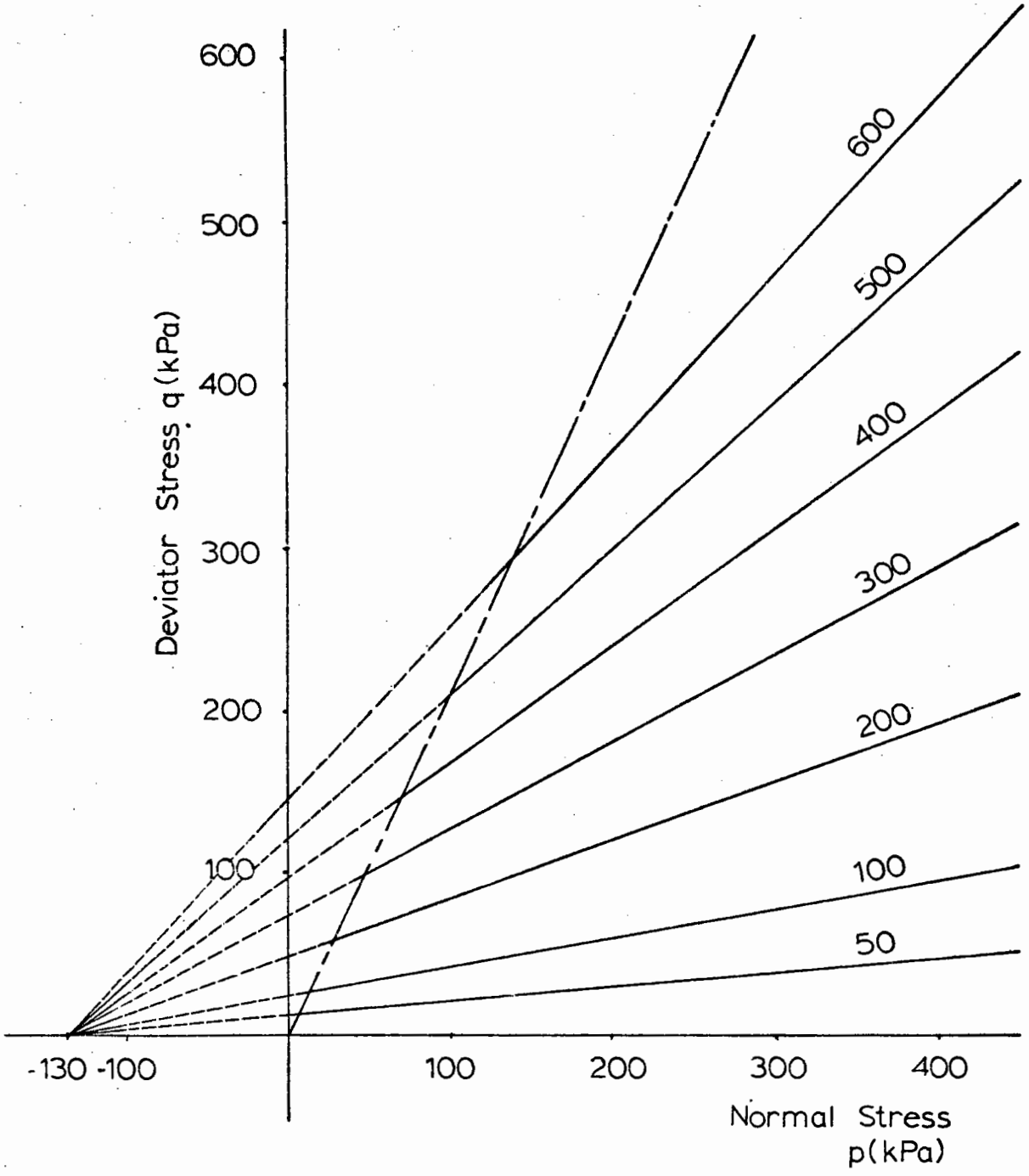

FIG. 3.18 CONTOURS OF NORMALISED SHEAR STRAIN IN (p,q) STRESS SPACE ($\mu\varepsilon$)

$$\varepsilon_n = D\left[\frac{q}{p + E}\right] \tag{3.11}$$

where $D = 5.5 \times 10^{-4}$ and $E = +130$ kPa.

On applying the stress path length correction, the resilient shear strain is given by:

$$\varepsilon_r = D\left[\frac{q_2}{p_2 + E} - \frac{q_1}{p_1 + E}\right]\left[\frac{(p_r^2 + q_r^2)^{\frac{1}{2}}}{p_m}\right]^n \tag{3.12}$$

where p_1, q_1 and p_2, q_2 are the initial and final stress states in kPa and $n = 0.45$.

Comparisons of the predicted and measured resilient shear strains for the compression region are shown in Figs 3.19 to 3.22. The model tended to underpredict slightly at high p_m (384 kPa) but was generally satisfactory.

Comparison with graded material: The form of equations for the volumetric and shear strain contours is similar to that obtained by Pappin (1979) (see Section 3.5). On comparing the contours of volumetric strain for the graded and uniform material, it was found that generally the latter gave greater strains as p increased.

Shear strains for the uniform material were almost twice those obtained from the graded material for any given p and q. One would expect greater straining to take place in the single size material because of increased voids ratio and less particle contact. The voids ratio of the graded material was 0.19 whereas that of the single size material was 0.68.

3.4.4 Triaxial Extension

To examine the triaxial extension region, consider the view down the space diagonal as shown in Fig. 3.23. This is effectively a plane

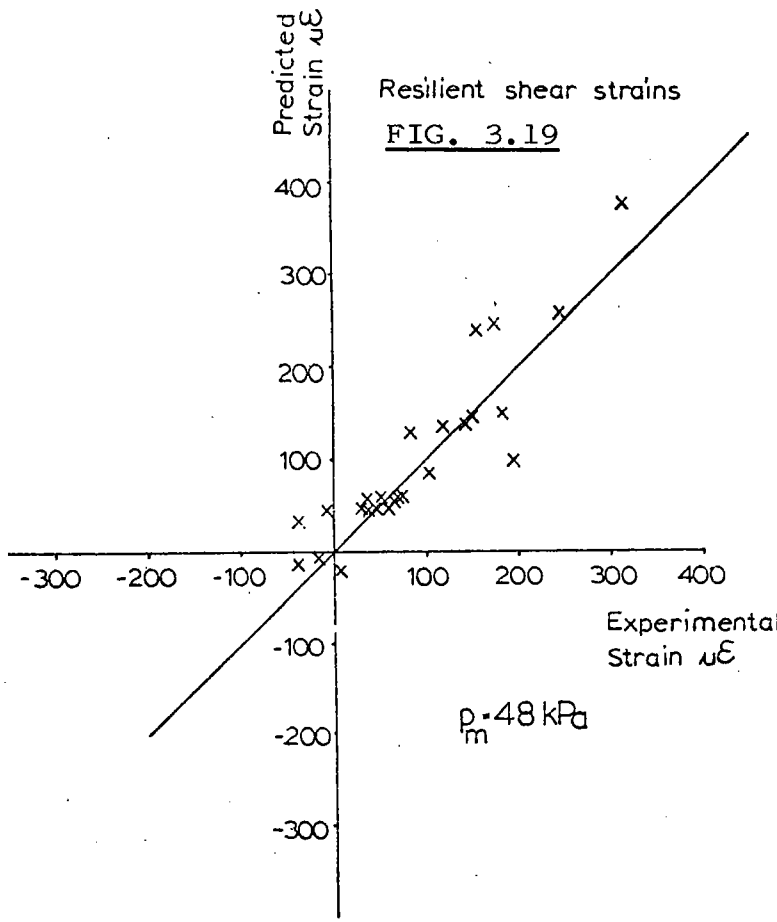

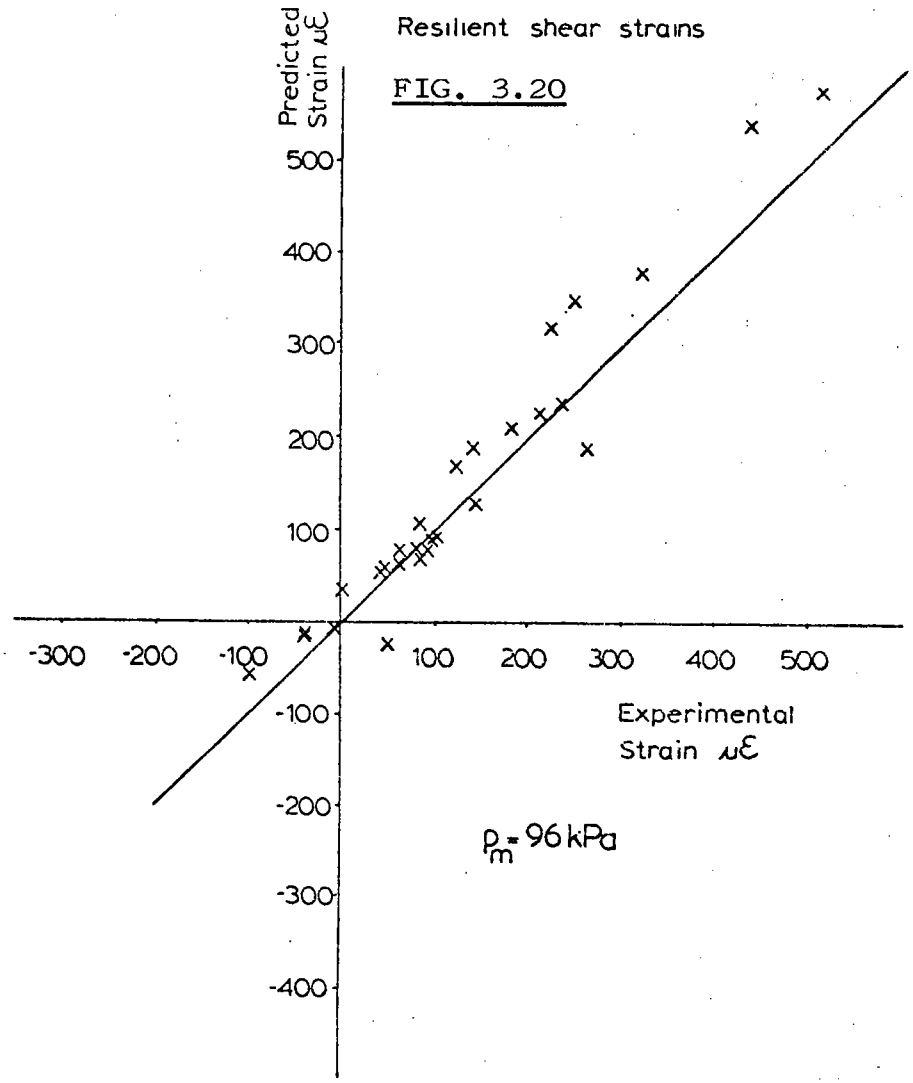

COMPARISON OF PREDICTED AND EXPERIMENTAL RESILIENT SHEAR STRAINS

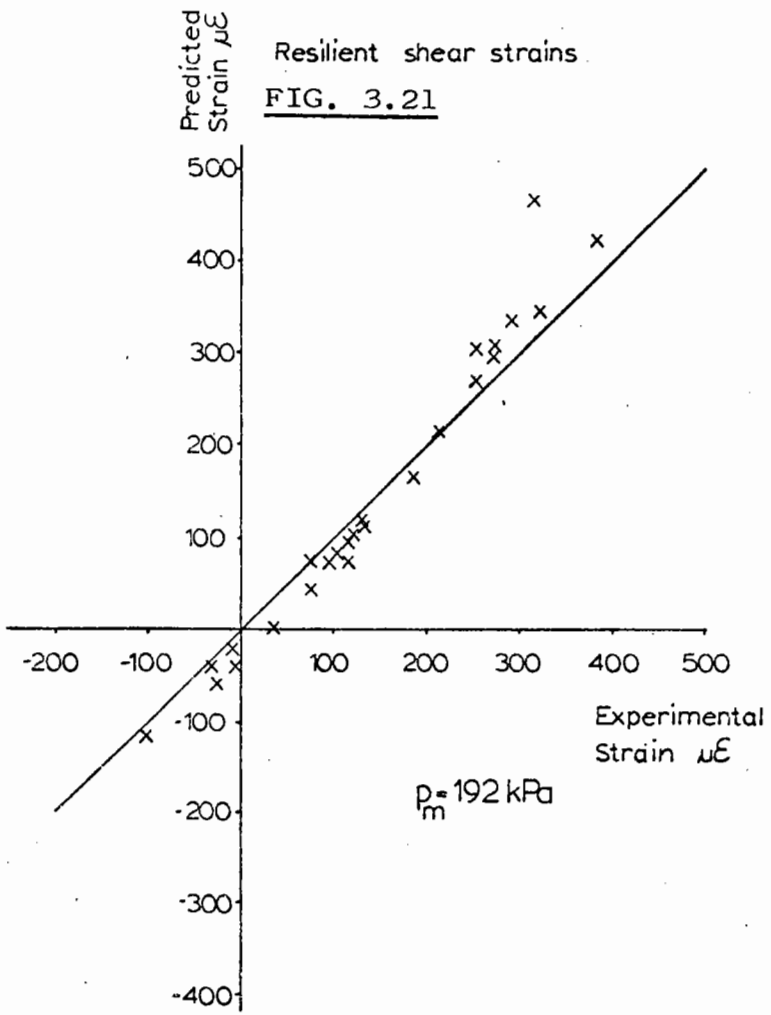

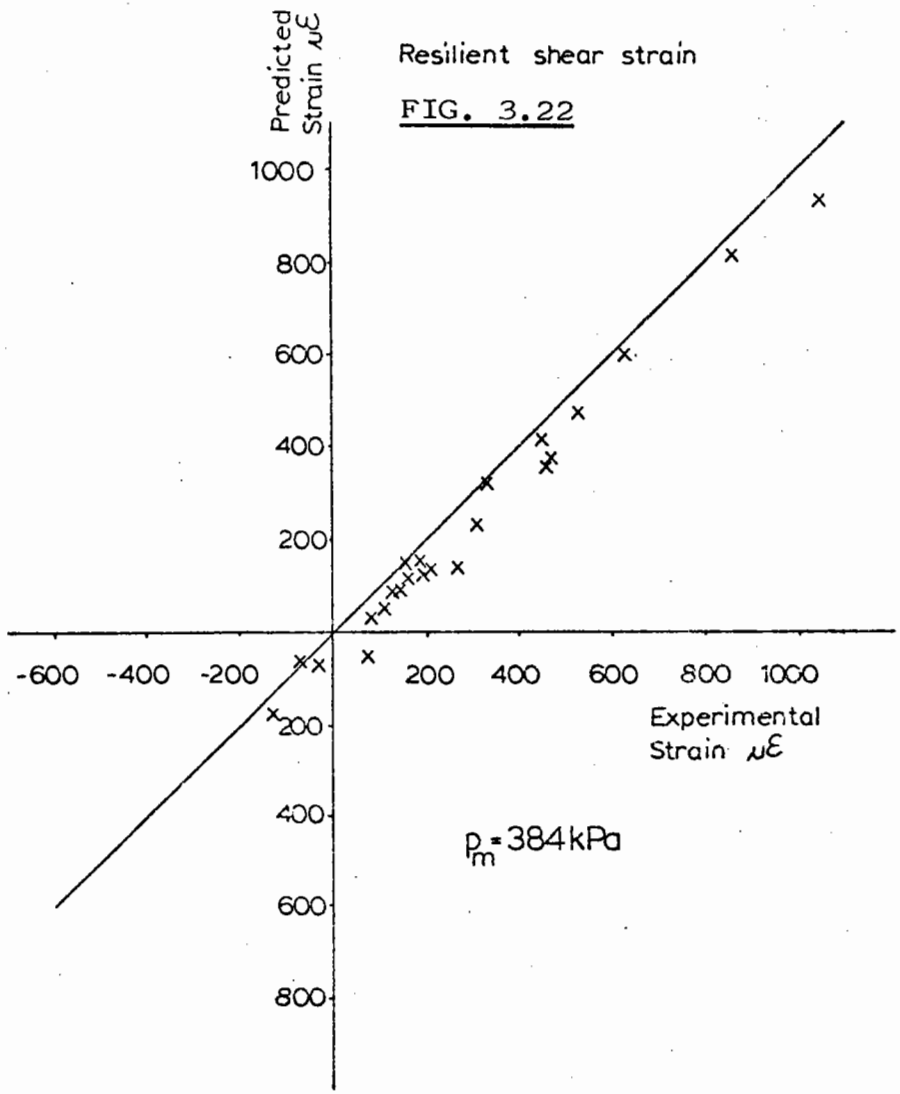

COMPARISON OF PREDICTED AND EXPERIMENTAL RESILIENT SHEAR STRAINS

where the deviator stress q increases equally in all directions when moving from point O. The line OC corresponds to all stress paths in triaxial compression and line OE to all stress paths in triaxial extension. When q is defined in terms of the triaxial stress conditions (Equation 3.4), triaxial extension gives a negative value ($\sigma_r > \sigma_a$), whereas in three-dimensional stress space deviator stress is always positive. Pappin observed that the resilient response of the graded material was not the same in triaxial compression as in extension, but found that the extension strain contours could be correlated with compression contours using a correction based on the major to minor principal stress ratio (σ_1/σ_3).

To apply this correction, any general stress point $\sigma_1 > \sigma_2 > \sigma_3$ with its corresponding p and q, must be converted to a triaxial compression condition $\bar{\sigma}_z > \bar{\sigma}_x = \bar{\sigma}_y$ with its corresponding $\bar{p}$ and $\bar{q}$, such that $\bar{\sigma}_z/\bar{\sigma}_x$ is equal to σ_1/σ_3 and $\bar{p} = p$. If this is accomplished, the stress point $\bar{\sigma}_z > \bar{\sigma}_x = \bar{\sigma}_y$ should be equivalent to $\sigma_1 > \sigma_2 > \sigma_3$ for all stress strain characteristics.

Pappin determined these equivalent stresses $\bar{\sigma}_z > \bar{\sigma}_x = \bar{\sigma}_y$ in the following manner.

$$\text{Let } \bar{p} = \frac{\bar{\sigma}_z + 2\bar{\sigma}_x}{3} = p = \frac{\sigma_1 + \sigma_2 + \sigma_3}{3} \tag{3.13}$$

then if

$$\frac{\bar{\sigma}_z}{\bar{\sigma}_x} = \frac{\sigma_1}{\sigma_3} \tag{3.14}$$

the equivalent deviator stress may be written as:

$$\bar{q} = \bar{\sigma}_z - \bar{\sigma}_x = \left(\frac{\sigma_1}{\sigma_3} - 1\right) \bar{\sigma}_x \tag{3.15}$$

and the equivalent stress ratio $\bar{q}/\bar{p} = \bar{q}/p$ as:

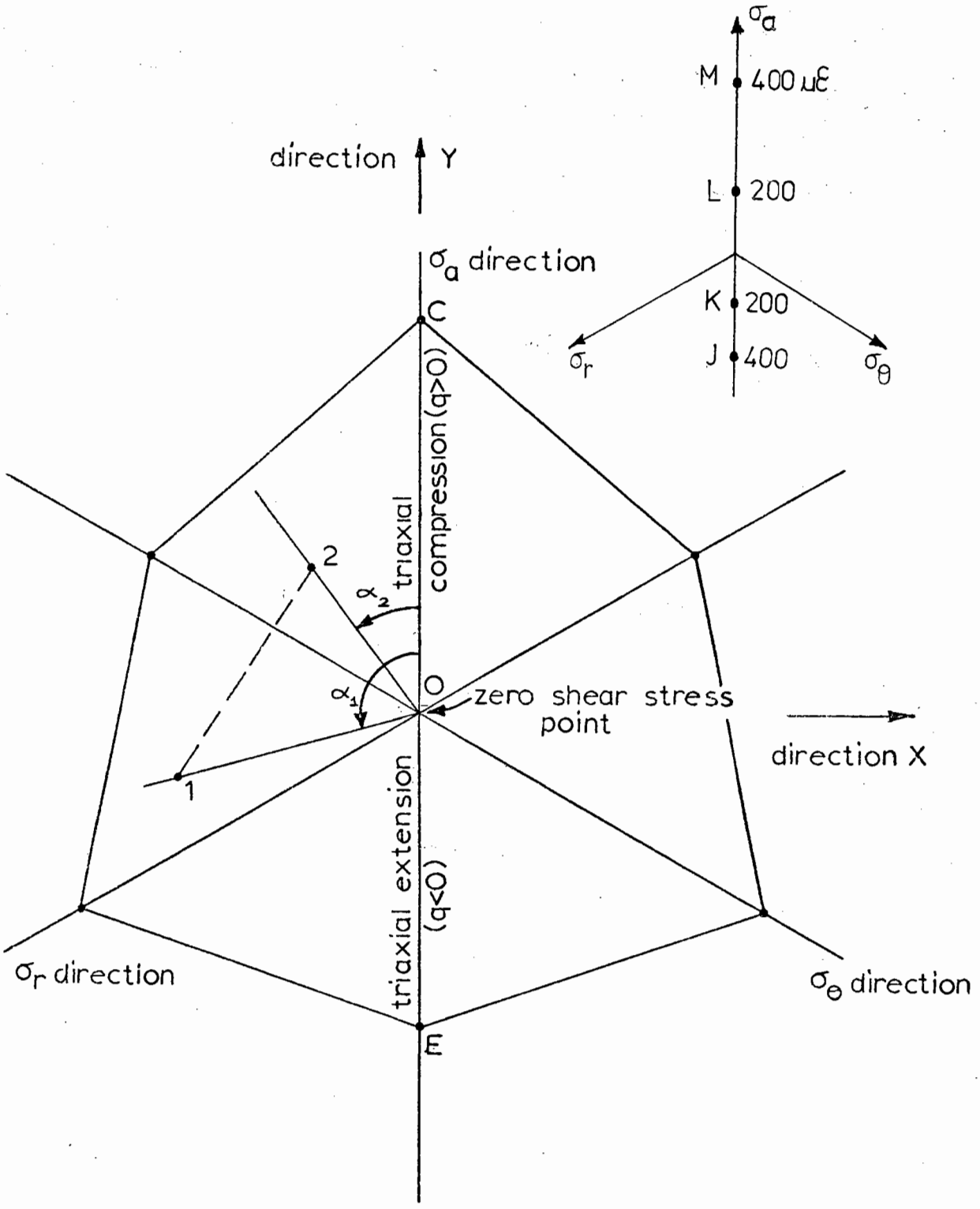

FIG. 3.23 VIEW DOWN SPACE DIAGONAL ONTO A p= CONSTANT PLANE

$$\bar{q}/p = \frac{3\left(\frac{\sigma_1}{\sigma_3} - 1\right)\bar{\sigma}_x}{\frac{\sigma_1}{\sigma_3}\bar{\sigma}_x + 2\bar{\sigma}_x} = \frac{3\sigma_1 - 3\sigma_3}{\sigma_1 + 2\sigma_3} \tag{3.16}$$

i.e. any stress condition to be analysed can be reduced to the triaxial compression condition with stress states p, $\bar{q}$ determined by using Equations 3.13, 3.14 and 3.16.

To use these equations specifically for the triaxial extension condition where p and q are defined in terms of σ_a and σ_r:

$$\sigma_1 = \sigma_r = p - q/3 \tag{3.17}$$

$$\sigma_3 = \sigma_a = p + 2q/3 \tag{3.18}$$

By applying the above equations:

$$\bar{q} = \frac{-q}{1 + q/3p} \tag{3.19}$$

Volumetric strains: The transformed stresses for the data on the single sized material were inserted directly into the equation for the volumetric strains and the results calculated. Comparisons of predicted and experimental strains are shown in Fig. 3.25 to be satisfactory.

Shear strains: In calculating shear strains, the stress path length correction was obtained by using the original values of p and q and the transformed value of q was inserted in the remainder of the contour equation. Satisfactory comparisons of experimental strains with values predicted using this procedure are shown in Fig. 3.24.

3.4.5 Triaxial Compression-Extension

Fig. 3.23 shows the view down the space diagonal ($\sigma_1 = \sigma_2 = \sigma_3$), the three principal stresses having orthogonal axes. As described in

Triaxial Resilient Shear Strains
Extension Region

x without stress ratio correction

• with stress ratio correction

FIG. 3.24

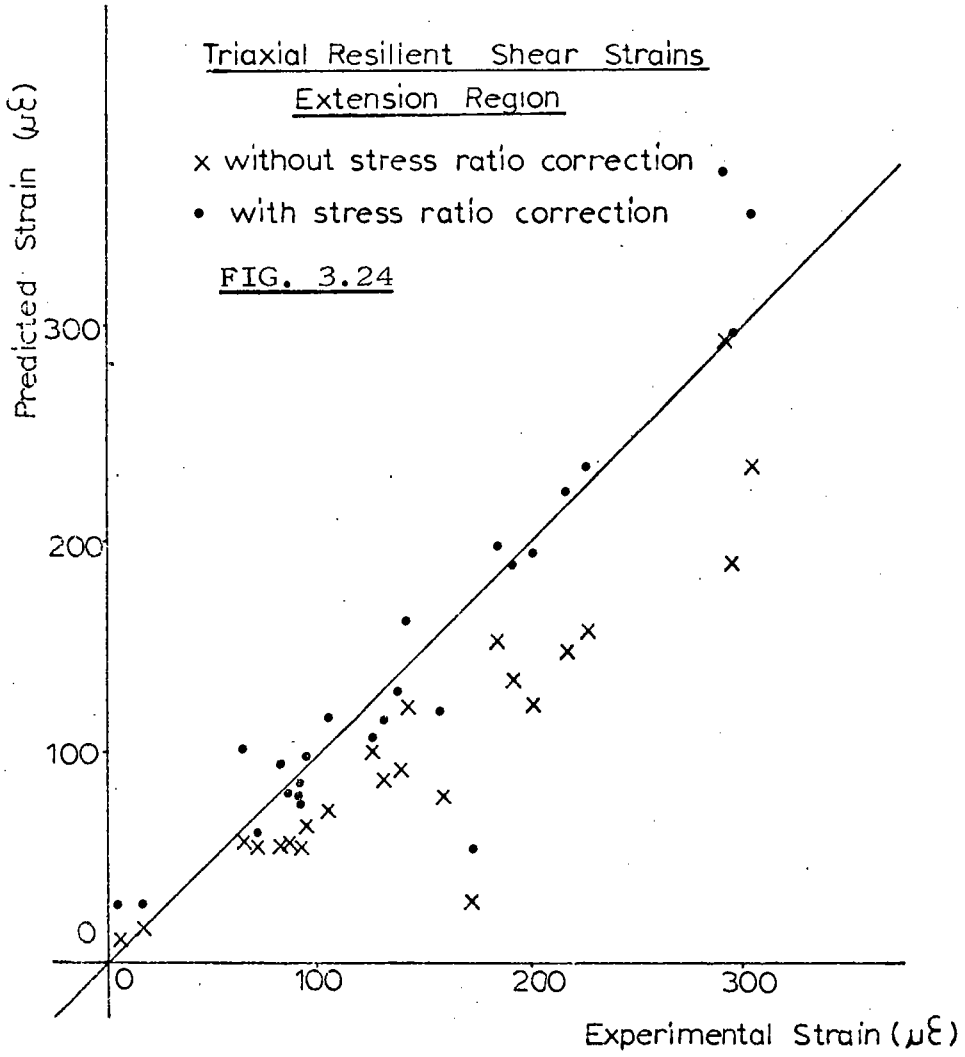

Triaxial Resilient Volumetric
Strains - Extension Region

FIG. 3.25

x without stress ratio correction

• with stress ratio correction

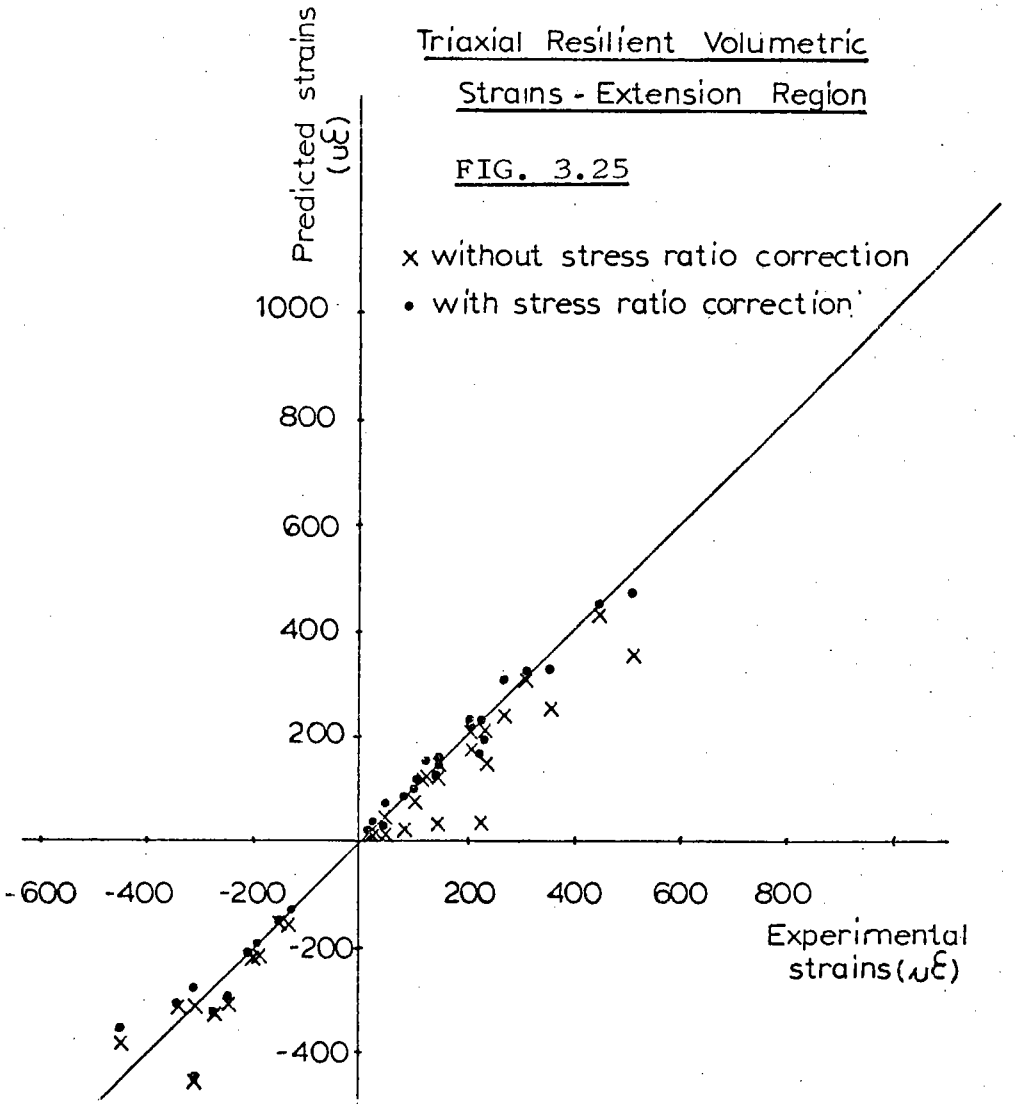

Section 3.4.4, triaxial compression and triaxial extension tests occur along the lines OC and OE respectively. Values for resilient shear strains as predicted by the contour model are shown for points in the compression and extension regions.

Consider points J, K, L and M. It is assumed that there is zero shear strain at zero shear stress. By using the procedure described previously, the resulting shear strain in travelling from points L to M and K to J is 200 $\mu\varepsilon$. If, however, the same procedure is applied to a stress path travelling from points K to L, the model will predict zero shear strain, when in fact the actual strain is 400 $\mu\varepsilon$. For paths completely in compression, or completely in the extension region, the resilient shear strain is determined from the difference in contour values for each end of the stress path. However, for paths which are of the compression-extension type, the resilient shear strain is equal to the sum of the contour values. A procedure was required which would recognise the stress state of any path, apply the stress ratio correction (Section 3.4.4) if necessary, and sum or subtract the contour values for each end of the stress path as required. The following procedure was adopted:

Consider points 1 and 2 in general three-dimensional stress space. The coordinates of each point in terms of directions X and Y may be found using the following equations:

$$X = \frac{\sqrt{3}}{2}(\sigma_\theta - \sigma_r) \tag{3.20}$$

$$Y = \frac{2\sigma_a - \sigma_\theta - \sigma_r}{2} \tag{3.21}$$

The coordinates X and Y enable an angle α to be calculated which is anticlockwise from the positive Y direction to the line connecting the stress point and the origin. Assuming that the directions of stress

and strain coincide, shear strain contour values for points 1 and 2 may be determined using the model and applying a stress ratio correction as necessary. Let ε_n be the normalised resilient shear strain produced by the stress path connecting points 1 and 2, then using the cosine rule:

$$\varepsilon_n^2 = \varepsilon_1^2 + \varepsilon_2^2 - 2\varepsilon_1\varepsilon_2 \cos(\alpha_2 - \alpha_1) \qquad (3.22)$$

where ε_1 and ε_2 are the shear strain contour values for points 1 and 2.

The resilient shear strain ε_r may then be obtained using the correction previously described (Equation 3.10) but using a stress path length ℓ_r defined as:

$$\ell_r = \sqrt{(X_2 - X_1)^2 + (Y_2 - Y_1)^2 + (p_2 - p_1)^2} \qquad (3.23)$$

It can be seen that for paths entirely in compression or extension, $\cos(\alpha_2 - \alpha_1) = +1$ and Equation 3.22 reduces to:

$$\varepsilon_n = (\varepsilon_1 - \varepsilon_2) \qquad (3.24)$$

For paths of the compression-extension type, $\cos(\alpha_2 - \alpha_1) = -1$ and Equation 3.22 reduces to:

$$\varepsilon_n = (\varepsilon_1 + \varepsilon_2) \qquad (3.25)$$

Chapter 4 describes how the above procedure has been extended to paths away from the vertical axes.

Comparisons of predicted and experimental results for triaxial compression-extension paths are shown in Fig. 3.26. The procedure described above is shown to be satisfactory.

The normalised shear strain contours obtained by Pappin (1979) for the graded material were expressed as:

$$\varepsilon_n = 2.4\left[\frac{q}{p + 13}\right] \times 10^{-4} \qquad (3.26)$$

COMPARISON OF PREDICTED AND EXPERIMENTAL RESILIENT SHEAR STRAINS FOR TRIAXIAL COMPRESSION-EXTENSION

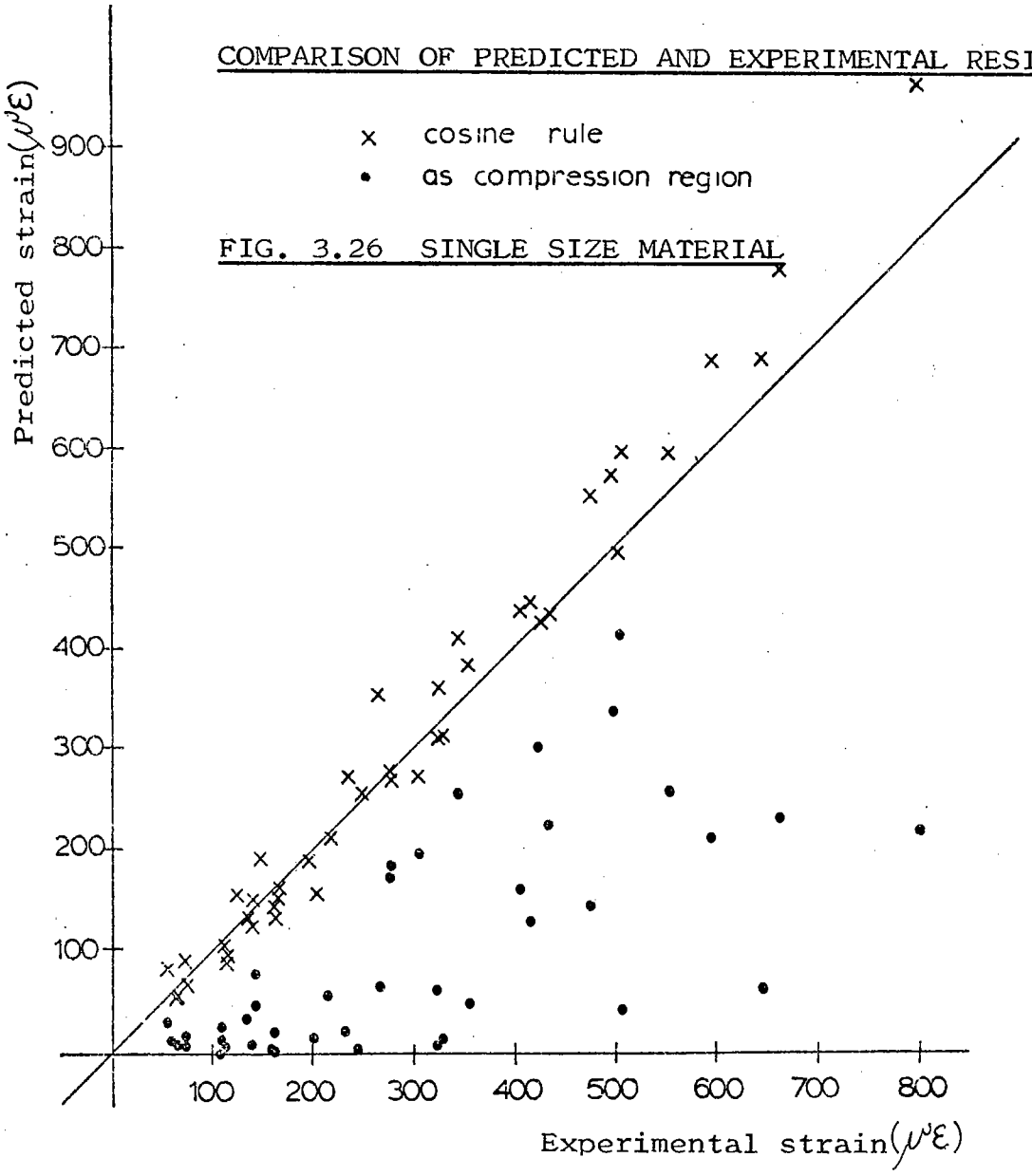

FIG. 3.26 SINGLE SIZE MATERIAL

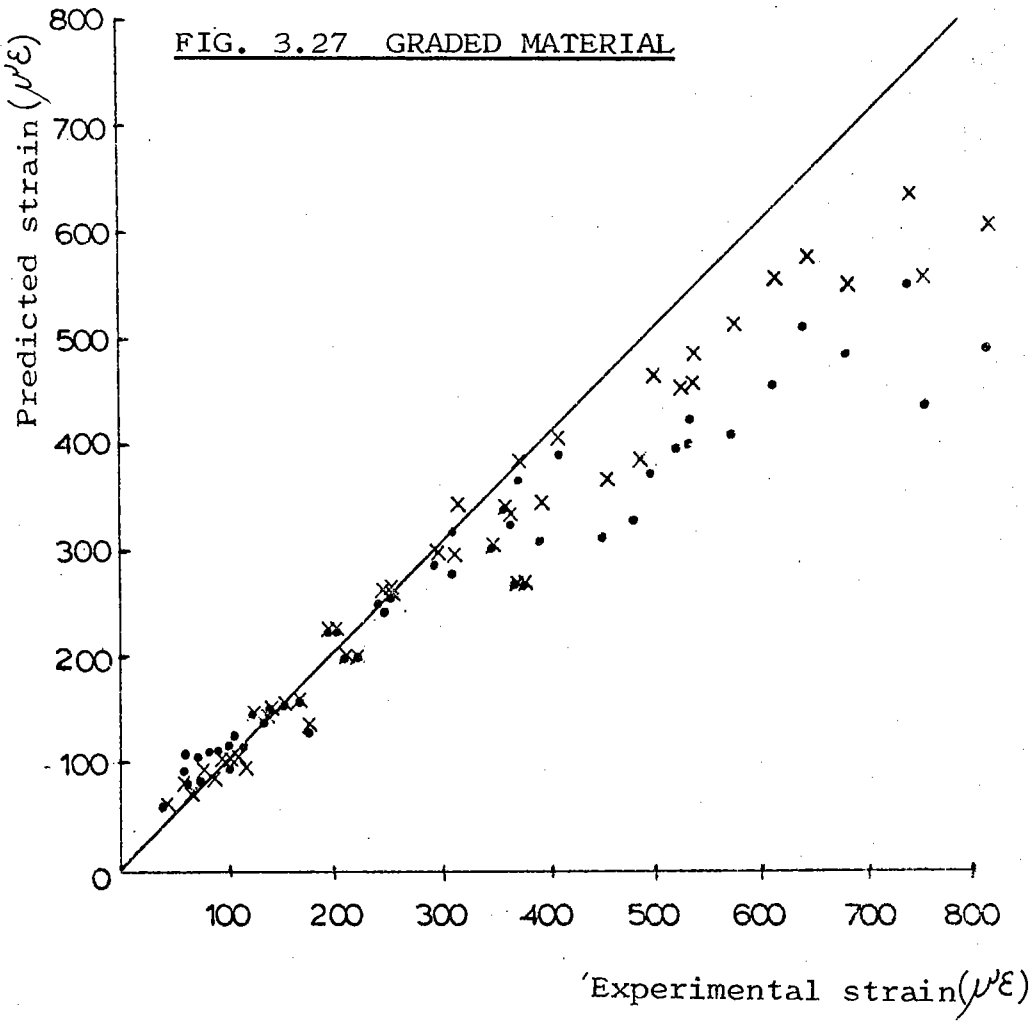

FIG. 3.27 GRADED MATERIAL

For stress paths of the compression-extension type joining points (p_1, q_1) and (p_2, q_2) in (p,q) stress space, Pappin predicted shear strain ε_1 for point (p_1, q_1) as:

$$\varepsilon_1 = 2.4\left[\frac{q_1}{p_1 + 13}\right] \times 10^{-4} \tag{3.27}$$

ε_r was calculated as:

$$\varepsilon_r = 2.4\left[\frac{q_2}{p_2+13} - \frac{q_1}{p_1+13}\right] \times \text{stress path length correction} \times 10^{-4} \tag{3.28}$$

and ε_2 for point (p_2, q_2) as:

$$\varepsilon_2 = \varepsilon_1 + \varepsilon_r \tag{3.29}$$

The final predicted resilient shear strain was then obtained from the sum of ε_1 and ε_2. This method was cumbersome and involved extra computations for paths of the compression-extension type. The method described above, involving the cosine rule, proved to be superior when applied to the graded material, as shown in Fig. 3.27.

Resilient volumetric strains are almost entirely dependent on changes in p. After transforming the values of deviator stress as required (Equation 3.19), the difference in contour values for each end of a stress path was found to be satisfactory in computing the resilient volumetric strain.

3.5 TESTS ON OTHER MATERIALS

The test programme described in the previous section was carried out to investigate the resilient strain behaviour of a further two materials. Comparisons of the results obtained for the well graded material (Pappin 1979) and the single size material had shown that the general concept of contour models was applicable to both materials,

the only difference being in the numerical constants. Tests conducted at the Transport and Road Research Laboratory (Mayhew 1978) also produced a similar type of model. It was decided to test a gravel and a smaller size fraction of the crushed limestone to further examine whether the model type, although developed empirically, could be applied generally to various gradings and types of granular materials.

The gravel was from Woodhall Spa and its properties are presented in Table 3.2.

Table 3.2 Woodhall Spa gravel

Property	Value	Size fraction*
Specific Gravity	2.26	10/5
Aggregate crushing value	18%	as BS 812
Saturated moisture content	7.17%	10/5
Angularity	5.0	10/6.3
Flakiness	38.1%	10/6.3
Elongation index	32.6%	10/6.3
Aggregate impact value	20%	as BS 812
Average chalk content (by wt)	66.0%	10/5

* Y/X, passing Y mm retained on X mm British Standard Sieves.

The size fraction tested was that passing a 10 mm and retained on 5 mm British Standard Sieves. The material is described as a "sandy hoggin" containing elongated glassy flint particles and rounded smooth chalk particles.

The contour models developed for the single size crushed limestone were applied directly to the triaxial results obtained for the gravel. The general concept of contours was found to apply but strains were consistently underpredicted by about 50%. After adjusting the equation constants, satisfactory contour models to predict resilient volumetric

strain v_c and normalised resilient shear strain ε_n were obtained as:

$$v_c = \left(\frac{p}{A}\right)^{0.5}\left[1 - B(q/p)^C\right] \quad (3.30)$$

$$\varepsilon_n = D\left[\frac{q}{p + E}\right] \quad (3.31)$$

where A, B, C, D and E are constants

$A = 5.49 \times 10^{+7}$ kPa

B and C are as defined in Equation 3.6

$D = 8.25 \times 10^{-4}$

E is as defined in Equation 3.11.

Typical comparisons of predicted and experimental strains are shown in Figs 3.28 and 3.29, and the models are shown to be satisfactory.

Problems with particle size in the simple shear apparatus resulted in a test programme being conducted on a smaller grading of the single size crushed limestone (Chapter 6). In order that some correlation of results could be obtained, a test programme to determine resilient properties was also conducted on this material. The size fraction was that passing No. 7 and retained on No. 14 British Standard sieves. Again the contour models developed for the 3 mm single size material were applied directly to the smaller grading and a comparison of predicted and experimental results made. The same equation constants as for the 3 mm material were found to be adequate for the 1.5 mm material. Generally the smaller material shows a greater scatter of results, but this is to be expected as only one specimen was tested. Typical comparisons of predicted and experimental strains are shown in Figs 3.30 and 3.31. The results would suggest that for the crushed limestone, it may be possible to apply the same contour model to all size fractions provided that the angularity and ratio of particle size within the fraction are similar to that for the 3 mm material.

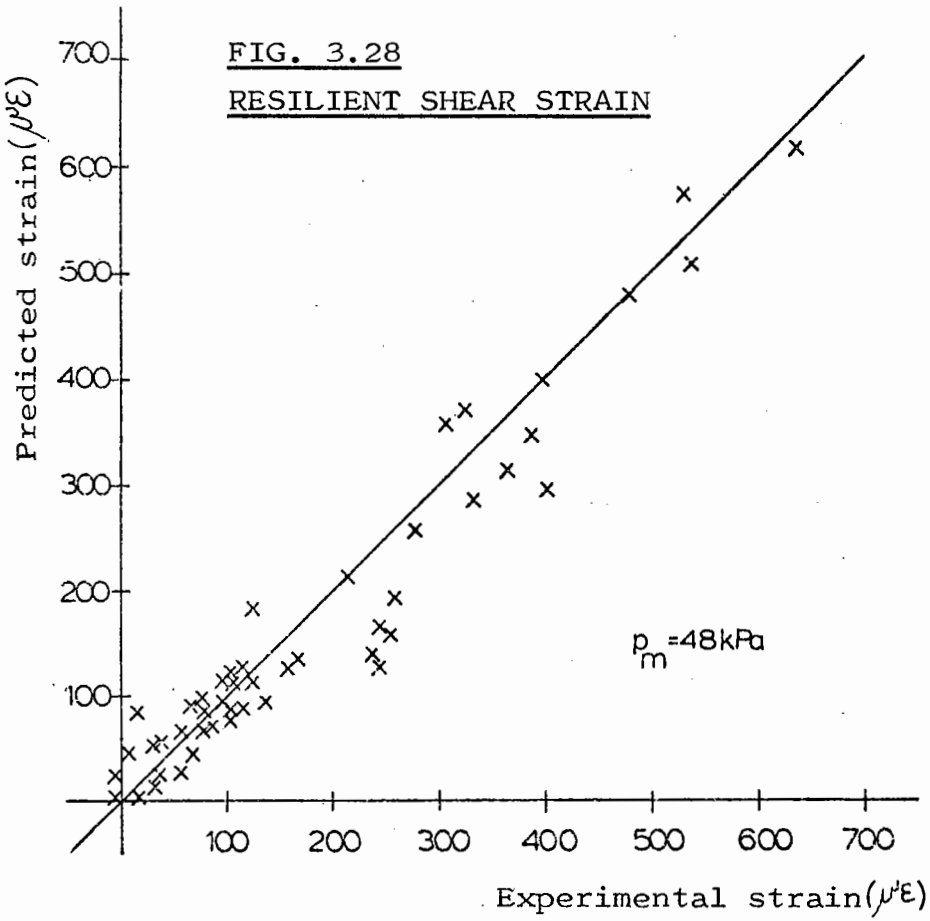

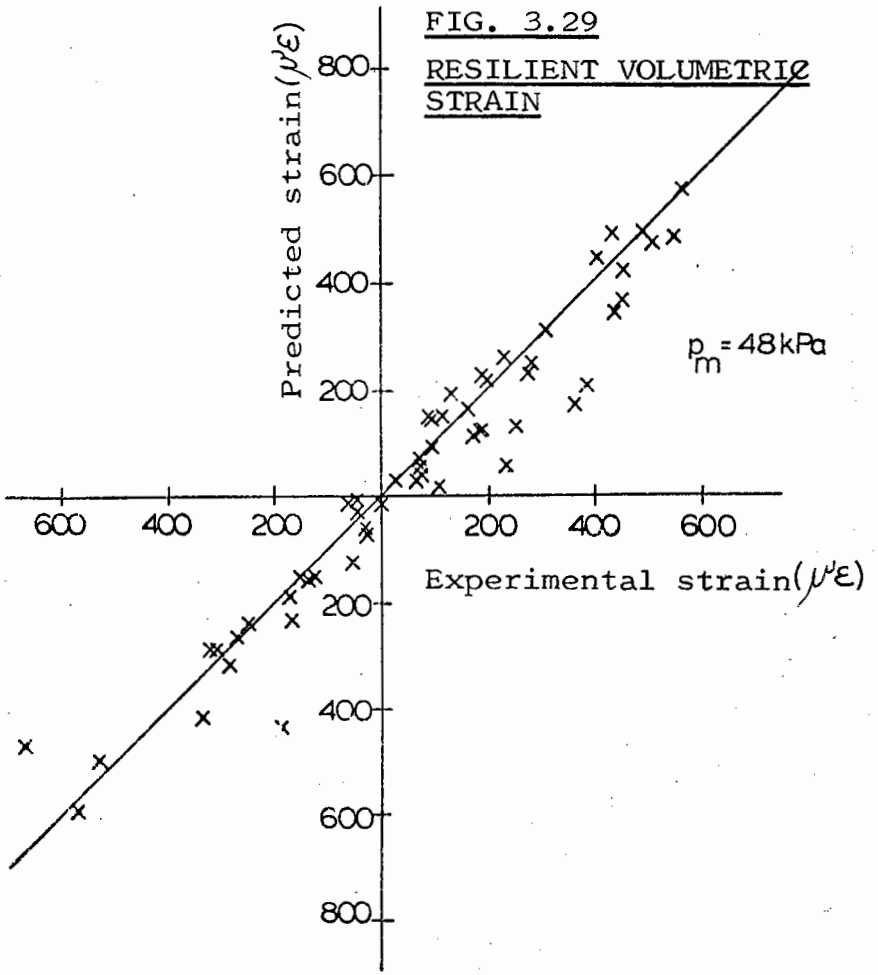

COMPARISON OF PREDICTED AND EXPERIMENTAL STRAINS FOR WOODHALL SPA GRAVEL

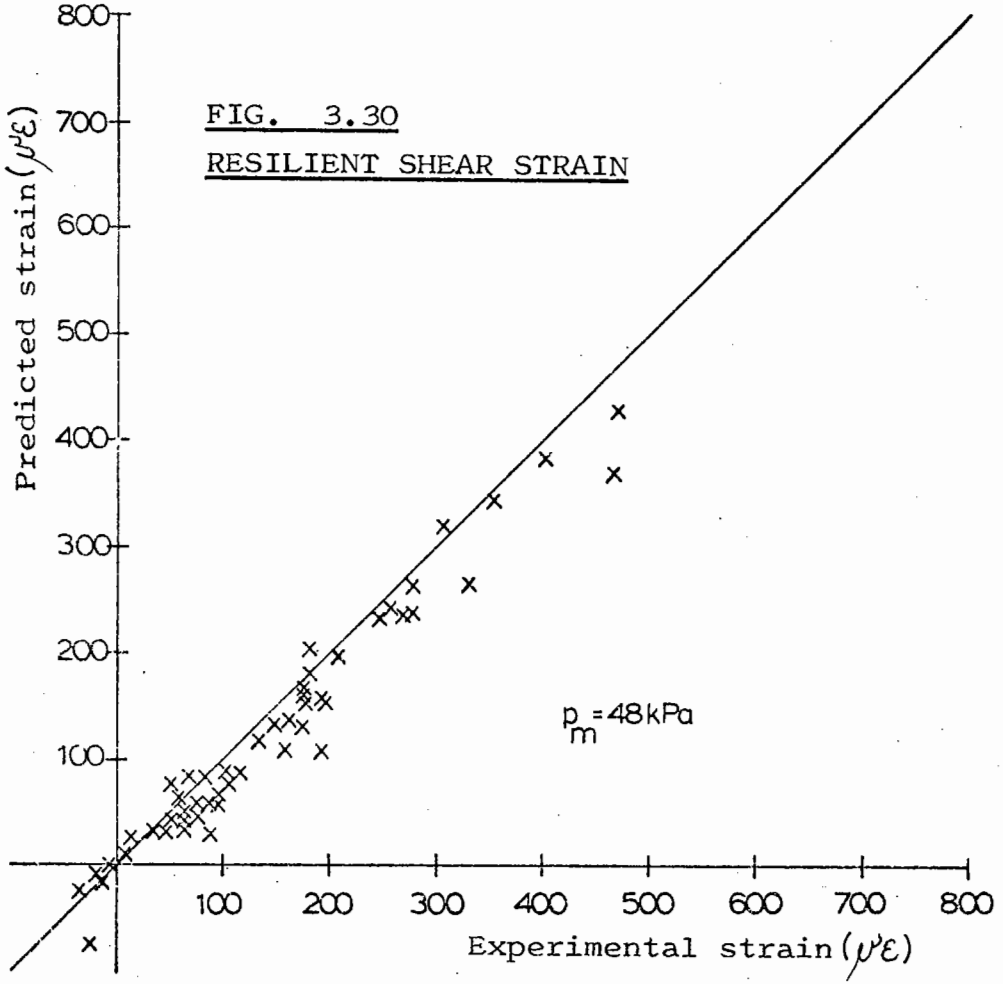

FIG. 3.30

RESILIENT SHEAR STRAIN

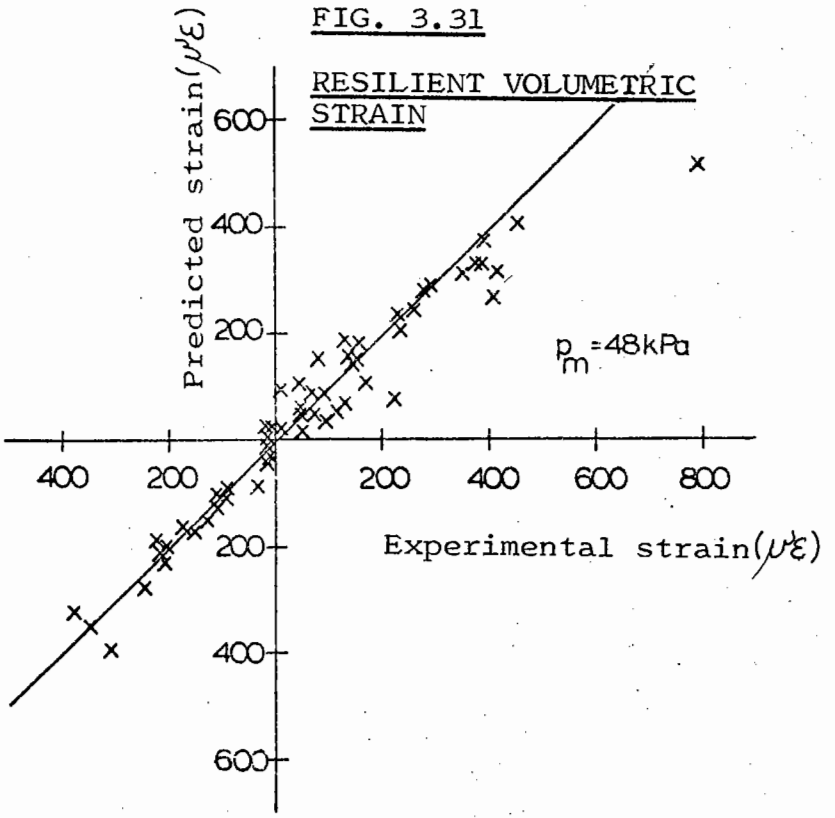

FIG. 3.31

RESILIENT VOLUMETRIC STRAIN

COMPARISON OF PREDICTED AND EXPERIMENTAL STRAIN FOR 1.5 mm LIMESTONE

Full results for the gravel and crushed limestone are presented in Appendix 3B.

3.6 ZERO AXIAL STRAIN TESTS

One of the objectives of the project was to compare results obtained from the triaxial apparatus with those from the biaxial shear box (Chapter 4). However, the latter involves plane strain conditions, so an attempt was made to reproduce these in the triaxial apparatus. The equipment had the facility to compare the load command signal with feedback taken from the axial strain measurements enabling zero axial strain tests to be conducted.

A number of stress paths were selected from those used previously and a short zero axial strain, repeated load test programme conducted on the 3 mm single size crushed limestone. The results were analysed defining volumetric and shear strain as:

$$v = 2\varepsilon_{rad} \tag{3.32}$$

$$\varepsilon = -\frac{2}{3}\varepsilon_{rad} \tag{3.33}$$

where ε_{rad} = radial strain.

The contour models developed from the full resilient test programme were then applied to the results and comparisons of predicted and experimental resilient strains are shown in Figs 3.32 and 3.33.

The predictions are generally high, although this may be attributed to the fact that only one specimen was tested. The specimen had already been subjected to 100 000 cycles of stress to determine permanent strain behaviour. The results obtained would suggest a stiffened response which is in agreement with the findings of Section 3.9.

The model was shown to be applicable to triaxial plane strain

FIG. 3.32 ZERO AXIAL STRAIN TEST

RESILIENT SHEAR STRAIN

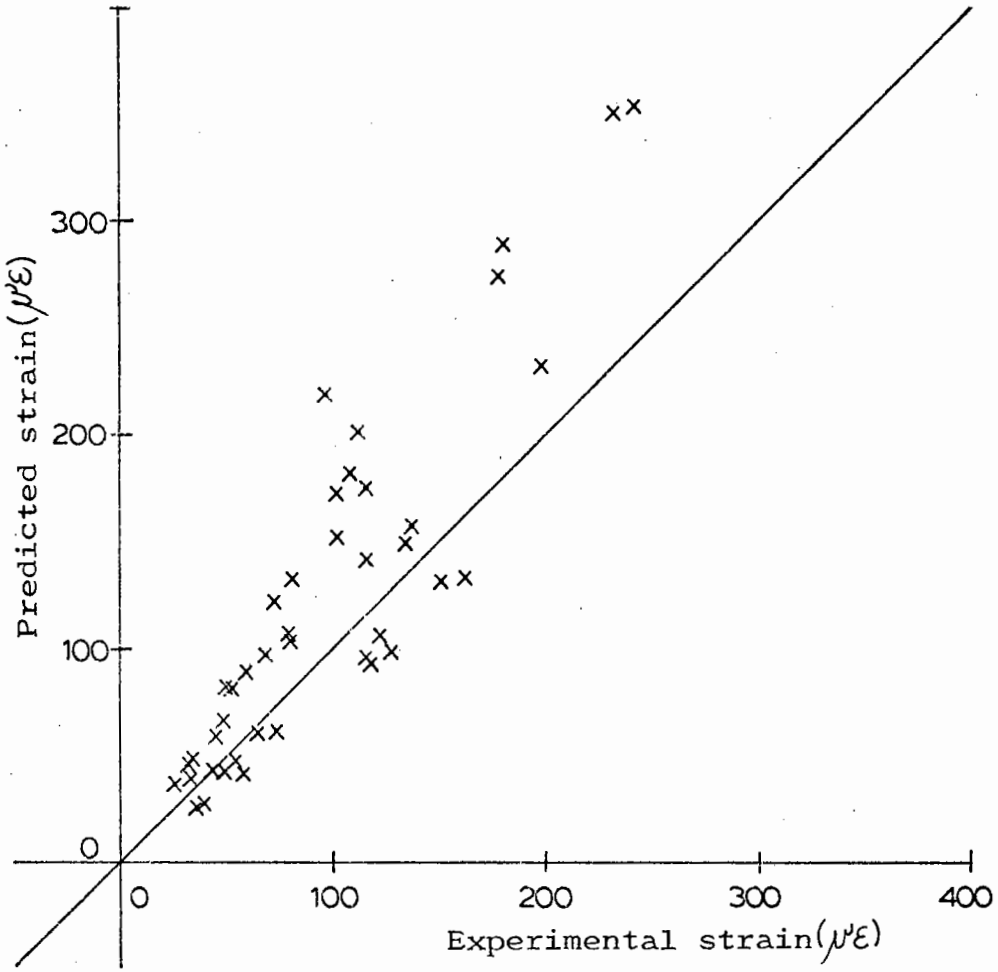

FIG. 3.33 ZERO AXIAL STRAIN TEST

RESILIENT VOLUMETRIC STRAIN

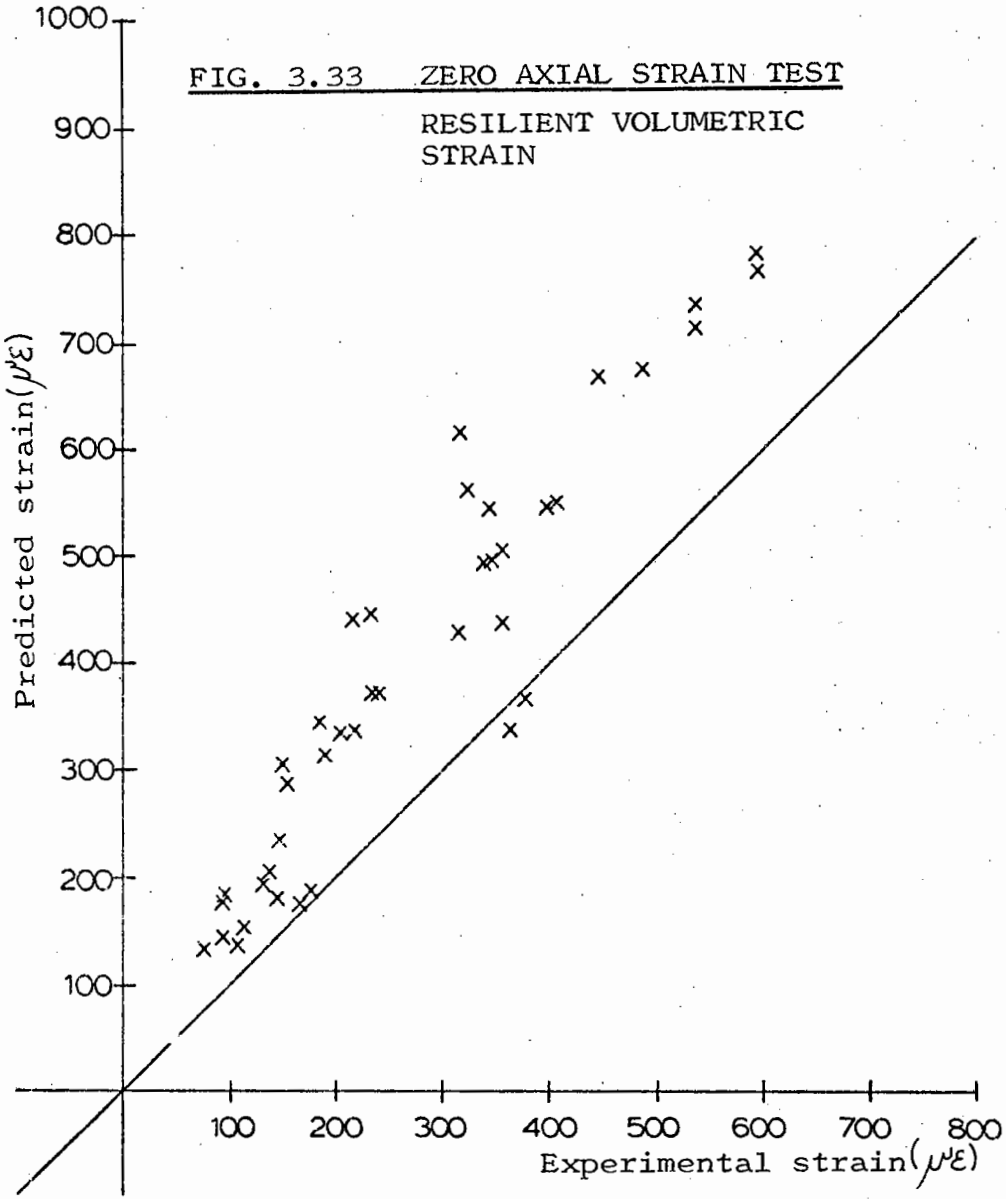

conditions and was subsequently successfully applied to a full resilient test programme in the biaxial shear box (Chapter 4).

3.7 PERMANENT STRAIN BEHAVIOUR

A testing programme to investigate permanent strain behaviour was carried out using the stress paths shown in Fig. 3.34. The programme was designed so that tests were carried out at two p_m values. The initial intention was to repeat the stress paths applied by Pappin (1979), enabling a direct comparison of results to be obtained for the different gradings. However, on testing path PA, it was found that excessive strains were developing in the single size material, so rather than risk damaging the instrumentation it was decided to test at a higher p_m value. All the tests involved a frequency of 1 Hz, with at least 100 000 cycles of stress applied. Three tests were conducted for each stress path and the results were averaged. On completing the required quota of cycles for each test, some specimens were subjected to a monotonic failure test to investigate the effect of permanent strain on the shear strength of the material. These, along with observations of the resilient strain behaviour throughout each test, are discussed in Sections 3.8 and 3.9. Typical plots of permanent shear and volumetric strains (test path PA2) are shown in Figs 3.35 and 3.36. Full results for all the paths are presented in Appendix 3C.

3.7.1 Test Results

It was found that differences in permanent strains occurred during the first few cycles for tests following the same stress path. This was more pronounced for tests using the biaxial shear box (Chapter 4) but, to be consistent the following procedure was adopted for results

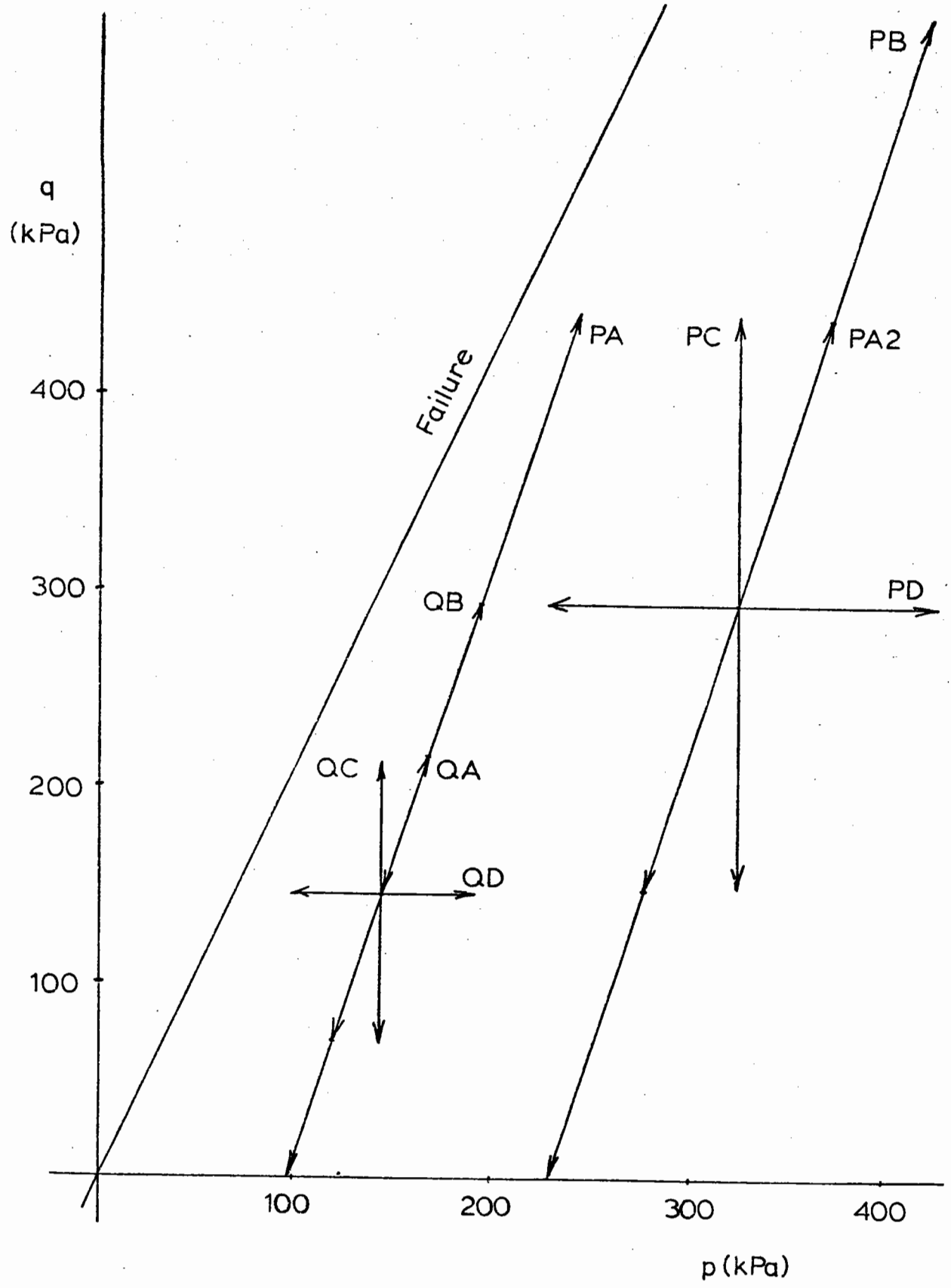

FIG. 3.34 STRESS PATHS TO INVESTIGATE PERMANENT STRAIN BEHAVIOUR

FIG. 3.35

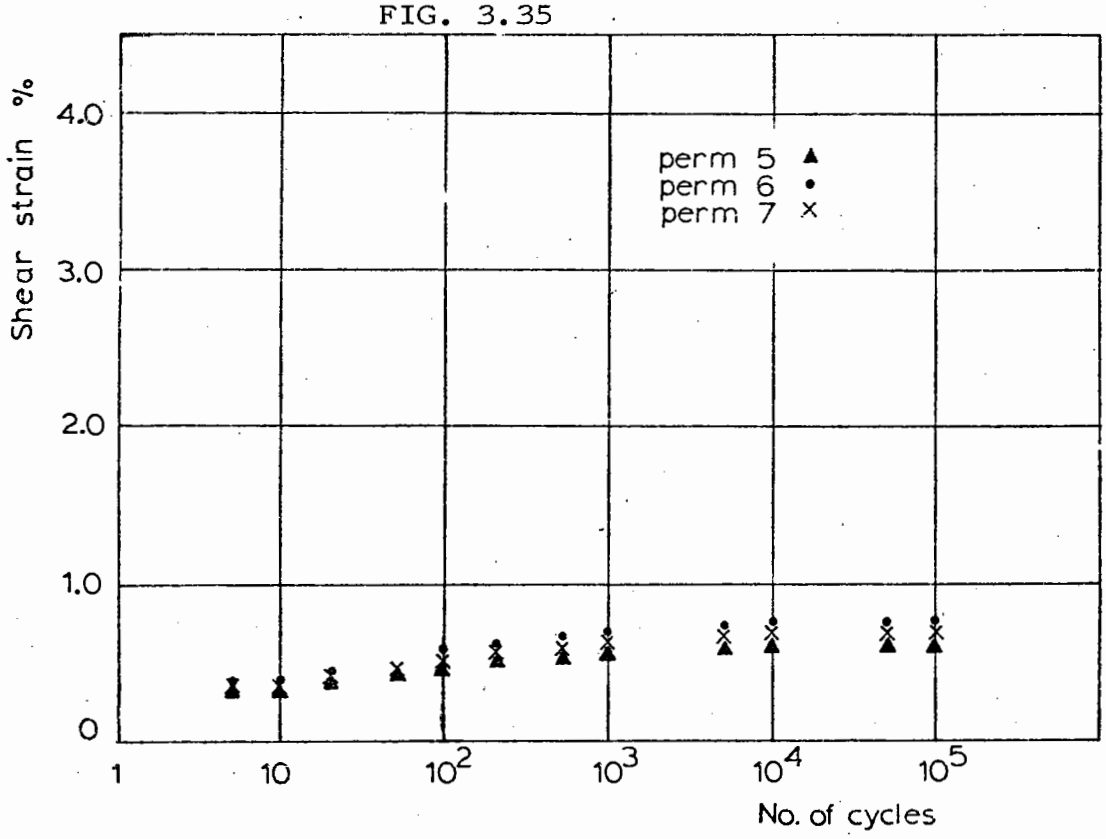

FIG. 3.36

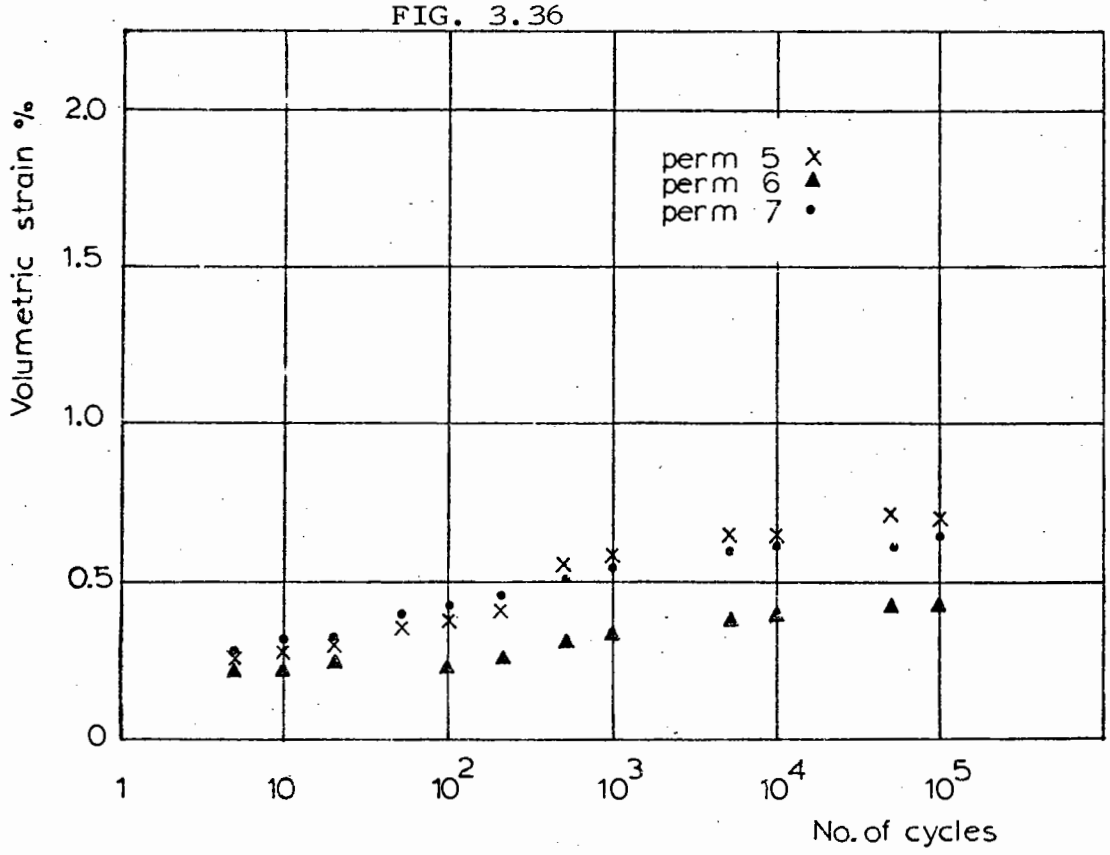

TYPICAL PERMANENT STRAIN RESULTS - PATH PA2

from both pieces of apparatus. It was decided to ignore these initial discrepancies as, in a real situation, initial loading cycles occur during construction and therefore have no direct relation to the situation when the pavement is surfaced and opened to traffic. The rate of increase of permanent strain after a particular number of cycles was thought to be more useful than an absolute strain value. On comparing results from the biaxial shear box and triaxial apparatus, ten cycles seemed an appropriate number to choose as an arbitrary point to determine the increase of permanent strain rate. The results from each test path have been plotted with a common origin at 10 cycles and a curve representing the subsequent average development of permanent strain drawn. Figs 3.37 and 3.38 show the averaged permanent volumetric and shear strains for each test path plotted against the logarithm of the number of cycles.

3.7.2 Permanent Shear Strain

Previous work at Nottingham: Pappin (1979) selected 100 cycles as an arbitrary point to determine the rate of permanent strain. The permanent strain results from each test were then plotted so that at 100 cycles the strains were the same, and a curve representing the average rate of permanent strain for each stress path was plotted. The shapes of the curves were similar and each curve was normalised by dividing by the strain rate at 100 cycles. A shape function (fnN) was then calculated for the normalised curves, so that by multiplying the shape function (fnN) by the appropriate strain rate the final permanent shear strain for each stress path could be calculated at a given number of cycles. A final expression for permanent shear strain was derived as:

$$\varepsilon_p = (fnN) \times \ell_r \times (q/p)_{max}^{2.8} \times 10^{-4} \qquad (3.34)$$

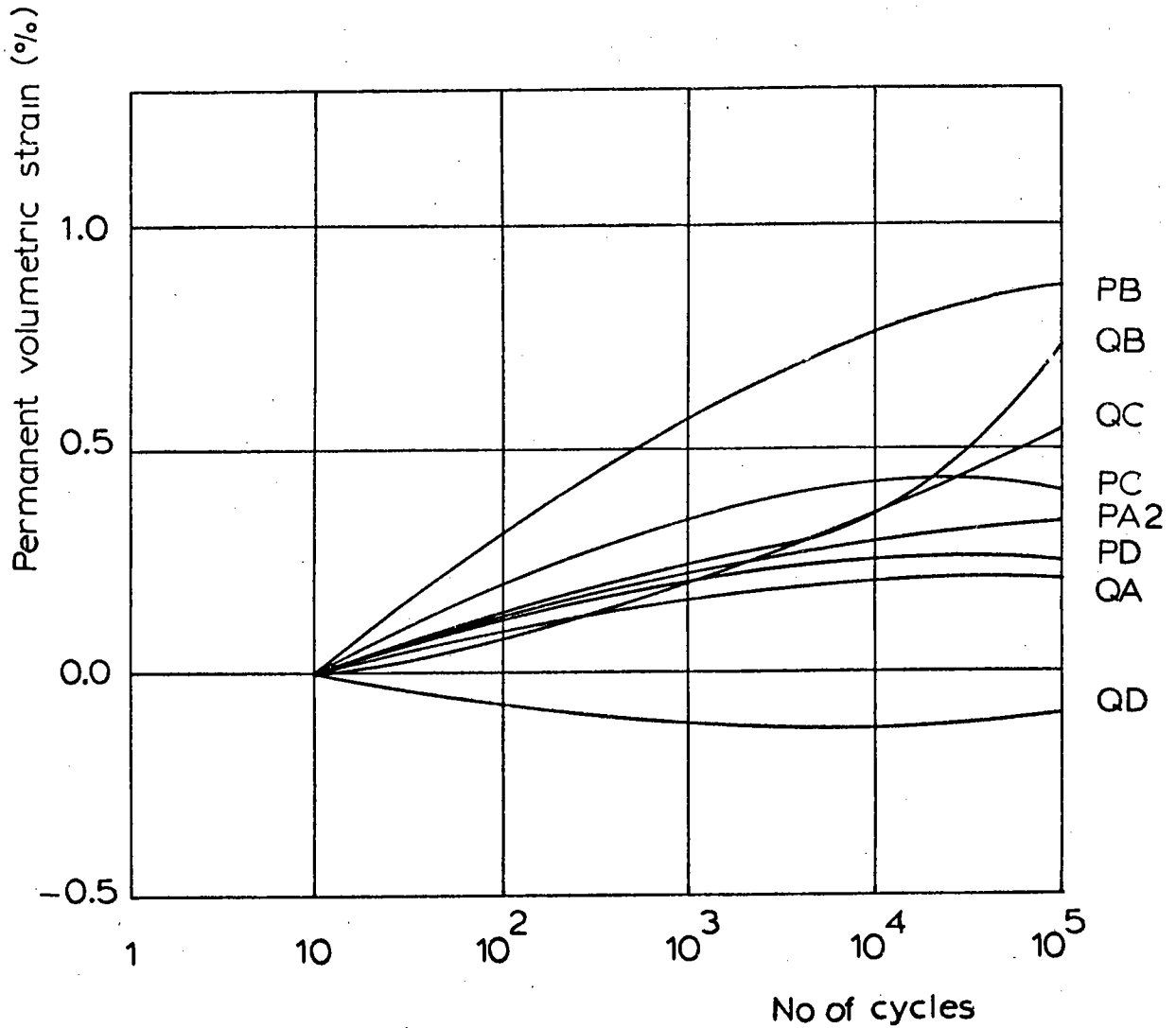

FIG. 3.37 AVERAGED PERMANENT VOLUMETRIC STRAINS

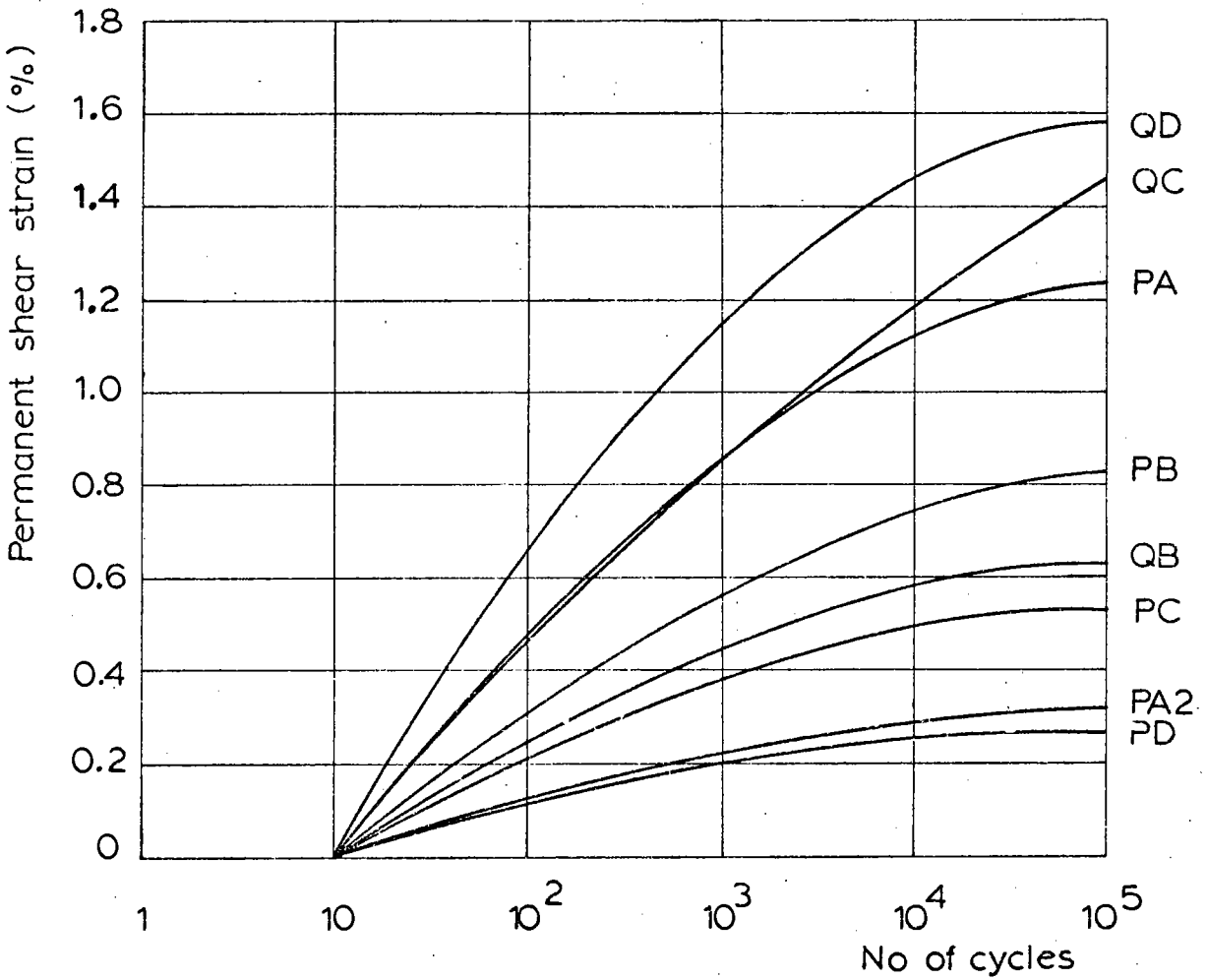

FIG. 3.38 AVERAGED PERMANENT SHEAR STRAINS

where ε_p is the permanent shear strain %

fnN is the shape function which depends on the number of stress cycles N

ℓ_r is the stress path length defined as:

$$\ell_r = (p_r^2 + q_r^2)^{\frac{1}{2}} \tag{3.35}$$

where

$$p = \frac{\sigma_1 + \sigma_2 + \sigma_3}{\sqrt{3}} \tag{3.36}$$

$$q = \frac{\left[(\sigma_1-\sigma_2)^2 + (\sigma_2-\sigma_3)^2 + (\sigma_3-\sigma_1)^2\right]^{\frac{1}{2}}}{\sqrt{3}} \tag{3.37}$$

The curves shown in Fig. 3.38 were found to be of similar shape to those obtained by Pappin (1979) for the well graded material. Following the procedure he used, an average shape function (fnN) for all the curves was determined. Each curve was normalised by dividing the permanent strain value at cycle N (ε_{pN}) by the strain rate at 100 cycles ($\dot{\varepsilon}_{p100}$) where:

$$\text{strain rate} = \frac{\Delta \text{strain}}{\Delta \text{ no. of cycles}} \tag{3.38}$$

The strain rate at 100 cycles for each test path was:

stress path	PA2	PB	PC	PD	QA	QB	QC	QD
strain rate $\times 10^{-6}$	5.1	8.9	8.0	4.5	4.3	9.0	15.0	23.7

Table 3.3

The resulting normalised strain value at cycle N was called the shape function and was found to be fairly uniform for all the stress paths. An average shape function (fnN) was therefore determined as in Table 3.4.

No. of cycles	10^2	10^3	10^4	10^5
shape function (fnN)	286	507	651	740

Table 3.4

The permanent strain at cycle N could then be determined from:

$$\varepsilon_{p_N} = fnN \times \dot{\varepsilon}_{p_{100}} \tag{3.39}$$

The strain rate at 100 cycles may only be determined by laboratory testing and to generalise the model, it was necessary to relate $\dot{\varepsilon}_{p_{100}}$ to some readily available parameters.

The permanent shear strain model developed by Pappin related permanent shear strain rate at 100 cycles to the stress path length and the variable (q/p)max. An attempt was made to establish a similar relationship; however, as shown in Table 3.5, it was possible to have stress paths with identical (q/p)max but completely different strain rates.

Table 3.5

Stress path	(q/p)max	Strain rate at 100 cycles $\dot{\varepsilon}_{p_{100}} \times 10^{-6}$
PD	1.28	4.5
PA2	1.17	5.1
PC	1.35	8.0
PB	1.38	8.9
QA	1.28	4.3
QB	1.5	9.0
QC	1.5	15.0
QD	1.5	23.7

Further investigation revealed that strain rate did not depend on (q/p)max but on the minimum normal stress distance A of the stress path from the failure envelope in (p,q) stress space (Fig. 3.39). A was defined as:

$$A = p_R - \frac{q_R}{2.1} \tag{3.40}$$

where p_R, q_R = p,q from (q/p)max, i.e. not necessarily p_{max} and q_{max}.

It is apparent that (q/p)max is still an important parameter but is inadequate on its own.

In the development of the resilient shear strain contour model (Section 3.4.3) the stress path length was defined as:

$$\ell_r = (p_r^2 + q_r^2)^{\frac{1}{2}} \tag{3.41}$$

and to be consistent this definition was also used for the permanent strain model. After dividing the strain rate by the stress path length, the result was plotted against A as shown in Fig. 3.40. It can be seen that there is a distinct threshold value for A below which the strain rate increases rapidly. Only two results were within this limit and it was decided to concentrate efforts on modelling the behaviour when A was greater than the threshold value. For values of A below the threshold, one would expect the curve of the line to be asymptotic to the vertical axes. More tests are required in this region. The expression for permanent shear strain was derived as:

$$\varepsilon_p = (fnN) \times \ell_r \times (3200 - 9.14A) \times 10^{-11} \tag{3.42}$$

where ε_p is permanent shear strain

fnN is the shape function as indicated in Table 3.4

ℓ_r is $(p_r^2 + q_r^2)^{0.5}$

A is always greater than 50.

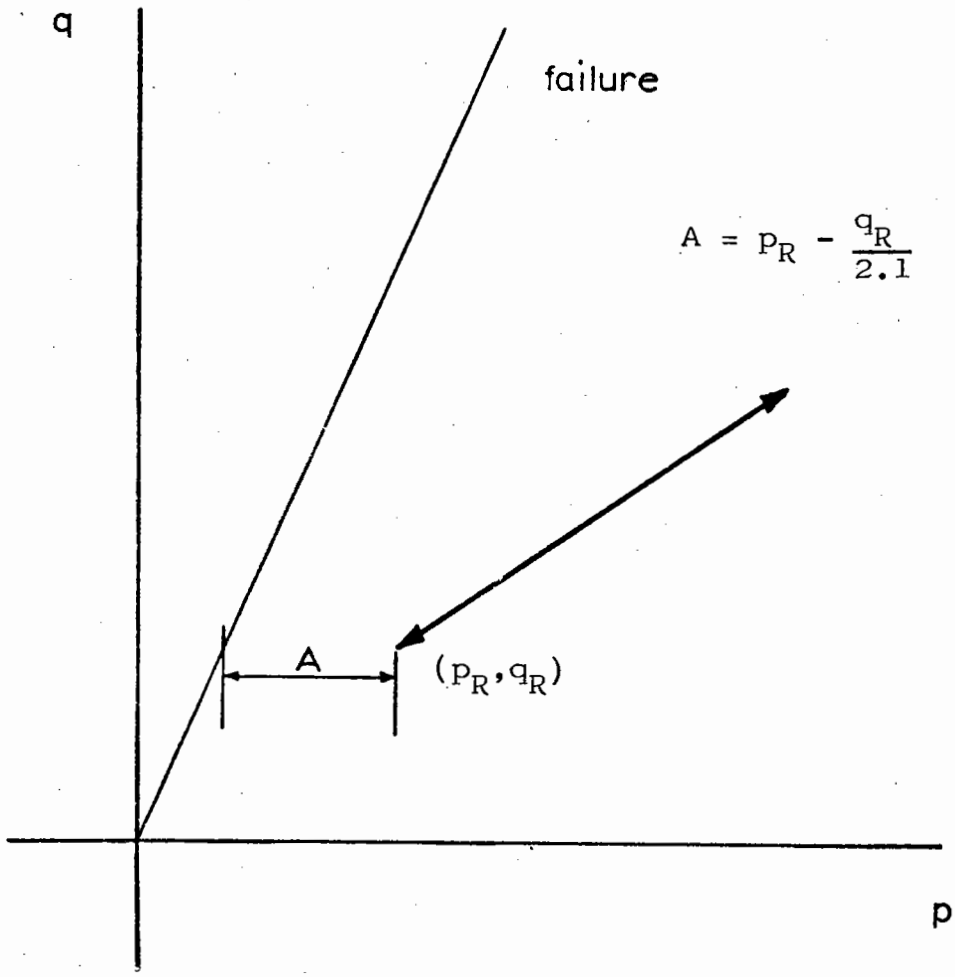

FIG. 3.39 DEFINITION OF DISTANCE A

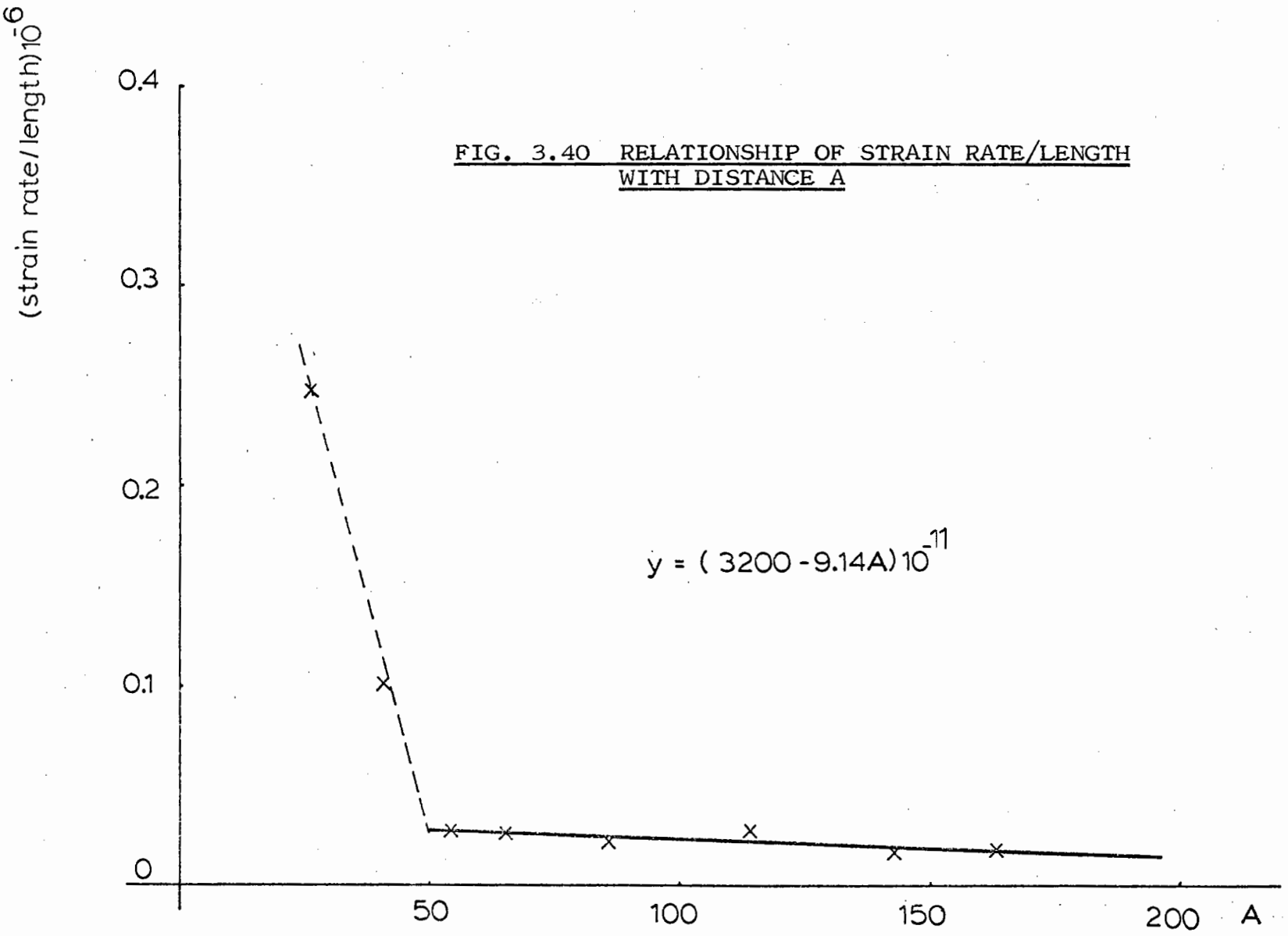

FIG. 3.40 RELATIONSHIP OF STRAIN RATE/LENGTH WITH DISTANCE A

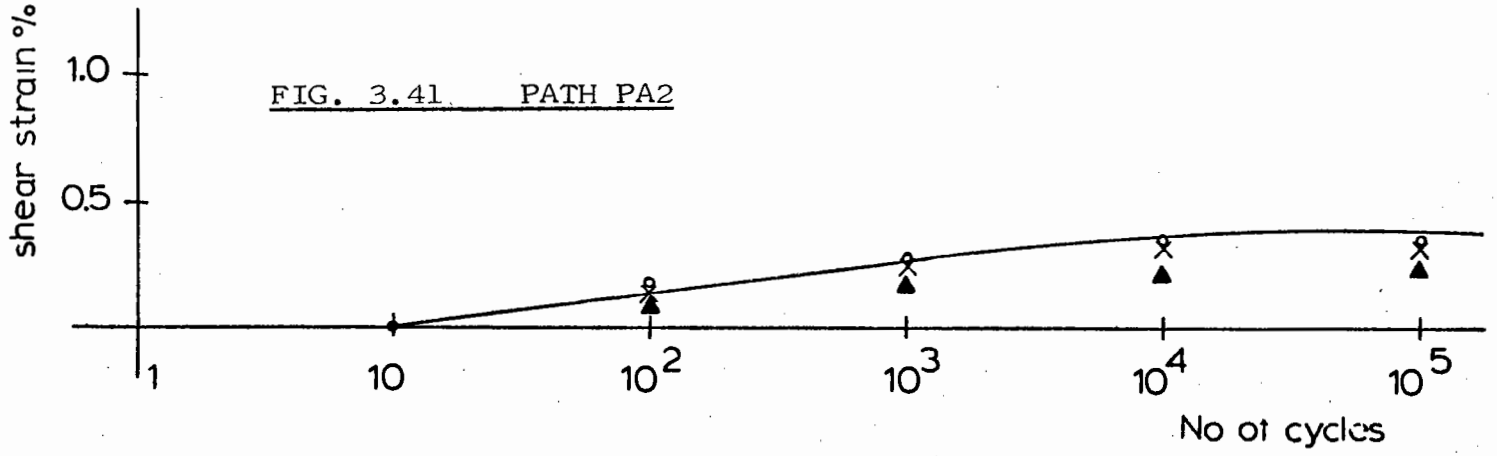

FIG. 3.41 PATH PA2

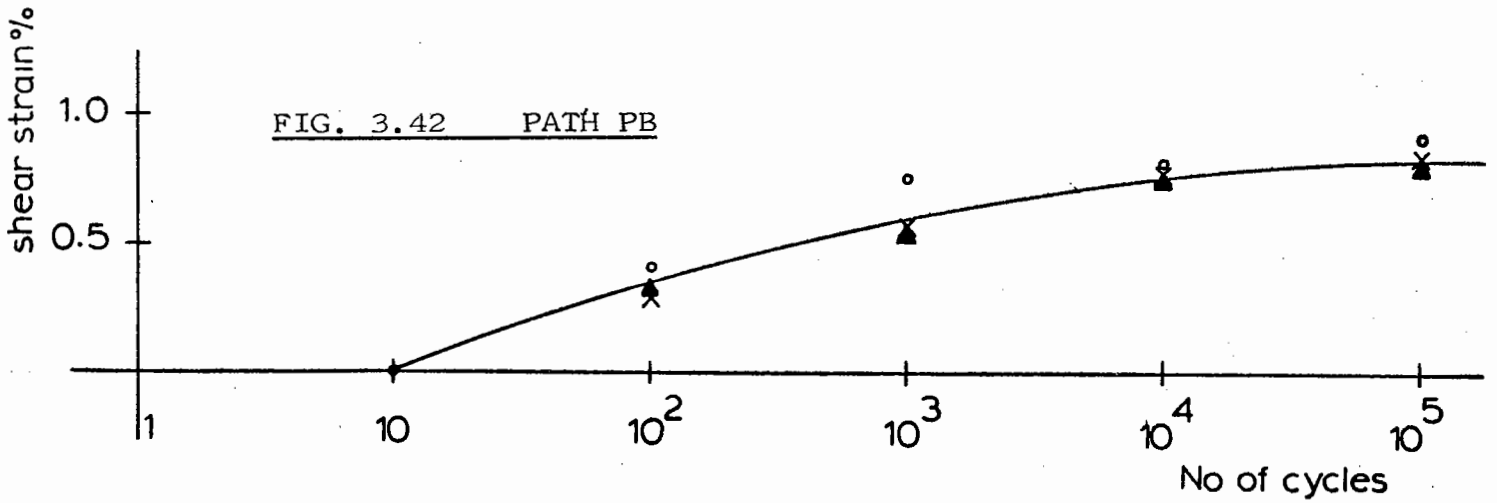

FIG. 3.42 PATH PB

PREDICTED AGAINST EXPERIMENTAL PERMANENT SHEAR STRAINS

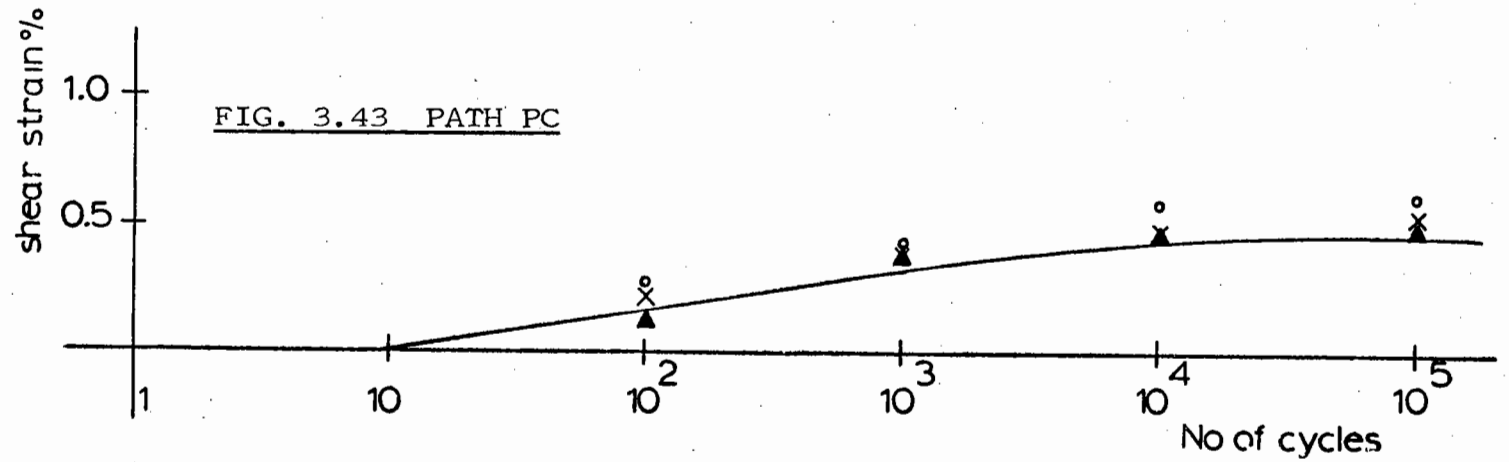

FIG. 3.43 PATH PC

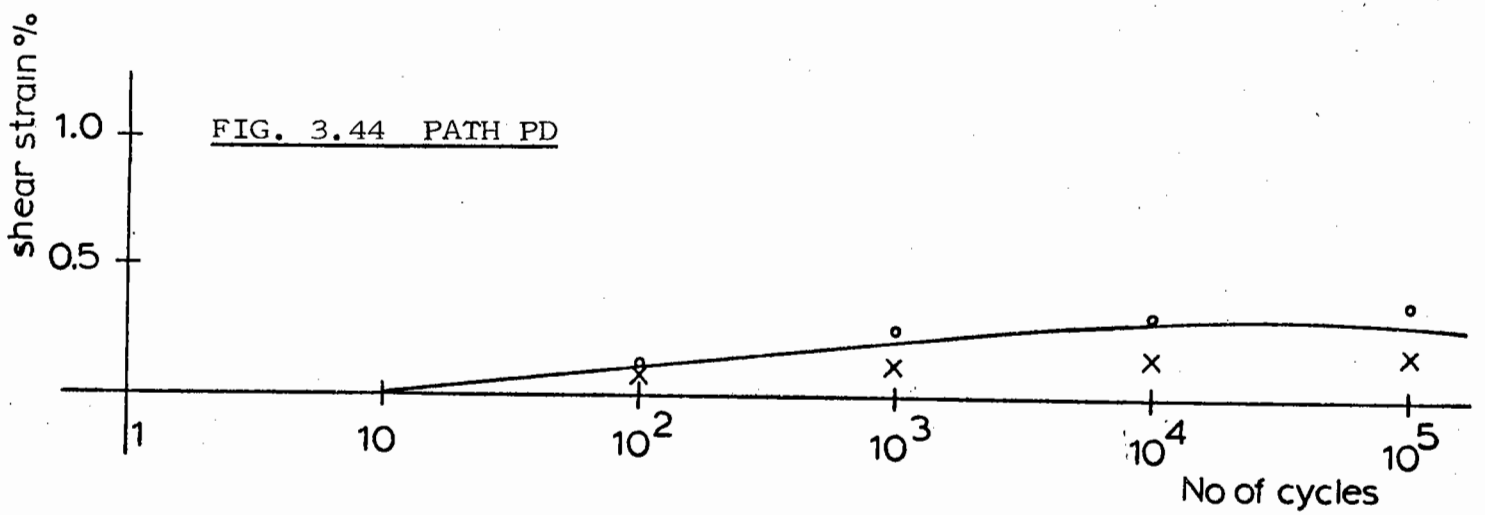

FIG. 3.44 PATH PD

PREDICTED AGAINST EXPERIMENTAL PERMANENT SHEAR STRAINS

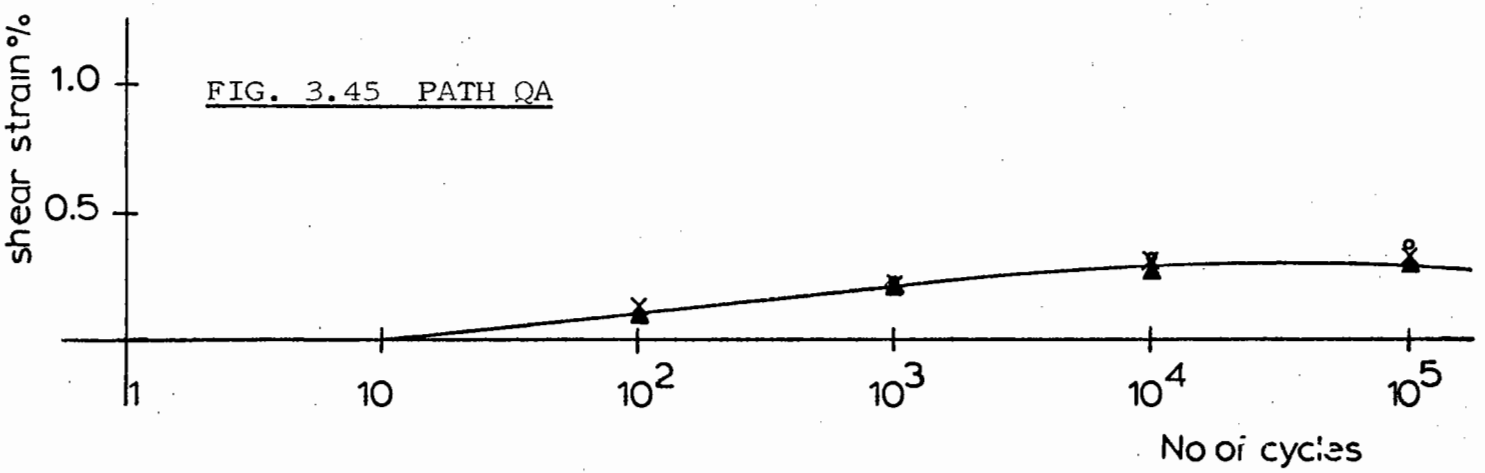

FIG. 3.45 PATH QA

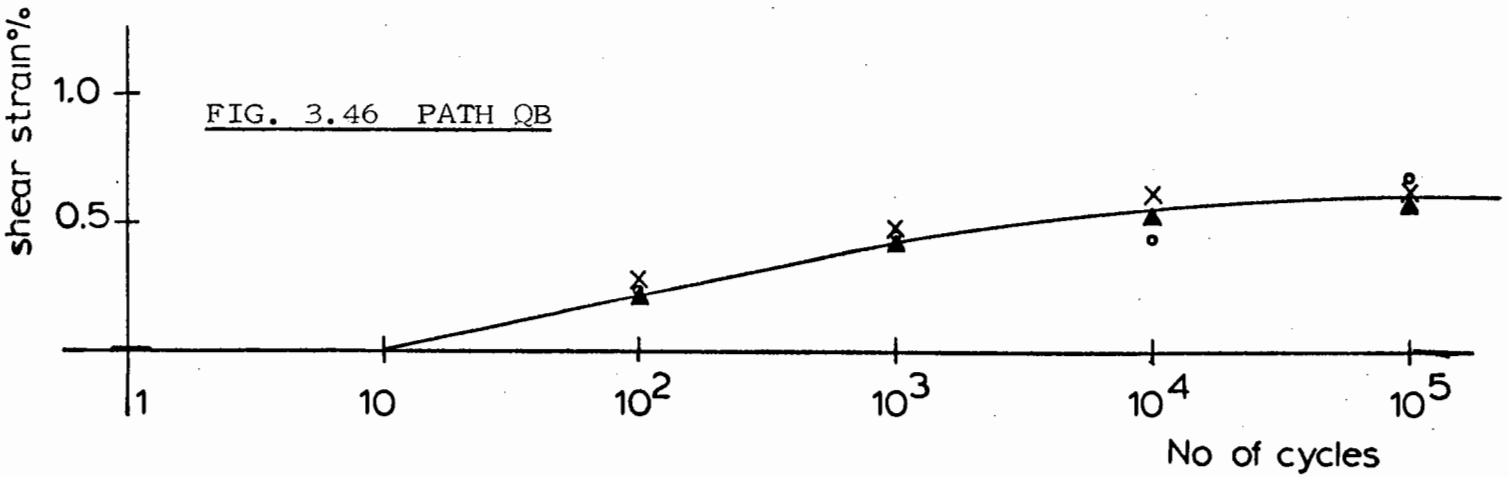

FIG. 3.46 PATH QB

PREDICTED AGAINST EXPERIMENTAL PERMANENT SHEAR STRAINS

Comparisons of predicted and experimental permanent shear strains for A > 50 are presented in Figs 3.41 to 3.46, and considering the approximations involved in the development of the model, are generally quite good.

The existence of a threshold value has important consequences in design consideration for structures containing single size materials. The permanent strain programme conducted by Pappin on the well graded material was reanalysed using the above procedure. The test paths used by Pappin are shown in Fig. 3.47. A plot of strain rate divided by stress path length against A is shown in Fig. 3.48. Most of the stress paths conducted on the graded material were inside the threshold limit as determined for the single size material. However, the well graded material did not appear to exhibit the same dramatic increase in strain rate. The relationship between strain rate and distance A was not as clearly defined and more testing is required.

3.7.3 Permanent Volumetric Strain

Fig. 3.37 shows the average permanent volumetric strains against the logarithm of the number of cycles. As for the shear strain results, the curves could be normalised by dividing by the strain rate at 100 cycles and an average shape function determined. Several attempts were made to model permanent volumetric strains but no satisfactory relationship could be found. Difficulties arose when trying to model a parameter which could be either dilatant or compactive. Attempts to relate volumetric behaviour and static monotonic tests also failed.

3.8 RESILIENT RESPONSE DURING PERMANENT STRAIN TESTS

Resilient strain was monitored throughout each of the permanent strain tests described in the previous section. The results from path PA2

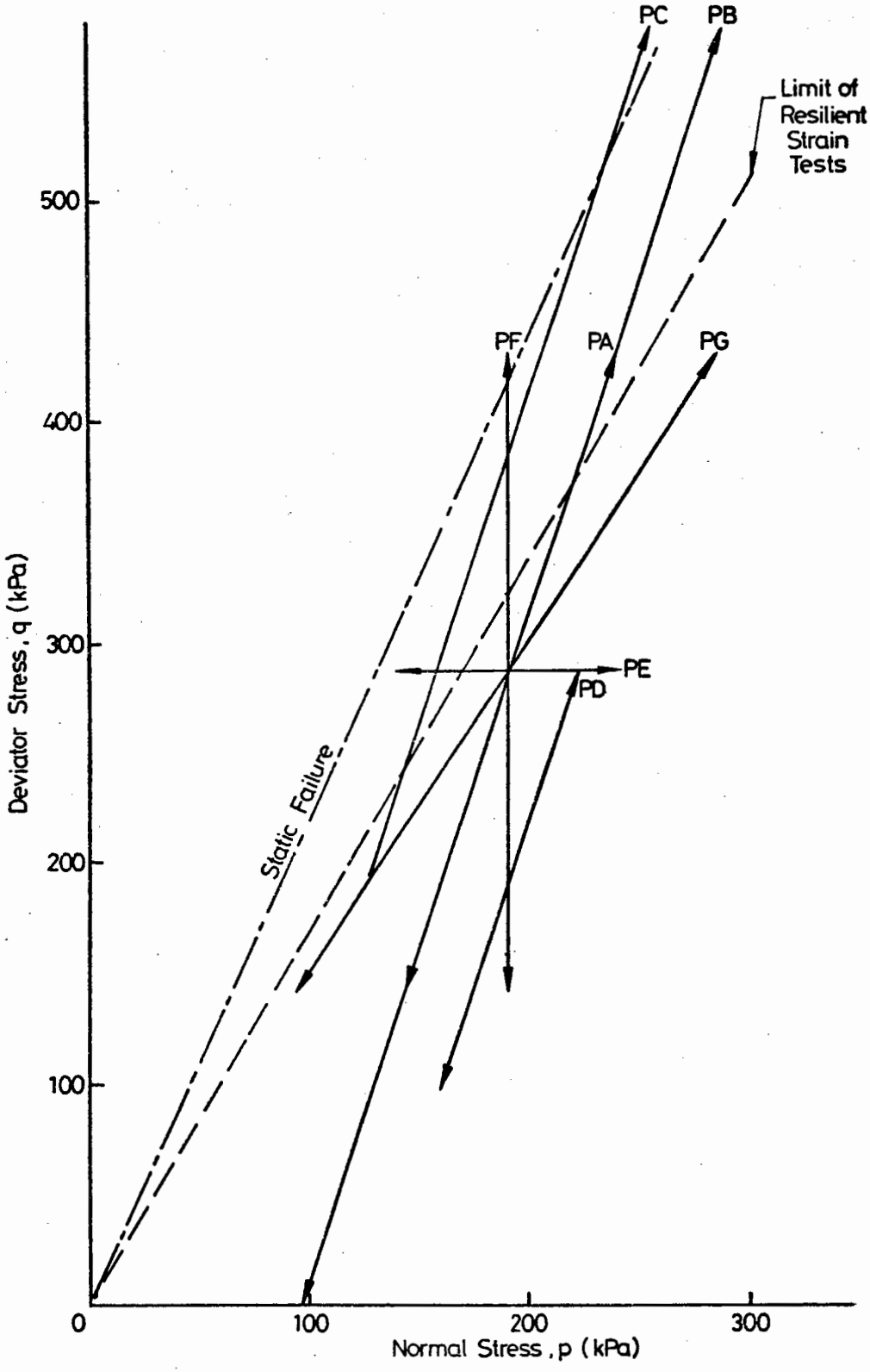

FIG. 3.47 STRESS PATHS TO INVESTIGATE PERMANENT STRAIN BEHAVIOUR (PAPPIN 1979)

FIG. 3.48 RELATIONSHIP OF STRAIN RATE/LENGTH WITH DISTANCE A FOR GRADED MATERIAL

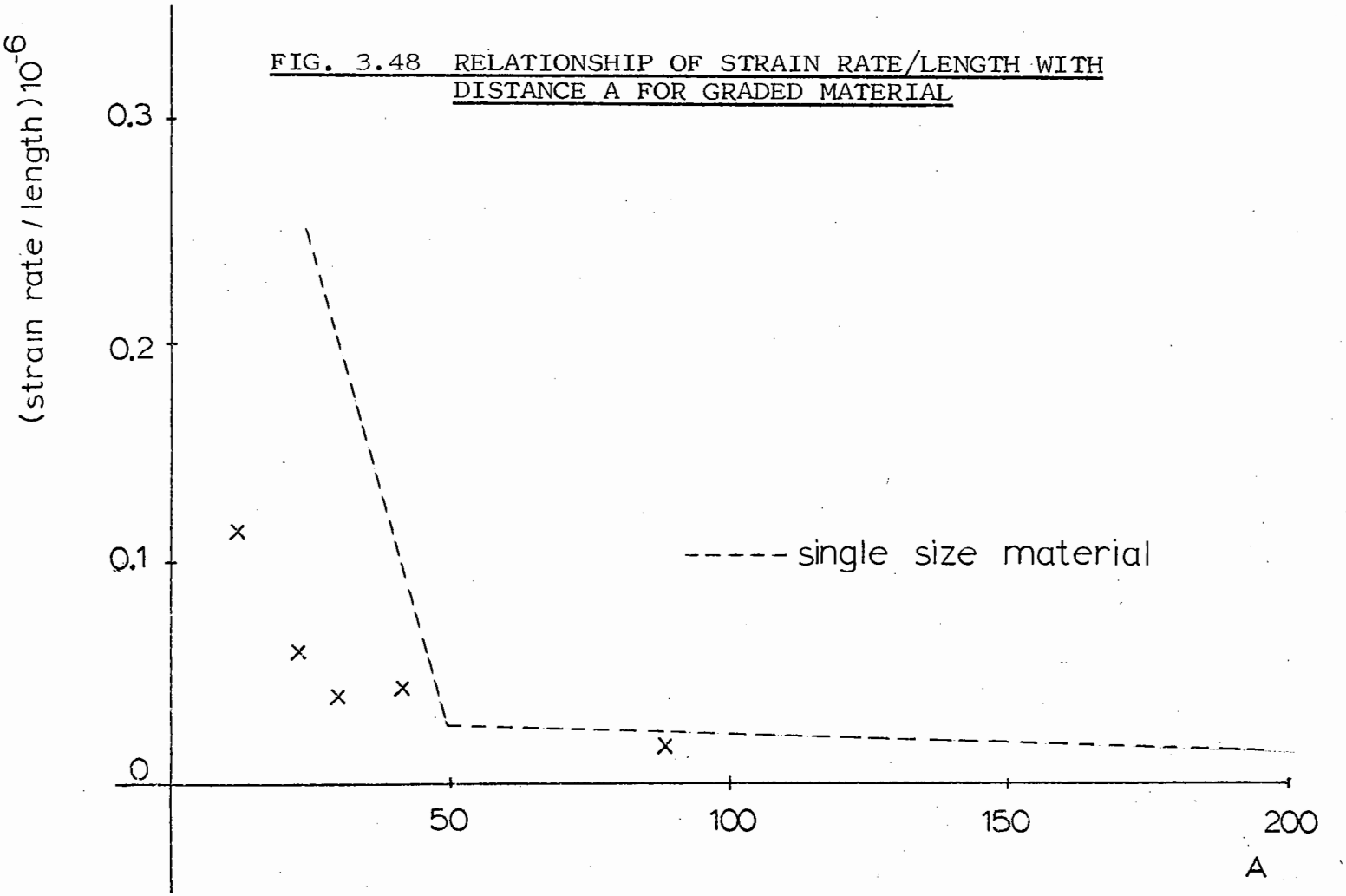

are shown in Figs 3.49 and 3.50. Full results for all the test paths are presented in Appendix 3D.

Resilient strains were fairly uniform and reached a steady value after about 200 cycles. This was typical for paths outside the threshold value described in Section 3.7. For paths near to, or inside the threshold, it was found that resilient strains showed significant scatter and tended not to stabilise. Typical results for a path inside the threshold (QC) are shown in Figs 3.51 and 3.52.

Pappin (1979), testing a well graded material, observed that where large permanent strains occurred, resilient strains required more cycles to reach a steady value. The resilient response, however, still stabilised even for specimens which failed. This may be related to the lack of a distinct threshold value (Fig. 3.48) as was identified for the single size material.

3.9 EFFECT OF PERMANENT STRAINING ON OTHER MATERIAL PROPERTIES

Several of the test specimens were subjected to monotonic failure tests after the investigation of their permanent strain behaviour was completed. Fig. 3.53 shows a typical failure plot. Superimposed is the result obtained from the monotonic tests described in Section 3.3. Generally, the specimens showed an initial stiffened response but failure results were similar to those obtained in Section 3.3.

Raymond and Williams (1978) conducted repeated load triaxial tests on dolomite ballast and found that stiffening of the ballast occurred under repeated loading. This agreed with field observations in which traffic loading caused an increase in track stiffness and strength.

The results obtained for the 3 mm material would suggest that permanent straining has little effect on the static failure strength.

FIG. 3.49

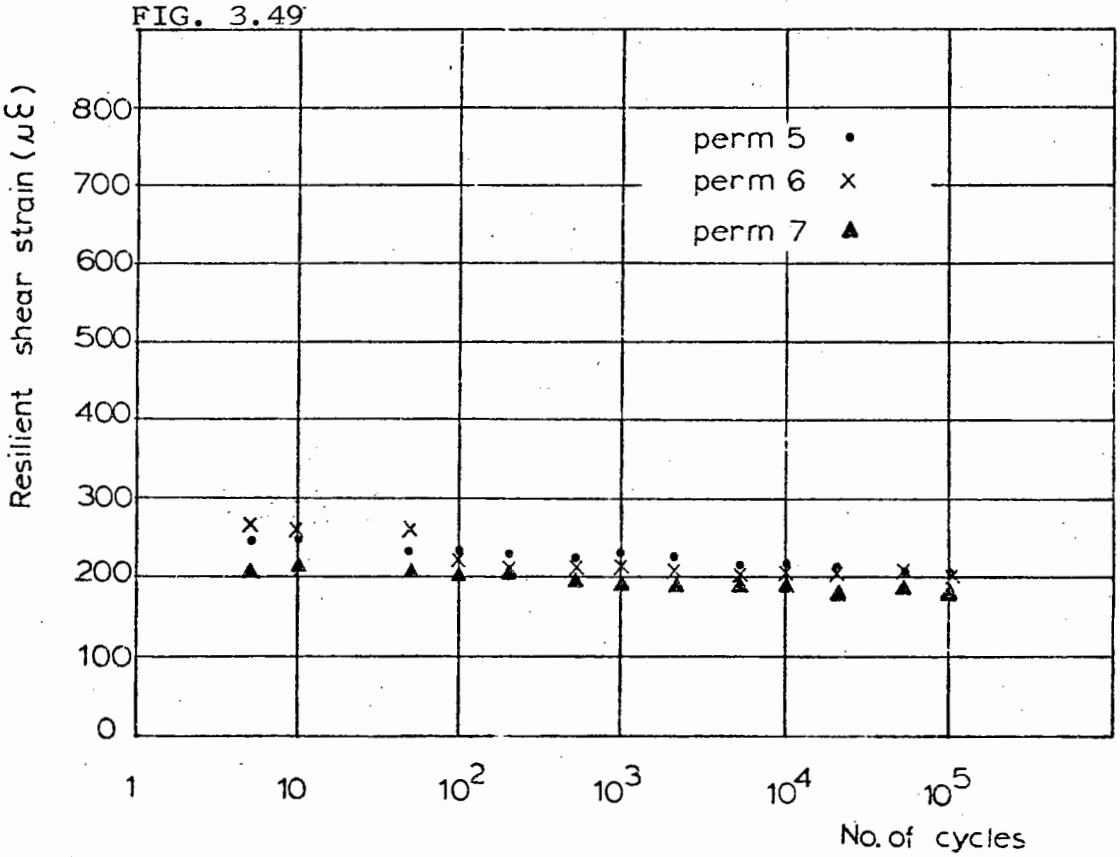

TYPICAL RESILIENT SHEAR STRAIN RESPONSE DURING PERMANENT STRAIN TEST - PATH PA2

FIG. 3.50

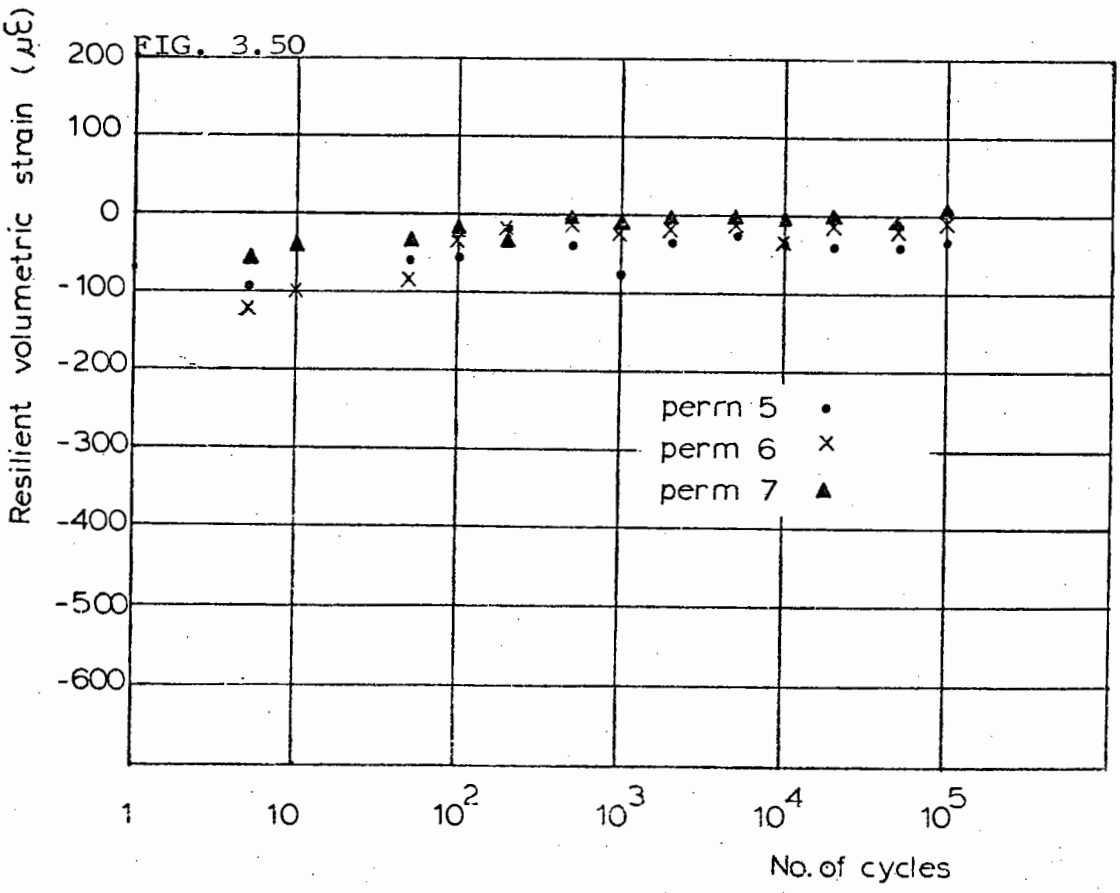

FIG. 3.51

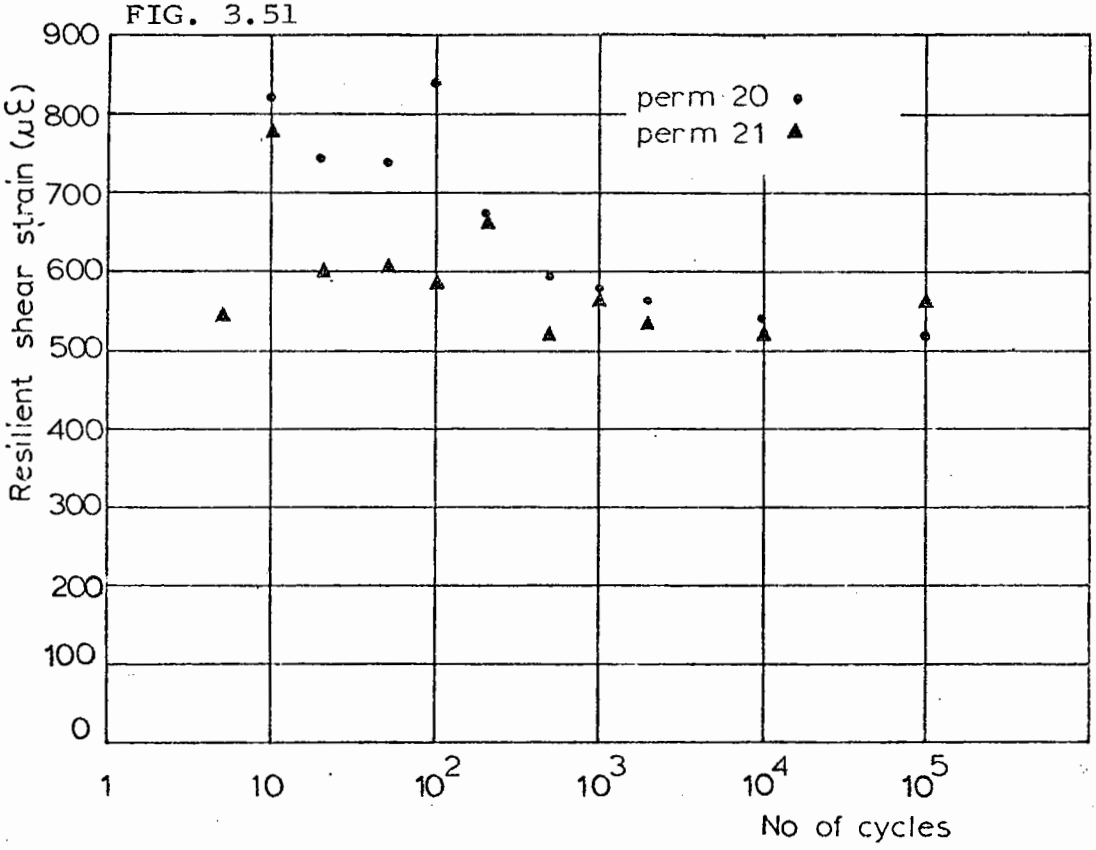

TYPICAL RESILIENT STRAIN RESPONSE DURING PERMANENT STRAIN TEST - PATH QC

FIG. 3.52

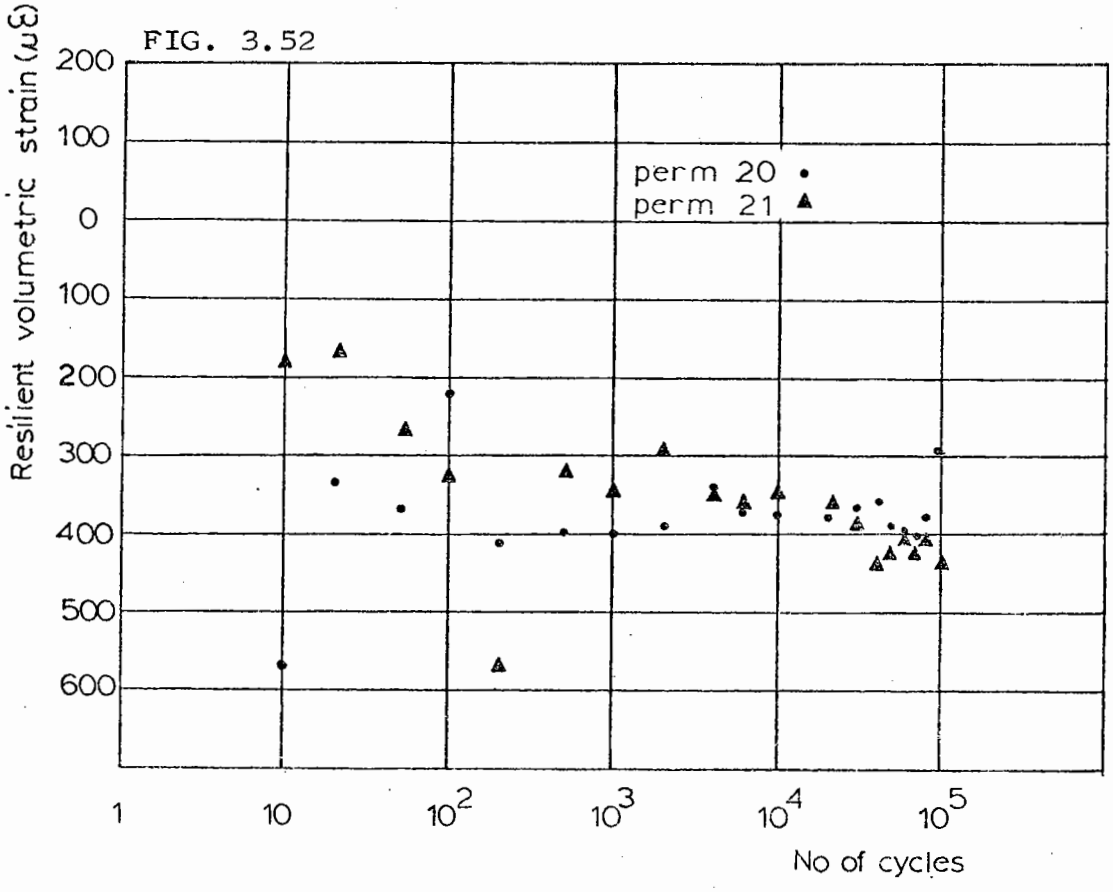

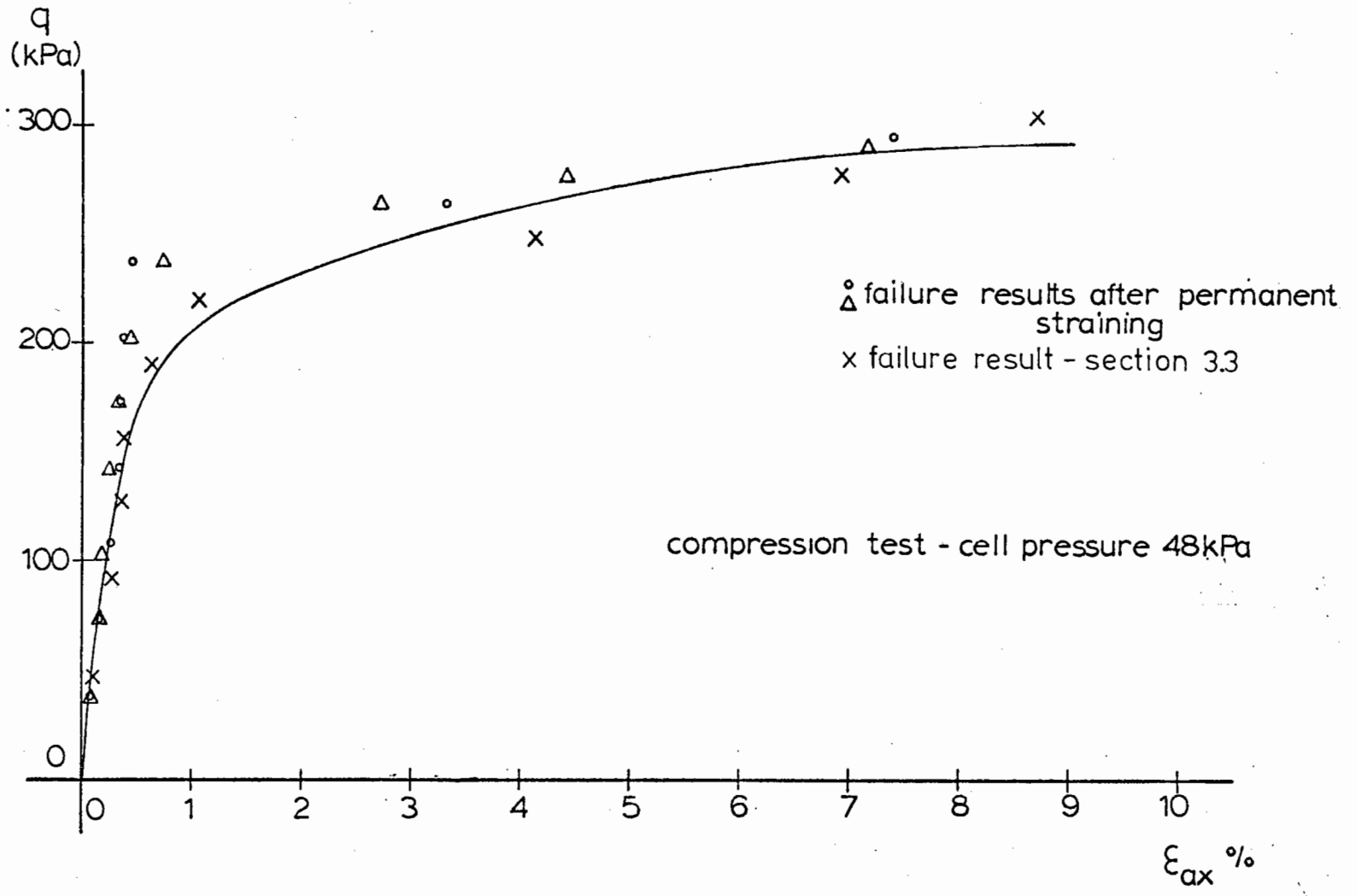

FIG. 3.53 TYPICAL MONOTONIC FAILURE RESULT AFTER PERMANENT STRAIN TEST

However, for stresses below failure, a stiffened response was observed. This would agree with the zero axial strain tests of Section 3.6. Ansell (1977) testing the same material in the simple shear apparatus found that although shear modulus increased significantly and porosity decreased throughout a test, the static shear strength of the material remained relatively unaffected.

CHAPTER FOUR

THE BIAXIAL SHEAR BOX

4.1 INTRODUCTION

A biaxial shear box capable of applying three independent principal stresses to a cubical specimen was developed by British Rail at the Technical Centre in Derby.

This chapter contains details of modifications to the apparatus and presents results from a testing programme to investigate resilient strain behaviour. The resilient contour models developed from the triaxial tests, described in Chapter 3, were applied to the biaxial stress situation. A test programme to determine permanent strain behaviour resulted in a permanent shear strain model which was also compared with that obtained in the triaxial apparatus.

4.2 THE ORIGINAL APPARATUS

The biaxial shear box was developed at the British Rail Technical Centre, Derby to study the behaviour of granular material under a three-dimensional stress system. It was intended to reproduce as closely as possible the stress conditions in railway ballast during both traffic loading and maintenance procedures.

The apparatus as designed by BR and made available for this project is shown in Fig. 4.1. The ballast specimen takes the form of a 100 mm cube retained by six rigid plane boundaries, constrained to move on three mutually perpendicular axes. Loads were applied to the sample via six air rams attached directly to the boundaries.

The four horizontal rams were mounted permanently in a rigid frame, but the two vertical rams were removable to allow access to the specimen. The weight of the vertical rams and specimen boundaries was

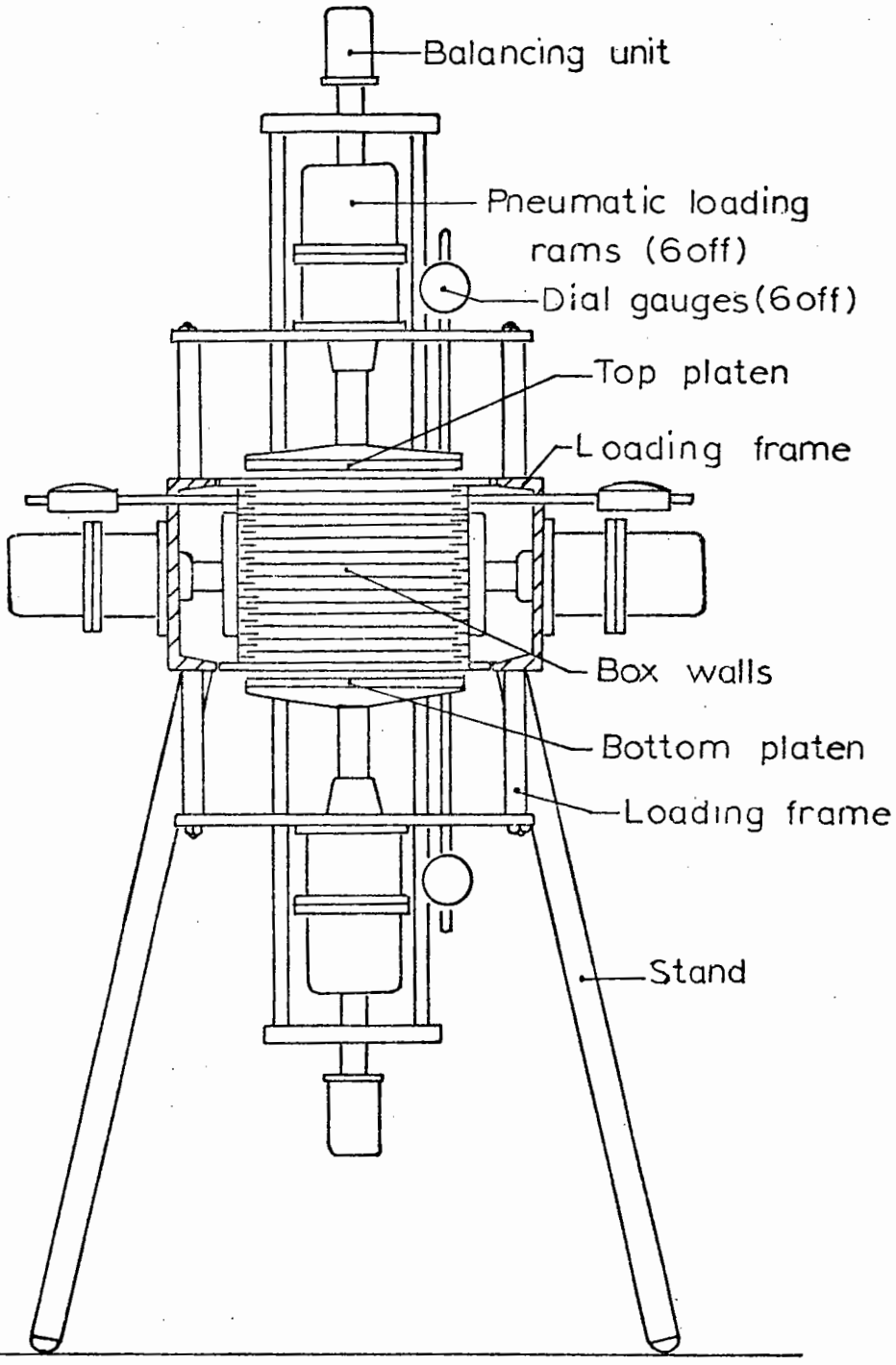

FIG. 4.1 THE ORIGINAL APPARATUS

counterbalanced by auxiliary actuators thrusting against the horizontal mounting frame. The vertical specimen boundaries consisted of a stack of plates interleaved at the corners to allow relatively large deformations to take place (see Plate 4A). The horizontal specimen boundaries were set up with limited initial clearance from the vertical boundaries, allowing only relatively small deformations to take place in the vertical direction. The apparatus is thus regarded as a biaxial shear box rather than a true triaxial machine. In order to minimise friction between the ballast and the specimen boundaries, polished stainless steel plates were fixed to the walls leaving only sufficient of the interleaving exposed to allow about 12% compressive strain in the horizontal directions. Steel rollers placed in the corners of the box prevented particles getting trapped in the exposed interleaved sections. Deformations of the boundaries were measured using dial gauges.

The test specimens were prepared by compacting the material in four layers, each layer receiving twenty blows from a small drop hammer. The specimen was made by locking the vertical boundaries and raising the lower horizontal boundary to give approximately 1 mm clearance below the lower edge of the vertical boundaries. The specimen was then compacted until 1 mm proud of the upper edge of the vertical boundaries. The upper horizontal boundary was then placed in position, the required initial horizontal stresses applied and the boundaries released.

4.3 MODIFICATIONS TO APPARATUS

4.3.1 Replacement of Dial Gauges

Deformations under repeated loading could not be monitored accurately using dial gauges and these were replaced by ±12 mm linear variable differential transformers (LVDTs).

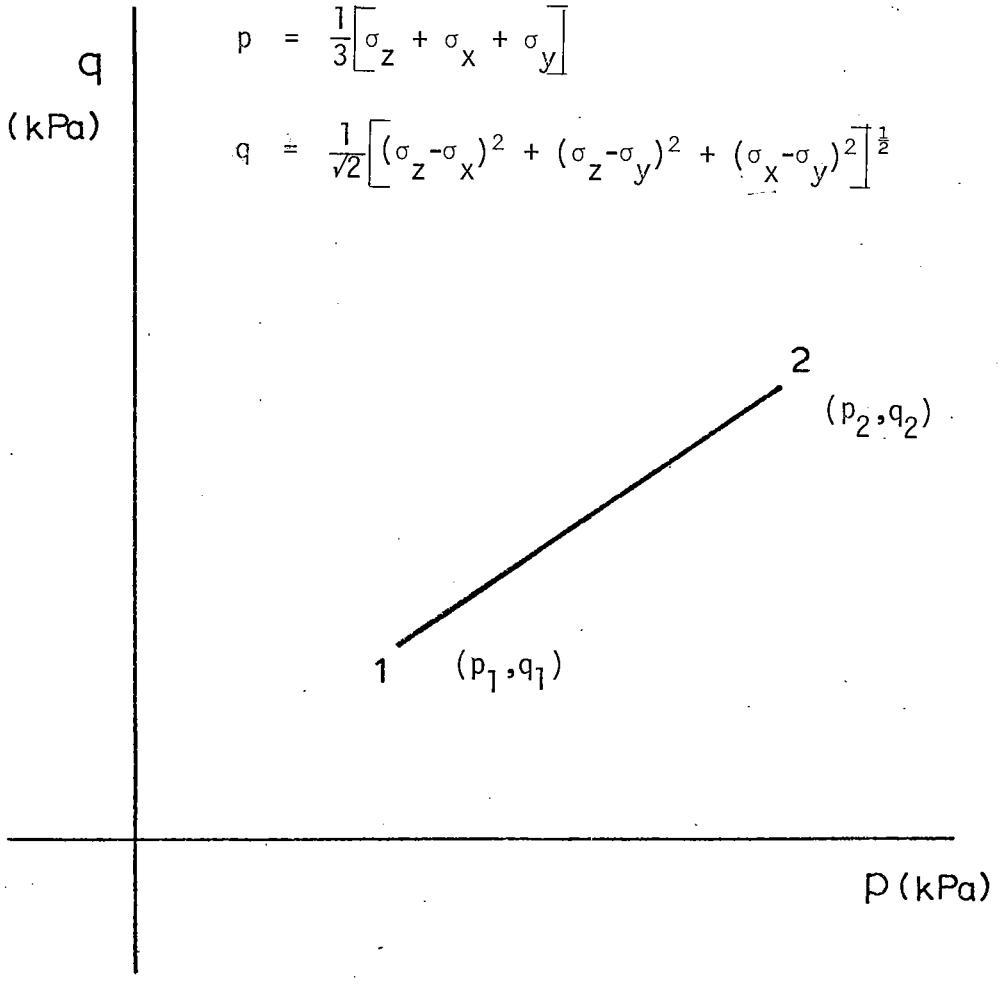

FIG. 5.2 GENERAL STRESS PATH

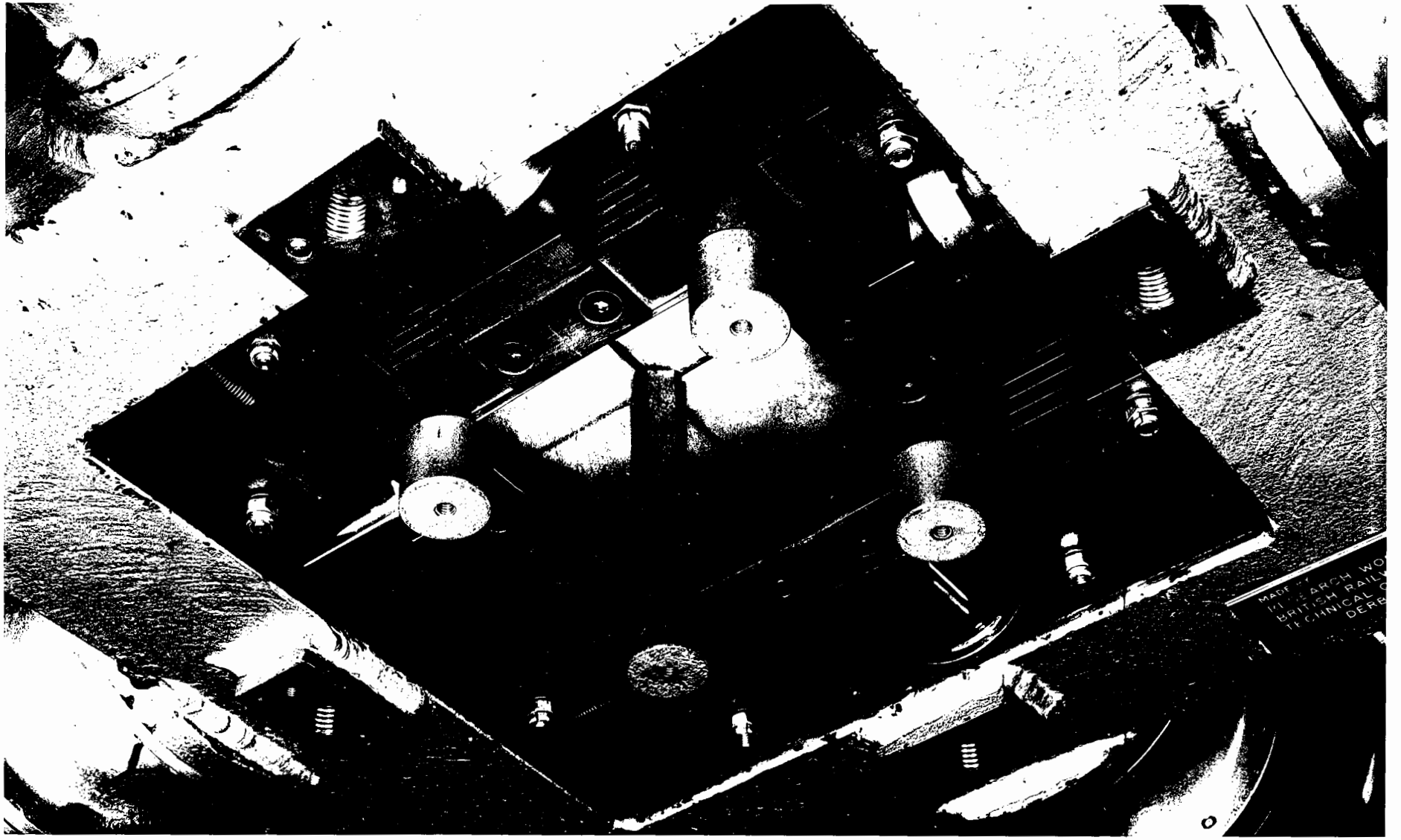

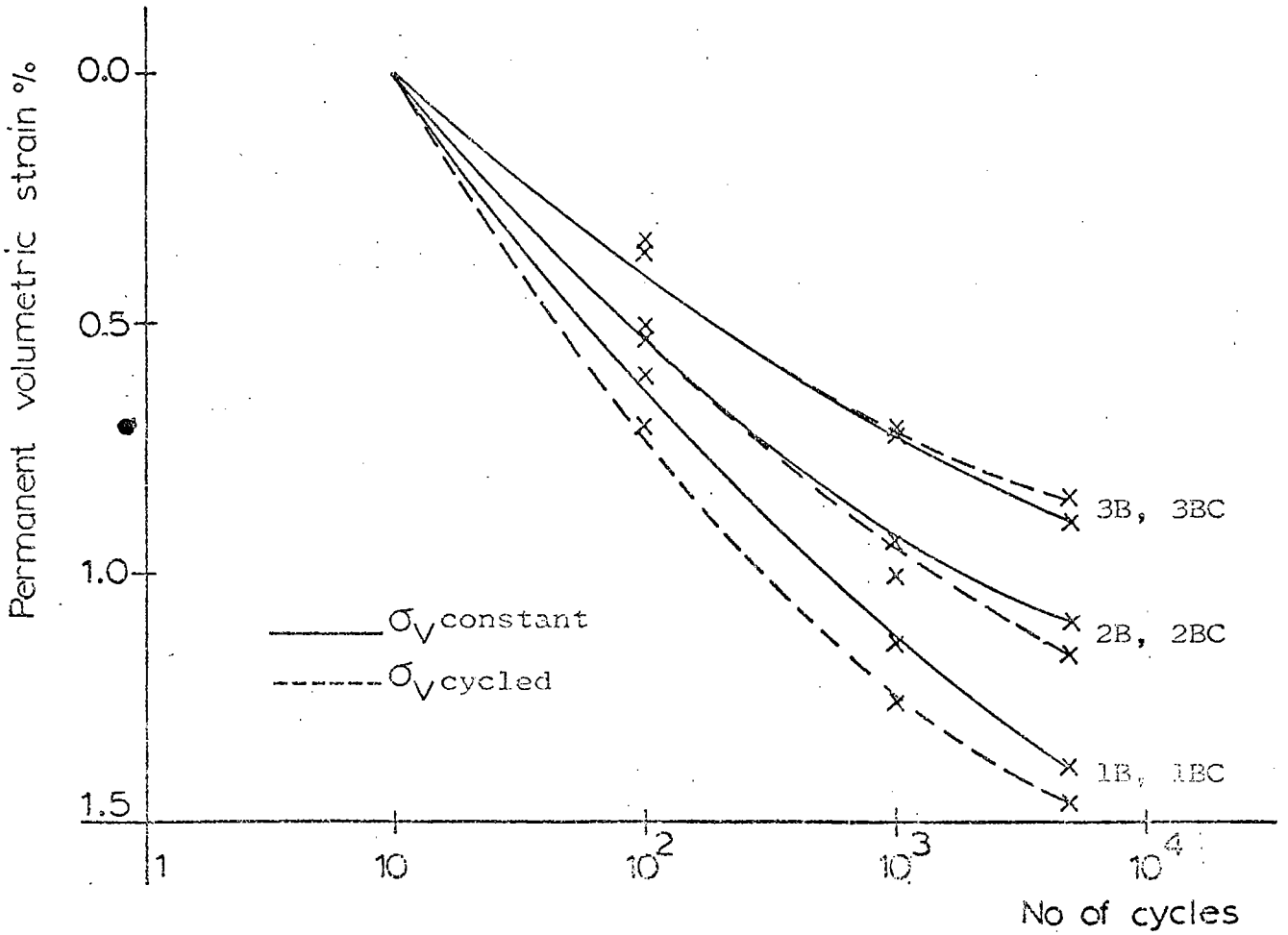

FIG. 6.48 COMPARISONS OF PERMANENT VOLUMETRIC STRAIN FOR BIDIRECTIONAL TEST SERIES ON 1.5 mm MATERIAL

4.3.2 Removal of Vertical Loading Rams

The restricted movement of the sample in the vertical direction limited the triaxial applications of the apparatus and it was decided to replace the existing top and bottom loading rams with a fixed boundary containing a load cell. This modification imposed plane strain in the vertical direction.

4.3.3 Development of Load Cell for Horizontal Boundaries

The mode of deformation of the specimen is shown in Fig. 4.2. It was felt that there would be stress concentrations in the corners of the specimen and it was therefore necessary to develop a load cell to measure normal stress over the central portion of the specimen only. A circular load cell was designed as shown in Fig. 4.3. The loading face was 60 mm diameter and the load was transmitted to four pillars of minimum section 3 x 1 mm thick. The load cell was machined from aluminium HE 15W. The load cells were designed for a working stress of 300 kPa and gave a maximum deflection of 0.001 mm under full load.

Since the load cells did not form a complete boundary to the specimen, it was necessary to calibrate them against the material under test. The problem was to find a method of calibration in which a known stress was applied to the material and, via the material, to the load cell. It was thought that the most satisfactory method would be to measure the stress at the base of a triaxial specimen (Brown 1969). A finite element analysis by Richards (1975) of a triaxial specimen, revealed that stresses near the loading platen were reasonably uniform. A calibration apparatus was designed incorporating the load cell in the base of a triaxial cell as shown in Fig. 4.4. The bottom platen was made of steel and the clearance gap around the load cell filled with silicone rubber to prevent trapping of particles. Load was applied to the specimen via a proving ring and loading ram.

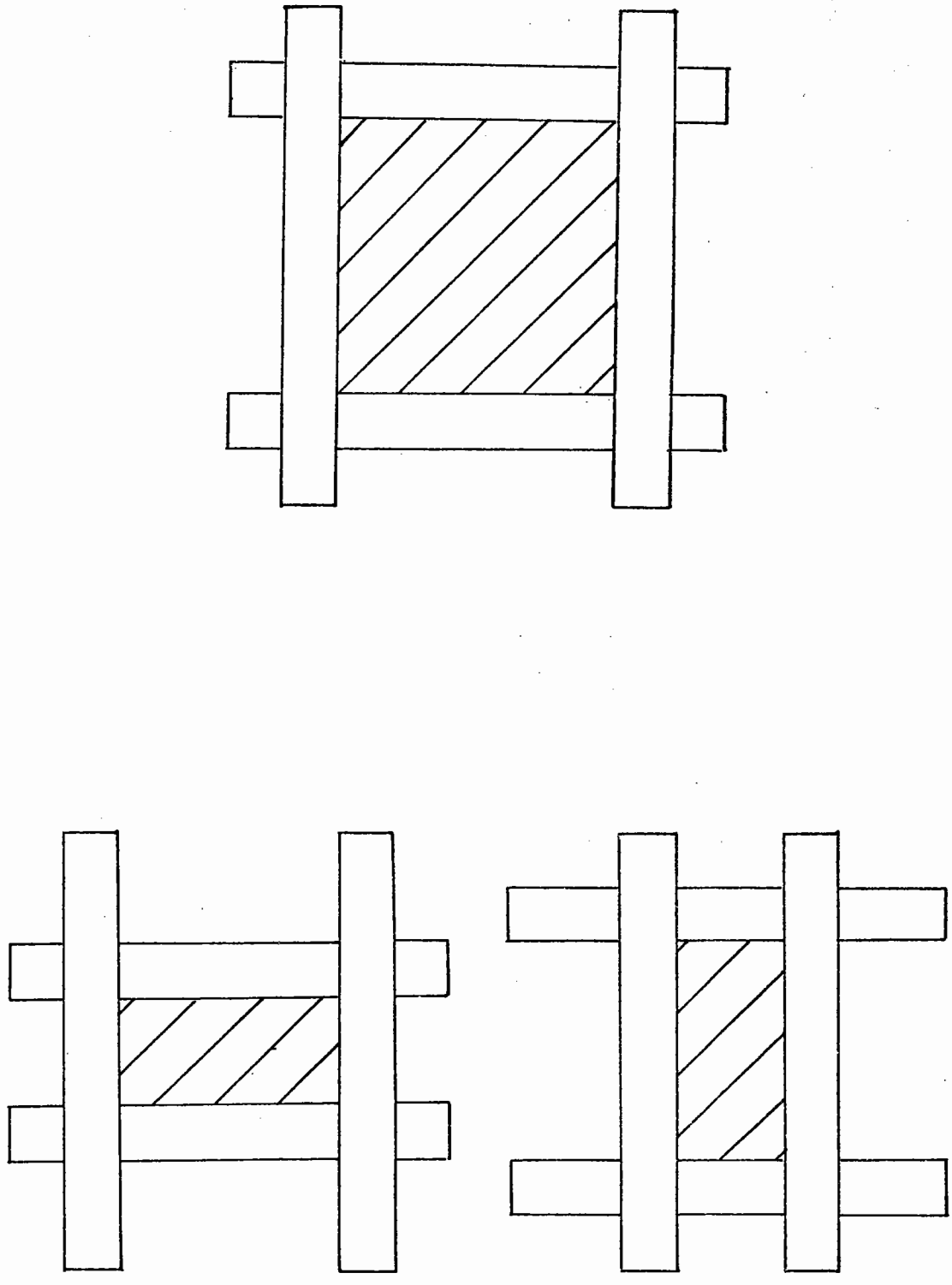

FIG. 4.2 MODE OF DEFORMATION IN THE BIAXIAL SHEAR BOX

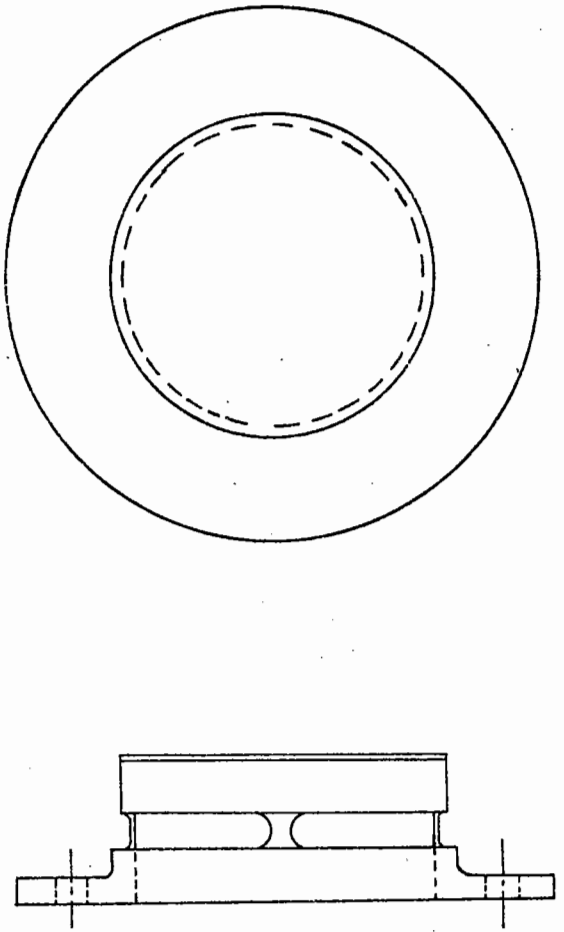

FIG. 4.3 LOAD CELL DESIGN NO. 1

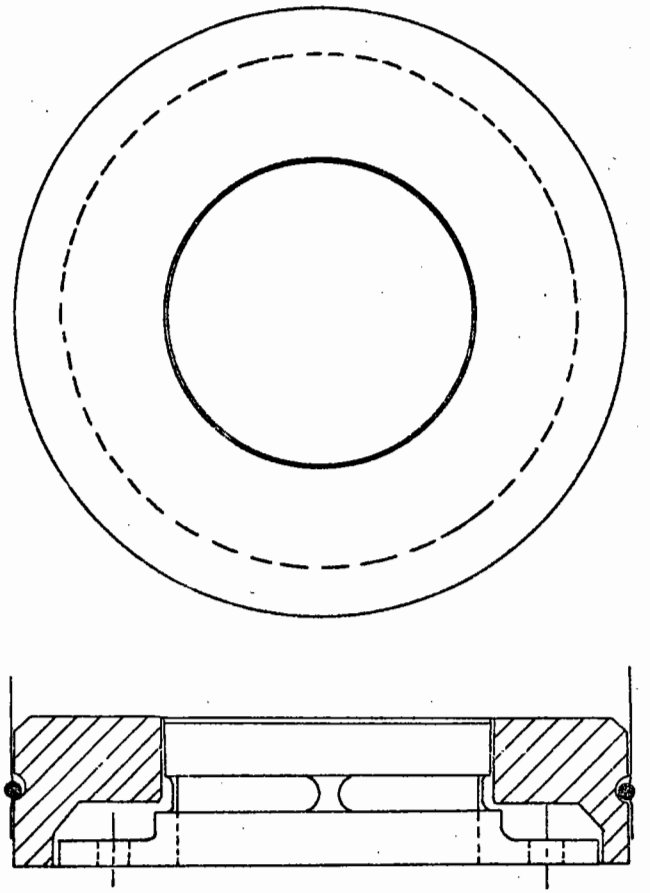

FIG. 4.4 LOAD CELL INCORPORATED IN BASE OF TRIAXIAL CELL

The specimen was compacted by vibration to the same density as required for testing, i.e. 1.62 Mg/m^3. Before calibration commenced, the specimen was stressed a number of times to overcome any initial seating problems. Various loads were then applied to the specimen at different cell pressures and the load cell output monitored. Different calibration curves were obtained for different constant cell pressures. Some difficulty was also encountered with repeatability. Calibrations of load cells for use in the simple shear apparatus produced even greater problems (Chapter 6) and it was generally decided that a load cell covering the entire area of the sample would have to be developed.

A load cell was designed as shown in Fig. 4.5. The loading face was 170 mm diameter and initially the sample acted over the shaded area. The load cell was machined from aluminium alloy HE 15W. Allowance was made for a 10 mm increase in sample dimensions in both directions. The loading face transmitted the load to a compression cylinder of 160 mm diameter and 1 mm wall thickness. The load cell was designed for a working stress of 500 kPa giving 0.001 mm deflection under full load. This corresponded to a maximum specimen strain in the vertical direction of 20 $\mu\varepsilon$. This was thought insufficient to violate the plane strain condition of the test. The cylinder was strain gauged with 350 Ω Technimeasure FLE-1-350 strain gauges. Using the load cells as the complete horizontal boundaries, meant that a calibration against the material was not required. The face of the load cell in contact with the aggregate was covered with a 1 mm thick stainless steel plate to reduce friction and prevent degradation of the aluminium cap. However, seating problems were encountered with this design and after several attempts to modify its shape, it was abandoned.

Attention was then given to the load rams used in the triaxial testing apparatus. These were basically steel rods attached to the top

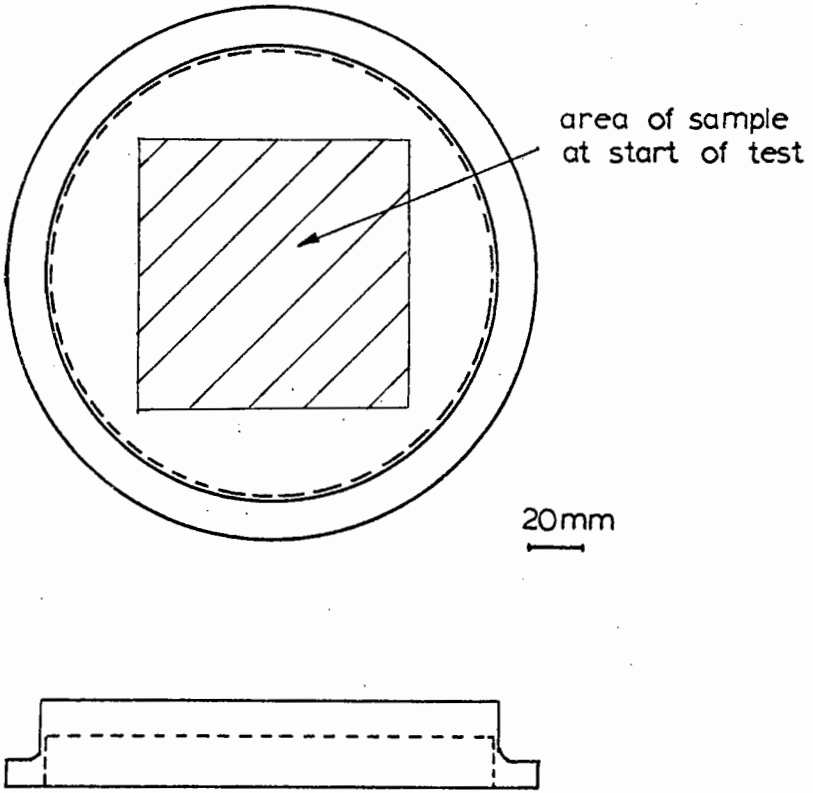

FIG. 4.5 LOAD CELL DESIGN NO. 2

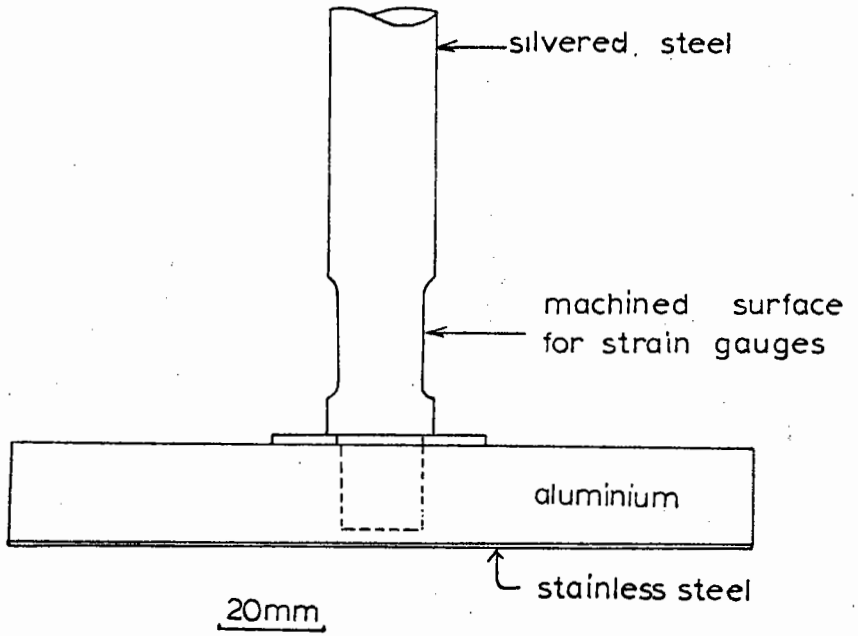

FIG. 4.6 LOAD CELL DESIGN NO. 3

platen of the cell as shown in Fig. 4.6. Boyce (1976) and Pappin (1979) found these to be satisfactory and sufficiently non-sensitive to eccentric loading and it was decided to design something similar for use in the biaxial shear box.

The load cell was designed for a working stress of 500 kPa giving 0.001 mm deflection under full load. Maximum specimen strain in the vertical direction was then 20 $\mu\varepsilon$ as before. Clamps were designed to hold the load cell in position as shown in Fig. 4.7. As previously, the face of the load cell in contact with the aggregate was covered with a 1 mm thick stainless steel plate to reduce friction and prevent degradation of the aluminium platen.

4.3.4 The Pneumatic Control System

The control system designed by British Rail could apply repeated loading to any of the three axes. However, a serious limitation was that the same magnitude of stress had to be used if repeated loading was required in more than one direction. Following the removal of the top and bottom loading rams and their replacement by fixed boundary load cells, it was decided to operate the biaxial shear box using the pneumatic controls already existing for the simple shear apparatus (Chapter 6, Section 6A.4).

A measure of the load applied by each ram was obtained by monitoring the air pressure using conventional pressure gauges. These were not very accurate and a pressure transducer was placed in the air line adjacent to each loading ram. This gave a much more accurate measurement of air pressure and enabled the electrical outputs to be recorded permanently on a U.V. recorder.

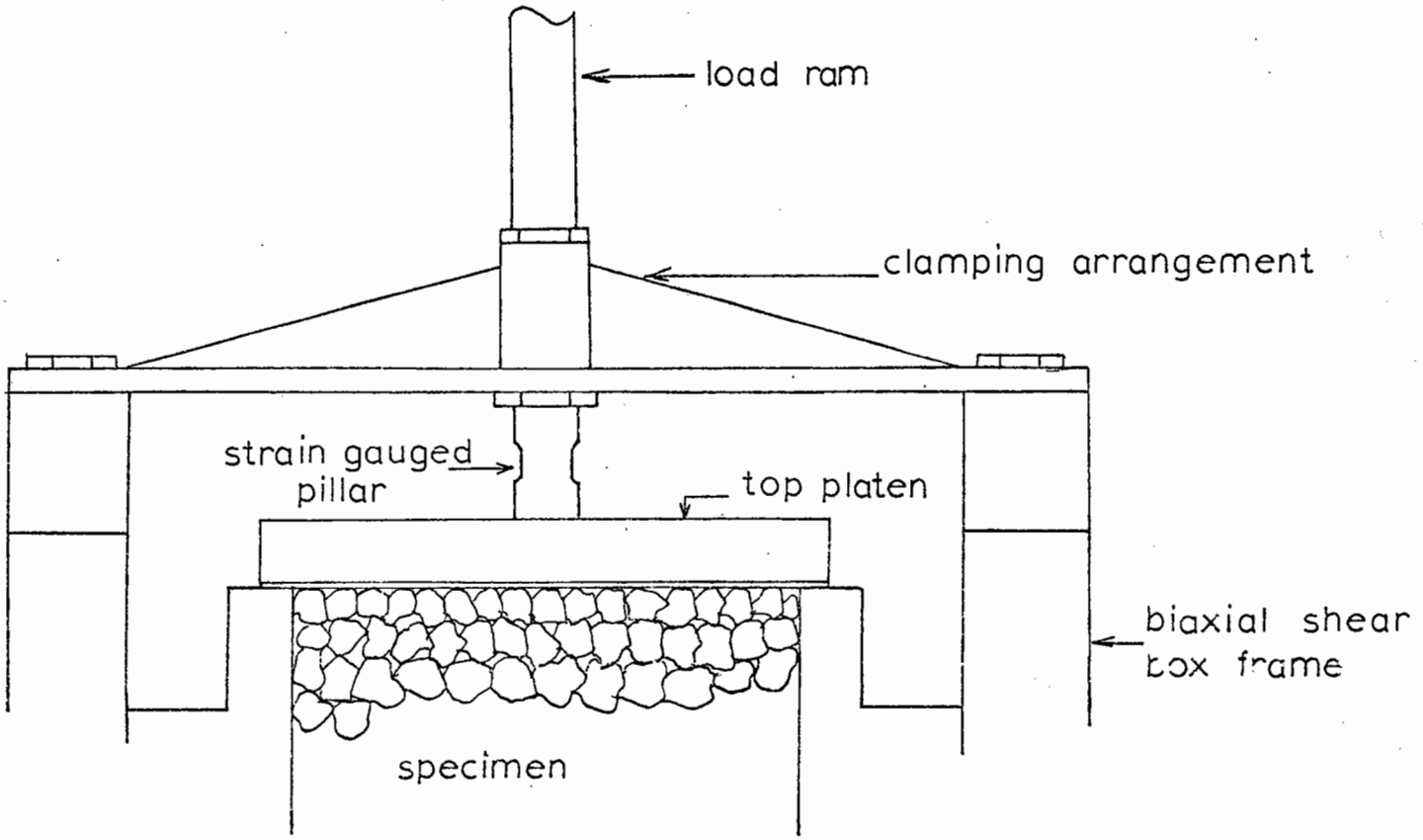

FIG. 4.7 CLAMPING ARRANGEMENT FOR BIAXIAL LOAD CELL

4.3.5 Data Monitoring

Following modifications, the biaxial shear box had 10 output signals. These were monitored using the system existing for the simple shear apparatus. Permanent records of all the signals could be obtained using a U.V. recorder.

4.4 MATERIAL AND SPECIMEN PREPARATION

The material was as used for the triaxial test series (Chapter 3). The test specimens were prepared by compacting the material in four layers, each layer receiving 10 blows from a small drop hammer acting through a metal plate. The specimen was made by locking the vertical boundaries, and compacting the material until 1 mm proud of the upper edge of the vertical boundaries. The upper horizontal boundary was then placed in position and the vertical boundaries released. The top platen was then bolted down, the vertical boundaries moving automatically to accommodate any specimen deformation. By monitoring the load cell and LVDT outputs the initial stress state and dimensions of the specimen could be obtained. The above procedure produced the required average density of 1.62 Mg/m^3.

4.5 MONOTONIC FAILURE TESTING

Monotonic tests to failure were conducted using the stress conditions shown in Table 4.1. Generally, failure did not occur until one of the stresses approached zero. This was thought to be caused by specimen interlock due to the angularity of the particles. The estimated failure points were plotted on a p = constant plane as shown in Fig. 4.8. The triaxial compression and extension failure points are included and the Mohr-Coulomb failure criterion for a compression failure ratio q/p = 2.1 is also presented. The Mohr-Coulomb criterion

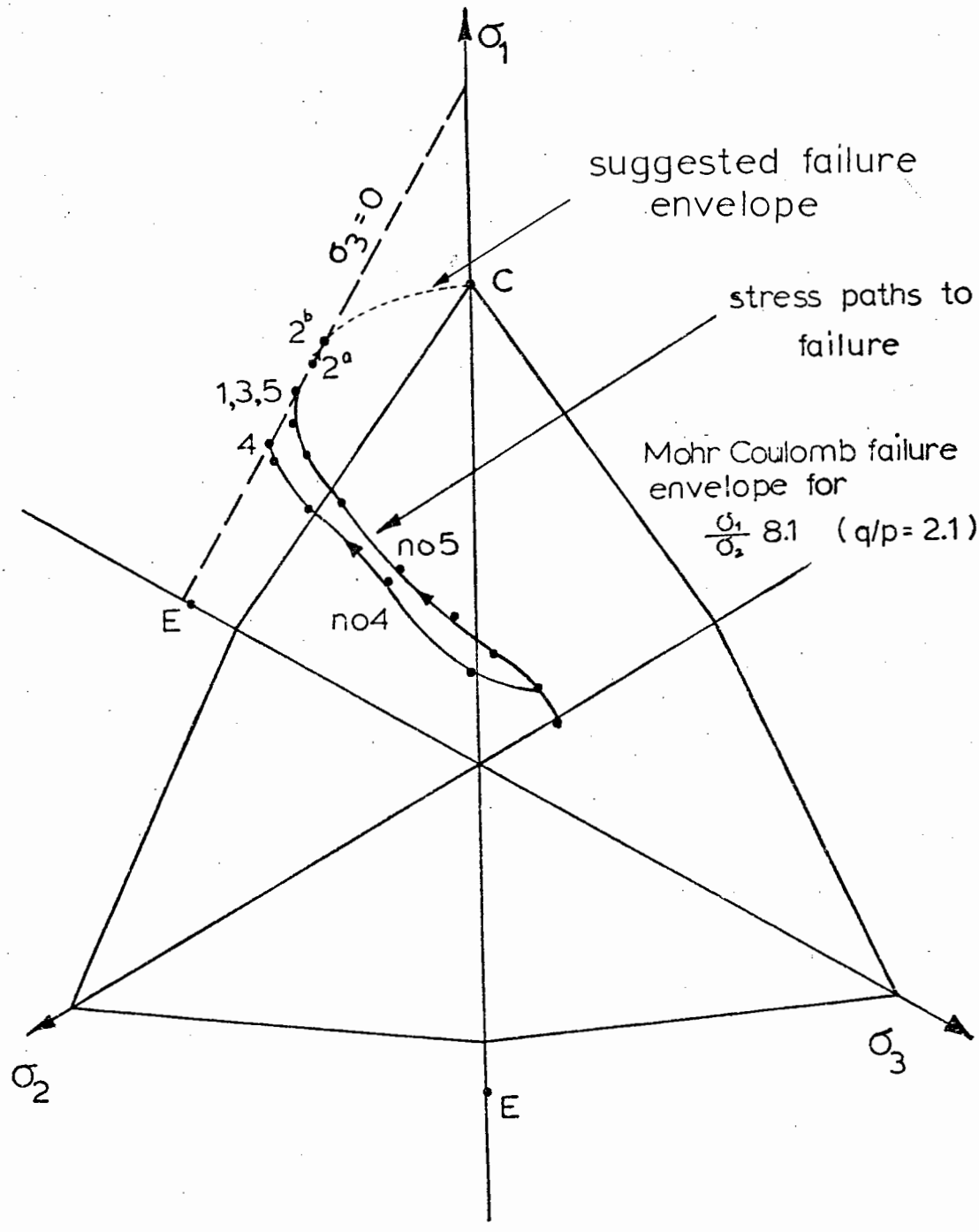

FIG. 4.8 MONOTONIC FAILURE TEST RESULTS ON A p= CONSTANT PLANE

Table 4.1

Test No.	Stress state	
	σ_x (kPa)	σ_y (kPa)
1	500	500
	σ_y reduced to failure	
2	0	0
	σ_x increased to failure	
3	356	356
	σ_y reduced to failure	
4	214	214
	σ_y reduced to failure	
5	428	428
	σ_y reduced to failure	

was found to be conservative for all results from the biaxial shear box as it was for triaxial extension (Section 3.3).

The biaxial shear box failure points were on a $\sigma_3 = 0$ line which also coincided with the triaxial extension failure result. Test No. 2 was carried out with initial stresses zero and then increasing one of them. The resulting stress path to failure can be seen to move along the $\sigma_3 = 0$ line in Fig. 4.8 from point 2a to point 2b. Stress paths to failure are also presented for tests Nos 4 and 5. No information is available for the region from 2b to c on Fig. 4.8, but combining biaxial and triaxial failure results would suggest a failure envelope as shown.

4.6 RESILIENT STRAIN BEHAVIOUR

4.6.1 Preliminary Repeated Load Tests

The resilient behaviour of the material over a number of cycles was observed for several preliminary repeated load stress paths. The resilient strains were found to reach a steady value after 50 to 100 cycles.

Applying several stress paths to the specimens at different stages of testing produced similar results. It was, therefore, decided that a test programme to investigate the resilient behaviour of the material, similar in principle to that used on the triaxial apparatus, was feasible. Before commencing resilient testing it was decided to apply 300 cycles of stress to each specimen, thus enabling the specimen to reach a steady state and hence produce reliable resilient strain measurements.

4.6.2 Full Test Programme

In the biaxial shear box two of the applied stresses are controlled and the third is measured. A testing programme using the stress paths shown in Fig. 4.9 was devised for the two applied stresses and conducted on four different specimens. It was not possible to test all the stress paths indicated, because of problems in operating the solenoid valves controlling the passage of air to the load rams.

Permanent records of the resilient strains and the stresses in the vertical direction were obtained on an ultra violet (U.V.) chart recorder. The permanent strains were recorded on two flat bed paper chart recorders. The air pressures applied to the load rams were monitored using two digital voltmeters. This gave a record of σ_x, σ_y and σ_z and the strains ε_x and ε_y on the specimen for each stress path applied. The applied stresses σ_x and σ_y and the measured stress σ_z were converted to p and q as:

$$p = \frac{1}{3}(\sigma_x + \sigma_y + \sigma_z) \tag{4.1}$$

$$q = \frac{1}{\sqrt{2}}\left[(\sigma_x-\sigma_y)^2 + (\sigma_x-\sigma_z)^2 + (\sigma_y-\sigma_z)^2\right]^{\frac{1}{2}} \tag{4.2}$$

Full test details are presented in Appendix 4A.

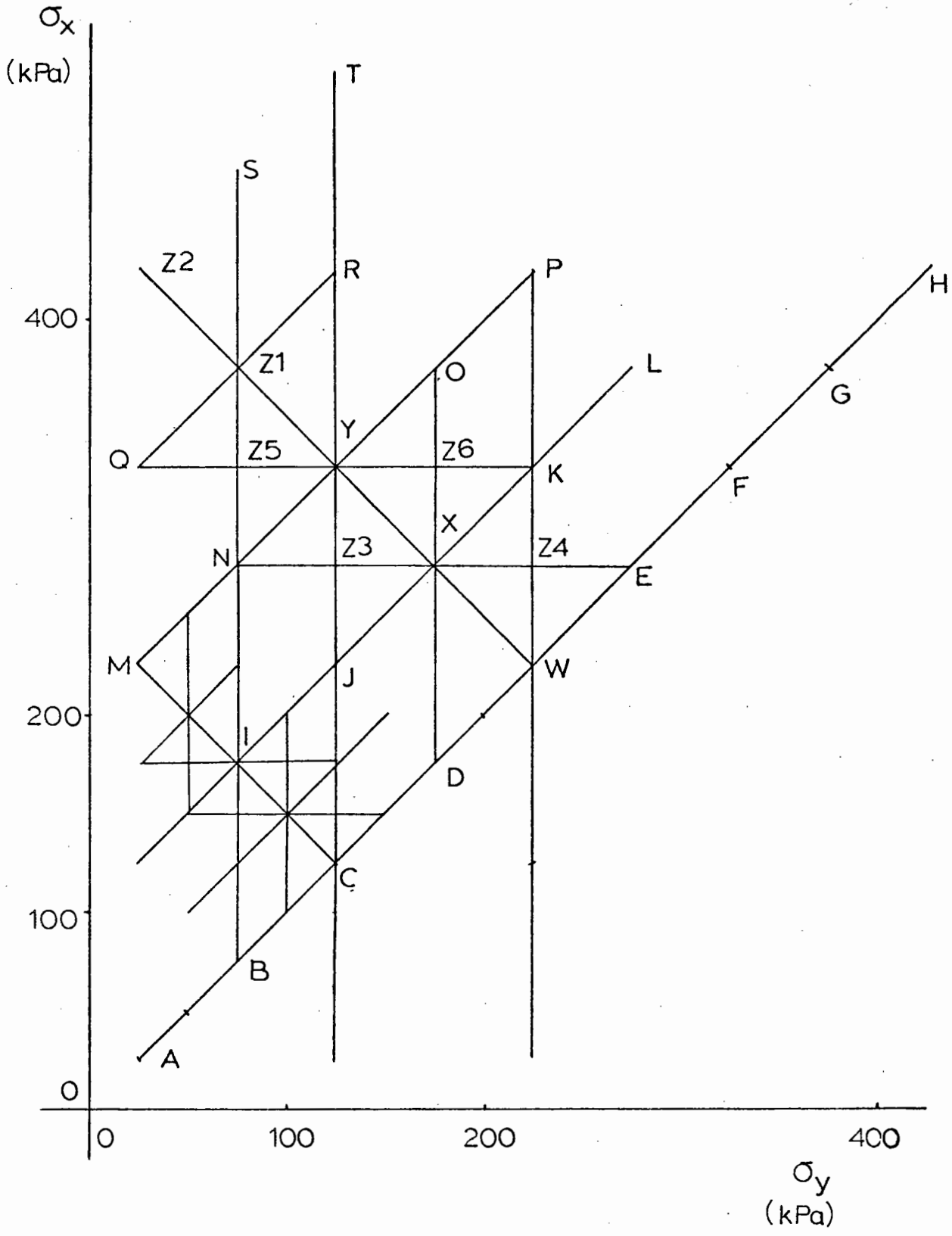

FIG. 4.9 STRESS PATHS TO INVESTIGATE RESILIENT STRAIN BEHAVIOUR

4.6.3 Shear Strain

Chapter 3 contains details of the method to predict resilient shear strain using the contours developed from repeated load triaxial testing. The method required the stress path coordinates in the X and Y directions and the angle α as shown in Fig. 4.10 (Equations 3.20 and 3.21). Assuming that zero shear strain occurred at zero shear stress and that the direction of strain coincided with that of stress, a strain path could be drawn from the zero shear stress point to each end of the stress path, i.e. 0 to 1 and 0 to 2 in Fig. 4.10.

If stress conditions were such that both ends of the stress path lay on the same plane taken radially through 0, then the resilient shear strain was either the sum or difference of the strain contour values for each end of the path. All tests in the triaxial apparatus lay on such a plane and the above method was shown to apply. In analysing results from the biaxial shear box it was found that the majority of paths did not lie on the same plane but crossed several planes, e.g. stress paths 1 to 2. As in the triaxial model, vector methods were employed and the resilient shear strain ε_r computed as:

$$\varepsilon_r = \left[\varepsilon_1^2 + \varepsilon_2^2 + 2\varepsilon_1\varepsilon_2 \cos(\alpha_2-\alpha_1)\right]^{\frac{1}{2}} \times L_c \qquad (4.3)$$

where ε_1 = shear strain contour value at point 1

ε_2 = shear strain contour value at point 2

L_c = stress path length correction.

The stress path length correction and stress ratio correction developed from the triaxial tests were also applied to the biaxial results. Predictions of resilient shear strain using the above method are plotted against experimental strains in Fig. 4.11. Comparisons are obviously not as good as for the triaxial results, but it would appear that the contour model developed for triaxial conditions can be extended, with

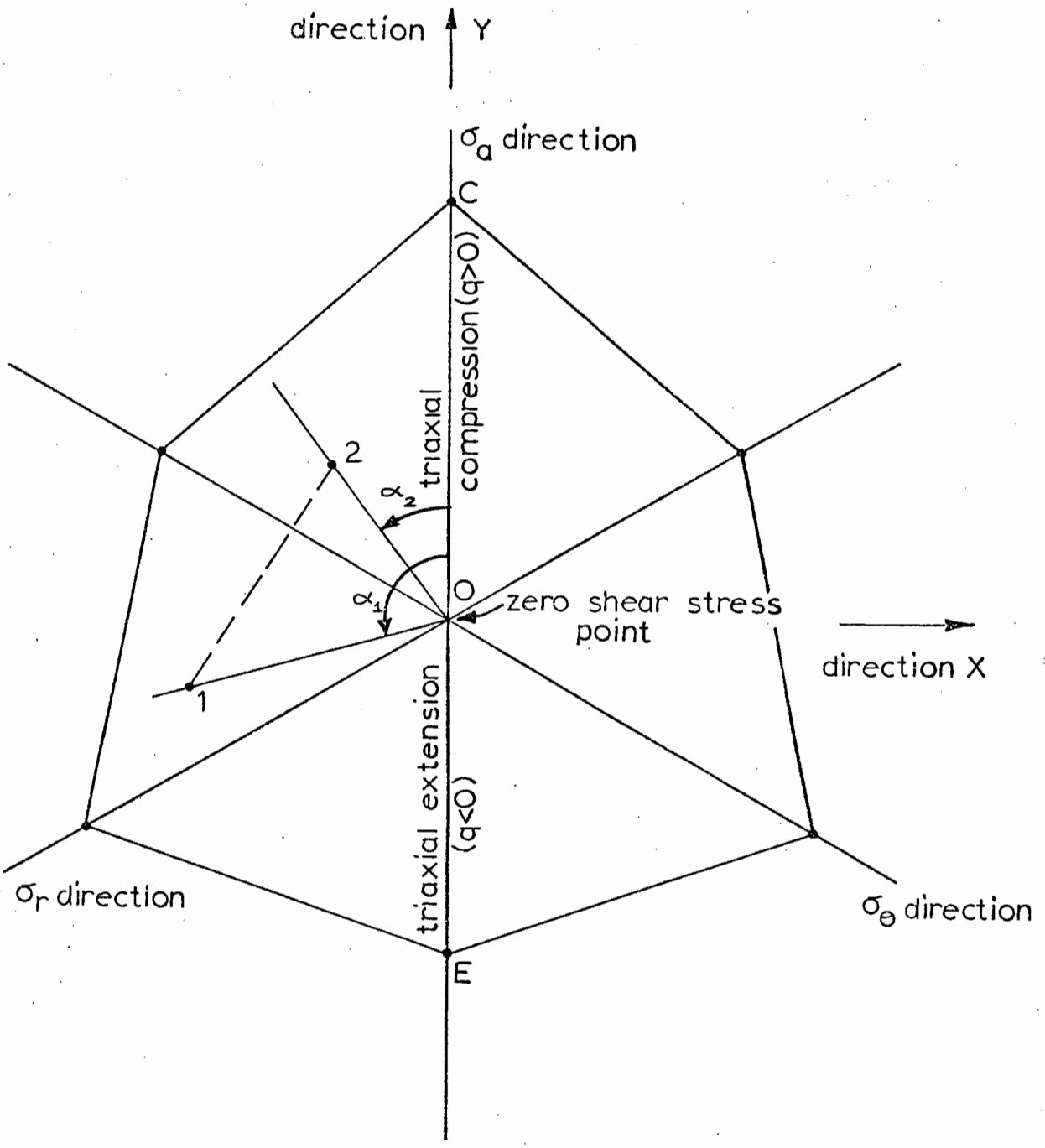

FIG. 4.10 VIEW DOWN THE SPACE DIAGONAL ONTO A p= CONSTANT PLANE

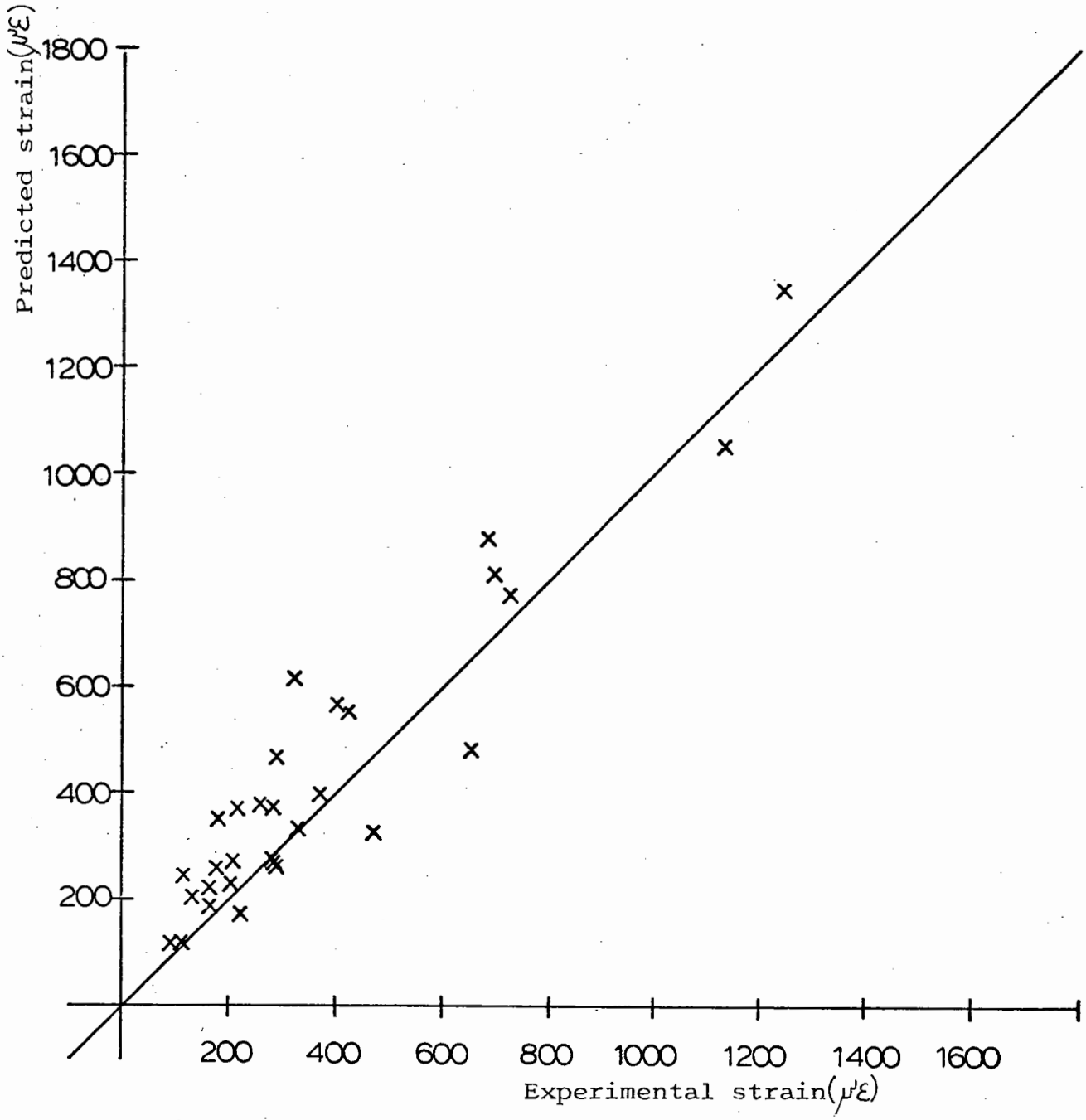

FIG. 4.11 COMPARISON OF PREDICTED AND EXPERIMENTAL RESILIENT SHEAR STRAINS

some confidence, to biaxial plane strain conditions.

4.6.4 Volumetric Strain

As for the triaxial case, volumetric strains were almost entirely dependent on changes in p so the orientation of the stress path as projected onto a p = constant plane had little effect. Resilient volumetric strain was therefore taken as being equal to the difference in contour value between each end of the stress path. Fig. 4.12 shows a plot of predicted against experimental resilient volumetric strain for the biaxial shear box results. Comparisons are not as good as those obtained for the shear strain but experimental conditions in the biaxial are less accurately controlled than in the triaxial apparatus and when this is taken into consideration, the comparisons are considered reasonable.

4.6.5 Comparison of Load Pulse

Stress application in the triaxial apparatus was in the form of a sine wave and was well controlled by means of a servo-hydraulic feedback system. In the biaxial shear box, loading was applied via air rams, which because of the compressibility of air, tended to produce a "saw-tooth" wave shape. Since the model developed under the sine wave loading has been extended to biaxial conditions and predicts strains reasonably well, the shape of the load pulse would appear to be of little importance in testing granular materials. This is encouraging, since in many situations, finance is not readily available to develop the complex apparatus necessary to produce sine waves.

4.7 PERMANENT STRAIN BEHAVIOUR

The previous section contained details of the test paths used to

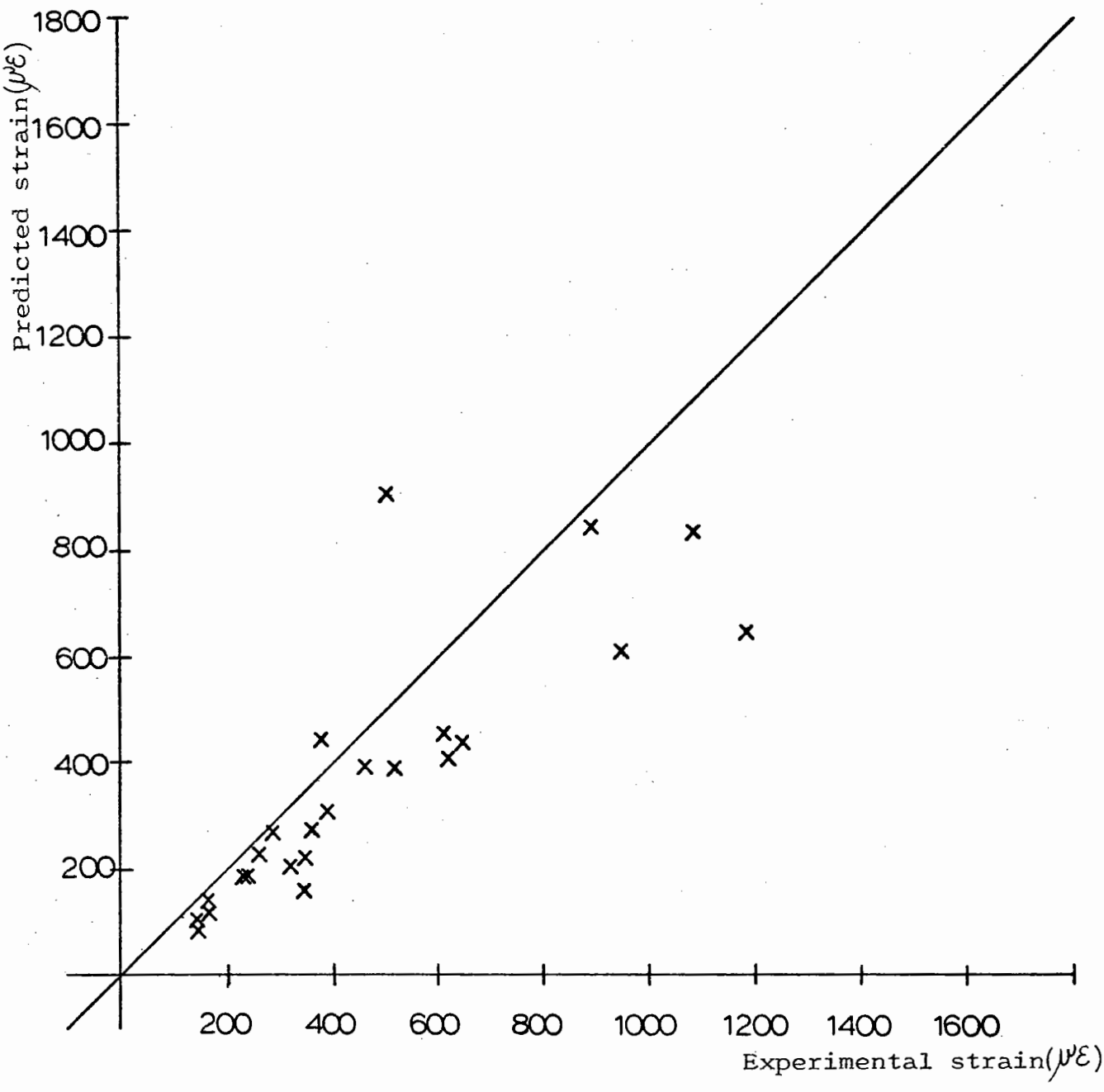

FIG. 4.12 COMPARISON OF PREDICTED AND EXPERIMENTAL RESILIENT VOLUMETRIC STRAINS

carry out a resilient test programme. Several of these paths were selected to form a testing programme to investigate the permanent strain behaviour of the material in the biaxial shear box. Fig. 4.13 shows the stress paths selected for the test programme. Three specimens were tested to 5000 cycles for each stress path. The applied stresses σ_x and σ_y and the measured stress σ_z were converted to p and q using Equations 4.1 and 4.2 and the permanent strain test paths plotted in (p,q) stress space as shown in Fig. 4.14.

4.7.1 Test Results

Typical plots of permanent shear and volumetric strains against the logarithm of the number of cycles are shown in Figs 4.15 and 4.16. Complete results are presented in Appendix 4B. As for the triaxial results, an average curve representing change in strain rate was drawn for each test path assuming zero strain at 10 cycles. These are presented in Figs 4.17 and 4.18. Volumetric and shear strains were defined as in Section 2.4. The curves were normalised by dividing by the strain rate at 100 cycles and an average shape function determined. The shape function was very similar to that for the triaxial test results.

stress path	BP2	BP3	BP4	BP6	BP8	BP9
strain rate $\times 10^{-6}$	10.0	2.5	4.33	4.17	5.67	10.7

Table 4.2

No. of cycles	10^2	10^3	5×10^3
shape function	249	484	610

Table 4.3

TEST NO.		STRESS PATH	TEST NO.		STRESS PATH
BP1	=	CF	BP6	=	LJ
BP2	=	AH	BP7	=	LR
BP3	=	UK	BP8	=	MP
BP4	=	VP	BP9	=	BD
BP5	=	JR	BP10	=	EG

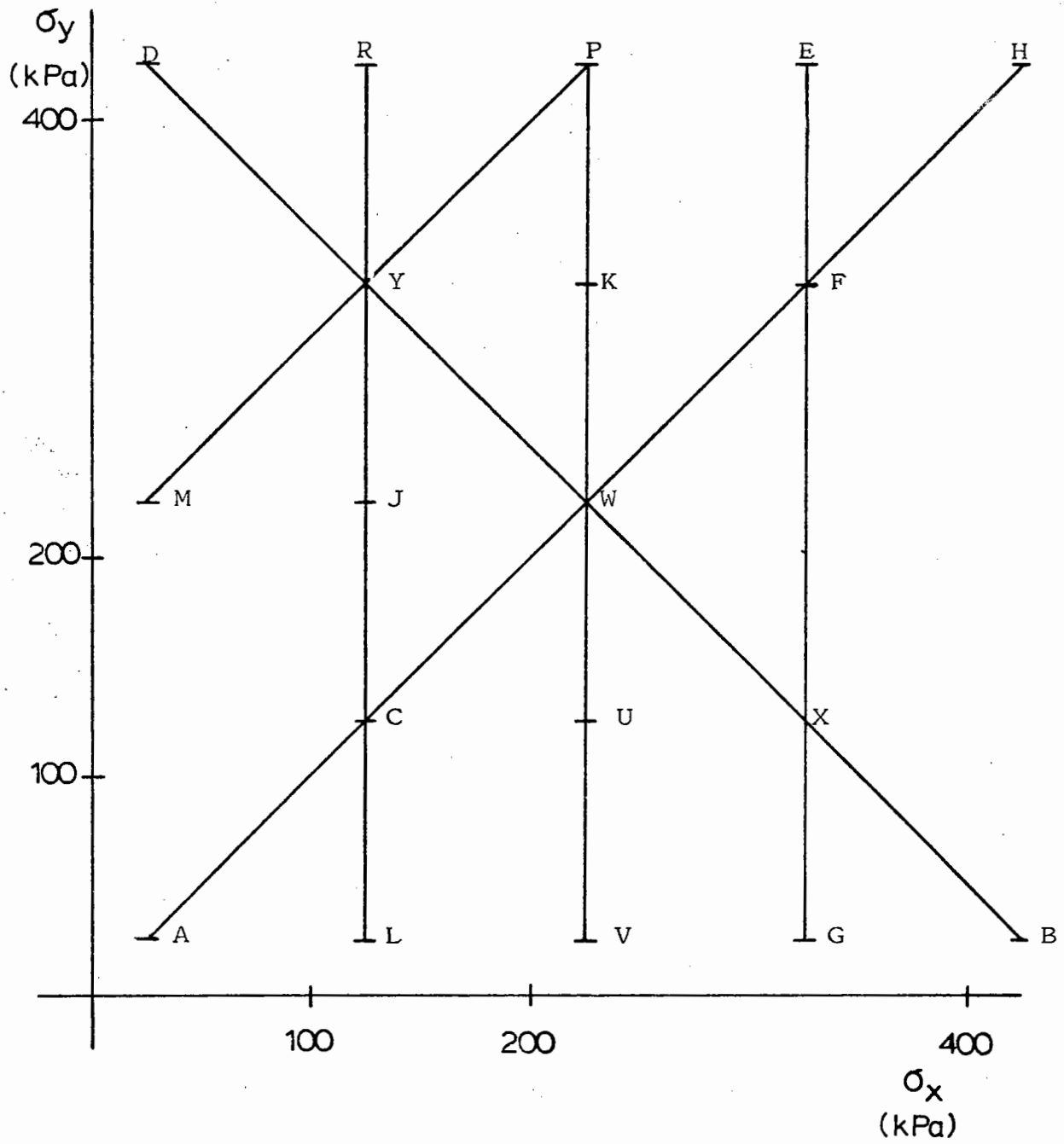

FIG. 4.13 STRESS PATHS TO INVESTIGATE PERMANENT STRAIN BEHAVIOUR

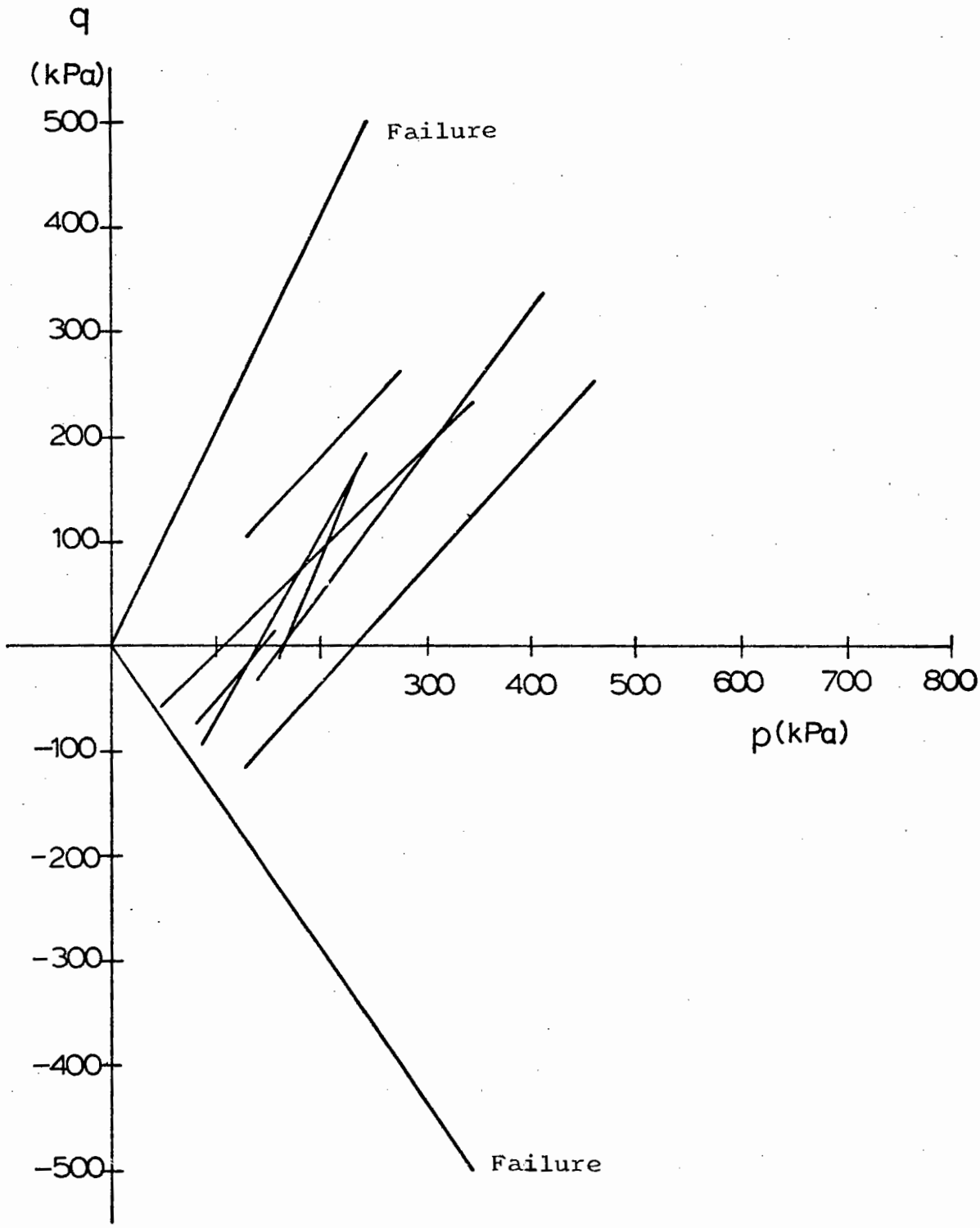

FIG. 4.14 PERMANENT STRAIN TEST PATHS IN (p,q) STRESS SPACE

FIG. 4.15

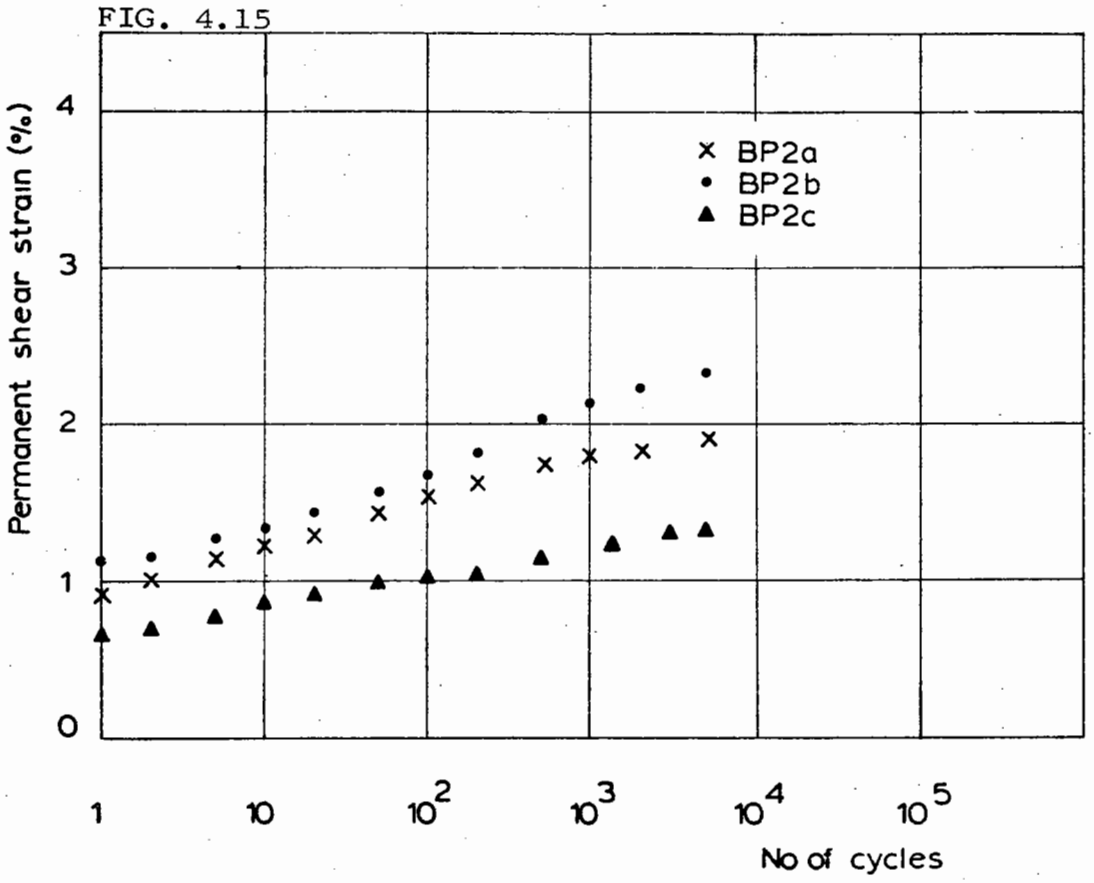

TYPICAL PERMANENT STRAIN RESULTS

FIG. 4.16

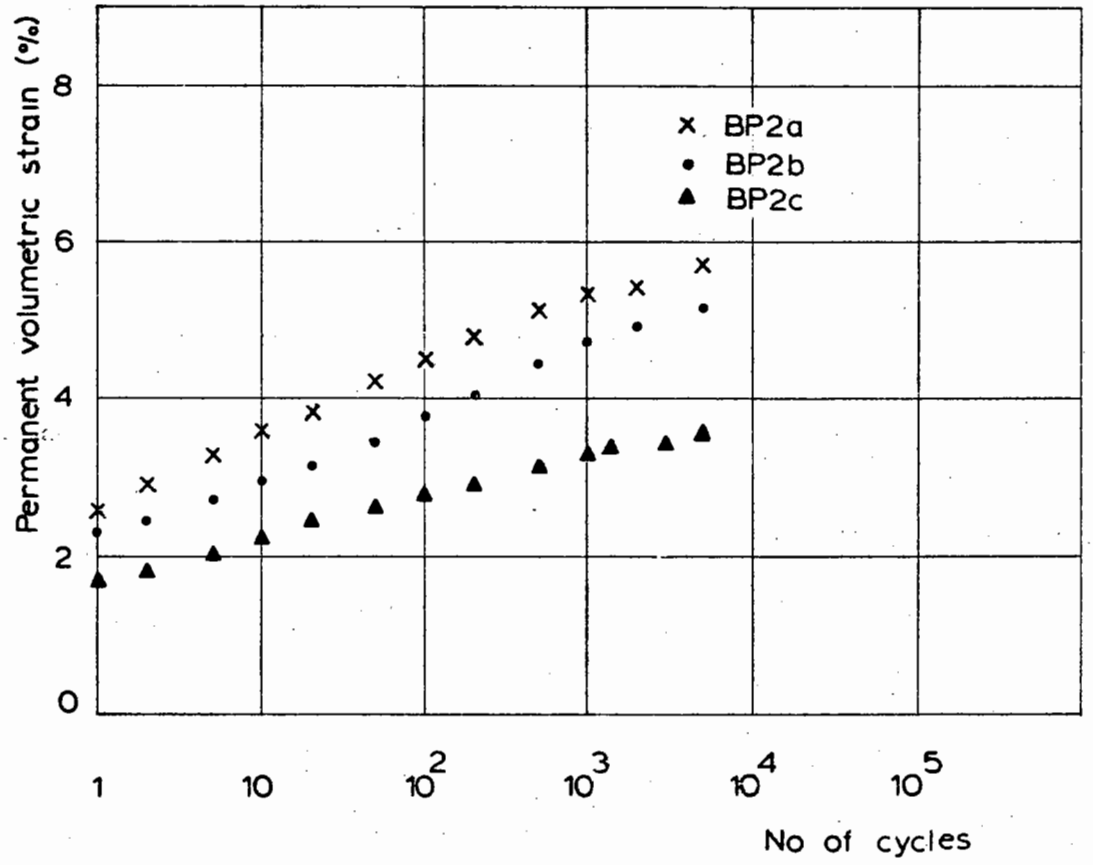

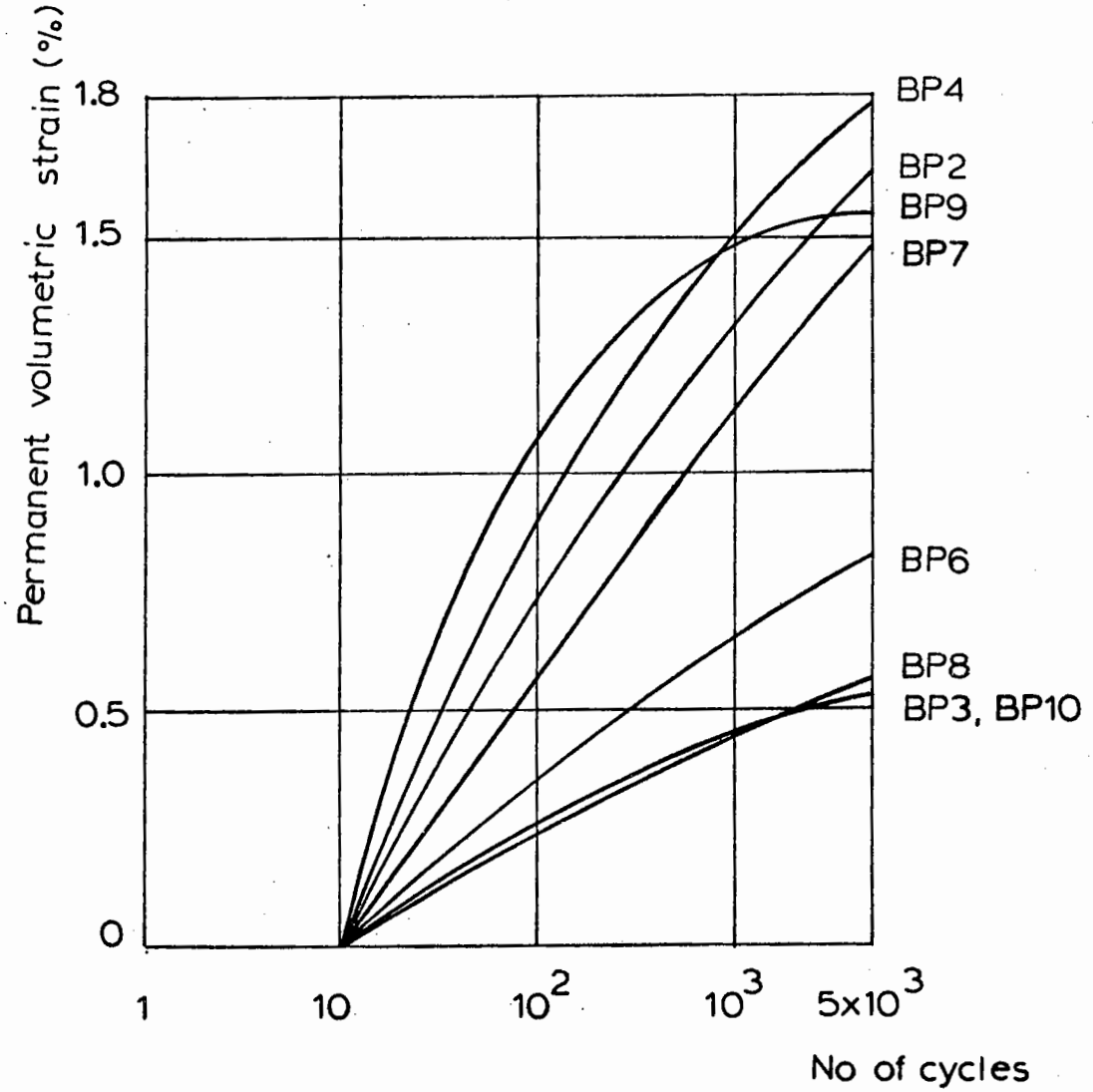

FIG. 4.17 AVERAGED PERMANENT VOLUMETRIC STRAINS

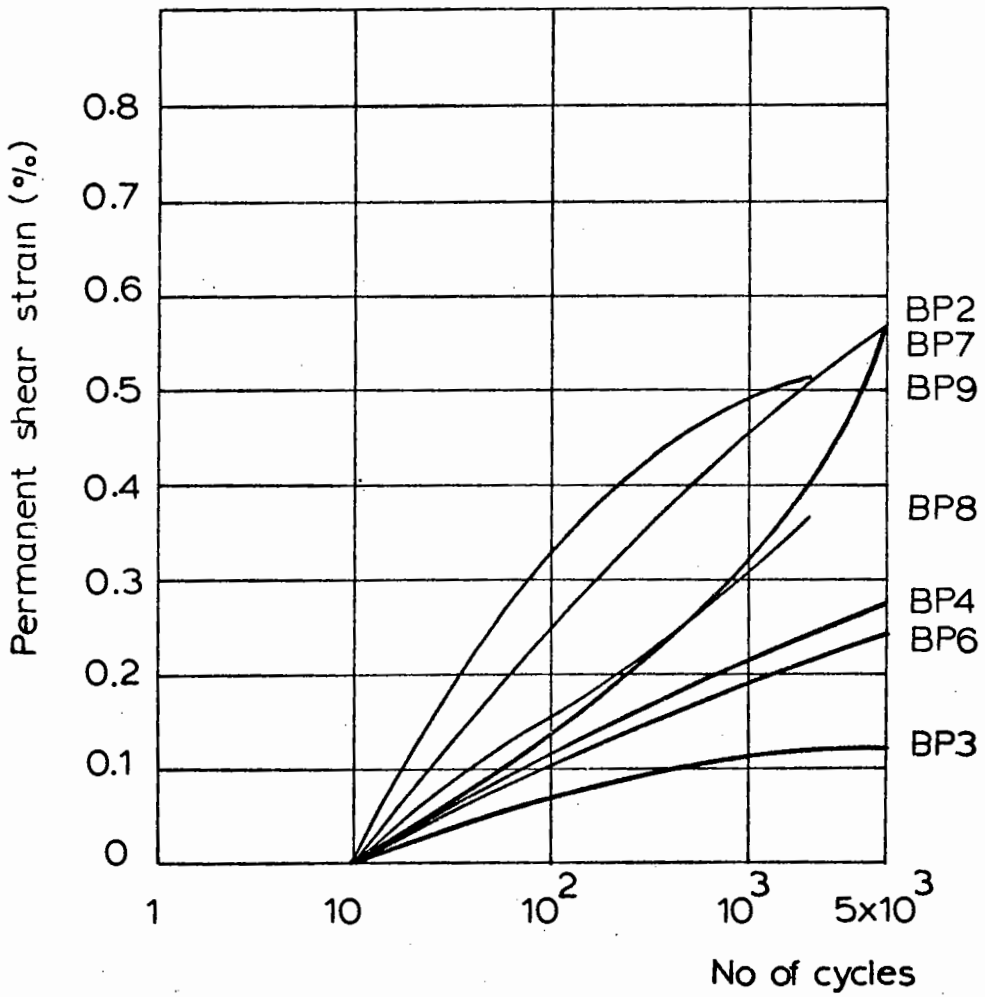

FIG. 4.18 AVERAGED PERMANENT SHEAR STRAINS

4.7.2 Permanent Shear Strain

The model developed from the triaxial permanent strain test program was applied to the biaxial results. The model required a value for A to be found for each path. (A was the minimum normal stress distance of the stress path from the failure envelope in (p,q) stress space - Chapter 3.) In the triaxial test programme all the paths were in the compressive stress region. Fig. 4.14 shows that most of the biaxial stress paths were of the compression-extension type. A was defined for the extension stress region as:

$$A = p_R - \frac{q_R}{1.47} \qquad (4.4)$$

where p_R and q_R were as defined previously but with the sign ignored. The strain rate at 100 cycles divided by the stress path length was plotted against A as shown in Fig. 4.19. The length of the stress path was as defined in Equation 3.8.

The ratio strain rate/stress path length appeared to be a constant independent of A and did not appear to have a threshold value as exhibited in the triaxial test programme. If the monotonic tests to failure for the triaxial and biaxial apparatus are compared, it can be seen that the triaxial tests behaved in the conventional way with strain rate increasing as failure was approached. For the biaxial tests, however, failure did not occur until one of the principal stresses became zero. This may have been the effects of three independent principle stresses and the plane strain nature of the apparatus which is also influencing the permanent strain behaviour of the material. The model for predicting permanent shear strain was:

$$\varepsilon_p = (fnN) \times \ell_r \times 0.017 \times 10^{-6} \qquad (4.5)$$

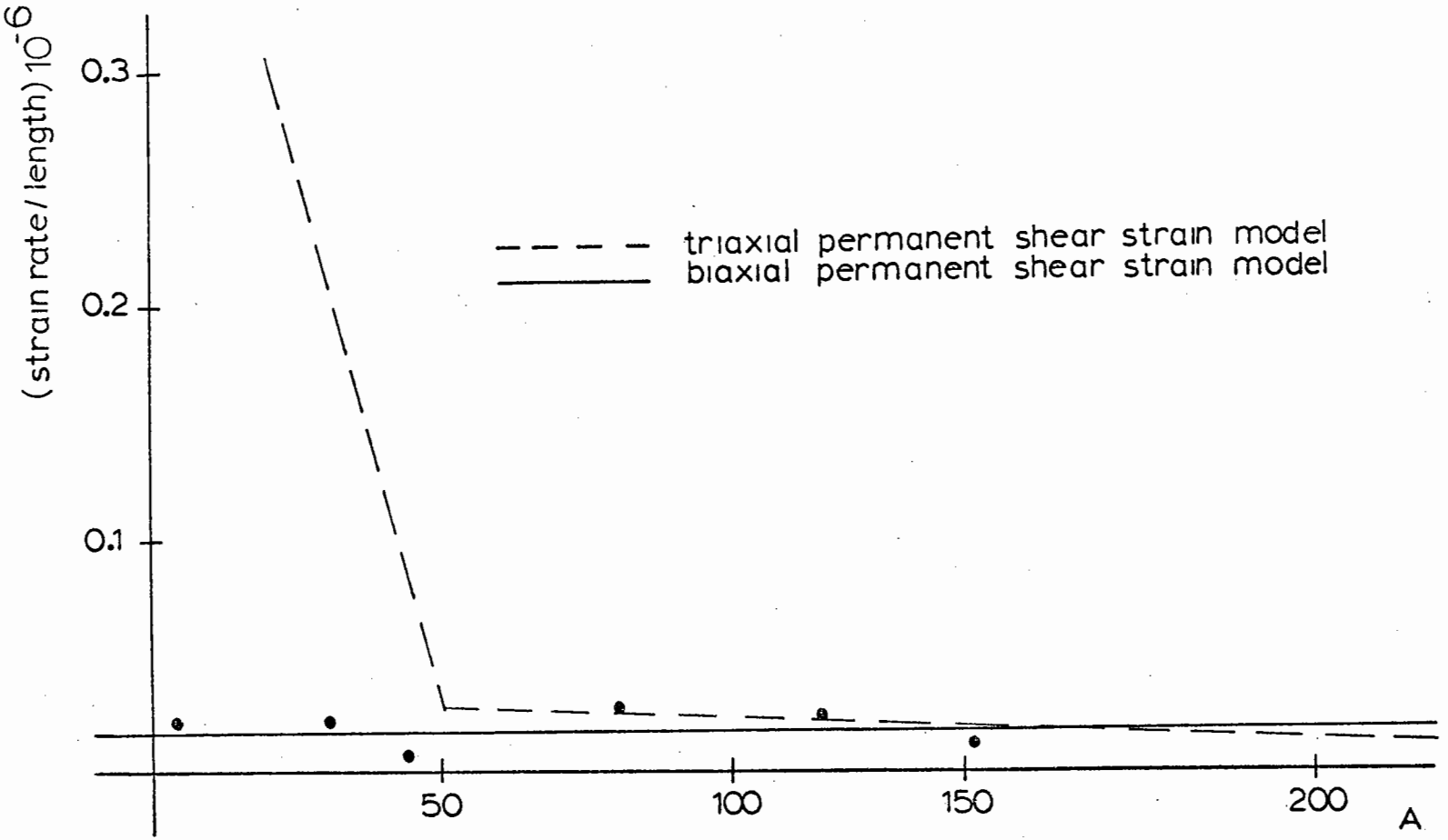

FIG. 4.19 RELATIONSHIP OF STRAIN RATE/LENGTH WITH DISTANCE A

where fnN is the shape function as used for the triaxial results, and ℓ_r is the stress path length.

Figs 4.20 to 4.25 show comparisons of predicted and measured permanent shear strain against the logarithm of the number of cycles for each stress path. Predictions are generally poor, but one must consider that the model is based on results which showed considerable variation. Plotted on each diagram are the permanent shear strain values obtained from separate tests on the same stress path. The scatter evident from these plots and the further approximations necessary in determining an average shape function and distance A do not contribute towards producing an accurate result. However, the model gives some indication of the development of permanent shear strain with predictions generally falling inside the region of experimental scatter.

4.7.3 Permanent Volumetric Strain

As for the triaxial test programme, no satisfactory relationships emerged to enable change of volumetric strain with number of cycles to be adequately modelled.

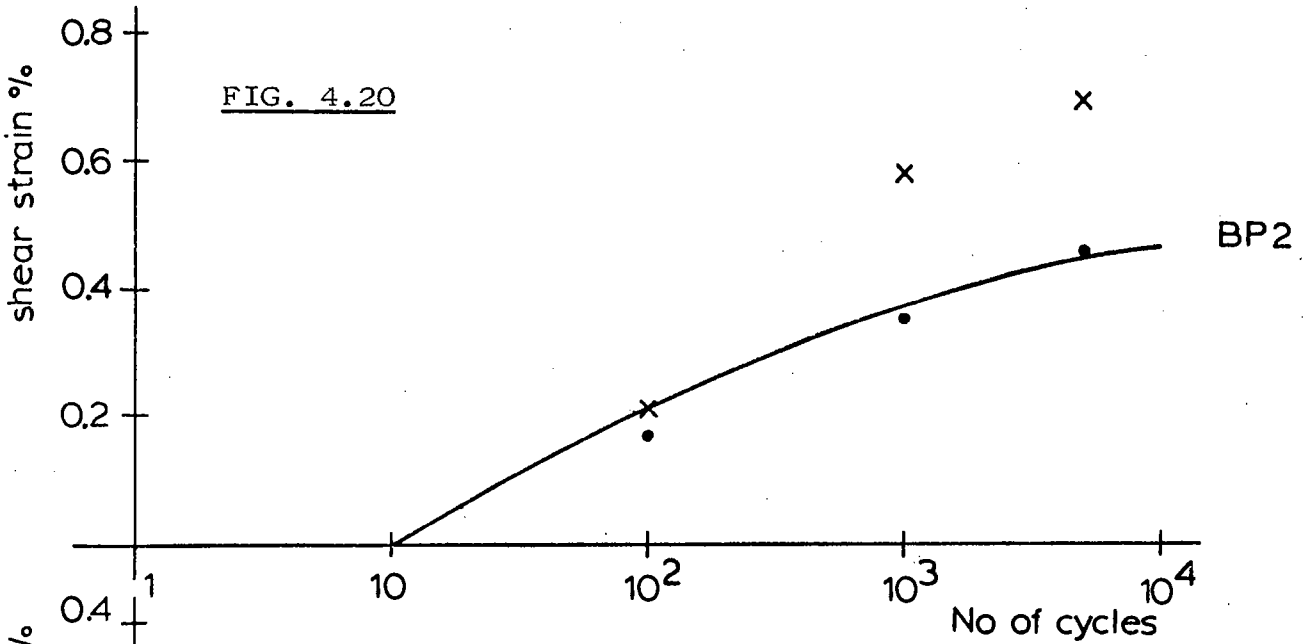

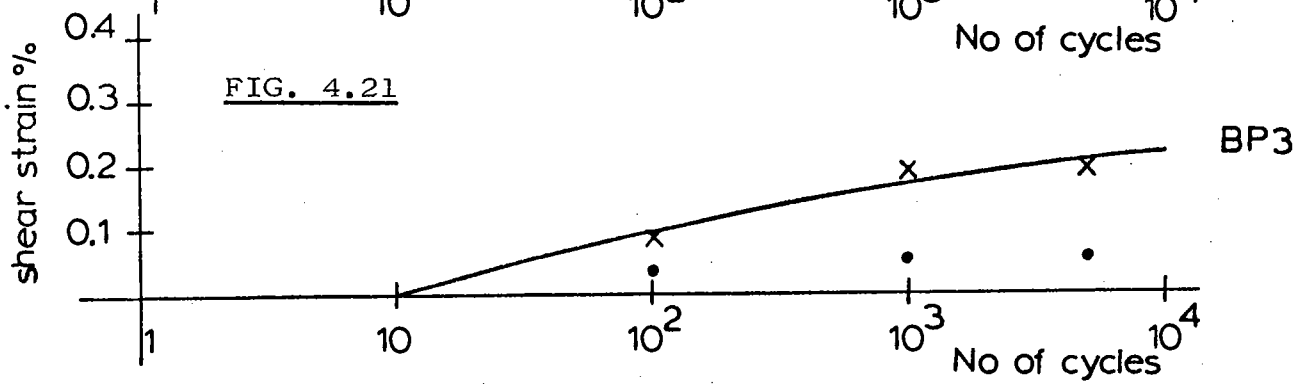

PREDICTED AGAINST EXPERIMENTAL PERMANENT SHEAR STRAINS

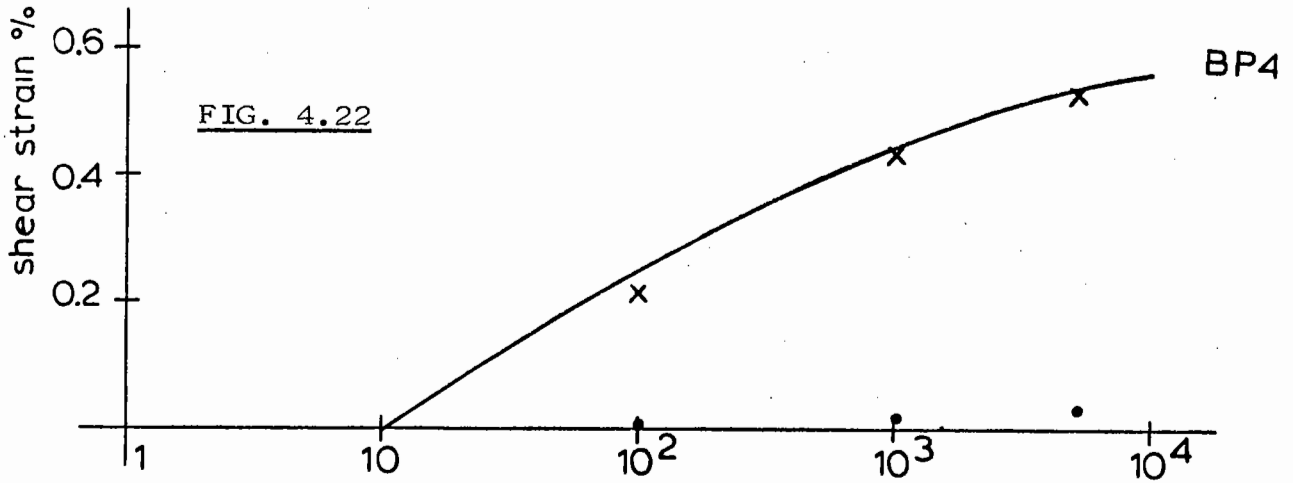

FIG. 4.22

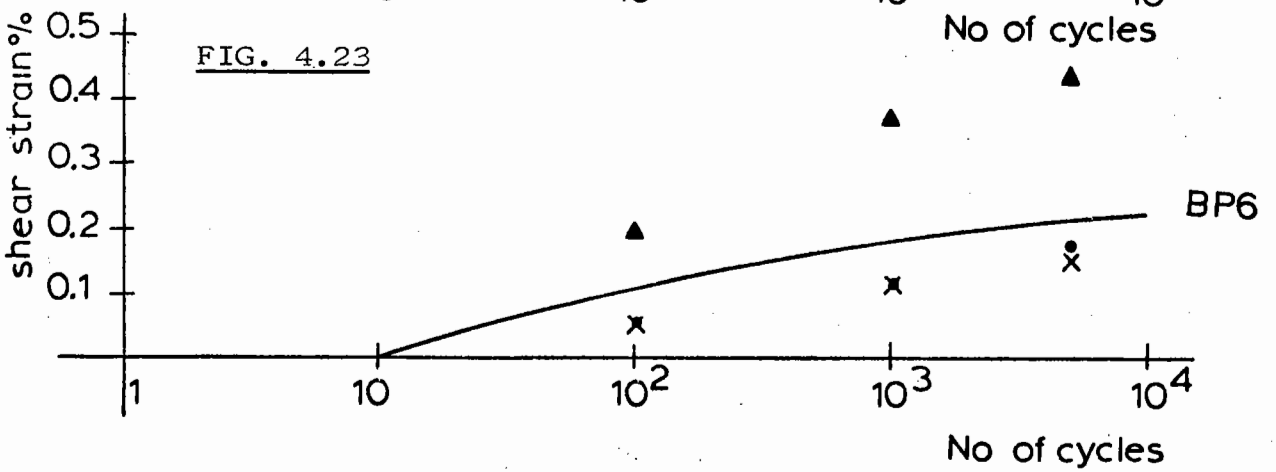

FIG. 4.23

PREDICTED AGAINST EXPERIMENTAL PERMANENT SHEAR STRAINS

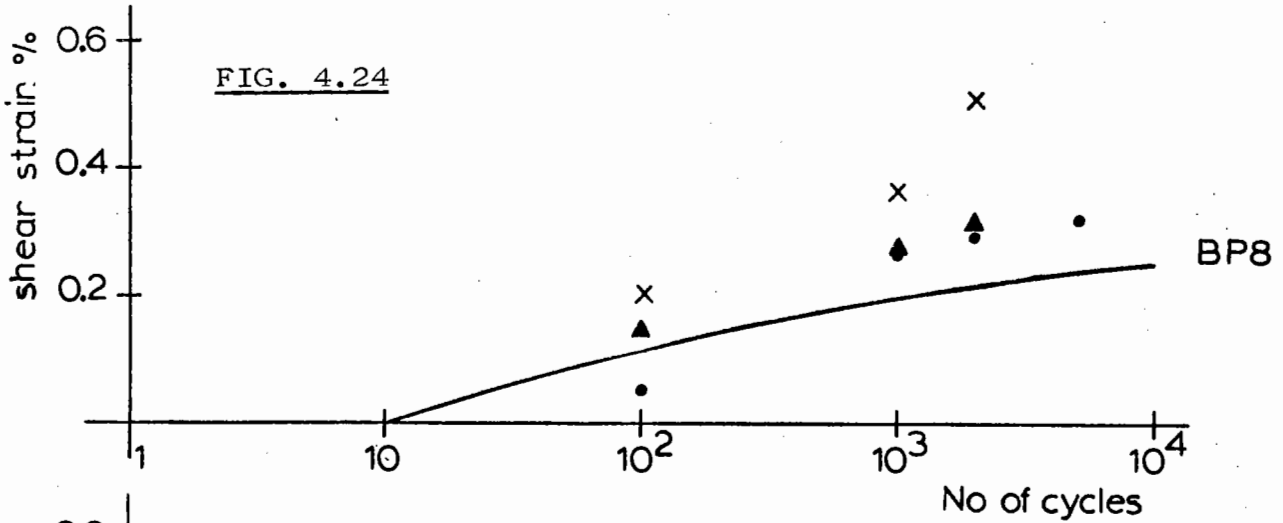

FIG. 4.24

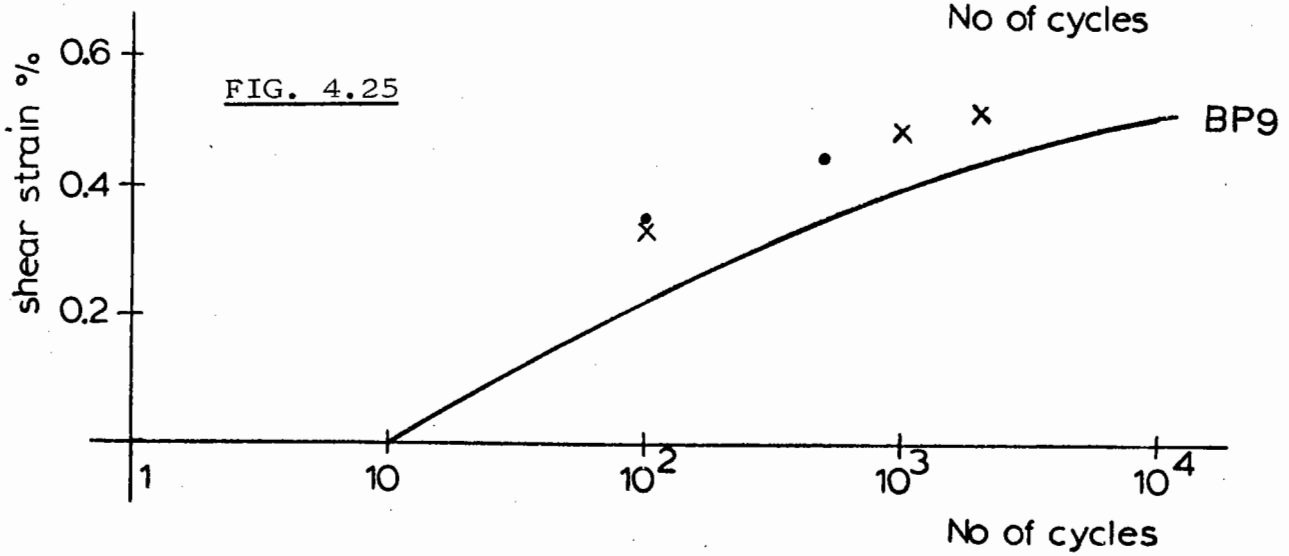

FIG. 4.25

PREDICTED AGAINST EXPERIMENTAL PERMANENT SHEAR STRAINS

CHAPTER FIVE

COMPARISON OF TWO NON-LINEAR MODELS

5.1 INTRODUCTION

A simple model of the type:

$$M_R = K_1 \theta^{K_2} \tag{5.1}$$

is described. M_R is the resilient modulus and θ is the sum of the principal stresses. K_1 and K_2 are material constants determined from laboratory testing. The model is commonly referred to as a "K-theta" model and has been used extensively in the United States (Hicks and Monismith 1971, Raad and Figueroa 1980).

Predictions of strains for both triaxial and biaxial conditions using the K-theta model, are compared with those produced by the contour model described in Chapter 3. Comparisons are made for both the single size and well graded crushed limestone materials.

5.2 DEVELOPMENT OF THE K-THETA MODEL

A commonly used non-linear stress-strain model for granular materials is that relating resilient modulus M_R and stress level in the form of Equation 5.1.

The resilient modulus is usually obtained from tests at constant confining stress with the deviator stress pulsed from zero to various peak values.

$$M_R = q_r/\varepsilon_{zr} \tag{5.2}$$

where q_r = repeated deviator stress

$\theta = \sigma_z + 2\sigma_x = 3\sigma_x + q_r$

σ_z = peak axial stress

σ_x = constant confining stress

ε_{zr} = resilient axial strain

K_1 and K_2 are material constants.

The tests are generally conducted in a triaxial apparatus with dynamic load and axial deformations being monitored throughout the test. After about 200 cycles, the resilient deformations tend to stabilise and the M_R value is then computed as in Equation 5.2. Fig. 5.1 shows a typical stress path used to determine the above relationship. The resilient test programme carried out on the crushed limestone contained several stress paths of this type, enabling K-theta models to be established for the single size and graded materials. Details of the test results and computations are given in Appendix 5A. The models obtained were:

single size material: $M_R = 19454\theta^{0.5}$ (5.3)

graded material: $M_R = 8634\theta^{0.69}$ (5.4)

where M_R and θ are in kPa. Each model was developed from the results of several stress paths.

The K-theta model is widely used to predict the response of unbound granular materials in numerical analysis of pavement structures. However, it has the limitation that the stress paths used in its development cover a very restricted range when compared to the situation in the pavement. The philosophy behind the extensive testing programme described in Chapter 3, was that contour models could be developed and applied with confidence to any general stress situation.

In order to test the validity of the K-theta model over a wide range of stresses, the models were used to predict resilient shear and volumetric strains for the complete range of paths used in the complex test programme (Chapters 3 and 4).

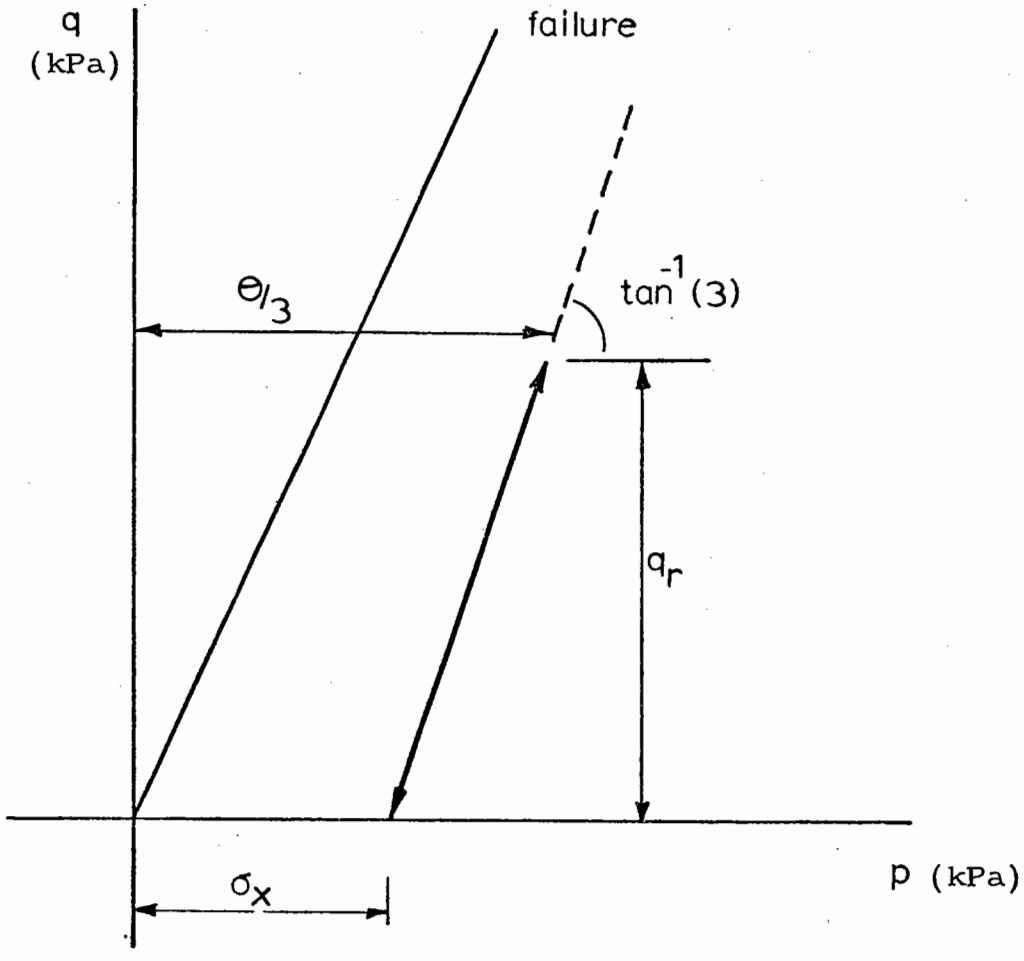

FIG. 5.1 TYPICAL STRESS PATH TO DETERMINE K-THETA MODEL

5.3 USE OF K-THETA MODEL

The K-theta model would appear to be applied to numerical analysis using a tangent modulus approach. The value of M_R is generally determined from the peak stress state for any path under investigation. The complex contour models described previously employ a secant approach. However, the purpose of this investigation was to compare the performance of each model, as generally used to characterise non-linear behaviour. A comparison was therefore made between a secant contour and tangent K-theta model. For completeness, Section 5.3.2 describes a secant approach to the use of the K-theta model as well.

5.3.1 K-theta Model - Tangent Modulus

Having established the relationship

$$M_R = K_1 \theta^{K_2} \tag{5.1}$$

generalised Hooke's Law was used to calculate the resilient principal strains and hence the resilient shear and volumetric strains for each stress path. An average Poisson's ratio of 0.32 was determined from the triaxial tests described above. Consider the stress path shown in Fig. 5.2. Assuming triaxial conditions, $\sigma_x = \sigma_y$ and hence $\varepsilon_x = \varepsilon_y$. θ, defined previously, is in terms of the peak axial stress σ_z and the constant confining stress $\sigma_x = \sigma_y$. For general conditions in which confining stress is not always constant, θ is defined as the sum of the peak stresses, i.e.

$$\theta = \sigma_z + 2\sigma_x \tag{5.5}$$

where σ_z and σ_x are peak values.

The resilient principal strains ε_{zr} and ε_{xr} were found from:

$$\varepsilon_{zr} = \left[(\sigma_{z2}-\sigma_{z1}) - 2\nu(\sigma_{x2}-\sigma_{x1})\right]/K_1(\sigma_{z2}+2\sigma_{x2})^{K_2} \quad (5.6)$$

$$\varepsilon_{xr} = \left[(\sigma_{x2}-\sigma_{x1})(1-\nu)-\nu(\sigma_{z2}-\sigma_{z1})\right]/K_1(\sigma_{z2}+2\sigma_{x2})^{K_2} \quad (5.7)$$

where ν = Poisson's ratio = 0.32 as determined from the triaxial tests.

σ_{z1}, $\sigma_{x1} = \sigma_{y1}$ are principal stresses at point 1.

σ_{z2}, $\sigma_{x2} = \sigma_{y2}$ are principal stresses at point 2.

The resilient shear strain ε_r was then found as:

$$\varepsilon_r = \frac{2}{3}(\varepsilon_{zr} - \varepsilon_{xr}) \quad (5.8)$$

and the resilient volumetric strain v_r as:

$$v_r = \varepsilon_{zr} + 2\varepsilon_{xr} \quad (5.9)$$

The model thus used applies a tangent modulus to a given stress path, the modulus being determined by the peak stress state. Comparisons of results for the full contour model and the tangent K-theta approach, as used for the single size material, are shown in Figs 5.3 to 5.10. The results obtained using a secant approach as described in Section 5.3.2 are also included.

It is clear that the K-theta model is often inadequate when compared with predictions using the resilient contour models. Taking into consideration the simplistic approach in determining the K-theta model, predictions of resilient shear strain are surprisingly good. However, the model is often inaccurate when applied to the prediction of volumetric strain. No account is taken of changes in q, so if p does not vary, the model predicts zero strain. Full details of the results are presented in Appendix 5B.

5.3.2 K-theta Model - Secant Modulus

In applying the secant approach, a modulus value for each end of

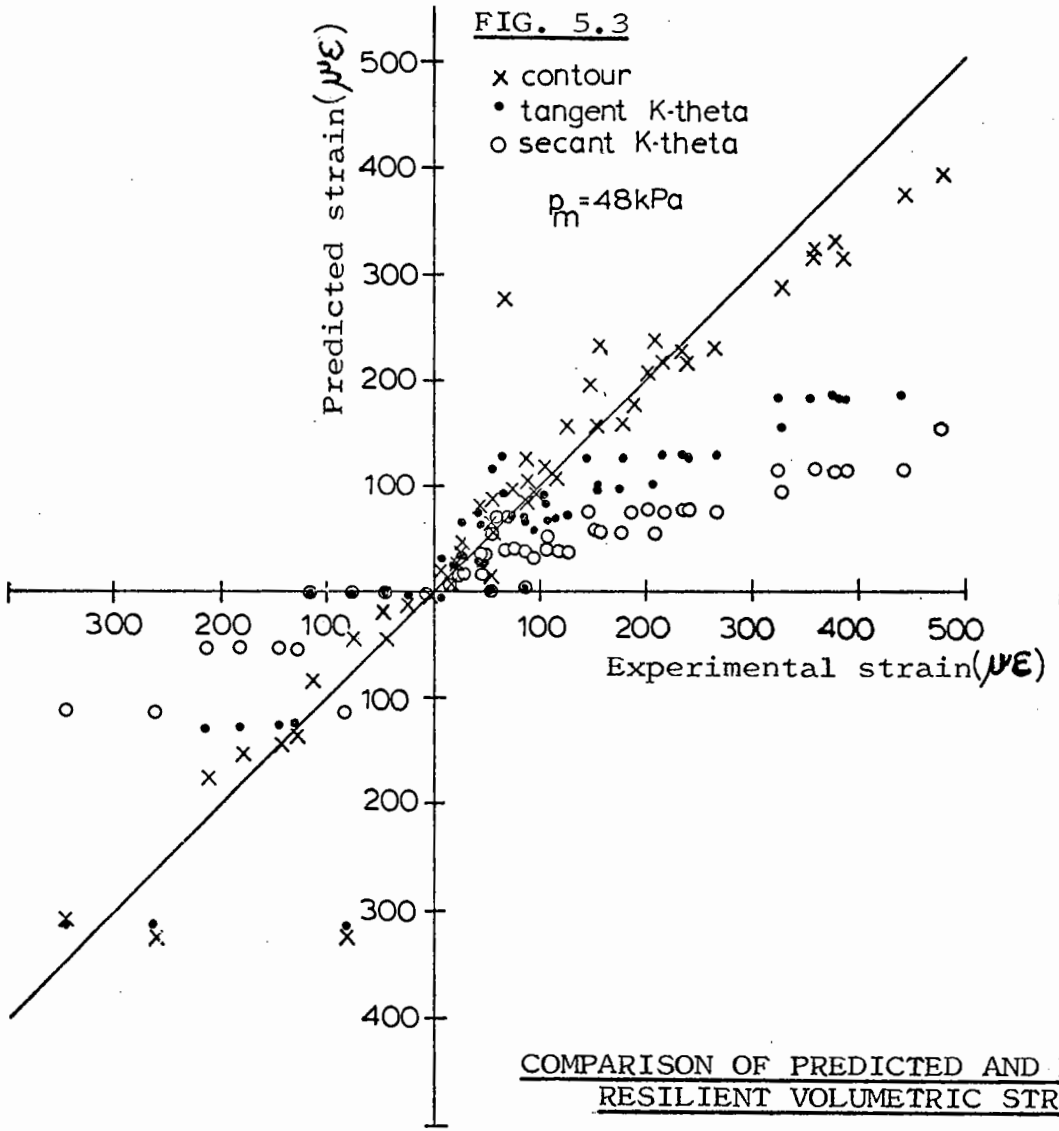

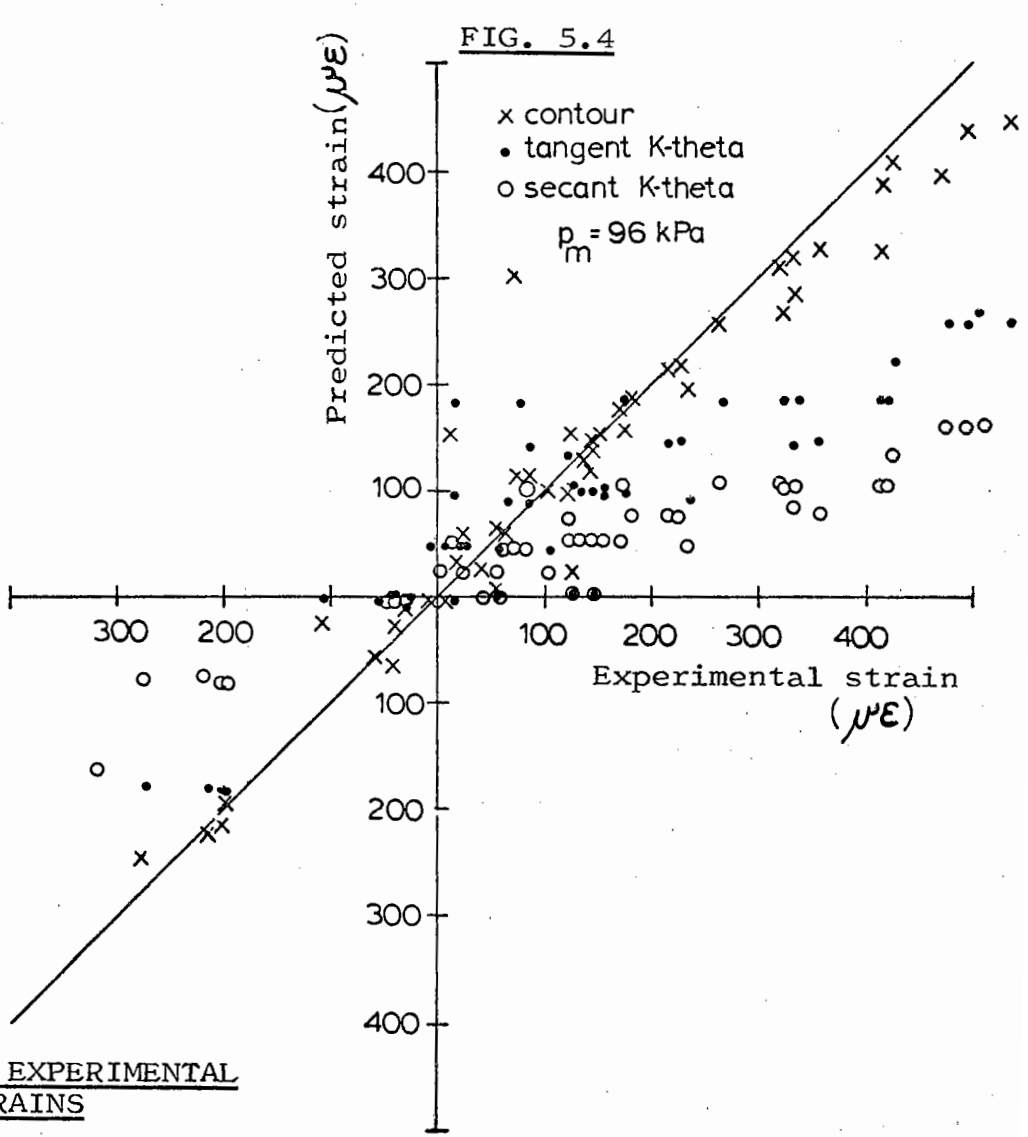

COMPARISON OF PREDICTED AND EXPERIMENTAL RESILIENT VOLUMETRIC STRAINS

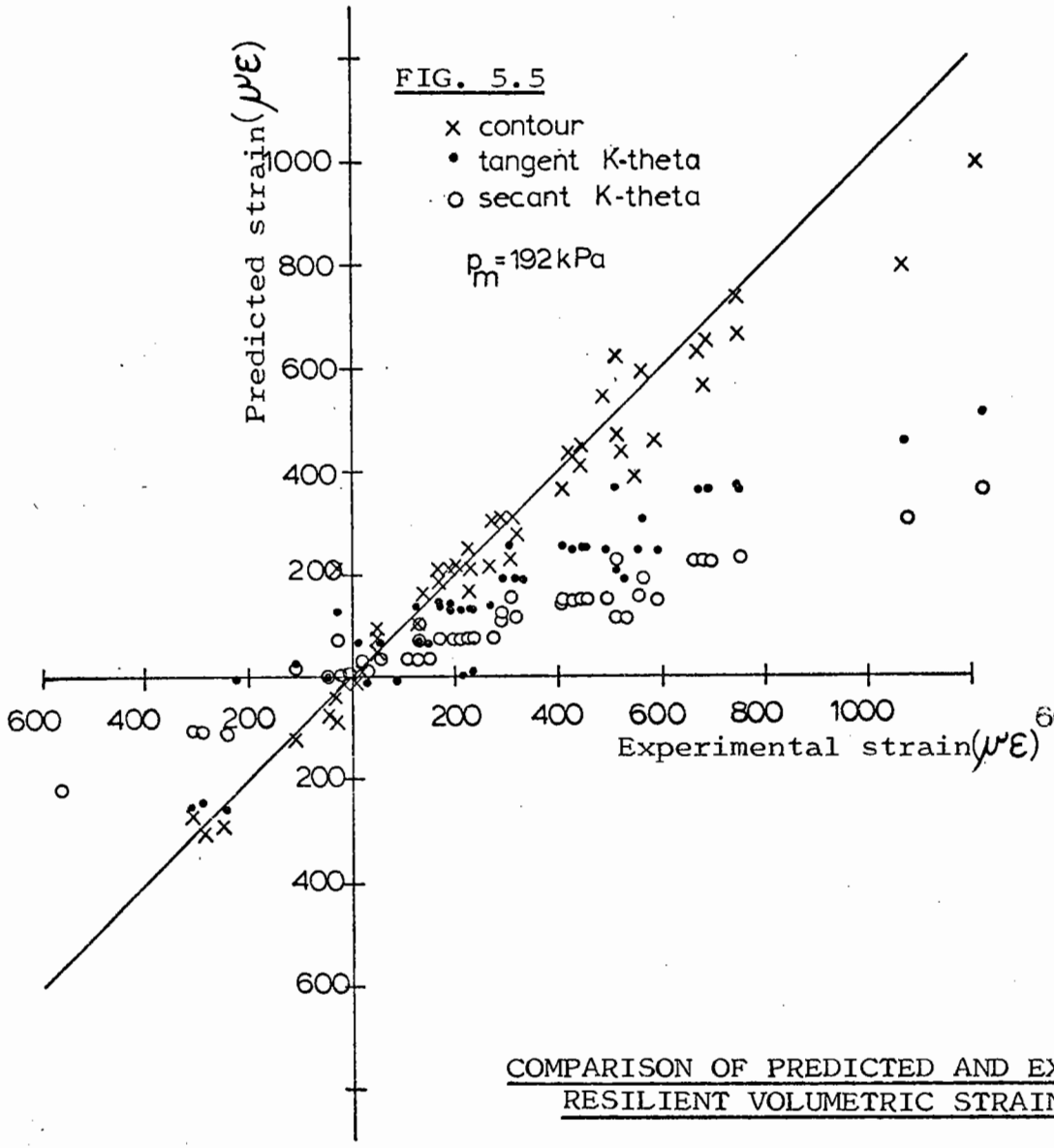

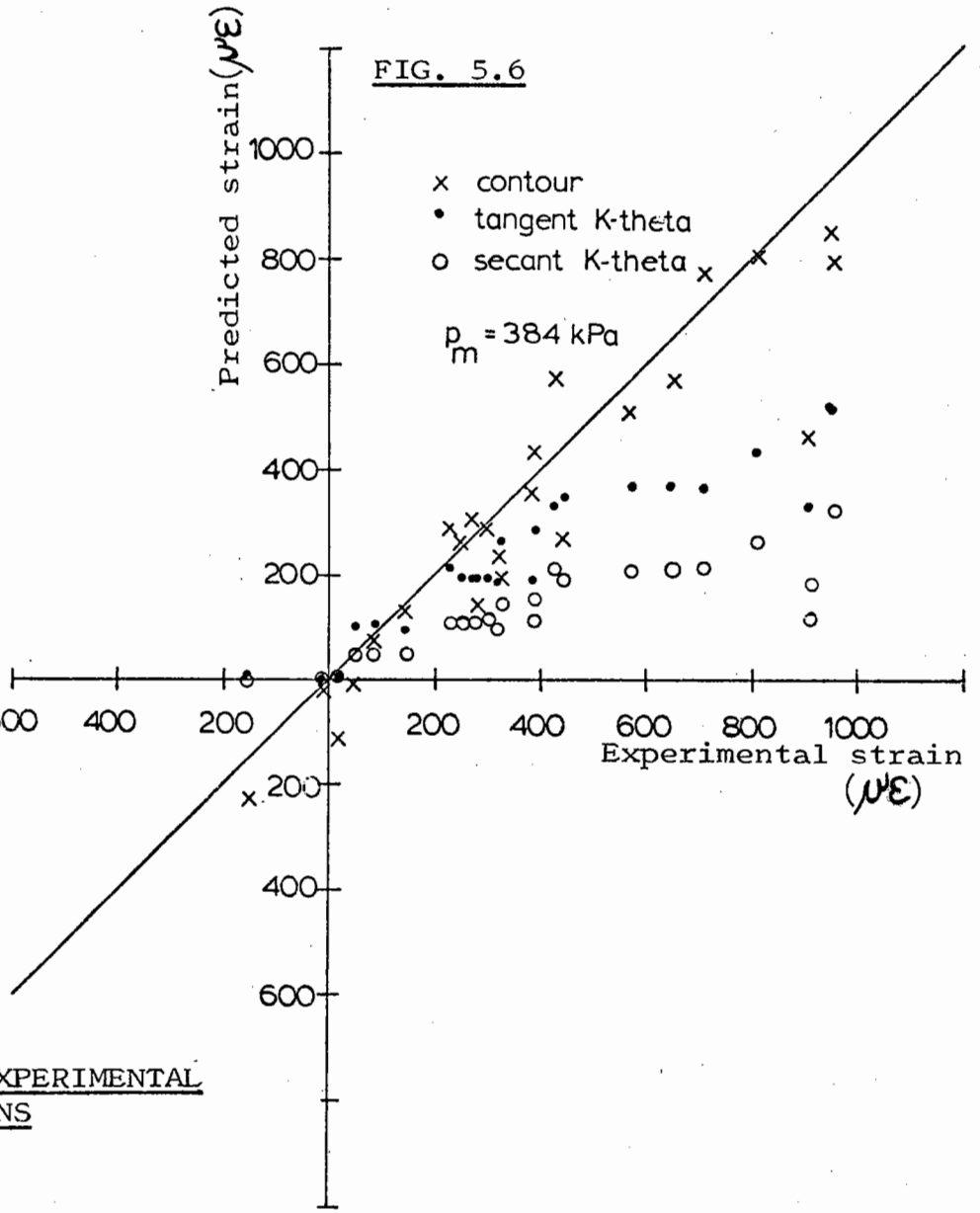

COMPARISON OF PREDICTED AND EXPERIMENTAL RESILIENT VOLUMETRIC STRAINS

COMPARISON OF PREDICTED AND EXPERIMENTAL RESILIENT SHEAR STRAINS

FIG. 5.7

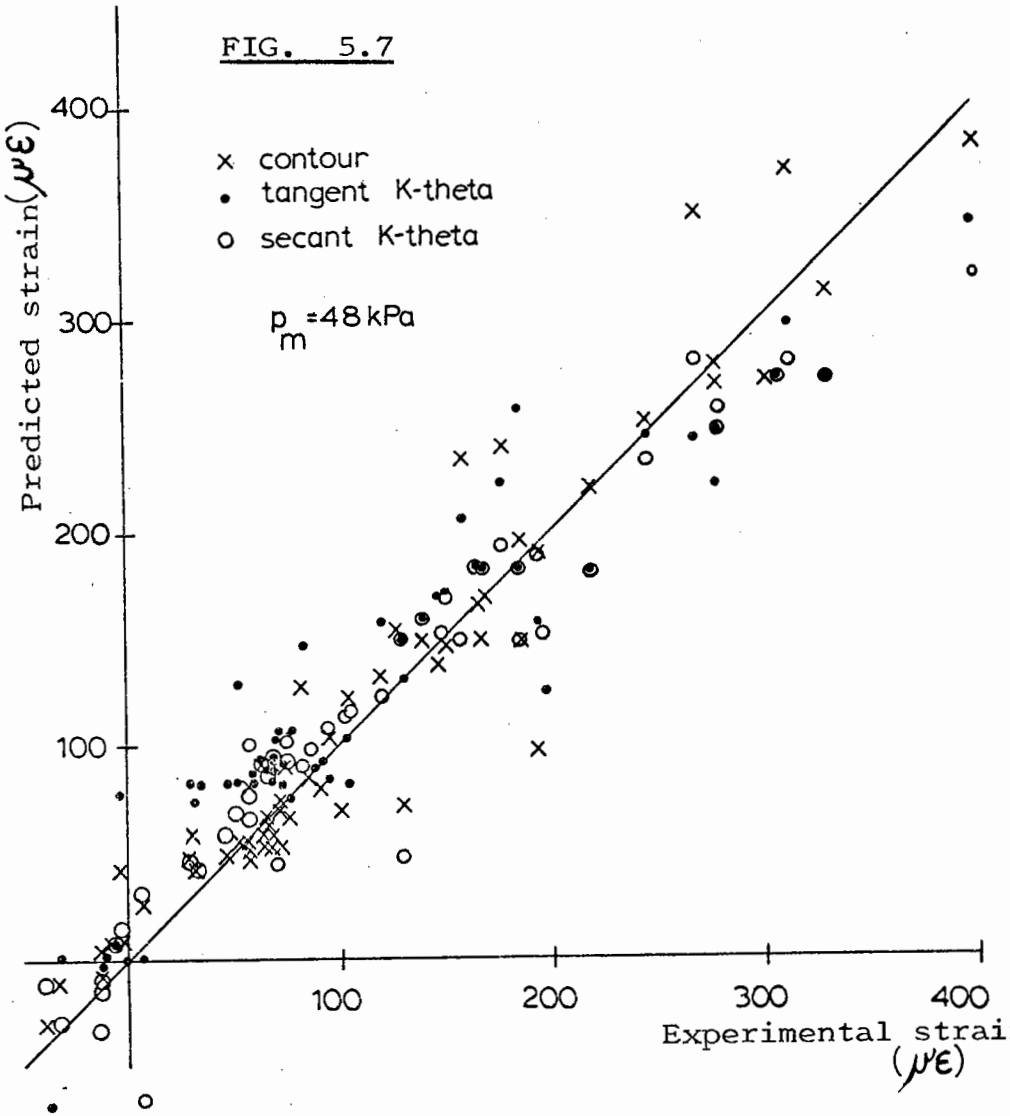

FIG. 5.8

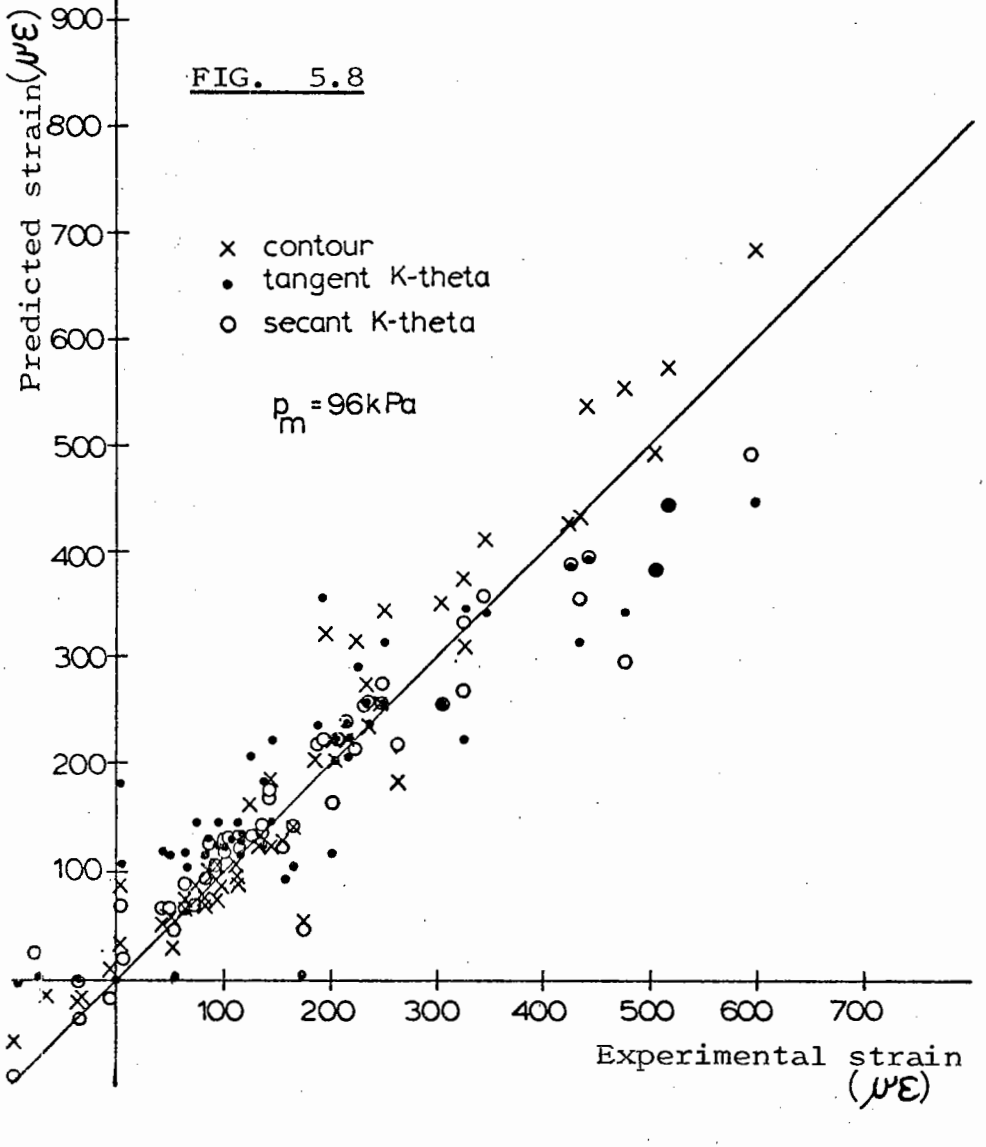

COMPARISON OF PREDICTED AND EXPERIMENTAL RESILIENT SHEAR STRAINS

FIG. 5.9

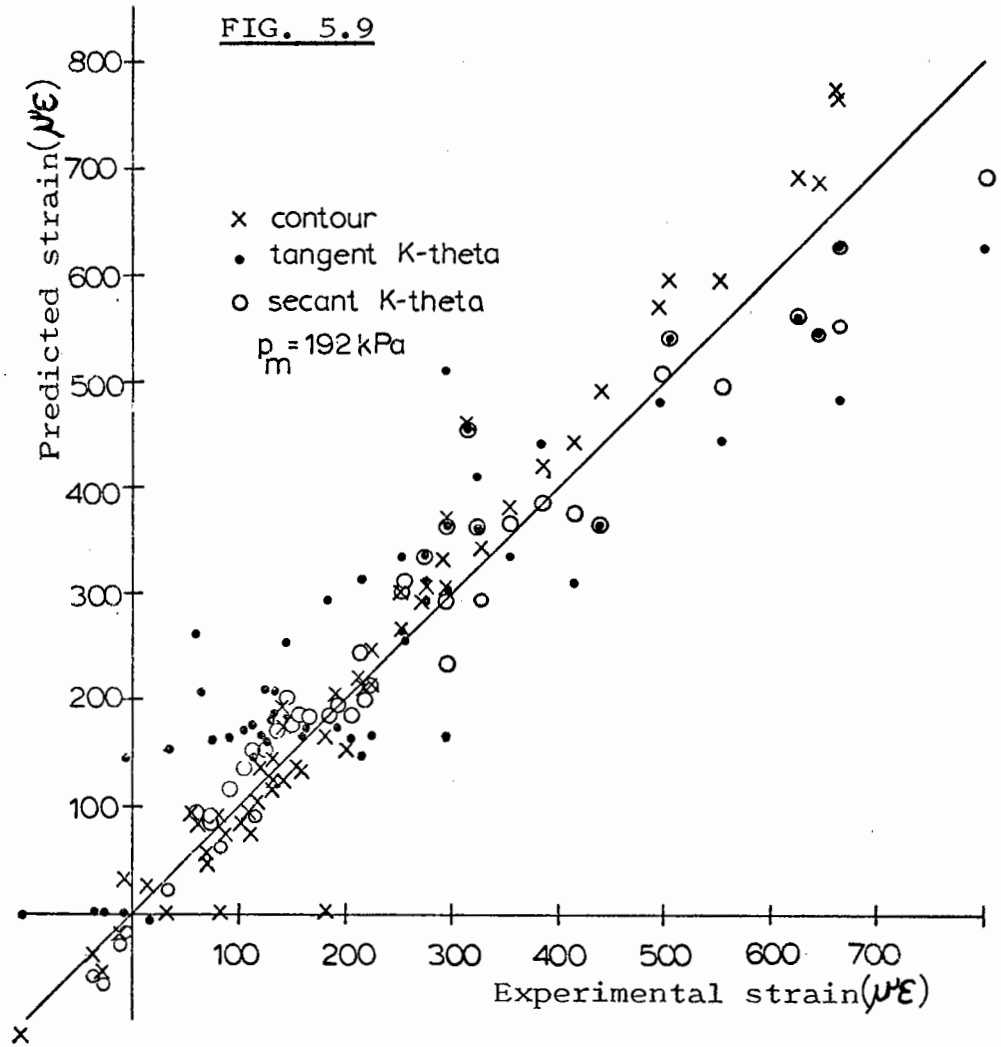

FIG. 5.10

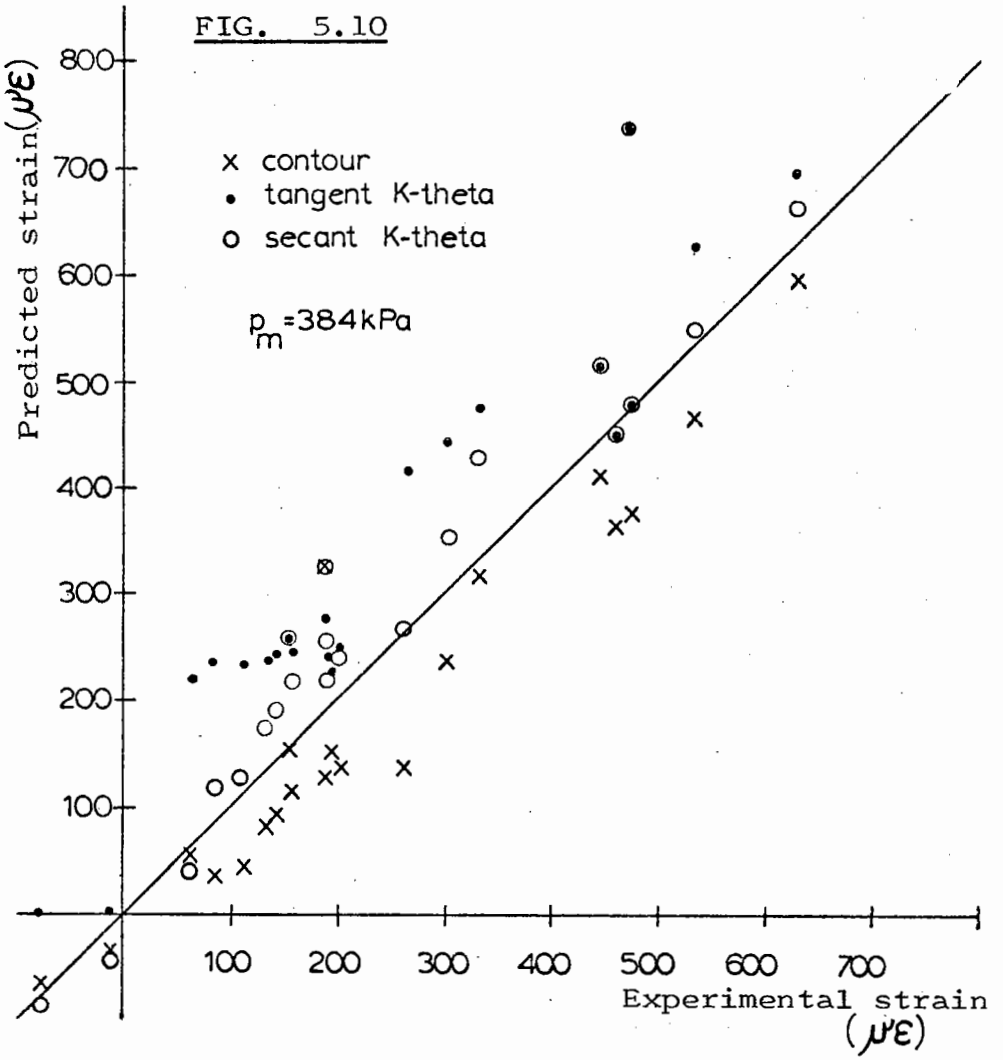

the stress path was determined and the corresponding strain state calculated. The resilient strain was defined as the difference in strain value of each end of the stress path. This approach was similar to that used for the contour model.

The modulus for point 1 in Fig. 5.2 is given by:

$$M_{R1} = K_1(\sigma_{z1} + 2\sigma_{x1})^{K_2} \tag{5.10}$$

Hence the principal strains ε_{z1} and ε_{x1} for point 1 can be calculated:

$$\varepsilon_{z1} = (\sigma_{z1} - 2\nu\sigma_{x1})/K_1(\sigma_{z1} + 2\sigma_{x1})^{K_2} \tag{5.11}$$

$$\varepsilon_{x1} = (\sigma_{x1}(1-\nu) - \nu\sigma_{z1})/K_1(\sigma_{z1} + 2\sigma_{x1})^{K_2} \tag{5.12}$$

where $\nu = 0.32$ as previously determined.

The shear strain ε_1 and volumetric strain v_1 at point 1 may then be found:

$$\varepsilon_1 = \frac{2}{3}(\varepsilon_{z1} - \varepsilon_{x1}) \tag{5.13}$$

$$v_1 = \varepsilon_{z1} + 2\varepsilon_{x1} \tag{5.14}$$

For point 2, the modulus is given by:

$$M_{R2} = K_1(\sigma_{z2} + 2\sigma_{x2})^{K_2} \tag{5.15}$$

and using a similar procedure, the shear and volumetric strain at point 2 may be calculated as ε_2 and v_2 respectively.

The resilient shear strain ε_r and resilient volumetric strain v_r resulting from stress path 1 to 2 are therefore defined as:

$$\varepsilon_r = \varepsilon_2 - \varepsilon_1 \tag{5.16}$$

$$v_r = v_2 - v_1 \tag{5.17}$$

Typical comparisons of predictions obtained using the contour models and secant K-theta are shown in Figs 5.3 to 5.10 along with results from the tangent K-theta model. Full details of the results are presented in Appendix 5B.

It is immediately apparent that the secant approach reduces the scatter of results in predicting resilient shear strain when compared with the tangent model. However, both are still less accurate than the contour model. Predictions of volumetric strain using the secant K-theta model consistently underpredicted by about 300%,although once again there were many paths where the model predicted zero strain. A similar behaviour was observed for the graded material, as described later. A further examination of the resilient shear strain results revealed that on applying a stress path length correction (Chapter 3, Section 3.4.3), the K-theta model performed as accurately as the contour model. However, this is not generally used in applying the model and was ignored for these comparisons.

Secant and tangent K-theta models were used to reanalyse the results for the well graded material and typical comparisons are shown in Figs 5.11 and 5.12. The pattern of behaviour was similar to that observed for the single size material. Full results are presented in Appendix 5C.

5.4 K-THETA MODEL APPLIED TO BIAXIAL TEST RESULTS

The biaxial shear box applies three independent principal stresses to the specimen as described in Chapter 4. However, the apparatus involves plane strain conditions and shear strain and volumetric strain are defined as:

$$\text{shear strain } \varepsilon = \frac{\sqrt{2}}{3}\left[\varepsilon_y^2 + \varepsilon_x^2 + (\varepsilon_y - \varepsilon_x)^2\right]^{\frac{1}{2}} \qquad (5.18)$$

FIG. 5.11 RESILIENT SHEAR STRAIN

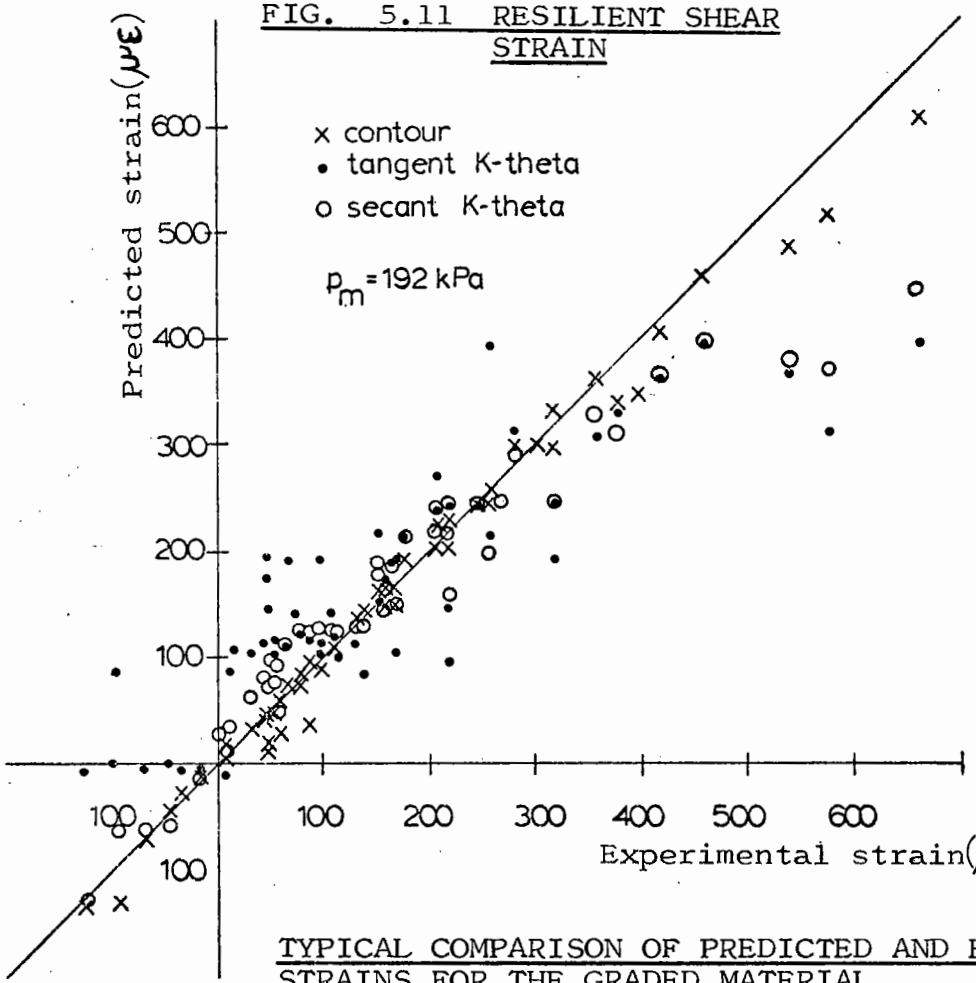

FIG. 5.12 RESILIENT VOLUMETRIC STRAIN

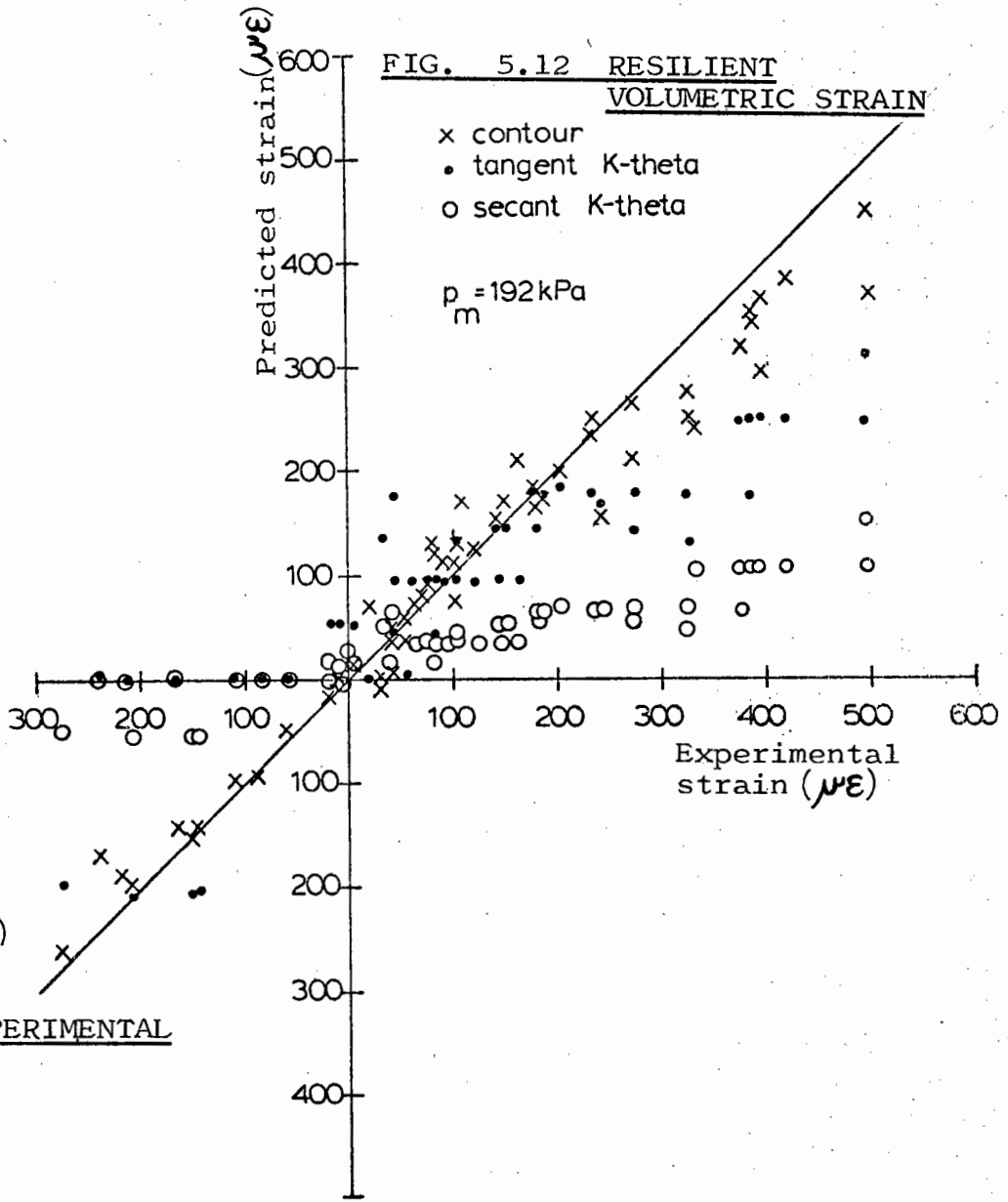

TYPICAL COMPARISON OF PREDICTED AND EXPERIMENTAL STRAINS FOR THE GRADED MATERIAL

$$\text{volumetric strain } v = \varepsilon_y + \varepsilon_x \tag{5.19}$$

where ε_y and ε_x are the principal strains in the x and y directions.
$\varepsilon_z = 0$.

5.4.1 K-theta Model - Tangent Modulus

The same procedure as for the triaxial results was adopted with θ expressed as:

$$\theta = \sigma_x + \sigma_y + \sigma_z \tag{5.20}$$

where σ_x, σ_y and σ_z are peak values.

The resilient principal strains ε_{xr} and ε_{yr} were obtained from:

$$\varepsilon_{xr} = \left[(\sigma_{x2}-\sigma_{x1}) - \nu((\sigma_{y2}-\sigma_{y1})+(\sigma_{z2}-\sigma_{z1}))\right]/K_1(\sigma_{x2}+\sigma_{y2}+\sigma_{z2})^{K_2} \tag{5.21}$$

$$\varepsilon_{yr} = \left[(\sigma_{y2}-\sigma_{y1})-\nu((\sigma_{x2}-\sigma_{x1})+(\sigma_{z2}-\sigma_{z1}))\right]/K_1(\sigma_{x2}+\sigma_{y2}+\sigma_{z2})^{K_2} \tag{5.22}$$

where $\nu = 0.32$ as previously determined.

σ_{x1}, σ_{y1}, σ_{z1} are principal stresses at point 1.

σ_{x2}, σ_{y2}, σ_{z2} are principal stresses at point 2.

The resilient shear strain ε_r and resilient volumetric strain v_r were obtained from:

$$\varepsilon_r = \frac{\sqrt{2}}{3}\left[\varepsilon_{yr}^2 + \varepsilon_{xr}^2 + (\varepsilon_{yr} - \varepsilon_{xr})^2\right]^{\frac{1}{2}} \tag{5.23}$$

$$v_r = \varepsilon_{yr} + \varepsilon_{xr} \tag{5.24}$$

Figs 5.13 and 5.14 show comparisons of predicted and experimental strains using a tangent approach. Also included are comparisons for the secant model as described in the following section. The model is generally shown to be inadequate in predicting both shear and volumetric strains. Full results are presented in Appendix 5D.

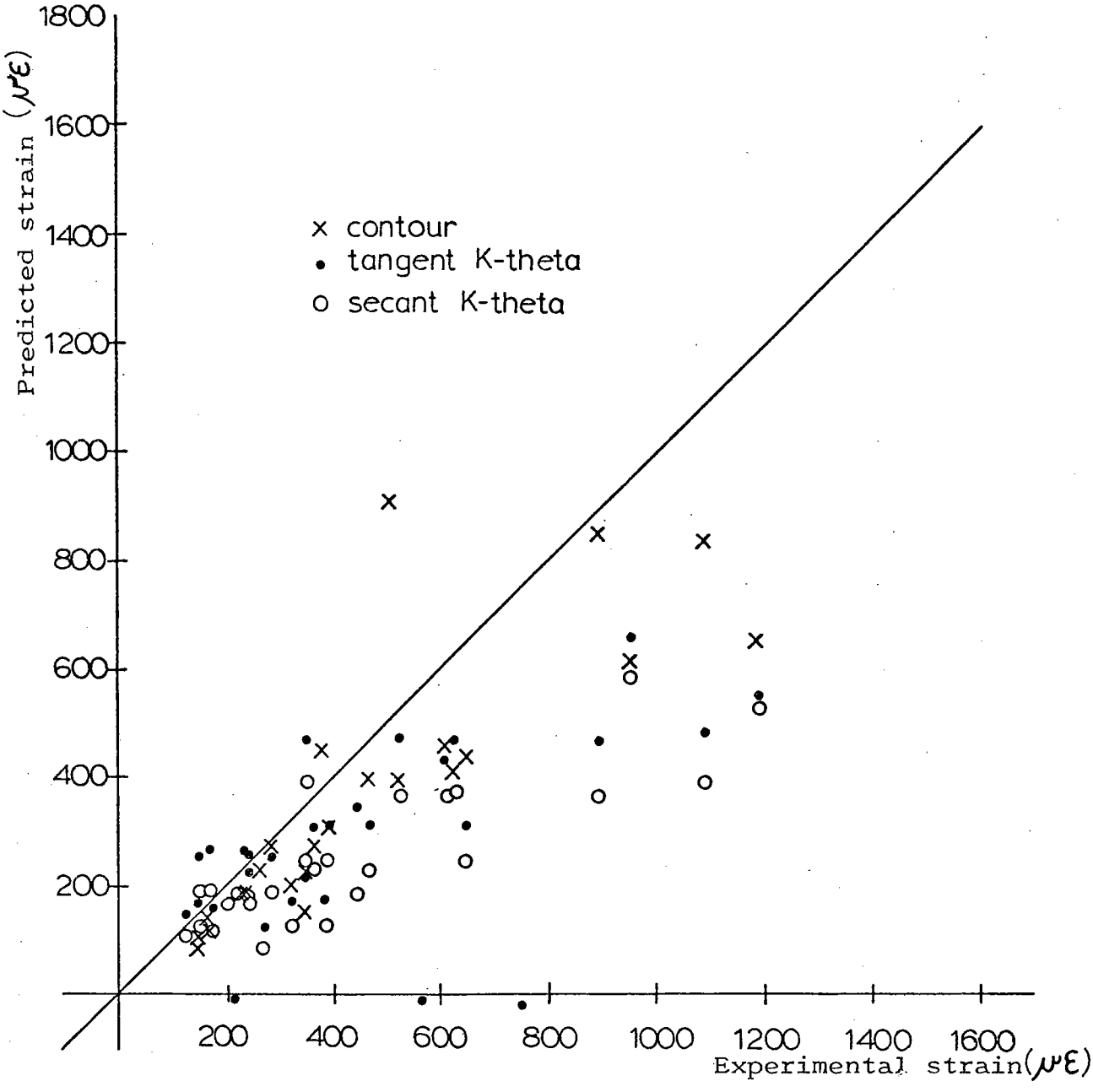

FIG. 5.13 COMPARISON OF PREDICTED AND EXPERIMENTAL RESILIENT VOLUMETRIC STRAINS FOR THE BIAXIAL TEST RESULTS

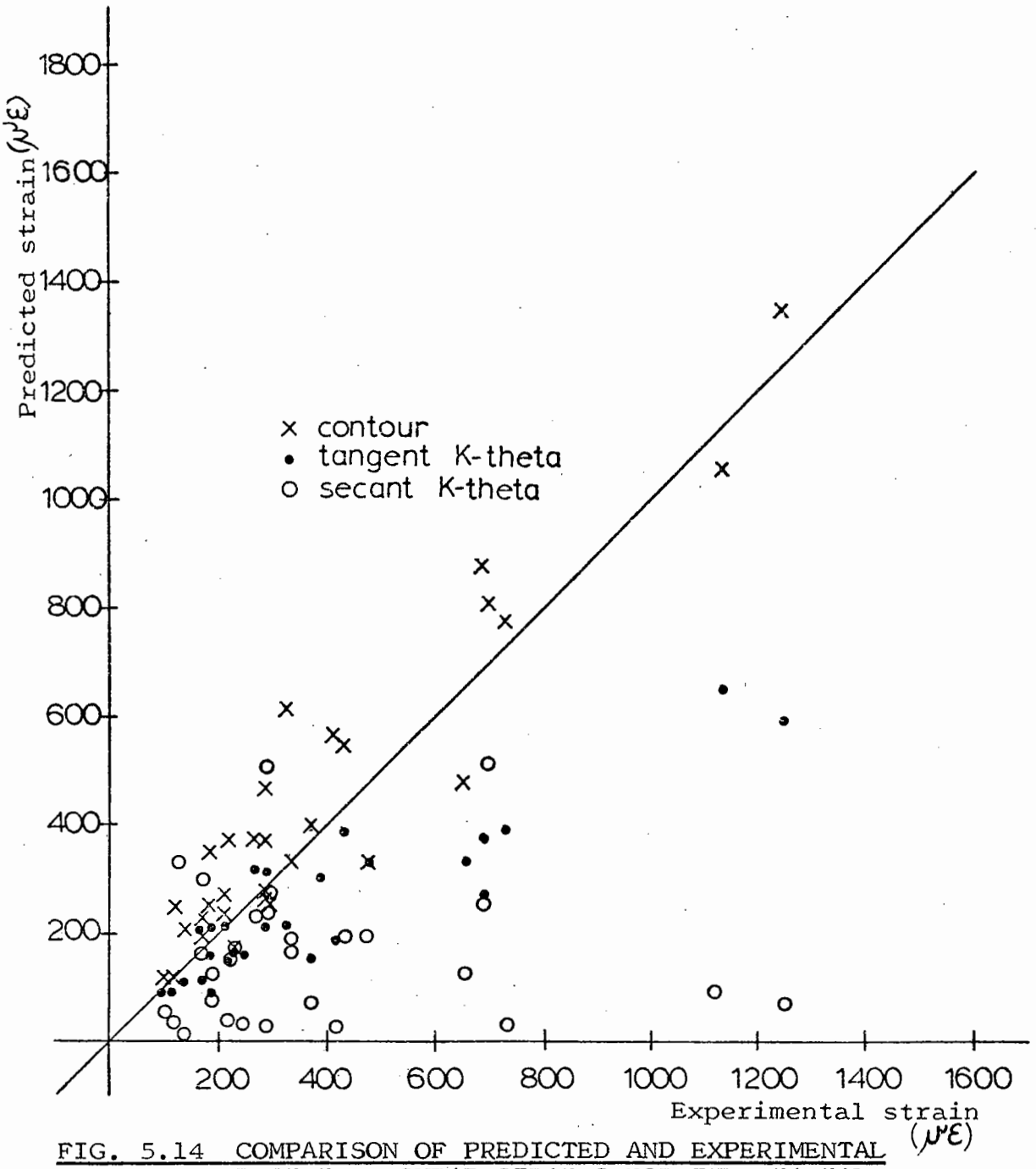

FIG. 5.14 COMPARISON OF PREDICTED AND EXPERIMENTAL RESILIENT SHEAR STRAINS FOR THE BIAXIAL TEST RESULTS

5.4.2 K-theta Model - Secant Modulus

The secant approach described in Section 5.3.2 was then applied to the biaxial test results. A modulus value for each end of the stress path was determined and the corresponding strain state calculated. For point 1:

$$M_{R_1} = K_1(\sigma_{x1} + \sigma_{y1} + \sigma_{z1})^{K_2} \tag{5.25}$$

and

$$\varepsilon_{x1} = \left[\sigma_{x1} - \nu(\sigma_{y1}+\sigma_{z1})\right]/K_1(\sigma x_1 + \sigma_{y1} + \sigma_{z1})^{K_2} \tag{5.26}$$

$$\varepsilon_{y1} = \left[\sigma_{y1} - \nu(\sigma_{x1}+\sigma_{z1})\right]/K_1(\sigma_{x1} + \sigma_{y1} + \sigma_{z1})^{K_2} \tag{5.27}$$

where $\nu = 0.32$ and M_R, K_1, K_2, ε_x and ε_y are as previously defined.

The shear strain ε_1 and volumetric strain v_1 at point 1 were obtained from:

$$\varepsilon_1 = \frac{\sqrt{2}}{3}\left[\varepsilon_{x1}^2 + \varepsilon_{y1}^2 + (\varepsilon_{y1}-\varepsilon_{x1})^2\right]^{\frac{1}{2}} \tag{5.28}$$

$$v_1 = \varepsilon_{y1} + \varepsilon_{x1} \tag{5.29}$$

For point 2, the modulus is given by:

$$M_{R_2} = K_1(\sigma_{x2} + \sigma_{y2} + \sigma_{z2})^{K_2} \tag{5.30}$$

and using a similar procedure, the shear strain ε_2 and volumetric strain v_2 at point 2 may be determined.

The resilient shear strain ε_r and resilient volumetric strain v_r were obtained from Equations 5.16 and 5.17. Figs 5.13 and 5.14 show comparisons of predicted and experimental strains using the secant approach. Contrary to the triaxial situation, the secant model was found to be less accurate when predicting shear strains than the tangent model. Triaxial resilient volumetric strains were consistently underpredicted by about 300%

for both the single size and graded materials. However, this trend was not apparent in the biaxial results. Full results are presented in Appendix 5D.

5.4.3 Comparison of K-theta Model for Triaxial and Biaxial Results

Generally the K-theta model is less accurate for biaxial conditions. However, it must be noted that measurements of strain in the biaxial shear box showed considerable scatter. These inaccuracies were reflected in the comparisons of predicted and experimental strains as obtained using the contour model (Chapter 3). Any considerations of the merits of the K-theta model should therefore be confined to the triaxial results where stresses and strains were accurately controlled and measured.

5.5 DISCUSSION

The K-theta model has been shown to predict resilient shear strains quite accurately, but is totally inadequate when applied to volumetric strain. It can be argued that the resilient modulus M_R is essentially a shear modulus and therefore one would not expect accurate predictions of volumetric strain. The limited testing required to determine the model and the fact that it can be applied generally to all stress conditions make the K-theta approach very attractive. However, Chapter 7 contains details of comparisons between the contour and K-theta models when used to compute the response of the granular layer in a pavement structure using finite element analysis. The K-theta model is shown to be inadequate when predicting stresses in the granular layer.

CHAPTER SIX

THE SIMPLE SHEAR APPARATUS

6.1 INTRODUCTION

A simple shear apparatus was developed by Ansell (1977) at the University of Nottingham. A description of the original equipment along with a detailed account of modifications to enable end and lateral stresses to be measured on the specimen is given. Additional loading facilities are described to cycle applied vertical and shear loads.

The chapter is divided into three sections. Section A describes the original equipment and gives details of recent modifications. Section B describes the stress behaviour of 3 mm and 1.5 mm single size crushed limestone specimens and also includes predictions of the stress state around the specimen using a method developed at Cambridge (Wood, Drescher and Budhu, 1979). An attempt to express simple shear stress paths in terms of the stress invariants p and q is also presented. Section C contains details of the strain behaviour of the two materials and compares results with those obtained by Ansell.

SECTION A - APPARATUS DEVELOPMENT

6A.1 REVIEW OF EXISTING APPARATUS

Schematic diagrams of the Mk2 simple shear apparatus (Ansell 1977) are shown in Figs 6.1 and 6.2. The specimen space was 210 x 140 x 30 mm deep. The end plates of the box were pivoted and designed to accommodate 36% shear strain either side of the central position. The top platen of the shear box contained three contact stress transducers measuring normal stress. Each was mounted on a separate crosshead carrying linear bearings which engaged with hardened steel rods on the main frame of the box. Each crosshead could move independently but provision was made to

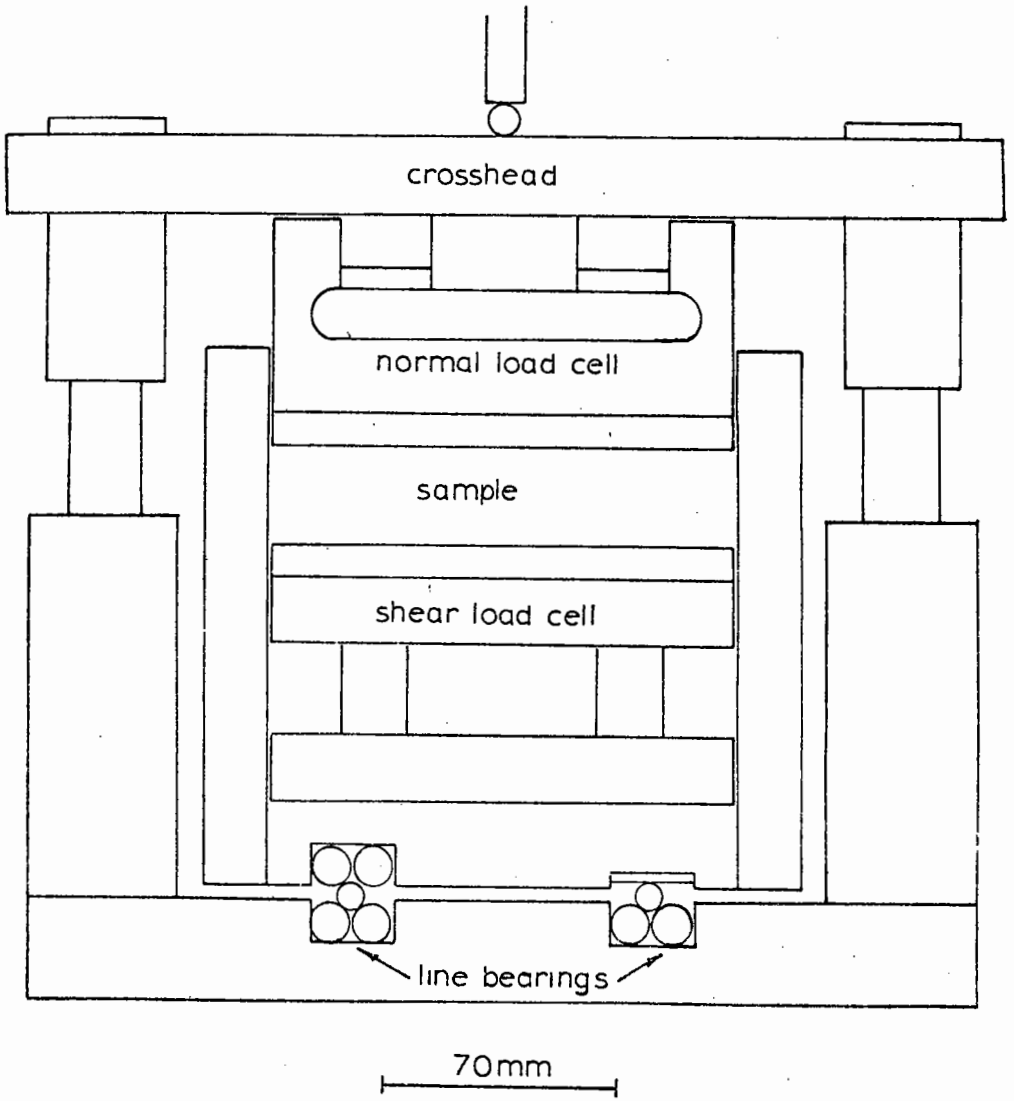

FIG. 6.1 SCHEMATIC TRANSVERSE SECTION OF THE SIMPLE SHEAR APPARATUS

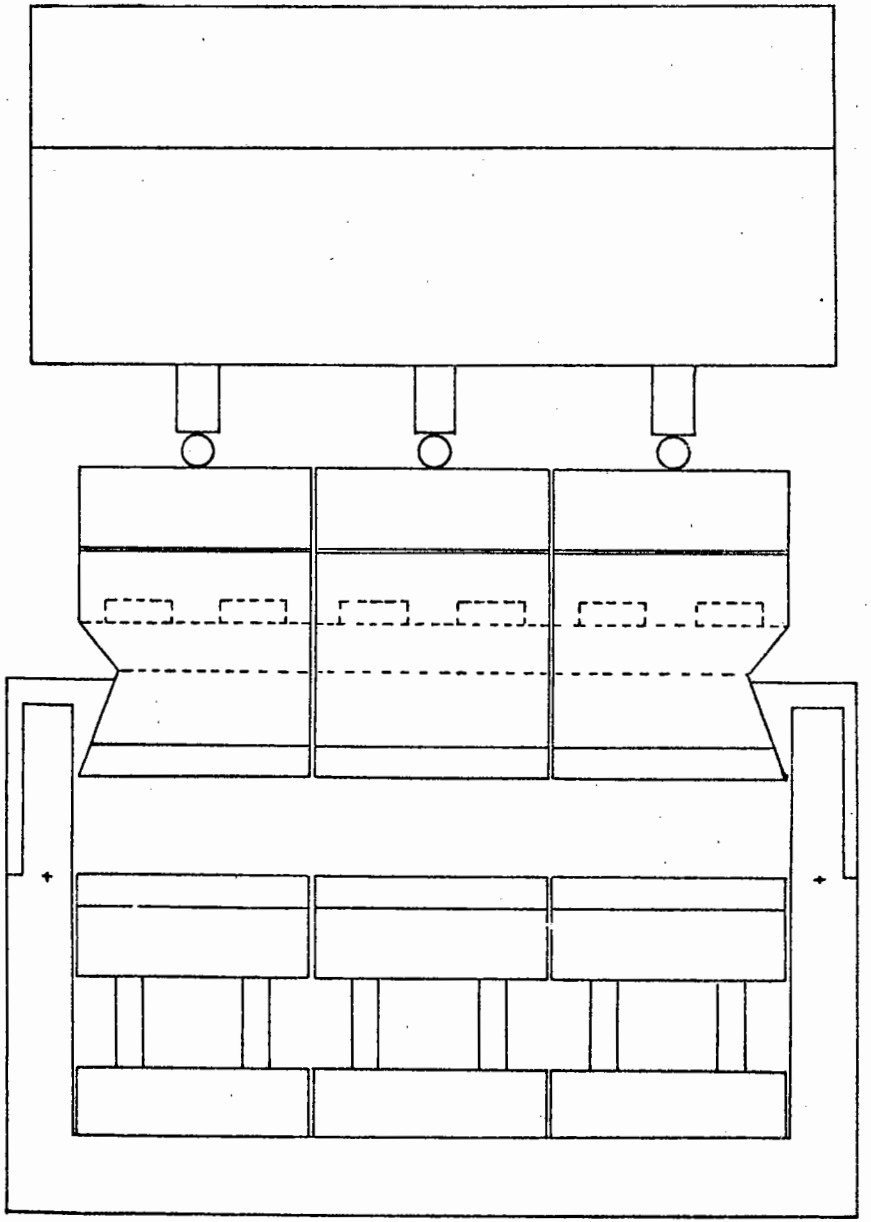

FIG. 6.2 SCHEMATIC LONGITUDINAL SECTION OF THE SIMPLE SHEAR APPARATUS

bolt all three together for sample preparation. The top platen was split into three parts to allow differential dilation of the specimen to occur when failure conditions were approached near the ends. This allowed accurate measurement of stresses over the central portion of the specimen. The base of the box contained three contact stress transducers measuring shear stress. To provide a good interface between the transducer loading plates and the specimen, each load plate had a layer of the test material fixed to it by Araldite.

The shear loads were provided by a single acting air ram at each end of the apparatus. The normal loads were provided by three loading rams operated from a common regulated air pressure line. All of the rams incorporated Bellofram rolling diaphragms and the loading rods were carried by linear bearings to reduce frictional losses. The loading frame of the Mk2 apparatus was made up of rolled steel channel sections and the cross member carrying the vertical loading rams was removable.

Sample deformations were monitored using four LVDTs. Horizontal movement of the lower half of the shear box was measured using a ±12 mm linear range LVDT with the core extension lightly spring-loaded against the shear box. The LVDT was supported by a clamp fixed to the main frame. The vertical movement of the crossheads was measured using three ±5 mm linear range LVDTs mounted in a clamp supported by pillars fitted to the side of the main frame.

There were 10 output signals from the assembled apparatus: 3 from the normal load cells, 3 from the shear load cells, 3 from the vertical LVDTs and 1 from the horizontal LVDT. Permanent records of any four outputs could be obtained using two Bryans Southern, Series 2800, two-pen flatbed chart recorders. Generally, these were used to monitor the outputs from the central normal and shear load cells, the central vertical

LVDT and the horizontal LVDT. Two Solartron A220 digital voltmeters (DVM) connected to a two gang, multi-channel selector switch enabled any required voltage to be monitored by simply selecting the relevant channel and the appropriate range on the DVM.

The general arrangement of the compressed air control equipment is shown in Fig. 6.3. A supply pressure of up to 350 lbf/in^2 was available. Fairchild Kendall Model 10 precision regulators were used throughout the equipment. Asco type 8321 NC solenoid valves actuated by an electronic timing switch controlled the flow of air to the shear rams. No provision had been made for cycling the vertical load. The loading waveforms produced by the control equipment are shown in Fig. 6.4. Waveform (a) corresponds to the unidirectional repeated load tests and waveform (b) to bidirectional repeated load tests.

6A.2 MATERIAL AND SPECIMEN PREPARATION

The material previously tested at Nottingham was the single size crushed limestone described in Chapter 3 and used for the triaxial and biaxial testing programmes. The same material was used in the simple shear apparatus to provide some continuity with the previous work, although as Section B describes, problems were later encountered when attempting to measure lateral stress.

The shear box with the end plates locked in the vertical position and minus the top platen was clamped to the vibrating table. A soft 3 mm diameter PVC sleeving was inserted along the lower edge of each end plate to prevent particles from being trapped by the movement of the end plates. A known weight of material was scooped into the box and the surface levelled. The top platen with the three independent sections locked together was then placed in position and the specimen compacted using 4 cycles of the vibration amplitude. This produced an average

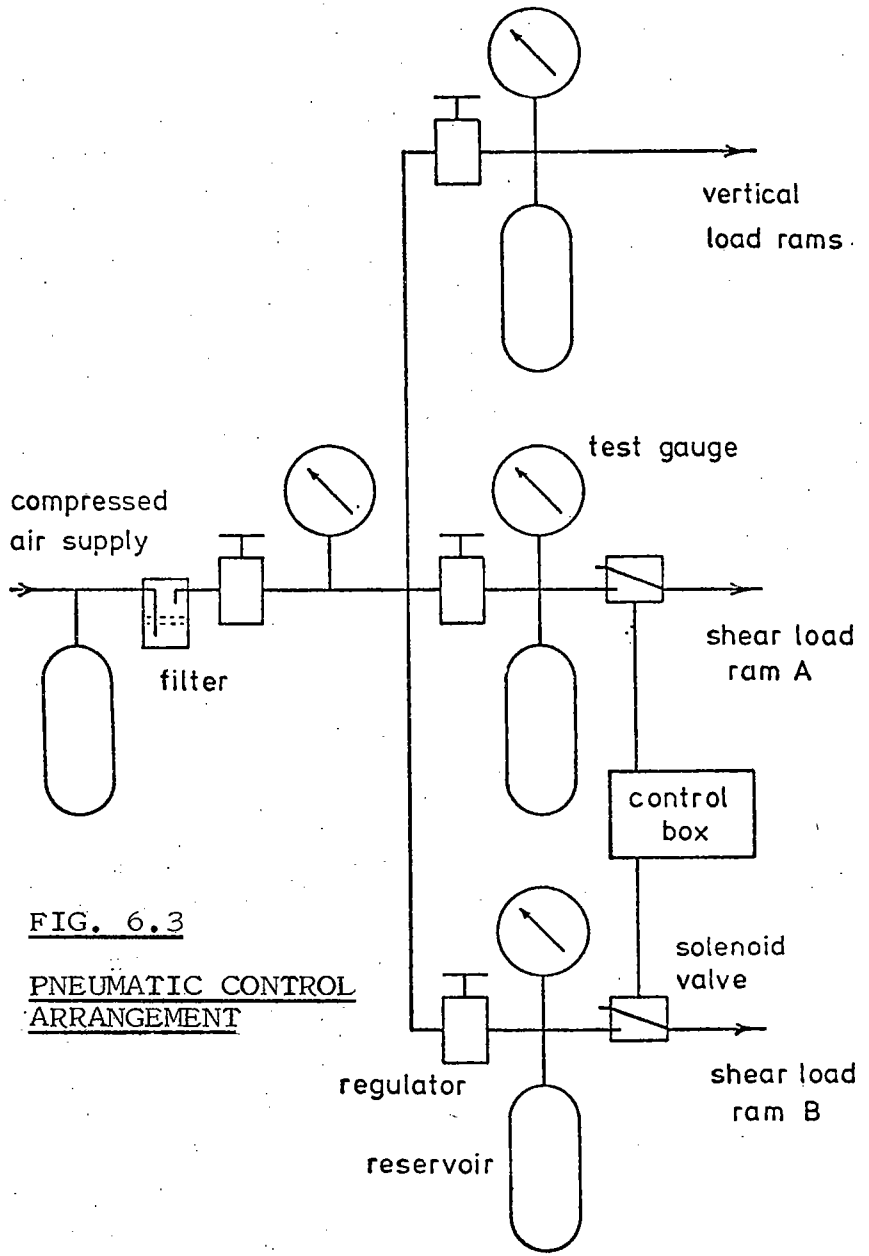

FIG. 6.3

PNEUMATIC CONTROL ARRANGEMENT

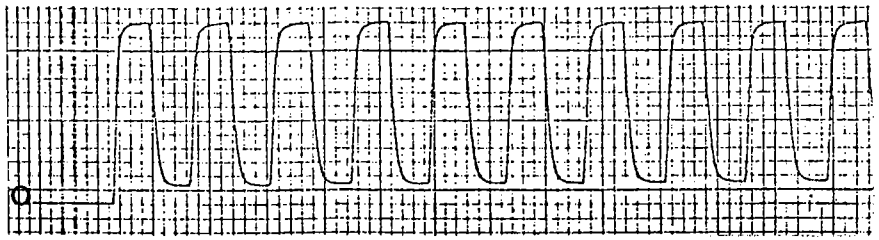

(a) Waveform for unidirectional load

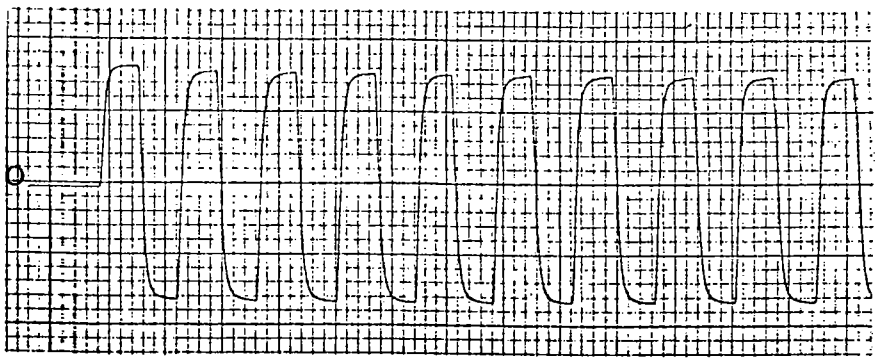

(b) Waveform for bidirectional load

FIG. 6.4 WAVEFORMS FOR REPEATED LOAD TESTS

specimen density of 1.62 Mg/m^3. The shear box was then transferred to the main loading frame and the LVDTs and vertical loading rams clamped into position. Initial specimen depth was measured using a vernier and a fixed reference point. Preliminary testing with various quantities of material enabled the distance of the reference point from the base of the specimen to be established.

6A.3 PRELIMINARY TEST PROGRAMME

6A.3.1 Definition of Parameters

It is necessary to define the various parameters used to describe the test conditions and associated response of the material. The same parameters as chosen by Ansell were used in order to facilitate comparisons of results. Fig. 6.5(a) shows a generalised shear stress pulse and Fig. 6.5(b) shows a shear deformation response to this loading. The waveforms in each case have been idealised.

Mean shear stress	$= \tau_m$
Cyclic shear stress	$= \tau_c$
Repeated shear stress	$= \tau_r$
Mean shear stress ratio, R_m	$= \tau_m/\sigma$
Cyclic shear stress ratio, R_c	$= \tau_c/\sigma$
Applied normal stress	$= \sigma_v$
Permanent shear strain	$= \gamma_p$
Resilient shear strain	$= \gamma_r$
Permanent volumetric strain	$= v_p$
Resilient volumetric strain	$= v_r$
Shear modulus, G	$= \tau_r/\gamma_r$
Cyclic shear stress ratio at cycle N, $R_c(N)$	$= \frac{\tau_c(N)}{\sigma_v(N)}$

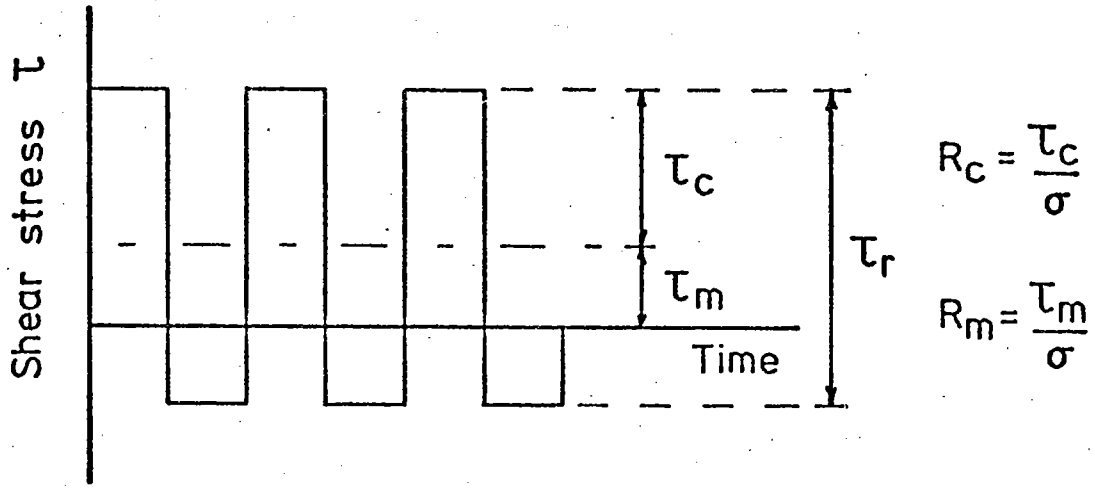

(a) Idealised repeated load waveform

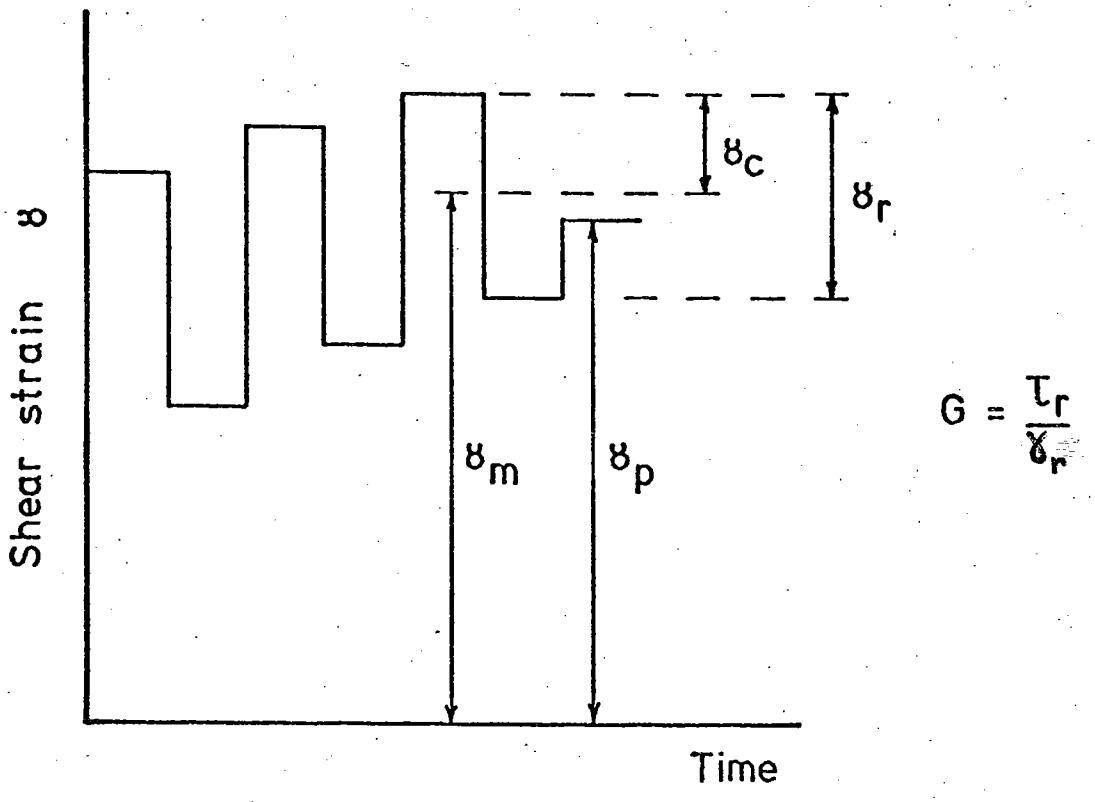

(b) Idealised response to (a)

FIG. 6.5 IDEALISED WAVEFORMS

Ansell observed that the cyclic shear stress ratio tended to decrease throughout a test. Correlating cyclic shear stress ratio and permanent shear strain at several points indicated that the cyclic shear stress ratio at cycle 10, $R_c(10)$, could be used as a representative value and this was adopted for all the repeated load tests.

Resilient shear strain γ_r was defined as the peak to peak shear strain and for unidirectional loading this is the correct definition. For bidirectional loading, however, the material is being loaded in two directions and a definition of resilient shear strain is not apparent. Ansell used the peak to peak shear strain for both bidirectional and unidirectional loading and on comparing results found the definitions to be compatible. In order that no confusion should arise when comparing results of the present test series with those obtained previously, the same definition has been used and the shear strain produced in bidirectional loading has been called resilient shear strain.

The question of correlating results from the simple shear apparatus with those from triaxial and biaxial equipment remains unsolved. Some doubt is expressed as to the validity of comparing two situations having entirely different boundary conditions and loading regimes. Although principal stresses may be calculated for the simple shear apparatus, it is difficult to obtain any correlation between shear strain defined as rotation of the end plates in the simple shear apparatus and shear strain as obtained from principal strains in the triaxial apparatus.

6A.3.2 Repeating Original Tests

A number of the tests conducted by Ansell were repeated as a preliminary investigation to ensure that the specimen preparation and test procedures were being performed correctly. The test conditions are

presented in Table 6.1. They involved unidirectional and bi-directional modes of testing. A comparison between the results that were obtained and those of Ansell are presented in Figs 6.6 to 6.11. Full test details are given in Appendix 6A.

The results did not correspond exactly to those of Ansell but the general trend was similar. Ansell does not make reference to the repeatability of results in the simple shear test and it was therefore decided to carry out a repeatability study.

6A.3.3 Repeatability Series

The series R tests were all unidirectional. An attempt was made to produce identical stress conditions over the central third by applying 600 kPa air pressure to the shear rams and 1000 kPa air pressure to the normal rams in each test. The resulting stresses over the central third at cycle 10 are presented in Table 6.2. As can be seen, the cyclic shear stress ratio at cycle 10, $R_c(10)$, varied for each test. This may have been due to different packing arrangements of particles for each sample during compaction or differing degrees of contact between the loading plates and the sample boundaries. The cyclic shear stress ratios varied from 0.31 to 0.37. Typical test results are compared in Figs 6.12 and 6.13. It should be noted that although tests having almost identical $R_c(10)$ value are compared, the normal stress applied to the sample is often slightly different. Research by Silver and Seed (1971) and Youd (1972) would seem to suggest that minor changes in normal loading have no significant effect on test results. However, the series R tests did not produce enough data to verify these findings.

The test results were not exactly repeatable and the difference between results for the preliminary testing programme (Section 6A.3.2)

TABLE 6.1 - REPEATING ORIGINAL TESTS

UNIDIRECTIONAL TEST SERIES A

Test No.	σ_v	τ	$R_c(10)$	ρ (Mg/m^3)
A100	83.03	32.75	0.19	1.63
A102	86.38	43.05	0.25	1.53
A103	92.29	66.44	0.36	1.62
A104	93.63	36.49	0.19	1.61
A105	185.26	117.91	0.32	1.62
A106	183.92	96.38	0.26	1.62

BIDIRECTIONAL TEST SERIES B

Test No.	σ_v	τ	$R_c(10)$	ρ (Mg/m^3)
B100	92.29	54.27	0.29	1.58
B101	92.96	122.58	0.66	1.64
B102	187.26	277.93	0.74	1.62
B103	185.93	150.66	0.41	1.61

ρ = compacted density

FIG. 6.6 SERIES A

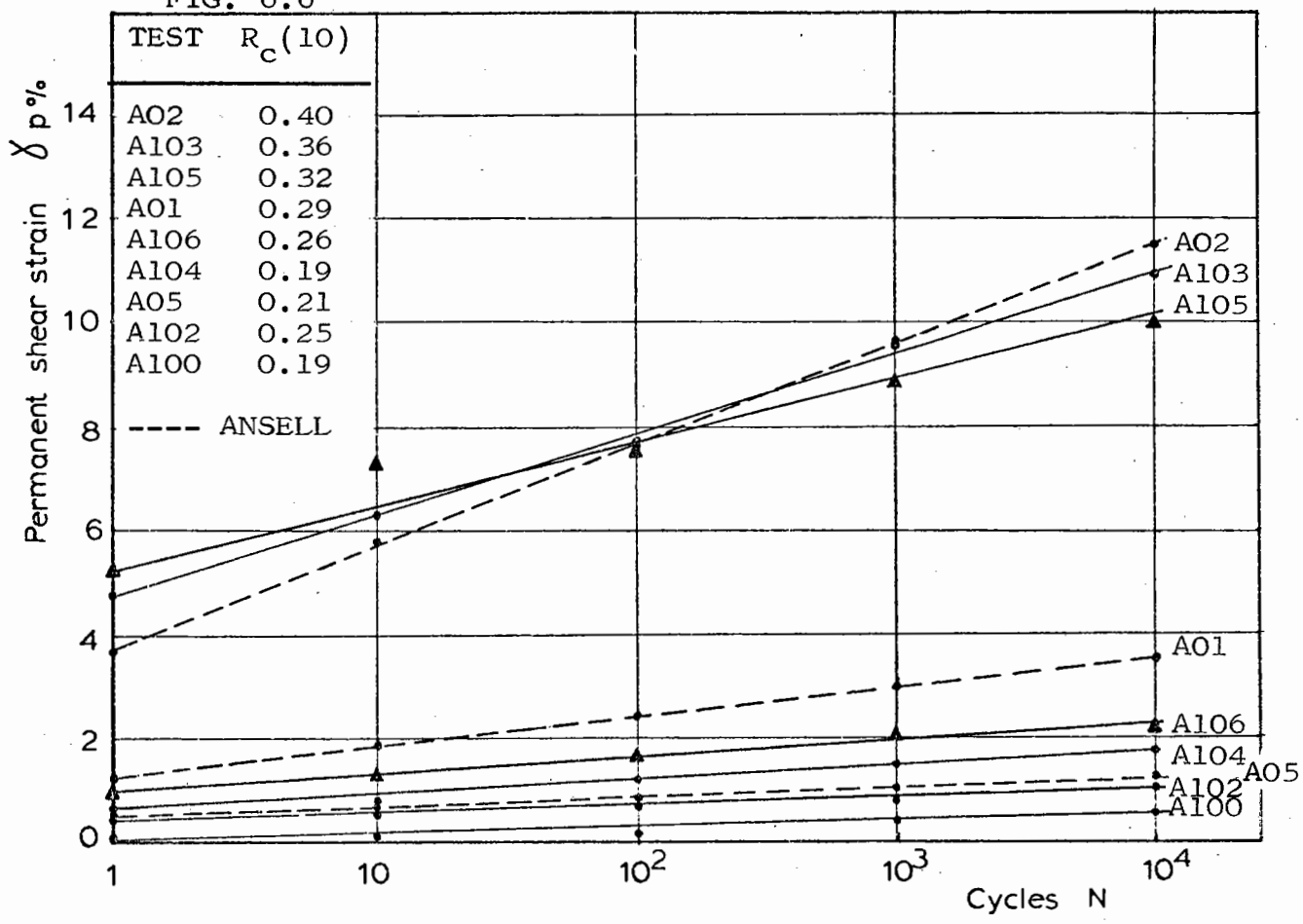

PRELIMINARY TEST SERIES

FIG. 6.7 SERIES A

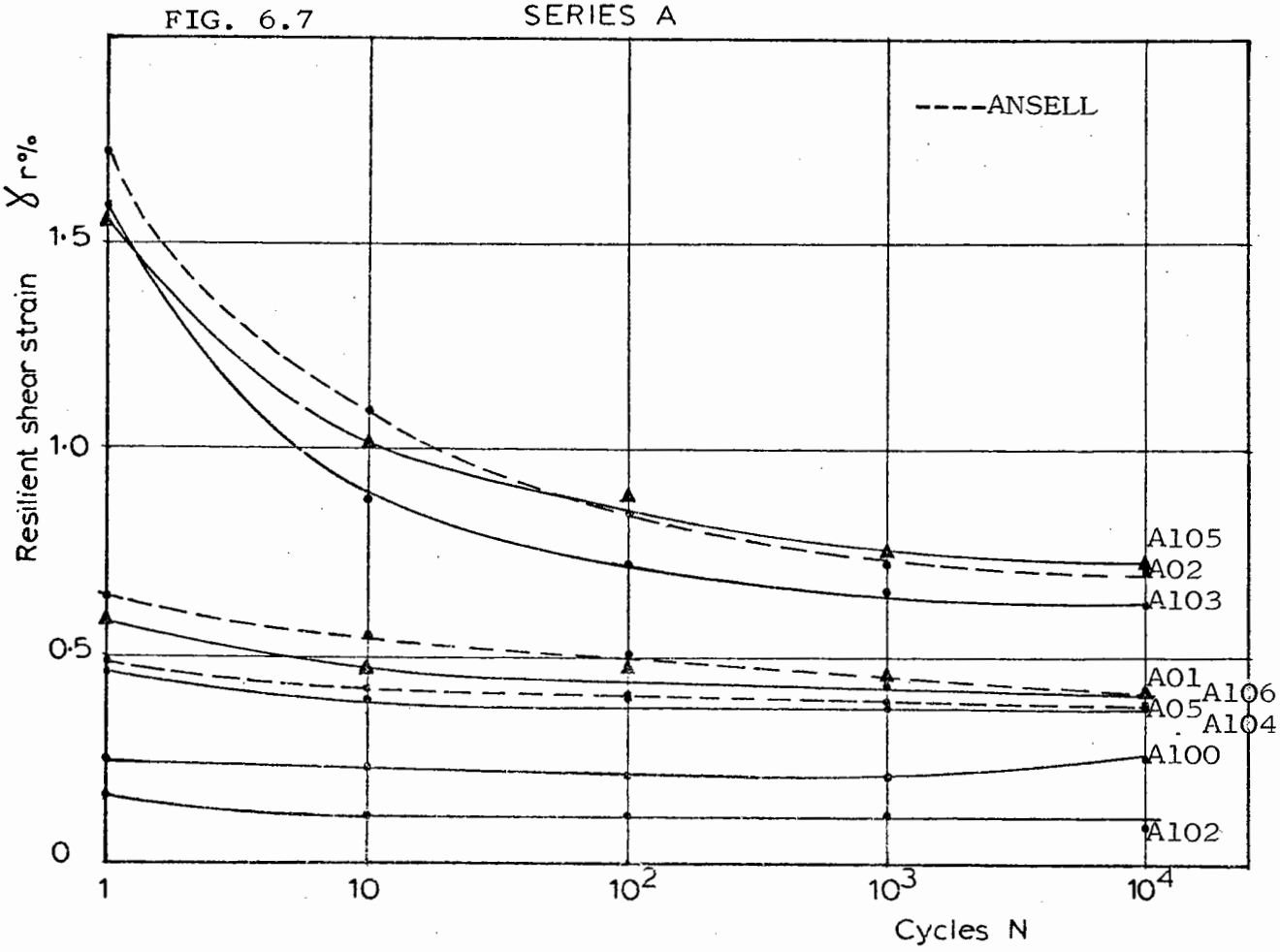

FIG. 6.8

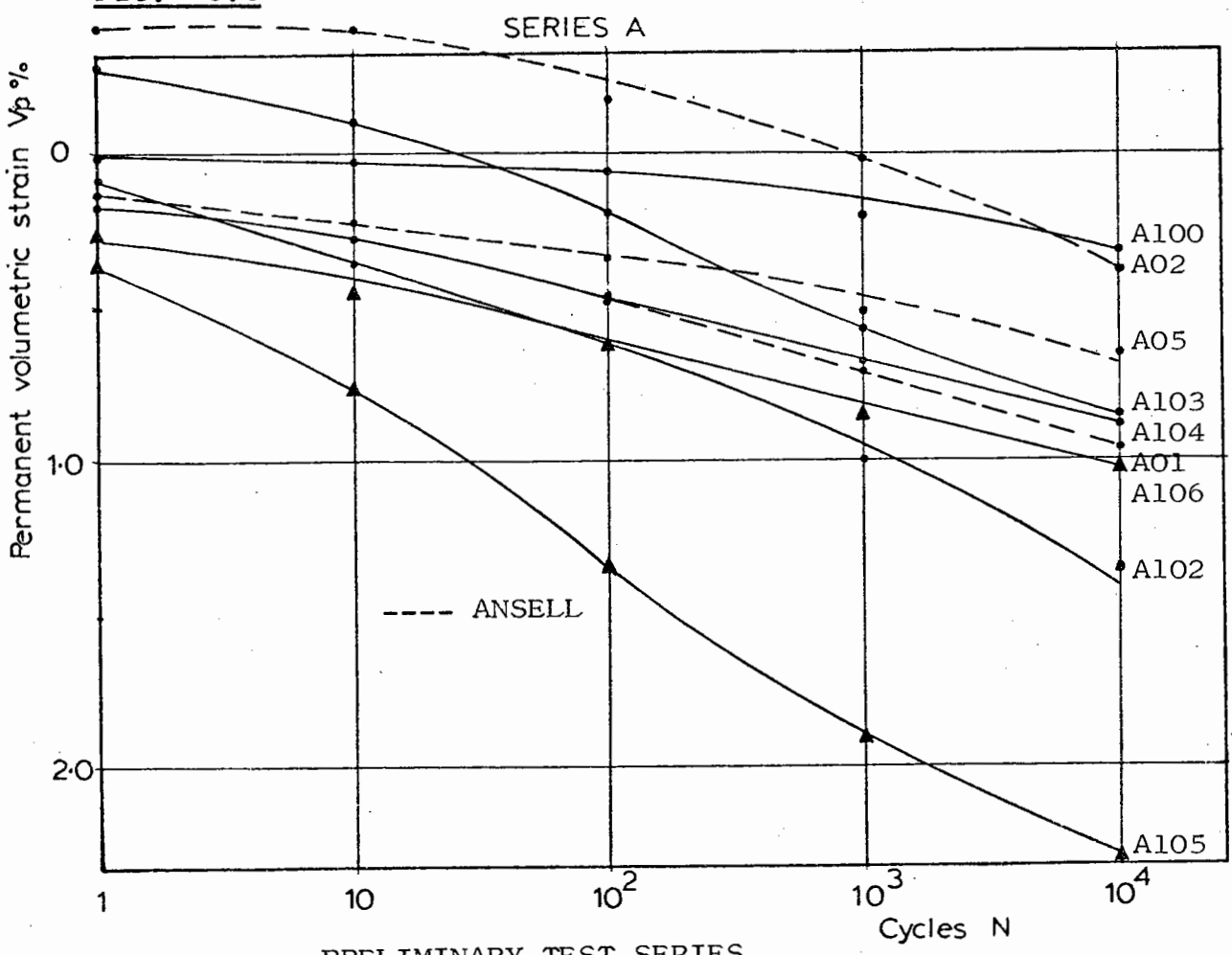

PRELIMINARY TEST SERIES

FIG. 6.9

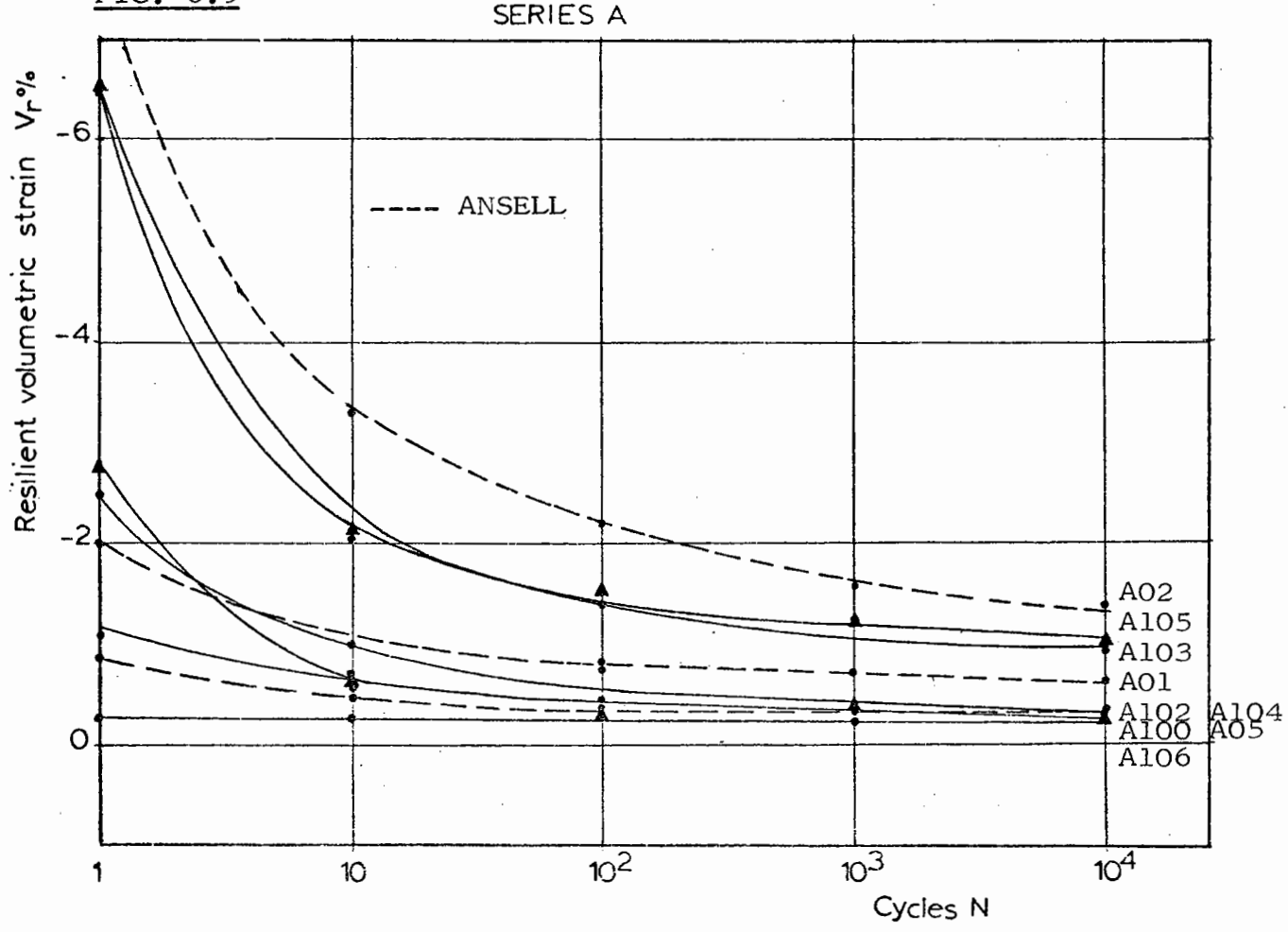

FIG. 6.10 SERIES B

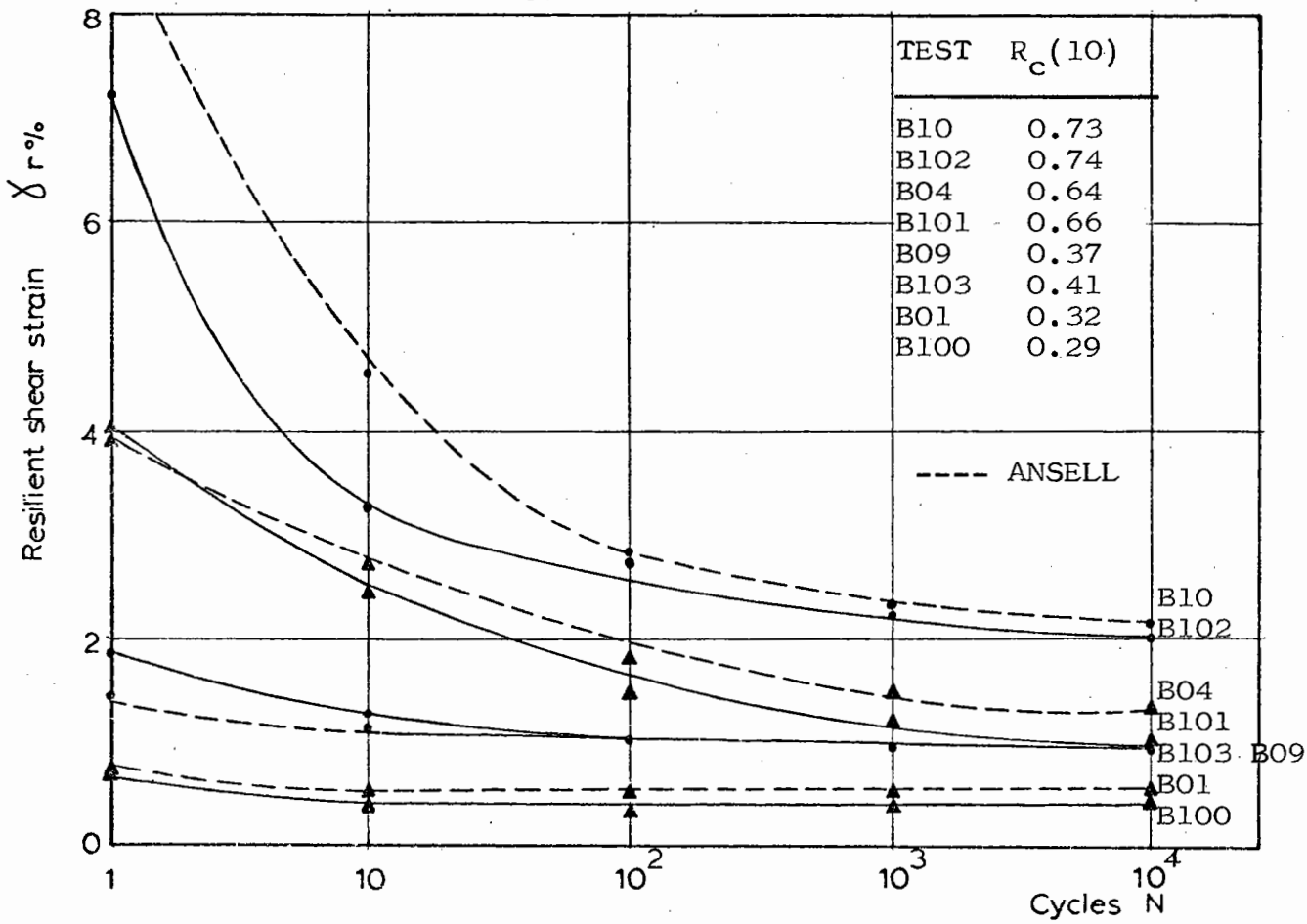

PRELIMINARY TEST SERIES

FIG. 6.11 SERIES B

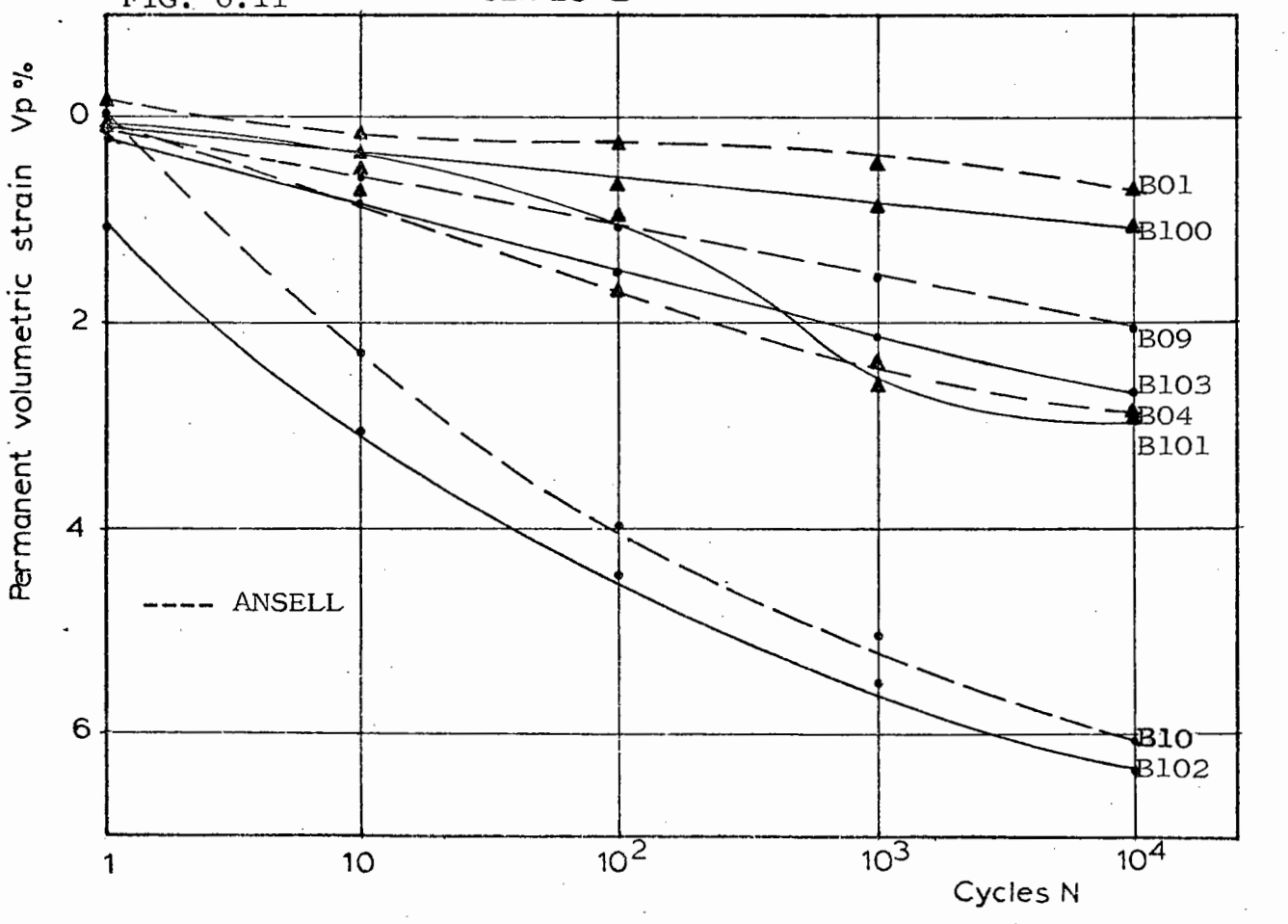

TABLE 6.2 TEST RESULTS FOR REPEATABILITY SERIES R

Test No.	σ_v	τ	$R_c(10)$	ρ (M_g/m^3)
R1	187.93	126.33	0.34	1.62
R2	189.27	142.24	0.37	1.61
R3	190.61	125.40	0.33	1.62
R4	137.56	181.25	0.37	1.61
R5	181.25	126.33	0.35	1 62
R6	187.26	122.59	0.33	1.62
R7	189.27	131.95	0.35	1.61
R8	187.93	134.75	0.36	1.60
R9	116.97	187.49	0.31	1.62
R10	128.20	181.46	0.35	1.62

ρ = compacted density

FIG. 6.12 (a) SERIES R

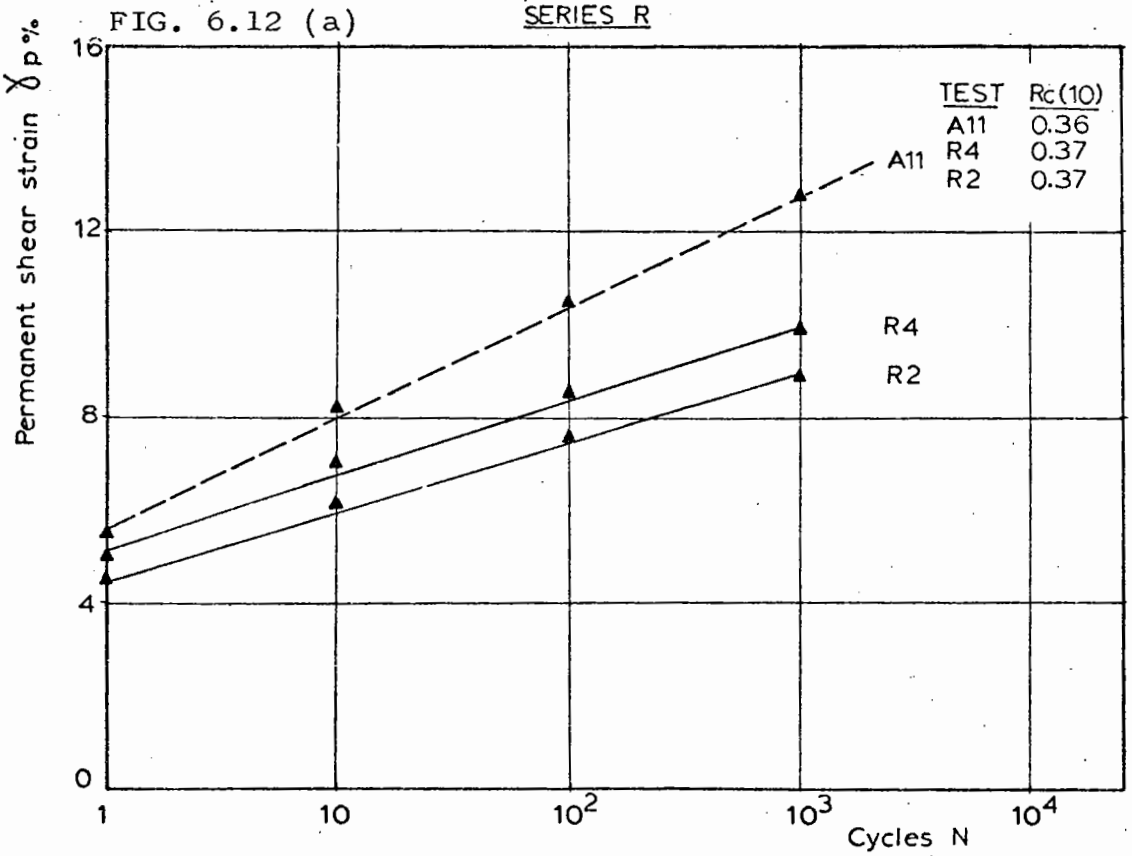

FIG. 6.12 (b) SERIES R

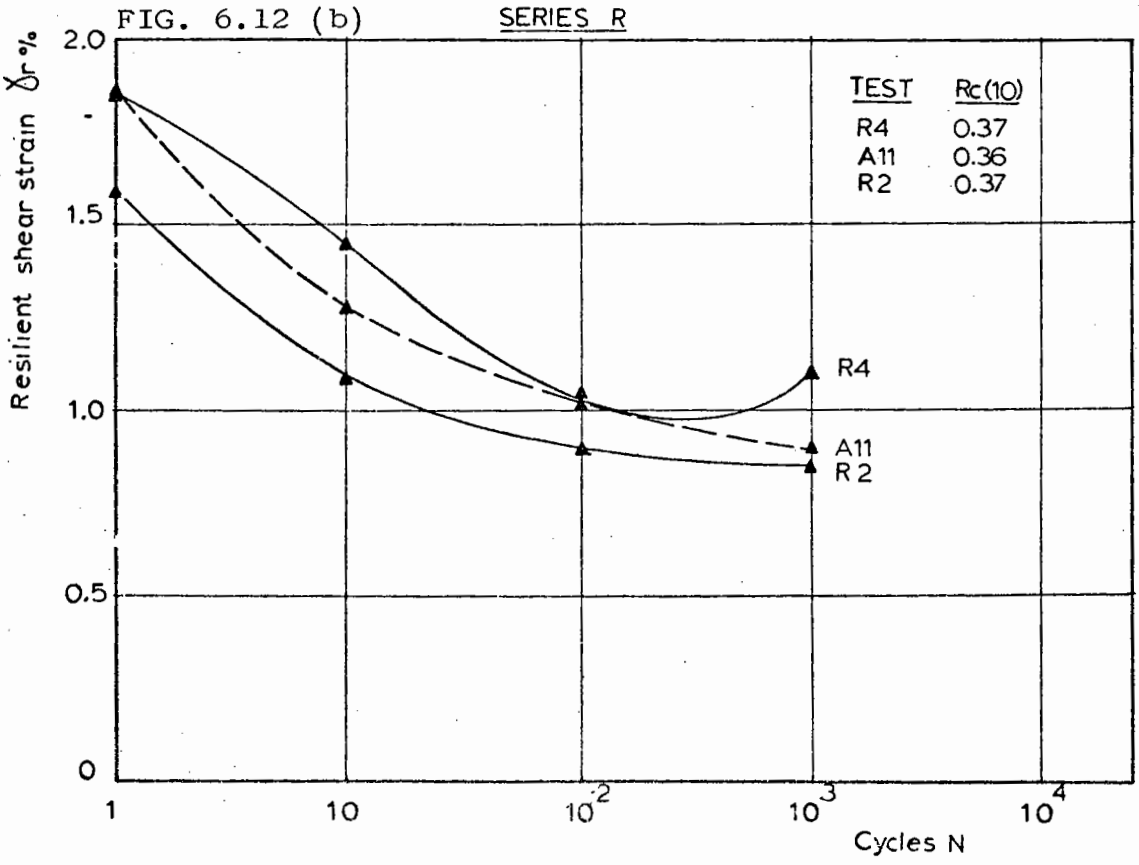

TYPICAL RESULTS FROM REPEATABILITY SERIES

FIG. 6.13 (a)

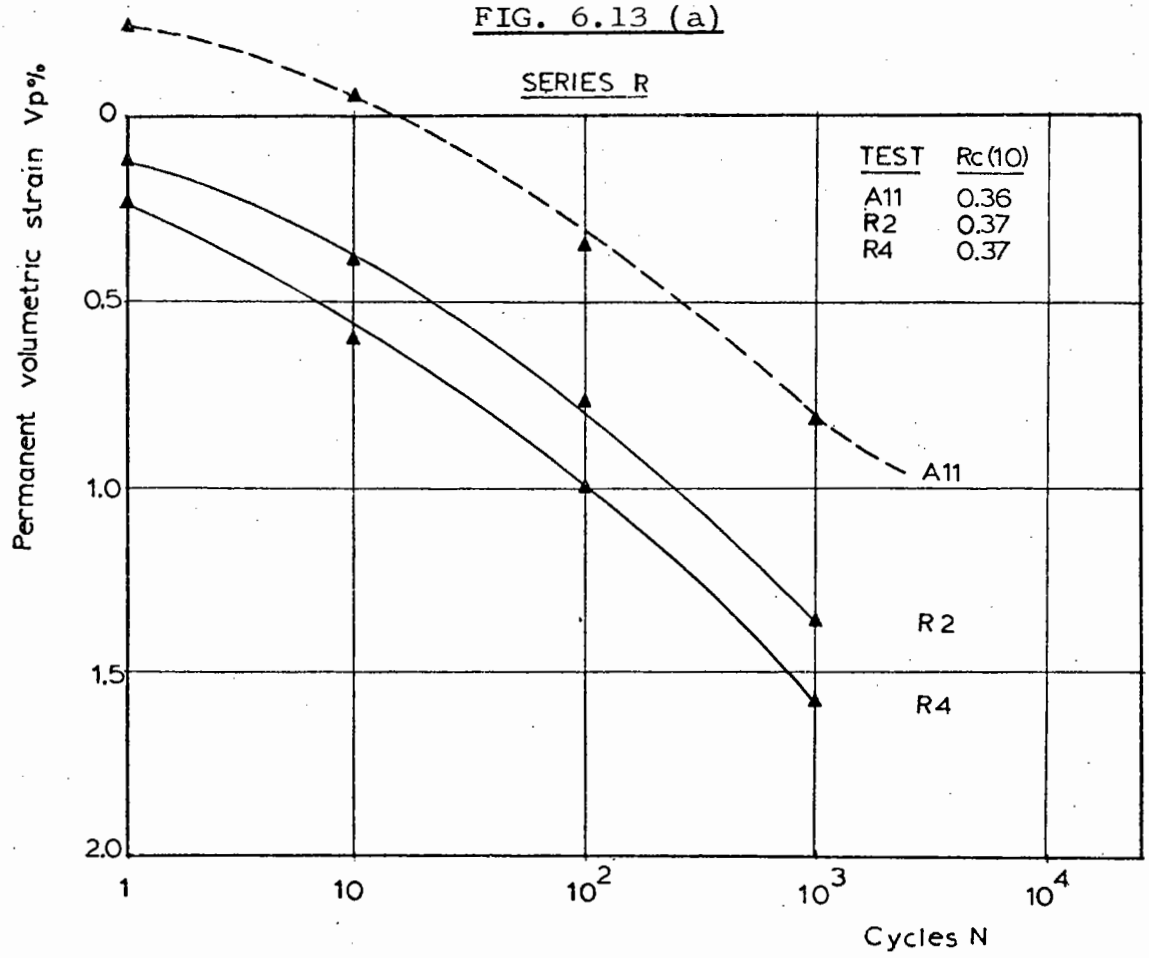

FIG. 6.13 (b)

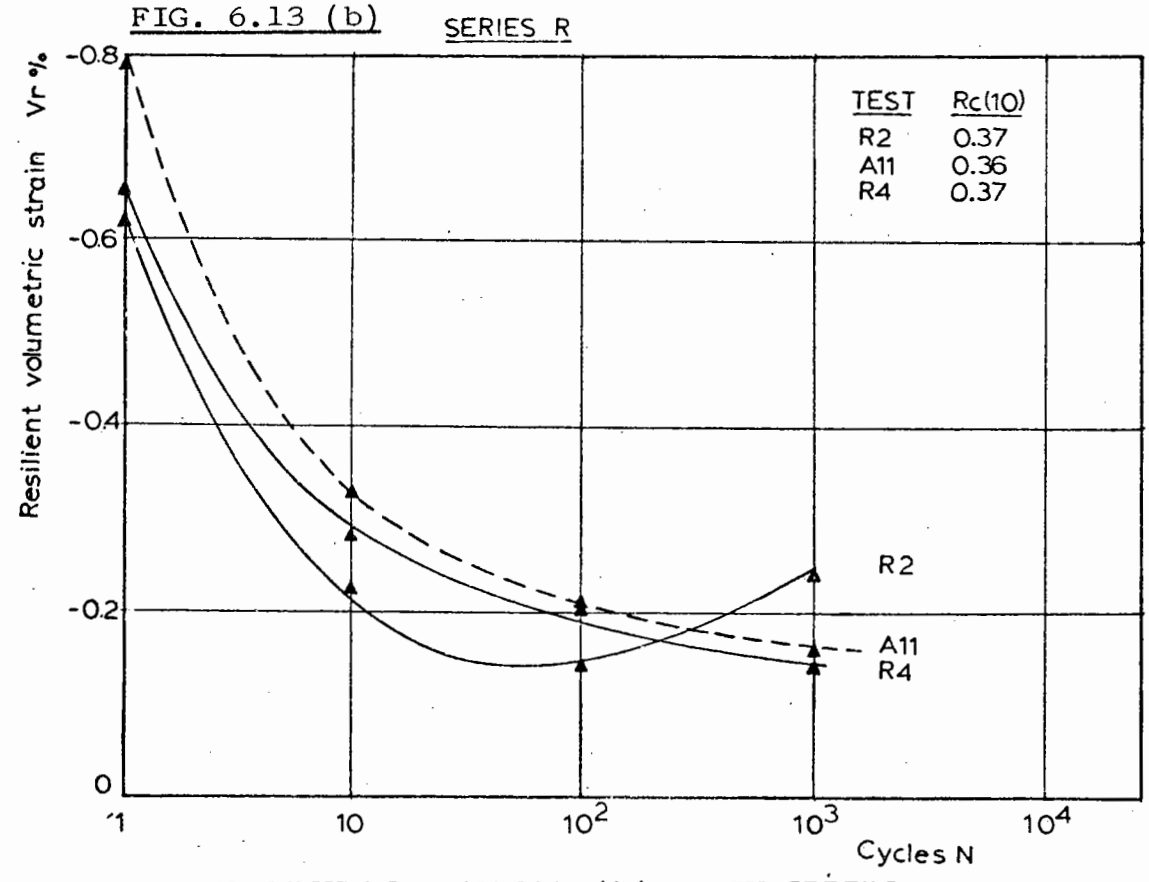

TYPICAL RESULTS FROM REPEATABILITY SERIES

and those obtained by Ansell fell within the range of scatter for any one test. Full details of the test results are presented in Appendix 6B.

There was considerable variation in the strains produced at cycle 1 for similar stress paths; however, the procedure described in Chapters 3 and 4 may be used and comparisons made of strain rates rather than absolute strain values.

6A.4 MODIFICATIONS TO THE APPARATUS

6A.4.1 Cycled Vertical Load

The stress conditions beneath a rolling wheel load are presented in Fig. 6.14. The Mk2 apparatus, as designed by Ansell, produced shear stress reversal but the normal stress, σ_v, was constant. In order to more closely simulate the in situ stress conditions, it was necessary to incorporate a cyclic normal load into the system. The nature of the response of the material to different cyclic shear stress ratios required the phasing of the normal and shear stress pulses to be such that the shear stress did not build up ahead of the normal stress causing very large shear deformations to occur.

The stresses under a rolling wheel load are approximately sinusoidal. This type of waveform could have been produced using a servo-hydraulic loading system and phasing of the normal and shear pulses would have been considerably easier. However, such a system is much more expensive. Fig. 6.14 shows that normal stress and shear stress increase and decrease simultaneously. The use of compressed air in the simple shear apparatus produces a saw-tooth waveform and to increase normal and shear stress together, while retaining control over the application, would have required an extremely long cycle time. It was decided that if cycle times were to be kept to a reasonable length, the normal stress and shear stress would have to be applied independently of each other. Two waveforms

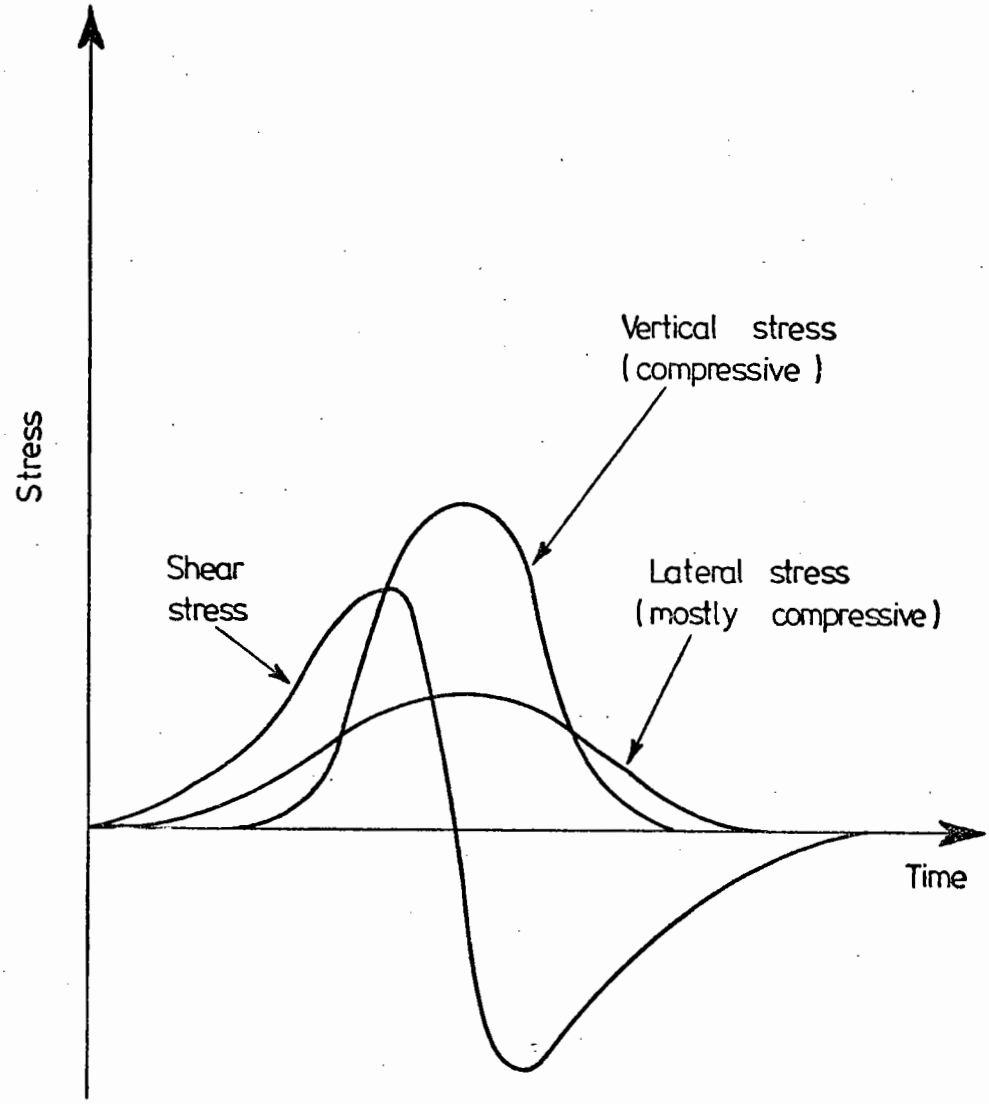

FIG. 6.14 STRESS CONDITIONS BENEATH ROLLING WHEEL LOAD

were considered as shown in Fig. 6.15. The timing mechanism was modified and another solenoid valve incorporated in the system to facilitate cyclic normal loading. Initially, the waveform was of type A. The "on" time of each pulse was variable as was the "off" time. In observing the in situ waveform in Fig. 6.14, it can be seen that the normal stress remains at maximum as the shear stress changes direction. Waveform A did not behave in this manner. An attempt was made to produce type B phasing. The electronic timing mechanism needed to be redesigned to accommodate this and was replaced by a series of adjustable cams wired to micro-switches controlling the solenoid valves. This produced waveform B with a cycle time of 5.7 seconds. Facilities were also available to conduct unidirectional tests with cyclic normal load. The normal load could be cycled between a maximum value and zero or between a maximum and minimum value as desired. This was made possible by applying a back pressure to the solenoid valve exhaust. A similar modification made it possible to cycle the shear load between a maximum and minimum value. The resulting stress paths are shown in Fig. 6.16. The modified air controlled system is shown in Fig. 6.17.

6A.4.2 Development of Transducers to Measure the Stress Around the Specimen

The existing apparatus enabled the normal stress on the top of the sample and shear stress on the base of the sample to be measured. To make a satisfactory comparison of triaxial, biaxial and simple shear test results, a knowledge of the principal stresses or stress invariants on the sample is required. To calculate these for the simple shear test, the horizontal normal stresses must be measured.

There were two approaches to the development of lateral load cells. One method was to use the same technique as employed for the measurement

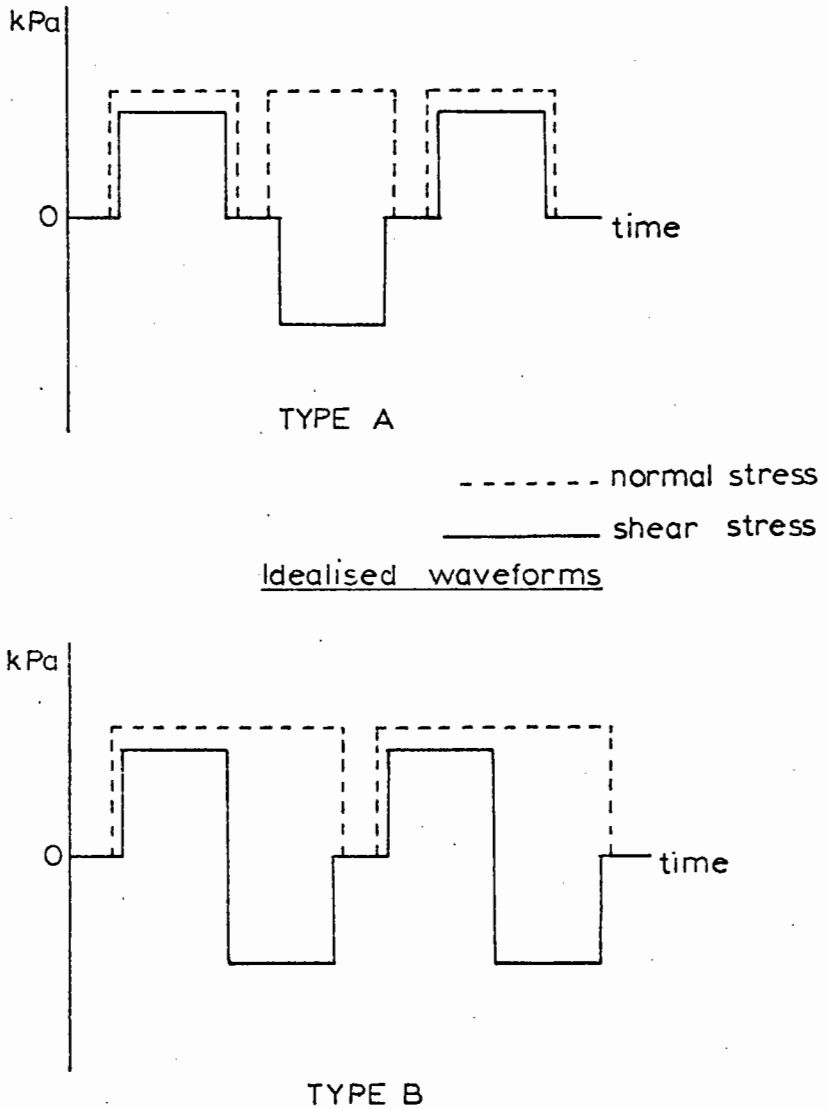

FIG. 6.15 PHASING OF NORMAL AND SHEAR STRESS PULSES

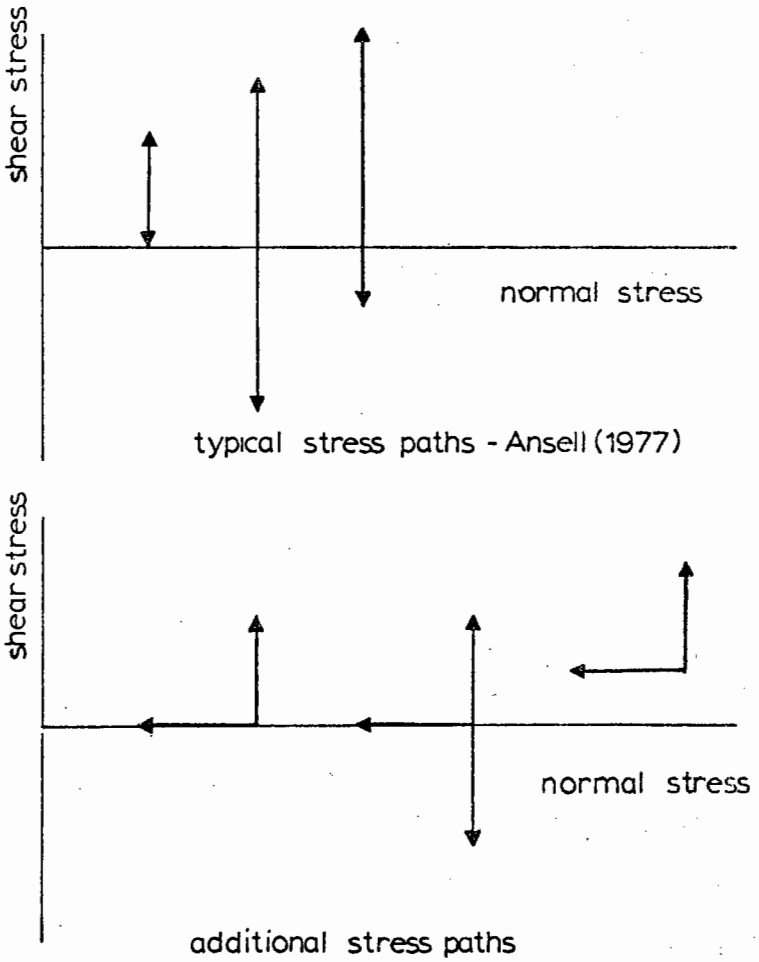

FIG. 6.16 TYPICAL STRESS PATHS FOR REPEATED LOAD TESTS

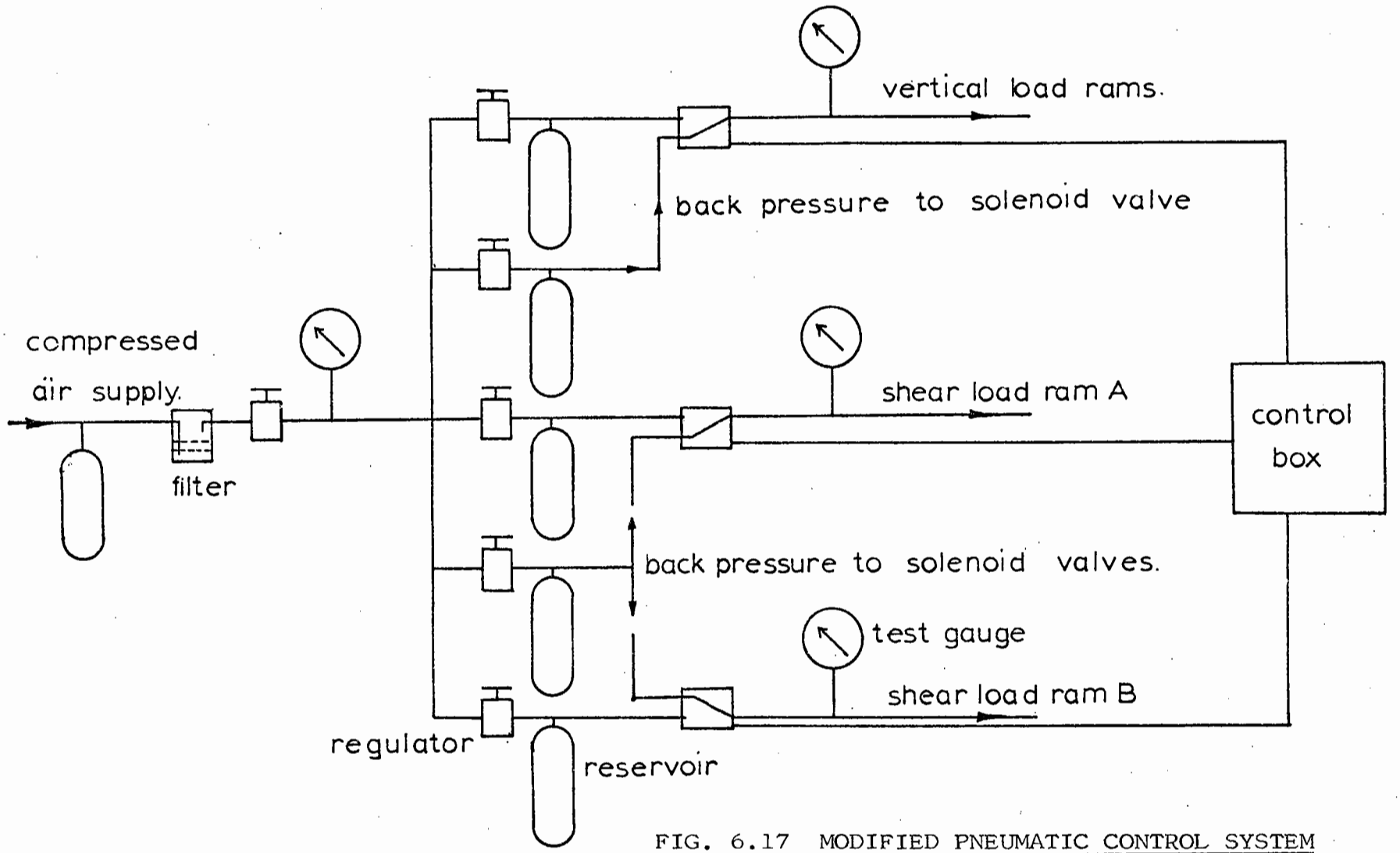

FIG. 6.17 MODIFIED PNEUMATIC CONTROL SYSTEM

of normal and shear stress on the top and bottom of the sample, i.e. design load cells which when stacked together formed the sample boundary. Rigidly mounting these load cells would have been extremely difficult because of the limited space available between the sides of the shear box and the main frame. The alternative method was to make smaller load cells which measured the stress at specific points around the boundary of the sample. This involved mounting the load cells in the wall and end plates of the shear box, ensuring they were flush with the surface. It was decided to make a first attempt to measure the lateral stresses using the latter method.

The existing transducers to measure the normal stress on the sample had performed satisfactorily and it was decided to develop smaller load cells of similar design to measure the lateral stress. The load cells were machined from solid blocks of aluminium alloy, HE 15W. The basic measuring elements in the load cells were four webs 5 mm x 2 mm x 10 mm long acting as fixed end beams (Fig. 6.18a). They were strain gauged as near their roots as possible. The face of the load cell in contact with the material was protected by a 1 mm thick stainless steel plate. This reduced friction and also protected the aluminium cell from the abrasive aggregate under test. The load cells were mounted in recesses machined in the sides of the shear box and held in place by two bolts. A clearance of 0.1 mm was allowed around each cell. To prevent trapping of particles the clearance gap was filled with silicone rubber. Three load cells were mounted in each side of the shear box and one at each end. The load cells were incorporated in the base of a triaxial cell and calibrated against the material as described in Chapter 4, Section 4.3.3. The load cells were found to over-register at low stresses and under-register at higher stresses. The calibrations were compared with those obtained from dead weight loading. One explanation for the load cell

under-registration is that due to excessive deflection of the cell compared to the rigid boundary around it, the material was arching over the face of the load cell and causing a stress reduction. Due to difficulties with repeatability of results it was impossible to obtain a satisfactory calibration. The calculated deflection of the load cell was 0.032 mm. This was checked by direct measurement of the deflection under dead weight loading. The deflection under 0.36 kN load (285 kPa stress) was measured as 0.031 mm. Tests running concurrently to develop a load cell for the biaxial shear box reinforced the decision to attempt to design a load cell having a similar stiffness to the walls of the shear box.

Attempts were made to use a load cell comprising a solid aluminium block (Fig. 6.18b). Semi-conductor strain gauges of type Technimeasure BG-3-350 were used and a calibration under dead weight loading carried out. The output was non-linear and very susceptible to temperature fluctuations. Inadequate temperature control of the laboratory made further investigation of this method unnecessary.

A circular piston type load cell as shown in Fig. 6.18c was designed. The load cell employed direct compression elements and the calculated maximum deflection for a design stress of 350 kPa was 5×10^{-4} mm. The maximum specimen depth was 30 mm and this influenced the choice of a 25 mm diameter loading face. The active face transmitted the load to four pillars of dimensions 2.5 mm x 0.5 mm thick. The simple design made machining from a solid block of aluminium HE 15W relatively simple. However, problems were again encountered with calibration against the material.

Consideration was given to a circular load cell of similar design but large enough to form a complete boundary to the specimen. This was the approach finally adopted for the biaxial load cell design (Section 4.3.3.)

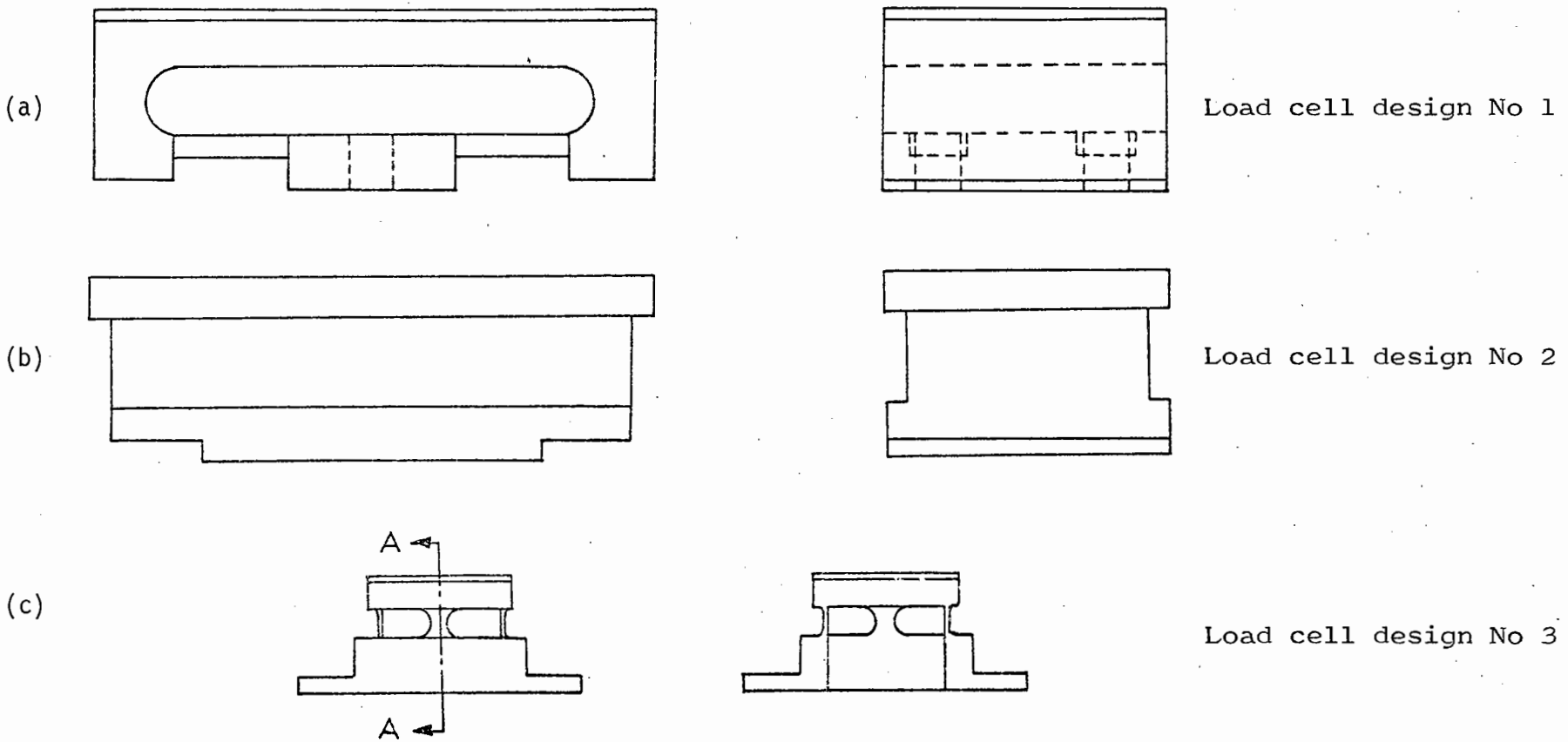

FIG. 6.18 PRELIMINARY LOAD CELL DESIGNS

The cells had two sides cut away as shown in Fig. 6.19a. The cells were designed for a maximum load of 1.8 kN and were machined from a solid block of aluminium HE 15W. The solid cap transmits the load to four strain gauged pillars each 4 mm x 1.6 mm thick. Four dummy gauges were placed on the unstressed cell base. The maximum deflection of the load cells under full load was calculated as 0.001 mm corresponding to 14 $\mu\varepsilon$ in the lateral direction. This was considered small enough to essentially retain plane strain conditions. The design of the load cells enabled them to be stacked as shown in Fig. 6.19b and their circular design meant that they could be manufactured quickly and easily on a lathe. Since the design of the shear box end plates required that they be held in position by the sides, the load cells were restricted to the area shown in Fig. 6.19b. This meant that as the end plates rotated outwards, the load cells did not completely form the sample boundary. However, stress conditions are complex at the ends and generally the stresses on the central portion are considered reasonably uniform. Taking this into consideration it was thought satisfactory to mount the load cells as shown in Fig. 6.19b. The top caps of the load cells were covered with a 1 mm thick stainless steel plate to reduce friction and wear on the aluminium surface. The new design did not require calibration against the material and was calibrated by dead weight loading only. A typical calibration is shown in Fig. 6.20. The normal and shear transducers effectively measure stress since their entire surface areas are in contact with the test material. However, the lateral cells measure load since as the sample changes thickness, the contact area changes. A knowledge of the sample depth enables stresses to be calculated during a test. The sample acts on the hatched area shown in Fig. 6.19b. The design and depth of the load cells ruled out any possibility of using them in the end plates of the shear box.

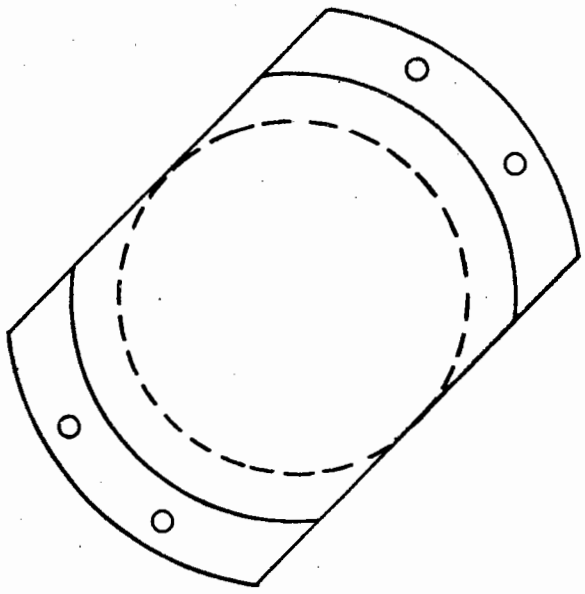

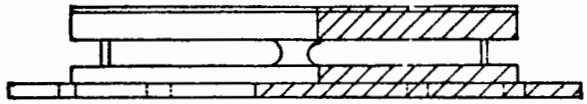

FIG. 6.19 (a) SIMPLE SHEAR LATERAL LOAD CELL

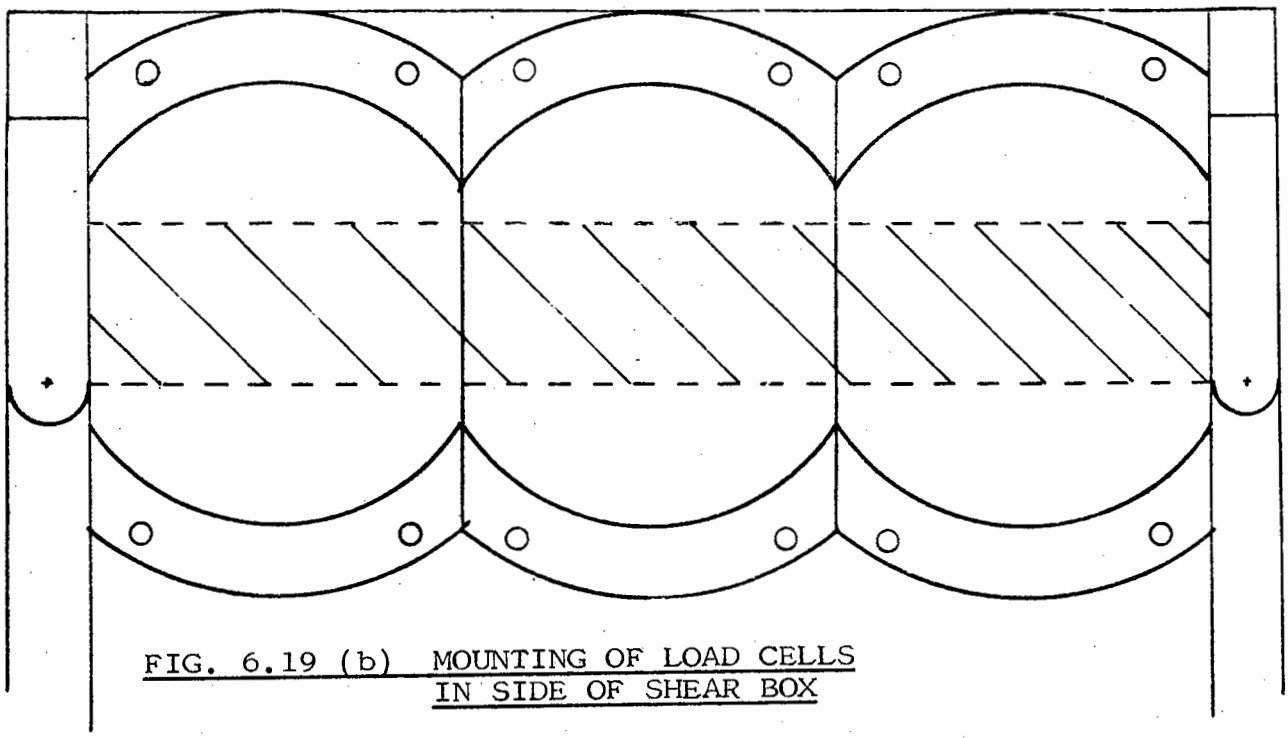

FIG. 6.19 (b) MOUNTING OF LOAD CELLS IN SIDE OF SHEAR BOX

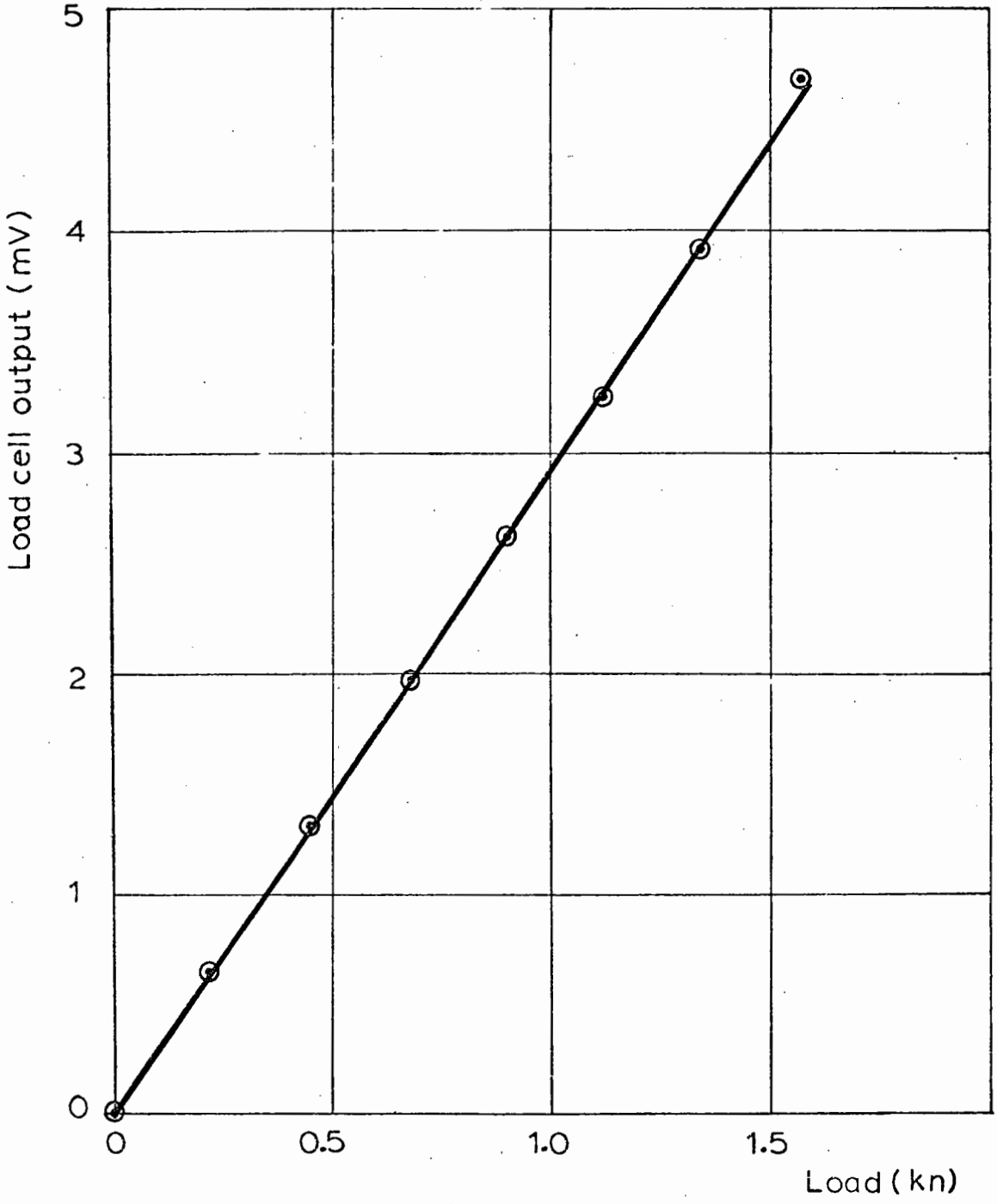

FIG. 6.20 TYPICAL CALIBRATION FOR LATERAL LOAD CELL

6A.4.3 Hinged End Plate Arrangement

The original rotating ends (Ansell 1977) were made from steel plate having locating holes drilled on the axis at each end. The end pieces were hinged between the sides of the lower half of the box using these holes. Spring loaded stub axles mounted in the sides held the end plates in semi-cylindrical slots cut in the ends of the shear box. The effect of the concentric semi-cylinders was to allow the end plates to tilt backwards or forwards while maintaining a seal at the lower edge. The top platen fitted between the hinged end plates. These were held in contact with the top platen by the clamp arrangement shown in Fig. 6.21. This arrangement caused the specimen to deform as a parallelogram in the manner required for simple shear.

This system was inadequate in that the aluminium clamping frame flexed considerably during testing, thus allowing limited straining of the specimen in the longitudinal direction. As the end plates were only 20 mm in thickness, the arrangement as originally designed made it almost impossible to satisfactorily mount end load cells. The design was such that the end plates rested against the top platen and during shearing were pushed by the top platen thus providing the rotation. Since the top platen is composed of normal stress transducers it was felt that a system where the top platen did not come into contact with the end plates would be more satisfactory. Hence, it was decided to design a new arrangement for end rotation and end stress measurement.

A new system of slots and bearings was designed as shown in Fig. 6.22. This allowed load cells similar to those used to measure normal stress on the top of the specimen to be adopted. The slots were designed so that the points of rotation were always in line with the top and bottom corners of the specimen, i.e. as the sample compacted or dilated, the top corner hinge also moved up or down by a similar distance. The load cells formed

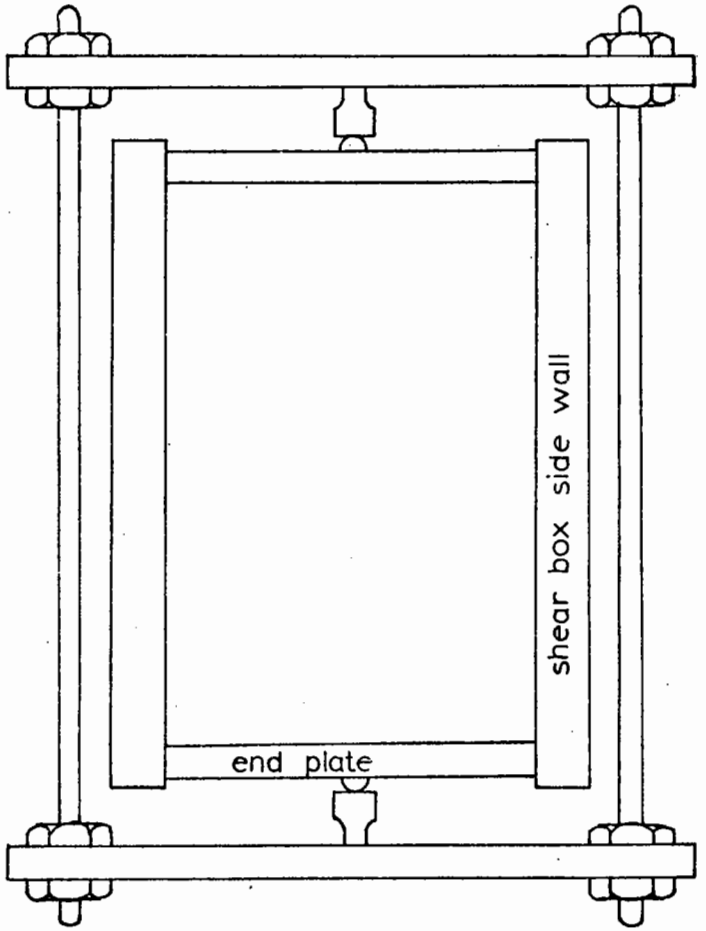

Diagrammatic plan view of simple shear box with clamp arrangement for end plates as used by Ansell.

FIG. 6.21 SIMPLE SHEAR APPARATUS HINGED END PLATES (ANSELL 1977)

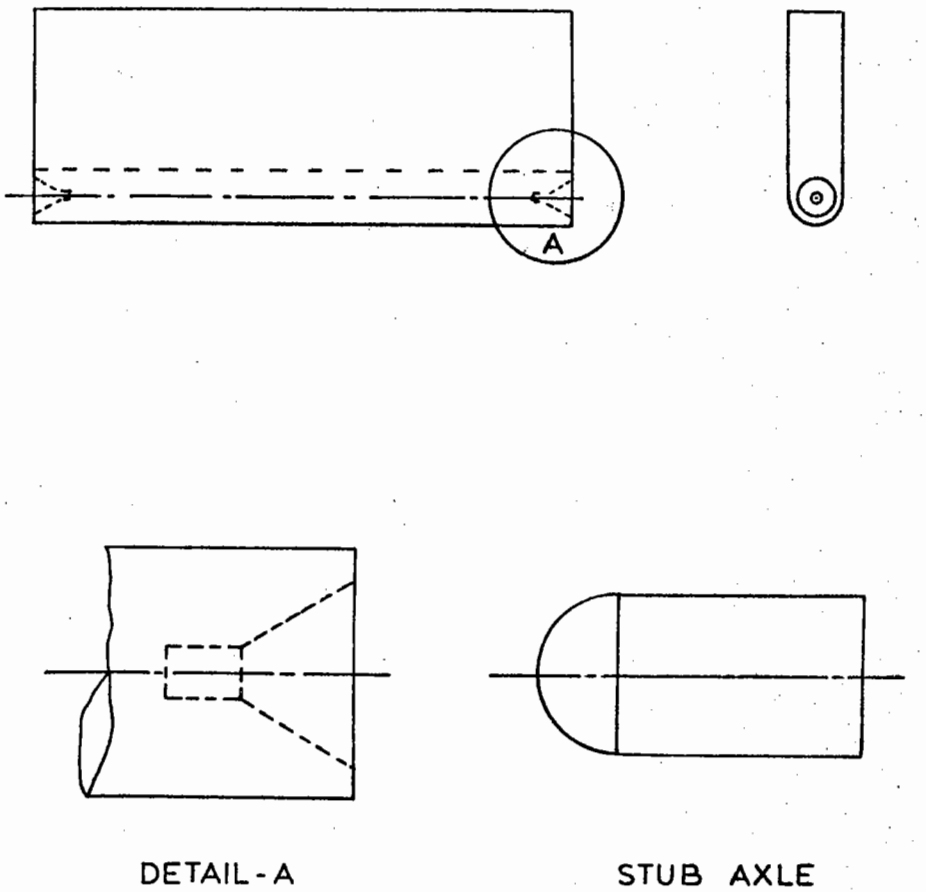

Detail of end flap and stub axle for simple shear box.

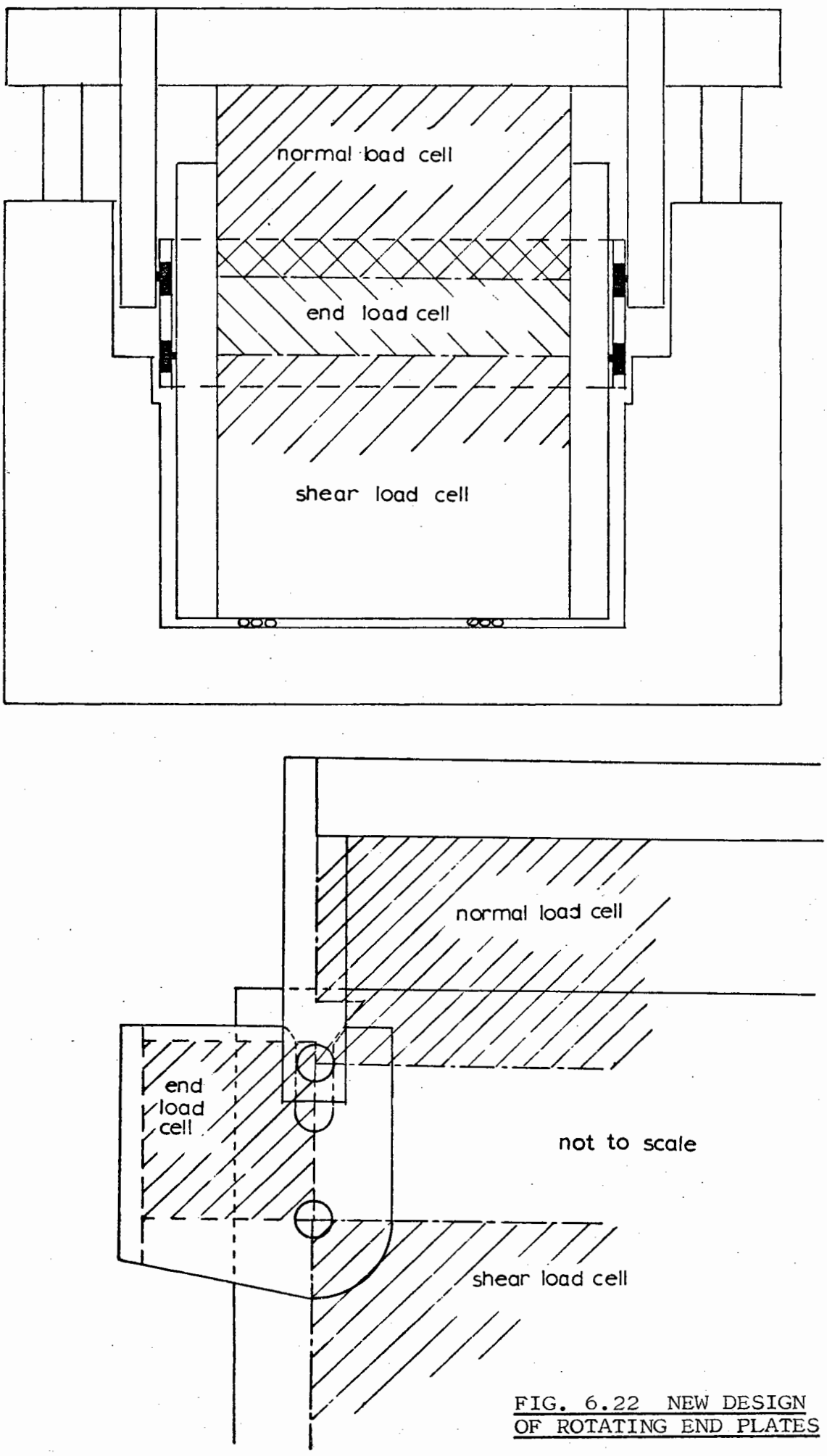

FIG. 6.22 NEW DESIGN OF ROTATING END PLATES

the complete sample boundary at each end and a knowledge of the specimen depth enabled the end stress to be calculated. The load cells were not as stiff as those used in the sides of the shear box and hence were not ideal. However, it was hoped that they would provide some indication of the stress in the longitudinal direction.

6A.4.4 Data Monitoring

The original data monitoring system could keep a permanent record of any four output signals. In order to satisfactorily investigate stress conditions around the sample during a test, it was necessary to have a permanent output of at least the central transducers and end load cells. An ultra violet (U.V.) recorder was used to monitor the stress on the central portion of the specimen and on the ends. Records of the vertical and shear deformations of the specimen were obtained using the two existing chart recorders.

SECTION B - STRESS BEHAVIOUR

6B.1 TESTS WITH GLASS BALLOTINI

Having designed and installed the lateral load cells and new hinged end assembly, several preliminary tests were conducted with glass ballotini to ensure that the apparatus was functioning properly before testing of the 3 mm crushed limestone commenced.

Full details and results are presented in Tables 6.3 and 6.4. Several tests were conducted with the end plates locked in the vertical position. Vertical stress σ_v was then increased in steps to a peak value. Bidirectional simple shear tests were carried out to 150 cycles both with σ_v constant and with σ_v cycled. Lateral and end stresses along with σ_v and the shear stress τ were monitored throughout the tests.

GLASS BALLOTINI STATIC LOADING TESTS - TABLE 6.3

σ_v (kPa)	TEST 1 (kPa)					TEST 2 (kPa)			
	L2	L8	E1	E2		L2	L8	E1	E2
0	0	0	0	0		0	0	0	0
57	18	18	18	14		22	23	6	8
114	33	29	13	14		37	35	10	11
171	45	40	16	17		49	47	12	14
228	61	52	19	18		59	56	16	14
285	68	61	21	21		71	70	18	19
228	68	57	21	20		71	66	18	19
171	65	54	21	20		67	63	17	17
114	63	52	20	18		62	56	16	14
57	50	40	18	17		49	50	12	14
0	10	18	10	12		15	21	5	8

GLASS BALLOTINI CYCLIC LOADING TESTS - TABLE 6.4

σ_v (kPa)	TEST 1 (kPa)					TEST 2 (kPa)				cycle
	L1	L2	E1	E2		L1	L2	E1	E2	
285	68	70	24	19		73	69	27	26	1
	88	87	30	22		88	96	32	29	2
	100	104	31	23		100	118	34	30	5
	126	130	36	28		100	130	36	32	10
	154	166	44	34		98	139	38	33	20
	168	183	49	39		88	148	38	35	50
	176	200	52	43		88	156	40	35	100
	176	209	54	44		88	166	41	35	150

TEST 1 σ_v = 285 kPa constant
τ = $\pm$ 4 bar

TEST 2 σ_v = 285 kPa cycled between 285 kPa and zero
τ = $\pm$ 4 bar

Generally, there was good correlation between stresses on either side and at each end of the specimen. The test results were quite repeatable. Defining K_o in the conventional manner as the ratio of lateral to vertical stress, it can be observed from Table 6.3 that K_o decreases with increasing applied vertical load. The range of values was from 0.36 to 0.24. Jakey (1948) developed an equation to predict the coefficient of earth pressure K_o at rest in silos. K_o was estimated from:

$$K_o = 1 - \sin \phi' \qquad (6.1)$$

where ϕ' is the angle of internal friction of the material. ϕ' for the glass Ballotini was 9^o (Cooper 1973) giving a predicted K_o of 0.84. Equation 6.1, however, has been developed for a situation where the granular materials were loosely packed and must be treated with caution when applied to the densely packed material in the simple shear apparatus.

Lateral stresses were found to be consistently greater than end stresses. This may be a function of the material behaviour or may be due to the fact that the load cells used to measure end stress were less stiff than those employed in the sides of the apparatus. However, it is not thought that this effect is as severe as the results suggest and it is quite likely that there is a difference between stresses in the two lateral directions. During shearing, it was observed that one of the lateral load cells produced a considerable increase in output towards the end of each test. On recalibrating, it showed considerable hysteresis and was replaced before testing continued.

Experiments were short and consequently the results for each test were obtained at approximately the same temperature. It was not until the full test series was in progress, that the lateral load cells were found to be temperature sensitive. A calibration was obtained enabling

temperature corrections to be applied and all the results presented for the simple shear apparatus have been temperature corrected.

6B.2 TESTS ON 3 mm CRUSHED LIMESTONE

The same 3 mm crushed limestone material as tested by Ansell (1977) and subsequently used in the main triaxial and biaxial test series, was subjected to the stress paths shown in Fig. 6.23. The tests were of the bidirectional type and the programme was conducted with vertical stress constant or cycled between a maximum and zero. The pattern of loading was described in Section 6A.4.1. The lateral and end stresses were plotted against the logarithm of the number of cycles in Figs 6.24 to 6.26.

Measurements of lateral stress were poor, with as much as 300% difference in stress measurements across the specimen. There was also considerable difference between the measured lateral and end stresses. Measurements of stress were not repeatable and were deemed unreliable. The main reason for the lack of accuracy in monitoring lateral and end stress, was thought to be related to the material size and shape. A ratio of specimen depth to particle size of 10:1 was selected by Ansell when designing the apparatus. As he was not able to measure lateral or end stresses, the apparatus yielded satisfactory results for the parameters observed. The limestone was described as a nominally 3 mm size material. It was thought that the angularity of the crushed limestone particles was causing them to lock together, thus preventing equal transmission of stress to the sides and ends of the shear box. This was not helped by the relatively large particle size and as it was impossible to increase the specimen depth because of the apparatus design, attempts were made to find a material for which a testing programme could be conducted with full stress measurements.

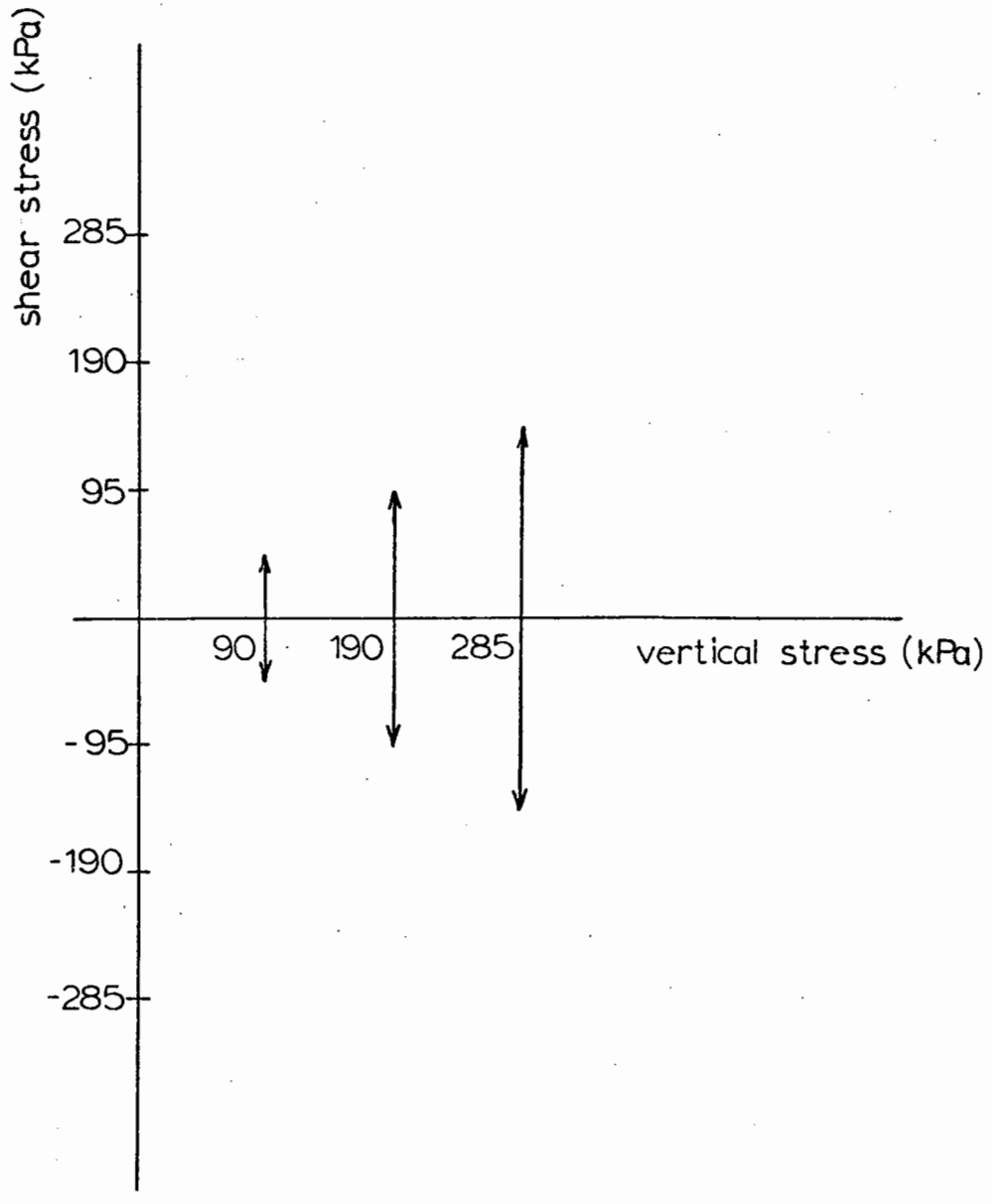

FIG. 6.23 BIDIRECTIONAL TEST SERIES - 3 mm MATERIAL

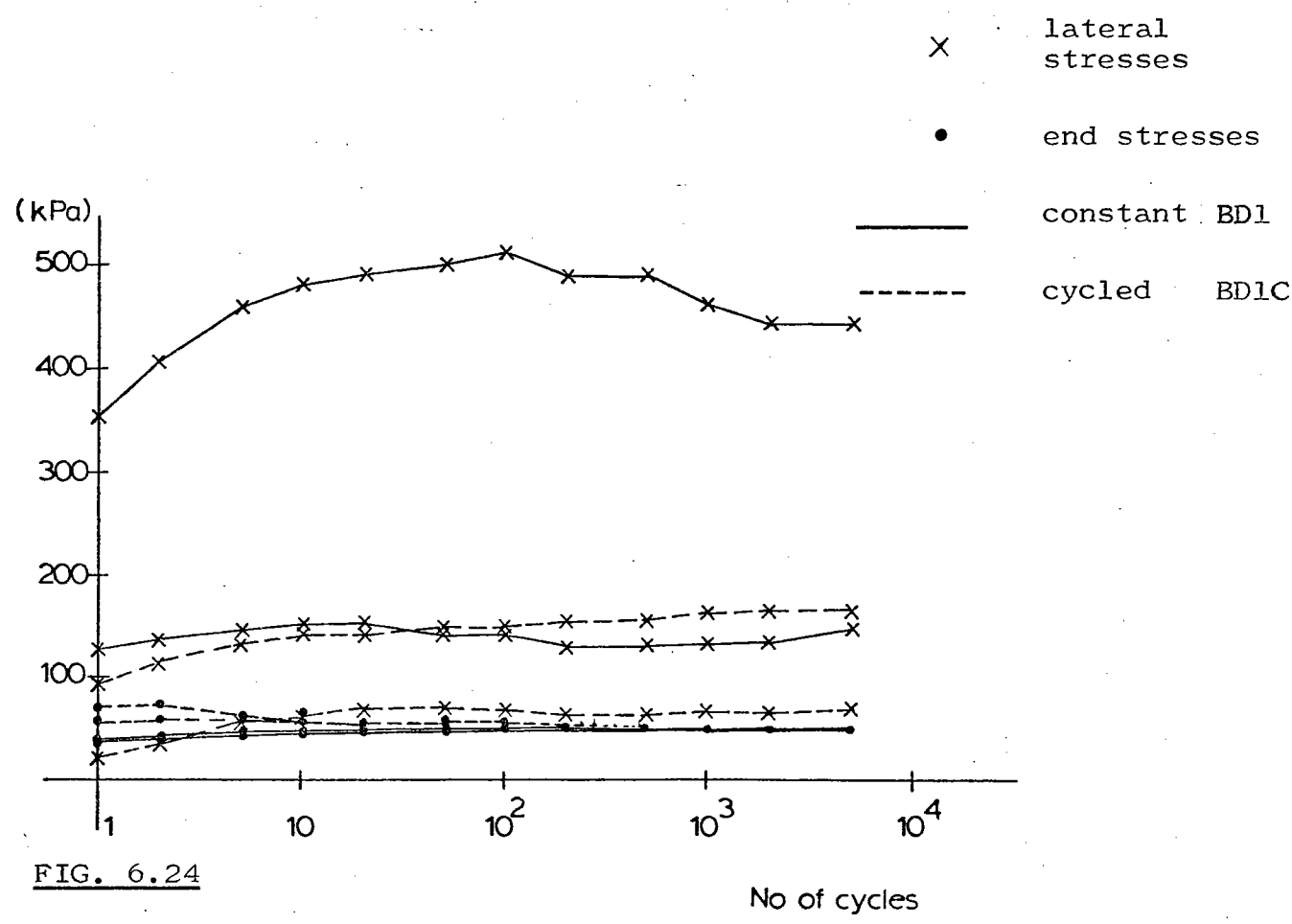

FIG. 6.24

MEASURED LATERAL AND END STRESSES FOR BIDIRECTIONAL TESTS ON 3 mm MATERIAL

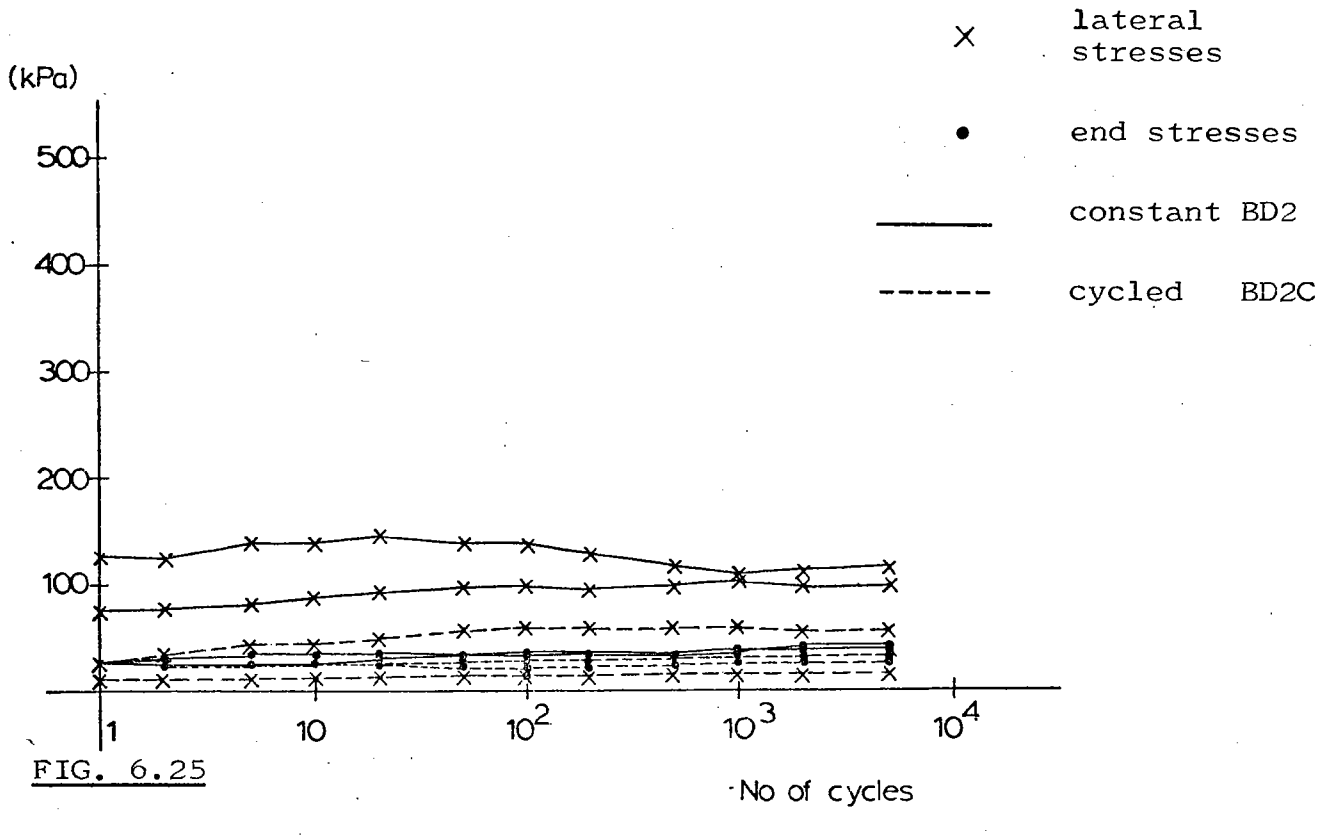

FIG. 6.25

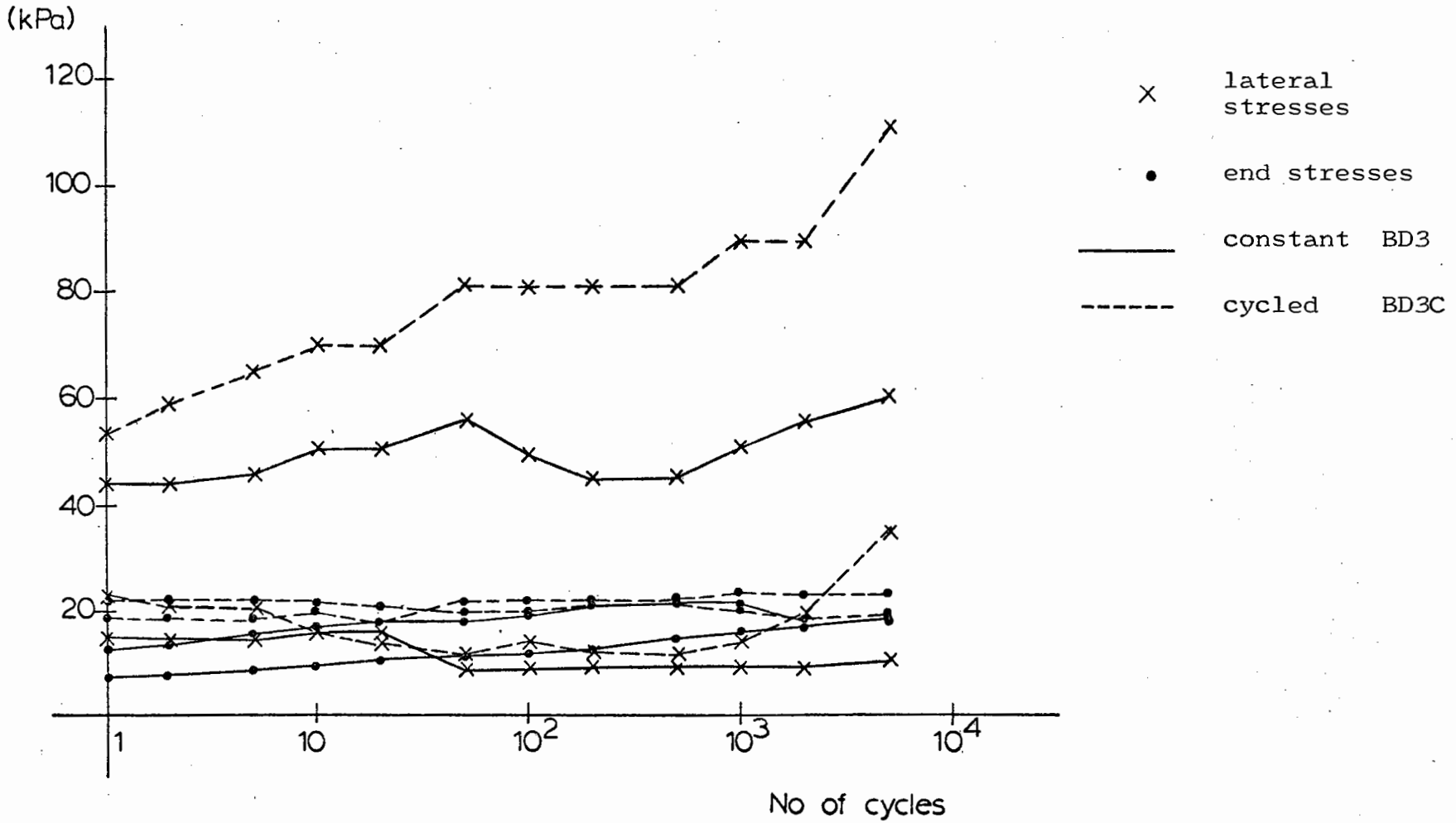

FIG. 6.26 MEASURED LATERAL AND END STRESSES FOR BIDIRECTIONAL TESTS ON 3 mm MATERIAL

6B.3 CHOICE OF NEW MATERIAL

Simple shear tests were conducted on several materials, in an attempt to find a grading suitable for the dimensions of the shear box. A rounded sand of approximately 1.25 mm particle size was tested, along with a graded crushed limestone (Ballidon) containing particles ranging from 3 mm to dust.

The sand was found to give much more consistent readings of lateral and end stress. However, it was thought preferable to test the same Chipping Sodbury limestone throughout the project and a size fraction suitable for the shear box was chosen. After several attempts it was found that the material passing No. 7 and retained on No. 14 British Standard sieves, gave the most consistent results. Subsequent tests in the triaxial apparatus (Chapter 3, Section 3.5) showed that the contour models developed for the 3 mm material were also applicable to the smaller size fraction. The particles were nominally 1.5 mm size and each specimen was compacted by vibration to a density of 1.62 Mg/m^3.

6B.4 TEST PROGRAMME FOR 1.5 mm CRUSHED LIMESTONE

A short test programme was devised such that comparisons could be made with previous results (Ansell 1977) but including additional tests to utilise the new loading facilities of the apparatus. The test paths are shown in Fig. 6.27. The programme was conducted with constant vertical stress (σ_v) and also with σ_v cycled between zero and maximum. Both bidirectional and unidirectional tests were performed, although because of time limits, only one specimen could be tested for each stress path. However, the series conducted previously had shown that test results were quite repeatable.

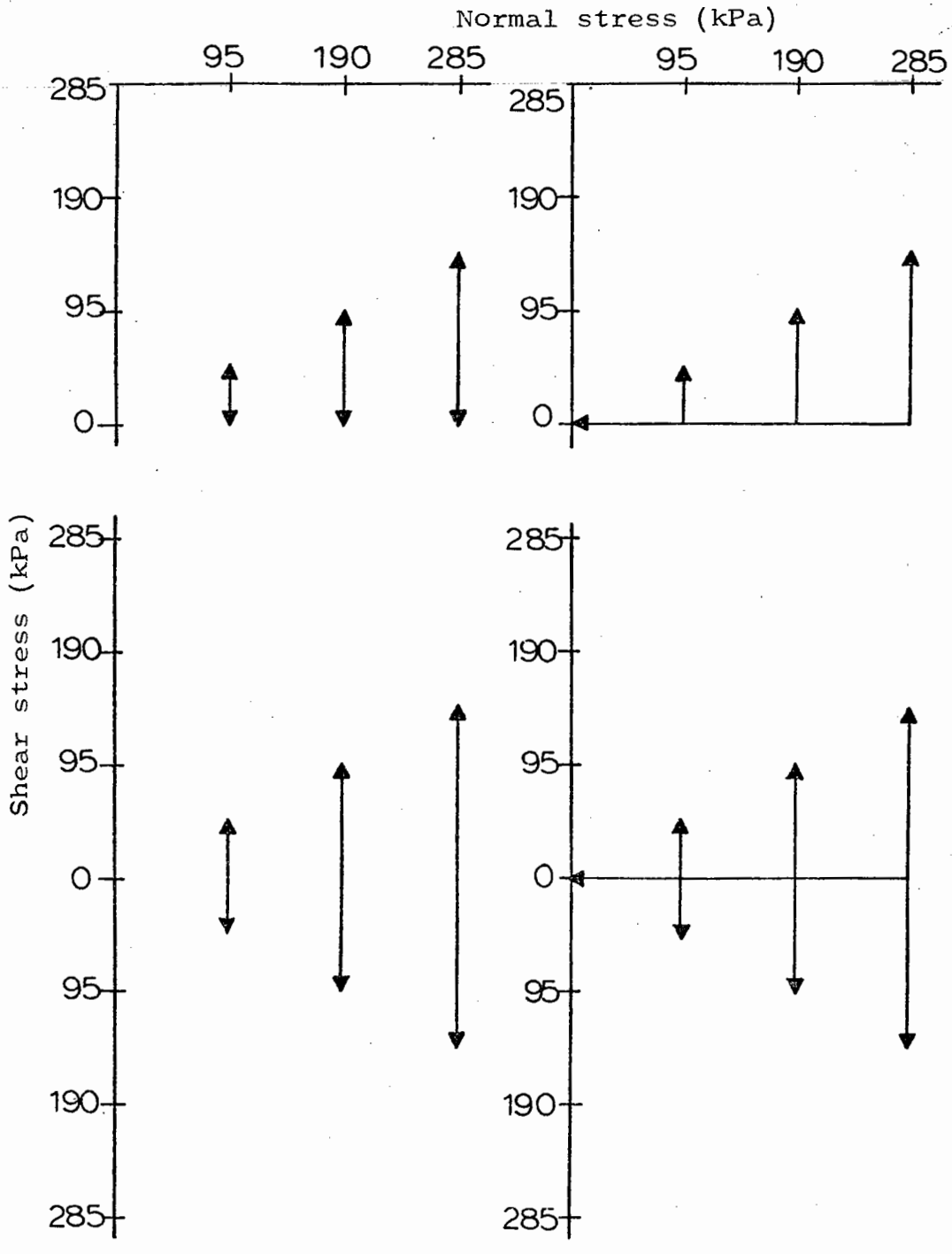

FIG. 6.27 TEST PROGRAM FOR 1.5 mm MATERIAL

6B.5 MEASUREMENT OF LATERAL AND END STRESSES

Figs 6.28 to 6.33 and 6.34 to 6.39 show the variation of measured lateral and end stresses for each of the tests conducted. Generally, the lateral stresses on each side of the specimen were similar and an average measurement of lateral stress was plotted. End stresses tended to vary with the direction of shearing and consequently the measured stresses for each end of the specimen are presented.

Table 6.5 shows the initial K_o state of several of the specimens. Measurements were taken after applying the vertical load, with the end plates vertical, and no shear stress on the specimens.

Table 6.5

σ_v (kPa)	Lateral stress (kPa)		Average K_o	End stress (kPa)		Average K_o
	L1	L2		E1	E2	
285	35.5	45.3	0.14	12.2	13.2	0.04
285	40.9	44.8	0.15	9.4	10.5	0.03
190	19.7	37.4	0.15	6.6	7.0	0.04
190	23.7	29.6	0.14	5.7	6.2	0.03
95	15.5	32.9	0.25	8.4	4.3	0.07
95	17.8	21.7	0.20	2.9	3.5	0.03

Using Equation 6.1, the predicted K_o value is 0.22. This would suggest that measured end stresses are in error and lateral stresses only approach the predicted value at low vertical loads. One would immediately assume that the load cells were deflecting under increased loading causing a bridging effect to take place. This is probably the case for the end load cells, although the specimen boundaries, if deflecting, would do so uniformly since they consist entirely of load cell faces. However, the maximum calculated deflection of each lateral load cell (assuming $K_o = 1$) was only $4\mu\varepsilon$. Figs 6.28 and 6.29 also

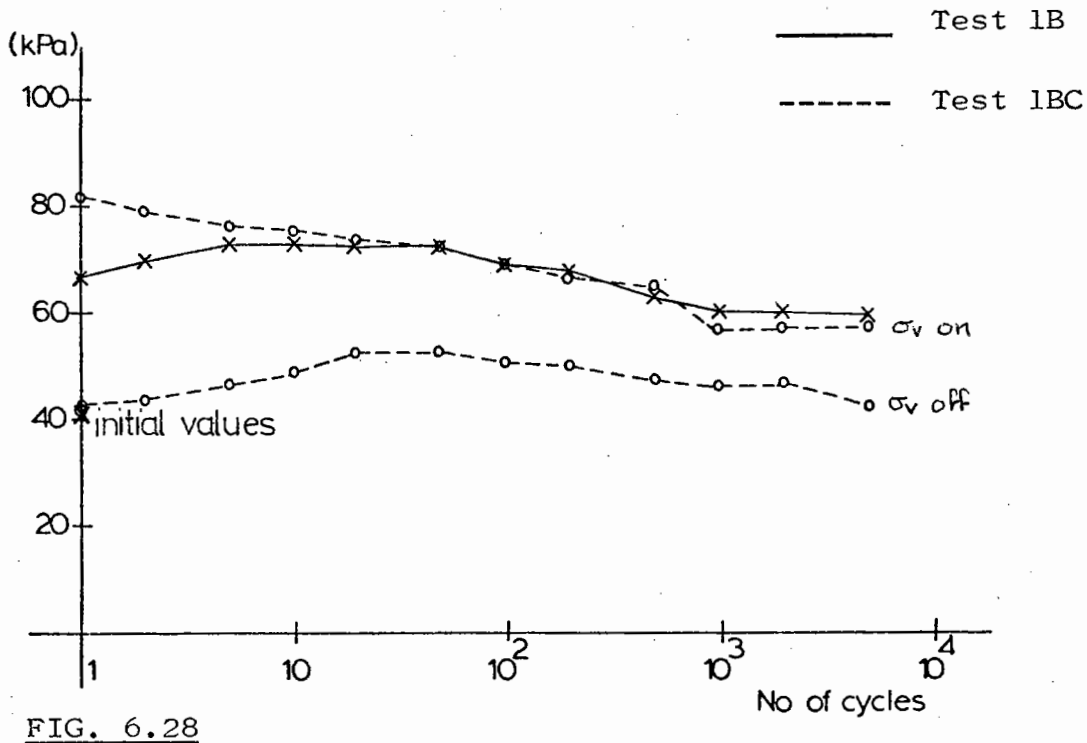

FIG. 6.28

MEASURED LATERAL STRESSES FOR BIDIRECTIONAL TESTS ON 1.5 mm MATERIAL

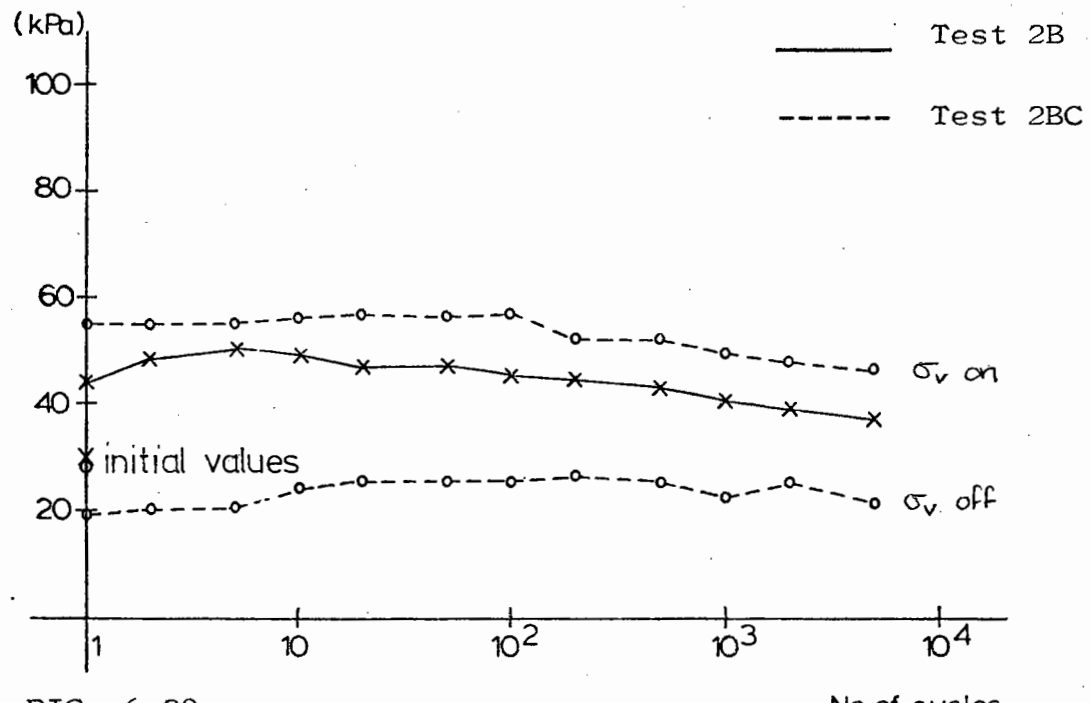

FIG. 6.29

FIG. 6.30 MEASURED LATERAL STRESSES FOR BIDIRECTIONAL TESTS ON 1.5 mm MATERIAL

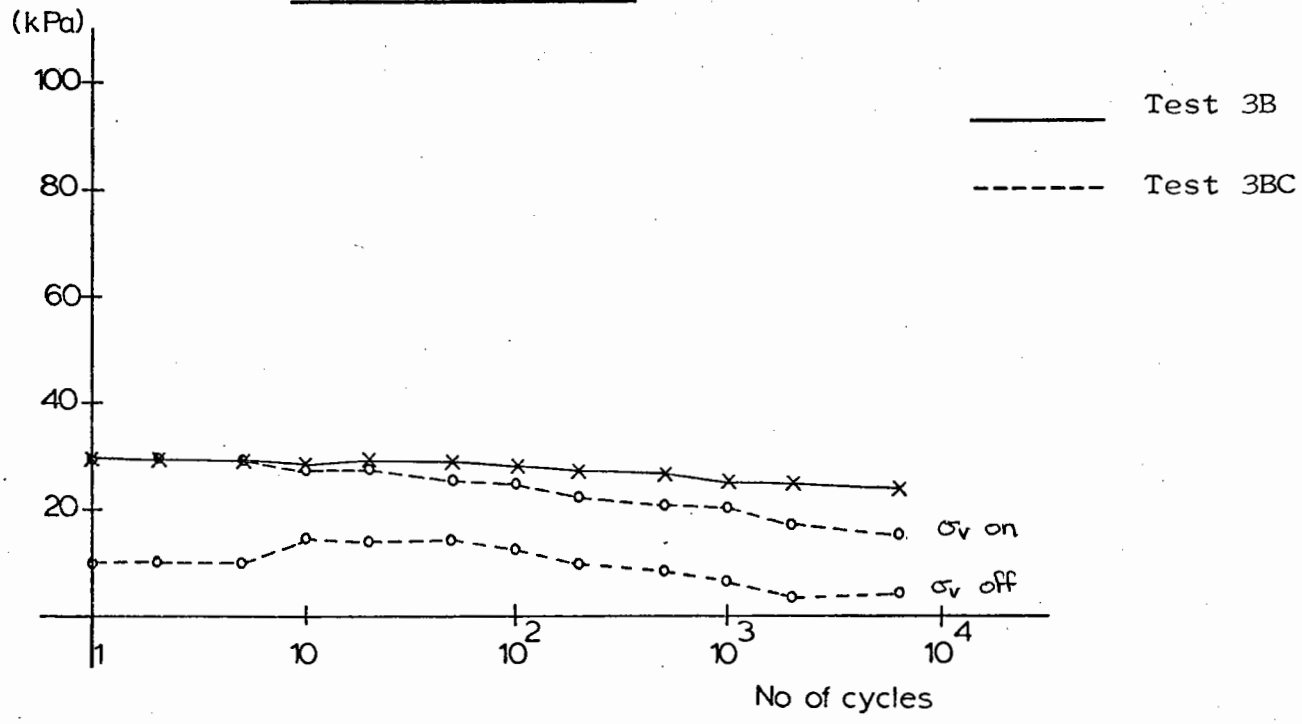

MEASURED END STRESSES FOR BIDIRECTIONAL TESTS ON 1.5 mm MATERIAL

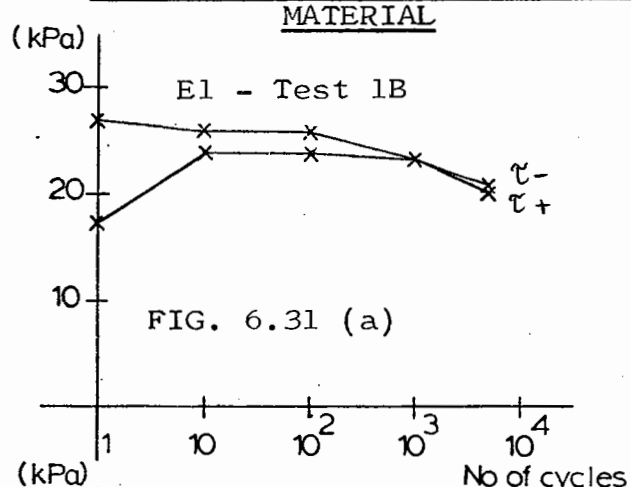

FIG. 6.31 (a)

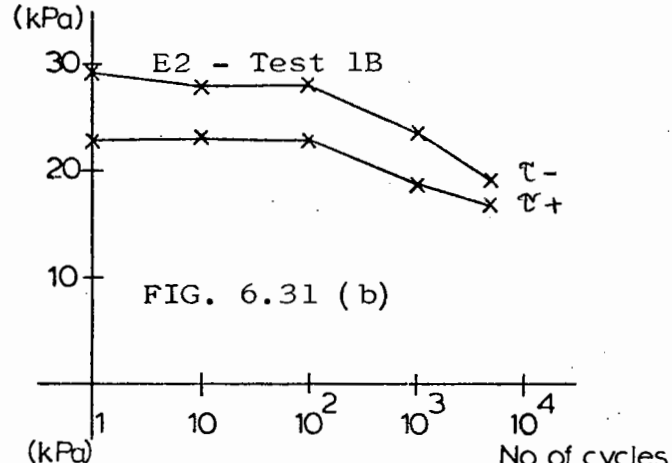

FIG. 6.31 (b)

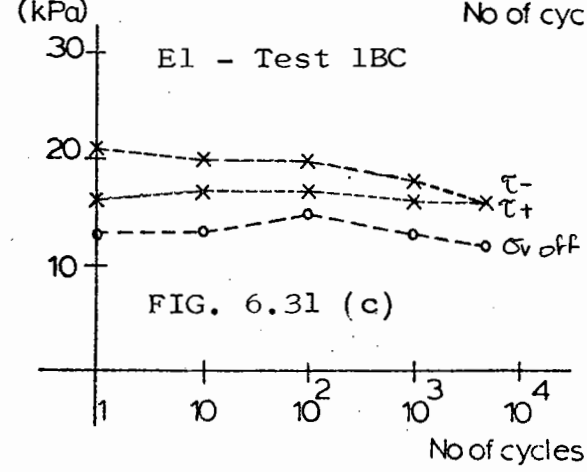

FIG. 6.31 (c)

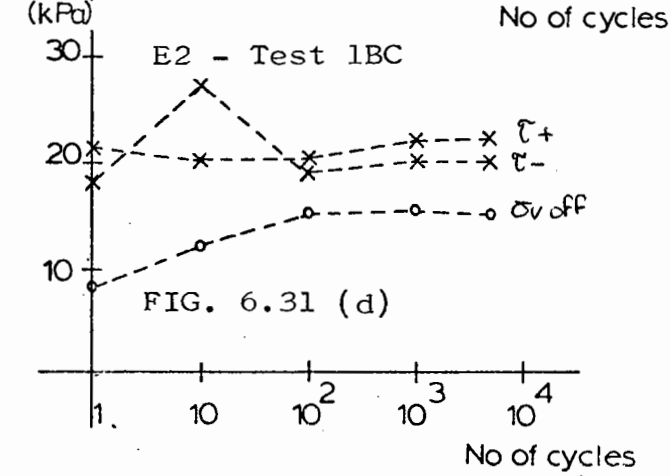

FIG. 6.31 (d)

MEASURED END STRESSES FOR BIDIRECTIONAL TESTS ON 1.5 mm MATERIAL

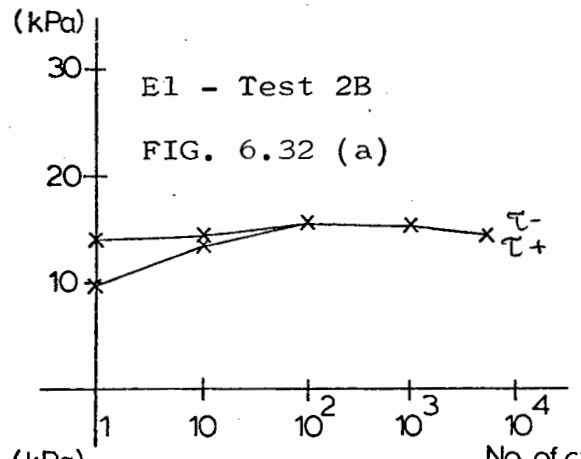

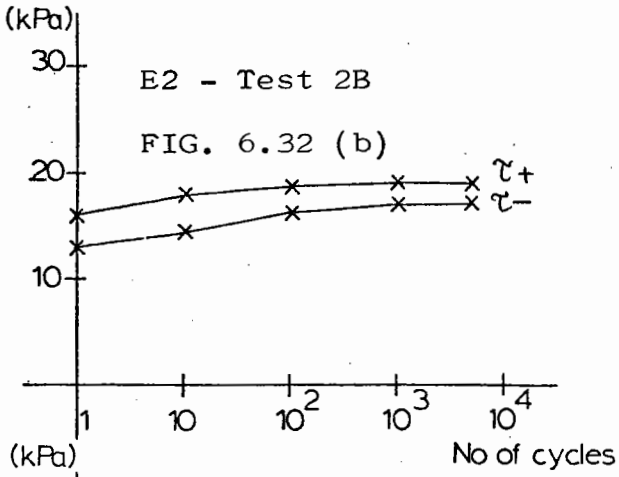

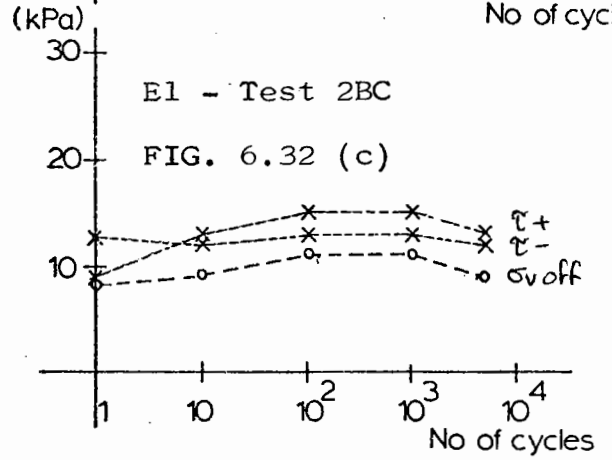

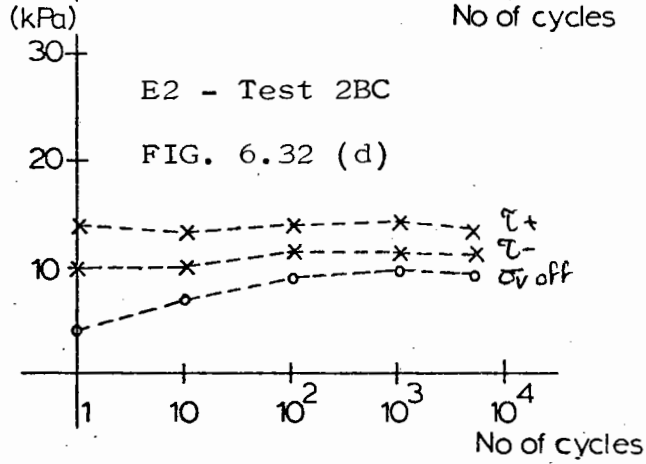

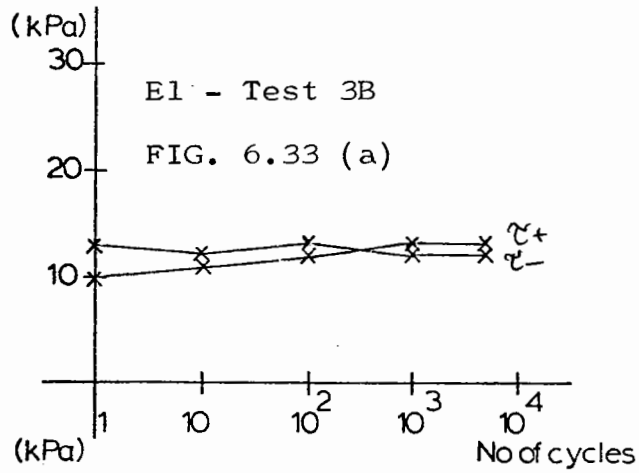

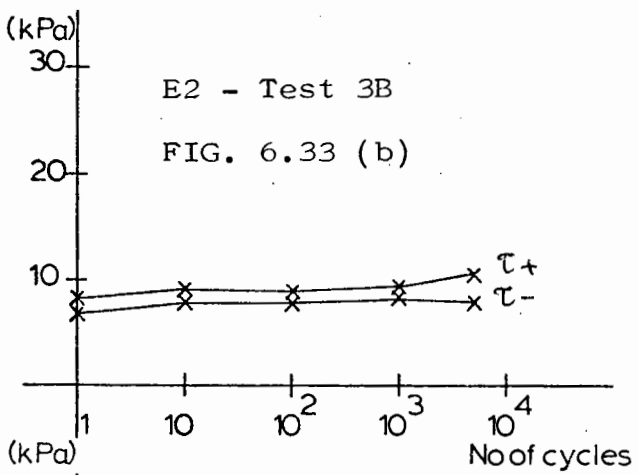

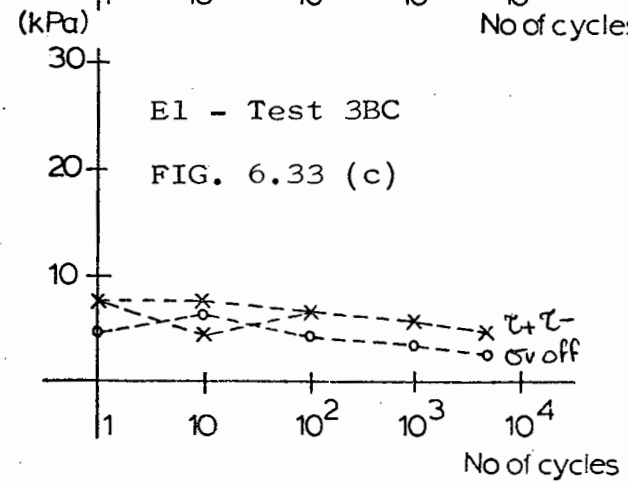

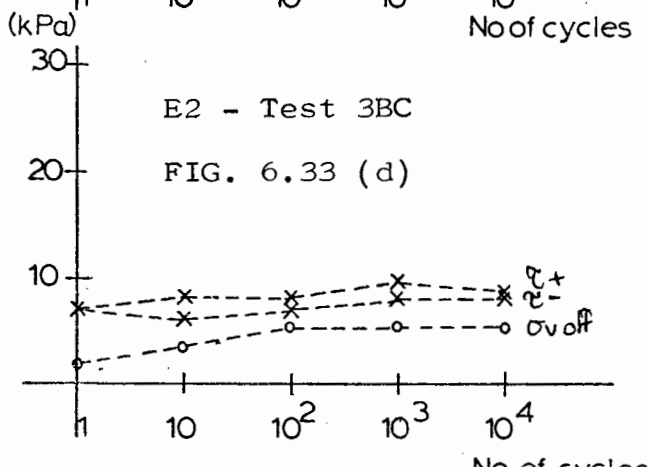

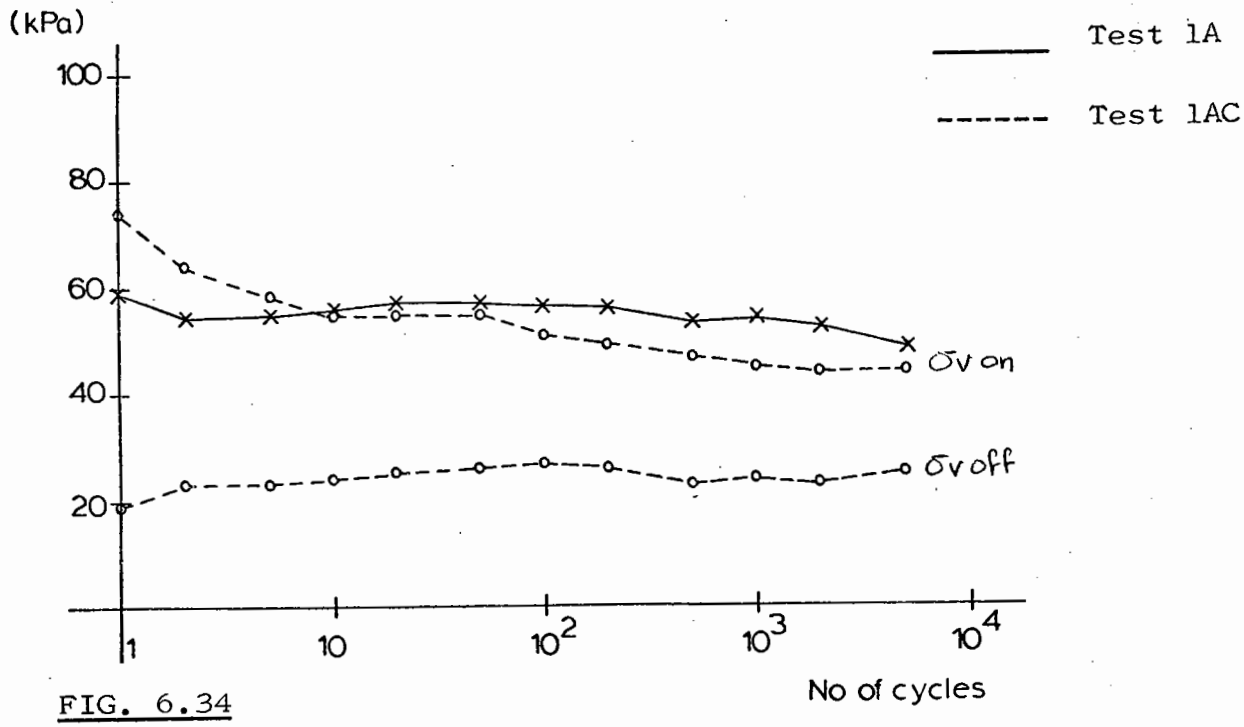

FIG. 6.34

MEASURED LATERAL STRESSES FOR UNIDIRECTIONAL TESTS ON 1.5 mm MATERIAL

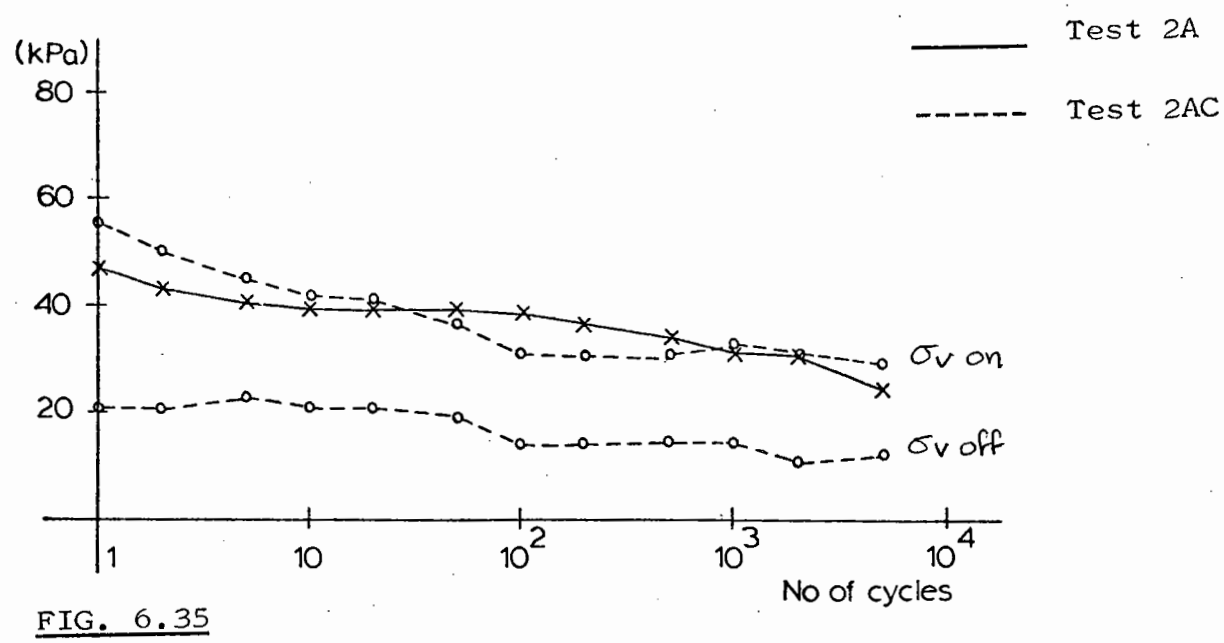

FIG. 6.35

FIG. 6.36 MEASURED LATERAL STRESSES FOR UNIDIRECTIONAL TESTS ON 1.5 mm MATERIAL

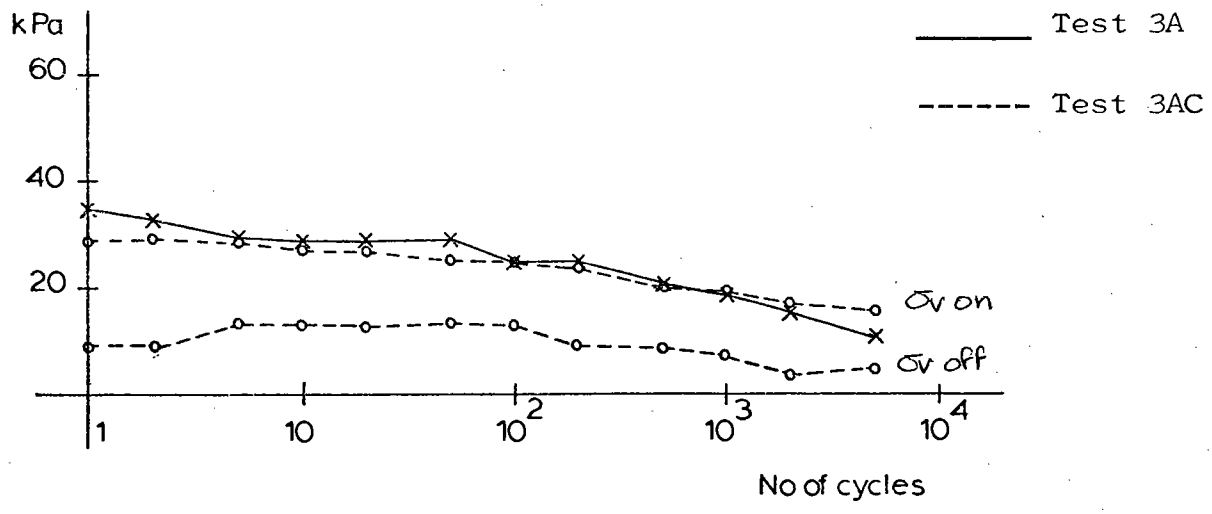

MEASURED END STRESSES FOR UNIDIRECTIONAL TESTS ON 1.5 mm MATERIAL

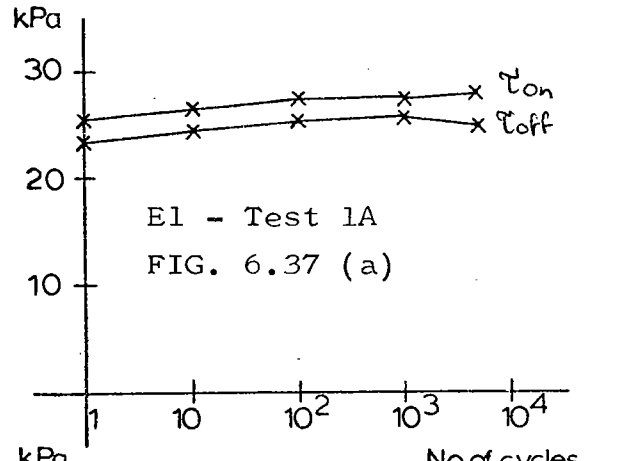

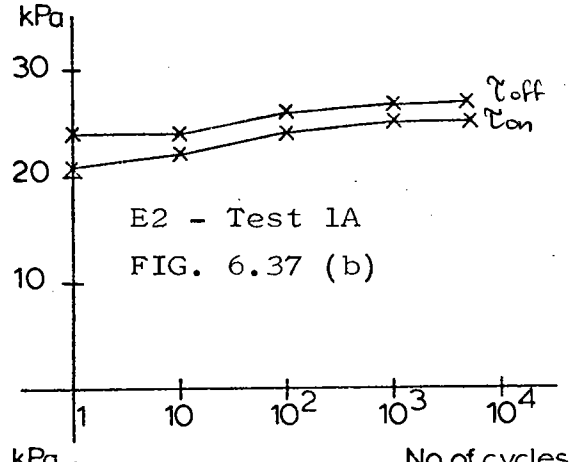

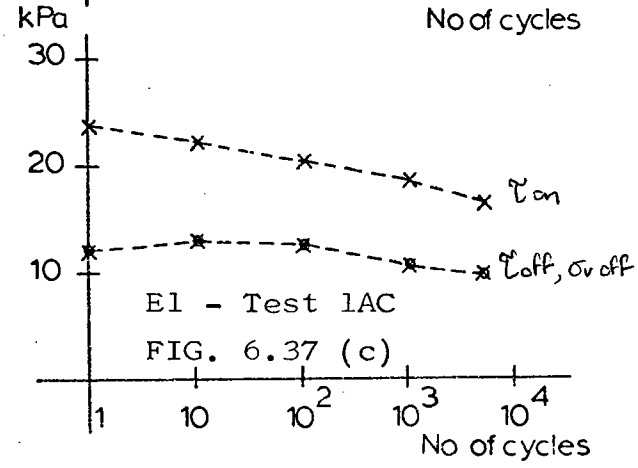

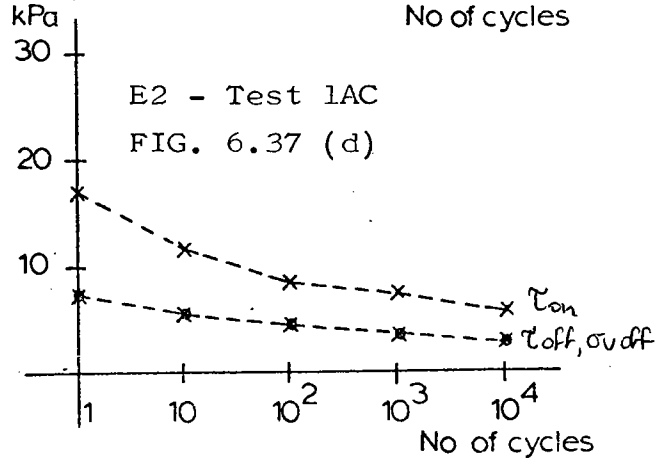

MEASURED END STRESSES FOR UNIDIRECTIONAL TESTS ON 1.5 mm MATERIAL

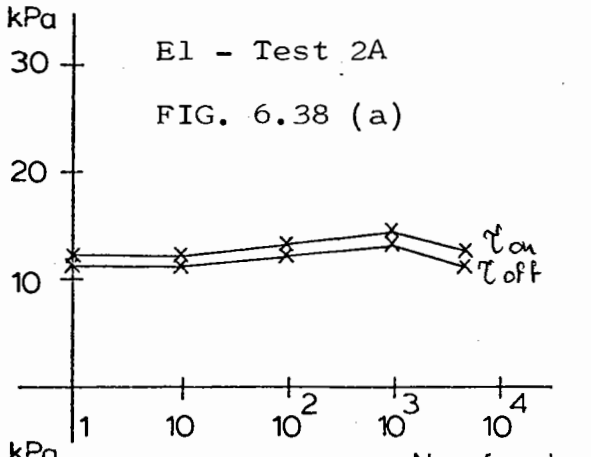

E1 - Test 2A

FIG. 6.38 (a)

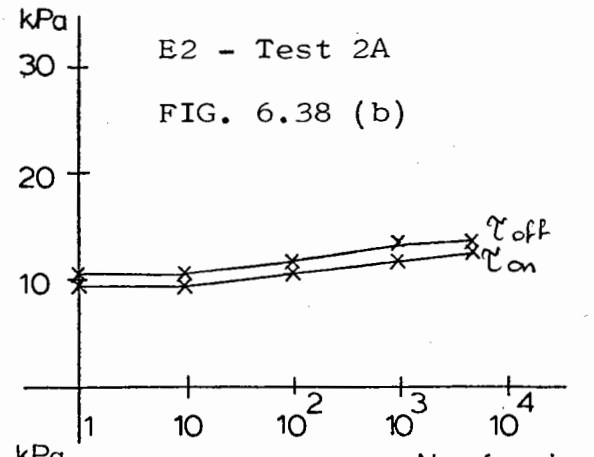

E2 - Test 2A

FIG. 6.38 (b)

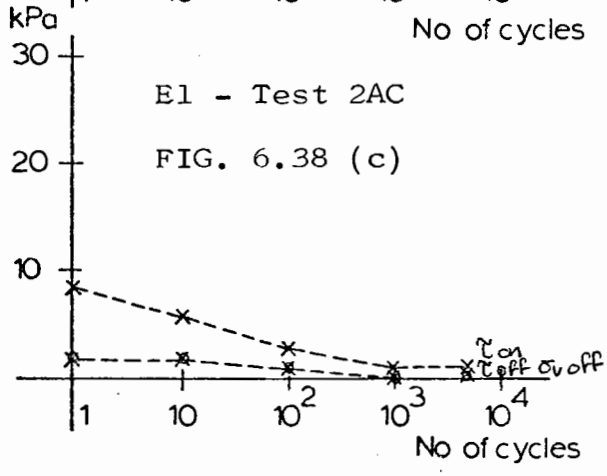

E1 - Test 2AC

FIG. 6.38 (c)

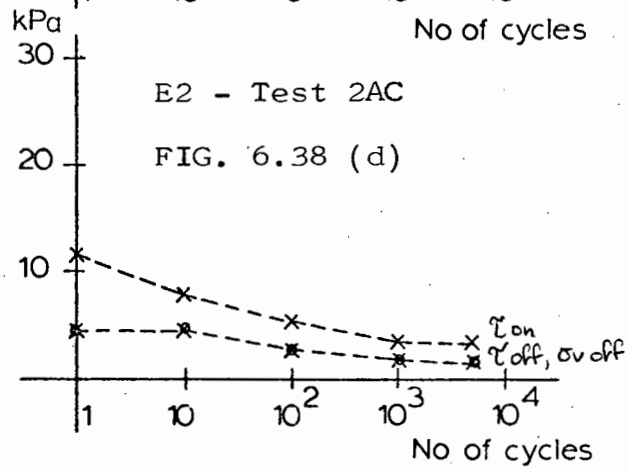

E2 - Test 2AC

FIG. 6.38 (d)

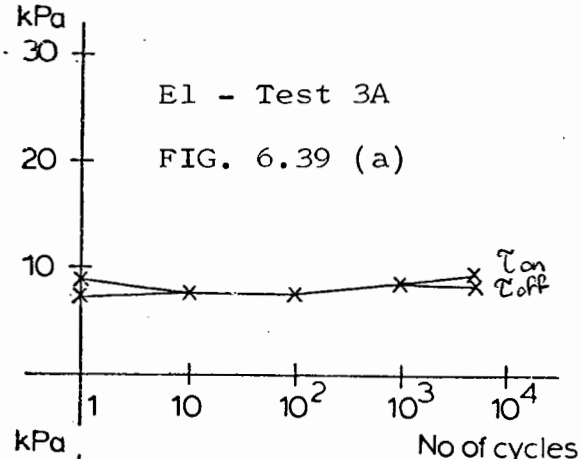

E1 - Test 3A

FIG. 6.39 (a)

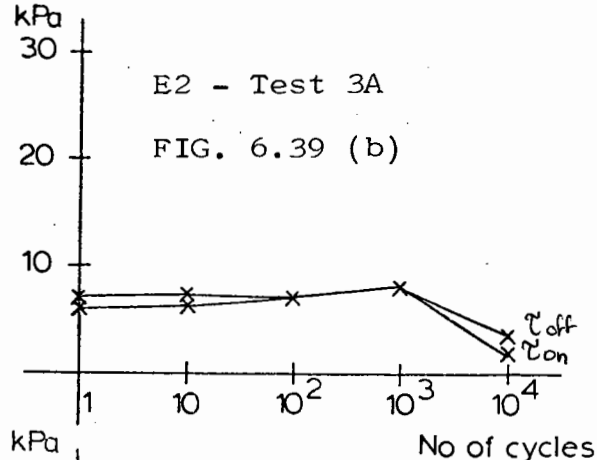

E2 - Test 3A

FIG. 6.39 (b)

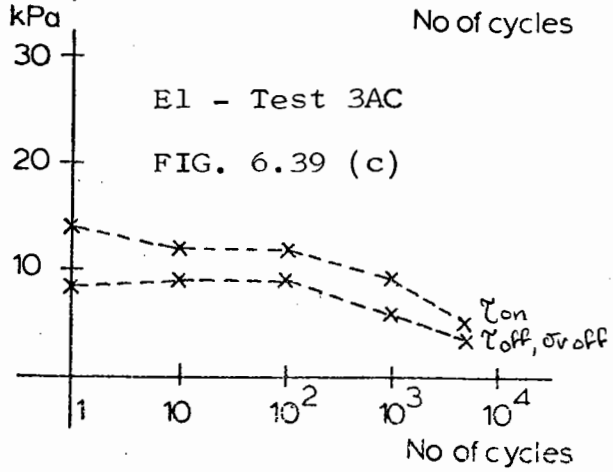

E1 - Test 3AC

FIG. 6.39 (c)

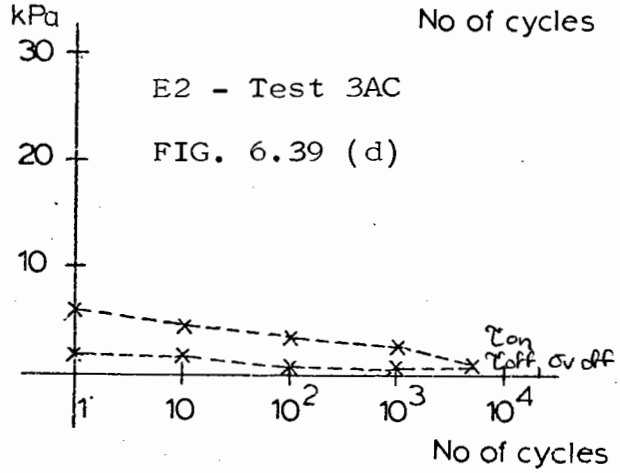

E2 - Test 3AC

FIG. 6.39 (d)

contain the initial readings of stress and it can be seen that once shearing had commenced, the measured lateral stress increased dramatically with the first cycle, but tended to decrease as the test progressed. It was thought that the material locked together during the initial compaction by vibration, and the action of shearing the specimen released the particles to transmit stress laterally. Subsequent shearing caused reorientation of the particles to take place which increased compaction and the specimen locked together again. This was evident on removing the top platen after testing when the material was normally found to be rigidly locked together. This effect may be partly overcome if the initial compaction of the specimen were carried out using shear reversal. The specimen would then be subjected to similar stress paths as during the test and particles would initially be correctly orientated. However, Youd (1975) who investigated the lateral stresses in sands during cyclic loading, found that the ratio of lateral normal stress to vertical normal stress nearly doubled during the first shear cycle for strain amplitudes near 1%. The tests were performed in a Norwegian Geotechnical Institute type of simple shear apparatus (Chapter 2).

Although the absolute values of end stresses are probably inaccurate, the general trend of results for measured stress throughout a test may be of interest.

Lateral Stress for unidirectional and bidirectional tests with both cycled and constant σ_v, tended to decrease slightly over the 5000 cycles as shown in Figs 6.29 and 6.35. This is thought to be due to the locking together of the specimen through compaction as described previously.

End Stress for the bidirectional test series, remained constant or showed a very slight increase (Fig. 6.32). A different pattern emerged for the

unidirectional test programme. Comparing Figs 6.32 and 6.38 it can be seen that for tests in which σ_v remained constant, average end stresses behaved in a similar manner to that observed for the bidirectional tests. If, however, σ_v was cycled, average end stresses decreased considerably throughout a test and this trend was consistent for all tests with cycled vertical load. No explanation can be offered other than the relative vertical motion of the top platen sections as σ_v increased and decreased was causing loosening of the specimen to take place at each end of the shear box. During testing, the ends of the specimen may also be subjected to greater particle reorientation.

Results, therefore, of lateral stress measurement, are thought to be quite accurate, although measured end stresses were consistently less. It should be noted, however, that stresses as measured on the ends of the shear box may not necessarily give a true indication of the stress state on the central portion of the specimen.

Attempts were made to predict the stress state around the specimen using only the measured values of shear stress and vertical stress for the central third.

6B.6 PREDICTION OF STRESSES (WOOD, DRESCHER & BUDHU, 1979)

The Cambridge simple shear apparatus has been developed to a stage where accurate measurements of the stresses around the boundary of the soil specimen enable a complete description of the stress state on the central part of the specimen to be computed. Over a number of years, tests on various materials have been conducted and observations made relating the ratio of shear to normal stress R and the angle of inclination of the principal axes. It is not proposed to produce a detailed description here; only major equations will be presented.

It was found that plotting the ratio of shear to normal stress, $\tau/\sigma_v = R$ against tan ψ, where ψ is the inclination to the horizontal of the plane on which the major principal stress acts, produced a straight line:

$$R = k \tan \psi \tag{6.2}$$

where k is a constant for the material under test. Assuming that, at the critical state, principal axes of strain increment and stress coincide, so that $\psi = \pi/4$ (Fig. 6.40), then:

$$R_{cv} = \sin \phi_{cv} = k \tag{6.3}$$

where ϕ_{cv} is the angle of friction for constant volume shearing and R_{cv} is the corresponding value of τ/σ_v equal to the critical state value of t/s, where

$$t = \frac{\sigma_1 - \sigma_3}{2} \tag{6.4}$$

and

$$s = \frac{\sigma_1 + \sigma_3}{2} \tag{6.5}$$

From Equation 6.2 and the geometry of Mohr's circle of stress, the following relationships can be determined:

$$\frac{\sigma_1}{\sigma_v} = 1 + R^2/k \tag{6.6}$$

$$\frac{\sigma_3}{\sigma_v} = 1 - k \tag{6.7}$$

To use these equations to predict σ_1 and σ_3 obviously requires a value of k. This may be determined for a particular material by performing a simple shear test and assuming that at the peak value of R (for example), the principal axes of strain increment and stress coincide.

Tests were conducted for the 1.5 mm size material at σ_v = 95 kPa, 190 kPa and 285 kPa, and an average value of k determined as 0.949.

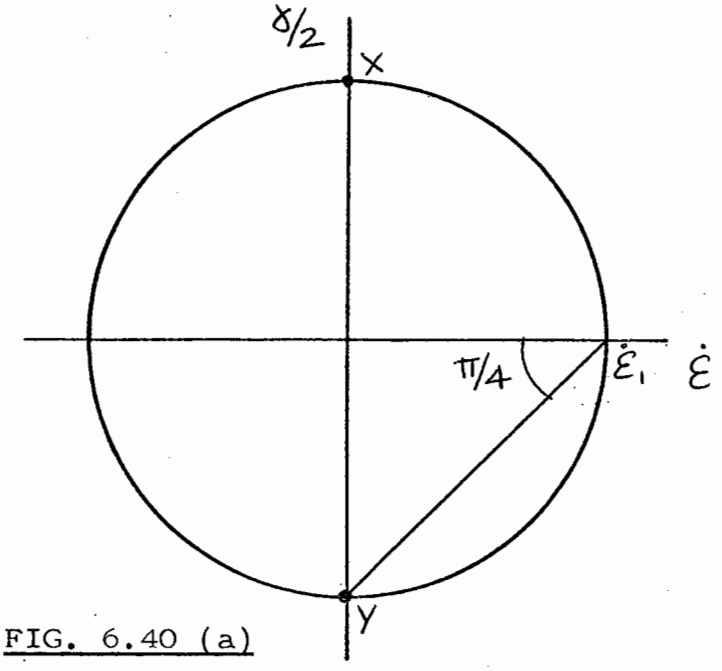

FIG. 6.40 (a)

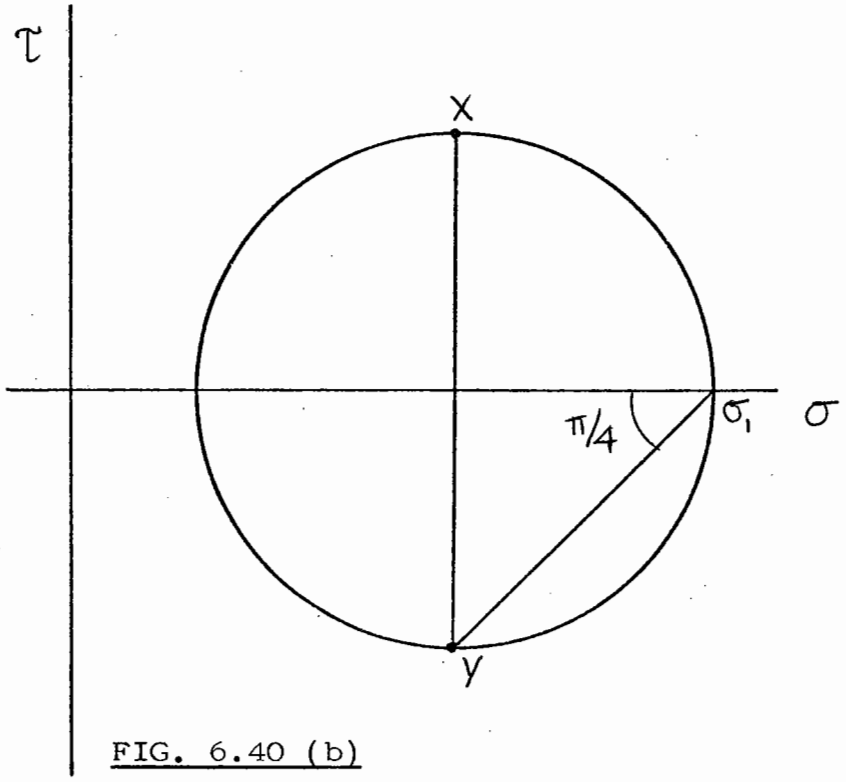

FIG. 6.40 (b)

MOHR'S CIRCLES OF (a) STRAIN INCREMENT AND (b) STRESS FOR THE CRITICAL STATE CONSTANT VOLUME SHEARING WITH $\xi = \psi = \pi/4$ (WOOD, DRESCHER & BUDHU 1979)

Table 6.6

Test	σ_v	τ/σ_v(max) = k
A	95	1.067
B	190	0.906
C	285	0.874

Table 6.7 shows the calculated values of principal stress from which the end stress was estimated and compared with the measured values. The predicted values are considerably greater than those measured. No consistent pattern emerges to enable a correction to be applied to future measured results.

To completely describe the stress state around the specimen, σ_2 is also required. Wood et al (1979) also describe a method for estimating σ_2, although serious doubts are expressed concerning its accuracy.

$$\frac{\sigma_2}{\sigma_v} = k_1 + \frac{k_1}{2k}(R^2 - k^2) \qquad (6.8)$$

where R and k are as previously defined. If the coefficient of earth pressure at rest K_o is known, then k_1 may be estimated from:

$$k_1 = \frac{2K_o}{1 + K_o} \qquad (6.9)$$

where K_o may be obtained from:

$$K_o = 1 - \sin \phi' \qquad (6.10)$$

Table 6.7 also compares predicted and measured values of σ_2. It is assumed that no shear force acts on the vertical lateral face of the shear box and hence measurements of lateral stress are measurements of the intermediate principal stress. The measured lateral stresses appear

TABLE 6.7 PREDICTED AND MEASURED STRESSES FOR 1.5 mm MATERIAL

TEST	σ_v (kPa)	R	PREDICTED (kPa)		σ_E (kPa)		σ_2 (kPa)	
			σ_1	σ_3	PREDICTED	MEASURED	PREDICTED	MEASURED
1B	284	0.48	354.1	14.5	83.6	25.7	66.6	73.2
1BC	282	0.47	351.3	14.5	80.8	21.4	66.1	75.8
2B	190	0.48	242.3	9.9	57.3	15.1	45.6	42.3
2BC	190	0.47	240.2	9.9	55.2	12.6	45.2	56.4
3B	97	0.39	112.5	4.9	20.4	10.3	21.2	28.4
3BC	97	0.45	117.7	4.9	25.7	7.2	22.1	27.9
1A	285	0.46	348.5	14.5	78.0	24.6	65.6	55.9
1AC	283	0.48	354.2	14.5	83.7	16.8	66.6	55.7
2A	190	0.48	244.8	10.0	57.8	11.1	46.0	39.7
2AC	190	0.50	269.1	10.9	66.9	6.8	50.6	42.2
3A	97	0.62	136.3	4.9	44.3	6.9	25.5	28.8
3AC	97	0.46	140.6	5.9	31.5	8.3	26.4	21.6

to be of the same order of magnitude as those predicted using Wood et al (1979).

6B.7 REPRESENTATION OF STRESS PATHS IN (p,q) STRESS SPACE

The predicted values of σ_1, σ_2 and σ_3 enabled the stress conditions of the simple shear apparatus to be expressed in terms of the invariants p and q. Since measurements of lateral stress were considered reasonably accurate (Section 6B.6), it was decided to use the predicted values of σ_1 and σ_3 and the measured lateral stress. For simplicity, only paths having constant σ_v were considered.

Fig. 6.41 shows the simple shear conditions as represented by Mohr's circle of stress. The stress path under consideration was a unidirectional path as illustrated by the insert.

Initially there was no shear on the specimen and σ_v and σ_E (the vertical and end stress) were principal stresses. The test results indicated that the lateral stress remained constant during shear reversal for stress paths with constant σ_v. Since no shear stress was assumed to act on the vertical lateral face of the box, the measured lateral stress could be considered as a principal stress. The beginning of the stress path was therefore represented by p_1 and q_1 where:

$$p_1 = \frac{1}{3}(\sigma_v + \sigma_E + \sigma_L) \qquad (6.11)$$

$$q_1 = \frac{1}{\sqrt{2}}\left[(\sigma_v-\sigma_E)^2 + (\sigma_v-\sigma_L)^2 + (\sigma_E-\sigma_L)^2\right]^{\frac{1}{2}} \qquad (6.12)$$

σ_v, σ_E and σ_L are the vertical, end and lateral stresses respectively and are principal stresses. Lateral stress was assumed to remain constant on application of shear stress, when the Mohr's Circle (Fig. 6.41) expanded to positions σ_1 and σ_3. Hence the end of the stress path was represented by p_2 and q_2:

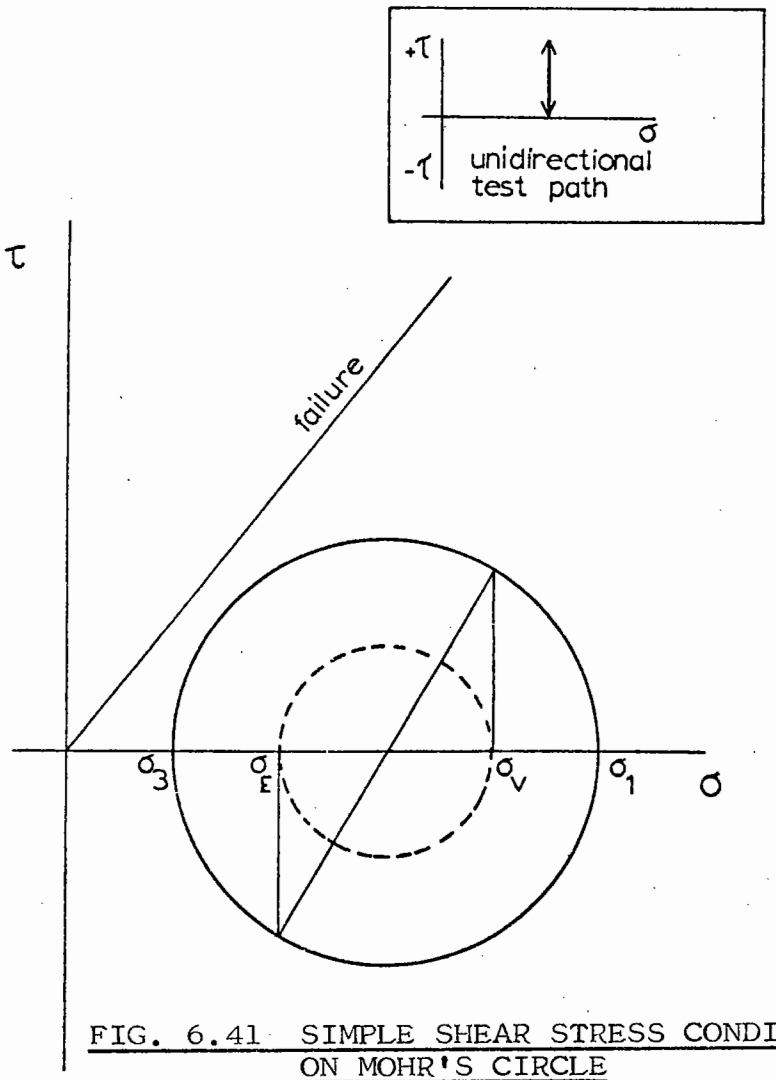

FIG. 6.41 SIMPLE SHEAR STRESS CONDITIONS ON MOHR'S CIRCLE

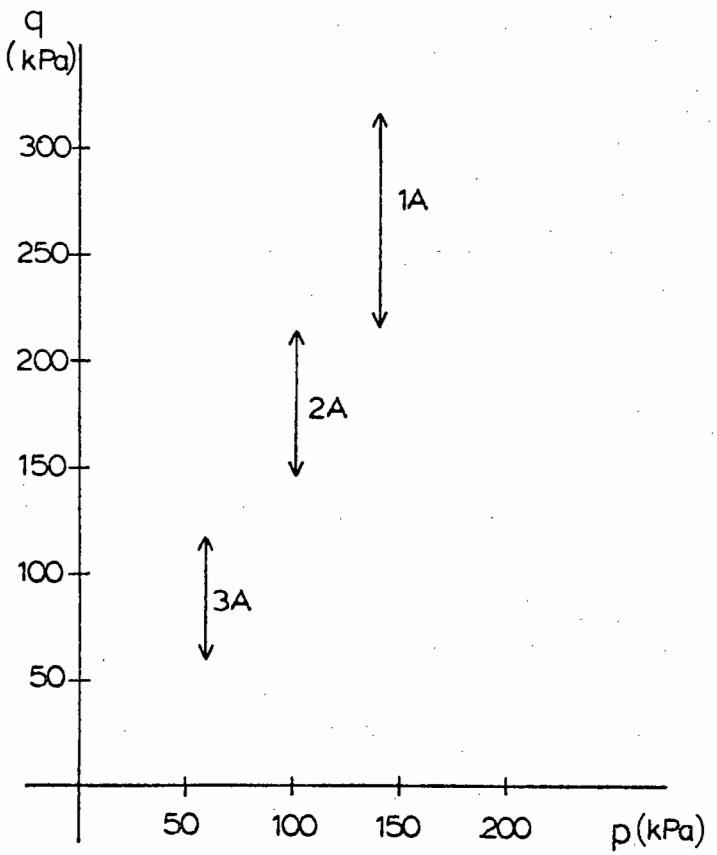

FIG. 6.42 SIMPLE SHEAR STRESS PATHS IN (p,q) STRESS SPACE

$$p_2 = \frac{1}{3}(\sigma_1 + \sigma_3 + \sigma_L) \tag{6.13}$$

$$q_2 = \frac{1}{\sqrt{2}}\left[(\sigma_1-\sigma_L)^2 + (\sigma_1-\sigma_3)^2 + (\sigma_3-\sigma_L)^2\right]^{\frac{1}{2}} \tag{6.14}$$

where σ_1 and σ_3 are the predicted major and minor principal stress and $\sigma_L = \sigma_2$ is the measured lateral stress. Using this procedure, the stress paths may be represented by expanding Mohr's circles (Fig. 6.41) or a series of straight lines perpendicular to the p axes in (p,q) stress space as shown in Fig. 6.42. Table 6.8 gives the p and q values for each of the three unidirectional tests with σ_V constant.

Bidirectional tests produced the same p and q values, but during shear reversal the path repeated itself in (p,q) stress space. Hence, one bidirectional stress path was equal to two repetitions of a unidirectional path.

It was found that using this approach, lateral stress tended to switch position as intermediate and minor principal stress for each stress path. Initially, lateral stress was the minor principal stress σ_3, but on shearing became the intermediate stress. This, however, did not affect the calculated values of p and q for the beginning and end of each stress path.

An attempt was then made to correlate the simple shear results with the resilient and permanent strain models produced in the triaxial apparatus. A closer examination of the stress paths as determined for (p,q) stress space revealed that all were near to or exceeded the failure ratio q/p = 2.1 as determined from triaxial compression monotonic failure tests (Section 3.3). It is the author's opinion, therefore, that no comparison can be made between triaxial and simple shear results on the basis of (p,q) stress representation. The simple shear test paths are outside the validity of the triaxial and resilient and permanent strain

TABLE 6.8 (p,q) REPRESENTATION OF STRESS PATHS

TEST	σ_v(kPa)	p_1(kPa)	q_1(kPa)	p_2(kPa)	q_2(kPa)	(q/p)max
1A	285	140	219	140	316	2.26
2A	197	101	149	101	215	2.13
3A	97	59	63	59	117	1.98

ANSELL'S RESULTS

TEST	σ_v(kPa)	p_1(kPa)	q_1(kPa)	p_2(kPa)	q_2(kPa)	(q/p)max
A01	95	53	65	53	116	2.19
A03	95	67	57	67	150	2.24
A04	95	42	79	42	91	2.17
A09	190	85	158	85	183	2.15
A10	190	94	144	94	205	2.18
A11	190	120	117	120	264	2.20
A13	285	150	204	150	328	2.19
A14	285	126	240	126	272	2.16
A16	285	197	170	197	440	2.23

TABLE 6.9 (p,q) REPRESENTATION OF STRESS PATHS

models. An analysis of Ansell's results (1977) revealed that almost all of the paths tested on the 3 mm crushed limestone were for conditions in excess of failure as defined for (p,q) stress space (Table 6.9).

It must also be considered, however, that the assumptions made in predicting the stress state around the specimen may be in error and that the predicted (p,q) values are not a true representation of the simple shear stress state. This cannot be checked under present circumstances. If, however, the predicted stresses are of the correct order, strains produced in the simple shear apparatus are less severe than would occur in the triaxial apparatus under failure conditions. The plane strain nature of the biaxial apparatus (Chapter 4) affected permanent straining such that no threshold value was obtained and permanent strain tests could be conducted right up to failure with no significant increase in permanent strain rate (Fig. 4.19). It is thought that a similar condition exists in the simple shear apparatus and although loading patterns are different, it is possible to conduct tests beyond the failure state as defined for the axisymmetric triaxial case.

Section C, however, contains details of the strain behaviour of the material in the simple shear apparatus and compares results obtained with those of Ansell (1977).

SECTION C - STRAIN BEHAVIOUR

6C.1 TESTS ON 3mm CRUSHED LIMESTONE

A preliminary testing programme was conducted on the 3 mm crushed limestone as used by Ansell (1977) and in the triaxial and biaxial test programmes of Chapters 3 and 4. The series was designed to investigate lateral stress behaviour (Section 6B.2) but contained some tests with cycled vertical loading. The series, therefore, was useful to investigate the effects of a cycled vertical stress. The tests were all of the

bidirectional type as shown in Fig. 6.23 and the programme was conducted with σ_v constant or cycled between a maximum and zero.

Brown and Ansell (1980) found that shear reversal resulted in increased compaction. This was also commented on by Youd (1972) who suggested that shear reversal was one of the most effective means of compaction. However, in both cases, tests were conducted with constant vertical stress. Fig. 6.43 shows a comparison of the resilient shear strains for each of the tests on the 3 mm material. The shear stress and resilient shear strain was essentially the same for each stress path at a given σ_v value. The differences in permanent volumetric strain shown in Fig. 6.44 were, therefore, entirely due to the effects of vertical stress.

Ansell placed great importance on strains resulting from cycle 1, but the repeatability series described in Section 6A.3.3 showed that large variations occur between strains observed at cycle 1 for tests with similar stress conditions. To be consistent with the procedure adopted for analysis of the triaxial and biaxial results, it was decided to investigate changes in strain, rather than absolute values. Subsequently, the results in Fig. 6.45 were plotted such that the permanent volumetric strain for each test was zero at cycle 10. It is immediately apparent that cycling σ_v causes considerable increases in compaction. There were no unidirectional tests conducted on the 3 mm crushed limestone in this programme, but Section 6C.2 describes tests on a 1.5 mm single size material, where it is shown that a similar effect is evident for both bidirectional and unidirectional loading conditions.

It would, therefore, appear that compaction may be further increased by a repeated vertical stress.

The test results from the modified apparatus compared favourably with those obtained by Ansell (1977) and inspired some confidence that

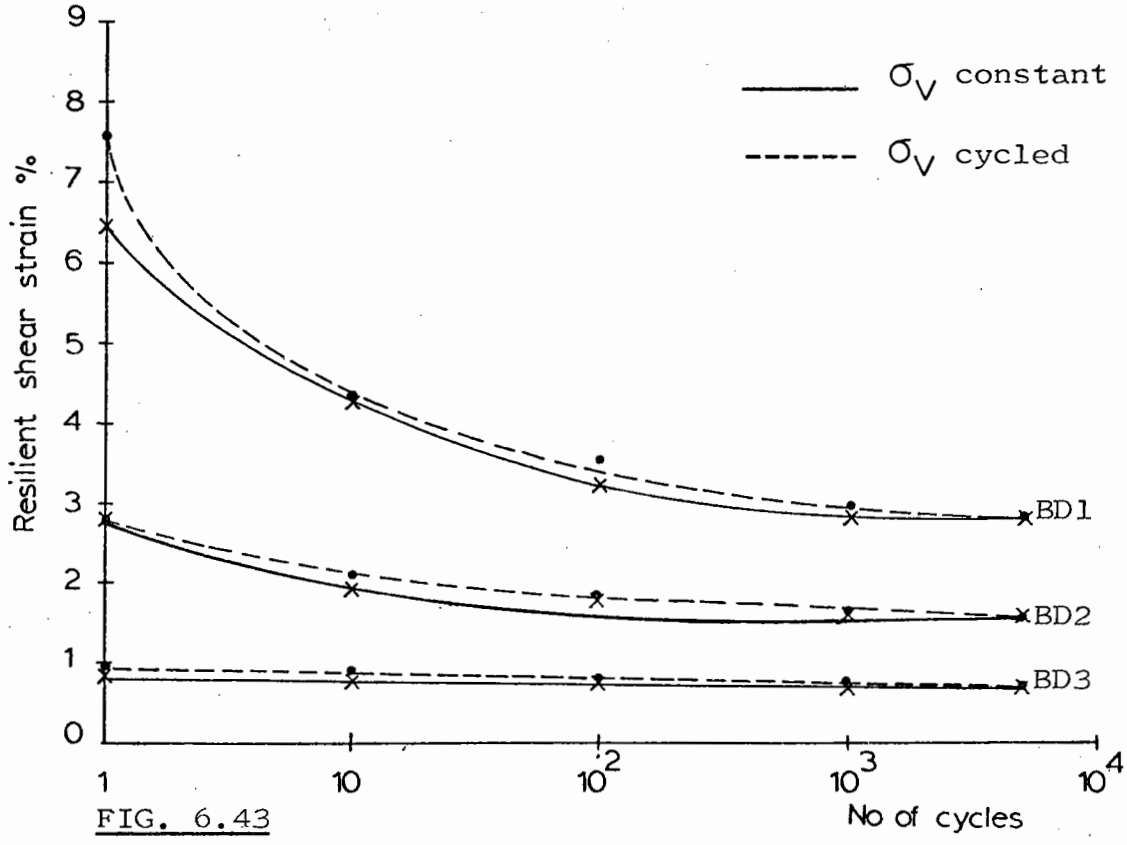

FIG. 6.43

RESULTS FROM BIDIRECTIONAL TEST SERIES ON 3 mm MATERIAL

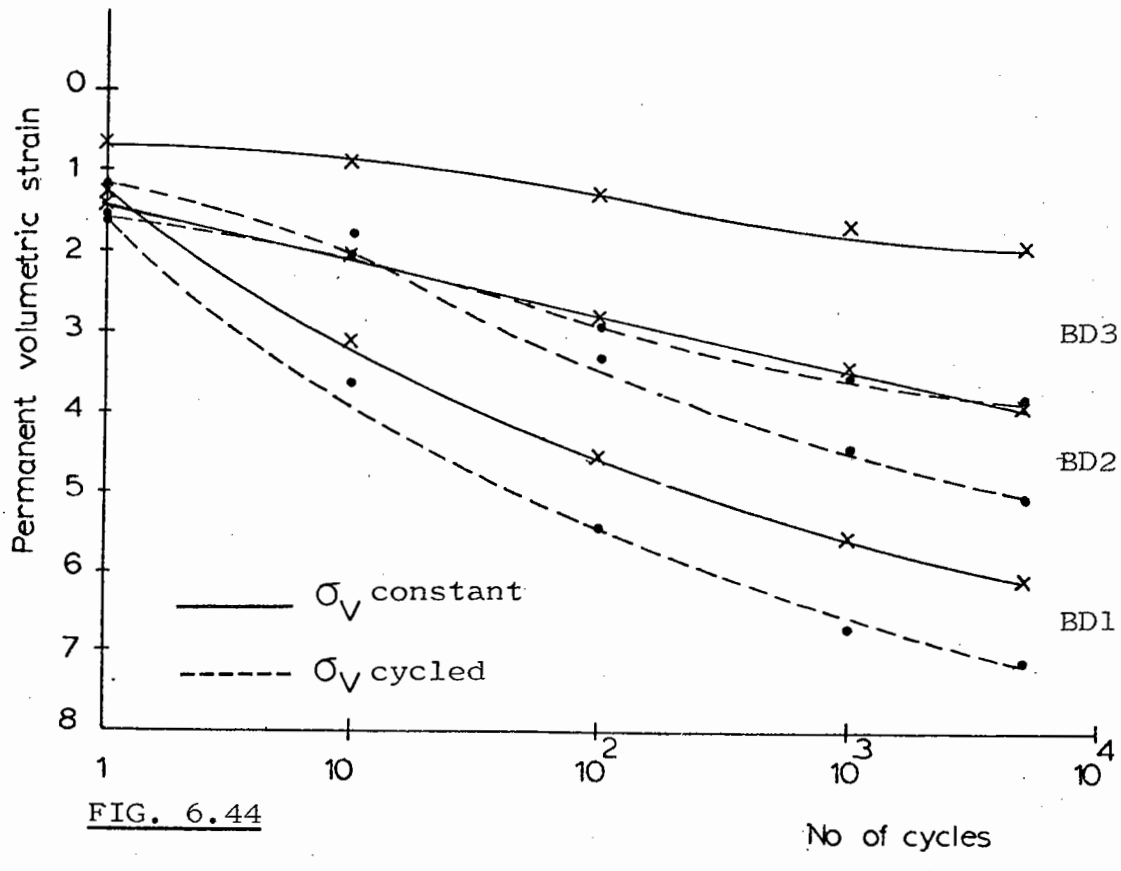

FIG. 6.44

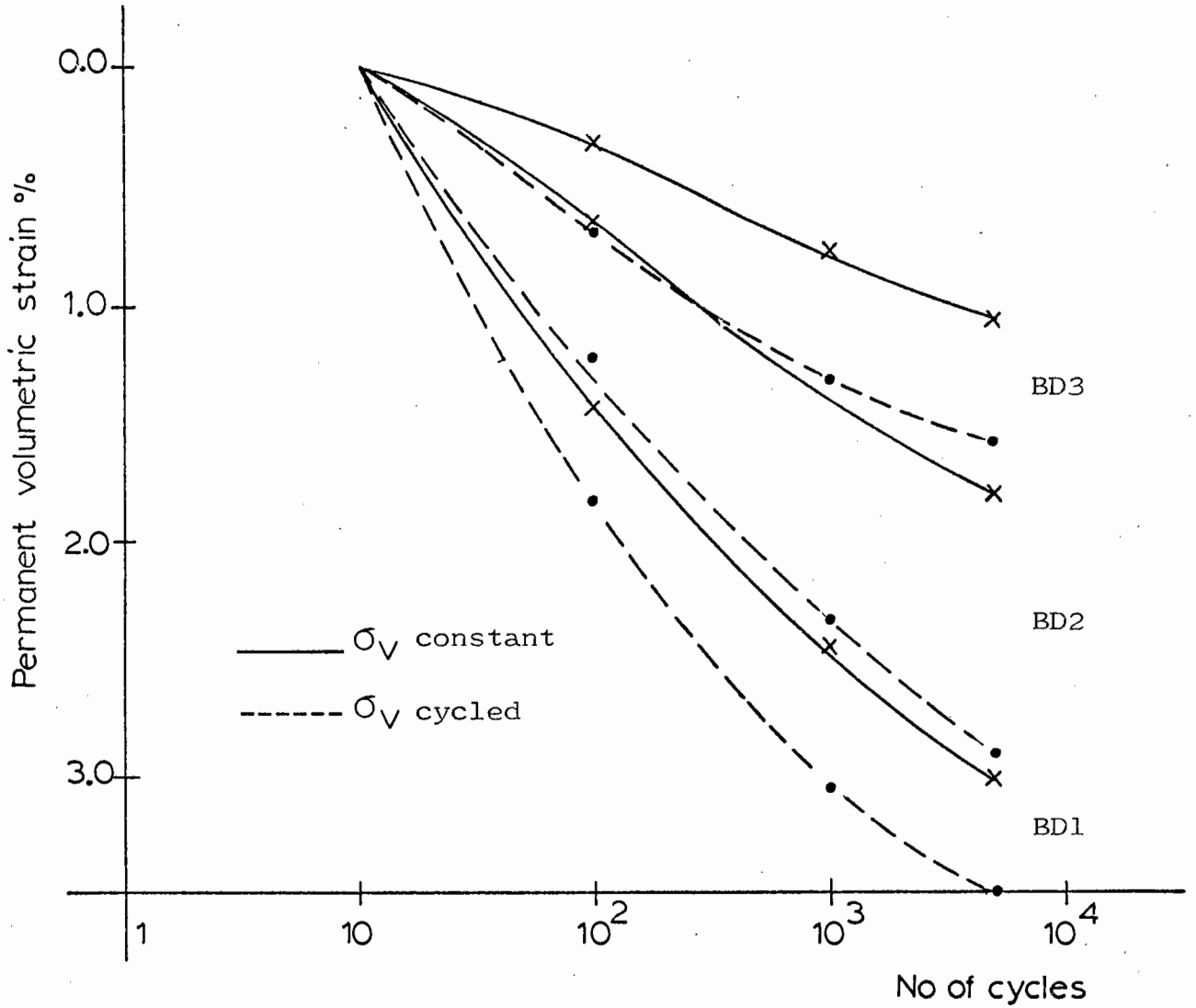

FIG. 6.45 COMPARISONS OF PERMANENT VOLUMETRIC STRAIN FOR BIDIRECTIONAL TEST SERIES ON 3 mm MATERIAL

material characteristics and not apparatus effects were being investigated.

6C.2 TESTS ON 1.5mm CRUSHED LIMESTONE

Following the investigation into lateral stress measurement (Section 6B.3), a 1.5 mm crushed limestone material was chosen on which to perform a more complex test programme. Both bidirectional and unidirectional tests were performed with constant σ_v and cycled σ_v. The repeated load stress paths applied to the specimens are shown in Fig. 6.27. As indicated in Section 6B.4, only one test was conducted on each stress path.

Bidirectional Tests

These were tests in which the shear load pulse was symmetrical about zero. The specimen was subjected to a shear pulse alternately in each direction. This produced a shear reversal in the material. The series involved six tests, three with σ_v constant and three with σ_v cycled. The resilient shear strain and permanent volumetric strain were plotted against the logarithm of the number of cycles as shown in Figs 6.46 and 6.47.

The procedure of zeroing test results at 10 cycles was again adopted and a plot of permanent volumetric strain against stress cycles is shown in Fig. 6.48. The results are not as distinctive as those obtained for the 3 mm material, but the trend again suggests that cycling vertical stress increases compaction.

Unidirectional Tests

These were tests in which shear loading was applied in one direction only. The test paths are shown in Fig. 6.27. The three paths were tested both with σ_v constant and cycled as for the bidirectional programme.

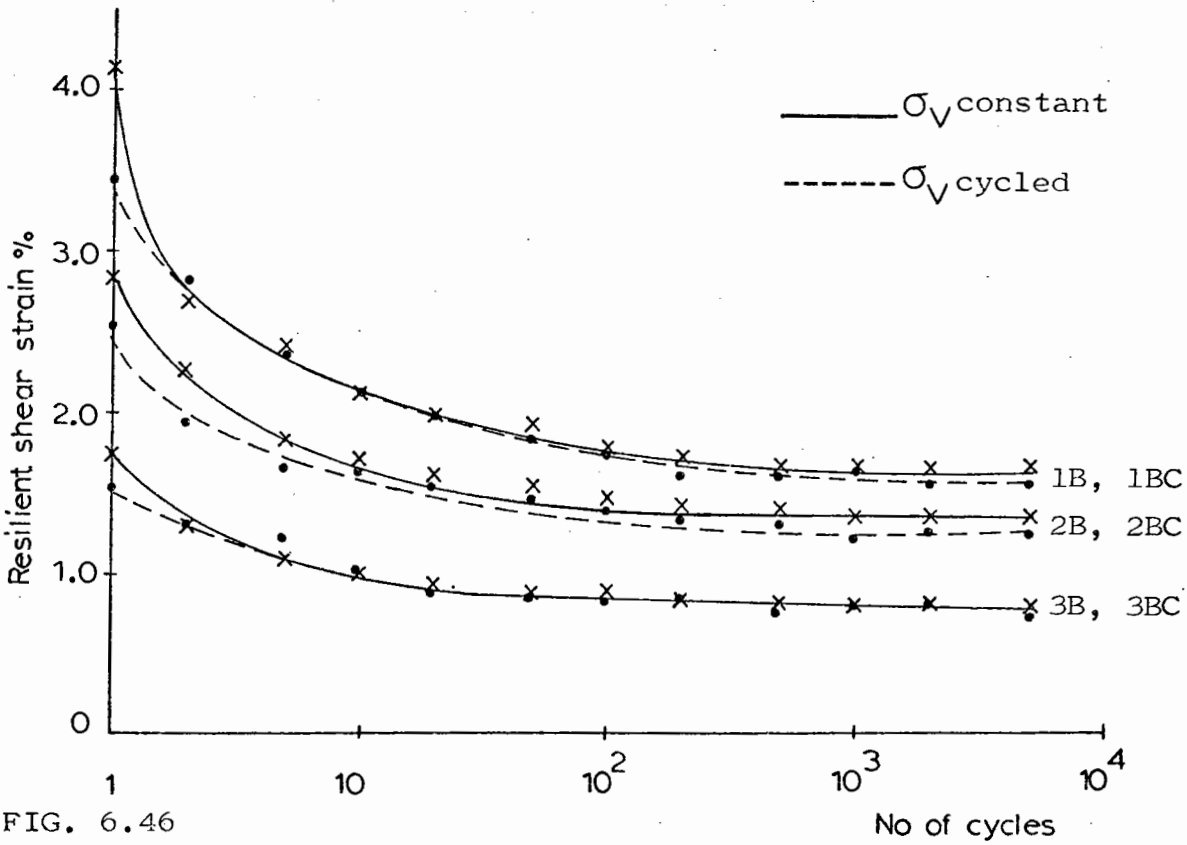

FIG. 6.46

RESULTS FROM BIDIRECTIONAL TEST SERIES ON 1.5 mm MATERIAL

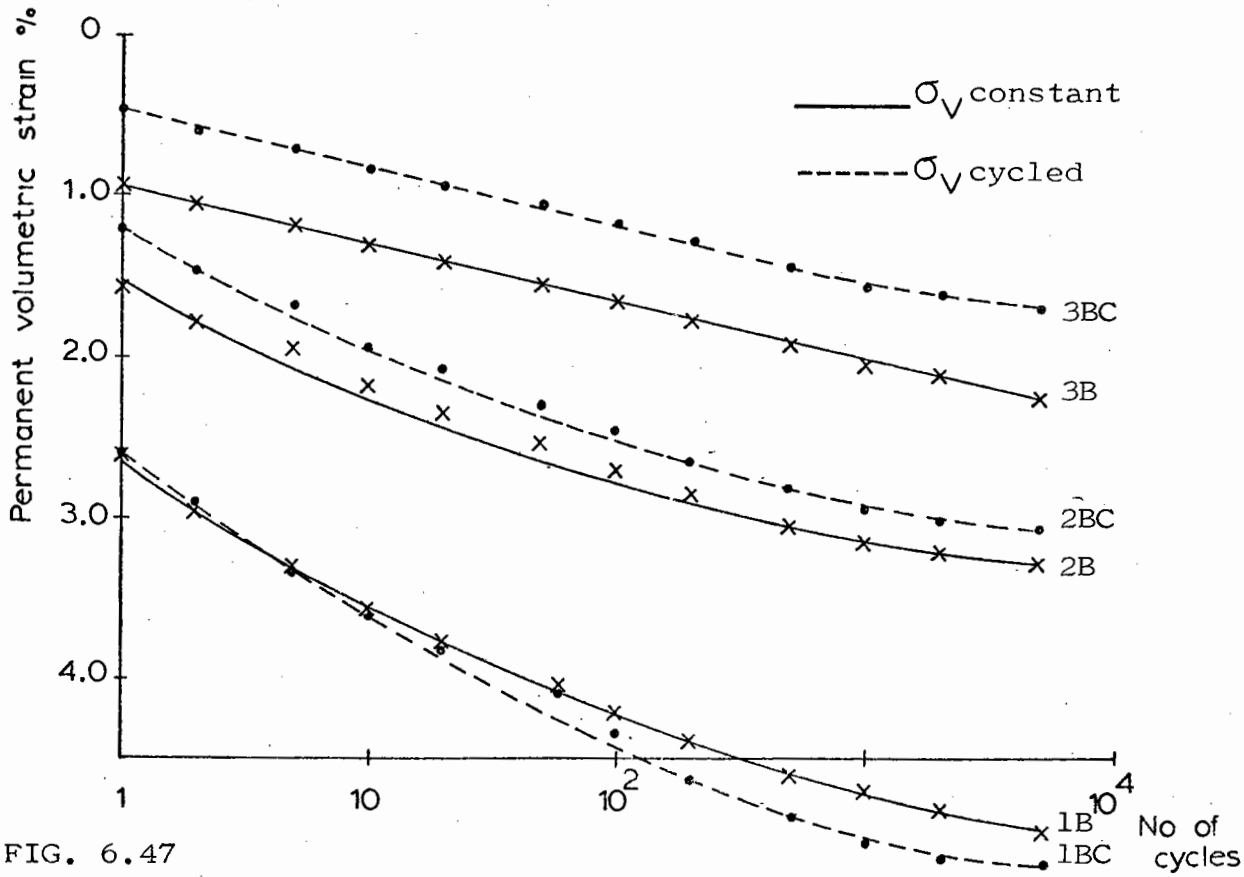

FIG. 6.47

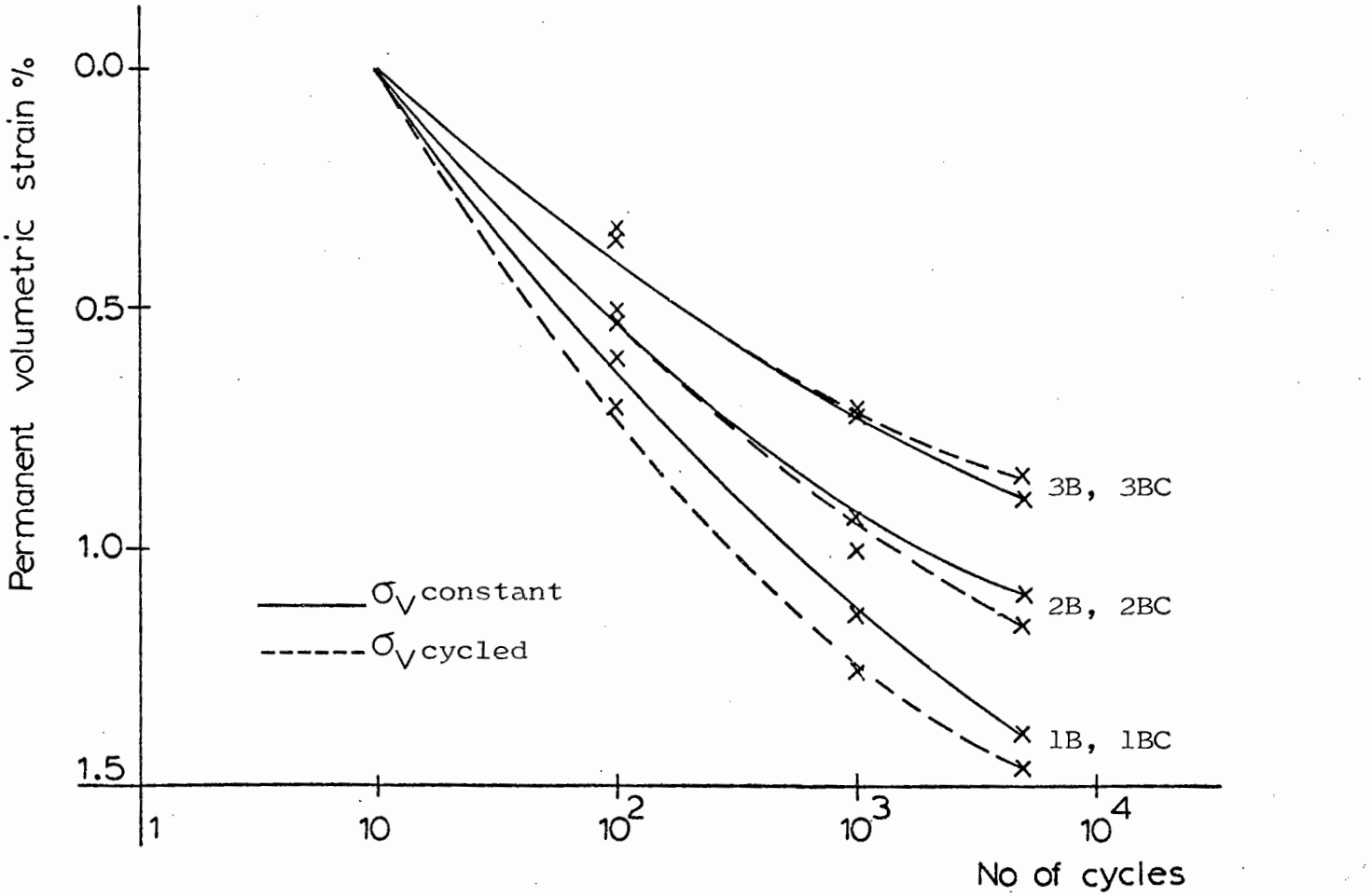

FIG. 6.48 COMPARISONS OF PERMANENT VOLUMETRIC STRAIN FOR BIDIRECTIONAL TEST SERIES ON 1.5 mm MATERIAL

Plots of permanent shear strain, resilient shear strain and permanent volumetric strain, against the logarithm of the number of cycles are shown in Figs 6.49 to 6.51. The material did not exhibit any significant resilient volumetric strain.

Observations on the bidirectional test series, suggested that resilient shear strain was unaffected by the pattern of vertical loading, the results being repeatable for σ_v constant and σ_v cycled. However, this was not the case for the unidirectional tests. Fig. 6.50 shows that resilient shear strains for tests with σ_v cycled were generally greater than if σ_v was constant. This would suggest that there may be some rearrangement of particles within the specimen as σ_v is unloaded and reapplied. The permanent shear strain behaviour (Fig. 6.49) was also significantly altered by the application of a repeated vertical load. Tests with constant σ_v behaved in a similar manner to those conducted by Ansell. Fig. 6.51 shows the development of permanent volumetric strain for each test and is replotted in Fig. 6.52. Again the trend would suggest that cycling σ_v increases compaction. On comparing the volumetric strain results of the unidirectional series with those of the bidirectional, the findings of Ansell are reinforced in that shear reversal tends to produce greater compaction. However, the effect is not so marked as for the 3 mm material. This is discussed in Section 6C.3 where further comparisons are made between the strain behaviour of the 3 mm and 1.5 mm materials.

Insufficient tests have been conducted to quantify the effects of a repeated vertical stress. However, results obtained would suggest that the new loading conditions signficantly affect the pattern of strain behaviour.

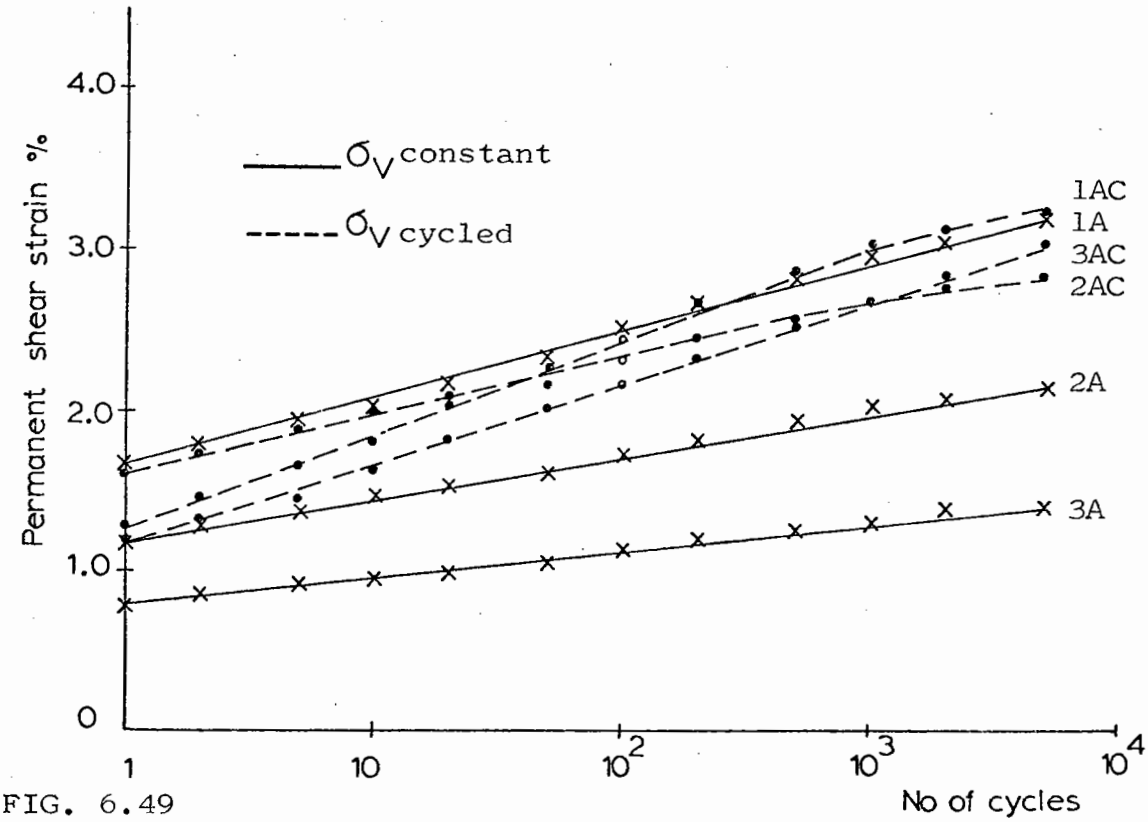

FIG. 6.49

RESULTS FROM UNIDIRECTIONAL TEST SERIES ON 1.5 mm MATERIAL

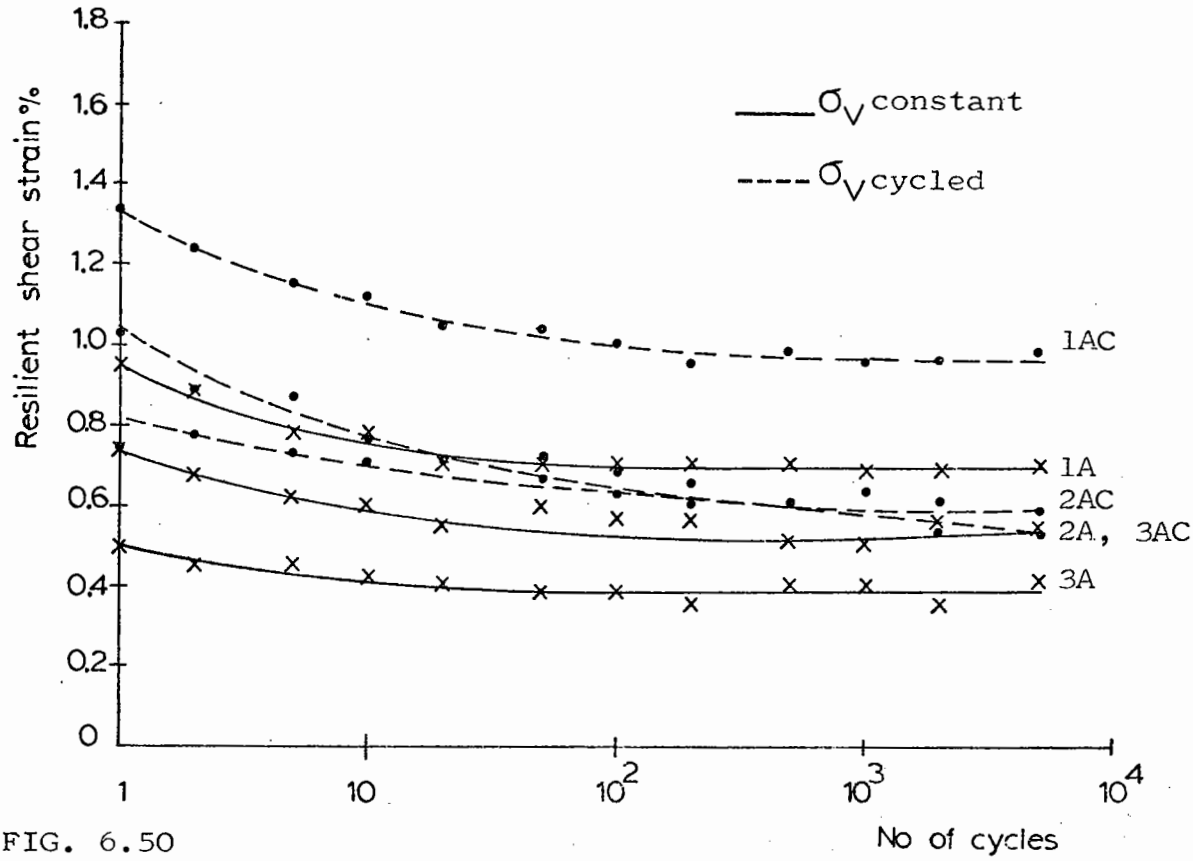

FIG. 6.50

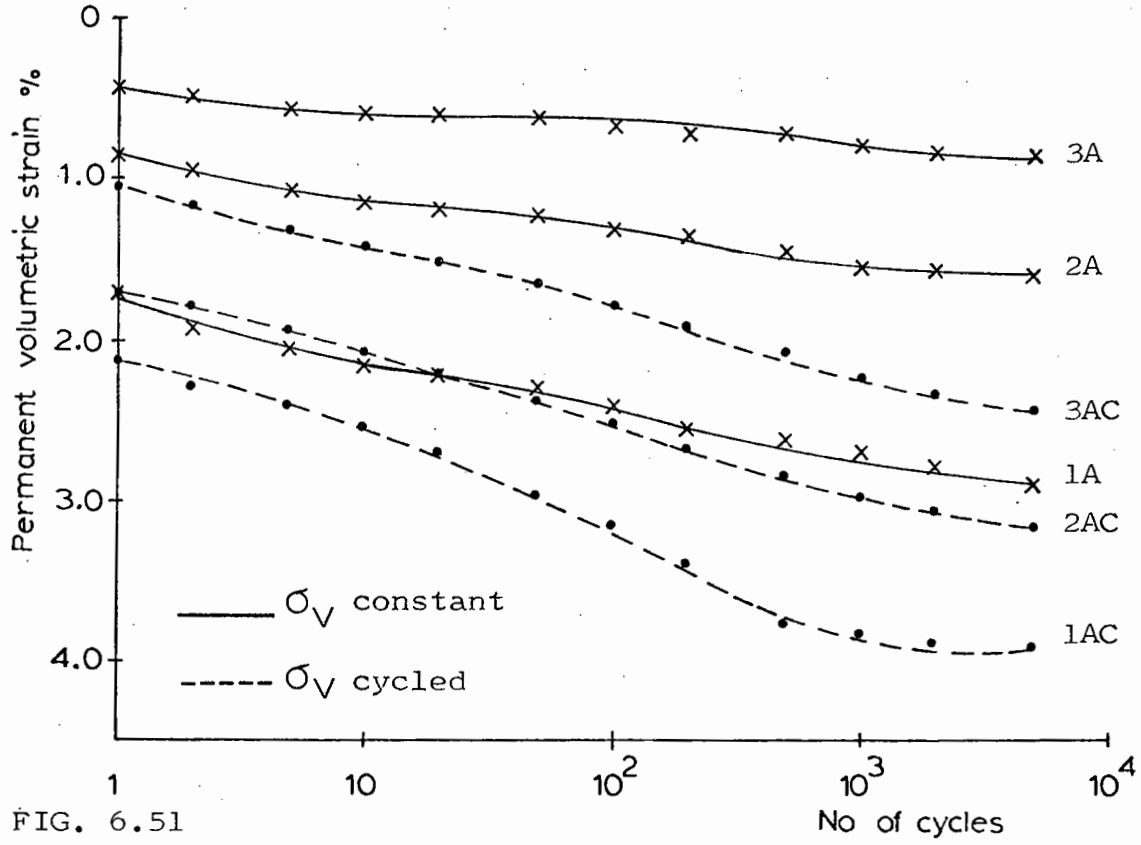

FIG. 6.51

COMPARISONS OF PERMANENT VOLUMETRIC STRAIN FOR UNIDIRECTIONAL TEST SERIES ON 1.5 mm MATERIAL

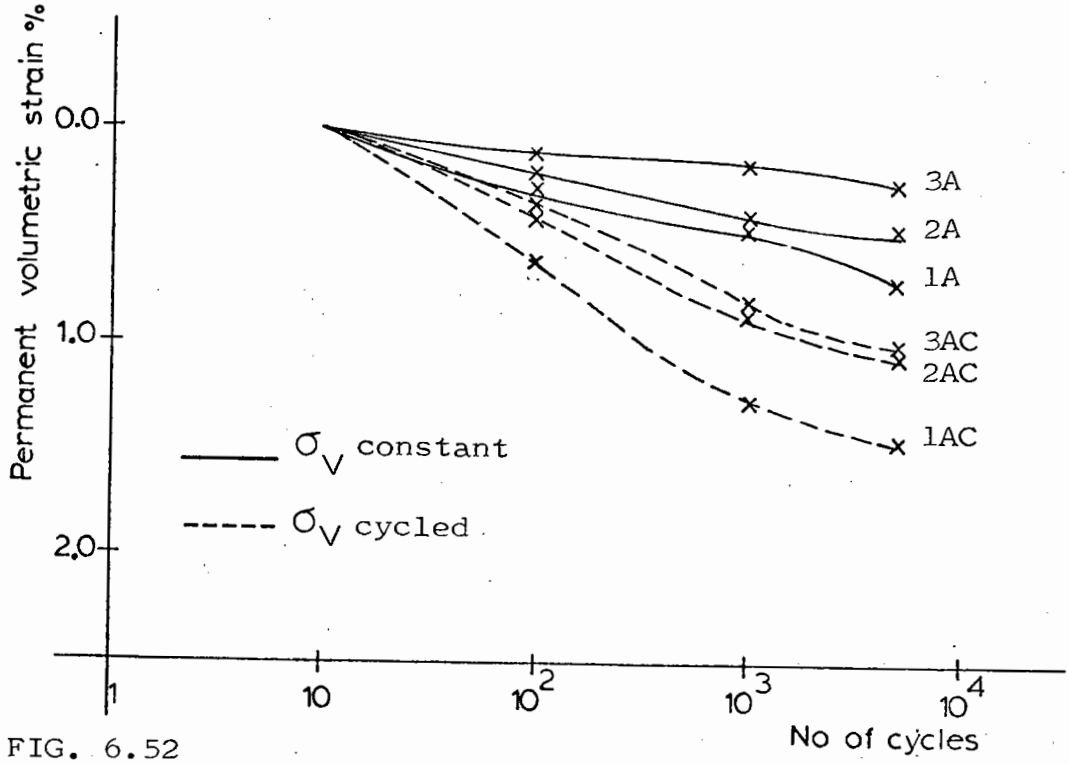

FIG. 6.52

6C.3 COMPARISON OF 3mm AND 1.5mm MATERIALS

Resilient Strains: A comparison of the resilient behaviour of the 3 mm and 1.5 mm materials showed that both behaved similarly under triaxial conditions (Chapter 3, Section 3.5). By defining a cyclic shear stress ratio R_c at cycle 10 as described in Section 6A.3.1, a comparison of the resilient behaviour of the two materials may be obtained for simple shear conditions.

Figs 6.53 and 6.54 show plots of resilient shear strain against the logarithm of the number of cycles for both materials under bidirectional and unidirectional loading conditions, respectively. Only tests with σ_v constant are compared, as Ansell did not have the facility for repeated vertical loading. It was not possible to directly compare tests having the same cyclic shear stress ratio, but general trends can be observed. Consistent with the triaxial findings, the results showed that the resilient shear strain behaviour of the two materials was similar. Resilient volumetric strains for the 1.5 mm material were not measured with sufficient accuracy to be included in this presentation.

Permanent Strains: No permanent strain tests were carried out on the 1.5 mm material using the triaxial equipment, although a comparison of permanent strain behaviour for the two materials may be made in the simple shear apparatus.

By assuming zero strain at 10 cycles, results for the 3 mm and 1.5 mm materials are compared in Figs 6.55 to 6.57. The lines of permanent strain against the logarithm of the number of cycles in effect represent the rate of straining for each test path.

Considering permanent volumetric strain, it is immediately apparent from Figs 6.55 and 6.56 that for both bidirectional and unidirectional tests, the rate of strain for the smaller material is considerably less than that of the larger. However, the general trend of increasing rate

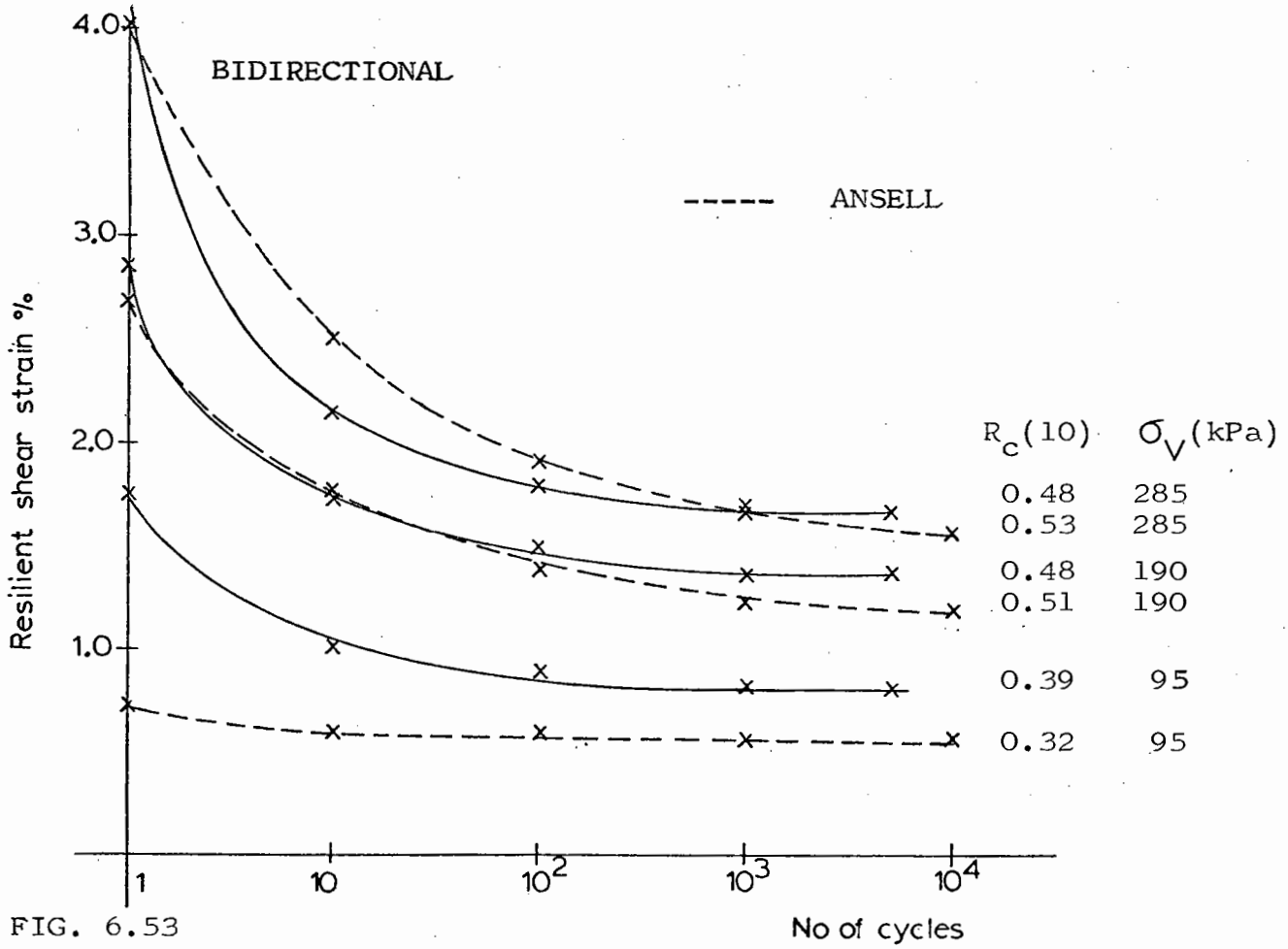

FIG. 6.53

COMPARISONS OF RESILIENT SHEAR STRAINS FOR 1.5 mm MATERIAL AND 3 mm MATERIAL

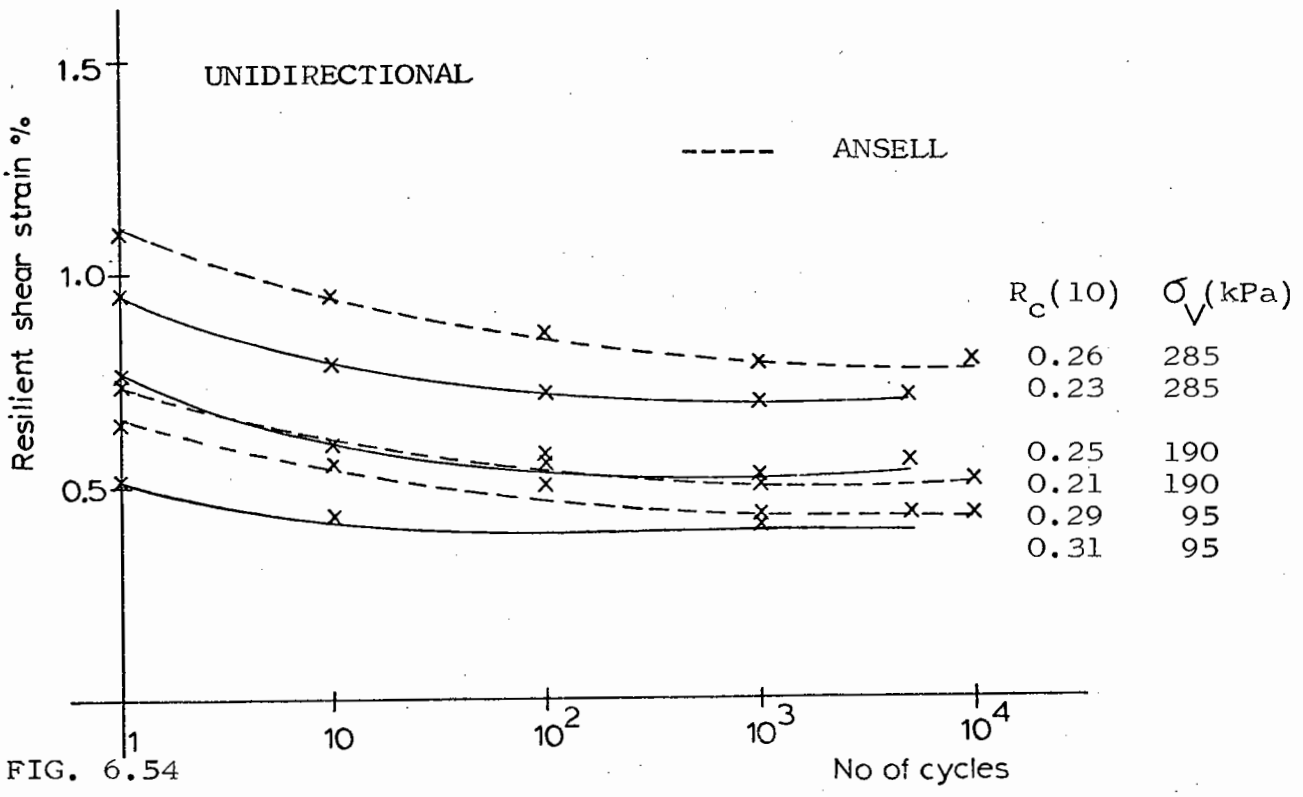

FIG. 6.54

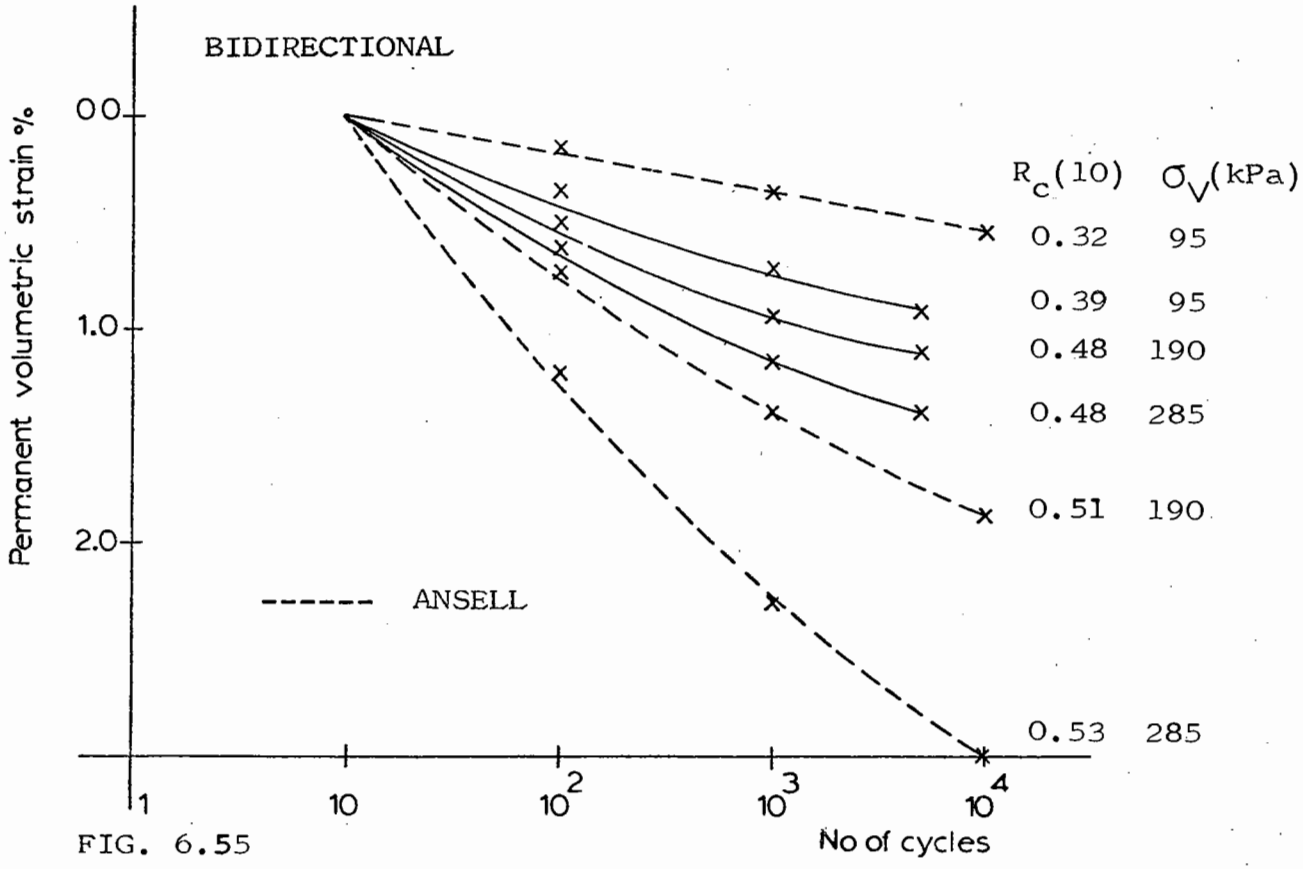

FIG. 6.55

COMPARISONS OF PERMANENT VOLUMETRIC STRAINS FOR 1.5 mm MATERIAL AND 3 mm MATERIAL

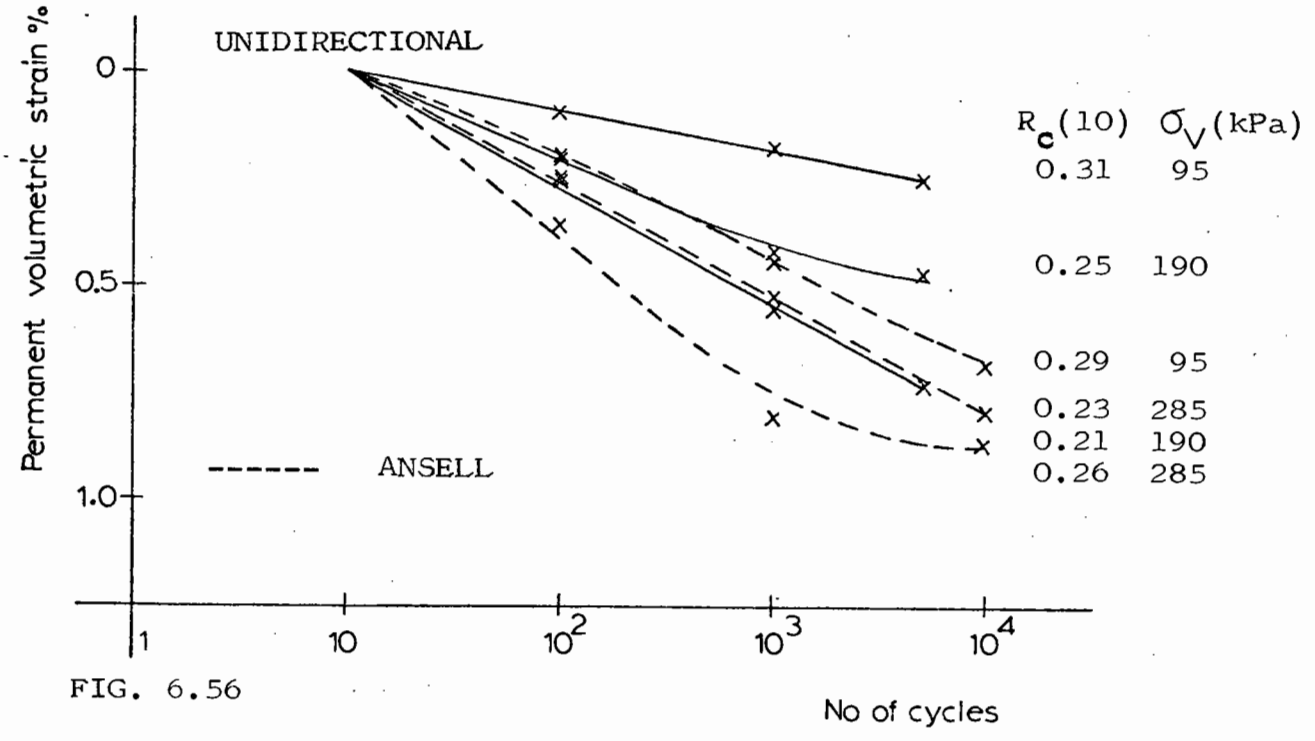

FIG. 6.56

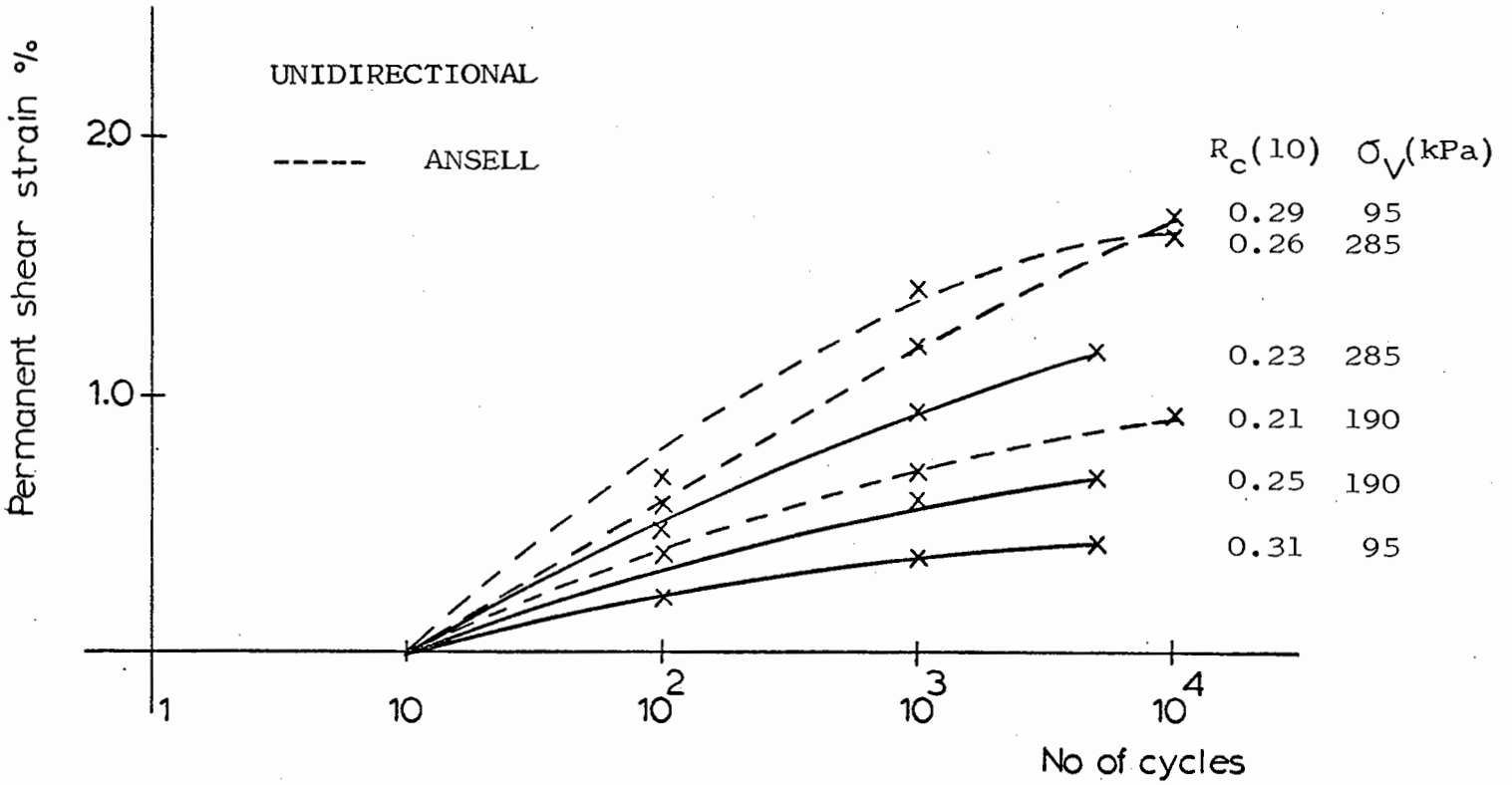

FIG. 6.57 COMPARISONS OF PERMANENT SHEAR STRAINS FOR 1.5 mm MATERIAL AND 3 mm MATERIAL

of compaction with increasing vertical stress, is common to both materials. If cycle 1 is considered, the smaller material produced greater volumetric strains over a complete test. It would be expected that the rate of straining of the 3 mm material should be greater because of less particle contacts and hence greater interparticle forces. However, as shown by Ansell, the 3 mm material exhibited a strongly dilatant behaviour and it is thought that this tendency towards dilation has contributed to the reduced initial compaction. The small material did not exhibit any dilatant behaviour throughout the present test series, and compacted continuously. The results, however, would indicate that after the first cycle, the smaller material develops less permanent strain than the 3 mm material. Permanent strain, repeated load triaxial tests on graded and single size material have shown that the graded material produces considerably less permanent strain (Chapter 3). The simple shear results presented above would suggest that a smaller material, which inherently produces increased particle contact, contributes towards the same effect.

In application to the railway situation, these findings would reinforce the viewpoint that a wider grading, whilst not drastically affecting drainage or riding quality, would result in significant reductions in the rate of permanent strain development.

Fig. 6.57 shows a comparison of the build up of permanent shear strain with number of cycles for the 3 mm and 1.5 mm materials. Again, the rate of straining of the smaller material is considerably less than that of the larger. On first examination, the results would appear to conflict, in that whilst the smaller material shows a definite reduction in permanent strain rate with decreasing vertical load, the larger material does not show the same tendency. However, the results from Ansell's tests were chosen in order that results from tests having similar R_c values could be compared, it is unfortunate that the σ_v = 95 kPa

result does not reflect the general trend of his findings.

It would therefore appear that whilst the resilient response of the two materials is similar, the permanent strain behaviour is considerably different.

CHAPTER SEVEN

APPLICATION OF RESILIENT STRAIN MODELS TO PAVEMENT ANALYSIS

7.1 INTRODUCTION

During recent years computers have been increasingly used for the analytical design of road pavements. Pavement design is basically a process where a pavement structure is selected, checked by some means and modified, if required, to ensure that predetermined failure levels will not be exceeded during the design life of the structure. The finite element method is often used during the design process to investigate the resilient and permanent strain response of structures containing non-linear layers. However, the accuracy of the system largely depends on that of the stress-strain models used to characterise the various materials which constitute the pavement.

The main contribution towards material characterisation has come from laboratory testing and whilst considerable work has been conducted on asphaltic materials, attention is now being directed more towards the granular layer and subgrade.

It is not the author's intention to give a detailed description of the finite element method, but rather to compare results from analysis of a selection of pavements. Two programs have been used, BISTRO (Peutz et al, 1968), which employs layered elastic methods, and SENOL (Pappin, 1979) which employs finite element methods. The granular layer has been modelled as linear elastic in BISTRO and non-linear in SENOL. The non-linear models used, were the contour models described in Chapter 3 and the K-theta model from Chapter 5. Most of this chapter will be devoted to discussing the use of, and results obtained from, SENOL.

7.2 SENOL: SEcant NOn Linear finite element analysis

The finite element program SENOL was developed by Pappin (1979) to accommodate the contour models described in Chapter 3. The philosophy behind the development of the resilient models has, therefore, influenced the structure of the program.

The resilient contour models are based on the fact that all stresses and strains are referred to a common origin. Body forces must, therefore, be considered, as they will give rise to stresses and strains in the pavement before any load is applied. This is shown by Fig. 7.1, where point A corresponds to the body force position and point B to the state when loading is applied.

Generalised Hooke's Law equations, if used to calculate a modulus of elasticity E and Poisson's ratio ν, assume that the material is linear elastic. Measured stresses and strains, however, may be combined in order to characterise a material without making a linear assumption. Brown and Bush (1972) suggest that bulk modulus (K) and shear modulus (G) are suitable parameters to describe the behaviour of a granular material.

Bulk modulus K is defined as:

$$K = \frac{\Delta P}{\Delta V}$$

and shear modulus G is defined as:

$$G = \frac{\Delta q}{3\Delta \varepsilon}$$

The non-linear models described in Chapter 3 produce a secant K and G. A bulk modulus K_1 and shear modulus G_1 may therefore be calculated from stress OA (Fig. 7.1) to give a strain at point A. Similarly, after the addition of the load, K_2 and G_2 may be calculated from stress OB to determine the strain at point B. The strain caused by the addition of load only is obtained by deducting the strain at A from the strain at B.

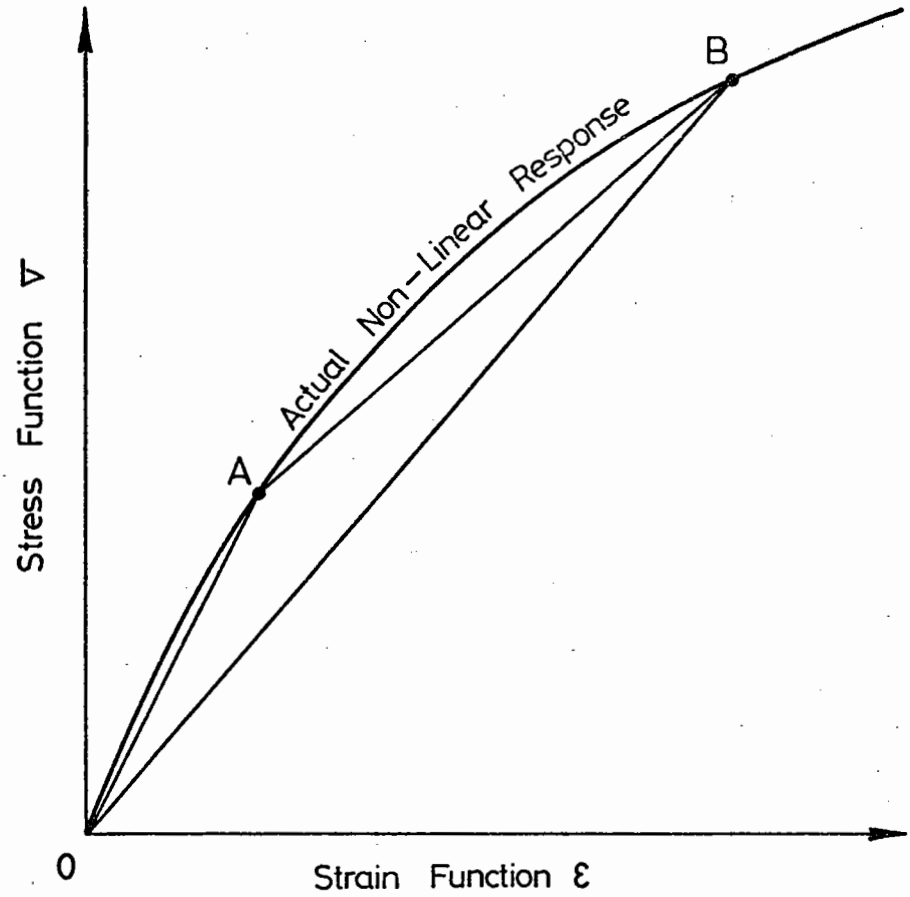

FIG. 7.1 SCHEMATIC ILLUSTRATION OF A NON LINEAR RESPONSE

This is a secant approach and is the method adopted for the SENOL program.

Full details of the program and the assumptions made in determining the initial body force condition are presented by Pappin (1979) and Brown, Brodrick and Pappin (1980). A brief summary of the main sections of the program is presented below.

The pavement was considered as an axisymmetric system and divided into a series of rectangular elements. Fig. 7.2 shows a typical layout of the elements, material layers, loading and boundary conditions.

Fig. 7.3 shows a flow chart. Following the philosophy outlined above, stresses and strains were calculated (step 3) for body forces before the application of wheel load (step 6). The program assumed initial elastic properties for each element (step 2), the vertical stress on an element being calculated using the depth of the element and the density of the overlying materials. Horizontal stresses were obtained using an assumed value of K_o. An initial octahedral shear strain was then obtained for the granular layer and subgrade using estimated values of bulk and shear modulus. After solving for stress and strain (step 3), new element properties were calculated (step 4) and a final solution for body force conditions determined and stored.

The wheel loading (step 6) was then applied in ten increments and when full loading was achieved an iteration process carried out using a variable damping factor. An error check was incorporated to determine when the convergence was adequate.

A non-linear model developed at Nottingham (Brown et al, 1975) was used to characterise the cohesive layer (subgrade) while the asphalt layer was treated as linear elastic, the value of Young's modulus being taken as the dynamic stiffness and Poisson's ratio as 0.4.

The contour and K-theta models were used to characterise the granular layers. The contour models provided values of bulk modulus and shear

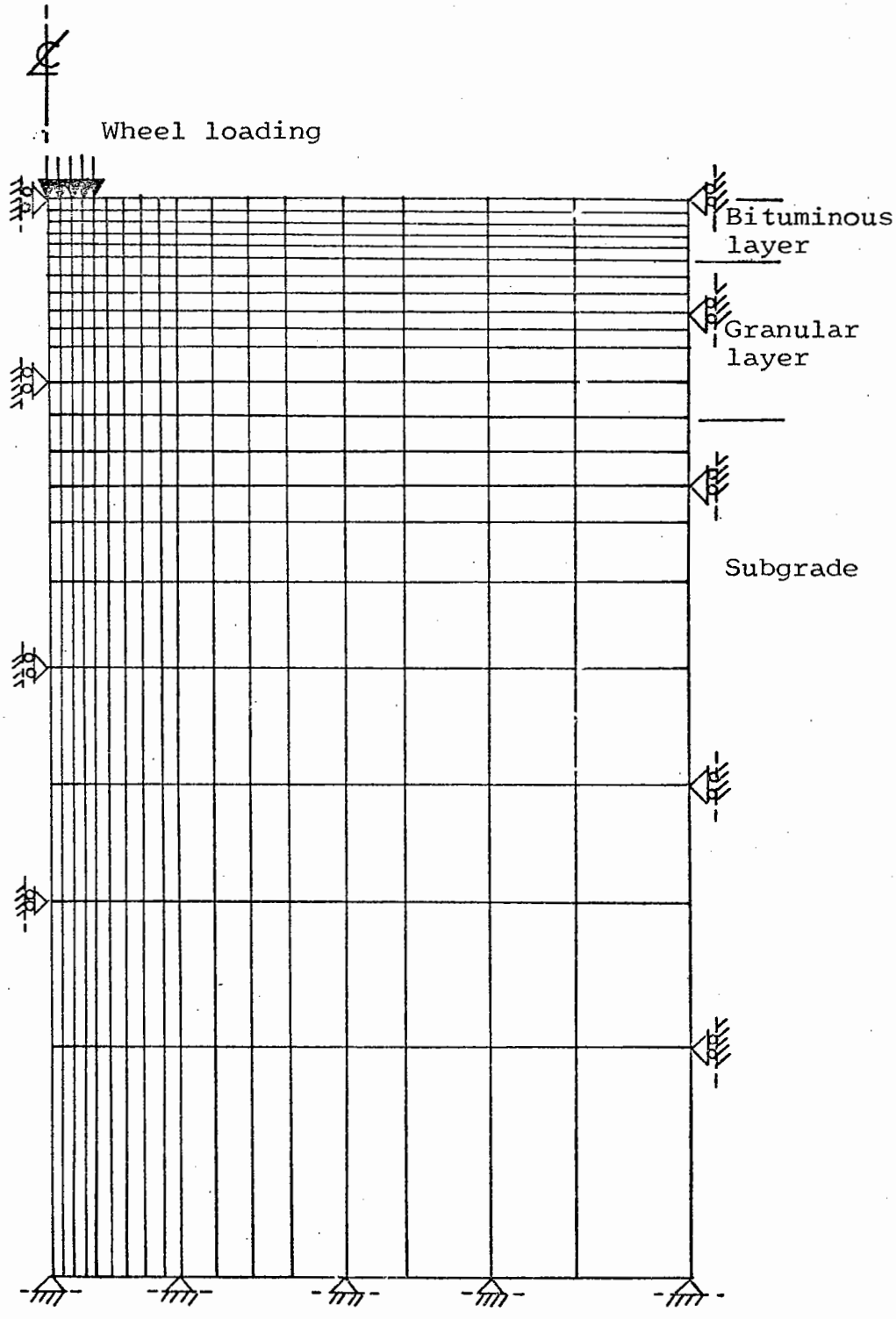

FIG. 7.2 TYPICAL FINITE ELEMENT LAYOUT

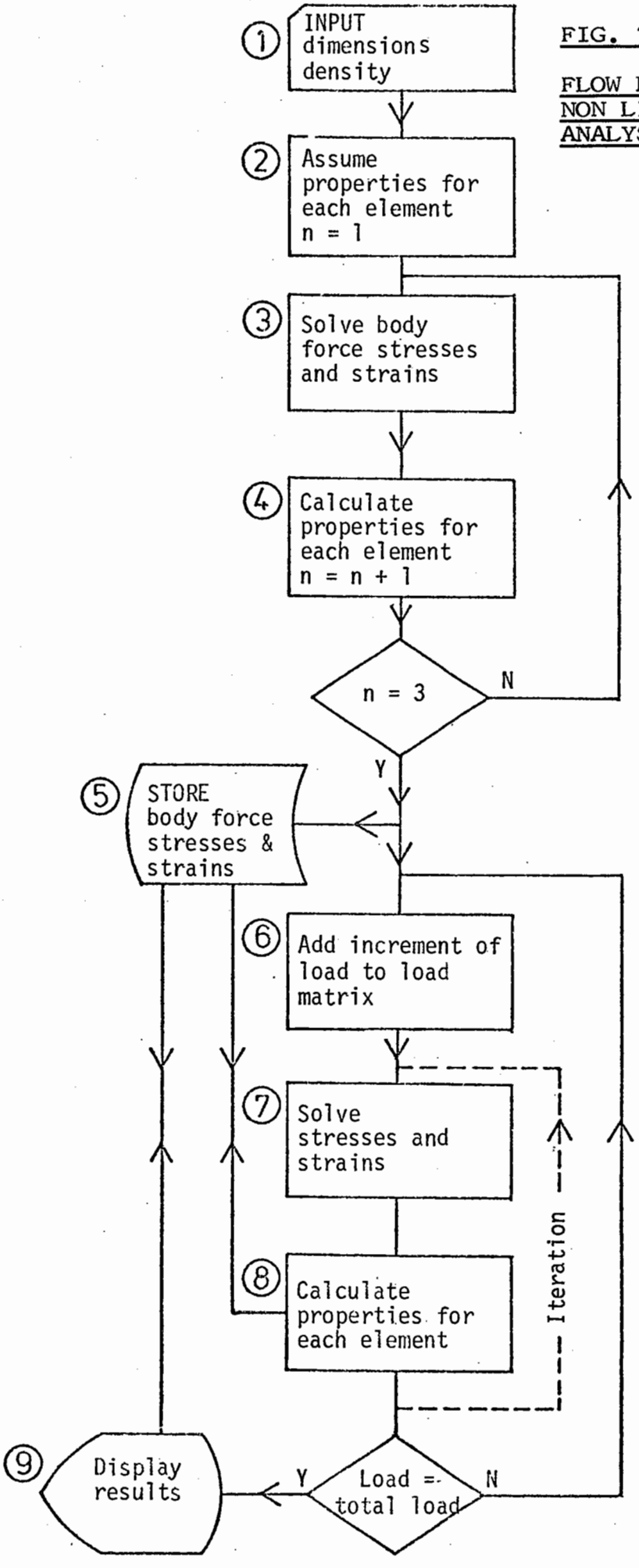

FIG. 7.3

FLOW DIAGRAM FOR NON LINEAR PAVEMENT ANALYSIS

modulus, while the K-theta model was incorporated in the program as a Young's modulus E and Poisson's ratio ν. Resilient modulus was assumed analogous to E and Poisson's ratio was assumed constant at 0.3 (Chapter 5). A similar approach was used for both models in that a solution was first obtained for body forces and then load applied. The K-theta model was therefore effectively used with a secant modulus (Chapter 5).

7.3 PAVEMENTS SELECTED FOR ANALYSIS

Following an extensive parametric study involving the analysis of many pavement structures (not yet published), several were selected to compare results obtained by using resilient contour and K-theta models to characterise the granular layer. Much of the work described in previous chapters has been devoted to investigating the behaviour of a single size material. However, in this chapter, the contour models developed by Pappin (1979) and the K-theta model from Chapter 5, as determined for the well graded material, were used in analysis. The well graded crushed limestone conformed with the specifications for wet-mix base material commonly used in Britain. Section 7.5 describes an attempt to use the models developed for the single size material to analyse a railway track situation. Table 7.1 gives a summary of the pavements selected for analysis.

7.4 RESULTS AND DISCUSSION

The tensile strain at the base of the asphaltic layer (ε_t), the maximum vertical strain in the subgrade (ε_z) and the vertical displacement of the structure (w_z) were compared for analysis using the contour models and K-theta model. These parameters were chosen because ε_t is related to the fatigue life of the asphalt, ε_z provides some indication of permanent strain development and w_z is a parameter which can be measured in situ.

Table 7.1

Layer	Pavement Number					
	1	2	3	4	5	6
ASPHALT						
E (kPa)	4×10^6	4×10^6	7×10^6	7×10^6	12×10^6	12×10^6
ν	0.4	0.4	0.4	0.4	0.4	0.4
thickness (mm)	200	200	100	100	100	100
GRANULAR						
*E (kPa)	5×10^4	5×10^4	5×10^4	1.75×10^5	5×10^4	5×10^4
*ν	0.3	0.3	0.3	0.3	0.3	0.3
thickness (mm)	700	200	700	200	450	200
SUBGRADE						
E (kPa)	3×10^4	5×10^4	2×10^4	7×10^4	2×10^4	7×10^4
ν	0.4	0.4	0.4	0.4	0.4	0.4

* It should be noted that these values of E and ν were used to analyse the initial condition for body forces. Once loading was applied, the non-linear contour models and K-theta models were used to characterise the material behaviour.

Single wheel loading in all cases was taken as 500 kPa with a radius of 160 mm. The results from the finite element program are presented for the contour and K-theta models in Table 7.2. Also included are results using the BISTRO program. The finite element program on completion calculates an equivalent tangent modulus for each element and the ratio of this modulus to that of the subgrade are presented for the top and bottom of the granular layer as R in Table 7.2. The BISTRO program treats the entire structure as linear elastic and requires a value of modulus to be selected for the granular layer. The modulus was taken as the average of the values obtained for that pavement using the resilient contour model analysis. These are also presented in Table 7.2.

PAVEMENT	MODEL	ε_t ($\mu\varepsilon$)	ε_z ($\mu\varepsilon$)	w_z (mm)	R TOP	R BOTTOM
1	Contour	141	216	0.42	2.7	4.5
	K-theta	121	182	0.42	6.0	3.6
	Bistro	141	235	0.54	4	
2	Contour	138	315	0.35	1.6	1.9
	K-theta	135	343	0.38	2.5	2.0
	Bistro	162	391	0.52	1.5	
3	Contour	236	506	0.79	5.5	5.5
	K-theta	167	385	0.70	14.5	4.0
	Bistro	220	445	0.90	5.5	
4	Contour	213	583		1.7	1.4
	K-theta	183	586	0.48	3.1	1.7
	Bistro	230	664	0.62	1.5	
5	Contour	164	513	0.69	3.6	5.7
	K-theta	139	479	0.71	8.8	3.1
	Bistro	174	658	1.0	4.5	
6	Contour	144	422	0.41	1.5	1.4
	K-theta	129	451	0.40	3.0	1.7
	Bistro	159	520	0.54	1.5	

TABLE 7.2 RESULTS FROM COMPUTER ANALYSIS

From the results there appears to be little difference in the overall performance of the contour and K-theta models. The K-theta approach tends to underpredict the tensile strain at the base of the asphaltic layer but compares well for vertical strain in the subgrade and the total vertical displacement of the structure. A superficial comparison would suggest that the K-theta model is adequate. However, the main purpose of the models is to characterise the non-linear behaviour of the granular layer and a closer inspection was made of stress and strain predictions.

If the modulus values for the granular layer are compared for each method, it is immediately apparent that similar stress patterns are not predicted. From experience in using the program, a rule of thumb has emerged where pavements which are 'safe' tend to produce modulus values which increase through the granular layer, but pavements which have failed, tend to show decreasing modulus values. The latter trend was shown in pavements analysed using the K-theta approach.

An examination of individual elements revealed that many were in a failure state. Static failure tests on the granular material produced a maximum q/p ratio of 2.2. Fig. 7.4 shows comparisons of elements in the granular layer of pavement 3 where predicted q/p ratios were greater than 2.2. A significant number of these elements had q/p greater than 3, which implied that one of the principal stresses was less than zero and hence tension was being developed.

Turcke and Raymond (1979) have developed a three-dimensional finite element model to analyse railway track structures. However, the method employs a tangent modulus and predicts tensile stresses in the railway ballast. Since granular materials cannot sustain tension, they use a technique applying fictitious restraining forces in an attempt to overcome the problem. Raad and Figueroa (1980) using a K-theta model in finite

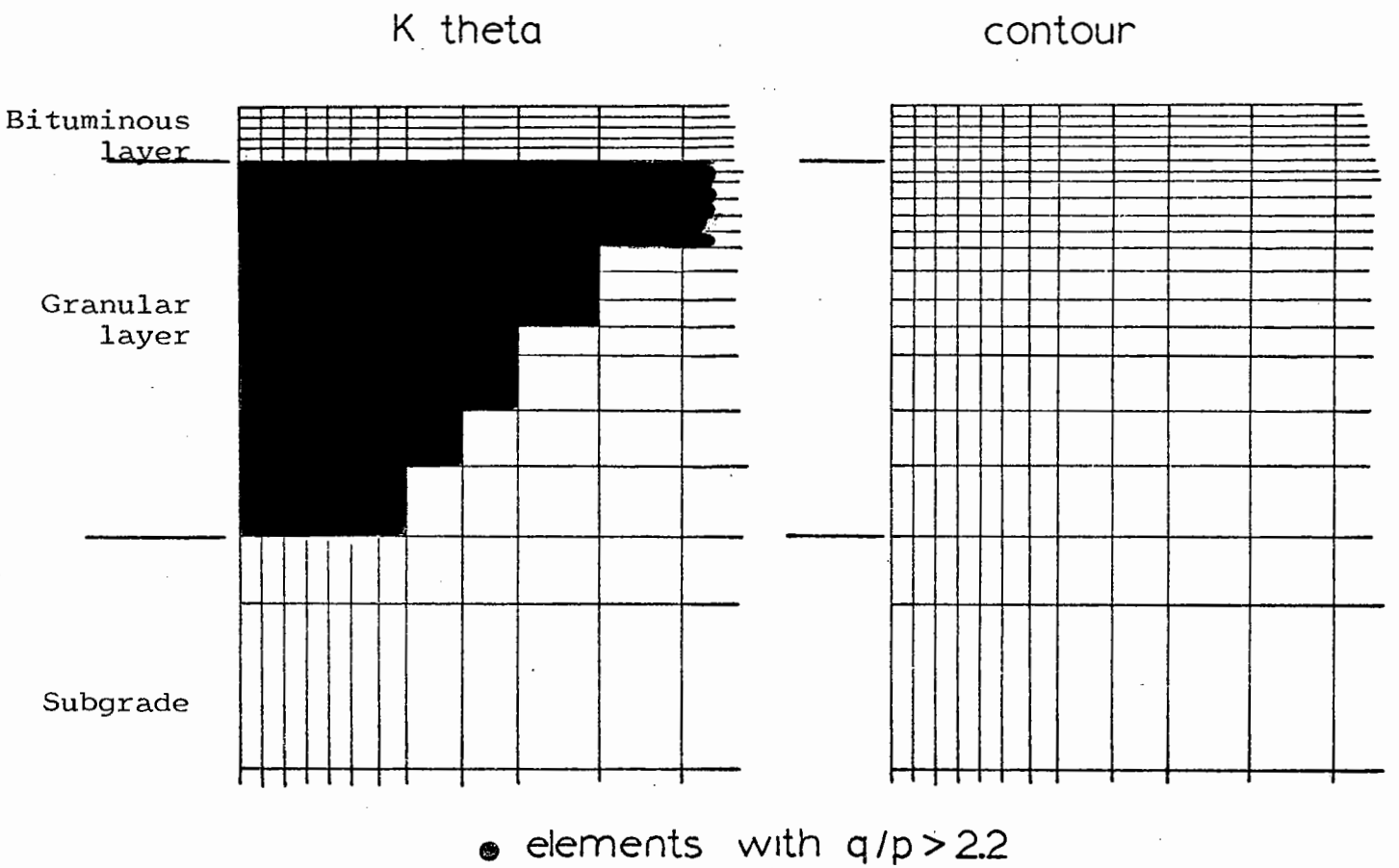

FIG. 7.4 COMPARISON OF FAILED ELEMENTS IN GRANULAR LAYER

element analysis of pavement structures, adjust the predicted stresses so that no element exceeds the Mohr Coulomb failure condition. The need to make adjustments to predicted stresses in the granular layer suggests that the K-theta models used to characterise the material are over simplified.

The contour models did not predict tensile stresses in the granular layer (Fig. 7.4). It is thought that this results from their greater accuracy in predicting resilient volumetric strain (Chapter 5). It has, therefore, been possible, in practice, to assess the suitability of pavement designs on the basis of the development of failure zones in the granular layer. Such an assessment would not be possible using a K-theta approach.

The above considerations would suggest that the use of a non-linear model of the type $M_r = K_1\theta^{K_2}$ will adequately predict the overall strain situation in a pavement structure. However, the model is limited in its application to predicting stresses within the granular layer. Any analysis of permanent strain behaviour requires a knowledge of the transient stress state in the structure and the use of the K-theta model is likely to lead to inaccurate results.

7.5 AN ATTEMPT TO MODEL A RAIL TRACK STRUCTURE

The Pavement Test Facility at the University of Nottingham has been used extensively in the development of predictive design procedures for flexible pavement deformation. A detailed description of the facility is given by Brown et al (1977, 1980). Briefly, a loaded rolling wheel attached to a carriage guided between two reaction beams acts on a pavement structure contained in a test pit. A schematic diagram is shown in Fig. 7.5. An attempt was made to use the existing facilities to apply sleeper loading to a single size material in order to test the

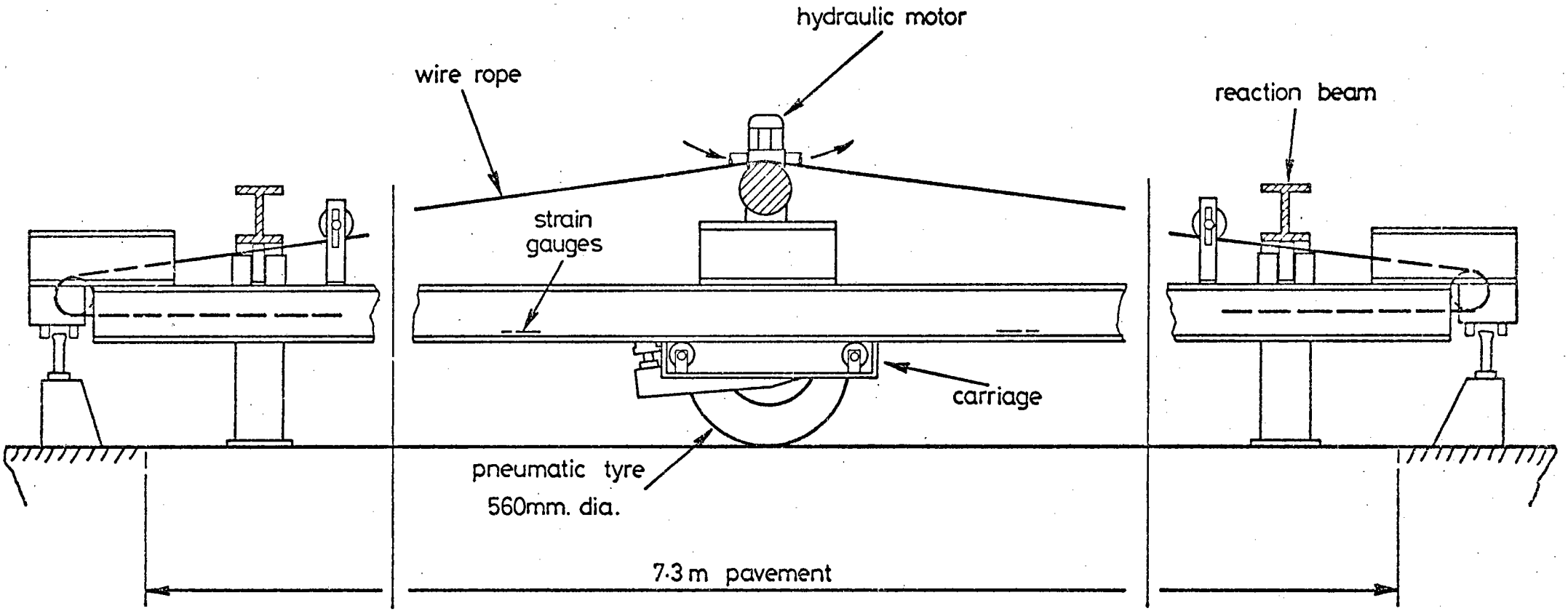

FIG. 7.5 SCHEMATIC DIAGRAM OF TEST PAVEMENT

ability of the models developed in Chapter 3 to predict resilient strains under transient loading.

The test pit was 15 m x 7 m in plan and contained a subgrade of silty clay (Keuper Marl). On top of this was placed 230 mm of 3 mm single size crushed limestone material. The limestone was obtained from Ballidon quarry, Derbyshire, and although not the same as that used in the tests described in previous chapters, was the most readily available at the time. A series of model sleepers 0.1 m square by 1.0 m long were placed on top of the ballast as shown in Fig. 7.6. Loading was applied using the existing wheel, running along a 150 mm wide by 50 mm deep plank laid across the sleepers and fastened securely at each end of the pit. Bison strain coils and Nottingham pressure cells were installed to monitor strains and stresses (Brown and Brodrick, 1973) at the depths shown in Fig. 7.6. 50 000 passes of a 10 kN wheel load were applied to the structure and transient stresses and strains monitored throughout. Appendix 7A contains full details of the results.

Fig. 7.7 shows the measurements of resilient vertical strain. The strain at the top of the ballast was of the order of 2000 $\mu\varepsilon$. This was extremely high, but on observing the ballast during loading, the top few centimetres could be described as being in a failure state. Strains decreased through the granular layer to about 300 $\mu\varepsilon$ at the base. Also shown in Fig. 7.7 are the measured strains after differing numbers of cycles. It can be seen that strains changed little throughout the test and did not exhibit the stiffened response described by Raymond and Williams (1978).

The measured transient stresses are shown in Fig. 7.8. The difference between the vertical stress and that measured in the longitudinal and lateral directions is immediately apparent. The general trend observed in the simple shear apparatus was that vertical loading produced

FIG. 7.6 POSITION OF TRANSDUCERS IN MODEL RAILWAY TRACK STRUCTURE

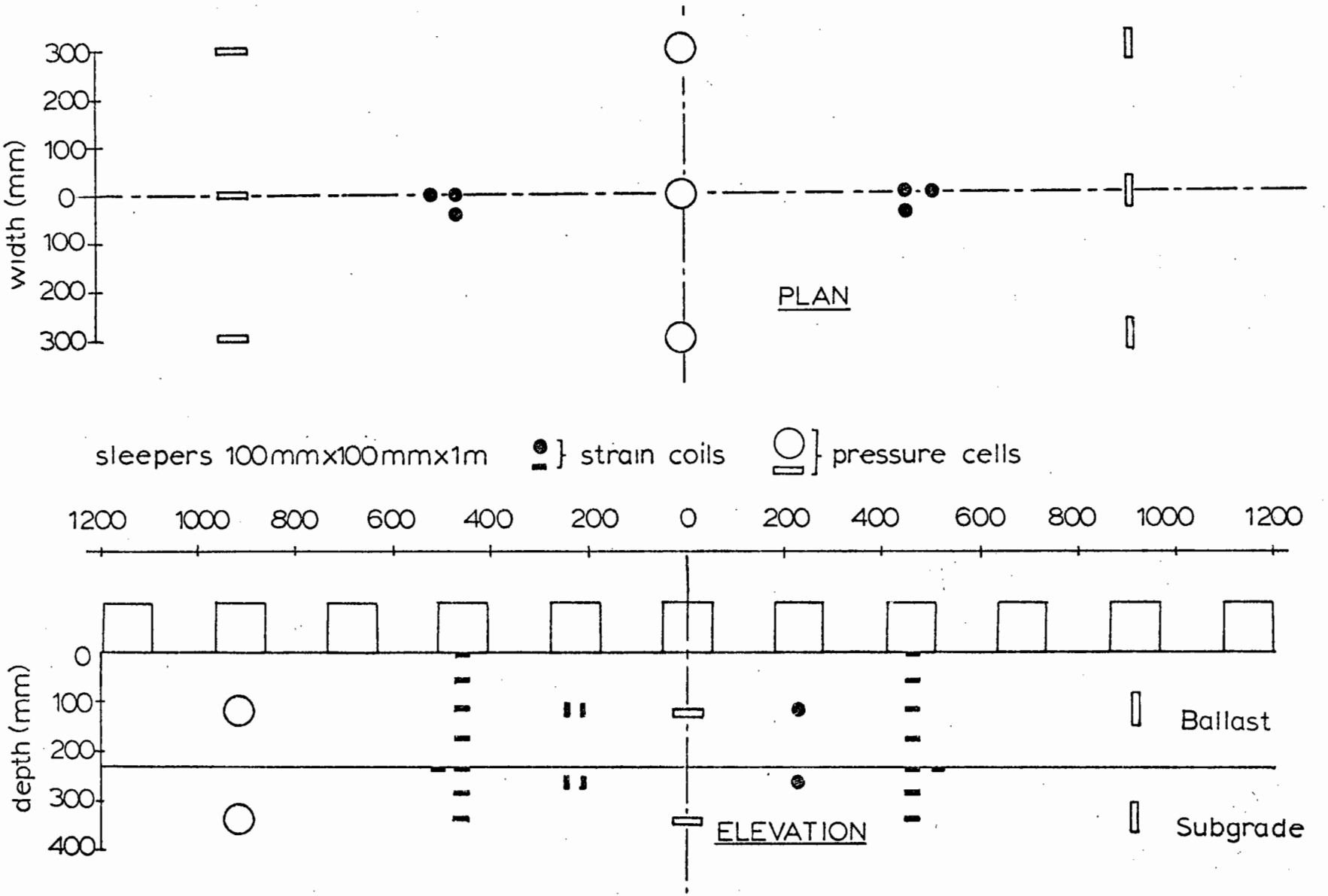

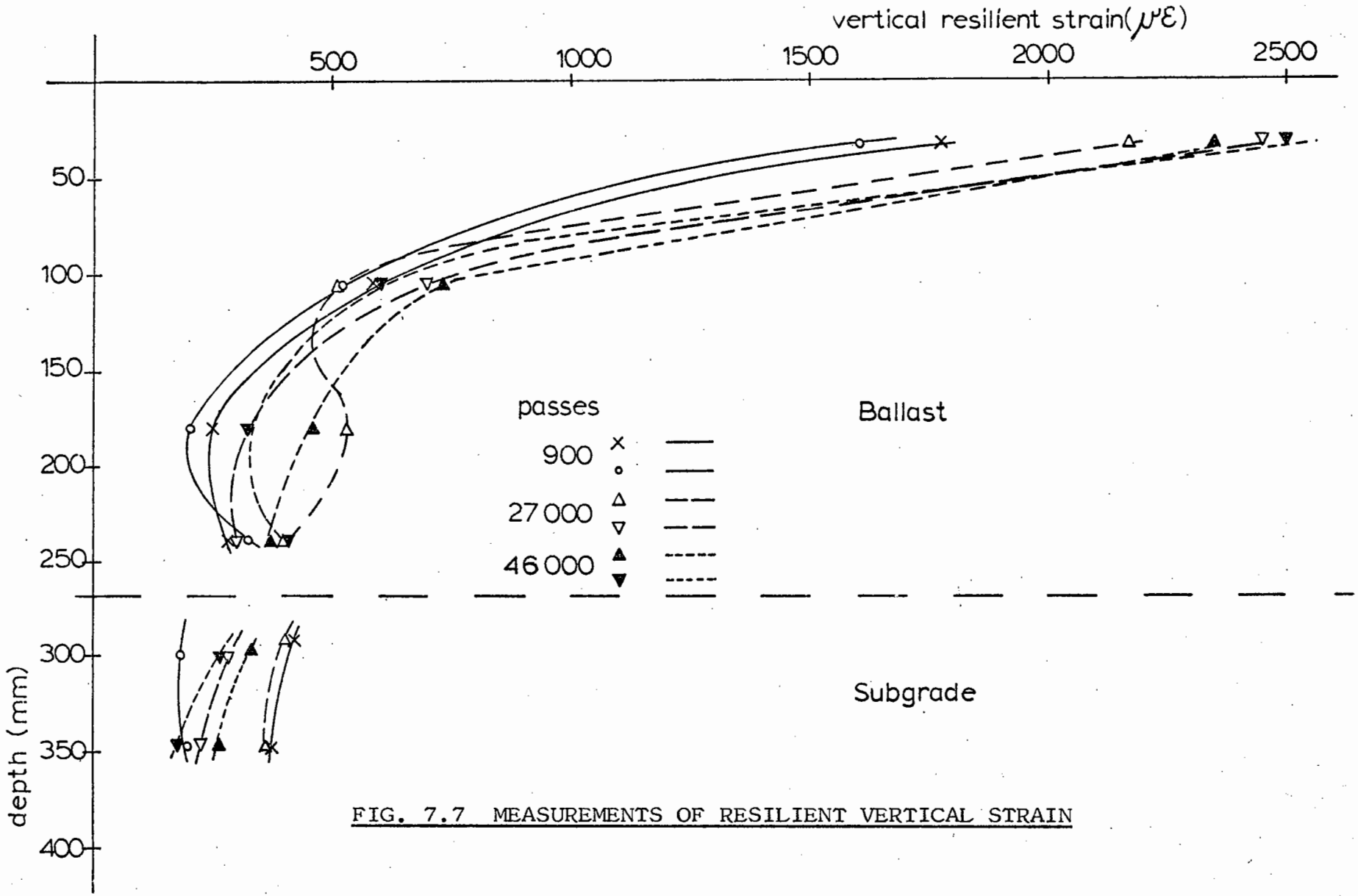

FIG. 7.7 MEASUREMENTS OF RESILIENT VERTICAL STRAIN

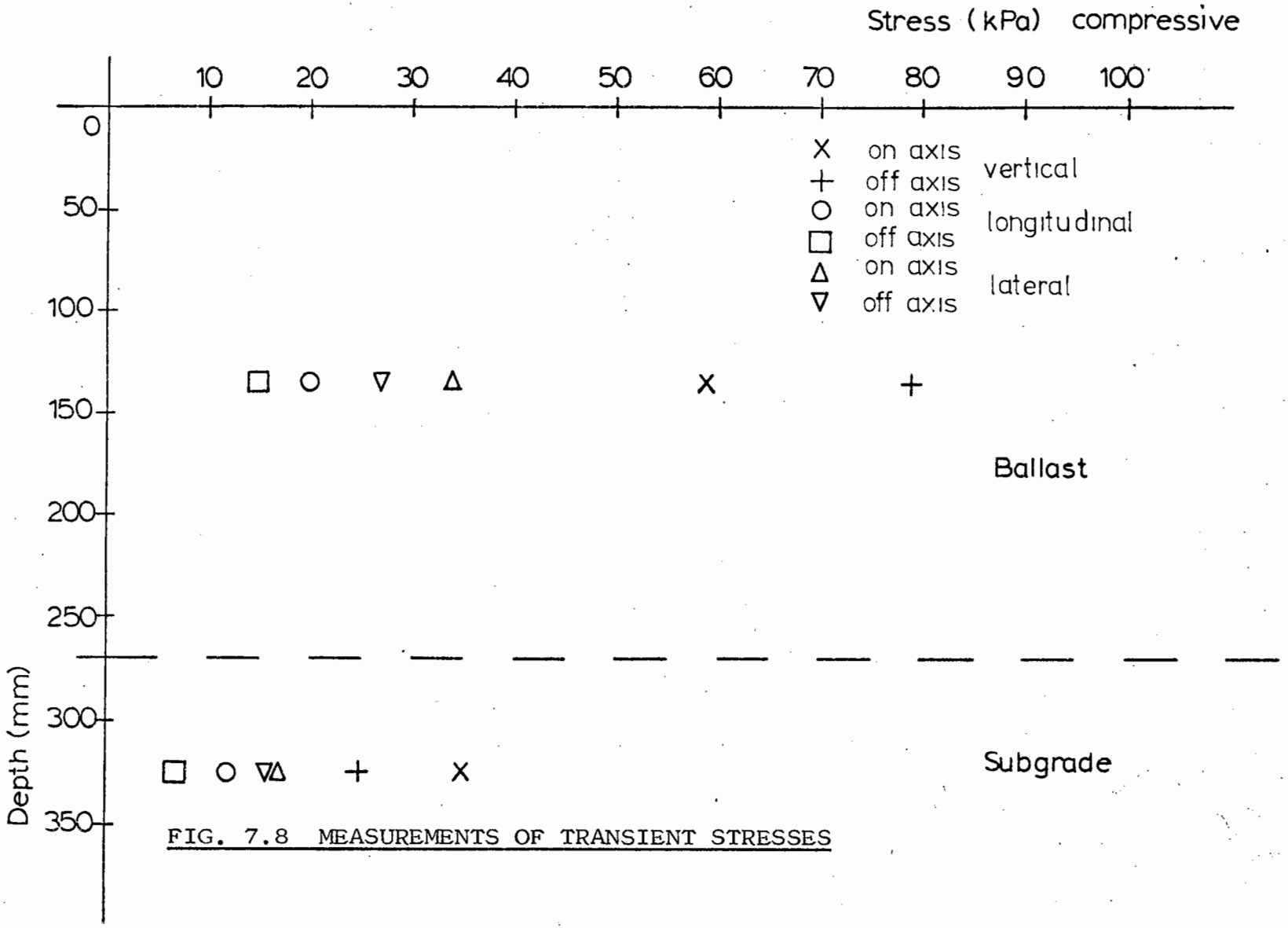

FIG. 7.8 MEASUREMENTS OF TRANSIENT STRESSES

different stresses in the sides and ends of the shear box. However, taking into consideration the difficulties in measuring stresses in a granular material, the readings obtained from the test pavement for lateral and longitudinal directions are of the same order of magnitude. As expected, transient stresses decreased with depth in the structure.

An attempt was made to use the SENOL finite element program to predict stresses and strains in the rail track structure. The previously described analysis of pavements using the SENOL program assumed axisymmetric conditions in all cases. However, it is generally accepted that for the type of loading existing in a railway track structure, plane strain is a closer approximation. Some speculation exists as to which direction may be considered as plane strain but for all analysis presented below, was assumed to be the direction of travel, i.e. transverse section.

The structure was modelled as shown in Fig. 7.9. A typical Young's Modulus for the sleeper was taken as 10 000 MPa with a Poisson's ratio of 0.3 (Turcke and Raymond 1979, Selig et al 1979). The non-linear contour models developed in Chapter 3 were used to characterise the ballast behaviour and the subgrade modulus was taken as 30 000 kPa.

Considerable difficulties were experienced in reproducing the stress pattern as measured in the model track structure. This was not surprising since the method of load application was a compromise between that for a pavement structure and a rail track structure. In practice, the sleepers tended to tilt and flex with the passage of the wheel. This could not be modelled using the present computer program. Generally, it was found that using the SENOL approach, loading was dispersed in the first layer (sleeper) and the predicted stress in the granular material was minimal. It was then decided to increase the applied load so that the predicted stresses in the granular material were of the same order as

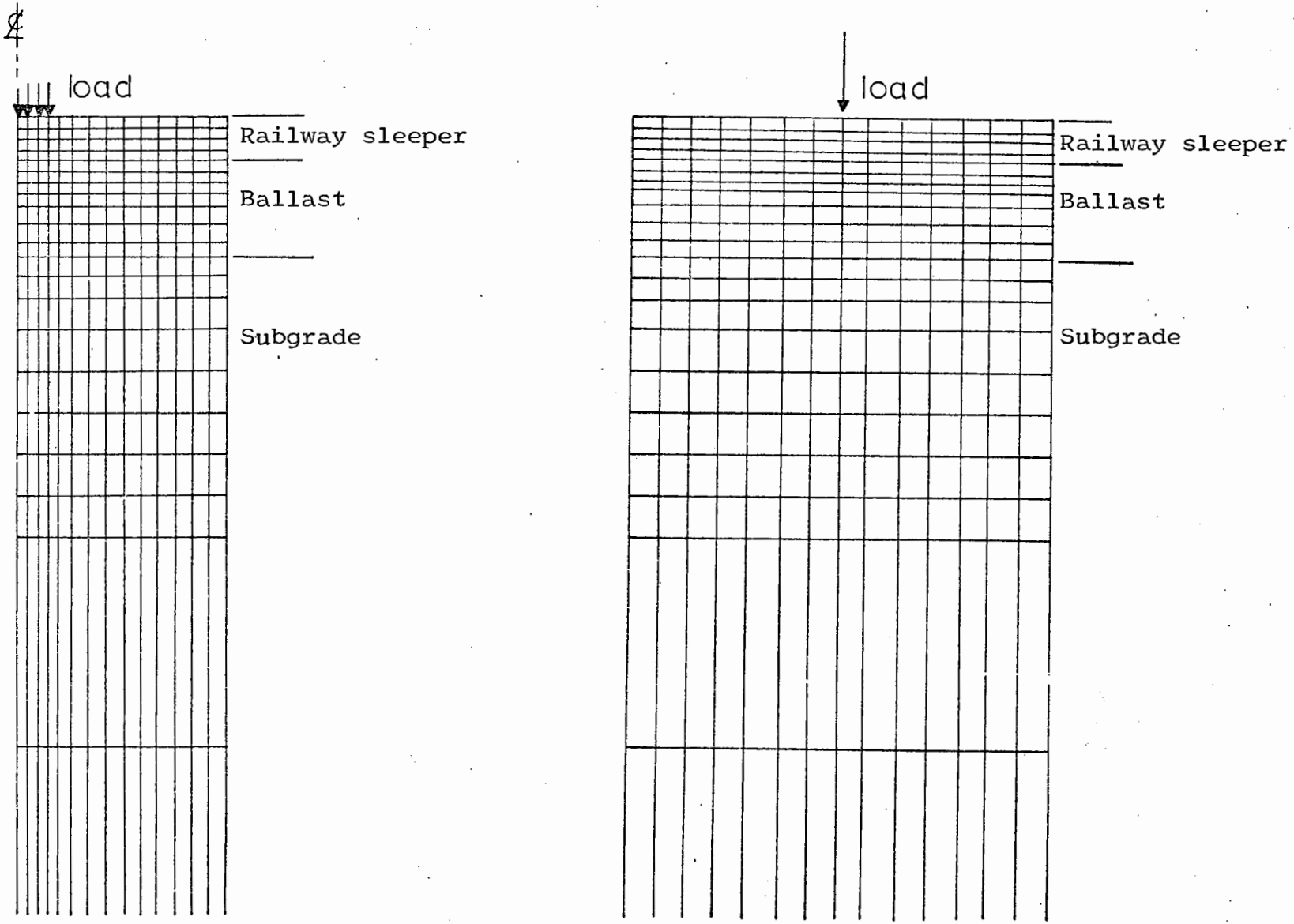

FIG. 7.9 FINITE ELEMENT LAYOUTS FOR MODEL RAILWAY TRACK STRUCTURE

those measured in the test pit. However, it was found that when stresses approached the magnitude of those measured, the program did not converge, suggesting excessive strains were developing in the granular layer. Observations of the 3 mm material during the test indicated that at least the top few centimetres were in a failure state.

The test procedure and method of loading imposed severe limitations on the application of the results. In practice, sleepers tend to be within the ballast as opposed to resting on top in the manner of the trial structure. However, the exercise was useful in highlighting the problems associated with computer analysis of railway track structures.

CHAPTER EIGHT

DISCUSSION AND RECOMMENDATIONS

The repeated load triaxial test facility required no modifications and performed satisfactorily throughout the project. Due to the brittle nature of the araldite strain rings, care had to be taken to ensure that radial strains were kept within acceptable limits. This severely restricted the use of the triaxial equipment when monitoring static failure tests, particularly for the single size material which exhibited large strains at failure. If an extensive investigation of monotonic behaviour is to be conducted, then more attention must be directed towards developing an alternative method to measure radial strain.

The conversion to plane strain conditions in the biaxial shear box has been successful and the load cells designed to measure stress in the vertical direction performed well during testing. However, work will have to be carried out to investigate the effects of friction within the sliding parts of the apparatus. The semi-cylindrical rods used to prevent trapping of particles in the corners of the shear box may be causing friction and restricting movement of the sides. It is quite possible that this is having an effect on the measured monotonic failure strains and may be contributing towards the experimental scatter produced by the apparatus.

Considerable work has been carried out to develop satisfactory load cells to measure lateral and end stress in the simple shear apparatus. Several designs were considered which measured stress at specific points on the boundary of the specimen. Problems were encountered in designing a load cell with adequate stiffness to prevent arching of the material and yet produce a measurable output. Calibration against the material was carried out by inserting the load cell in the base of a triaxial specimen. The difficulties in obtaining repeatable results may have

been due to non-uniform stresses in the triaxial specimen or the relatively large particle size. The final load cell design, which formed a complete boundary to the specimen, was found to perform adequately on reducing the size of the material being tested. The exercise highlighted the necessity of a large particle size to specimen depth ratio. A more suitable load cell is required to measure the end stress. The original design of the apparatus made mounting of transducers in the sides and ends of the shear box extremely difficult and it may only be possible to produce an adequate system by redesigning the loading equipment to provide more space around the specimen.

The monotonic behaviour of a 3 mm single size crushed limestone has been investigated under triaxial and biaxial test conditions for initial specimen densities of approximately 1.62 Mg/m^3. Previous research (Pappin 1979) produced triaxial results for well graded specimens of the same material. A comparison of failure results showed the single size material to be of similar strength in compression but stronger in triaxial extension. Biaxial failure tests on the single size material produced results which were in excess of those predicted using the Mohr-Coulomb criterion. It is thought that this may be related to the angularity of the particles causing specimen interlock. It is suggested that a full examination of the monotonic behaviour of the material be carried out as this may have relevance to the permanent strain behaviour described below. It may also be possible to relate permanent strain developed by repeated loading to that produced in static failure testing.

The resilient behaviour of a number of granular materials has been investigated for triaxial test conditions. Contours of resilient strain have been drawn in the compression region of (p,q) stress space and appear to have a similar shape for all the materials tested. The contours

have been satisfactorily extended to triaxial compression-extension stress paths and also to the $\sigma_1 \neq \sigma_2 \neq \sigma_3$ plane strain conditions of the biaxial shear box. However, more work is required to determine the effects of particle shape and a complete investigation of the effects of dry density on the resilient behaviour of the materials has yet to be conducted.

Permanent strain behaviour has been partially investigated in the triaxial apparatus and results for a single size material have been compared with those for a graded material. A threshold value was determined for the distance of the stress path from the failure envelope and specimens subjected to stress conditions inside the threshold showed a rapid increase in permanent shear strain development. The specimens were observed to be in a state of dilation or little volume change and it is thought that the threshold is related to the volumetric strain behaviour of the material. A closer examination of the monotonic strain behaviour may provide more insight on the permanent strain response. The tests would necessarily involve accurate measurements of axial and radial strain.

Permanent strain tests on the biaxial shear box did not exhibit any threshold value and stress paths could be tested close to failure with no dramatic change in permanent strain behaviour. Results from the simple shear apparatus, when compared with triaxial results, showed reduced straining for conditions in excess of failure. Failure in both cases is as defined by triaxial testing. It is thought that the more complex boundary conditions of the biaxial and simple shear apparatus are having an effect on the permanent strain response and more investigation is required.

3 mm and 1.5 mm single size materials were tested in the simple shear apparatus and results compared for both constant and cycled vertical

stress conditions. The findings of Ansell (1977) were reinforced in that repeated shear reversal increased compaction; however, it would appear that compaction is best achieved by a combination of repeated shear reversal and cycled vertical load.

Tests to investigate permanent strain behaviour in the triaxial apparatus showed that a graded material produced less permanent strain than a single size material. This would suggest that for application to railways, a wider grading of ballast would reduce permanent strain development and hence maintenance costs.

The effects of stress rotation have not been investigated, mainly because of doubts concerning the accuracy of the measured and predicted stresses around the simple shear specimen. It is suggested that on designing a suitable load cell to measure end stress, a test programme be conducted using similar stress levels to those applied in the triaxial and biaxial equipment.

An adequate comparison of results from all three pieces of equipment will only be possible if the same size of material is tested throughout. In the work described in previous chapters, the 3 mm single size material was common to all three test methods, but was found to be unsuitable for the simple shear apparatus when measuring lateral and end stresses. The situation has been improved by reducing the particle size to approximately 1.5 mm. The simple shear and biaxial equipment was initially designed for larger sized particles and has considerable clearance gaps throughout. If smaller materials are to be considered, it will be necessary to enclose the specimen in a membrane.

An investigation has been carried out into the use of a simple model relating resilient modulus and stress level as:

$$M_R = K_1 \theta^{K_2} \qquad (8.1)$$

where M_R is the resilient modulus, θ is the sum of the principal stresses and K_1 and K_2 are material constants. This is commonly referred to as the "K-theta" model. It is thought that in practice, for any particular stress path, resilient strains are determined using a modulus value obtained from peak stress conditions. This approach is satisfactory for short stress paths, but does not take account of the change in resilient modulus when travelling along a stress path of considerable length. Chapter 5 shows that it is more accurate to analyse resilient strains by considering the modulus value for both the beginning and end of each stress path. Generally, the "K-theta" model predicted resilient shear strains quite accurately but was inadequate for prediction of resilient volumetric strain.

The main application of the resilient and permanent strain models is in computer analysis and some non-linear finite element work has been described. Results from analysis of a selection of road pavements using the K-theta model have been compared with those obtained using the resilient contour models described previously. Generally, both methods gave similar results for the overall strain behaviour of each structure, but the K-theta model was shown to be inadequate for predicting stresses in the granular layers. It is thought that this may be related to the inaccuracy of the model in predicting volumetric strain. The complexities and cost of finite element analysis make it unsuitable for routine design procedures; however, it may be possible to use the advanced non-linear finite element method to calibrate results from simpler linear elastic analysis. The application of the resilient models to analysis of railway track structures is an area which requires major investigation. This would involve a scaling factor and comparisons of the resilient behaviour of commonly used ballast and the 3 mm material are needed before full size structures can be modelled.

CHAPTER NINE

CONCLUSIONS

A laboratory testing programme was completed on several granular materials using triaxial, biaxial and simple shear equipment. Non-linear behaviour models were developed and incorporated in pavement analysis. The main conclusions of the work described in this thesis are listed below.

9.1 TRIAXIAL TESTING

Triaxial tests were conducted on a 3 mm single size crushed limestone at a density of 1.62 Mg/m^3.

9.1.1 Failure Tests

(a) The material was found to have an angle of shearing resistance of 51^o. This was equivalent to a q/p failure ratio of 2.1.

(b) Static failure strength was virtually unaffected by permanent strain caused by large numbers of load applications.

9.1.2 Resilient Strain Behaviour

(a) Resilient strains could be expressed as a series of contours in the compressive region of (p,q) stress space. The resilient strain was obtained from the difference in contour value at the beginning and end of each stress state. Resilient volumetric strain was obtained from:

$$v_r = \left[\left[\frac{p_2}{A}\right]^{0.5}\left(1 - B(q_2/p_2)^C\right) - \left(\frac{p_1}{A}\right)^{0.5}\left(1 - B(q_1/p_1)^C\right)\right]$$

where $A = 1.23\times10^{+8}$ kPa, B = 0.033, C = 3.5.

Shear strains were influenced by stress path length. After normalising this effect the resilient strains were obtained from:

$$\varepsilon_r = D\left[\frac{q_2}{p_2+E} - \frac{q_1}{p_1+E}\right]\left[\frac{(p_r^2 + q_r^2)^{0.5}}{p_m}\right]^{0.45}$$

where $D = 5.5\times10^{-4}$, $E = 130$ kPa.

(b) A general stress state could be converted to an equivalent triaxial compression state by using a correction based on the ratio of the major to minor principal stresses (σ_1/σ_3).

(c) For stress paths of the compression-extension type, it was necessary to use vector methods to obtain resilient shear strain values. Resilient volumetric strains were adequately predicted by the difference in contour strain for the beginning and end of each stress state.

9.1.3 Permanent Strain Behaviour

(a) The strain rate for permanent shear strain was found to be related to the stress path length and the minimum normal stress distance of the stress path from the failure envelope in (p,q) stress space. No satisfactory relationship was established for volumetric strain.

(b) A threshold value exists above which large permanent shear strains develop.

9.1.4 Effect of Permanent Strain on Resilient Behaviour

Resilient strains were found to stabilise after several hundred cycles of load for stress states below the threshold value. Above the threshold, resilient strain behaviour was erratic.

9.1.5 Triaxial Testing of Other Granular Materials

Repeated load testing of a gravel and a smaller size fraction of the crushed limestone produced resilient strain contours of similar shape to those described above.

9.2 BIAXIAL TESTING

Biaxial tests with the three principal stresses different were conducted on the 3 mm crushed limestone at a density of 1.62 Mg/m^3.

9.2.1 Failure Tests

(a) Failure did not occur until one of the principal stresses was zero. This corresponded to the triaxial extension failure state.

(b) The combined failure results from triaxial and biaxial testing showed the Mohr Coulomb failure criterion to be conservative.

9.2.2 Resilient Strain Behaviour

(a) The resilient strain contours developed for the axisymmetric triaxial case were found to apply to the three-dimensional stress conditions of the biaxial shear box.

(b) Resilient shear strains had to be computed using vector methods (as for triaxial compression-extension). It was sufficient to obtain resilient volumetric strains as the difference in contour strain for the beginning and end of each stress state.

9.2.3 Permanent Strain Behaviour

(a) A linear relationship exists between permanent shear strain rate and the product of stress path length and minimum normal stress distance of the stress path from the failure envelope in (p,q) stress space. No satisfactory relationship was obtained for volumetric strain.

(b) No threshold value was observed in the biaxial shear box.

9.3 COMPARISONS OF NON-LINEAR MODELS

Predictions using the resilient contour models were compared with those from a frequently used model of the type $M_R = K_1\theta^{K_2}$. Comparisons were made for both single size and graded materials.

(a) The simple model $M_R = K_1\theta^{K_2}$ is likely to lead to inaccurate results because the triaxial tests used in its development do not cover an adequate range of stress paths.

(b) When incorporated in a non-linear finite element program for pavement analysis, the contour models were superior in predicting stresses within the granular layer. The simple model often predicted tensile stresses. However, the simple model was shown to be adequate in predicting the overall strain response of the structure.

9.4 THE SIMPLE SHEAR APPARATUS

Unidirectional and bidirectional tests were conducted on specimens of 3 mm and 1.5 mm particle size crushed limestone at initial densities of 1.62 Mg/m^3.

9.4.1 Apparatus Development

(a) The loading equipment has been modified so that both cyclic normal and shear loading can be applied to the specimen between zero and a maximum, or some mean value and maximum.

(b) A more satisfactory rotating end plate arrangement has been incorporated in the shear box.

(c) Load cells have been designed and installed in the sides and ends

of the shear box enabling the stress distribution around the specimen to be measured.

(d) The ratio of particle size to specimen depth was found to be unsatisfactory for lateral stress measurement. A smaller material was therefore selected for testing.

9.4.2 Stress Behaviour

(a) The modifications carried out to measure lateral and end stresses, enabled an estimate to be made of the stress state on the central portion of the apparatus. When compared with predictions obtained using a technique developed at Cambridge, end stress measurements appeared to be less accurate.

(b) It was possible to calculate simple shear stress paths in terms of p and q. Stress conditions, however, were always greater than the failure state as determined from triaxial testing.

(c) Lateral stresses remained constant during shearing but tended to decrease with number of shear cycles.

9.4.3 Strain Behaviour

(a) For tests in which vertical stress was constant, patterns of strain behaviour were similar to those obtained previously by Ansell (1977) for both unidirectional and bidirectional tests.

(b) Cycling vertical stress caused considerable increases in compaction for the 3 mm material. Results for the 1.5 mm material were not so distinctive.

(c) For all tests, the 3 mm material showed significantly greater straining than the 1.5 mm material.

REFERENCES

Adegoke, C.W., Chang, C.S. and Selig, E.T. (1979), "Study of analytical models for track support systems", Transportation Research Record 733, pp 12-20.

Allen, J.J. and Thompson, M.R. (1974), "Resilient response of granular materials subjected to time dependent lateral stresses", Transportation Research Record 510, pp 1-13.

Ansell, P. (1977), "Cyclic simple shear testing of granular material", Ph.D. thesis, University of Nottingham.

Arthur, J.R.F., Chua, K.S. and Dunstan, T. (1977), "Induced anisotropy in a sand", Geotechnique 27, No. 1, pp 13-30.

Arthur, J.R.F., Chua, K.S. and Dunstan, T. (1979), "Dense sand weakened by continuous principal stress direction rotation", Geotechnique 29, No. 1, pp 91-96.

Bjerrum, L. and Landva, A. (1966), "Direct simple-shear tests on Norwegian quick clay", Geotechnique 16, No. 1, pp 1-20.

Bishop, A.W. (1958), "Test requirements for measuring the coefficient of earth pressure at rest", Proceedings of the Brussels Conference 58 on Earth Pressure Problems, Vol. 1, pp 2-14.

Boyce, J.R. (1976), "The behaviour of granular material under repeated loading", Ph.D. thesis, University of Nottingham.

Bransby, P.L. (1973), Cambridge contact stress transducers, Lecture Notes for Course on "Research Techniques and Equipment in Soil Mechanics", CUED/C-SOILS/LN2, Department of Engineering, University of Cambridge.

Brown, S.F. (1969), Discussion on pressure cell calibration, Proceedings, Conference on In Situ Investigation of Soil and Rock, British Geological Society, pp 243-245.

Brown, S.F. (1974), "Repeated load testing of a granular material", Journal Geotech. Eng. Div., ASCE, Vol. 100, GT7, pp 825-841.

Brown, S.F. and Bush, D.I. (1972), "Dynamic response of model pavement structure", Trans. Eng. Journ., ASCE, Vol. 98, TE4, November, pp 1005-1022.

Brown, S.F. and Brodrick, B.V. (1973), "The performance of stress and strain transducers for use in pavement research", Research Report to SRC.

Brown, S.F., Lashine, A.K.F. and Hyde, A.F.L. (1975), "Repeated load triaxial testing of a silty clay", Geotechnique 25, No. 1, pp 95-114.

Brown, S.F. and Ansell, P. (1980), "The influence of repeated shear reversal on the compaction of granular material", International Conference on Compaction, Paris.

Brown, S.F., Brodrick, B.V. and Pappin, J.W. (1980), "Permanent deformation of flexible pavements", Final report to European Research Office, US Army.

Cornforth, D.H. (1964), "Some experiments on the influence of strain conditions on the strength of sand", Geotechnique 14, pp 143-167.

Green, G.E. and Reades, D.W. (1975), "Boundary conditions, anisotropy and sample shape effects on the stress-strain behaviour of sand in triaxial compression and plane strain", Geotechnique 25, No. 1, pp 333-356.

Heukelom, W. and Klomp, A.J.G. (1962), "Dynamic testing as a means of controlling pavements during and after construction", Proc. Int. Conf. on the Struct. Design of Asphalt Pavements, pp 667-679.

Hicks, R.G. (1970), "Factors influencing the resilient response of granular materials", Ph.D. thesis, University of California.

Hicks, R.G. and Monismith, C.L. (1971), "Factors influencing the resilient response of granular materials", Highway Research Record No. 345, pp 15-31.

Hill, R. (1950), Plasticity, Oxford Univ. Press.

Jakey, J. (1948), "Pressure in Silos", Proc. 2nd Int. Conf. Soil Mech., Vol. 1, Rotterdam, pp 103-107.

Lee, K.L. (1970), "Comparison of plane strain and triaxial tests on sand", Journal of the Soil Mech. and Found. Div., ASCE, Vol. 96, pp 901-923.

Mayhew, H. (1978), Private Communication.

Pappin, J.W. (1979), "Characteristics of a granular material for pavement analysis", Ph.D. thesis, University of Nottingham.

Peutz, M.G.F., Van Kempen, H.P.M. and Jones, A. (1968), "Layered systems under normal surface loads", Highway Research Record No. 228, pp 34-45.

Phillips, S.J. (1975), "Repeated loading of railway ballast", B.Sc. thesis, University of Nottingham.

Prevost, J.H. and Hoeg, K. (1976), "Reanalysis of simple shear soil testing", Canadian Geotechnical Journal, Vol. 13, No. 4, pp 418-429.

Pyke, R. (1978), "Some effects of test configuration on measured soil properties under cyclic loading", Geotechnical Testing Journal, ASTM, Vol. 1, No. 3, pp 125-134.

Raad, L. and Figueroa, J.L. (1980), "Load response of transportation support systems", Transportation Eng. Journ., ASCE, Vol. 106, pp 111-128.

Raymond, G.P. and Davies, J.R. (1978), "Triaxial tests on dolomite railroad ballast", Geot. Eng. Div., ASCE, Vol. 104, GT6, pp 737-751.

Raymond, G.P. and Williams, D.R. (1978), "Repeated load triaxial tests on a dolomite ballast", Geot. Eng. Div., ASCE, Vol. 104, GT7, pp 1013-1029.

Richards, B.G. (1975), "The determination of experimentally based load-deformation properties of a mine fill", Research Paper No. 247,

Div. of Applied Geomechanics, CSIRO, Australia.

Roscoe, K.H. (1953), "An apparatus for the application of simple shear to soil samples", Proc. 3rd Int. Conf. on Soil Mech. and Found. Eng., Zurich, Vol. 1, pp 186-191.

Roscoe, K.H., Bassett, R.H. and Cole, E.R.L. (1967), "Principal axes observed during simple shear of a sand", Proc. of the Geotechnical Conf., Oslo, Vol. 1, pp 231-237.

Selig, E.T., Chang, C.S., Adegoke, C.W. and Alva-Hurtado, J.E. (1979), "A theory for track maintenance life prediction", Final report to US Department of Transportation, August.

Shenton, M.J. (1974), "Deformation of railway ballast under repeated loading (triaxial tests)", Report RPS, Soil Mech. Section, British Railways Research Dept., Derby.

Silver, M.L. and Seed, H.B. (1971), "Deformation characteristics of sands under cyclic loading", Soil Mech. and Found. Div., ASCE, Vol. 97, pp 1081-1098.

Sparrow, R.W. (1976), "A repeated load biaxial shear box for tests on railway ballast", Proc. of the 2nd Seminar on the Behaviour of Gran. Materials under Repeated Loading, Univ. of Nottingham.

Sutherland, H.B. and Mesdary, M.S. (1969), "The influence of the intermediate principal stress on the strength of sand", Proc. 7th Int. Conf. on Soil Mech. and Found. Eng., Vol. 1, pp 391-399.

Turcke, D.J. and Raymond, G.P. (1979), "Three dimensional analysis of rail track structure", Transportation Research Record 733, pp 1-6.

Wood, D.M., Drescher, A. and Budhu, M. (1979), "On the determination of the stress state in the simple shear apparatus", Geotechnical Testing Journal, ASTM, Vol. 2, No. 4, pp 211-222.

Wood, D.M. and Budhu, M. (1980), "The behaviour of Leighton Buzzard sand in cyclic simple shear tests", Proc. Int. Symposium on Soils under

Cyclic and Transient Loading, Swansea, Vol. 1, pp 9-21.

Youd, T.L. (1972), "Compaction of sands by repeated shear straining", Journ. Soil Mech. and Found. Div., ASCE, Vol. 98, pp 709-724.

Youd, T.L. (1975), "Lateral stresses in sands during cyclic loading", Geot. Eng. Div., ASCE, Vol. 101, pp 217-221.

APPENDIX A

TRANSDUCER CALIBRATIONS

TRIAXIAL EQUIPMENT

Load cell	0.477 Volts/100 kPa
Cell pressure	1.120 Volts/100 kPa
Axial strain LVDTs	21.11 Divisions/1% strain
Radial strain rings	21.11 Divisions/1% strain

BIAXIAL EQUIPMENT

	Pressure Transducers		Load Cells
1.	0.727 mV/bar	1.	80.25 N/Division
2.	0.705 mV/bar	2.	76.74 N/Division

	LVDTs
1.	0.525 Volts/mm
2.	0.550 Volts/mm
3.	0.540 Volts/mm
4.	0.554 Volts/mm

SIMPLE SHEAR EQUIPMENT

	Normal Load Cells		Shear Load Cells
1.	62.41 kPa/mV	1.	89.91 kPa/mV
2.	64.95 kPa/mV	2.	92.16 kPa/mV
3.	65.12 kPa/mV	3.	88.08 kPa/mV

	End Load Cells		Lateral Load Cells
1.	670.1 N/mV	3.	404.36 N/mV
2.	642.6 N/mV	4.	404.36 N/mV

LVDTs

Vertical

1. 0.722 Volts/mm
2. 0.694 Volts/mm
3. 0.644 Volts/mm

Horizontal

0.490 Volts/mm

APPENDIX 3A

TRIAXIAL RESILIENT STRAIN TESTS - 3 mm MATERIAL

No. of Tests	p_m (kPa)	q_m (kPa)	p_r (kPa)	q_r (kPa)	Resilient strains	
					Volumetric (Std Dev.) (με)	Shear (Std Dev.) (με)
2	48.09	0.01	16.65	2.06	105.26(3.3)	-8.92(0.1)
1	48.12	0.00	32.28	0.00	214.68(0.0)	-11.17(0.0)
3	48.13	-0.07	6.96	24.19	29.92(7.3)	68.57(8.4)
2	47.66	-0.18	-0.37	24.06	-8.08(11.6)	64.83(6.5)
3	47.96	-0.10	16.36	24.08	115.57(3.5)	67.49(15.6)
3	48.09	0.05	24.17	23.92	176.81(10.4)	74.53(13.8)
1	47.94	-0.16	48.76	24.13	372.41(0.0)	75.86(0.0)
2	48.02	0.10	-23.86	24.18	-182.47(14.6)	76.99(20.1)
3	48.15	0.12	-48.13	24.06	-87.21(365.8)	58.02(91.8)
3	48.50	0.17	13.33	48.10	93.90(17.8)	169.64(20.7)
3	47.82	-0.21	0.33	48.38	15.10(11.5)	165.66(17.8)
3	48.26	0.18	32.30	48.03	269.41(12.5)	194.01(34.3)
1	48.15	0.16	24.24	72.72	151.15(0.0)	268.68(0.0)
2	48.21	0.23	0.03	72.34	53.08(19.4)	330.23(40.0)
1	48.20	24.14	16.21	0.01	108.11(0.0)	-13.42(0.0)
1	48.18	24.10	31.86	-0.01	237.24(0.0)	-31.54(0.0)
3	47.83	24.29	7.01	24.32	21.33(12.9)	66.91(7.5)
3	47.97	24.12	-0.62	24.16	-27.14(4.3)	68.51(9.6)
3	47.98	24.25	16.59	24.42	85.49(7.5)	59.17(9.1)
3	48.22	24.30	24.24	24.34	152.59(1.5)	51.36(7.9)
3	48.12	24.22	48.45	23.99	356.66(17.7)	32.25(12.5)
3	48.38	24.65	-24.41	23.36	-216.08(1.6)	102.95(11.8)
3	48.21	24.49	-48.33	23.17	-537.75(30.6)	197.61(22.6)
3	48.14	24.21	14.01	48.34	46.61(11.9)	150.51(12.9)
3	48.12	24.10	0.08	48.57	-50.64(6.6)	166.75(12.2)
3	48.08	24.12	32.29	48.64	200.32(10.9)	140.89(19.1)
3	48.15	24.20	48.26	48.62	354.64(14.2)	129.19(20.2)
2	48.04	24.24	21.74	72.38	104.94(16.1)	278.42(17.6)
3	48.25	24.23	-0.09	72.38	-78.64(16.7)	307.30(24.7)
3	48.04	24.09	47.90	71.95	383.13(29.3)	278.86(21.4)
1	48.01	24.10	32.09	96.26	146.71(0.0)	403.19(0.0)
2	48.23	48.47	15.87	-0.96	89.70(39.2)	-13.92(15.8)
1	47.96	48.08	32.23	0.02	68.15(0.0)	6.83(0.0)
3	48.04	48.16	7.15	23.92	7.38(10.5)	57.69(5.8)
3	47.86	48.19	-0.62	23.97	-45.00(8.9)	72.78(4.0)
3	47.97	48.21	16.65	23.92	73.32(24.3)	46.19(4.8)
3	48.19	48.42	23.97	24.12	153.88(10.4)	30.23(4.6)
3	48.41	48.31	48.57	23.03	440.91(13.3)	-38.29(17.3)
3	48.11	48.19	40.10	24.18	328.40(8.4)	-4.36(8.3)
2	48.09	48.21	15.31	48.07	29.10(11.2)	147.11(11.9)
2	47.93	48.17	0.16	48.33	-116.54(15.3)	185.54(13.6)
2	48.29	48.34	31.78	47.99	189.96(8.8)	120.73(16.8)
1	48.02	48.02	47.73	47.35	382.47(0.0)	83.17(0.0)
3	47.88	48.07	21.69	72.06	51.25(13.5)	245.30(20.2)
2	48.19	48.25	48.33	72.27	326.41(9.8)	176.39(0.3)
3	48.05	48.10	72.06	72.02	546.85(131.3)	158.09(60.2)
3	48.26	47.86	29.06	96.22	58.54(25.8)	400.46(38.7)
3	48.00	47.93	63.83	95.67	472.17(44.4)	312.37(34.0)
3	48.25	72.31	7.67	23.78	1.01(5.0)	57.91(5.2)
3	48.04	72.20	16.19	23.66	69.65(38.3)	34.90(8.4)
1	48.20	-23.98	16.23	0.00	108.47(0.0)	-1.11(0.0)
1	47.85	-24.08	31.96	0.01	231.14(0.0)	6.08(0.0)
3	48.25	-24.06	6.40	24.32	46.71(15.6)	87.54(14.4)
3	48.02	-24.03	0.12	24.55	20.74(21.5)	92.49(22.1)
3	48.10	-24.08	16.56	24.19	123.43(13.8)	95.54(10.0)
3	48.07	-24.11	24.27	23.99	207.95(17.3)	105.79(11.9)
3	48.00	-23.94	-23.97	24.44	-147.80(18.4)	71.86(11.5)
3	48.06	-23.77	-48.37	24.65	-263.15(83.1)	130.66(55.3)
2	48.05	-23.98	0.01	47.90	87.95(35.0)	217.42(32.9)
3	47.85	-24.14	-47.85	48.06	-343.34(20.7)	185.47(24.1)
3	48.02	-48.21	-24.17	24.10	-130.59(30.1)	70.82(18.9)
1	95.85	-0.11	32.10	0.02	152.87(0.0)	-5.37(0.0)
1	95.92	-0.07	64.75	0.00	320.66(0.0)	-0.08(0.0)

3	95.94	0.06	14.18	48.29	58.69(21.1)	118.47(20.3)
3	96.37	0.13	-1.18	47.84	11.96(17.0)	115.41(17.8)
3	96.19	0.07	33.38	47.87	154.01(14.1)	114.52(24.3)
1	96.69	0.33	-15.26	48.41	271.40(0.0)	116.99(0.0)
3	96.24	0.15	96.75	47.72	542.92(67.1)	166.41(47.4)
3	96.27	0.39	-48.07	47.87	-218.20(7.7)	113.15(6.5)
3	96.54	0.29	-96.64	48.25	-504.08(24.3)	139.65(24.8)
1	96.81	0.86	32.35	97.01	158.67(0.0)	237.46(0.0)
3	95.77	0.03	0.18	95.96	59.32(36.3)	249.22(33.8)
3	95.98	-0.23	64.33	96.14	413.58(60.2)	324.58(63.0)
1	95.99	0.04	48.02	144.02	332.38(0.0)	475.23(0.0)
3	96.34	0.41	0.82	144.57	128.91(59.5)	503.23(80.8)
1	96.14	48.38	32.14	0.00	148.84(0.0)	-2.61(0.0)
1	95.64	47.74	64.16	0.00	78.86(0.0)	52.58(0.0)
3	95.58	48.05	14.90	48.49	28.93(20.9)	100.68(10.4)
3	95.71	48.42	0.09	48.86	-29.45(11.7)	104.78(11.0)
1	79.40	31.57	31.88	48.94	128.48(0.0)	85.65(0.0)
3	96.43	48.42	48.31	48.15	227.79(9.2)	81.68(7.4)
3	96.72	48.86	97.02	48.53	512.92(35.5)	67.55(18.6)
3	96.08	48.10	-47.53	48.35	-277.17(16.5)	142.04(3.5)
3	96.12	48.00	-95.70	48.33	-645.03(17.6)	265.38(13.4)
3	96.37	48.43	29.43	96.84	88.69(16.0)	219.54(18.7)
3	96.04	48.19	0.41	96.68	-40.97(18.4)	235.96(14.8)
3	96.38	48.48	64.43	97.06	337.08(28.6)	203.72(20.8)
2	96.56	48.41	96.68	96.46	527.82(13.4)	213.46(15.5)
1	96.04	48.00	47.86	143.62	181.41(0.0)	343.79(0.0)
3	96.30	48.56	-0.58	144.65	-41.05(13.3)	423.00(46.0)
3	96.38	48.55	97.10	144.75	543.24(37.2)	431.23(42.8)
1	96.50	48.97	64.39	193.18	321.85(0.0)	598.93(0.0)
3	96.06	96.15	32.20	0.31	172.45(13.2)	-35.65(0.5)
2	96.41	97.14	64.04	-1.95	420.07(8.8)	-99.12(13.8)
3	95.69	96.42	15.39	48.18	20.25(14.0)	92.36(10.7)
3	95.61	96.68	-0.95	48.12	-59.33(9.5)	101.36(7.0)
3	96.29	96.67	32.70	47.71	133.88(10.3)	64.79(11.0)
3	96.06	96.39	48.35	48.59	215.39(15.6)	50.28(12.3)
3	96.41	96.31	96.58	48.35	585.59(10.3)	-32.10(14.3)
3	95.86	96.15	80.16	48.01	428.61(11.5)	2.18(17.0)
3	96.18	96.43	29.34	95.85	64.97(15.5)	189.91(22.4)
3	95.60	95.71	0.61	96.00	-109.81(15.5)	235.30(19.6)
2	96.27	96.50	64.51	96.46	265.48(13.3)	144.78(8.4)
3	96.31	96.59	95.79	95.69	498.32(23.6)	125.38(14.2)
3	95.81	95.71	44.98	143.91	122.72(17.6)	326.37(33.2)
2	96.20	96.25	96.22	144.22	477.67(20.4)	250.37(11.3)
3	96.24	96.24	143.86	144.42	891.69(22.4)	223.04(32.3)
1	96.42	96.41	64.13	192.38	174.66(0.0)	514.31(0.0)
3	96.12	95.82	127.82	191.85	756.26(40.6)	440.78(40.9)
3	96.16	144.18	16.11	47.92	-0.95(15.8)	84.94(5.8)
3	96.36	144.82	32.77	47.96	141.70(7.8)	47.50(8.2)
1	95.69	-47.86	31.98	0.00	16.22(0.0)	-77.52(0.0)
1	95.92	-48.04	64.14	0.07	16.22(0.0)	174.22(0.0)
2	96.01	-47.66	13.82	47.59	106.87(1.6)	139.09(1.4)
3	96.00	-47.46	-0.09	48.35	47.64(11.4)	133.52(10.3)
1	95.03	-52.67	29.66	36.89	238.36(0.0)	158.44(0.0)
3	96.58	-47.70	48.96	48.04	359.30(50.6)	201.49(23.6)
3	96.38	-47.88	-48.84	48.05	-200.99(3.1)	91.47(11.9)
3	96.10	-47.92	-96.43	48.22	-313.95(226.9)	4.63(55.6)
3	96.21	-47.81	0.23	96.22	143.79(28.2)	305.77(14.8)
1	87.96	-48.28	-79.69	96.50	-458.73(0.0)	191.04(0.0)
3	96.10	-95.98	-48.25	48.17	-196.88(29.3)	71.39(21.6)
1	192.78	-0.02	64.37	0.05	-30.43(0.0)	84.86(0.0)
1	191.93	-0.22	128.78	0.05	-69.86(0.0)	185.04(0.0)
2	190.97	-0.75	30.97	96.41	126.00(27.9)	164.87(13.1)
3	191.26	-0.14	-1.38	95.36	27.71(14.0)	141.94(16.2)
3	191.86	-0.25	64.57	94.99	235.56(7.8)	160.43(24.4)
3	192.13	-0.13	96.54	97.03	288.85(147.5)	202.75(21.0)
3	191.49	0.25	194.84	94.75	745.17(79.6)	218.98(44.9)

3	193.07	0.62	-95.77	95.63	-294.81(8.0)	135.81(4.4)
3	192.12	0.21	-192.48	95.84	-685.02(34.0)	146.20(7.9)
1	193.10	2.23	64.50	193.49	272.82(0.0)	353.58(0.0)
3	192.31	0.29	-1.74	192.26	83.09(24.7)	325.61(16.3)
3	191.54	-0.82	128.14	191.09	590.60(26.8)	416.00(45.8)
1	193.42	0.94	95.66	287.09	528.00(0.0)	663.90(0.0)
2	192.89	1.82	-0.51	288.48	213.73(16.3)	646.69(31.3)
3	193.50	97.36	65.03	1.38	197.90(9.5)	-10.95(5.2)
2	193.21	97.33	128.28	0.03	423.50(5.7)	-29.32(2.4)
3	191.45	95.64	31.39	98.06	55.10(9.7)	134.86(12.2)
3	191.98	96.49	-0.75	96.02	-16.18(9.9)	132.65(11.6)
3	191.74	96.38	65.54	96.45	177.38(22.4)	121.25(12.9)
3	192.08	96.20	95.97	96.65	317.94(25.4)	123.78(19.0)
3	192.09	96.03	192.30	95.43	698.20(40.3)	116.62(18.9)
1	-277.55	-373.34	-94.69	97.15	-327.65(0.0)	166.41(0.0)
3	192.89	96.55	-192.51	97.04	-689.60(155.6)	259.83(49.5)
2	192.58	96.87	64.40	193.15	174.78(10.9)	275.78(10.5)
3	192.85	97.39	0.65	194.07	-26.96(10.6)	293.53(19.7)
3	192.41	96.45	128.77	192.41	442.98(40.8)	275.50(19.6)
2	193.32	97.27	192.51	193.48	675.37(4.6)	276.41(18.3)
1	192.03	97.87	96.26	288.67	326.94(0.0)	499.07(0.0)
2	192.02	96.69	0.03	288.19	-28.19(12.3)	508.74(14.2)
3	193.00	96.90	192.62	289.07	516.75(347.0)	551.48(41.8)
1	191.45	95.93	127.95	383.76	557.25(0.0)	800.86(0.0)
3	193.23	193.41	64.55	1.54	225.22(13.5)	-33.08(5.9)
2	193.13	192.55	128.27	0.20	491.77(17.9)	-103.18(10.3)
3	192.67	192.92	32.22	96.59	51.00(11.8)	116.57(3.5)
3	192.59	193.63	-0.50	97.74	-48.23(1.3)	133.94(10.1)
3	192.46	193.06	67.25	96.45	177.66(17.2)	90.49(7.7)
3	194.01	193.62	96.62	97.12	289.24(13.7)	73.86(3.0)
3	193.99	193.90	193.25	96.83	749.59(18.2)	-3.13(6.5)
3	192.34	192.63	161.51	97.01	562.22(13.2)	36.94(14.5)
3	193.57	193.01	62.02	191.33	128.64(6.5)	256.04(15.1)
1	184.12	168.07	15.50	241.58	-112.26(0.0)	315.21(0.0)
3	192.65	193.08	127.77	190.86	402.09(5.8)	213.90(13.6)
3	192.23	192.50	192.37	191.93	666.94(17.3)	182.07(17.6)
1	-108.42	-108.70	96.08	288.05	211.60(0.0)	451.31(0.0)
3	192.90	192.71	192.98	288.98	684.54(27.6)	384.45(20.6)
3	192.12	192.35	288.57	288.37	1214.48(23.7)	328.89(45.0)
1	191.55	191.14	127.71	382.94	305.27(0.0)	664.37(0.0)
3	192.00	191.90	257.09	384.32	1079.61(74.4)	628.95(41.3)
3	192.99	289.57	31.83	95.07	16.06(7.2)	109.39(7.1)
3	192.87	289.02	66.21	95.30	183.23(13.8)	71.71(6.7)
2	193.03	-95.67	64.23	-1.80	205.15(0.9)	18.00(1.7)
1	192.38	-95.23	128.26	0.00	454.70(0.0)	81.70(0.0)
2	192.71	-95.79	31.87	95.90	141.15(18.7)	193.68(20.4)
3	192.01	-95.64	-0.73	96.69	26.72(32.2)	143.89(36.6)
3	191.77	-96.50	64.63	94.69	276.18(36.2)	226.90(32.3)
3	192.39	-96.31	97.24	96.02	519.87(52.1)	295.35(48.6)
3	192.54	-95.85	-96.45	96.70	-246.57(14.4)	126.20(4.1)
3	192.04	-95.32	-193.93	97.81	-648.58(44.5)	60.76(16.7)
3	192.17	-96.24	-1.18	191.97	226.92(46.2)	440.20(26.8)
3	192.16	-96.57	-193.74	191.14	-574.85(43.6)	291.64(7.8)
3	192.50	-192.51	-96.81	96.38	-312.89(58.3)	65.89(8.1)
2	384.41	193.20	129.73	0.10	278.15(14.8)	-11.01(9.5)
2	383.32	193.89	63.02	194.83	143.46(23.9)	204.22(5.4)
3	383.50	192.46	-2.78	191.01	-2.41(15.0)	194.25(10.0)
3	384.94	193.84	131.06	195.49	300.65(18.8)	192.77(4.7)
1	229.49	36.82	190.30	191.90	427.11(0.0)	190.49(0.0)
2	385.04	195.77	118.58	385.58	320.07(20.6)	473.17(21.3)
1	185.58	-6.29	0.10	385.63	14.92(0.0)	471.76(0.0)
3	384.77	193.34	256.00	389.76	651.35(6.2)	460.28(35.3)
1	384.11	194.54	229.54	768.67	901.59(0.0)	1278.86(0.0)
3	385.43	386.94	127.51	0.06	387.09(84.0)	-78.39(40.8)
3	386.61	387.66	255.73	-0.03	707.55(64.9)	-137.96(9.0)
3	387.02	387.82	64.61	193.57	85.14(3.3)	160.81(7.5)

3	384.41	386.72	0.36	193.79	20.13(	116.4)	159.30(23.9)
3	385.44	385.25	132.01	193.54	255.69(	32.0)	135.89(10.3)
2	385.13	385.70	192.75	193.39	397.81(	22.4)	111.38(8.4)
3	385.48	386.56	319.70	195.01	801.14(	51.4)	61.16(13.0)
3	385.82	385.62	127.93	383.52	280.25(	89.7)	331.37(49.1)
2	384.97	386.93	2.24	385.73	-147.12(	18.9)	449.69(52.3)
3	385.78	386.46	256.90	385.66	575.33(	39.4)	307.93(20.8)
2	385.77	386.13	385.97	385.29	945.17(	62.0)	269.90(23.4)
2	383.17	384.88	178.03	575.95	327.82(	29.4)	630.03(42.5)
3	385.06	383.38	385.57	575.90	959.77(	58.8)	536.83(16.7)
2	384.98	384.81	241.70	766.75	441.20(	14.7)	1047.59(76.7)
2	385.60	385.15	512.19	769.15	1560.68(	61.3)	860.94(12.0)
3	385.31	577.26	64.12	190.37	50.29(	11.0)	144.44(3.2)
1	382.78	576.96	136.77	191.81	239.55(	0.0)	88.18(0.0)

APPENDIX 3B

TRIAXIAL RESILIENT STRAIN TESTS - OTHER MATERIALS

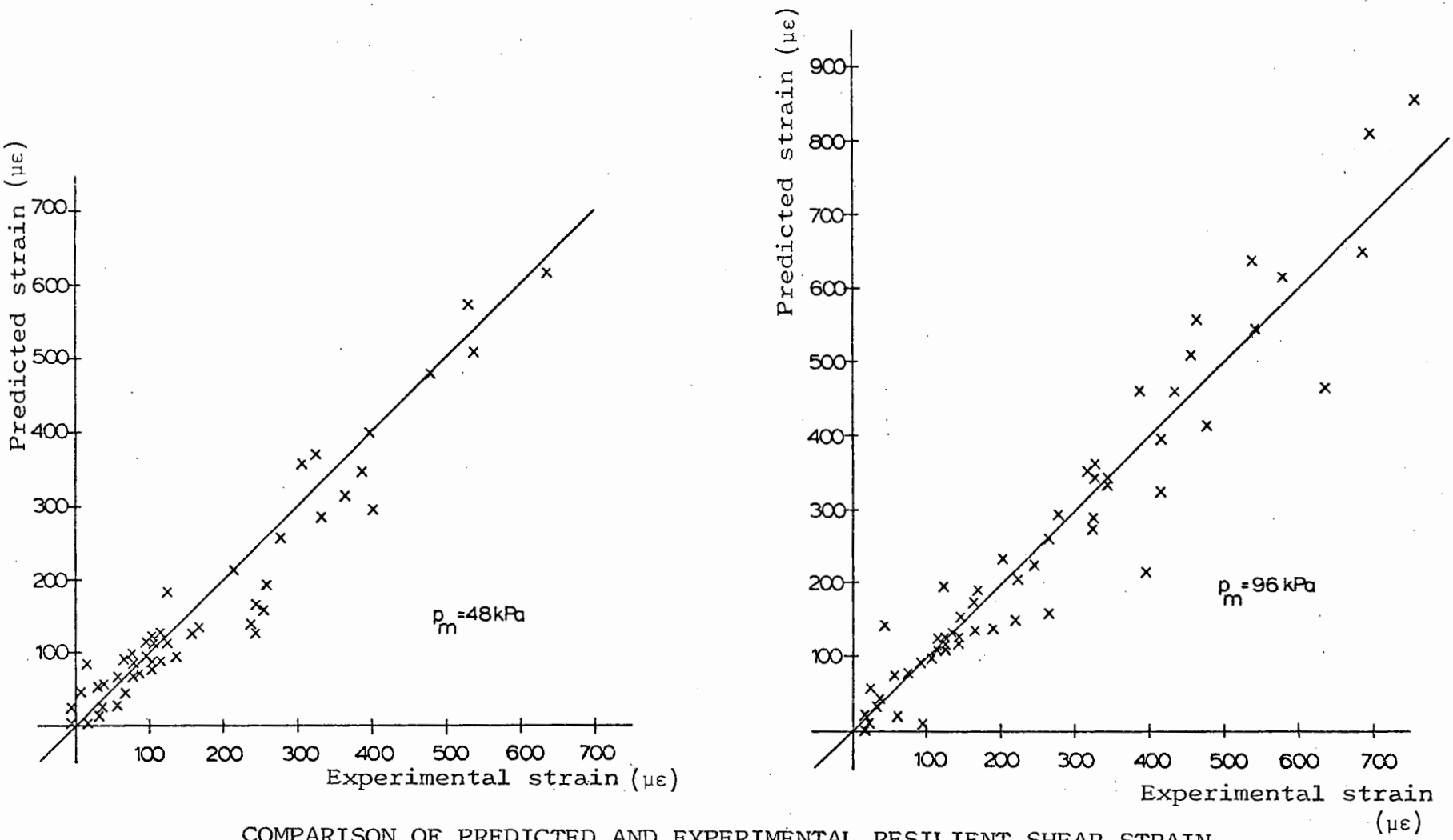

COMPARISON OF PREDICTED AND EXPERIMENTAL RESILIENT SHEAR STRAIN FOR WOODHALL SPA GRAVEL

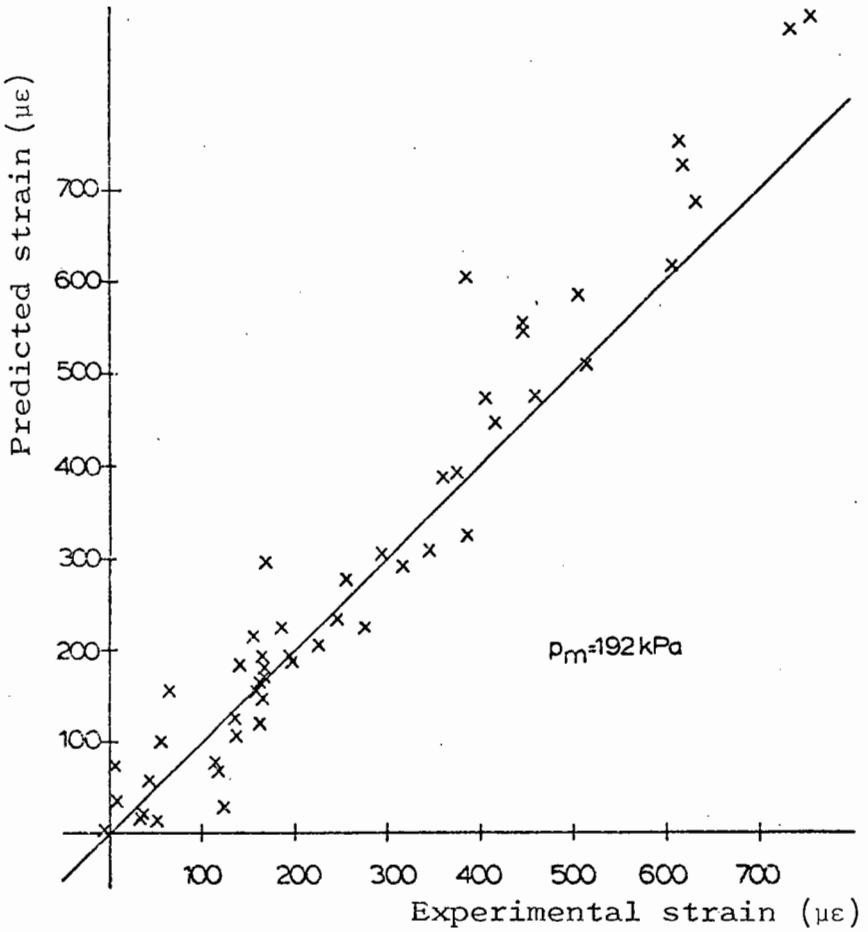

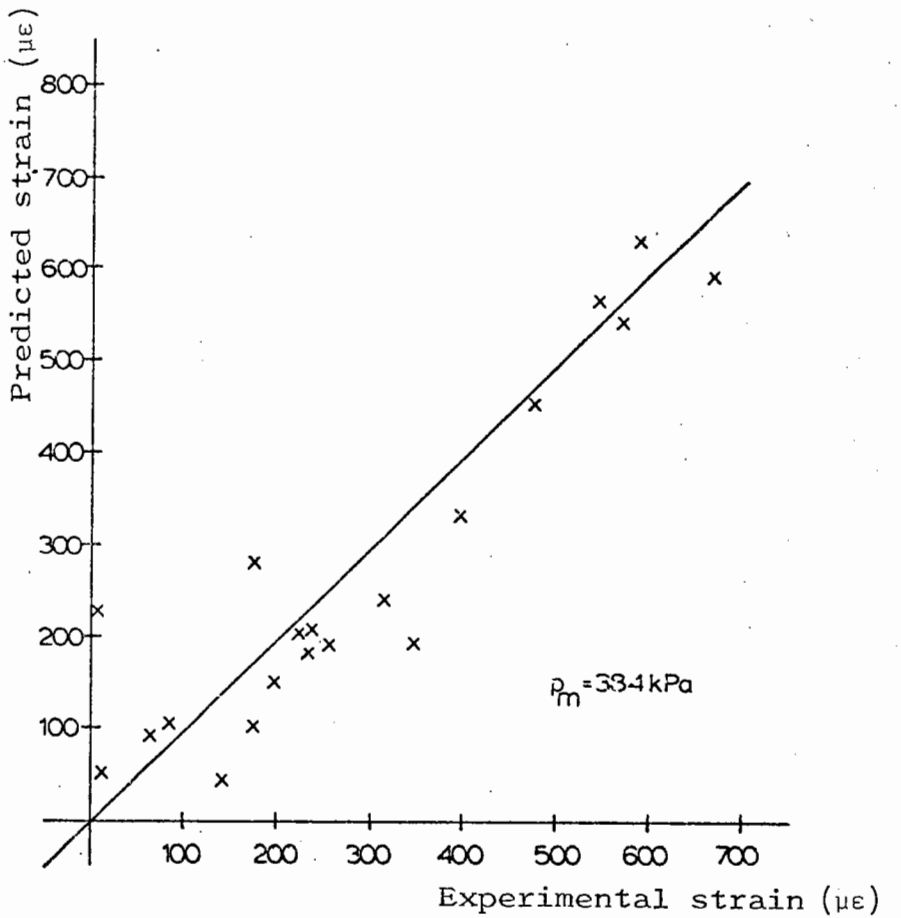

COMPARISON OF PREDICTED AND EXPERIMENTAL RESILIENT SHEAR STRAIN FOR WOODHALL SPA GRAVEL

COMPARISON OF PREDICTED AND EXPERIMENTAL RESILIENT VOLUMETRIC STRAINS FOR WOODHALL SPA GRAVEL

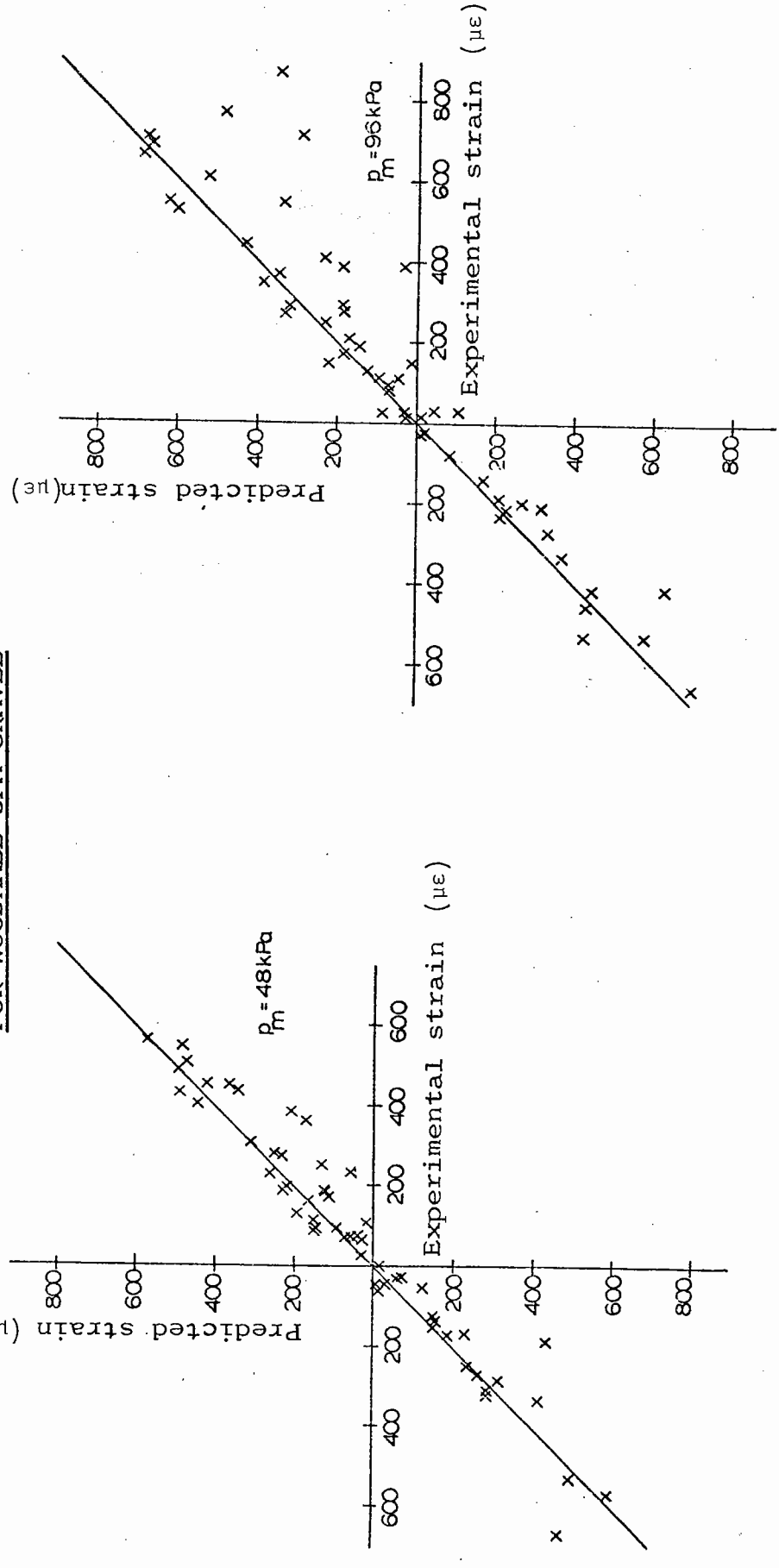

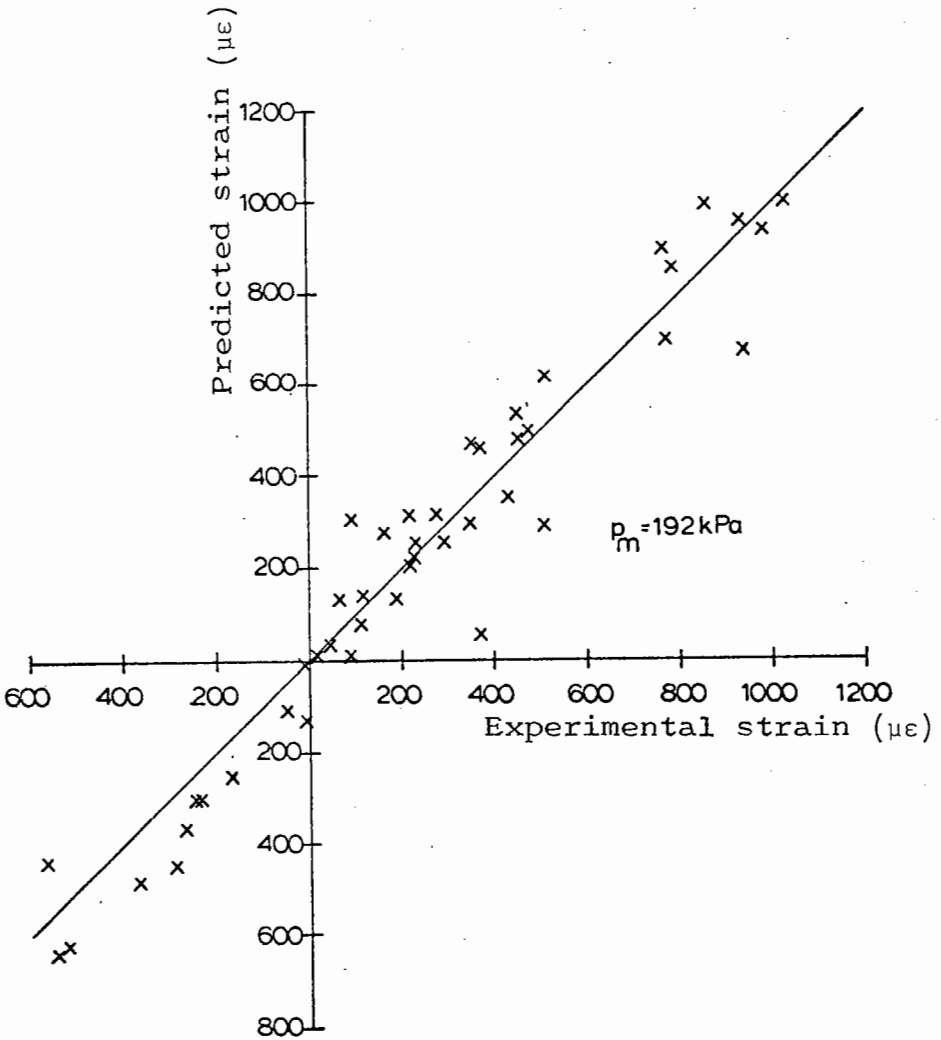

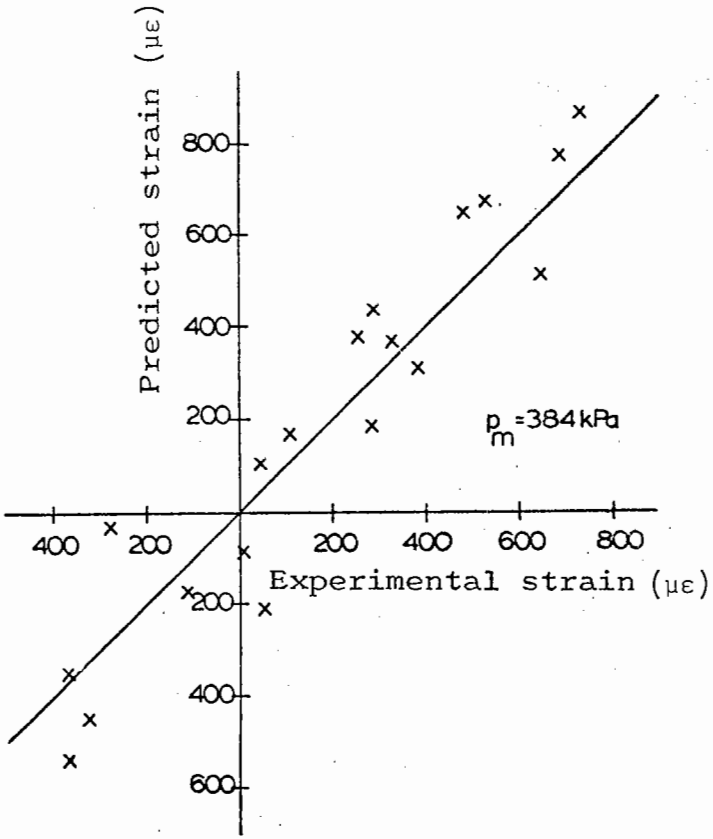

COMPARISON OF PREDICTED AND EXPERIMENTAL RESILIENT VOLUMETRIC STRAINS FOR WOODHALL SPA GRAVEL

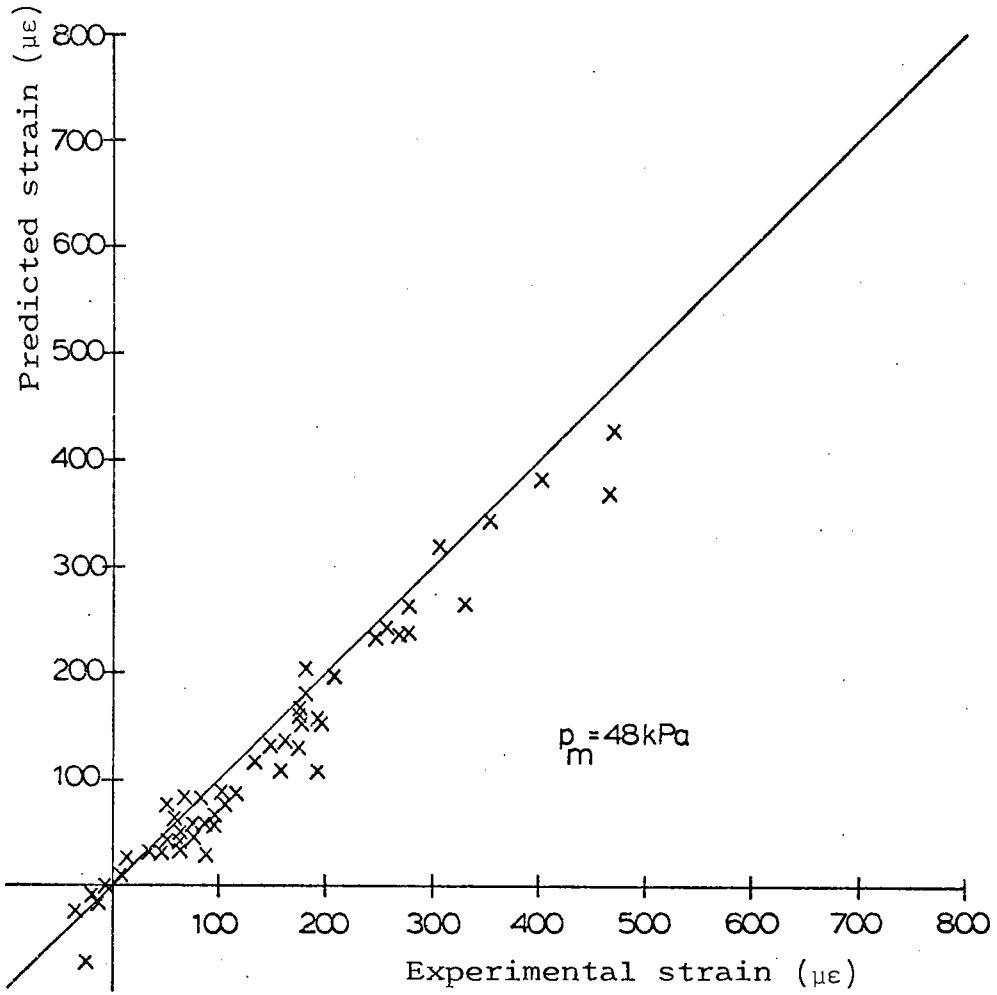

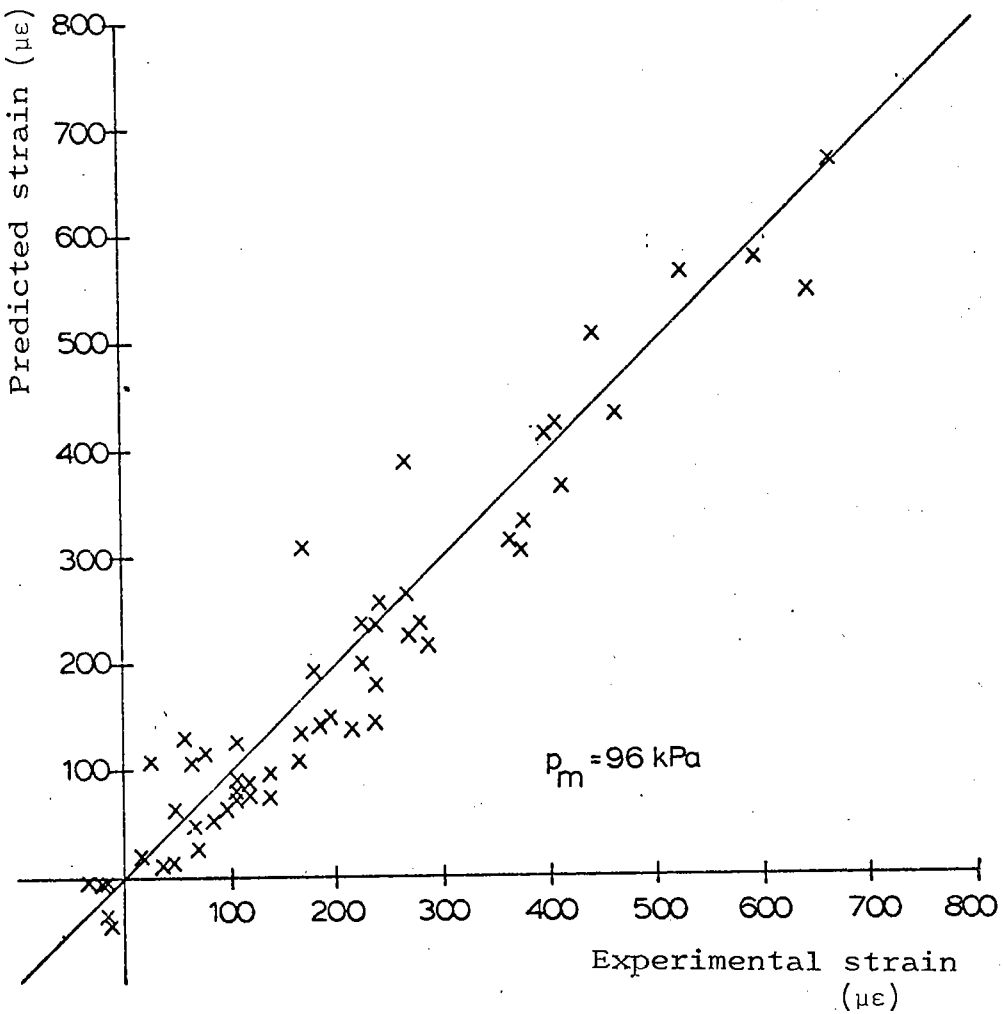

COMPARISON OF PREDICTED AND EXPERIMENTAL RESILIENT SHEAR STRAINS FOR 1.5 mm MATERIAL

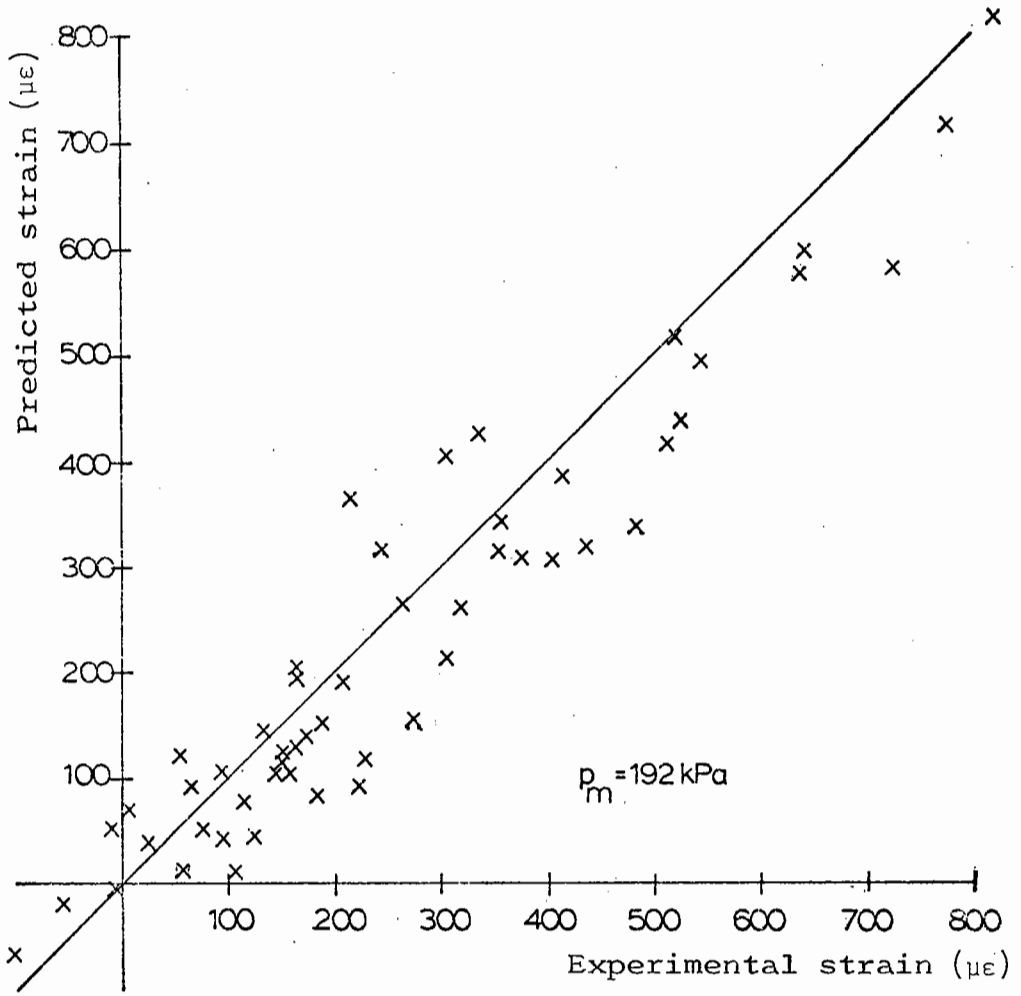

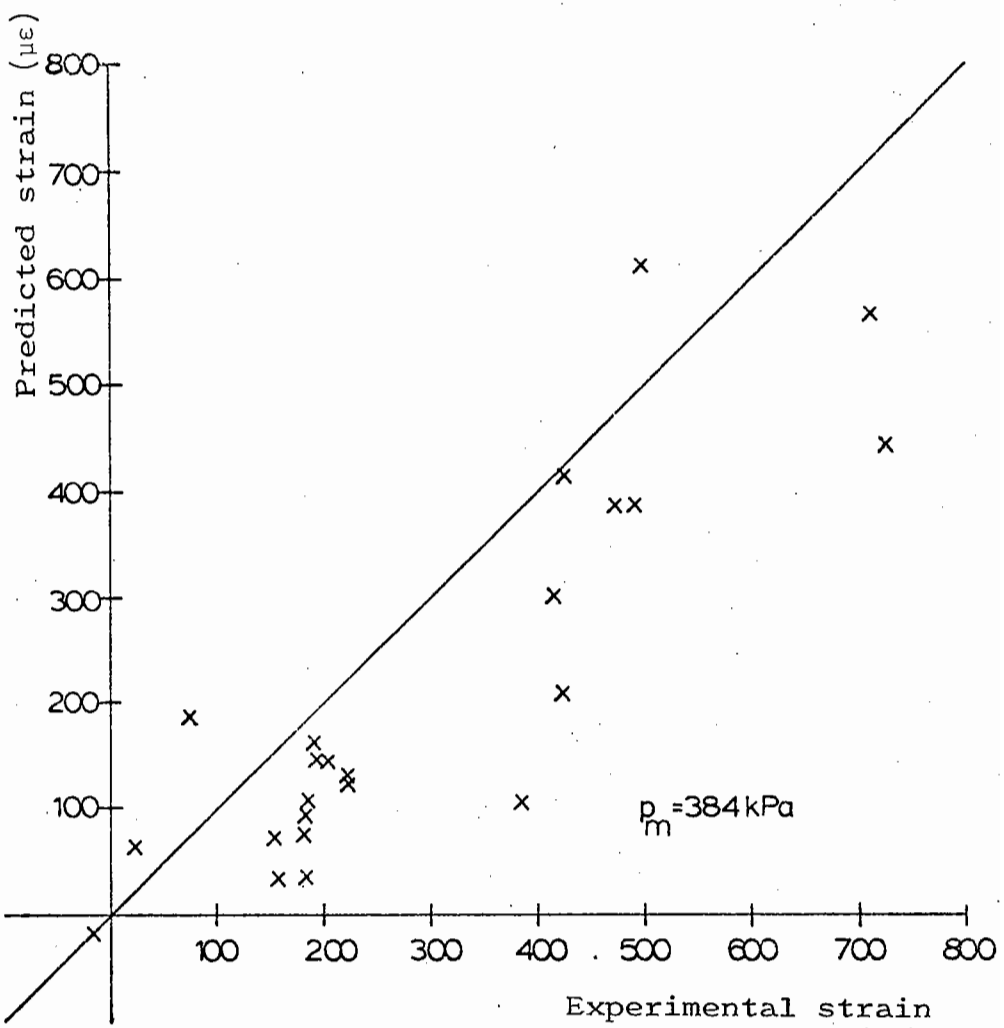

COMPARISON OF PREDICTED AND EXPERIMENTAL RESILIENT SHEAR STRAIN FOR 1.5 mm MATERIAL

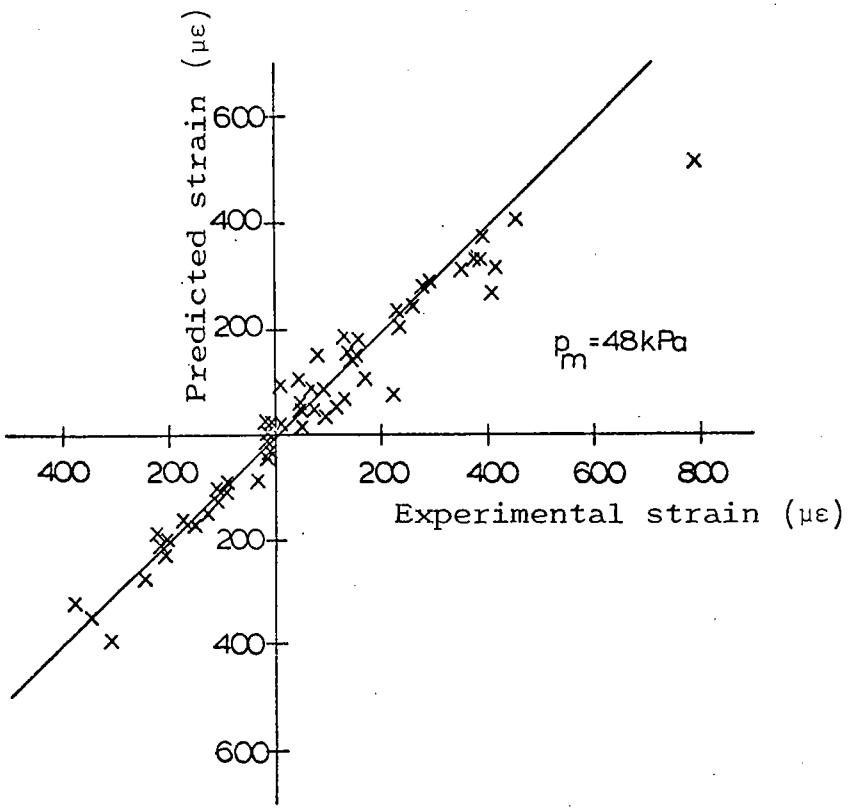

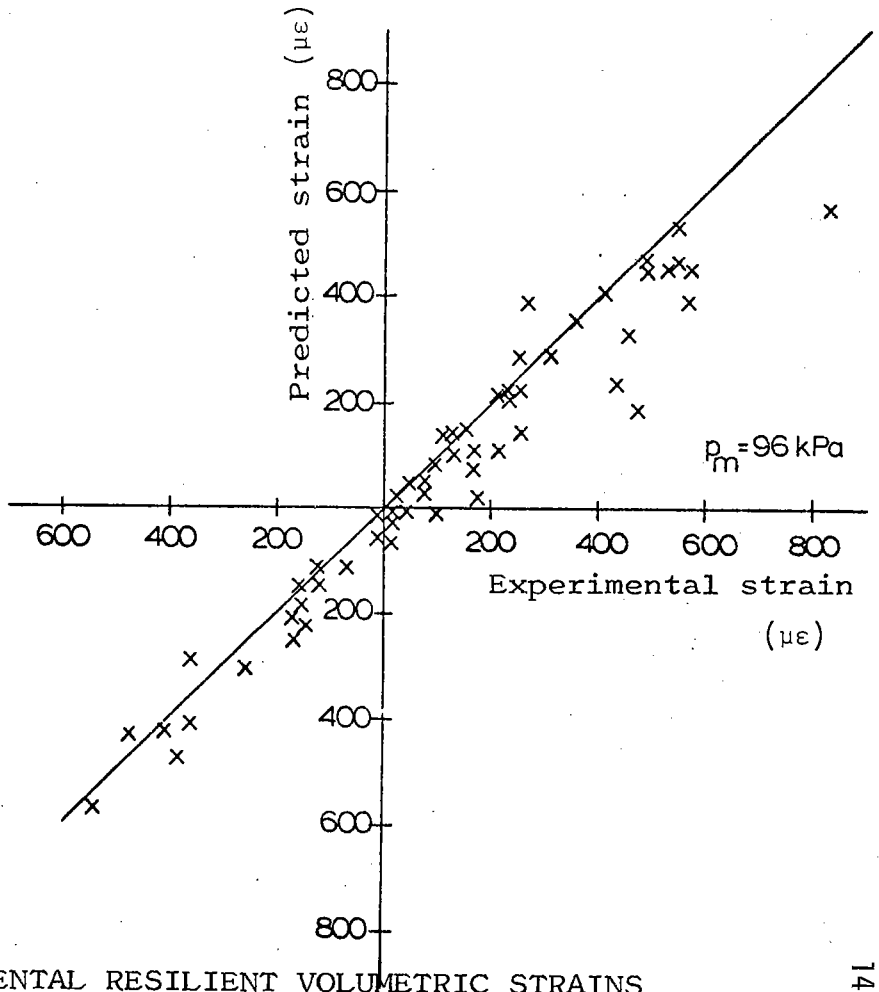

COMPARISON OF PREDICTED AND EXPERIMENTAL RESILIENT VOLUMETRIC STRAINS FOR 1.5 mm MATERIAL

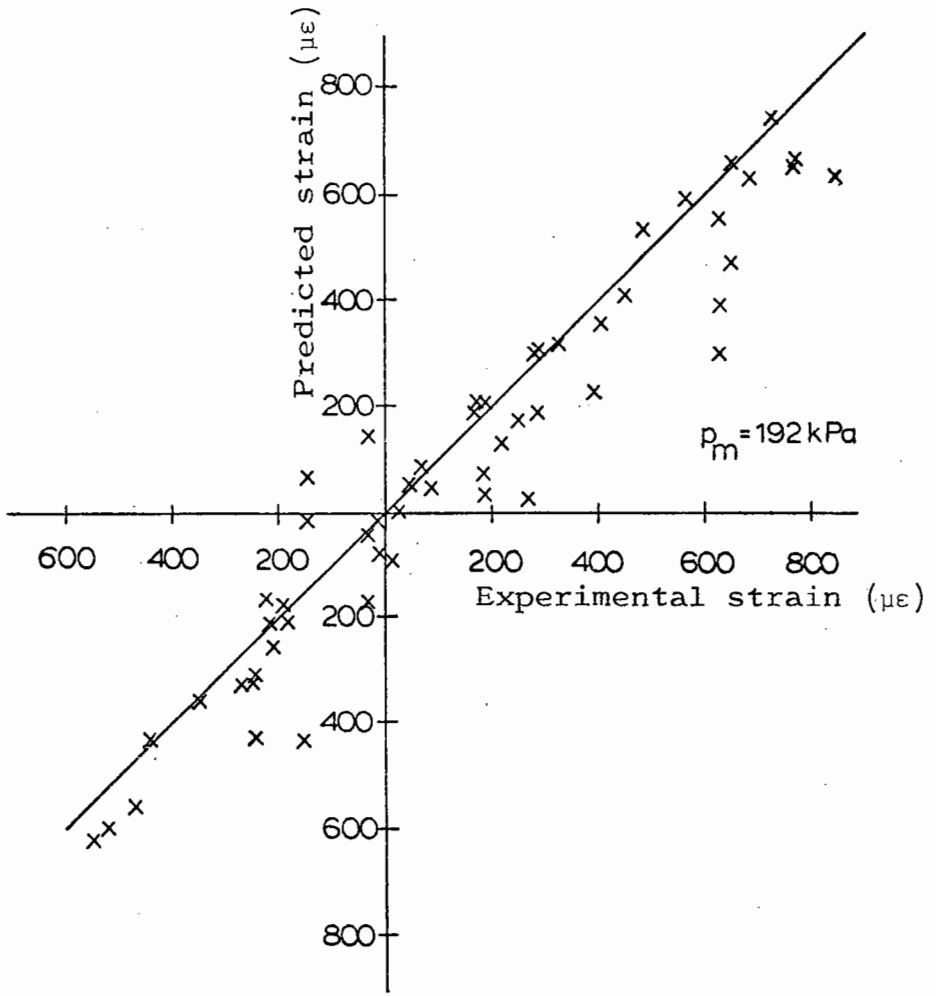

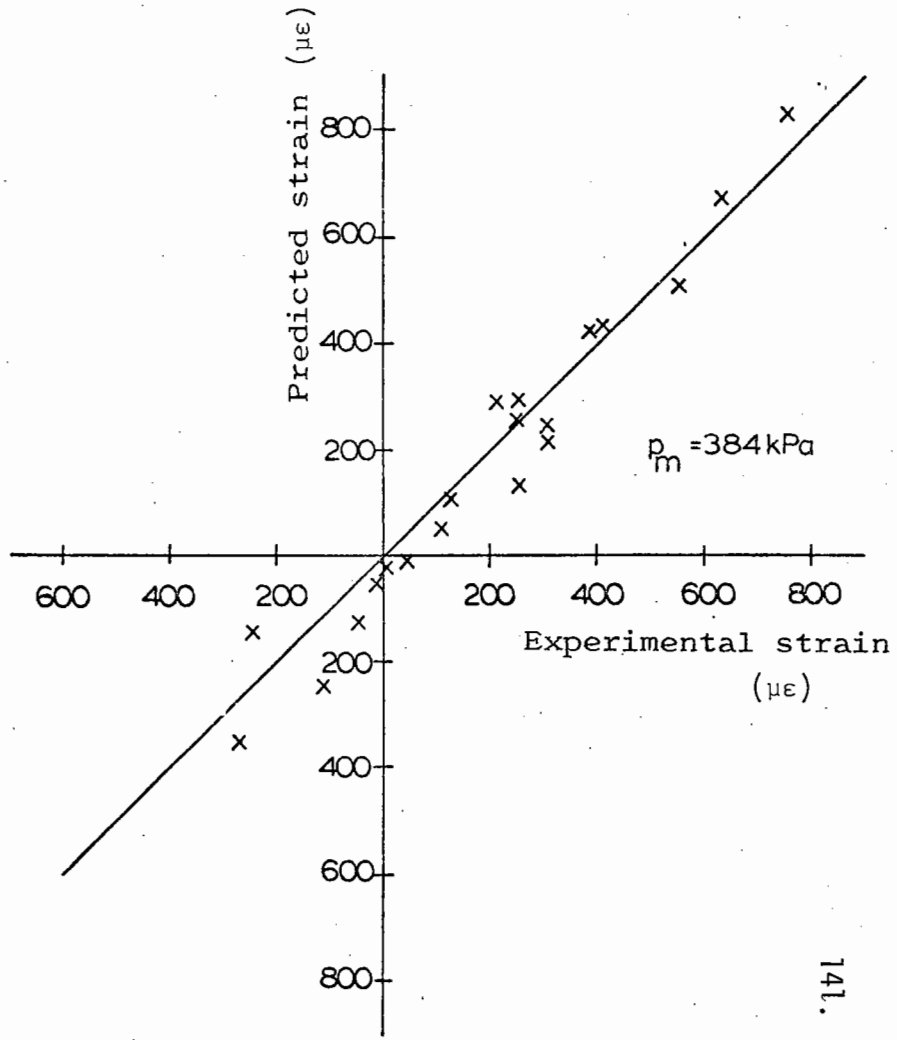

COMPARISON OF PREDICTED AND EXPERIMENTAL RESILIENT VOLUMETRIC STRAINS FOR 1.5 mm MATERIAL

APPENDIX 3C

TRIAXIAL PERMANENT STRAIN TESTS - 3 mm MATERIAL

TRIAXIAL PERMANENT STRAIN TESTS

PATH	p_m (kPa)	q_m (kPa)	p_r (kPa)	q_r (kPa)
PA	192	288	96	288
PA2	320	288	96	288
PB	320	288	192	576
PC	320	288	0	288
PD	320	288	192	0
QA	144	144	48	144
QB	144	144	96	288
QC	144	144	0	144
QD	144	144	96	0

TRIAXIAL PERMANENT STRAIN TESTS

PATH	TEST NO	PERMANENT SHEAR STRAIN % cycle 1	10	10^2	10^3	10^4	10^5
PA	1	1.23	2.21	2.98	3.33	3.64	3.43
	2	0.25	2.07	2.54	2.68	3.03	3.14
	3	0.85	2.34	2.72	3.11	3.33	3.39
PA2	1	0.24	0.36	0.46	0.55	0.59	0.61
	2	0.30	0.41	0.59	0.69	0.75	0.76
	3	0.25	0.37	0.49	0.62	0.68	0.69
PB	1	0.19	0.67	1.09	-	1.49	1.57
	2	0.46	0.82	1.10	1.41	1.59	1.65
	3	0.29	0.55	0.85	1.08	1.22	1.27
PC	1	0.24	0.36	0.63	0.76	0.84	0.87
	2	0.21	0.28	0.41	0.67	0.76	0.79
	3	0.30	0.42	-	0.85	0.96	1.02
PD	1	0.52	0.59	0.67	0.72	0.74	0.76
	2	-	-	-	0.55	0.60	0.62
	3	0.24	0.36	0.51	0.64	0.70	0.73
QA	1	0.29	0.54	0.66	0.78	0.87	0.92
	2	0.14	0.19	0.26	0.34	0.41	0.46
	3	0.10	0.21	0.35	0.46	0.51	0.55
QB	1	0.15	0.42	0.66	0.86	0.96	1.01
	2	0.28	0.46	0.75	0.95	1.08	1.08
	3	0.37	0.67	0.91	1.11	1.11	1.37
QC	1	0.29	0.53	0.98	1.34	1.59	1.80
	2	0.29	0.47	0.91	1.29	1.58	2.17
QD	1	0.17	1.09	2.16	2.39	2.64	2.66
	2	0.16	0.51	1.05	1.57	1.99	2.10
	3	0.39	1.32	1.88	2.32	2 82	2.86

TRIAXIAL PERMANENT STRAIN TESTS

PATH	TEST NO	PERMANENT VOLUMETRIC STRAIN % cycle 1	10	10^2	10^3	10^4	10^5
PA	1	-0.06	-0.24	-0.05	-0.04	-0.05	0.94
	2	0.02	-0.31	-0.41	-0.66	-0.32	-0.34
	3	0.14	-0.12	-0.18	-0.15	-0.05	-0.01
PA2	1	0.21	0.27	0.37	0.59	0.67	0.71
	2	0.17	0.24	0.23	0.34	0.39	0.44
	3	0.20	0.32	0.43	0.55	0.64	0.65
PB	1	0.14	0.51	0.86	-	1.37	1.49
	2	0.40	0.55	0.85	1.16	1.41	1.51
	3	0.14	0.23	0.45	0.68	0.86	0.95
PC	1	0.20	0.34	0.57	0.70	0.76	0.77
	2	0.09	0.13	0.21	0.48	0.55	0.55
	3	0.25	0.38	-	0.72	0.79	0.78
PD	1	-0.02	-0.07	0.05	0.11	0.15	0.15
	2	-	-	-	0.61	0.63	0.66
	3	0.19	0.29	0.41	0.54	0.57	0.58
QA	1	0.11	0.16	0.23	0.29	0.34	0.34
	2	0.04	0.02	0.07	0.11	0.16	0.25
	3	0.07	0.07	0.21	0.29	0.32	0.36
QB	1	0.09	0.22	0.35	0.51	0.68	0.82
	2	0.10	0.22	0.32	0.50	0.66	1.14
	3	-0.06	0.06	0.16	0.23	0.15	0.72
QC	1	0.16	0.19	0.36	0.51	0.68	0.78
	2	0.22	0.24	0.27	0.37	0.53	0.75
QD	1	0.10	-0.23	-0.42	-0.48	-0.44	-0.47
	2	0.15	0.07	-0.17	-0.25	-0.27	-0.34
	3	0.19	0.33	0.47	0.55	0.78	0.67

APPENDIX 3D

RESILIENT RESPONSE DURING TRIAXIAL PERMANENT STRAIN TESTS

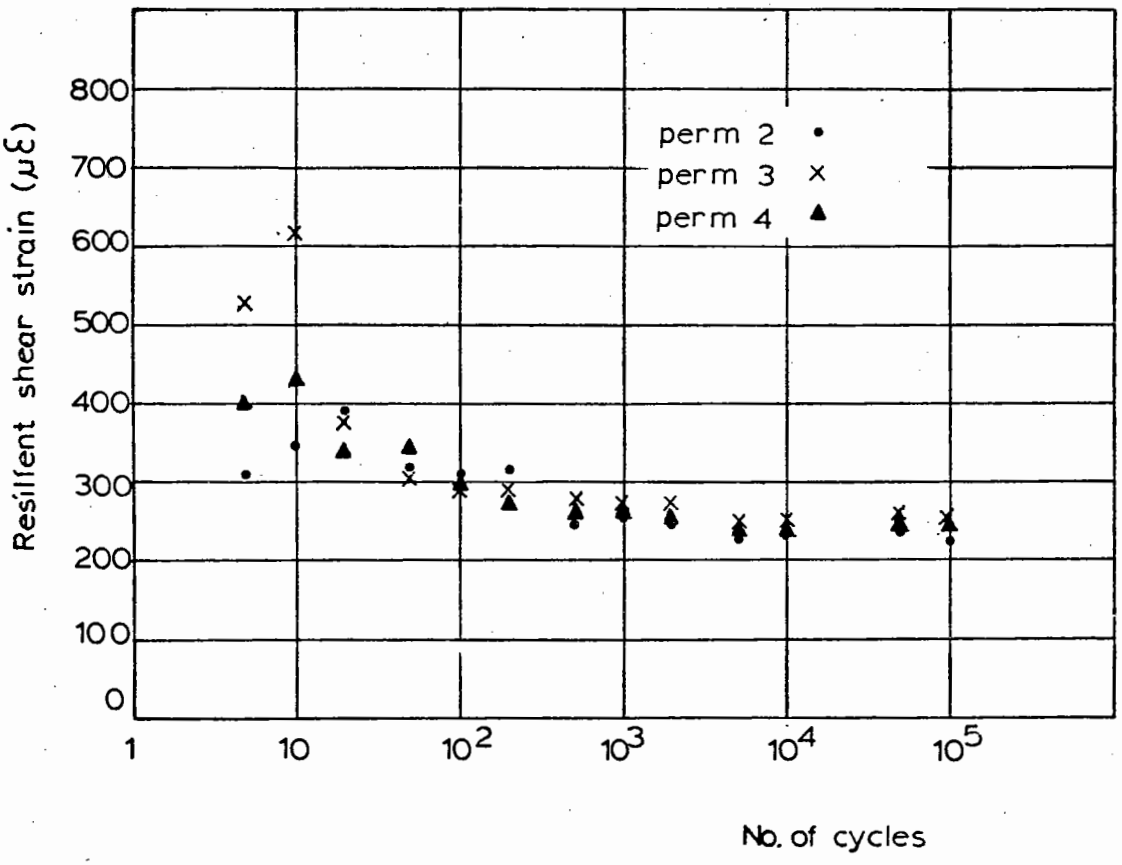

RESILIENT STRAIN RESPONSE DURING PERMANENT STRAIN TEST - PATH PA

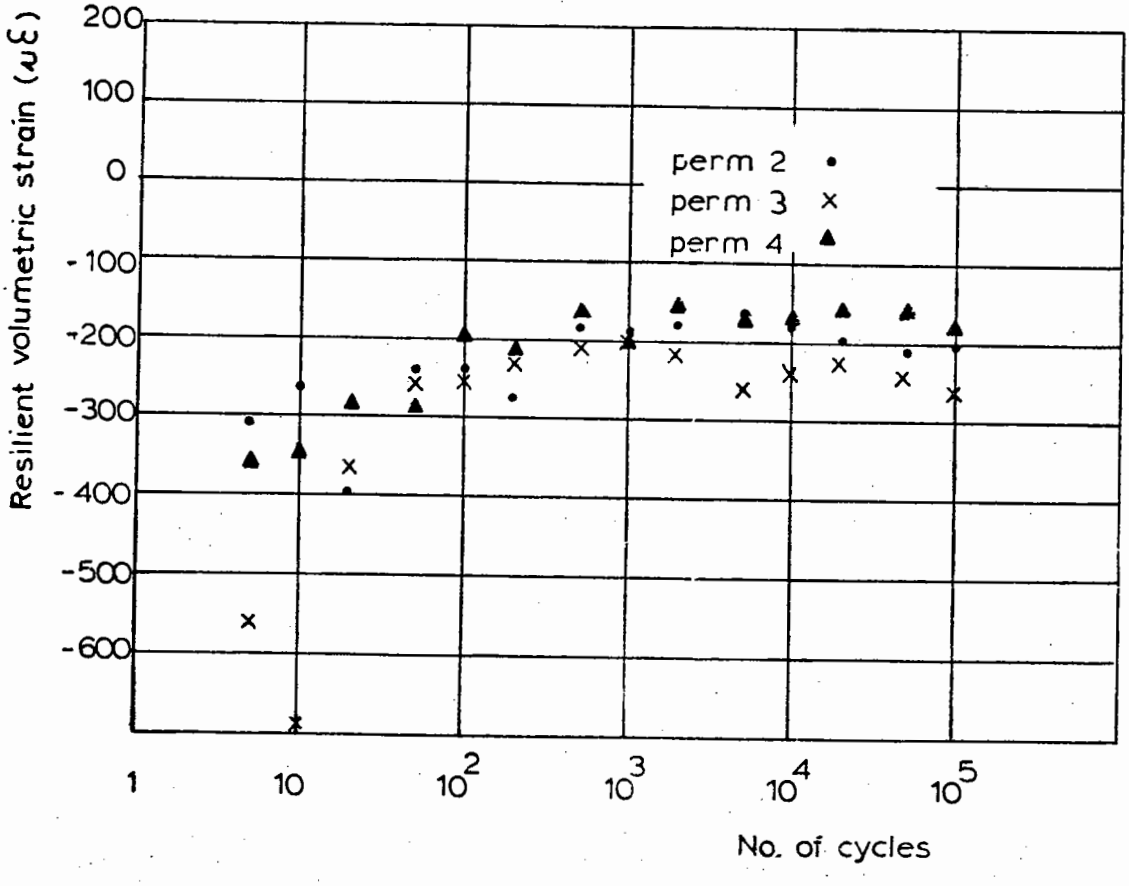

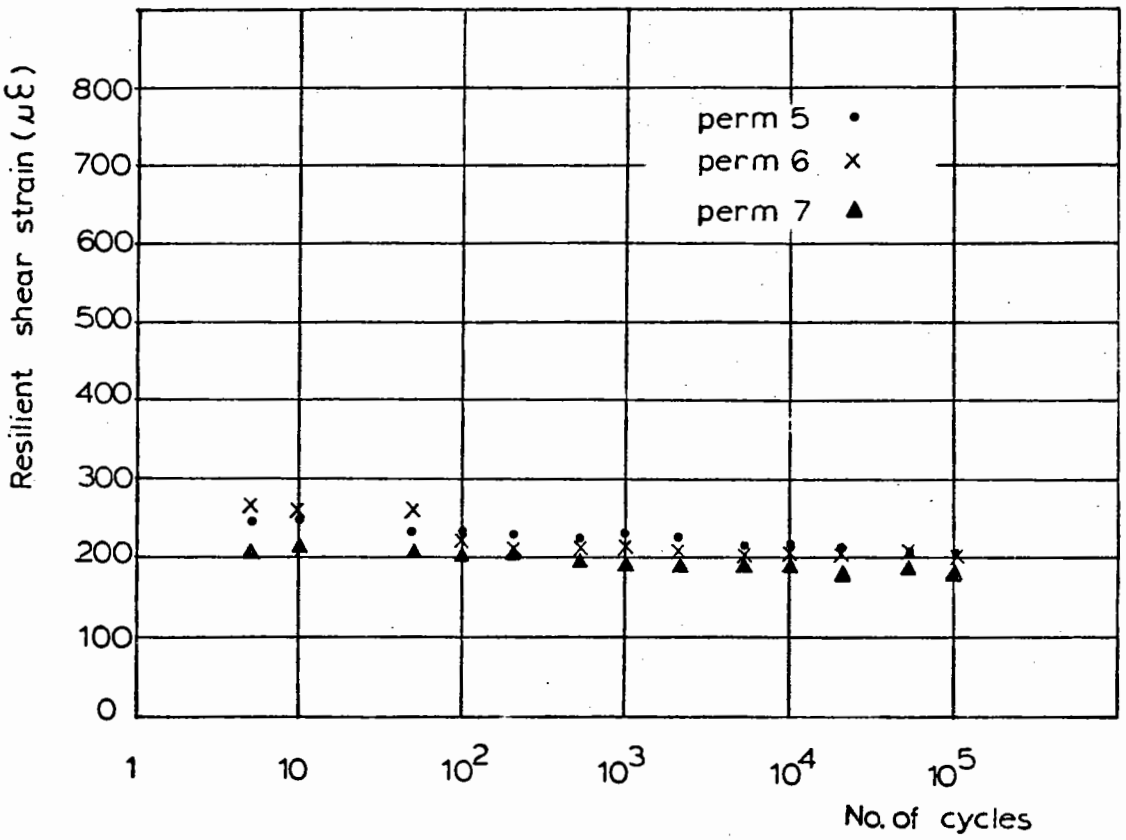

RESILIENT STRAIN RESPONSE DURING PERMANENT STRAIN TEST - PATH PA2

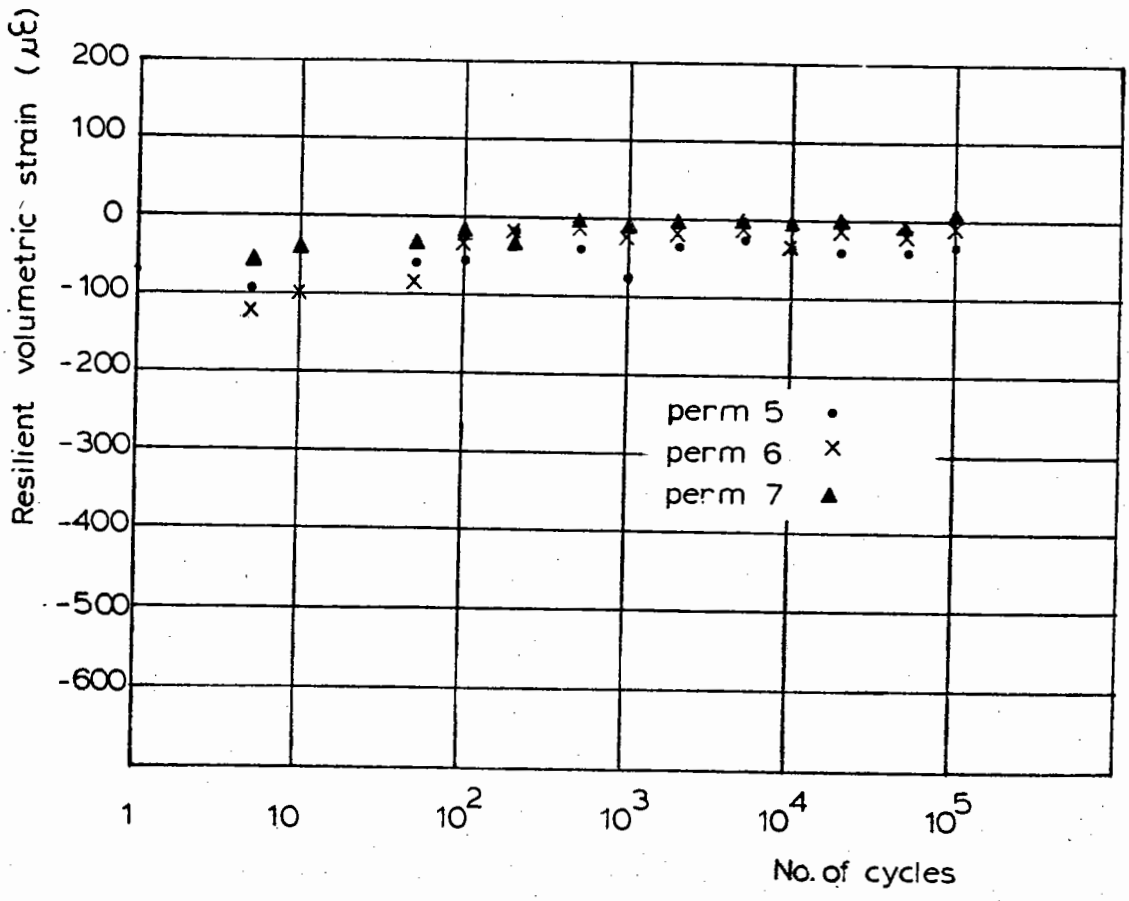

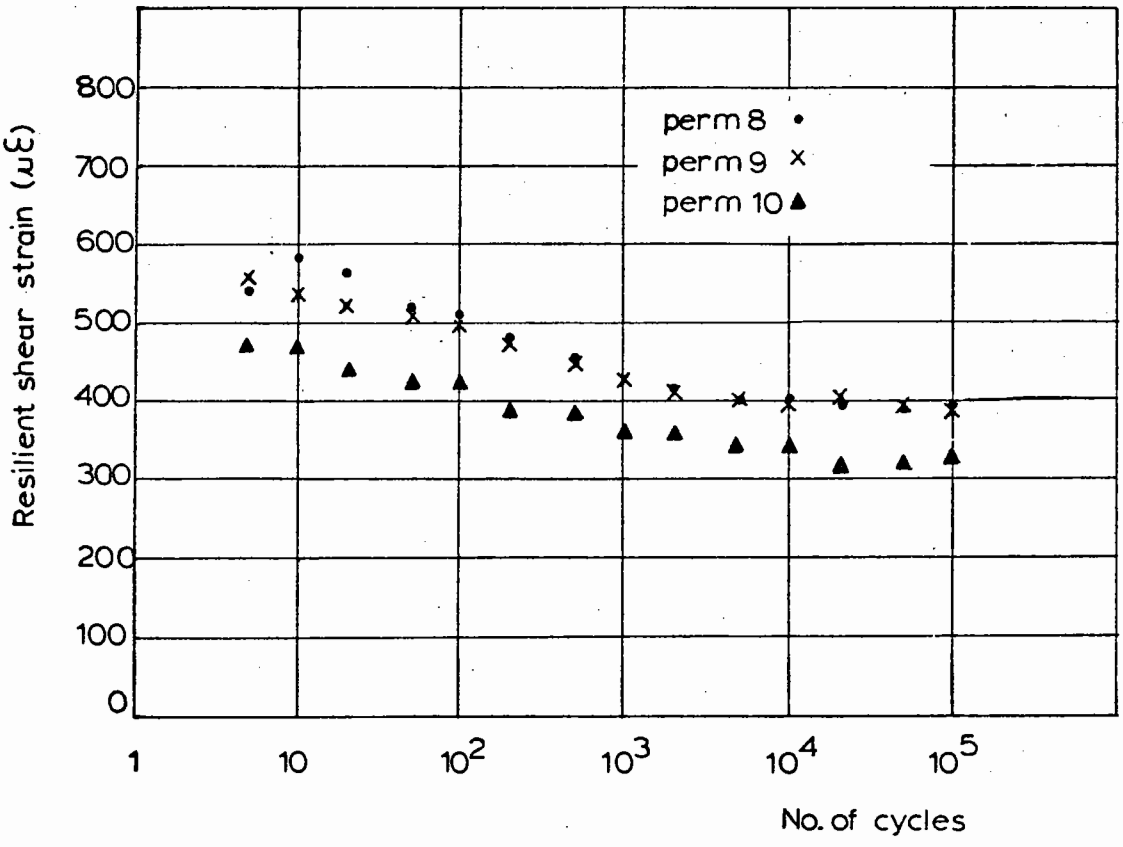

RESILIENT STRAIN RESPONSE DURING PERMANENT STRAIN TEST - PATH PB

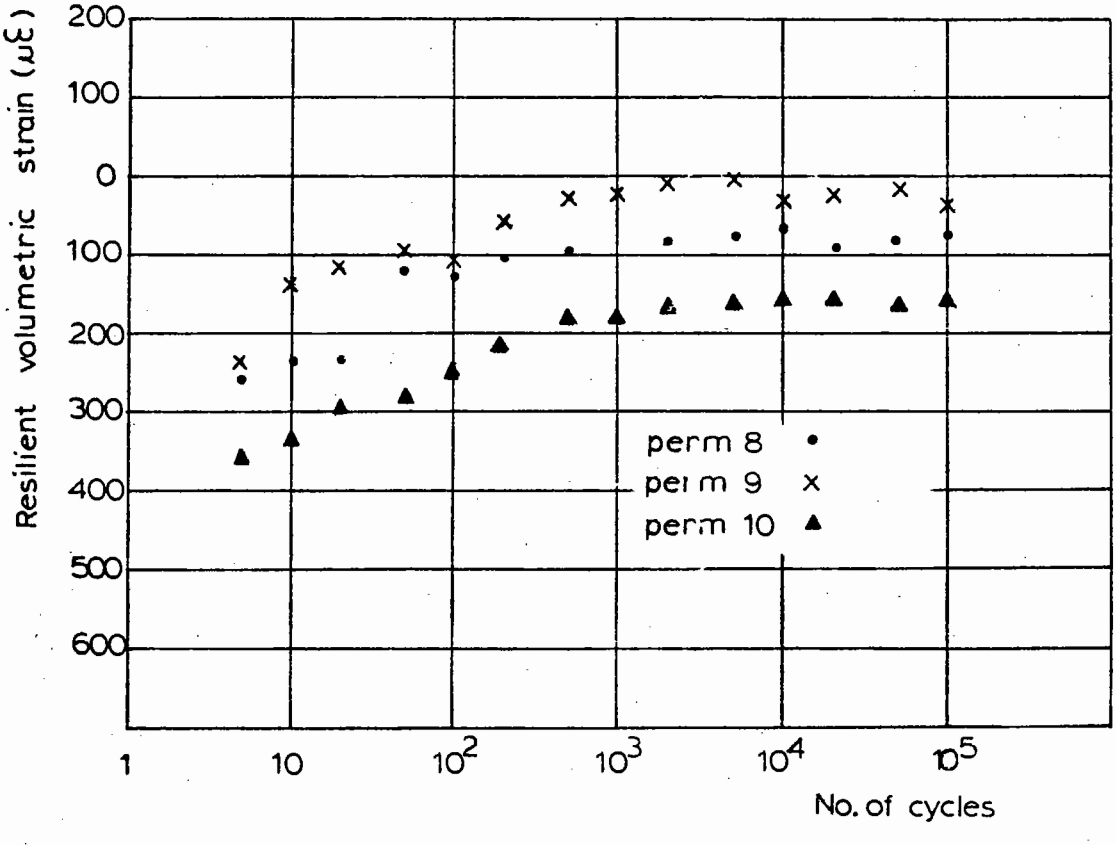

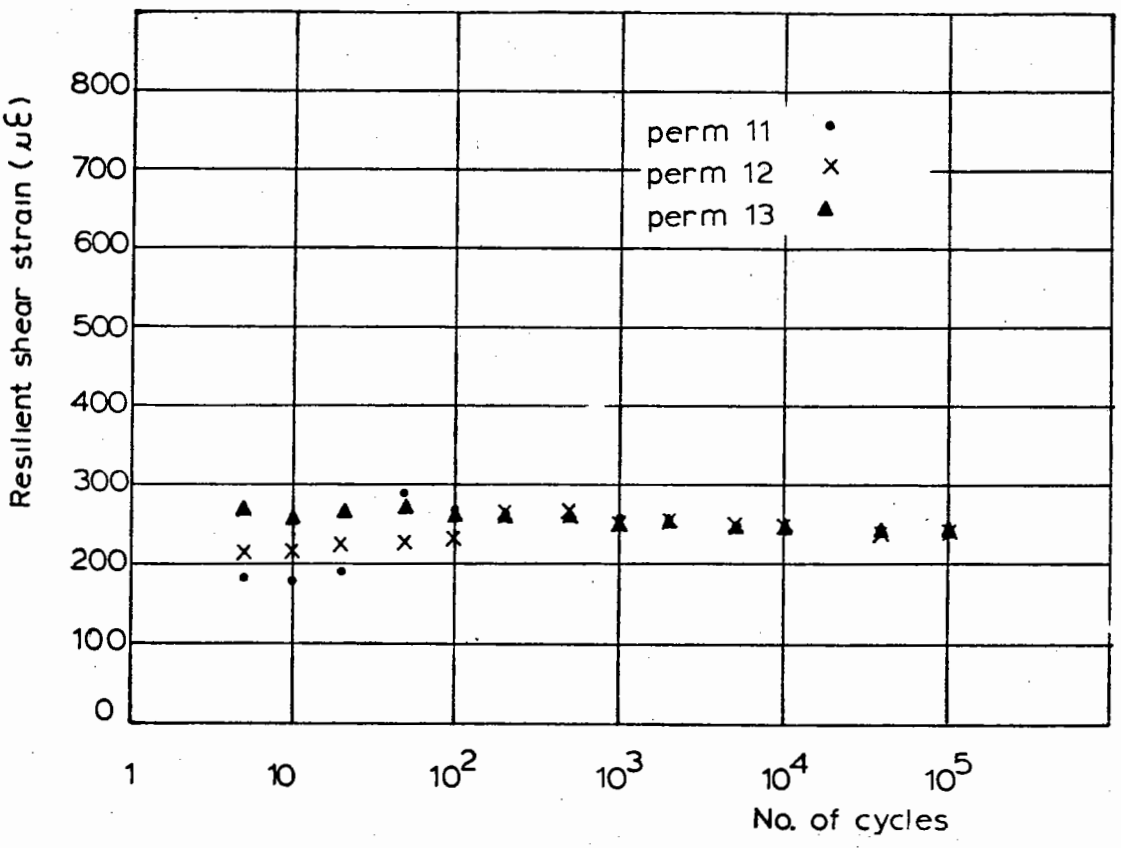

RESILIENT STRAIN RESPONSE DURING PERMANENT STRAIN TEST - PATH PC

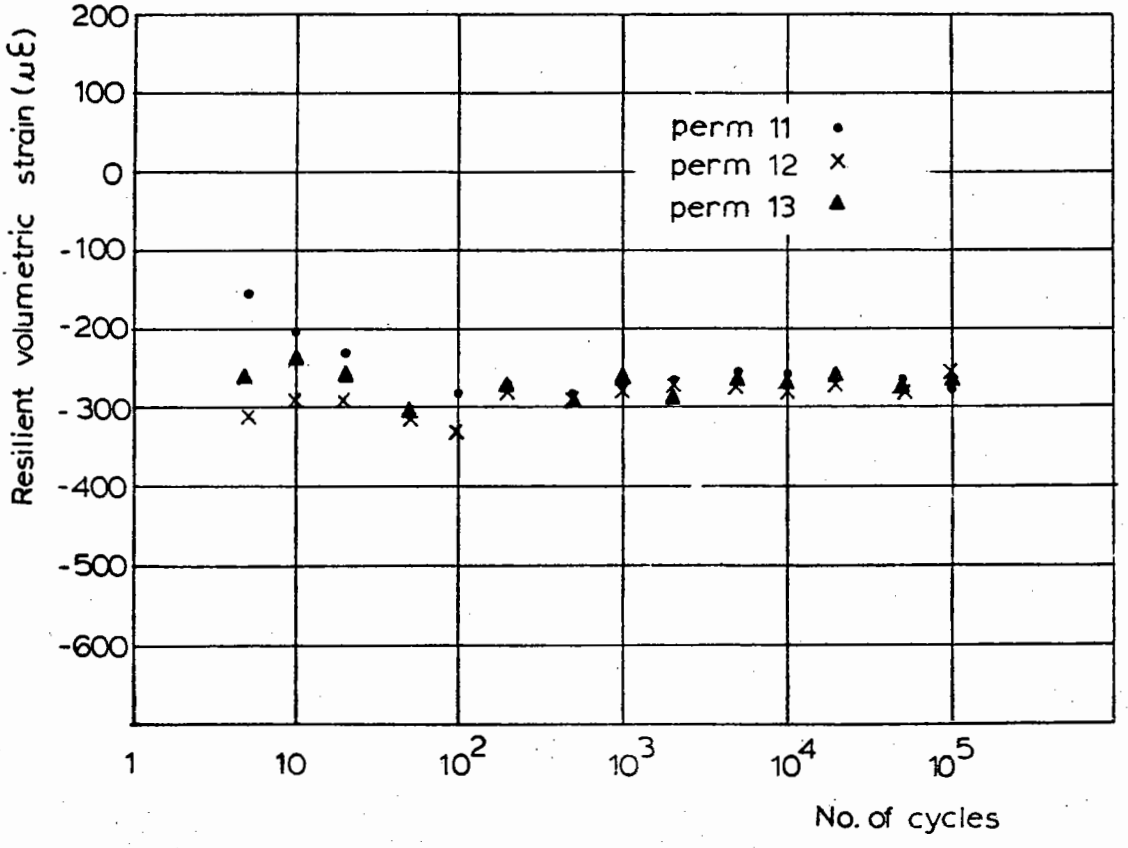

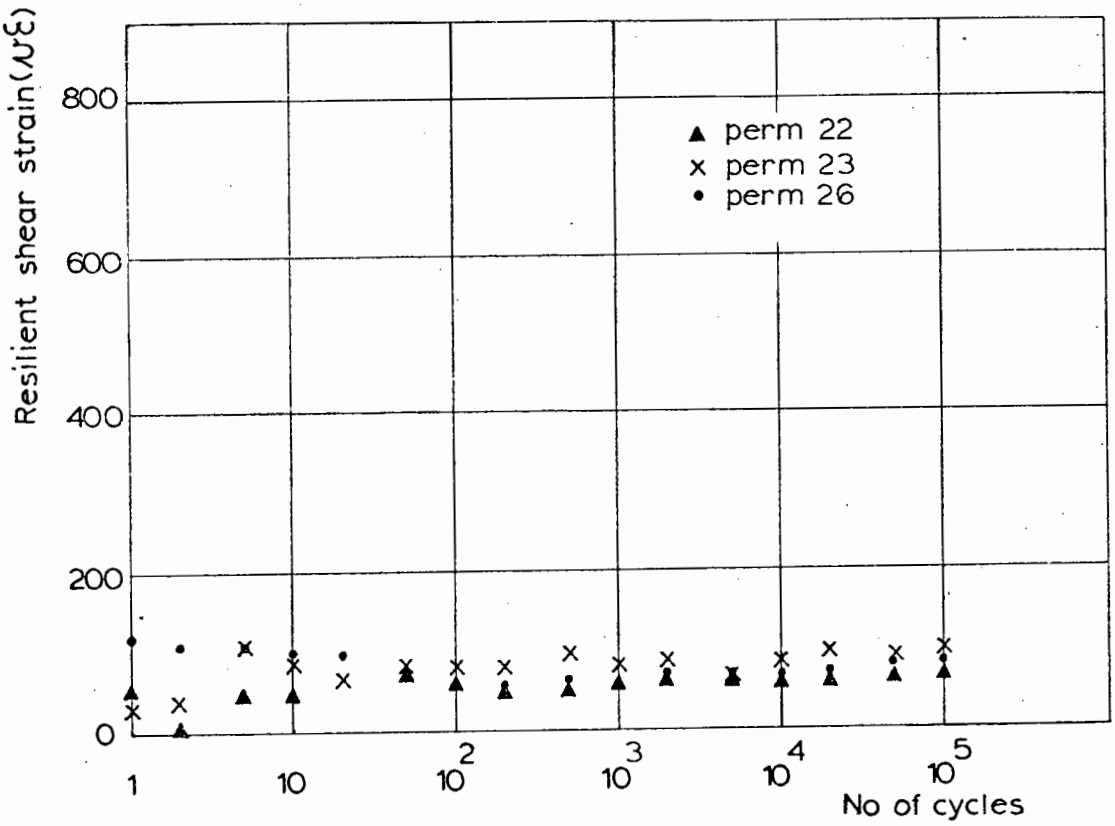

RESILIENT STRAIN RESPONSE DURING PERMANENT STRAIN TEST - PATH PD

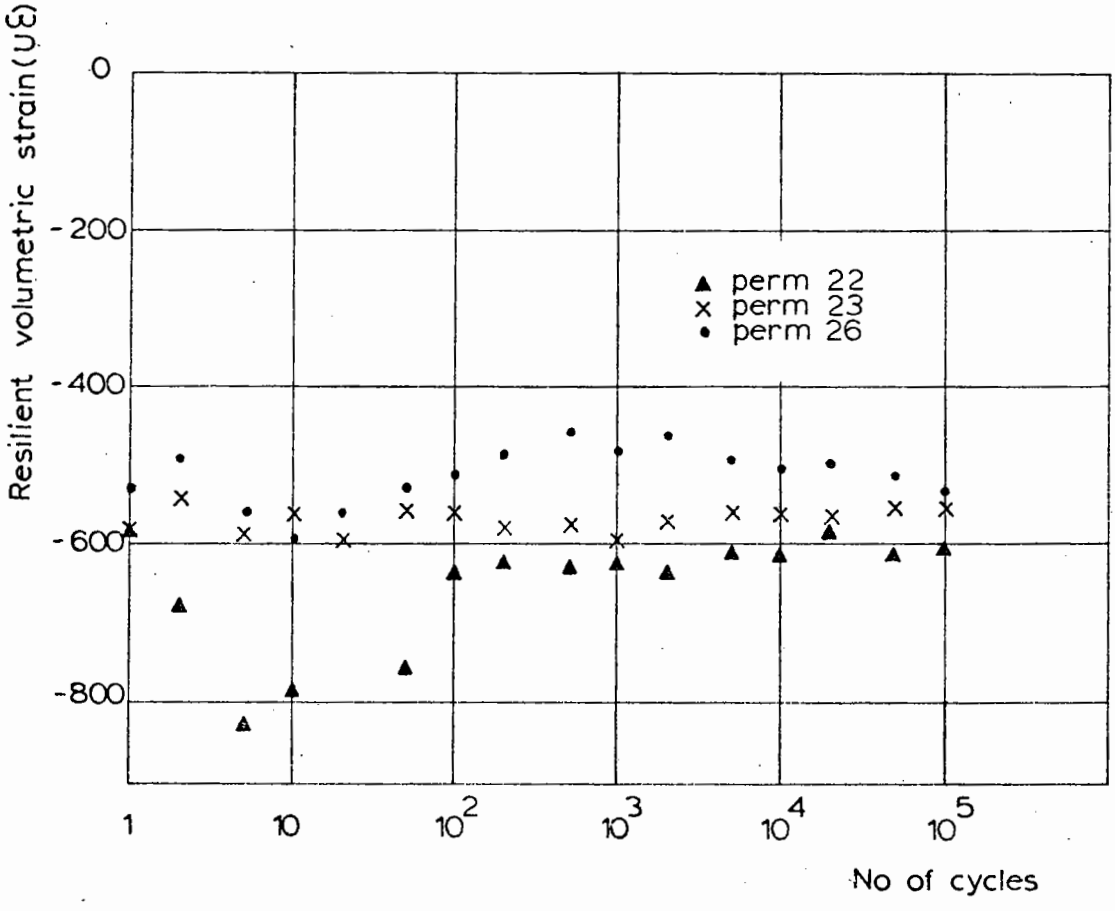

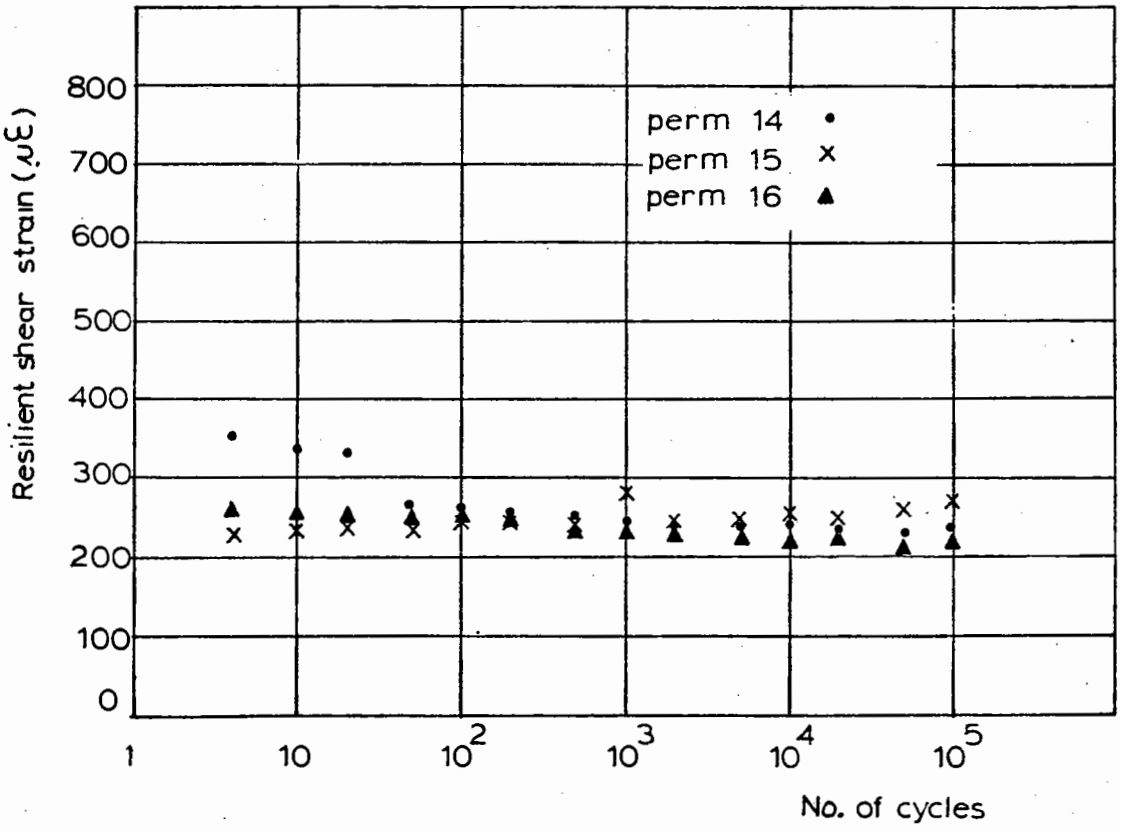

RESILIENT STRAIN RESPONSE DURING PERMANENT STRAIN TEST - PATH QA

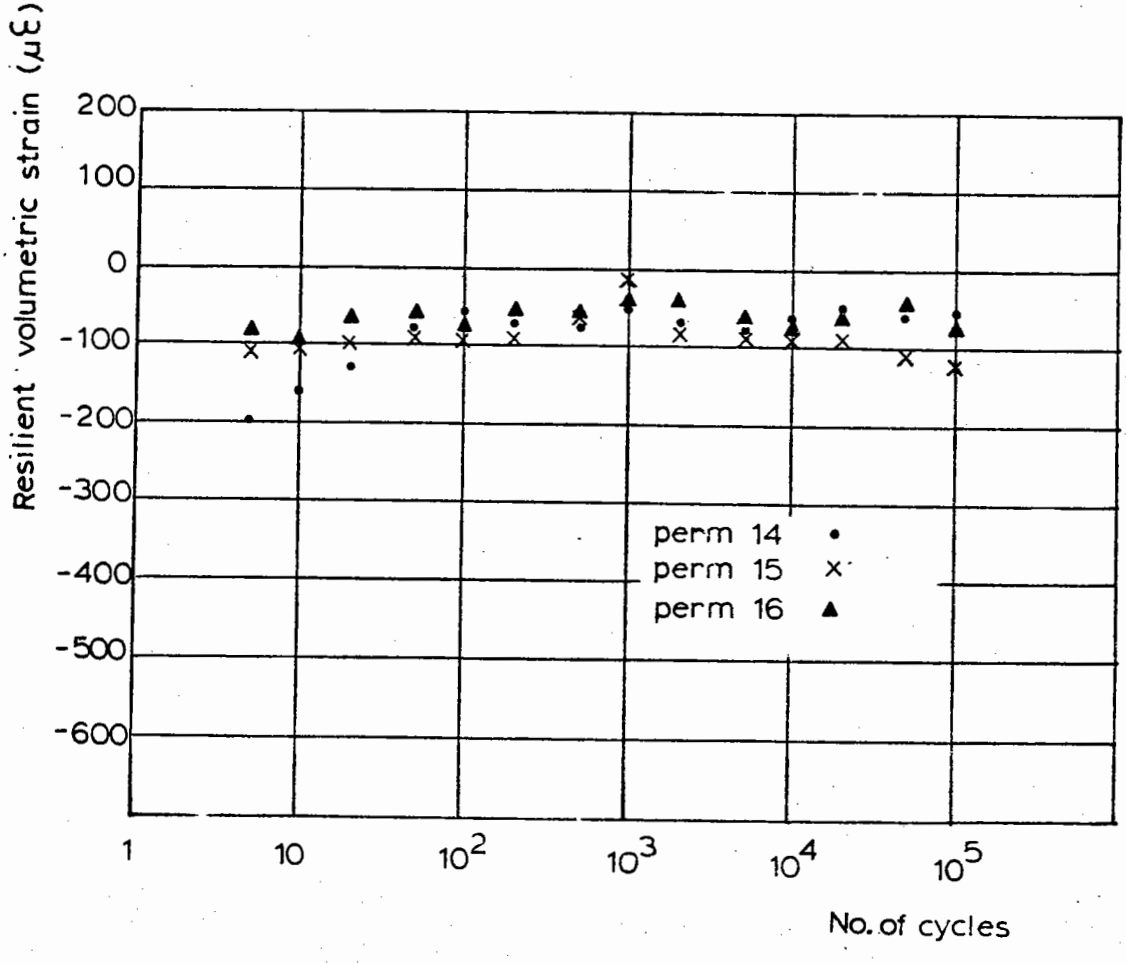

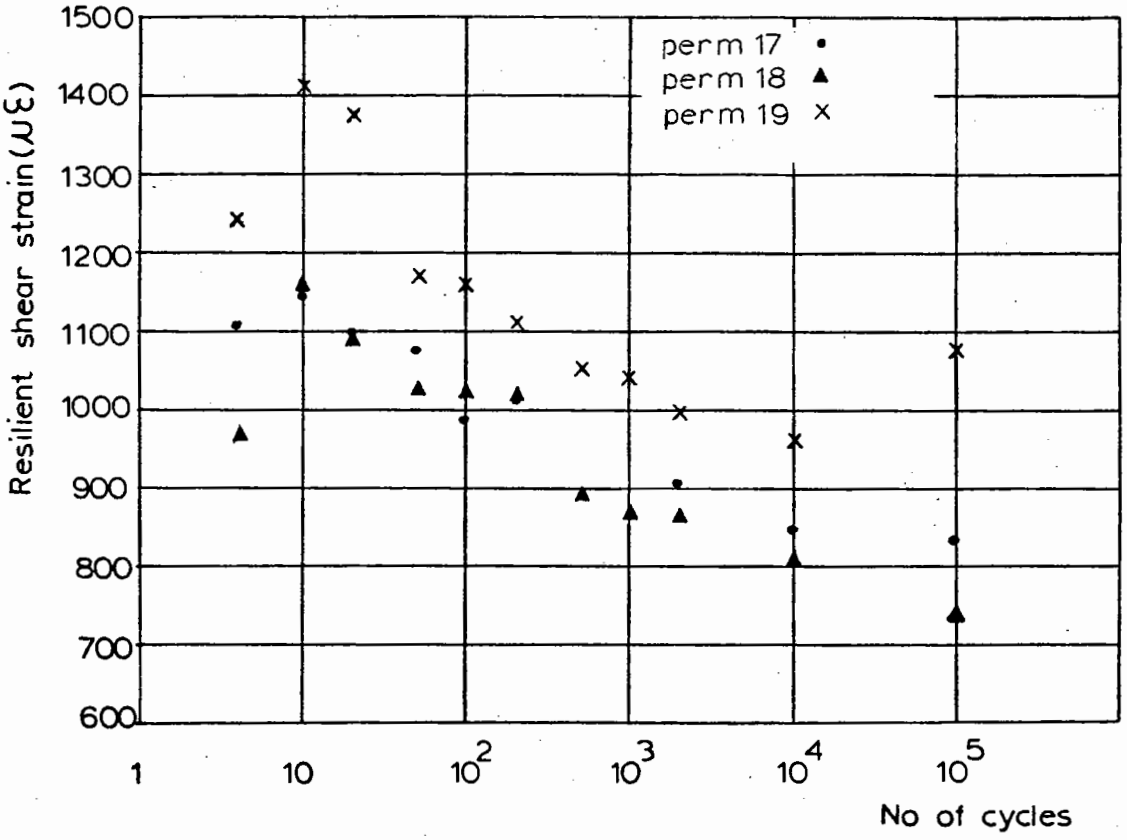

RESILIENT STRAIN RESPONSE DURING PERMANENT STRAIN TEST - PATH QB

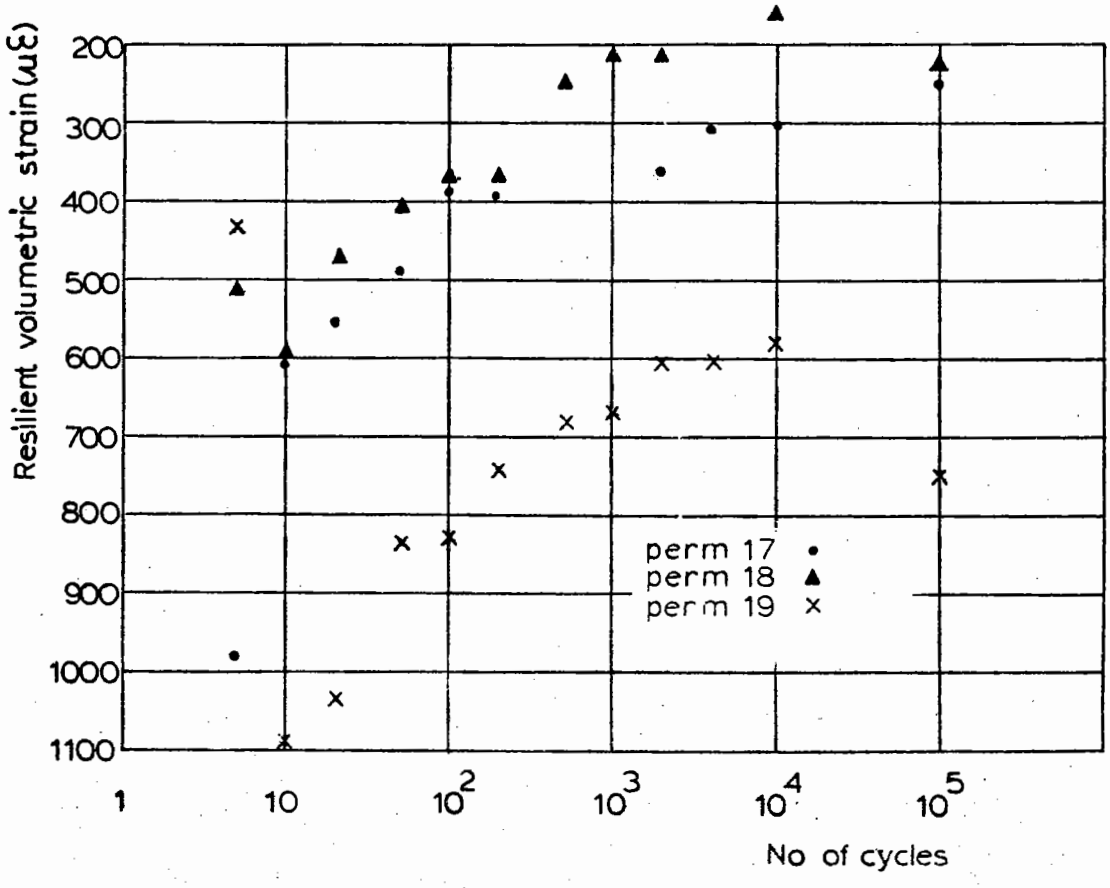

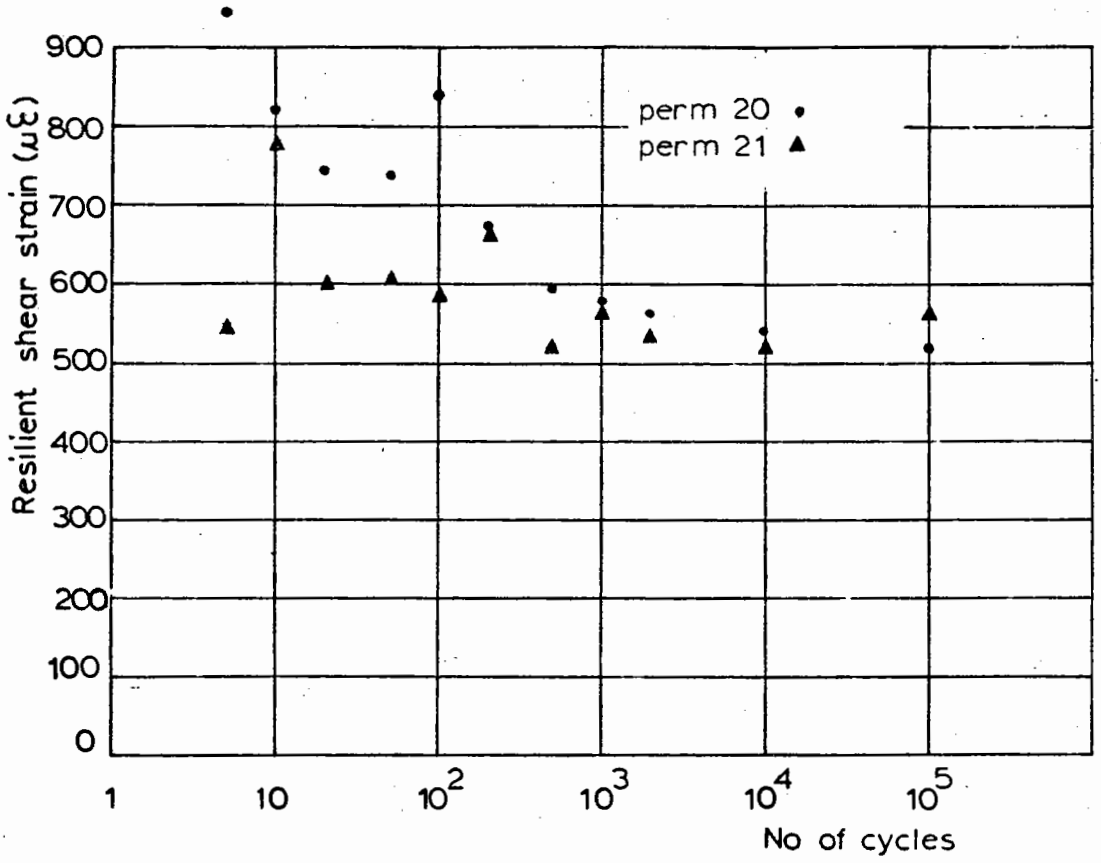

RESILIENT STRAIN RESPONSE DURING PERMANENT STRAIN TEST - PATH QC

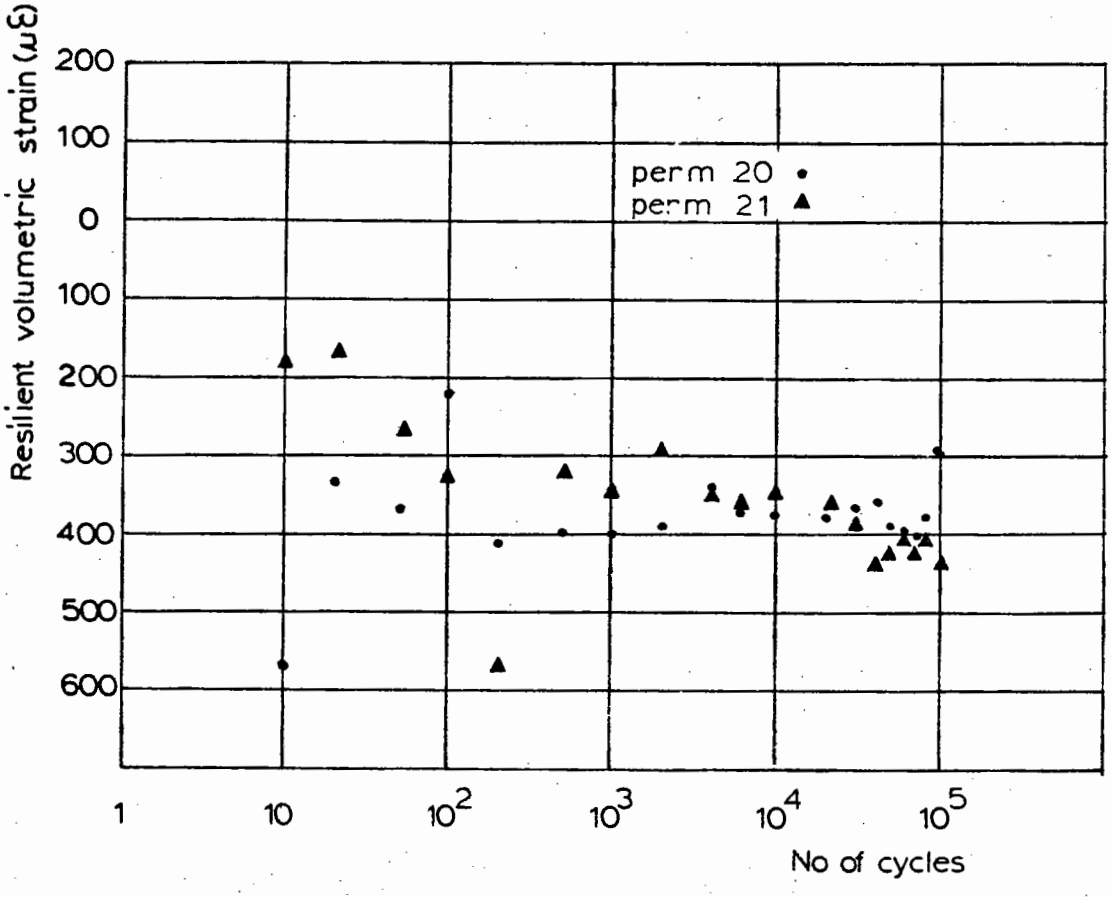

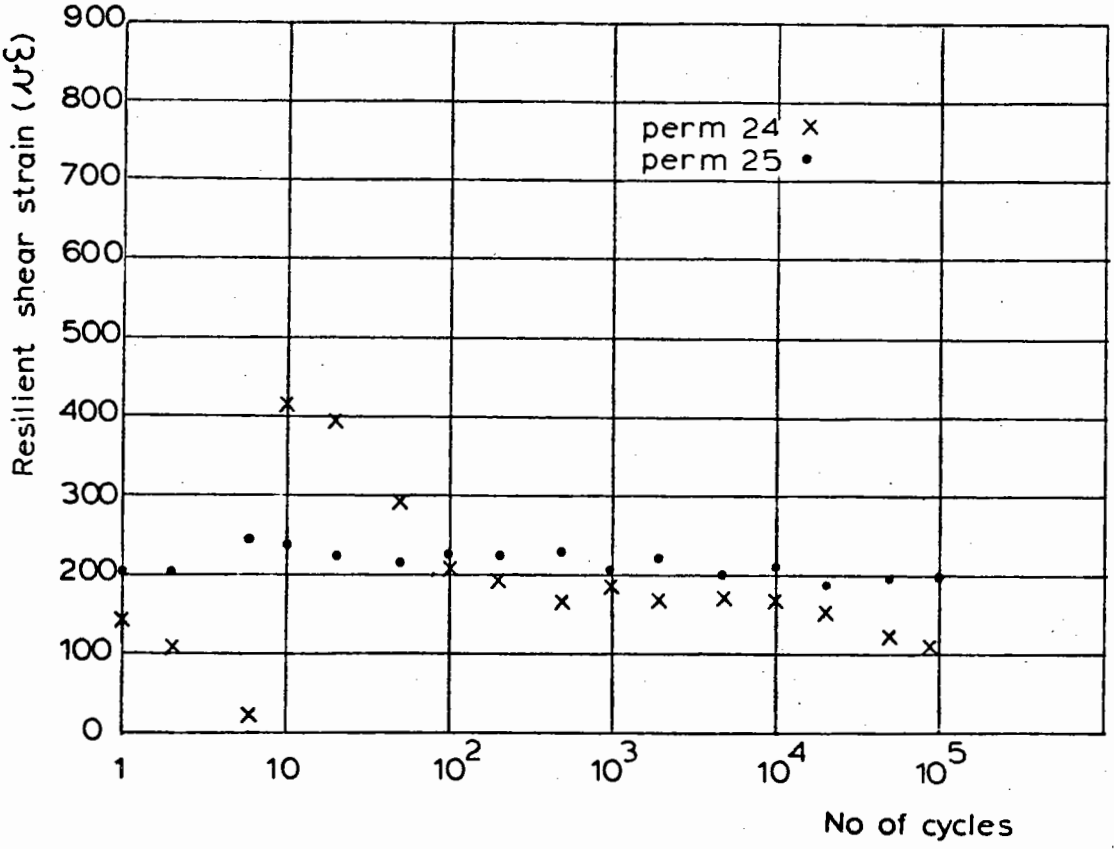

RESILIENT STRAIN RESPONSE DURING PERMANENT STRAIN TEST - PATH QD

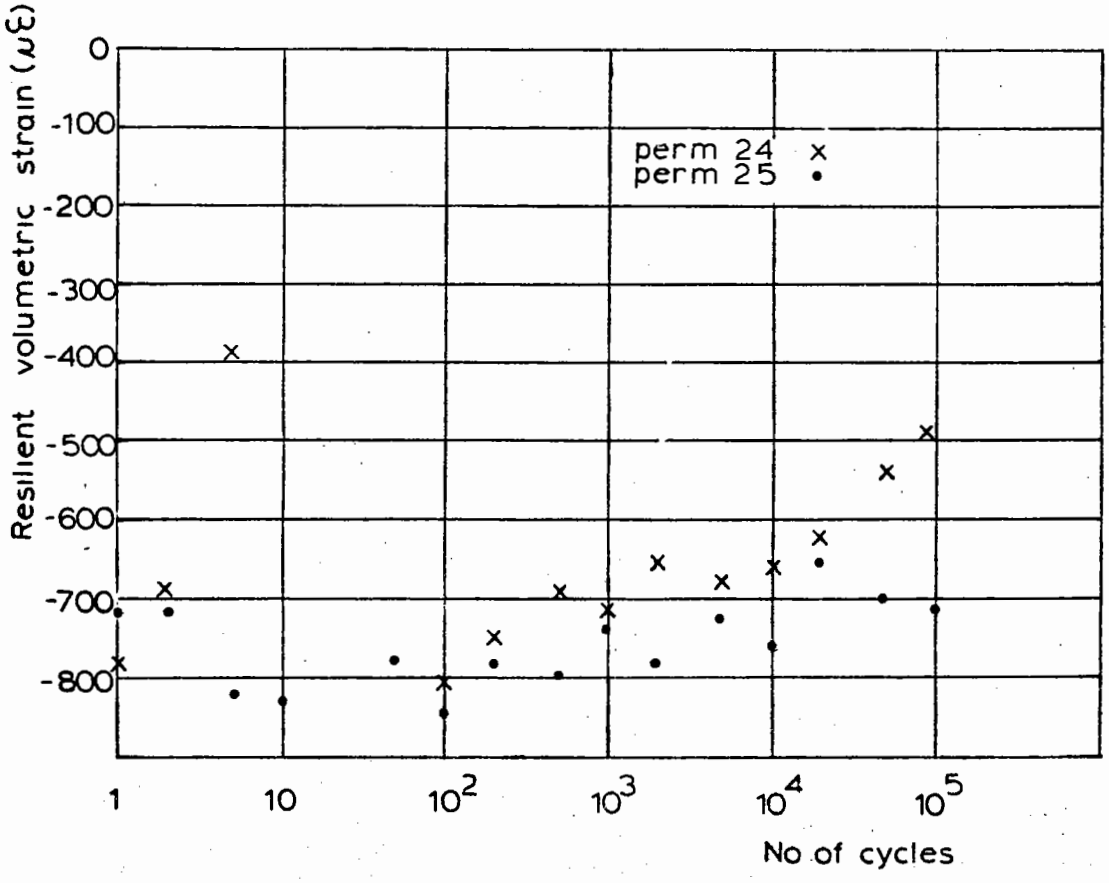

APPENDIX 4A

BIAXIAL RESILIENT STRAIN TEST RESULTS - 3 mm MATERIAL

No. of tests	Path	(kPa) p_m	q_m	p_r	q_r	Measured ($\mu\varepsilon$) v_r	ε_r
3	DE	178.28	140.18	71.89	84.34	244	100
3	CF	181.87	129.40	141.83	174.53	525	181
4	BG	186.08	116.79	214.45	256.69	955	329
4	AH	183.05	125.86	293.04	320.75	1981	683
4	UK	182.15	121.56	69.46	195.99	239	284
3	VP	189.26	107.24	139.37	391.36	1085	1244
4	IL	186.21	145.20	142.58	172.30	631	243
4	DO	186.37	144.81	69.49	195.94	174	262
3	NO	189.62	203.44	71.43	85.71	286	119
3	MP	187.64	206.41	143.26	170.24	893	370
3	JR	188.83	204.48	69.94	195.30	154	287
3	CT	195.66	194.48	140.03	390.40	357	692
4	QR	197.96	272.83	72.08	83.55	445	184
2	NS	174.79	270.97	73.38	190.94	241	286
3	YW	185.70	146.47	4.37	173.80	204	477
3	Z2W	193.54	197.53	5.51	347.10	753	1133
3	Z2Y	196.00	274.37	3.65	173.84	562	658
2	Z5Z6	193.71	197.06	37.51	94.38	267	229
3	CF(2)	107.93	51.22	72.80	81.59	397	138
4	BG(2)	105.99	57.04	109.68	120.98	617	217
4	AH(2)	104.52	61.47	146.97	212.14	1182	405
3	UK(2)	104.75	60.77	35.92	96.51	176	210
3	VP(2)	108.28	50.16	72.83	191.61	643	722
3	IL(2)	102.25	81.00	72.39	82.83	361	126
4	DO(2)	104.13	76.29	35.05	97.57	152	181
4	MP(2)	103.58	108.25	72.87	81.42	464	171
3	CT(2)	104.26	107.22	71.92	192.64	355	433
2	NE(2)	109.65	63.25	35.96	145.56	320	282
2	NS(2)	116.87	132.22	38.21	93.62	122	167
3	QK(2)	109.40	98.84	35.48	97.09	384	334

APPENDIX 4B

BIAXIAL PERMANENT STRAIN TESTS - 3 mm MATERIAL

BIAXIAL PERMANENT STRAIN TESTS

MEASURED AND APPLIED STRESSES (cycle 10)

	REPEATED (kPa)			MEAN (kPa)		
TEST	σ_x	σ_y	σ_z	σ_x	σ_y	σ_z
BP1A	200	200	38	225	225	176
BP2A	400	400	117	225	225	135
BP2B	400	400	92	225	225	279
BP2C	400	400	97	225	225	141
BP3A	200	0	30	225	225	137
BP3B	200	0	28	225	225	308
BP3C	200	0	27	225	225	148
BP4A	400	0	66	225	225	161
BP4B	400	0	61	225	225	320
BP4C	400	0	61	225	225	153
BP5A	200	0	28	325	125	293
BP5B	200	0	28	325	125	324
BP5C	200	0	29	325	125	161
BP6A	200	0	34	125	125	108
BP6B	200	0	33	125	125	111
BP6C	200	0	30	125	125	95
BP7A	400	0	61	225	125	140
BP7B	400	0	69	225	125	128
BP7C	400	0	67	225	125	145
BP8A	200	200	39	325	125	156
BP8B	200	200	39	325	125	164
BP8C	200	200	36	325	125	157
BP9A	400	400	31	225	225	368
BP9B	400	400	27	225	225	387
BP10A	400	0	55	225	325	195
BP10B	400	0	49	225	325	194

BIAXIAL PERMANENT STRAIN TESTS

TEST	PERMANENT VOLUMETRIC STRAIN %					
	cycle 1	10	10^2	10^3	$2x10^3$	$5x10^3$
BP1A	2.166	2.351	2.545	2.790	2.778	-
BP2A	2.655	3.627	4.588	5.378	5.417	5.722
BP2B	2.338	2.927	3.756	4.475	4.919	5.137
BP2C	1.741	2.266	2.804	3.295	3.477	3.548
BP3A	2.007	2.239	2.547	2.903	2.898	2.889
BP3B	4.038	4.286	4.611	4.827	4.941	5.021
BP3C	1.349	1.489	1.626	1.751	1.759	1.878
BP4A	2.466	3.638	4.785	5.692	5.871	6.011
BP4B	4.414	5.347	6.077	6.757	6.876	7.033
BP4C	1.554	2.266	2.821	3.321	3.403	3.493
BP5A	1.741	1.824	1.942	2.108	2.301	2.312
BP5B	2.000	2.136	2.198	2.179	2.319	2.342
BP5C	1.662	1.802	1.953	2.176	2.192	2.197
BP6A	1.830	2.195	2.485	2.787	2.818	2.925
BP6B	2.302	2.746	3.203	3.638	3.740	3.793
BP6C	1.058	1.317	1.587	1.842	1.905	2.043
BP7A	4.215	6.035	6.684	7.229	7.767	8.550
BP7B	3.250	3.659	4.148	4.633	4.705	4.775
BP7C	2.106	2.653	3.209	3.757	3.915	3.970
BP8A	1.518	1.578	1.647	1.859	2.001	-
BP8B	1.612	1.798	2.035	2.246	2.304	2.380
BP8C	2.030	2.244	2.499	2.766	2.823	-
BP9A	0.561	3.162	4.218	4.704	4.793	-
BP9B	0.723	2.780	3.883	-	-	-
BP10A	2.322	2.888	3.419	3.806	3.894	4.012
BP10B	4.555	4.911	4.850	4.855	4.853	4.823

BIAXIAL PERMANENT STRAIN TESTS

TEST	PERMANENT SHEAR STRAIN %					
	cycle 1	10	10^2	10^3	$2x10^3$	$5x10^3$
BP1A	0.734	0.800	0.867	0.957	0.986	
BP2A	0.903	1.213	1.529	1.793	1.809	1.907
BP2B	1.113	1.324	1.669	2.138	2.223	2.329
BP2C	0.673	0.864	1.039	1.223	1.287	1.322
BP3A	0.714	0.771	0.854	0.967	0.966	0.964
BP3B	2.251	2.342	2.426	2.505	2.545	2.575
BP3C	0.562	0.603	0.637	0.649	0.649	0.654
BP4A	1.527	1.504	1.709	1.933	1.991	2.026
BP4B	2.942	3.277	3.496	3.685	3.732	3.777
BP4C	1.400	1.396	1.391	1.403	1.411	1.421
BP5A	0.656	0.715	0.775	0.849	0.857	0.870
BP5B	0.669	0.712	0.735	0.744	0.783	0.793
BP5C	0.913	1.014	1.128	1.254	1.299	1.298
BP6A	0.933	1.015	1.068	1.129	1.136	1.157
BP6B	1.139	1.310	1.505	1.674	1.713	1.748
BP6C	0.474	0.518	0.574	0.629	0.649	0.695
BP7A	2.427	3.191	3.264	3.352	3.656	4.026
BP7B	1.168	1.284	1.454	1.614	1.634	1.659
BP7C	0.758	0.888	1.078	1.299	1.361	1.381
BP8A	1.242	1.423	1.623	1.783	1.923	
BP8B	1.237	1.363	1.410	1.627	1.649	1.676
BP8C	1.109	1.229	1.373	1.506	1.530	
BP9A	0.288	1.097	1.426	1.586	1.614	
BP9B	0.460	0.979	1.333			
BP10A	2.988	3.015	3.077	3.083	3.106	3.132
BP10B	2.000	2.139	2.294	2.491	2.532	2.587

BIAXIAL PERMANENT STRAIN TESTS

VARIATION OF σ_z (MEASURED STRESS) WITH NO. OF CYCLES.

TEST	MEAN (kPa) cycle 1	10	10^2	10^3	5×10^3
BP1A	182	176	174	171	-
BP2A	148	135	124	107	105
BP2B	287	278	272	261	265
BP2C	153	141	130	109	103
BP3A	138	137	137	124	129
BP3B	284	308	307	292	294
BP3C	144	148	147	142	141
BP4A	172	161	150	137	140
BP4B	319	320	312	369	302
BP4C	156	153	148	138	142
BP5A	290	293	290	281	280
BP5B	329	324	331	319	322
BP5C	156	161	162	159	163
BP6A	108	108	107	97	130
BP6B	126	111	109	97	100
BP6C	97	95	97	89	95
BP7A	142	139	129	123	124
BP7B	136	128	120	111	107
BP7C	154	145	138	127	129
BP8A	155	156	162	153	154
BP8B	162	164	162	159	163
BP8C	164	156	155	152	149
BP9A	371	367	363	349	356
BP9B	399	387	389	382	388
BP10A	197	195	194	180	185
BP10B	198	194	189	188	186

BIAXIAL PERMANENT STRAIN TESTS

VARIATION OF σ_z (MEASURED STRESS) WITH NO. OF CYCLES.

TEST	REPEATED (kPa) cycle 1	10	10^2	10^3	$5x10^3$
BP1A	50	38	37	32	-
BP2A	163	117	89	75	67
BP2B	115	92	71	61	59
BP2C	133	97	78	62	60
BP3A	37	29	27	30	21
BP3B	34	28	24	22	26
BP3C	32	27	25	24	24
BP4A	92	66	48	47	46
BP4B	84	61	49	32	44
BP4C	89	61	52	48	44
BP5A	39	28	27	27	28
BP5B	29	27	23	18	27
BP5C	34	29	28	28	24
BP6A	47	34	31	27	27
BP6B	31	33	27	25	26
BP6C	41	30	28	30	28
BP7A	103	60	56	50	-
BP7B	100	69	60	52	50
BP7C	100	67	58	52	47
BP8A	47	39	33	27	-
BP8B	54	39	32	33	34
BP8C	50	36	35	29	-
BP9A	38	31	33	33	28
BP9B	23	27	35	35	32
BP10A	67	55	46	47	43
BP10B	71	48	48	47	42

K-THETA MODELS : $M_R = K_1 \theta^{K_2}$

M_R = resilient modulus = q_r/ε_{ax} kPa $\theta = \sigma_1 + \sigma_2 + \sigma_3$ K_2 obtained from graph of log M_R against log θ.

Single Size Material : $M_R = 19454\ \theta^{0.5}$ kPa

PATH	p_m(kPa)	q_m(kPa)	p_r(kPa)	q_r(kPa)	θ (kPa)	ε_{ax} ($\mu\varepsilon$)	$M_R \times 10^6$(kPa)	K_1	K_2
1	48.14	24.21	14.01	48.34	165.44	166	0.291	22624	0.5
2	48.26	47.86	29.06	96.22	188.37	420	0.229	16685	0.5
3	96.37	48.43	29.43	96.84	333.26	249	0.388	21254	0.5
4	96.42	96.41	64.13	192.38	385.46	573	0.336	17114	0.5
5	192.58	96.87	64.40	193.15	674.34	334	0.578	22257	0.5
6	191.55	191.14	127.71	382.94	766.22	766	0.499	18027	0.5
7	385.05	195.77	118.58	385.58	1332.99	580	0.665	18214	0.5
Graded Material : $M_R = 8634\ \theta^{0.69}$									
1	98.25	54.04	34.59	94.81	346.64	188	0.504	8910	0.69
2	96.96	99.87	64.92	193.63	388.26	411	0.471	7701	0.69
3	50.15	30.24	18.26	46.79	177.83	135	0.347	9724	0.69
4	50.39	54.23	33.13	96.46	200.89	310	0.311	8012	0.69
5	192.96	199.52	128.69	385.92	771.92	471	0.819	8334	0.69
6	195.44	104.76	66.94	186.84	686.73	226	0.827	9123	0.69

APPENDIX 5B

TANGENT AND SECANT K-THETA PREDICTIONS - 3 mm MATERIAL

p_m (kPa)	q_m (kPa)	p_r (kPa)	q_r (kPa)	Secant		Tangent	
				v_r (με)	ε_r (με)	v_r (με)	ε_r (με)
48.09	0.01	16.65	2.06	38.62	7.84	71.05	7.16
48.12	0.00	32.28	0.00	75.68	-0.00	129.07	-0.00
48.13	-0.07	6.96	24.19	16.09	91.26	31.05	87.94
47.66	-0.18	-0.37	24.06	-0.86	91.02	-1.72	91.20
47.96	-0.10	16.36	24.08	38.00	91.89	69.98	83.93
48.09	0.05	24.17	23.92	56.31	92.27	99.87	80.53
47.94	-0.16	48.76	24.13	117.00	102.34	183.78	74.10
48.02	0.10	-23.86	24.18	-55.62	93.44	-127.30	105.12
48.15	0.12	-48.13	24.06	-115.08	101.26	-314.34	128.04
48.50	0.17	13.33	48.10	30.75	181.59	57.52	169.13
47.82	-0.21	0.33	48.38	0.76	182.72	1.53	182.40
48.26	0.18	32.30	48.03	75.61	188.59	129.00	156.30
48.15	0.16	24.24	72.72	56.44	280.36	100.08	244.63
48.21	0.23	0.03	72.34	0.07	272.10	0.14	272.05
48.20	24.14	16.21	0.01	37.55	-15.51	69.24	0.03
48.18	24.10	31.86	-0.01	74.62	-32.26	127.54	-0.03
47.83	24.29	7.01	24.32	16.25	85.28	31.36	88.65
47.97	24.12	-0.62	24.16	-1.43	91.69	-2.88	91.40
47.98	24.25	16.59	24.42	38.53	77.02	70.88	85.02
48.22	24.30	24.24	24.34	56.40	69.89	100.02	81.83
48.12	24.22	48.45	23.99	115.94	45.88	182.58	73.66
48.38	24.65	-24.41	23.36	-56.70	114.23	-130.08	101.43
48.21	24.49	-48.33	23.17	-115.51	152.52	-315.91	123.40
48.14	24.21	14.01	48.34	32.45	169.98	60.47	170.01
48.12	24.10	0.08	48.57	0.18	182.78	0.37	182.78
48.08	24.12	32.29	48.64	75.74	158.78	129.14	158.51
48.15	24.20	48.26	48.62	115.41	149.60	181.94	149.35
48.04	24.24	21.74	72.38	50.60	256.81	90.79	246.28
48.25	24.23	-0.09	72.38	-0.21	272.22	-0.42	272.26
48.04	24.09	47.90	71.95	114.63	248.12	180.95	221.47
48.01	24.10	32.09	96.26	75.31	346.70	128.51	314.11
48.23	48.47	15.87	-0.96	36.75	-34.15	67.87	-3.35
47.96	48.08	32.23	0.02	75.69	-65.57	129.05	0.07
48.04	48.16	7.15	23.92	16.54	76.77	31.90	86.95
47.86	48.19	-0.62	23.97	-1.44	91.67	-2.88	90.78
47.97	48.21	16.65	23.92	38.67	59.08	71.13	83.26
48.19	48.42	23.97	24.12	55.78	45.80	99.04	81.20
48.41	48.31	48.57	23.03	115.85	-12.39	182.59	70.54
48.11	48.19	40.10	24.18	94.83	12.71	155.68	76.49
48.09	48.21	15.31	48.07	35.49	153.42	65.72	168.15
47.93	48.17	0.16	48.33	0.37	182.01	0.74	182.16
48.29	48.34	31.78	47.99	74.33	124.11	127.15	156.45
48.02	48.02	47.73	47.35	114.22	91.48	180.44	145.85
47.88	48.07	21.69	72.06	50.56	234.94	90.72	245.58
48.19	48.25	48.33	72.27	115.54	194.53	182.11	221.89
48.05	48.10	72.06	72.02	182.78	148.49	251.88	205.13
48.26	47.86	29.06	96.22	67.83	317.43	117.55	317.13
48.00	47.93	63.83	95.67	157.98	279.15	228.86	279.50
48.25	72.31	7.67	23.78	17.71	67.93	34.06	86.05
48.04	72.20	16.19	23.66	37.57	43.45	69.26	82.47
48.20	-23.98	16.23	0.00	37.60	15.46	69.32	-0.00
47.85	-24.08	31.96	0.01	75.13	32.72	128.22	0.03
48.25	-24.06	6.40	24.32	14.77	97.61	28.60	88.55
48.02	-24.03	0.12	24.55	0.28	92.64	0.55	92.47
48.10	-24.08	16.56	24.19	38.41	108.03	70.69	84.14
48.07	-24.11	24.27	23.99	56.56	116.52	100.26	80.75

48.00	-23.94	-23.97	24.44	-55.89	70.93	-128.02	106.36
48.06	-23.77	-48.37	24.65	-115.82	49.73	-317.29	131.75
48.05	-23.98	0.01	47.90	0.02	180.48	0.05	180.46
47.85	-24.14	-47.85	48.06	-114.77	147.90	-313.55	256.61
48.02	-48.21	-24.17	24.10	-56.35	45.46	-129.23	105.00
95.85	-0.11	32.10	0.02	52.73	0.10	97.26	0.05
95.92	-0.07	64.75	0.00	107.54	0.07	183.23	0.00
95.94	0.06	14.18	48.29	23.22	129.01	44.78	124.25
96.37	0.13	-1.18	47.84	-1.93	127.28	-3.86	127.66
96.19	0.07	33.38	47.87	54.75	128.91	100.70	117.67
96.69	0.83	-15.26	48.41	-24.89	129.05	-51.83	133.97
96.24	0.15	96.75	47.72	163.69	141.65	257.87	103.64
96.27	0.39	-48.07	47.87	-79.14	130.81	-181.28	147.10
96.54	0.29	-96.64	48.25	-163.20	143.54	-446.06	181.47
96.81	0.86	32.35	97.01	52.88	259.86	97.55	238.35
95.77	0.03	0.18	95.96	0.29	256.09	0.59	255.97
95.98	-0.23	64.33	96.14	106.79	268.28	182.14	221.80
95.99	0.04	48.02	144.02	79.18	393.32	140.50	343.36
96.34	0.41	0.82	144.57	1.34	384.67	2.67	383.85
96.14	48.38	32.14	0.00	52.72	-21.92	97.25	-0.00
95.64	47.74	64.16	0.00	106.70	-46.07	181.97	-0.00
95.58	48.05	14.90	48.49	24.44	119.79	47.05	124.76
95.71	48.42	0.09	48.86	0.15	130.37	0.29	130.40
79.40	31.57	31.88	48.94	57.63	126.61	104.65	130.90
96.43	48.42	48.31	48.15	79.48	97.63	141.01	114.52
96.72	48.86	97.02	48.53	163.71	65.96	258.04	105.17
96.08	48.10	-47.53	48.35	-78.32	164.89	-179.15	148.49
96.12	48.00	-95.70	48.33	-161.90	219.39	-441.50	181.67
96.37	48.43	29.43	96.84	48.19	239.96	89.50	239.96
96.04	48.19	0.41	96.68	0.67	257.37	1.34	257.37
96.38	48.48	64.43	97.06	106.72	223.58	182.11	223.53
96.56	48.41	96.68	96.46	163.25	208.99	257.43	209.28
96.04	48.00	47.86	143.62	78.89	358.90	140.05	342.45
96.30	48.56	-0.58	144.65	-0.95	385.35	-1.90	385.54
96.38	48.55	97.10	144.75	164.19	352.30	258.52	314.02
96.50	48.97	64.39	193.18	106.58	490.19	181.92	444.73
96.06	96.15	32.20	0.31	52.84	-42.88	97.45	0.76
96.41	97.14	64.04	-1.95	106.04	-97.72	181.12	-4.49
95.69	96.42	15.39	48.18	25.23	108.16	48.51	123.75
95.61	96.68	-0.95	48.12	-1.56	129.81	-3.12	128.85
96.29	96.67	32.70	47.71	53.60	83.89	98.75	117.40
96.06	96.39	48.35	48.59	79.70	65.37	141.33	115.73
96.41	96.31	96.58	48.35	163.22	-9.99	257.34	104.97
95.86	96.15	80.16	48.01	134.32	16.86	220.36	107.54
96.18	96.43	29.34	95.85	48.09	217.77	89.32	237.76
95.60	95.71	0.61	96.00	1.00	255.61	2.00	256.01
96.27	96.50	64.51	96.46	106.92	175.85	182.38	222.21
96.31	96.59	95.79	95.69	161.88	131.16	255.67	208.11
95.81	95.71	44.98	143.91	74.16	330.14	132.55	345.55
96.20	96.25	96.22	144.22	162.77	275.11	256.73	313.54
96.24	96.24	143.86	144.42	257.62	211.96	355.57	290.85
96.42	96.41	64.13	192.38	106.19	443.04	181.34	443.25
96.12	95.82	127.82	191.85	223.56	396.34	323.86	396.07
96.16	144.18	16.11	47.92	26.35	95.65	50.58	122.59
96.36	144.82	32.77	47.96	53.70	62.28	98.92	117.96
95.69	-47.86	31.98	0.00	52.58	21.73	96.99	-0.00
95.92	-48.04	64.14	0.07	106.50	46.31	181.72	0.16
96.01	-47.66	13.82	47.59	22.62	136.26	43.66	122.51
96.00	-47.46	-0.09	48.35	-0.15	128.82	-0.29	128.91
95.03	-52.67	29.66	36.89	48.91	122.11	90.70	91.92
96.58	-47.70	48.96	48.04	80.50	164.38	142.62	114.03
96.38	-47.88	-48.84	48.05	-80.39	97.42	-184.54	147.93
96.10	-47.92	-96.43	48.22	-163.25	66.73	-446.65	181.99
96.21	-47.81	0.23	96.22	0.38	256.35	0.75	256.04
87.96	-48.28	-79.69	96.50	-140.02	222.89	-368.23	363.33
96.10	-95.98	-48.25	48.17	-79.52	64.66	-182.29	148.29

192.78	-0.02	64.37	0.05	74.56	0.10	137.56	0.09
191.93	-0.22	128.78	0.05	151.18	0.25	257.82	0.08
190.97	-0.75	30.97	96.41	35.95	182.77	69.08	175.24
191.26	-0.14	-1.38	95.36	-1.60	180.08	-3.20	180.41
191.86	-0.25	64.57	94.99	74.98	181.12	138.24	165.70
192.13	-0.13	96.54	97.03	112.52	187.42	199.57	163.44
191.49	0.25	194.84	94.75	233.93	200.07	367.41	145.58
193.07	0.62	-95.77	95.63	-111.33	184.38	-254.76	207.27
192.12	0.21	-192.48	95.84	-230.43	201.75	-630.05	255.62
193.10	2.23	64.50	193.49	74.65	366.82	137.72	336.62
192.31	0.29	-1.74	192.26	-2.01	362.08	-4.03	362.90
191.54	-0.82	128.14	191.09	150.57	377.64	256.89	312.15
193.42	0.94	95.66	287.09	111.10	551.60	197.40	482.72
192.89	1.82	-0.51	288.48	-0.59	542.47	-1.18	542.83
193.50	97.36	65.03	1.38	75.19	-28.65	138.64	2.40
193.21	97.33	128.28	0.03	150.04	-65.23	256.30	0.05
191.45	95.64	31.39	98.06	36.39	170.69	69.91	177.94
191.98	96.49	-0.75	96.02	-0.87	181.34	-1.74	181.16
191.74	96.38	65.54	96.45	76.13	152.30	140.20	168.11
192.08	96.20	95.97	96.65	111.86	139.45	198.53	162.91
192.09	96.03	192.30	95.43	230.22	92.30	363.04	146.80
192.89	96.55	-192.51	97.04	-229.94	311.64	-627.68	257.81
192.58	96.87	64.40	193.15	74.63	336.36	137.68	336.46
192.85	97.39	0.65	194.07	0.75	364.67	1.50	364.67
192.41	96.45	128.77	192.41	150.96	313.41	257.56	313.58
193.32	97.27	192.51	193.48	229.64	296.35	362.60	296.94
192.03	97.87	96.26	288.67	112.22	509.33	199.09	486.48
192.02	96.69	0.03	288.19	0.03	543.13	0.07	543.13
193.00	96.90	192.62	289.07	230.00	497.22	362.97	443.85
191.45	95.93	127.95	383.76	150.37	692.26	256.60	627.11
193.23	193.41	64.55	1.54	74.68	-58.85	137.78	2.68
193.13	192.55	128.27	0.20	150.06	-128.85	256.32	0.33
192.67	192.92	32.22	96.59	37.23	151.73	71.47	174.58
192.59	193.63	-0.50	97.74	-0.58	184.41	-1.16	184.06
192.46	193.06	67.25	96.45	77.99	118.96	143.35	167.52
194.01	193.62	96.62	97.12	112.05	92.45	198.94	162.94
193.99	193.90	193.25	96.83	230.13	-13.84	363.34	148.34
192.34	192.63	161.51	97.01	191.10	24.75	313.25	153.31
193.57	193.01	62.02	191.33	71.67	303.68	132.65	333.43
184.12	168.07	15.50	241.58	18.31	451.65	35.87	455.48
192.65	193.08	127.77	190.86	149.66	245.69	255.69	311.21
192.23	192.50	192.37	191.93	230.21	186.35	363.06	295.15
192.90	192.71	192.98	288.98	230.54	389.42	363.60	443.65
192.12	192.35	288.57	288.37	366.20	297.32	504.28	410.61
191.55	191.14	127.71	382.94	150.04	626.01	256.13	625.79
192.00	191.90	257.09	384.32	318.53	561.08	460.25	560.61
192.99	289.57	31.83	95.07	36.75	134.10	70.59	171.78
192.87	289.02	66.21	95.30	76.69	86.19	141.17	165.57
193.03	-95.67	64.23	-1.80	74.35	27.03	137.20	-3.13
192.38	-95.23	128.26	0.00	150.36	64.33	256.68	-0.00
192.71	-95.79	31.87	95.90	36.82	195.85	70.72	173.39
192.01	-95.64	-0.73	96.69	-0.84	181.89	-1.69	182.41
191.77	-96.50	64.63	94.69	75.06	211.74	138.38	165.20
192.39	-96.31	97.24	96.02	113.27	233.09	200.76	161.53
192.54	-95.85	-96.45	96.70	-112.29	139.44	-257.34	210.22
192.04	-95.32	-193.93	97.81	-232.36	97.25	-637.48	261.98
192.17	-96.24	-1.18	191.97	-1.36	361.11	-2.73	362.22
192.16	-96.57	-193.74	191.14	-232.03	292.49	-636.14	511.38
192.50	-192.51	-96.81	96.38	-112.73	91.02	-258.49	209.69
384.41	193.20	129.73	0.10	106.42	-44.08	196.17	0.12
383.32	193.89	63.02	194.83	51.63	239.20	99.17	249.82
383.50	192.46	-2.78	191.01	-2.28	255.67	-4.56	255.20
384.94	193.84	131.06	195.49	107.45	218.37	197.92	240.55
229.49	36.82	190.30	191.90	206.01	325.68	338.53	278.16
385.04	195.77	118.58	385.58	97.14	477.10	180.31	477.72
185.58	-6.29	0.10	385.63	0.12	739.30	0.24	739.20

384.77	193.34	256.00	389.76	212.20	450.25	362.35	449.52
384.11	194.54	229.54	768.67	189.88	978.89	329.39	898.78
385.43	386.94	127.51	0.06	104.45	-86.55	192.83	0.07
386.61	387.66	255.73	-0.03	211.43	-183.09	361.37	-0.03
387.02	387.82	64.61	193.57	52.68	214.48	101.13	246.87
384.41	386.72	0.36	193.79	0.29	257.89	0.59	258.07
385.44	385.25	132.01	193.54	108.16	170.94	199.14	237.89
385.13	385.70	192.75	193.39	158.67	129.96	281.55	230.17
385.48	386.56	319.70	195.01	267.03	38.79	438.80	218.09
385.82	385.62	127.93	383.52	104.74	428.80	193.34	472.28
384.97	386.93	2.24	385.73	1.83	511.94	3.65	512.69
385.78	386.46	256.90	385.66	212.67	351.92	363.11	444.16
385.77	386.13	385.97	385.29	326.05	264.38	514.23	418.27
383.17	384.88	178.03	575.95	146.76	661.12	262.60	692.22
385.06	383.38	385.57	575.90	326.03	549.63	514.10	625.68
384.98	384.81	241.70	766.75	199.96	889.72	344.45	890.36
385.60	385.15	512.19	769.15	447.18	792.25	648.07	792.98
385.31	577.26	64.12	190.37	52.39	189.76	100.60	243.36
382.78	576.96	136.77	191.81	112.48	118.77	206.38	235.84

APPENDIX 5C

TANGENT AND SECANT K-THETA PREDICTIONS - GRADED MATERIAL

p_m (kPa)	q_m/p_m	p_r/p_m	q_r/p_m	Secant		Tangent	
				v_r (με)	ε_r (με)	v_r (με)	ε_r (με)
98.11	0.06	0.31	-0.03	26.24	-7.80	76.21	-4.74
98.26	0.06	0.64	-0.06	54.51	-17.04	142.29	-8.94
98.51	0.07	0.15	0.49	12.51	94.28	38.37	90.67
98.45	0.06	0.01	0.50	0.61	98.13	1.97	97.94
98.74	0.07	0.31	0.48	26.29	91.83	76.36	84.56
98.40	0.07	0.50	0.49	42.34	94.87	115.65	82.44
99.03	0.07	0.97	0.46	85.55	94.10	199.75	68.06
98.03	0.06	-0.50	0.49	-42.02	104.26	-163.00	117.08
98.44	0.07	-0.97	0.51	-85.70	126.60	-415.94	156.38
98.41	0.07	0.29	0.98	24.73	189.75	72.27	173.06
98.31	0.06	0.00	0.99	0.08	193.11	0.24	193.05
98.30	0.07	0.64	0.98	54.98	196.86	143.28	157.32
97.50	0.06	0.44	1.47	37.22	290.88	103.61	249.47
97.31	0.05	0.01	1.53	0.84	297.69	2.69	296.73
97.95	0.55	0.32	-0.01	27.16	-25.26	78.60	-0.95
97.60	0.55	0.64	-0.03	54.33	-56.97	141.87	-4.70
97.66	0.55	0.16	0.51	13.40	87.15	40.94	93.48
98.04	0.55	0.32	0.49	27.24	73.40	78.82	86.81
98.04	0.54	0.01	0.52	0.49	100.41	1.56	100.63
98.41	0.55	0.49	0.49	41.36	61.05	113.42	82.11
99.03	0.55	0.96	0.47	84.73	21.25	198.41	70.73
98.27	0.55	-0.48	0.51	-40.66	140.61	-156.71	121.12
98.93	0.54	-0.96	0.51	-84.27	201.82	-405.39	157.38
98.18	0.56	0.30	0.95	25.58	164.92	74.50	168.22
97.92	0.55	-0.01	0.97	-1.08	190.60	-3.50	190.49
98.25	0.55	0.64	0.96	54.94	148.49	143.20	155.26
98.30	0.55	0.98	0.96	86.81	130.03	201.64	141.77
97.76	0.55	0.47	1.49	39.31	264.50	108.58	251.92
98.83	0.55	0.98	1.47	86.11	248.22	200.61	218.24
97.96	0.54	-0.01	1.52	-0.74	296.16	-2.38	296.42
97.98	0.55	0.61	1.96	52.19	356.30	137.38	318.26
98.58	0.55	0.02	1.99	1.80	387.58	5.77	386.29
97.90	1.04	0.32	-0.00	26.67	-45.64	77.33	-0.46
98.11	1.04	0.64	-0.01	54.68	-98.05	142.64	-0.84
97.70	1.04	0.16	0.49	13.46	73.09	41.11	90.36
97.81	1.04	0.00	0.49	0.24	94.28	0.78	94.59
98.13	1.04	0.31	0.47	26.44	48.24	76.75	82.91
98.17	1.04	0.49	0.49	41.86	25.65	114.55	81.19
99.00	1.03	0.94	0.47	83.06	-52.57	195.64	70.18
98.37	1.04	-0.48	0.51	-40.54	173.46	-156.13	120.56
98.11	1.03	0.32	0.97	26.51	147.56	76.92	171.24
98.12	1.03	-0.01	0.97	-0.70	180.97	-2.27	189.35
98.42	1.04	0.64	0.94	54.70	97.71	142.70	151.06
98.33	1.04	0.96	0.94	84.13	50.16	197.28	139.71
98.14	1.03	0.47	1.46	39.93	225.04	110.07	245.21
98.23	1.04	0.97	1.45	85.50	165.58	199.50	215.26
99.09	1.04	1.42	1.41	135.48	82.15	265.71	190.88
96.96	1.03	0.65	2.00	55.33	316.13	143.88	319.49
97.76	1.04	1.30	1.93	120.56	247.25	248.55	266.49
97.95	1.53	0.16	0.48	13.26	61.41	40.54	88.93
98.23	1.52	0.32	0.48	27.05	28.55	78.34	85.06
98.85	1.52	0.65	0.97	55.66	57.10	144.75	155.80
98.96	-0.40	0.31	-0.04	26.44	9.82	76.77	-6.80
98.53	-0.41	0.63	-0.10	53.86	17.61	140.96	-15.53

98.55	-0.42	0.14	0.48	11.72	102.86	36.06	90.32
97.96	-0.42	0.01	0.50	0.79	97.90	2.55	97.04
98.52	-0.41	0.31	0.47	25.78	110.26	75.02	83.00
98.16	-0.42	0.49	0.47	41.44	123.39	113.57	78.22
97.87	-0.43	-0.49	0.49	-41.49	69.64	-160.59	116.07
98.35	-0.42	-0.97	0.49	-85.76	45.08	-416.39	151.85
98.22	-0.42	-0.00	1.00	-0.09	195.84	-0.30	195.98
98.19	-0.42	-0.97	0.96	-85.43	151.62	-414.13	295.12
98.11	-0.90	-0.49	0.49	-41.66	35.74	-161.35	115.11
50.06	-0.36	0.30	-0.08	20.33	-1.28	59.32	-11.88
50.27	-0.36	0.56	-0.17	39.01	-5.04	104.31	-23.19
50.08	-0.37	0.12	0.47	8.05	79.07	24.95	71.28
49.99	-0.37	0 01	0.49	0.47	77.23	1.51	76.78
50.52	-0.35	0.29	0.46	19.57	84.65	57.33	66.10
50.15	-0.36	0.45	0.44	31.11	90.39	86.28	60.64
49.93	-0.37	-0.47	0.50	-32.23	62.18	-123.71	95.20
50.69	-0.35	-0.92	0.56	-65.61	58.89	-309.49	135.03
50.26	-0.36	-0.01	0.93	-0.90	147.44	-2.91	148.64
51.41	-0.30	1.00	1.07	72.30	243.25	166.98	129.04
50.31	-0.83	-0.48	0.47	-33.18	31.20	-127.99	89.92
49.71	0.10	0.29	-0.05	19.88	-11.69	58.14	-7.49
50.23	0.11	0.60	-0.09	41.76	-22.22	110.26	-11.53
49.94	0.11	0.14	0.49	9.68	75.62	29.75	73.50
50.01	0.11	-0.01	0.50	-0.80	78.96	-2.59	79.14
50.41	0.13	0.31	0.46	20.96	69.65	60.99	66.19
50.04	0.12	0.47	0.46	32.50	69.15	89.54	63.00
50.18	0.13	0.96	0.46	68.22	67.04	160.03	55.05
49.82	0.11	-0.49	0.50	-33.55	88.26	-129.77	96.04
50.19	0.11	-0.96	0.50	-68.84	106.56	-332.47	123.89
49.38	0.12	0.27	0.98	18.41	152.41	54.21	141.42
49.68	0.13	0.02	1.01	1.17	158.90	3.74	158.19
50.59	0.13	0.66	0.97	46.05	153.78	119.30	126.08
49.90	0.14	0.38	1.44	26.31	226.73	74.62	201.83
49.95	0.11	0.01	1.52	0.98	240.81	3.14	239.78
50.17	0.61	0.31	-0.02	21.42	-23.57	62.18	-2.18
49.87	0.60	0.62	-0.03	42.91	-48.58	112.67	-3.65
50.04	0.60	0.15	0.48	10.05	66.82	30.84	72.68
50.21	0.60	0.01	0.50	0.72	77.99	2.32	78.39
49.88	0.59	0.30	0.47	20.63	56.13	60.12	68.10
50.25	0.60	0.47	0.46	32.49	42.75	89.55	62.66
50.31	0.61	0.95	0.46	67.98	8.53	159.68	55.93
49.64	0.61	-0.51	0.49	-34.83	116.42	-135.74	95.58
50.42	0.59	-0.93	0.50	-66.62	164.95	-316.63	122.99
50.38	0.60	0.29	0.94	19.72	131.13	57.73	135.39
50.46	0.60	0.01	0.96	0.51	151.62	1.64	151.72
50.15	0.60	0.60	0.93	41.83	113.27	110.40	123.01
49.65	0.59	0.96	0.93	67.96	96.71	159.44	112.15
49.22	0.60	0.45	1.48	30.66	209.90	85.14	202.95
49.40	0.58	-0.00	1.48	-0.20	233.74	-0.66	233.79
50.22	0.60	0.92	1.38	65.52	179.42	155.55	168.58
49.78	0.59	0.57	1.89	38.94	275.06	104.10	251.84
50.41	0.61	0.02	1.95	1.51	303.53	4.84	307.63
50.26	1.08	0.30	-0.01	20.38	-37.43	59.47	-1.44
50.03	1.08	0.64	-0.02	44.07	-84.24	115.13	-2.55
49.71	1.09	0.15	0.48	10.48	58.41	32.06	72.68
49.85	1.08	0.00	0.49	0.33	76.60	1.07	77.04
50.10	1.08	0.30	0.46	20.50	37.64	59.77	66.07
49.72	1.08	0.48	0.46	32.89	16.10	90.43	62.66
50.18	1.07	0.97	0.46	69.13	-53.79	161.51	55.07
49.98	1.08	-0.48	0.48	-33.01	137.73	-127.25	91.86
50.06	1.08	0.31	0.98	21.24	119.35	61.70	139.84
50.17	1.07	-0.00	0.98	-0.04	155.57	-0.13	155.53
50.14	1.08	0.63	0.95	43.60	79.21	114.16	124.31
50.21	1.08	0.95	0.93	67.87	34.42	159.45	112.36
49.52	1.09	0.47	1.48	32.31	182.01	89.06	200.99
49.90	1.08	0.95	1.43	67.26	127.12	158.37	172.92

50.15	1.10	1.40	1.39	107.70	50.64	213.04	152.84
50.40	1.08	0.61	1.91	42.34	244.01	111.54	252.51
50.21	1.09	1.27	1.90	94.54	185.94	197.86	214.79
49.77	1.56	0.17	0.50	11.32	50.31	34.50	74.34
50.26	1.55	0.32	0.49	22.04	23.39	63.81	70.26
50.25	1.56	0.63	0.95	43.58	44.41	114.12	124.69
26.18	0.23	0.26	-0.09	14.77	-17.70	43.56	-11.07
26.14	0.23	0.56	-0.13	31.80	-30.17	85.06	-14.28
25.87	0.22	0.12	0.48	6.92	59.03	21.39	58.87
26.00	0.23	0.01	0.50	0.79	64.31	2.53	64.28
26.17	0.24	0.23	0.92	12.85	115.22	38.35	110.53
26.36	0.24	0.00	0.93	0.14	121.05	0.45	121.00
26.39	0.25	0.33	1.37	18.36	173.25	53.05	160.09
26.21	0.22	0.03	1.49	1.86	192.26	5.94	190.69
25.95	0.69	0.28	-0.07	15.79	-26.39	46.29	-7.84
26.12	0.68	0.56	-0.12	31.81	-52.52	85.08	-12.89
25.92	0.69	0.13	0.46	6.93	51.27	21.43	56.46
26.00	0.69	0.00	0.48	0.22	61.68	0.71	61.84
26.06	0.70	0.26	0.91	14.22	102.95	42.08	108.49
26.08	0.69	-0.01	0.94	-0.52	121.84	-1.69	121.66
25.99	0.69	0.38	1.38	21.05	157.82	59.85	157.75
26.11	0.68	0.02	1.44	1.10	185.40	3.52	185.33
25.85	0.70	0.50	1.89	27.95	220.46	76.37	208.94
25.99	0.66	0.04	1.95	2.17	249.36	6.90	248.28
26.23	-0.23	0.28	-0.13	15.42	-11.24	45.32	-15.30
26.25	-0.22	0.52	-0.27	29.54	-25.41	80.05	-29.84
26.17	-0.23	0.10	0.46	5.56	61.39	17.34	57.29
26.02	-0.23	0.01	0.48	0.45	62.44	1.44	62.10
26.00	-0.24	-0.02	0.92	-1.03	118.98	-3.35	120.14
25.94	1.14	0.29	-0.05	16.25	-36.59	47.52	-5.69
26.05	1.13	0.61	-0.04	34.21	-71.23	90.26	-4.34
25.74	1.17	0.14	0.48	7.93	46.59	24.37	58.50
25.99	1.16	0.01	0.49	0.66	62.37	2.12	63.34
26.07	1.16	0.28	0.93	15.54	92.28	45.64	109.90
25.87	1.15	-0.01	0.95	-0.70	124.17	-2.28	123.41
26.05	1.17	0.41	1.38	23.11	138.70	64.94	156.85
25.83	1.15	0.55	1.87	30.70	192.60	82.57	203.71
387.87	0.02	0.32	-0.02	41.58	-8.17	120.36	-6.06
385.47	0.01	0.15	0.49	19.23	147.47	58.94	140.16
386.34	0.02	0.01	0.47	1.25	139.31	4.03	138.87
382.70	0.01	0.30	1.00	38.45	301.86	112.12	271.11
377.71	0.01	0.00	1.05	0.62	309.53	2.01	309.01
384.99	0.01	0.45	1.49	58.15	455.22	161.43	385.02
382.61	0.52	0.32	-0.02	41.15	-39.51	119.18	-4.26
384.54	0.52	0.62	-0.04	81.10	-82.88	212.80	-8.91
387.78	0.51	0.16	0.51	20.51	136.36	62.66	144.77
386.06	0.51	0.00	0.52	0.00	155.79	0.00	155.79
389.32	0.51	0.31	0.99	39.50	266.21	114.94	267.50
386.94	0.52	0.00	1.00	0.22	297.96	0.70	297.97
387.78	0.50	0.47	1.49	60.21	410.70	166.35	385.70
380.26	0.48	0.03	1.60	4.15	470.72	13.24	468.59
395.70	0.53	0.61	1.94	79.79	546.23	210.38	486.28
382.13	1.00	0.32	-0.01	41.14	-70.08	119.16	-2.36
381.59	1.00	0.66	0.01	86.68	-146.48	224.28	2.29
384.80	1.01	0.16	0.50	20.62	117.39	62.96	142.45
384.02	1.01	0.01	0.51	1.51	148.52	4.84	150.34
386.27	1.00	0.32	1.00	41.32	235.57	119.66	269.44
383.26	1.01	-0.00	1.00	-0.13	298.80	-0.41	298.70
386.59	1.01	0.47	1.46	60.96	348.43	168.09	376.76
381.63	0.02	0.15	0.47	18.82	139.93	57.75	133.49
387.06	0.02	-0.00	0.47	-0.36	141.46	-1.16	141.59
387.26	0.00	0.30	0.99	38.55	298.32	112.43	267.52
379.95	0.00	-0.01	1.04	-0.66	307.53	-2.14	308.08
387.73	-0.00	0.46	1.48	59.14	455.37	163.82	382.75
194.19	0.03	0.32	-0.01	32.78	-5.08	95.11	-3.14
195.29	0.03	0.65	-0.04	68.77	-13.25	178.81	-7.63